PROCEEDINGS OF THE SECOND INTERNATIONAL SYMPOSIUM
ON ULTRA-CLEAN PROCESSING OF SILICON SURFACES

Marc Heyns (editor)
Marc Meuris & Paul Mertens (co-editors)

Proceedings of
the Second International Symposium on

Ultra-Clean Processing of Silicon Surfaces
(UCPSS '94)

Acco Leuven / Amersfoort

Conference organized by IMEC

First Edition : 1994

TW. 250.00.0
32 012 3262

Published by Uitgeverij Acco, Tiensestraat 134-136, 3000 Leuven (België)
For the Netherlands : Postbus 1285, 3800 BG Amersfoort / Hamersveldseweg 10a, 3833 GP Leusden

D/1994/0543/216 NUGI 841 ISBN 90-334-3262-5

Table of Contents

Preface

The First and Second International Symposium on Ultra Clean Processing of Silicon Surfaces (UCPSS) were held in Leuven (Belgium), September 17-19, 1992 and Bruges (Belgium), September 19-21, 1994 respectively. These symposia were organised by IMEC with the aim to provide a forum where the diverse groups who have been investigating Si-surfaces and ultra-clean technology from different points of view, could come together in order to improve the current understanding of the ultra-clean processing of silicon surfaces.

The scientific programme of UCPSS '94 consisted of 8 invited and 81 regular contributions which were selected out of 103 submitted abstracts. The meeting was attended by more than 250 scientists from 18 countries. The order and organisation of the presentations at the conference are maintained in these proceedings. Thanks are due to the programme committee for selecting the contributions and to the symposium authors and participants who made this symposium an informative and productive event.

The issues which were addressed at the UCPSS '94 symposium covered all aspects of ultra-clean Si-technology, cleaning, contamination control, Si-surface chemistry and topography and its relation with device performance and process yield. It was clearly noticeable that a lot of progress has been made in various areas over the last years and that the degree of fundamental understanding related to cleaning and contamination issues has come to a very high level.

The fundamental principles governing the metal adsorption and particle deposition from liquids onto Si-wafers were discussed by various authors. This work has come to such a level that it can now be effectively used as an instrument in the optimisation of wet cleaning technologies. Important progress was also reported on the understanding of the relation between various contaminants, cleaning strategies and yield (essentially of thin oxide layers). Various optimised cleaning and measurement techniques were proposed. Very interesting results were also presented on the initial oxidation steps on HF-treated surfaces. This work is a key contribution in the research directed to the reproducible growth of ultra-thin oxide layers. Particle densities, metal contamination and Si-surface roughness have been investigated extensively over the last few years. An important trend that could be noticed at the symposium was that a lot of attention also starts to be given to the causes and effects of organic contamination on Si-surfaces. The understanding at this point is, however, still rather fragmentary and a lot of work remains to be done.

An interesting aspect of the meeting was that the reports on fundamental research work were complemented with more practical oriented presentations where experiences from a production environment were shared. The confrontation of fundamental research with practical applications proved to be very productive and often resulted in lively discussions.

The success of the conference prompted us to start preparing for the Third International Symposium on Ultra Clean Processing of Silicon Surfaces (UCPSS '96). This will take place in Antwerp (Belgium) between September 23 and 25, 1996. The enthusiasm created by the first two meetings makes us look toward the Third Symposium with great excitement.

Marc Heyns
Conference Chairman

CONFERENCE ORGANISATION

Programme Committee

Marc Heyns (IMEC, Leuven, Belgium)
Carl Sofield (Harwell Laboratory, Oxfordshire, U.K.)
Jerzy Ruzyllo (Penn State Universtity, Pennsylvania, U.S.A.)
Ara Philipossian (Intel Corporation, Santa Clara, U.S.A.)
Tadahiro Ohmi (Tohoku University, Sendai, Japan)
Takeshi Hattori (Sony Corporation, Atsugi, Japan)

Local Organizing Committee

Marc Heyns (IMEC)
Marc Meuris (IMEC)
Paul Mertens (IMEC)
Stefaan Hendriks (Timshel Conference Service)

Sponsors and Supporting Organizations

The meeting received support from IMEC and from the IEEE Electron Devices Society.

The organisation of this symposium has been made possible with the financial support of the following companies : ASM International, BOC Limited, Fisons Instruments, FSI International, GeMeTec, Millipore, MSB, Norton Electronics, OCG, Olin Hunt, Ontrak Systems Inc., Semitool, Structural Europe, SubMicron Systems Inc. and Verteq.

TRENDS IN WAFER CLEANING TECHNOLOGY

Takeshi Hattori

Sony Corporation, Atsugi, Japan

1. Introduction

As device geometries continue to shrink and die sizes grow, microcontaminants such as particles and metallic and organic impurities have an ever-increasing impact on device yields. Keeping wafer surfaces scrupulously clean through the wafer processing cycle is, therefore, an essential prerequisite to obtaining high yields in the fabrication of VLSI devices.

Every wafer-processing step is a potential source of contamination. Only wet-chemical processing, or wet cleaning, between processing steps can reduce the number of particles on the surface of silicon wafers. Wet cleaning also removes metallic and organic contaminants as well as obstructive native-oxide films, which may not be quite a contaminant.

Wet cleaning is, therefore, the most repetitively applied processing step in any LSI fabrication sequence. Until recently, the fundamental processes involved in cleaning were not well understood and wet-cleaning procedures were too often applied on a trial-and-error basis. Recent progress in contamination detection techniques on the wafer surfaces have made it possible to evaluate and optimize cleaning processes based on scientific considerations. Hence, wafer cleaning has become a major area of concern and investigation [1,2]. This paper focuses on recent progress in wafer-cleaning technology and discusses the future prospects of this technology [3]. Special emphasis will be placed on the experience of the Japanese semiconductor industry [4].

2. Wet Cleaning: Chemistry

Although wet etching has been replaced by dry techniques for small-geometry applications, wafer cleaning by wet chemical means will continue to be the dominant technique for years to come. Although there is a strong interest in new vapor-phase cleaning and even newer completely dry-cleaning techniques, such processes remove only specific types of contaminants and presently offer little hope of removing small particles and some residues, at least not without a subsequent wet rinse. Ironically, the importance of wet cleaning has been more recognized as dry processes such as plasma etching have become popular.

Wafer cleaning chemistry has remained essentially unchanged over the past 25 years, the most prevalent method in the semiconductor industry still being the hydrogen peroxide-based wet-chemical process most notably the RCA Standard Clean, where wafers are sequentially immersed in the chemicals shown in Table I in order to remove organics, particles, metallics, and native oxides. Some examples of chemicals used in pre-oxidation wafer cleaning by Japan's major semiconductor companies are shown in Figure 1.

Table I. Typical chemicals for wet cleaning of wafers.

Contaminants	Chemicals
Organics	SPM (H_2SO_4/H_2O_2) = Piranha APM ($NH_4OH/H_2O_2/H_2O$) = SC-1
Particles	APM ($NH_4OH/H_2O_2/H_2O$)
Metallics	HPM ($HCl/H_2O_2/H_2O$) = SC-2 SPM (H_2SO_4/H_2O_2) DHF (HF/H_2O)
Native Oxides	DHF (HF/H_2O) BHF ($NH_4F/HF/H_2O$)

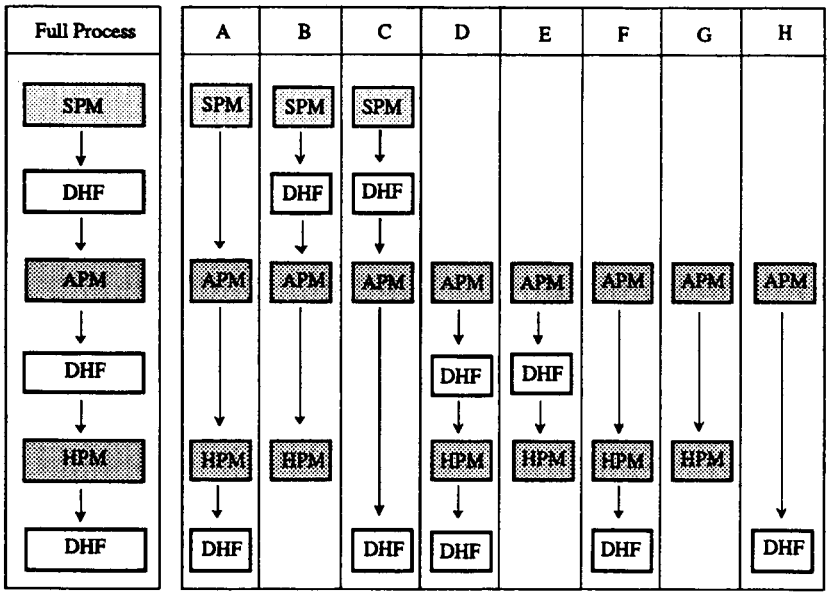

Figure 1. Sequence of chemicals used in pre-oxidation wafer cleaning by Japanese companies [4].

The advent of smaller geometries and contamination-sensitive features forced us to seek new methods of wet chemical processing. Continued improvements in performance and cost-effectiveness will be made by new chemicals and new equipment designs. It is for this reason that modified or alternative chemicals are being proposed and used with a varying degree of success. These include surfactant-added chemicals, HF-added piranha, chelate-added NH_4OH, diluted HCl, H_2O_2-added HF, IPA/ClHAc-added HF, ozonated water, and HF water. More recently, ecologically safe treatment in alkali and acid ionized water has been proposed.

Mechanical means, such as megasonics, centrifugal spraying, scrubbing, and pressurized fluids, and cryogenic particle jets, can be used to complement conventional simple immersion. Particularly, the use of megasonics in the SC-1 solution is very effective in removing particles adhering to the wafer. Some companies have been employing blush or water-jet scrubbing for wafer-frontside cleaning after oxide/metal film deposition on the wafer and/or wafer-backside cleaning.

3. Wet Cleaning: Equipment

To reduce the size of the wet bench and to reduce chemical consumption, simplification of the cleaning sequence has been attempted, particularly by eliminating the SC-2 step by using alternative chemicals. Consequently, the number of wet benches can be reduced as is shown in Figure 2. A single-bath system where the wafers are kept stationary and chemicals move across them will

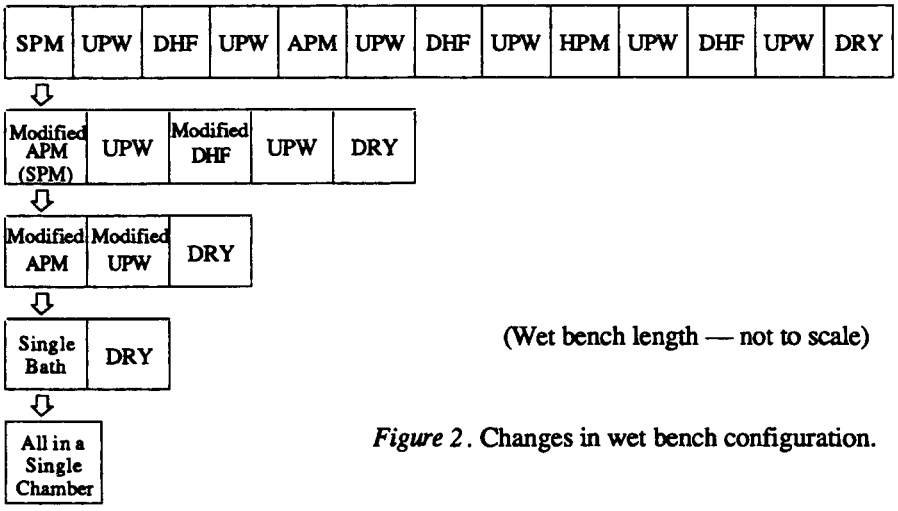

Figure 2. Changes in wet bench configuration.

minimize problems caused by repeated crossing through the particle-laden air/liquid boundary. But this configuration may bring about cross-contamination problems. Every configuration in Figure 2 is presently employed in the industry.

Wet chemical cleaning can reduce contaminants, but to achieve such results wafer carriers and baths as well as wet chemicals and the water must be clean. Although little attention has been paid to the impact of improper carrier use on device yields, adequate carrier cleaning is an important key to successful contamination control in wet chemical processing. Recently, carrierless wet benches have been put on the market and are particularly popular in Japan and even more in Korea. Carrierless wet benches allow smaller baths by eliminating the space needed for the carrier, thus trimming chemical consumption. But highly reliable transporting and chucking robotics is essential. Cleanliness of the wafer backside is another important factor in a scrupulously clean surface, particularly in the immersion-type wet bench (Figure 3).

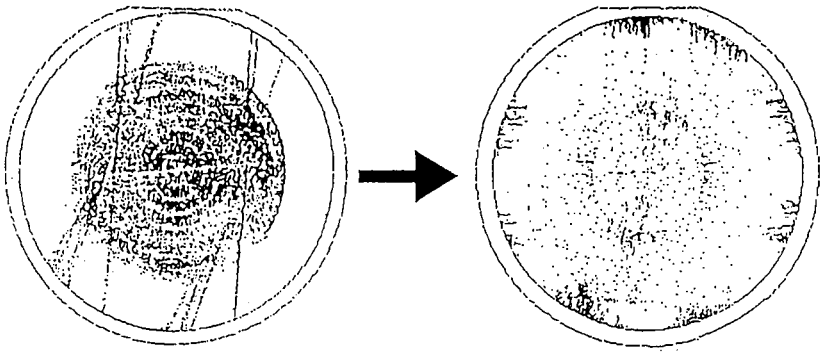

Figure 3. Transfer of particles from the back surface of a wafer to the front surface of the adjacent wafer during wet cleaning.

Wafer spin-processing equipment, much smaller than wet benches, must increase its throughput if it is to be applicable for general cleaning and its chemical consumption must be reduced. This equipment is very promising for ultra-dirty wafer cleaning applications after chemical-mechanical planarization.

The last step in wet cleaning is drying, an extremely critical step. While spin drying has been widely used, IPA vapor drying is preferred in the most advanced lines in order to prevent particle adhesion and watermark formation. The thermal design of the equipment and the purity of the solvent are extremely important in achieving good results. Other drying techniques, such as IPA direct-displacement and Marangoni drying, are being explored.

It should be noted here that even the most stringent wafer cleaning cannot solve every contamination-related problem, being useless for removing particles generated just before or during dry etching and film deposition. This is why a priority on the ultraclean processing of silicon surfaces is necessary throughout ULSI fabrication.

4. Dry Cleaning

While the use of advanced wet chemical cleaning techniques will persist for years to come, the research trend is toward a shift from liquid to vapor/gas-phase reactions. Gaseous reactions potentially offer more effective cleaning of smaller feature-size structures using significantly less chemicals and can be easily integrated with cluster tools, offering single-wafer processing capabilities.

Already, HF vapor-phase etching has been used for niche applications such as pre-silicide cleans. The addition of methanol to the anhydrous HF can suppress particulate and other residues on the silicon surface. Ultraviolet (UV)-excited dry cleaning and plasma-assisted dry cleaning have also been developed for specific applications, such as shown in Table II. More recently the formation of volatilizable organometallic chelates or complexes has been explored. Laser-assisted and gas-based particle removal is also in the research stage, but efficient ultra-small particle removal by dry means will be very difficult without causing substrate damage. No matter what technique is used —wet or dry— effective particle removal will continue to be a major challenge.

Table II. Typical methods for vapor/gas-phase cleaning.

Contaminants	Cleaning Methods
Organics	UV/O_3 Plasma O_2
Particles	?
Metallics	UV/Cl_2 HCl Vapor, NO/HCl Chlorine Oxidation/Anneal Organometallic Chelate
Native Oxides	HF Vapor (HF/H_2O, HF/CH_3OH) $UV/F_2/H_2$, H_2 Anneal Plasma H_2, NF_3, etc. Ar Sputter

5. Summary and Future Requirements

Although contamination prevention is always preferable, proper wafer cleaning of in-process wafers is indispensable for reducing surface particles as well as other contaminants. Wet cleaning will be continuously used for general purpose cleaning, particularly for the removal of particles and other heavy and gross contaminants, while dry cleaning will be used for application-specific cleaning and *in-situ* cleaning before certain wafer processes as part of integrated processes. Future efforts should be directed towards further reducing surface contamination to attain ultra-clean silicon surfaces. This will require advances in analytical tools and methods as well as revised or completely new cleaning methodologies.

Next-generation ULSI devices will have higher aspect-ratio structures, and more complicated and fragile structures such as fin-type DRAM capacitors. In addition, dirty CMP might be widely employed for planarization purposes. Cleaning of these structures will be a key issue in the near future. Several types of post-etch residues, watermarks, and process-induced damage must be prevented or removed, which could be ignored when feature sizes were larger than they are now.

Wafer cleaning does not only remove microcontaminants introduced by the previous processing steps but has also to prepare an optimum surface for the next processing step. The role of surface conditioning will become more important in the future. As we learn more about chemical reactions on the silicon surface from the scientific standpoint, we can begin to introduce new techniques, such as complete hydrogen termination of the silicon surface and surface passivation with ultrapure chemical oxides.

Not only from the performance point of view, but also from the standpoint of environmental concern, we must reconsider wafer cleaning to meet tougher future requirements. In the future, we hope to achieve complete recycling of waste chemicals instead of their disposal, use of less- or non-hazardous chemicals, and eventually and ideally ultraclean processing which requires no wafer cleaning procedures to remove contaminants.

REFERENCES

1. Extended Abstracts of the 1st International Symposium on Ultra Clean Processing of Silicon Surfaces (UCPSS'92), IMEC, Leuven, 1992.
2. J. Ruzyllo and R. E. Novak (eds.), Proceedings of the 1st, 2nd, and 3rd International Symposium on Cleaning Technology in Semiconductor Device Manufacturing, Electrochemical Society, Pennington (1990, 1992, and 1994, respectively).
3. T. Hattori, Semicon/Japan Technology Symposium'93 Proceedings, SEMI Japan, 1993, pp. 449-456.
4. T. Hattori et al. (eds.), Survey of the Wafer Cleaning Specifications of Semiconductor Manufacturers No.1, Science Forum, Tokyo, 1993, and also No.2, 1994 (in Japanese).

Recipes to avoid particle contamination during wet cleaning processes

L.Mouche*, B.Beneyton*, C.Paillet*, J.P.Joly*, F.Tardif*, D.Levy, K.Barla**, P.Patruno**, A.Tonti**, W.Sievert*****

INTRODUCTION

In the same way as chemical contamination, particles also induce detrimental effects in terms of IC manufacturing yield for 7 nm gate oxide, particularly during the critical steps as illustrated in figure 1. Although we can today foresee solutions for chemical contaminant removal such as using purer and purer chemicals or reactive gases, we have still not yet come up with technical solutions for ultimate removal of particles.
To decrease the final particle level, the simplest way is of course to avoid adding particles, firstly during the cleaning steps themselves.

PARTICLE DEPOSITION MECHANISMS IN CLEANING BATHS

During wet cleaning processes, silicon wafers are immersed in and removed from the solution vertically. Two possibilities of particle contamination can occur, within the solution and during the passage through the gas-liquid interface [1-2]. A previous fundamental study [3] identified the contamination mechanisms :
- The in-solution mechanism is the following : when they are attracted by the wafers, the particles close to the surface deposit quickly. This deposition creates a concentration gradient which triggers diffusion of the particles to the wafer. *Contamination by this mechanism is proportional to the particle concentration in solution and is dependent on immersion time.*
- The interface mechanism is the following : during the movement of the wafers through the interface, diffusion (which limits particle contamination in solution) is substituted by convection (figure 2) which can induce a high particle contamination if the wafers are not protected by a liquid layer. *Contamination by this mechanism occurs only during immersion of dry wafers.*

PRACTICAL RECIPES TO AVOID PARTICLE DEPOSITION

Natural particle contamination was studied in several baths (DI water, HF, $HF+H_2O_2$, SC2, $H_2SO_4+H_2O_2$). To highlight the major contamination mechanism in these baths, contamination curves were plotted as a function of immersion time and immersion number. An example is given in figure 5 for the HF bath. As deposition is independent from immersion time and proportional immersion number, we can say that interface contamination is preponderant in the HF bath.

---

*L.E.T.I (C.E.A - Advanced Technologies), MEL, CEN/G, 17 rue des Martyrs / F-38054 Grenoble
**SGS/Thomson Centre Commun, F-38290 Crolles
***Riedel-de Haën AG, D-3076 Seelze

Table 1 summarises the features of each studied bath and the best way we found to avoid contamination in critical baths. The experimental results which enabled us to draw up this table are presented and commented below :

- *DI water rinse.* Particle contamination is very low on hydrophilic wafers in overflow tank and also in Quick Dump Rinse tank (QDR) but after HF treatment (hydrophobic wafers) quick dump rinse is to be avoided because the wafers are not protected by a thin film of water and interface contamination occurs (see figure 3). For hydrophobic wafers, to prevent particle contamination we propose using the sequence DI water overflow tank 1 during ten seconds followed by DI water overflow tank 2. Using two overflow tanks enables the rinsing time and DI water use to be decreased (see figure 4).

- For *HF bath*, which is propitious to interface contamination (see figure 5), we propose dipping the hydrophilic wafers in a DI water overflow tank before HF. Figure 6 proves that this sequence enables good results to be obtained without using a recirculated-filtered bath. The same figure shows that similar results could be obtained with the mixture HF / H_2O_2.

- For *SC2,* which is propitious to in-solution contamination (see figure 7), the best way is to use a filtered bath. Using this technique, we decreased the contamination in a VLSI SC2 bath from 150 particles on a 100 mm substrate before filtration to less than 10 particles after filtration (figure 8).

- In $H_2SO_4+H_2O_2$, both contamination mechanisms seem to occur. Many parameters have to be optimised to minimise particle contamination (mixture proportions, temperature). We propose using a filtered bath and dipping wafers in a DI water overflow tank before $H_2SO_4+H_2O_2$. As shown in figure 9, the latter precaution could be sufficient to obtain good results.

CONCLUSION

The study of particle deposition mechanism enables recipes to be proposed to avoid particle contamination in critical baths (acid baths). A simple DI water dip pretreatment is a good way of preventing interface deposition (HF, CARO) and a filtered bath is necessary to minimize in-solution contamination (SC2, CARO).

Quick Dump Rinse followed by DI overflow tank for hydrophilic wafers and two DI overflow tanks for hydrophobic wafers seem to be the best sequences for rinsing the wafers.

REFERENCES :

1. D.J. Riley and J. Carbonel, "The deposition of contaminants from deionised water onto hydrophobic silicon wafers", Journal of the I.E.S., p 28, Nov/Dec (1991).
2. L.D. Michaels, V.B. Menon, R.P. Donovan and D.S. Ensor, "Particle deposition at the solid-liquid interface", Proceedings of Institute of Environmental Sciences, p 438, (1988) .
3. L.Mouche, F.Tardif and J.Derrien, "Particle deposition mechanism on silicon wafers during wet cleaning processes", Journal of the Electrochemical Society, Vol. 141, N°6, June, p 1684, (1994).

Solution	DI water overflow tank	QDR on hydrophilic wafers	QDR on hydrophobic wafers	HF 1% on dry wafers	UC+ (HF1%, H_2O_2 1%)	SC2 1:1:5 T=70°C	H_2SO_4:H_2O_2 3:1 T=140°C
Interface contam-ination	very low	very low	very high	high	very low	low	high
In-solution contam-ination	very low	-	-	very low	very low	high	high
Improve-ments	-	-	Two DI water overflow tank rinses	DI water dip before HF	-	filtered bath	DI water dip before CARO and filtered bath

Table 1. Features in terms of particle contamination of several baths used in wet silicon cleaning. Improvements proposed to minimise particle contamination in each bath.

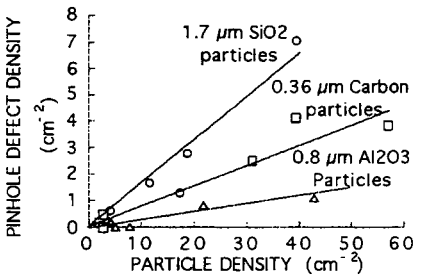

Figure 1. Particle impact on 7 nm dry oxide (hydrophobic wafers).

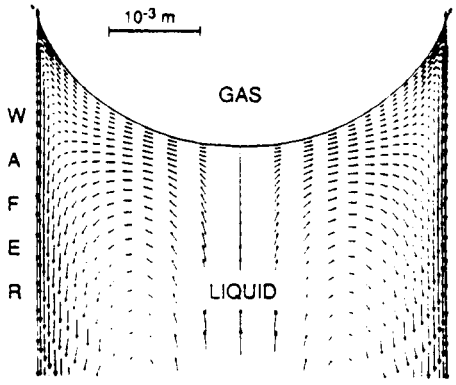

Figure 2. Hydrodynamics calculated by FIDAP software between two hydrophilic wafers dipped at the speed of 0.1 $m.s^{-1}$.

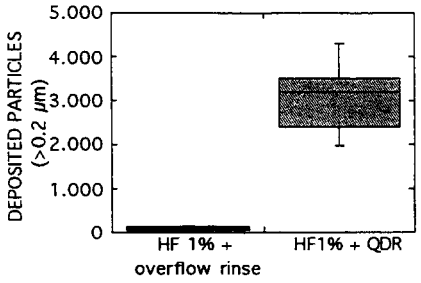

Figure 3. Impact of DI rinse water on particle contamination (hydrophobic wafers, 100 mm diameter).

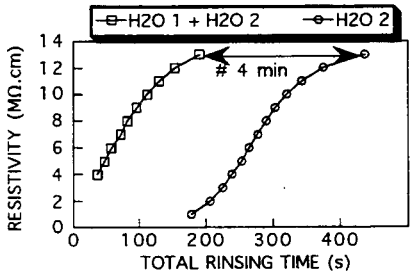

Figure 4. Rinse water resistivity as a function of total rinsing time after HF bath.

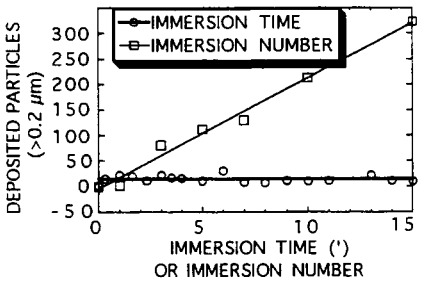

Figure 5. Particle contamination in HF 1% as a function of immersion time and immersion number (100 mm size wafers).

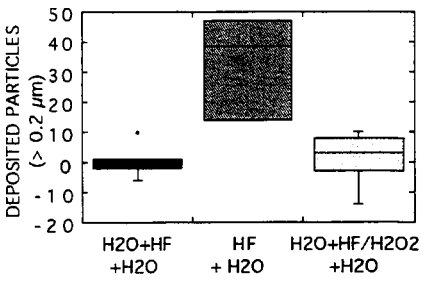

Figure 6. Particle contamination in HF and HF/H_2O_2 bath with or without DI water dip pretreatment (100 mm size initially hydrophilic wafers).

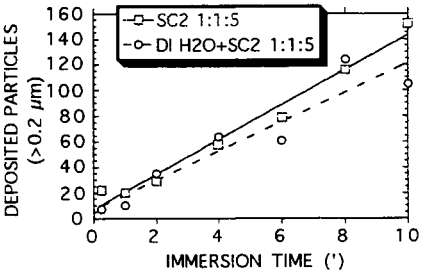

Figure 7. Particle contamination in SC2 VLSI 1:1:5 as a function of immersion time (T = 70°C), (100 mm size wafers).

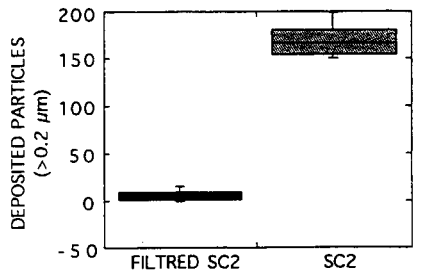

Figure 8. Impact of bath concentration on particle contamination in SC2 VLSI 1:1:5, (t = 10', T = 70°C), (100 mm size wafers).

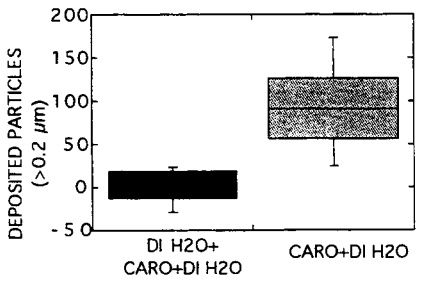

Figure 9. Particle contamination in CARO 3:1 bath with or without DI water dip pretreatment, T=140°C (100 mm size wafers).

Summary of HF-Last Wet Processing Using Direct-Displacement Technology

Gerald N. DiBello, Steven T. Bay, Christopher F. McConnell, Jennifer W. Parker, Ph.D., and Eric A. Cheney‡

The 10-20 Å chemical oxide layer remaining after traditional wet processing represents a significant fraction of an extremely thin gate oxide (<100Å). A final HF etch assures that the chemical oxide is removed and that a hydrogen-terminated surface remains. Early attempts at HF-last processing merely put the HF-etching processes after SC-1 and SC-2 cleaning operations. Yet, HF is known to be capable of removing most metals including Na, K, Ni, Fe, and Al. Cu, Au, and Cr may plate onto bare silicon if they are present in HF. Very pure HF solutions are available today and so SC-2 is no longer generally necessary.[1] SC-1 may be used to remove organic material prior to etching, but frequently, HF-only processing is all that is required.

HF-last processing has had a history of erratic particle performance. The difficulties with particle deposition can be attributed directly to the hydrophobic nature of the surface that is left after an HF process. Careful process and facility design will minimize particle deposition.

Chemical and Facility Requirements

For economic reasons, HF-last should be run using dilute HF solutions (between 100:1 and 250:1). Although excess chemical remains available for etching, as a result of the HF dissociation curve, the molecular HF concentration (as opposed to the ionic concentration) can be difficult to control. Since the polar HF molecule is required to break the silicon-oxygen bond, adding a small amount of HCl, a strong acid, to HF, a weak acid, inhibits the dissociation of the HF and promotes etching.[1]

In general, metals performance of HF-last processing is good. Excellent performance for Cr and Zn, and good performance for Fe and Ni. have been reported.[1,2] Care must be taken to eliminate metals that have a higher electronegativity than Si to eliminate plating.[3] A few percent of H_2O_2 or HCl in the HF-solution can reduce problems with metal plating.[2,4]

The temperature of the HF cleaning solution should be kept low (i.e., 35°C to 40°C) during native oxide removal for optimal etch control. Higher temperatures can also lead to bubble formation at the wafer surface and increase contamination from water heaters. The rate of diffusion of metals into silicon increases substantially with higher temperatures.

Exposure times to the HF solution should be minimized. The required time will depend on the native oxide to be removed. Extended soaking unnecessarily exposes the silicon to contaminants. Excessively long exposure to HF can cause surface roughening, especially at higher temperatures in the presence of elevated dissolved oxygen concentration.

HF-Last Processing Considerations

The most significant problem in HF-last processing is particle addition. Recent studies show that particle addition occurs primarily at gas/liquid interfaces.[5] Riley and Carbonell[6] investigated particle addition during three separate process steps: immersion, soaking, and withdrawal. With hydrophilic wafers almost all particle deposition occurs during the withdrawal of the wafer through the interface. Hydrophobic wafers appear to be even more sensitive than hydrophilic wafers to repeated exposure to gas/liquid interfaces, such as found when spray systems are used for rinsing .[5,7]

CFM Technologies Inc., West Chester, PA

‡ Hewlett-Packard Co., Corvalis, OR

Interfacial phenomena explain the particle addition associated with hydrophobic surfaces. The interfacial phenomena occurring on hydrophobic wafers revolves around two fundamental concepts: 1) contact angles occur at gas/liquid interfaces on particles; and 2) interfacial tension is an extremely powerful force when particles are very small. The same contact angle exists between a gas/ liquid/solid interface no matter what the shape and size of the solid. Consequently, small particles reside at gas/liquid interfaces where their surface energy is minimized and equilibrium is established. The dominance of interfacial tension for small particles is a direct result of scaling mathematics. Van der Waals forces and interfacial tension are directly proportional to the particle radius, R. Although these forces decline as particle size decreases, their relative magnitude becomes quite large for sub-micron particles (Table 1).

Table 1. Comparison of Forces Acting on a Sphere and a Sub-micron Particle.

Force	Scaling Factor	Dynes on 0.1m Sphere	Dynes on 0.1μm Sphere
Gravity	R^3	1.2E+6	1.2E-12
Buoyancy	R^3	4.8E+5	4.8E-13
Fluid Drag	R^2	1.0E+7	1.0E-5
Surface Tension	R	1.1E+3	**1.1E-3**
Van der Waals	R	1.3E+2	**1.3E-4**

Hydrophobic wafers do not easily penetrate a liquid. Rather, they draw the surface down into the bulk, and this surface is covered with surface-resident particles. Once immersed, hydrostatic forces combine with interfacial tension to ply these particles onto the wafer's surface. Upon withdrawal, the particles generally remain on the surface because the interfacial meniscus tends to invert upwards due to viscous forces. This inversion, can lead to more particle addition. A second immersion merely repeats the particle addition process.

Particle addition on hydrophobic surfaces is extremely problematic in the presence of droplets, as found during processing in spray-dump-rinsers and spin-rinser-dryers.[28] As droplets move across the wafer surface both receding (acting like an immersion) and advancing interfaces (acting like a withdrawal) sweep across the surface adding particles as they go. Bubbles in rinse-water can be even more detrimental. These bubbles may strike the surface, adhere, and travel if the fluid velocity is high enough. In bubbles, the leading edge is a withdrawal and the trailing edge is an immersion, both with attendant particle addition. The data shown in Figure 1 exemplify how harmful the presence of bubbles can be to hydrogen-terminated surfaces. Particle performance improved dramatically after a degasifier was installed to remove bubbles from ozonated rinse-water in an HF-last process.

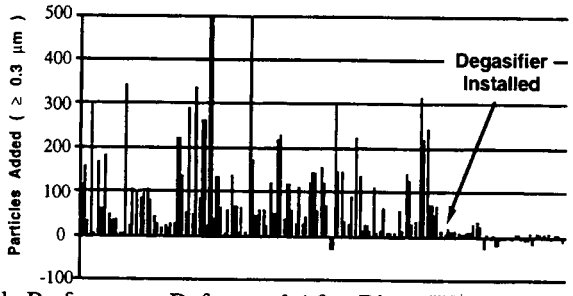

Figure 1. Particle Performance Before and After Rinse-Water Degasification.

The nature of the actual device structure on the wafer surface after the etching is completed must be considered when developing an HF-last process. Some wafers are entirely hydrophobic but many more have hydrophilic and hydrophobic regions. Processing that eliminates gas/liquid interfaces minimizes particle addition during wet cleaning regardless of whether the wafer surface is hydrophobic or hydrophilic.

Rinsing Hydrophobic Surfaces

The oxygen content of the water used for processing is critical. Dissolved oxygen (DO) levels in rinse water that are greater than 50 ppb will cause anisotropic etching of hydrogen-terminated surfaces. DO oxidizes the silicon which subsequently dissolves.[9] Surface oxidation resulting from high DO concentrations in HF solutions can also occur and can be confused with HF attack on the silicon surface.[3]

The temperature of the rinse should be kept low if DO levels are not below 50 ppb. Higher temperatures lead to increased surface roughening. Split lot experiments have shown that the surface roughness increases substantially as the temperature increases from 23°C to 75°C in an HF/SC-1/SC-2 recipe with a 5-minute post-HF rinse.[10] In these experiments, the gate oxide breakdown voltage resulting from higher HF rinse temperatures led to severely depressed yields.

Megasonic energy often is used to promote particle removal during rinse steps; however, the application of megasonics with hydrophobic wafer surfaces can be catastrophic. Sonoluminescence studies have shown that cavitation does occur during megasonics.[11] When hydrophobic surfaces are present, bubbles form directly ON the wafer surface, the implosion strikes the wafer surface, and creates numerous sub-micron defects in the substrate. Furthermore, inefficient wetting of the surface in an aqueous medium results in more nucleation sites for bubble formation.[12] Very high counts of tiny defects have been reported when megasonics are used in a rinse following HF processing.[13]

Drying and the Elimination of Watermarks

Watermarks are particularly troublesome with HF-last processing. Most watermarks are formed from silicon dioxide and other dissolved solids that precipitate out of DI water and deposit onto the wafer surface, primarily during drying processes (spin-rinse-dry, IPA vapor, etc.). Watermarks can be eliminated by preventing the evaporation of water from the wafer surface before the drying process and by using a non-evaporating drying technology.

Many drying techniques have been attempted to reduce the amount of water evaporation from substrate surfaces. Two separate studies comparing IPA Direct-Displace™ drying with conventional methods have shown that watermark formation is essentially eliminated with Direct-Displace™ drying.[14, 15] These striking results are attributed to eliminating gas/liquid interfaces during processing and preventing evaporation from the wafer during direct-displacement IPA drying.

Cost of Ownership

Consideration of cost of ownership, including throughput and cost per-wafer-pass, provides overwhelming justification for running HF-last processes. We determined the cost of ownership for various wet cleaning processes using the SEMATECH cost of ownership model. We examined the change in cost for different chemistries for a dual-vessel, fully-integrated, cleaning and drying system. A traditional four-chemical clean (H_2SO_4+H_2O_2/DHF/ SC-1/SC-2) represented the baseline cost in our study. We compared the cost of ownership of various simplifications of this process, finally considering HF-only processing. The relative savings with respect to baseline costs of various process changes are shown in Figure 2. With HF-only processing, substantial savings, resulting from higher throughput, reduced chemical and DI water consumption, and lower capital costs, cut two-thirds of the original base-line costs.

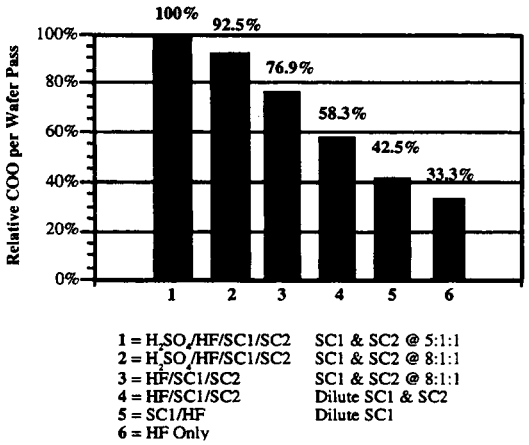

Figure 2. Comparative Cost of Ownership for Various Cleaning Sequences.

Conclusions

The atomically smooth, passivated surface resulting from an HF-last process provides technical motivation for using this method of surface preparation. Consideration of the hydrophobic nature of the surface, the physics of interfacial tension, and the chemistry occurring on the wafer surface allows HF-last processes to be developed that produce hydrogen terminated wafers in high yields. Cost of ownership considerations provide compelling reasons to implement HF-last or HF-only processes; HF-only processing represents only one third of the traditional cost.

References

1. Verhaverbeke, S. *Dielectric Breakdown in Thermally Grown Oxide Layers : Analysis, Effects of Contamination and Cleaning Strategy for Defect Reduction.* Katholieke Universiteit Leuven, IMEC. June 1993.
2. Christenson, K., Electrochem. Soc. Proc., 1991, V 92-12, , p.286-293.
3. Ohmi, T., T. Imaoka, T. Kezuka, and M. Itano, IES Conference, May 3-8, 1992, Nashville, USA.
4. Patruno, P., et al., Proc. Electrochem. Soc., 1993, V 94-7, p. 195-20.
5. McConnell, C.F., Microcontamination, Feb. 1991, p. 35-40.
6. Riley, D.J. and R.G. Carbonell, Microcontamination, Dec. 1990, p. 19-25.
7. Riley, D.J. and R.G. Carbonell, J. of IES, Nov./Dec. 1991, p. 28-34.
8. Roß, D., Proc. Electrochem. Soc., 1989, PV 90-7, p. 195-20.
9. Higashi, G.S., et al, ULSI Symposium-Hawaii 1993, Electrochem. Soc.
10. DiBello, G.N. et al., to be presented at Microcontamination, San Jose, CA, Oct. 1994.
11. *Ultrasound: Its Chemical, Physical and Biological Effects*, Edited by K. S. Suslick, 1988, VCH Pub.
12. Hagan, C.R.S.,et al., Ex. Abs., Electrochem. Soc., Fall 1993, V 93-2, p.782.
13. Personal Communication- Michael B. Olesen of Verteq, Inc., Anaheim, CA.
14. Sato, Y. and N. Miwa., Semicon/Kansai Kobe, Japan, June 1994.
15. Mackinnon, S., to be presented at Microcontamination, San Jose, CA, Oct. 1994.

THE IMPACT OF INTEGRATED PRE-CLEANS ON GATE OXIDE INTEGRITY

Sean O'Brien, George Brown, Charlotte Tipton
Semiconductor Process & Device Center
Texas Instruments

1. Abstract

Gate oxide integrity (GOI) as measured by ramped electric-field breakdown (Vbd) and constant current charge-to-breakdown (Q_{bd}) is characterized for several different wafer cleaning sequences. This study shows that a cleaning sequence which leaves a hydrophilic surface results in superior GOI for 65 Å gate oxide films to one which leaves a hydrophobic surface. HF-last cleans using unbuffered (HF), buffered (BHF), buffered surfactant (BSHF), and vapor + insitu rinse (VHF) are used to create a hydrophobic surface. These are compared with 3 sequences leaving hydrophilic surfaces: 80°C 1:1:5 SC1, 25°C 1:1:5 SC1/ megasonic, and 80°C 1:1:5 SC2. The H_2O_2-last process results in poor GOI despite leaving a hydrophilic surface. The other 3 oxidizing cleans produce high quality GOI, while the 3 HF-cleans result in inferior GOI. Elimination of the SC2 clean is also studied by implementing the pyroclean[1,2] a TI patented in-situ HCl vapor phase furnace process as a pre-clean step in oxide growth. This pyroclean process gives the best Q_{bd} of all processes studied.

2. Introduction

The sequence of wafer cleaning can have a dramatic impact on the electrical properties of gate oxide dielectric films. An integrated pre-gate clean (IPGC) includes removal of particles, metallics, and a sacrificial oxide film followed by drying. The concentration and purity of the chemicals used in these removal processes strongly influence device yield and electrical performance. In most processing situations particle removal cannot be the final step, since the SC1 solution (which is usually used for particle removal) deposits Fe on the wafer. The HF strip of the sacrificial oxide cannot be the final step, because the resulting patterned hydrophilic/hydrophobic surface typically generates unacceptable levels of watermarks. Thus the only acceptable final cleaning step appears to be metallic removal. If hydrophobic silicon is exposed this metallic clean must contain an oxidant, or else the watermark problem will not be eliminated. An alternative is to oxidize the surface prior to metallic cleaning.

This work studies the impact of a variety of IPGC sequences prior to the growth of 65 Å gate oxide films. The test wafers have a 350 Å dummy gate oxide which must be removed prior to gate oxide growth (dry O_2 850°C). In this test device flow the IPGC sequence is done prior to 3 furnace processes: growth of the LOCOS oxide sticking layer, dummy gate oxide, and the gate oxide. This test device incorporates isolation oxide, polysilicon capacitors with nested and

overlapping structures, and backside aluminum contact. For each set of wafers a SC1/megasonic-last control split is included.

Table I Pre-Gate Clean Sequences Studied in this Paper

Name	Sequence	HF	Dry
PFC	HF-Meg-SC2-Meg	4.9%	SRD
HF	SC2-Meg-HF	0.49%	VD
BHF	SC2-Meg-BHF	0.49% Buffered	SRD
BSHF	SC2-Meg-BSHF	0.49% Buff. Surfactant	SRD
VHF	SC2-Meg-SRD-Vapor HF	Vapor HF	Spin dry
SC2	HF-Meg-SC2	4.9%	SRD
SC1	HF-SC1	4.9%	SRD
Pyroclean	HF-Meg-SRD-Pyro oxidation	4.9%	SRD

3. Gate Oxide Integrity

This work indicates that there are essentially 2 classes of pre-cleans which determine gate dielectric quality. A clean which leaves the surface hydrophilic (such as SC1 or SC2) results in high quality films which meet or exceed the stringent reliability specifications for a manufacturable chip. A clean which leaves the surface hydrophobic results in poor quality films which fail in the intermediate regime. These devices represent the worst case scenario, they will pass all testing procedures at the manufacturer, then fail in the field long before the specified lifetime expires.

Within these 2 classes of cleans there does not appear to be a measurable difference between, for example, vapor and buffered HF. Any further tests to distinguish differences within a class would probably require drastically larger sample sizes (for better statistics) and possibly much larger capacitor area.

Elimination of the wet metallic removal clean by implementation of the pyroclean results in the best observed GOI. This process represents another step in the evolution from wet to dry wafer cleaning.

Oxide Breakdown Voltage (Ebd)

Ebd is probed with a ramped voltage source until a 100 mA/cm^2 current density is reached. If the capacitor does not suffer catastrophic failure it is labeled a survivor. Figure 1 shows the average breakdown voltage for 200 0.01 cm^2 capacitors and Figure 2 shows the survivor percentage.

The resolution of the electrical studies in this work is approximately 0.5 defects/cm^2. The SC1/megasonic-last control process is included in all 3 splits. Direct comparison between the 3 splits should not be made because the gate oxide thicknesses have been independently scaled. The legend indicates that p-type wafers were stressed with negative voltage, and n-type with positive.

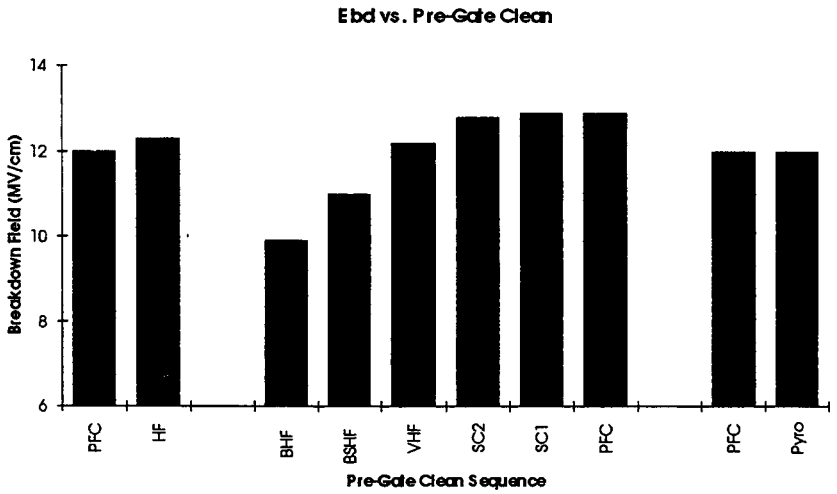

Figure 1 Average electric field breakdown for 3 sets of p-type wafers with a variety of integrated pre-gate cleans.

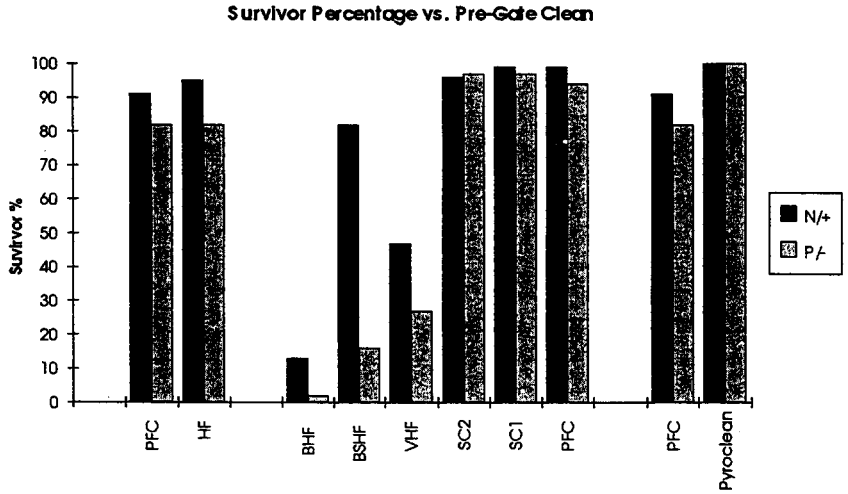

Figure 2 Survivor % of electric field breakdown testing for 3 sets of n- and p-type wafers with a variety of integrated pre-gate cleans.

Constant Current Charge to Breakdown (Q_{bd})

The Q_{bd} test used for this study is probed on 0.0005 cm^2 capacitors (20/wafer) in accumulation with substrate electron injection for n-type and gate injection for p-type wafers.

The BHF, BSHF, and VHF curves are almost identical. The primary distribution is much lower than the other cleans. The 0.49% HF wafers were cleaned in a superior tool, and the improved distribution indicates the equipment does play an important role in determining the final device performance, but in general hydrophobic wafers grow poor gate oxide films.

The 3 hydrophilic cleans show tight distributions with no tails, indicating consistent surfaces regardless of the H_2O_2 pH or temperature. The dielectric quality is excellent despite the thin chemical oxide remaining after clean which represents a significant fraction of the final gate oxide thickness. The pyroclean process grows superb dielectric films, the Q_{bd} distribution is consistently superior to any other wafer clean process.

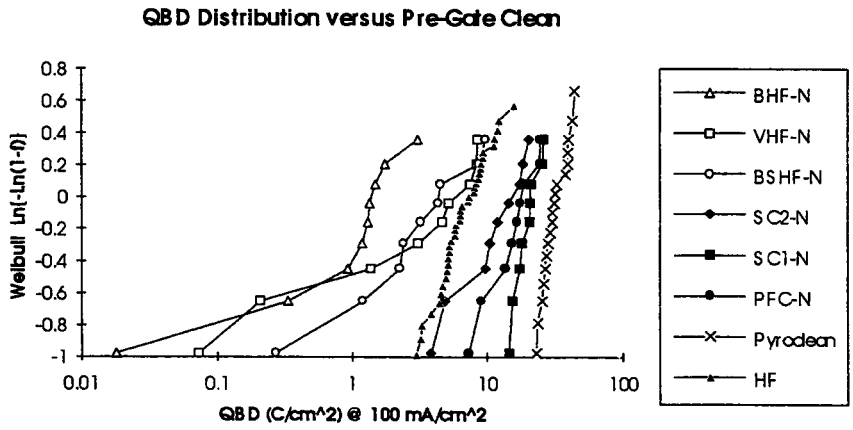

Figure 3 Weibull Q_{bd} distributions for n-type wafers with a variety of integrated pre-gate cleans.

4. Conclusion

Cleaning sequence and chemical type has been investigated using GOI measurements on 65 Å gate oxide films. A sequence which leaves a hydrophilic surface after the clean results in superior GOI to one leaving a hydrophobic surface. No significant difference was observed within these 2 classifications between various sequences or chemicals. The pyroclean, an insitu chlorine anneal process prior to oxidation, resulted in the best observed Q_{bd} values of all studied processes.

5. References

1. Nguyen et al, 1993 VLSI Symposium Proc. 8B-2, p. 109 (1993).

2. Meador, Breashears, Texas Instruments US Patent 4,544,416, (1985).

MARANGONI DRYING: A NEW CONCEPT FOR DRYING SILICON WAFERS

R. SCHILD[1], K. LOCKE[1], M. KOZAK[1] and M.M. HEYNS[2]

1. OVERVIEW

This paper is intended to discuss the experimental results obtained with MARANGONI DRYING, and to show that it is a cost effective and indeed a preferred way of drying wafers, especially after critical cleaning. The total use of IPA is absolutely minimal, only a few milliliters per run and the wafers do not suffer any dynamic forces. The drying is performed by a strong natural force in cold DI water, it is not due to evaporation of the water or condensation of IPA, and the wafers become totally dry.

Wafers are first rinsed to resistivity as in normal final rinsing. Then the wafers are separated from the carrier within the bath and raised at a pre-programmed speed through the surface of the over flowing cold final rinse bath. As this is happening nitrogen which has passed through a small IPA bubbler is directed onto the surface of the bath. The IPA absorbs into the surface of the water building up a higher concentration in the meniscus. This reduces the surface tension at the meniscus next to the wafer. The IPA on the surface of the water can dissolve into the bulk so that we have a gradient in surface tension between the meniscus at the wafer surface and the surface of the bath. The MARANGONI EFFECT states that a liquid will flow from a low surface tension area (1) to a region of higher surface tension (2). Whilst raising the wafer out of the bath this force will strip the water from the surface of the wafer. The strength of this force can be easily seen if you hold a cotton swab soaked in IPA above a wet wafer and watch the water strip itself away from the centre, leaving the wafer dry. A detailed discussion of the physical principle of Marangoni drying is given in [1] and [2].

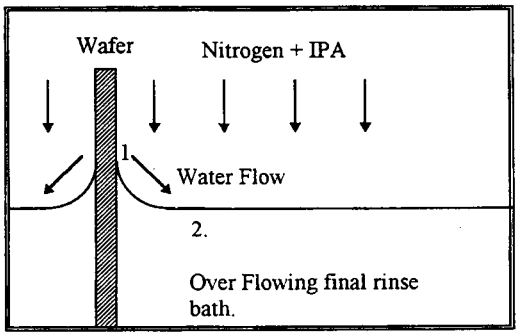

Figure 1. Idealised Marangoni Effect

[1] STEAG Microtech GmbH, Donaueschingen (Germany)
[2] IMEC, Leuven (Belgium)

2. ELECTRICAL CHARACTERISATION

Wafers were split during the gate oxide clean to receive a Marangoni dry and spin dry. The gate oxide was 650 Å with polysilicon to produce the top plate of the capacitor, with an Aluminium interconnect for probing. Both charge to breakdown and breakdown voltage were measured on hydrophobic and hydrophilic wafers. The defectivity results were significantly better for the Marangoni dryer, and the QBD showed an improvement. This suggests that the wafer surface is both cleaner in terms of particles and surface condition after Marangoni drying. The results are summarized in Table 1. and 2. which show the QBD values on different capacitor sizes.

Table 1. QBD Results Hydrophilic

	0.15 cm^2	**0.04 cm^2**	**0.01 cm^2**	**Std-Dev.**	**Def/cm^2**
Spin Dryer	89	92	95	1.3	0.4 ±0.1
MARANGONI	98	96	100	2	0.04 ±0.1

Table 2. QBD Results Hydrophobic.

	0.15 cm^2	**0.04 cm^2**	**0.01 cm^2**	**Std-Dev.**	**Def/cm^2**
Spin Dryer	90	97	96	1.4	0.5 ±0.2
MARANGONI	94	98	99	0.05	0.4 ±0.06

3. PARTICLE PERFORMANCE

The defect densities and the QBD values for larger capacitors in the charge to break down experiments suggest a good particle performance, even at very low particle sizes. The results for repeated particle testing down to 0.26μm of the Marangoni dryer are shown in graphical form below. As can be seen, both on hydrophilic and hydrophobic wafers within the standard deviation the Marangoni is particle neutral.

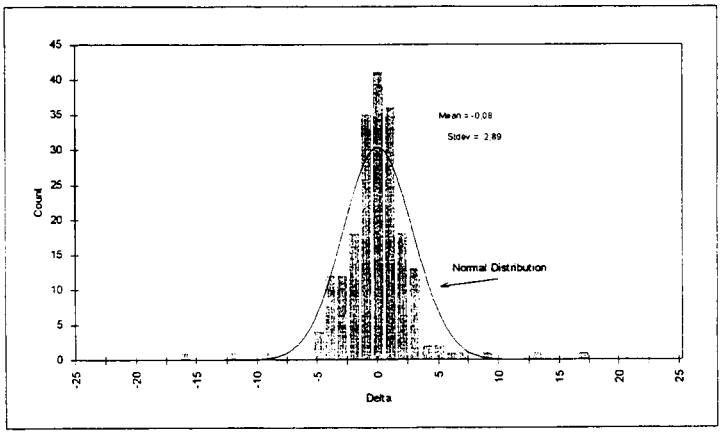

Figure 2. Particle Performance on Hydrophilic Surface

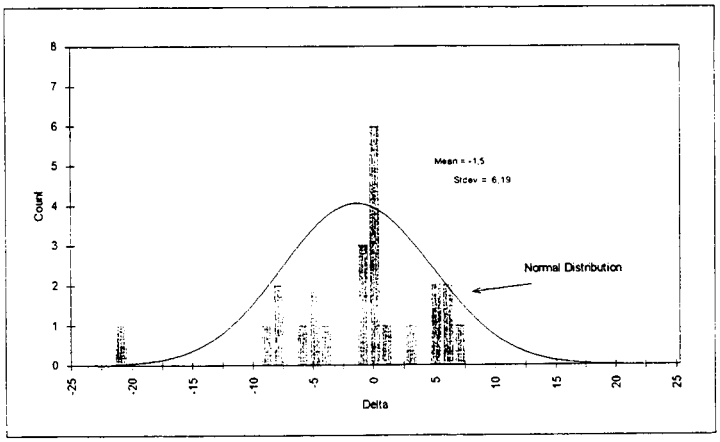

Figure 3. Particle Performance on Hydrophobic Surface

4. DRYING OF TEXTURED WAFERS

So far we have only referred to plain silicon wafers. The Marangoni relies on the IPA concentration gradient across the meniscus. This is very large compared to structures on the wafer and so is capable of drying them. Thomas Mask sets have been dried with 2000Å holes without any drying stains visible with dark field microscopy.

Also gated diode structures were dried in the Marangoni and a spin rinse dryer before Co and Ti sputtering and silicidation. The spin dried wafers showed

reproducible drying residues under the silicide at the border of the hydrophobic and the hydrophilic areas. None of these defects were seen on the Marangoni dried wafers. See photograph below.

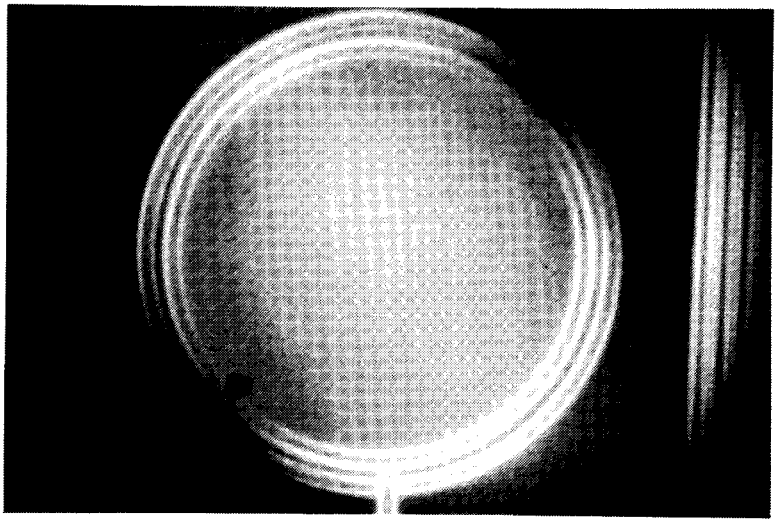

Figure 4. Top View of the Spin Dried Gated Diode Structure with Drying Residue

5. CONCLUSION

The experimental results show that Marangoni drying is capable of drying wafers with a superior cleanliness and without drying stains. Further testing with VPD-TXRF, TOF-SIMS for metals and ESCA, IR-Spectroscopy and SIMS for organics, showed that the Marangoni dryer had less or equal levels compared to spin dried reference wafers.
Due to the minimal use of IPA, safety and environmental problems are no longer an issue and the cost of ownership is very low. The design of this dryer with one robot arm, as the only moving part ensures very high reliability.
The capability to implement megasonic and chemical injection in the final rinse tank of the Marangoni dryer allows to integrate final stages of cleaning, rinsing and drying in one tank without exposing the wafers to air. This gives a promising future for further applications.

REFERENCES

1. Leenars A.F.M., Huethorst J.A.M. and van Oekel J.J., Langmuir 6 (1990) 1701
2. Marra J. and Huethorst J.A.M., Langmuir 7 (1991) 2748

PARTICLE REMOVAL EFFICIENCY FROM NATIVE OXIDES USING DILUTE SC-1 MEGASONIC CLEANING

S. L. Cohen [a], W. Syverson[b], S. Basiliere[b], M.J. Fleming[b], B. Furman[a], C. Gow[b], K. Pope[a], R. Tsai[a], and M. Liehr[a]

[a] IBM Research Division, T. J. Watson Research Center, Yorktown Heights, NY, and [b]IBM Microelectronics Division, Essex Junction, VT

1. INTRODUCTION

The control of equipment and processing cost will be increasingly important for future device fabrication. Concurrently, however, microcontamination targets are moving incessantly to lower levels of acceptable contamination, and additional yield detractors, such as surface roughness, have been identified. Only by providing a detailed understanding of processes and the impact of contamination on yield, can we hope to accommodate and balance both growing industry demands.

The industry standard wafer clean, the RCA clean, has recently become the focus of much attention, as it is recognized to generate substantial expense due to large chemical consumption. Furthermore, it was recently found to cause nano-scale roughening of silicon surfaces [1, 2] and to cause the creation of spikes and light point defects (LPDs), both potential yield detractors. [3] Both effects originate in the basic (NH_4OH/ H_2O_2) component of the clean. Radical deviations from the RCA clean have been suggested, i.e. all-acid cleans [4], or replacement of peroxide by O_3. Such suggestions are likely to be implemented in future (even near-term) generations of technology. Gas-phase cleans are yet other alternatives, but tend to find presently only niche applications. For immediate implementation in mature, qualified technologies one desires to minimize the risk of process changes. We believe that more subtle modifications of the standard RCA clean are more suited for such implementations. Recent characterization of the RCA clean in the regime of dilute chemical concentrations suggests that it is possible to minimize chemical consumption and surface roughening while maintaining high particle cleaning efficiency [5].

High efficiency particle removal has been postulated to require simply etching of a thin layer (20Å) of the substrate (eg, oxide) in the SC-1 solution. [4] In this same study it was also found that a combination of chemical oxidation (20Å) and oxide removal with HF led to excellent particle removal. The particles in that study were not well defined, however, and were deposited predominantly on thick oxide surfaces. The purpose of this paper is to compare particle removal efficiency for well-defined 0.3 µm silicon nitride (Si_3N_4) and 0.5 µm silicon dioxide (SiO_2) particles on native (chemical) oxide using dilute RCA chemistry, when the SC-1 chemical effects are aided by megasonics energy. While neither of these model particles by itself is representative of line contamination, together, they can be used to probe the range of contaminants present in a manufacturing line.

2. RESULTS

The particle removal results were obtained as part of a large design-of- experiment based study. Using BestDesign, (an IBM proprietary statistics package), 14 parameters of the RCA clean were varied and response functions were generated for oxide and nitride particle removal and surface roughening (among others). Standard 8-inch diameter Si(100) wafers were precleaned with an RCA-based clean in a spray processor to create a smooth, thin chemical oxide on the surface. The wafers were subsequently contaminated in a controlled way by a dip into DI water containing either the nitride or oxide particles. Initial particle counts prior to deliberate contamination were less than 50/wafer; 1500-3500 particles/wafer were deposited using this method as measured on a Tencor 5500 at 0.3μm sensitivity. Figures 1 and 2 show the uniformity and particle size distribution for the oxide and nitride particles.

Wafer cleaning conditions varied from a 'standard' clean (8:1:1; H_2O: NH_4OH: H_2O_2 ; H_2O: HCl: H_2O_2) to dilutions of 20X for the chemically active components; furthermore HF etches were added at times before the SC-1 step, or between the SC-1 and the SC-2 step. The chemical state of the surface was followed with contact angle measurements. High angle indicates hydrophobicity which suggests incomplete oxidation, whereas low angle indicates hydrophilicity and complete oxidation and OH termination. After an HF etch the surface state is a strong function of the subsequent processing. For an HF etch preceding an SC-1, immediate oxidation and -OH termination of the surface is assured as long as any NH_4OH is present in the SC-1 solution (within our experimental range), as Figure 3a demonstrates. However, for an HF step followed only by an SC-2, the surface contact angle suggests incomplete oxidation and -OH termination in the acidic solution. (Figure 3b).

The influence of electrostatic forces on particle adhesion can be detected in the preparation procedures used for the oxide and nitride particle wafers. For the nitride particle preparation, the concentration of nitride particles in water is approximately 2ppb by weight and the final particle concentration on the surface is a strong function of immersion time. A diffusion mechanism [6] is likely the dominant mechanism for adhesion whereby the positively charged nitride particles are attracted to the surface by electrostatic forces. By comparison, to obtain the same number of oxide particles on the wafers, the concentration in solution is closer to 100 ppm by weight. Additionally, the oxide particle deposition depends mostly on the concentration of particles in solution and is independent of immersion time. A film mechanism is most likely responsible for the adhesion of the oxide particles [6] since the electrostatic effects are expected to be less important for like materials.

The strong attraction of nitride particles to an oxide surface is explained by the zeta potential of the nitride and oxide particles as a function of pH [7]. At low and neutral pH the surface charge on the nitride particles is more positive than the oxide surface. At the higher pH's, the zeta potentials of the nitride and oxide materials converge thus minimizing the attractive forces. This data is consistent with AFM force vs. distance measurements , which show that silicon nitride tips are attractive towards oxide substrates at low pH, but repulsive at high pH's. [8] The repulsion at high pH is conducive to particle removal in the SC-1 solution since particle re-attachment is less likely. Differences in the shape and size of the nitride and oxide particles used in these experiments may also play a role in the particle adhesion strength. The oxide particles

are spherical (0.5μm) so there is a limited contact area between the particle and the surface. In contrast, the nitride particles are irregularly shaped and smaller (0.3μm) [9].

The importance of megasonic energy for nitride particle removal is shown in Figure 4 for comparison to similar studies[5]. In the absense of megasonics energy in the SC-1 , particle removal efficiency is less than 40% under all conditions used in our experiments. Increasing the temperature has less influence on particle removal than does the megasonic energy.

Particle removal efficiencies under many different cleaning conditions for nitride vs. oxide particles are compared in Figure 5. Each data point represents one cleaning experiment. The dotted line represents the case if oxide and nitride particle removal is identical. For most processes the oxide particles are easier to remove than the nitride particles. This is attributed mainly to the stronger electrostatic attraction of nitride particles for the surface as described above but may also be influenced by the particle shape/size. For each data point in Figure 5, the amount of substrate etched is the same on the nitride and oxide particle test wafers. Therefore, the particle removal efficiency can be strongly influenced by these electrostatic (and other) forces suggesting that the optimum amount of substrate etching required for cleaning will depend in a very specific way on particle adhesion forces.

The influence of surface etching on particle removal efficiency from these native oxide covered wafers is difficult to quantify since the only etch rate monitor used in these experiments was a thermal oxide substrate. Interestingly, a brief HF-only etch (followed by a rinse/dry) was not sufficient to remove either the nitride or oxide particles; this suggests that removal of the native oxide (and some limited etching of the oxide particles themselves) does not undercut and release the particles. The creation of a hydrogen passivated surface may also influence the particle adhesion forces in this case. Concurrently, in the absence of megasonics, these particles can be removed with the use of a sulfuric/ H_2O_2 (S/P) , HF step prior to the SC-1/ SC-2 sequence. This is consistent with previous suggestions that the S/P HF sequence can provide high efficiency particle removal by oxidation and etching of the underlying substrate[4]. Some oxidation and etching of the nitride particles may also be involved.

Further evidence that substrate etching contributes to particle removal from these surfaces is suggested by the appearance of surface 'spikes' or 'pillars' [3] observed in AFM images of native oxide substrates in the same cleaning cassette as the particle standards. Figure 6 is a 'calibration curve' showing the height of these 'pillars' vs. the etch depth of a thermal oxide substrate. These results are in agreement with previous work [10] which suggests that the etch rate of native oxide on silicon is significantly higher than thermal oxide. For a given run, the height of these pillars should give a lower limit of the amount of silicon etched away during the SC-1 step since these pillars are believed to arise from micromasking by bubbles during the SC-1 step [3]. Interestingly, the fact that some pillars are observed even in the presence of megasonic energy suggests that surface bubbles are not completely dislodged during megasonic cleaning.

3. SUMMARY

Silicon nitride and oxide particles deposited on native oxide surfaces can be used to monitor the effectivness of wet wafer cleaning processes. Removal of these particles is significantly

enhanced with the aid of megasonics energy in the SC-1 process. While substrate etching clearly is important for enhancing particle removal, electrostatic interactions and particle shape/size must be considered as well.

Acknowledgments: The authors gratefully acknowledge support from CFM Technologies for portions of this study as part of Sematech project J80.

1 T. Ohmi, Proceedings of the Inst. of Environ. Sci. 287-296 (1992).
2 M. Meuris, M. Heyns, P.W. Mertens, S. Verhaverbeke and A. Philipossian, Microcontamination 10(2), 31 (1992).
3 H.F.Schmidt, M. Meuris, P.W. Mertens, S. Verhaverbeke, M.M. Heyns, L. Hellemans, J. Snauwaert and K. Dillenbeck, Symp. on Cleaning Technology in Semi. Device Mfg., 184th ECS Mtg (New Orleans, LA, Oct 10-15, 1993).
4 M.M. Heyns, S. Verhaverbeke, M. Meuris, P.W. Mertens, H.F.Schmidt, M. Kubota, A. Philipossian, K. Dillenbeck, D. Graf, A. Schnegg and R. deBlank, Materials Research Society Meeting (San Francisco CA, Apr. 12-16, 1993).
5 P.J. Resnick, C.L.J. Adkins, P.J. Clews, E.V. Thomas and S.T. Cannaday, Symp. on Cleaning Tech.in Semi. Dev. Mfg., 184th ECS Mtg (New Orleans, LA, Oct 10-15 1993).
6 a) D. J. Riley, R.G. Carbonell, J. Colloid Interface Sci, (1993) b) D. J. Riley, R.G. Carbonell, Journal of the IES, 28, Nov/Dec 1991 c) R.P. Donovan, Spring MRS meeting procedings (San Francisco 1993).
7 D. Jan and S. Raghavan, Symp. on Cleaning Tech.in Semi. Device Mfg., 184th ECS Mtg (New Orleans, LA, Oct 10-15, 1993).
8 J.H. Hoh, J.P. Cleveland, C.B. Prater, J-P. Revel, P. Hansma, J. Am. Chem. Soc, 114, 4917(1992)
9 D. J. Guidotti, K.R. Pope, unpublished SEM data
10 S. Verhaverbeke, M. Meuris, H. Schmidt, M.M. Heyns, D. Graf, Semicon/ Japan, Chiba, Japan, Dec. 1-3, 1993.

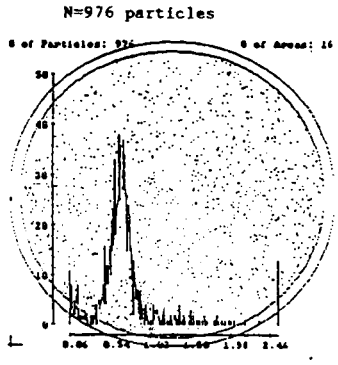

Figure 1: Light scattering cross section for oxide particles (Tencor 5500 > 0.3μm).

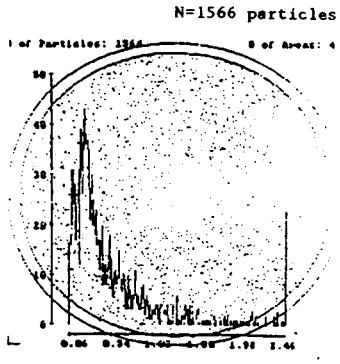

Figure 2: Light scattering cross section for nitride particles (Tencor 5500 > 0.3μm).

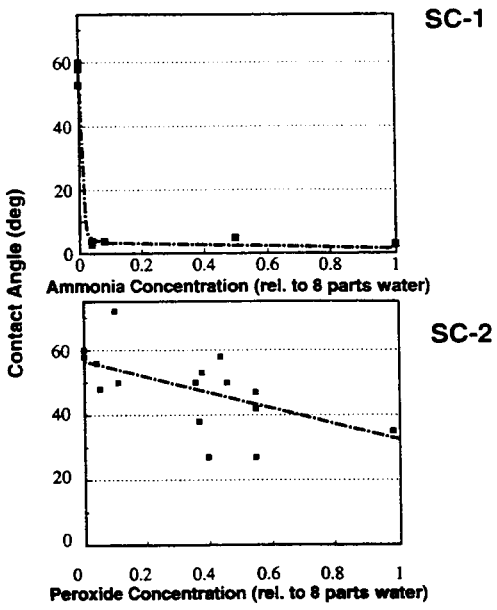

Figure 3: Contact angle for an HF cleaned surface exposed to various SC-1 and SC-2 solutions.

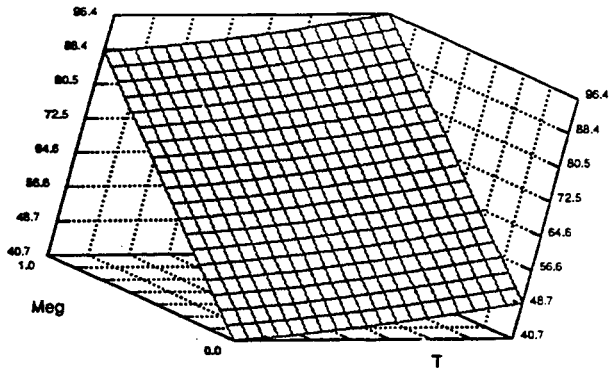

Figure 4. Response surface generated by **BestDesign** for silicon nitride particle removal as a function of megasonics power and SC-1 Temperature.

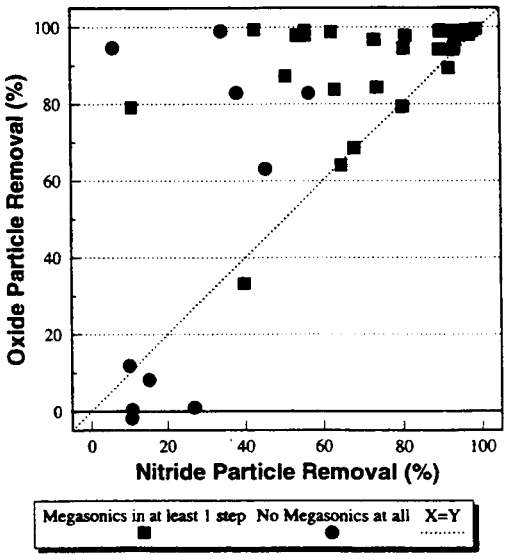

Figure 5: Removal efficiencies for oxide and nitride particles are compared for a large variety of dilute RCA cleaning conditions.

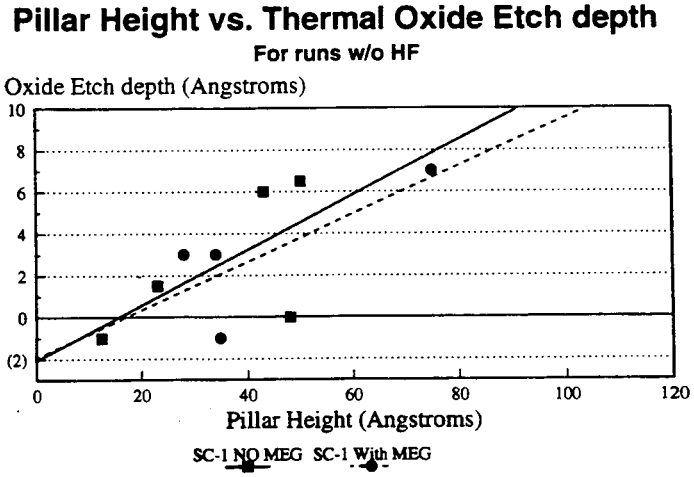

Figure 6. Correlation between native oxide etch rate (as measured by pillar height) and thermal oxide etch rate (from ellipsometry) for samples cleaned in the same cleaning cassette. Significant measurement error is involved for both of these techniques.

METAL REMOVAL WITHOUT PARTICLE ADDITION:
Optimization of the Dilute HCl Clean

T. Q. Hurd[1)*], P. W. Mertens[1)], L. H. Hall[2)], and M. M. Heyns[1)]
[1)] IMEC
Kapeldreef 75
B-3001 Leuven Belgium
*currently assigned to IMEC from Texas Instruments

[2)]Texas Instruments, Inc.
13546 N. Central
Dallas, TX 75243

Biographies

Trace Q. Hurd received his BS degree in Chemistry from Southern Methodist University in 1989. Since then he has worked at Texas Instruments in the Chemical Operations Department. Initially he worked on measurement and reduction of particle contamination in liquid chemicals. Currently he is researching advanced wafer cleaning techniques for Texas Instruments in the Ultra Clean Processing group in IMEC and is a graduate student pursuing a PhD in Chemistry.

Paul Mertens joined the Interuniversity MicroElectronics Center in 1984 to work on zone melting recrystallization for silicon-on-insulator applications. He developed a lamp based system to perform the zone melting process and subsequently studied different aspects of this process, including impurity redistribution and defect formation. From 1990 his main field of research has been the investigation of silicon wafer surface quality particularly for MOS applications. He received his MS degree in electrical engineering in 1984 and his PhD in 1991, both from the Katholieke Universiteit Leuven.

Lindsey Hall received his MS degree in Physical Organic Chemistry from the University of North Texas in 1980, and an MBA from Southern Methodist University in 1985. He has worked at TI for 14 years and is currently the Advanced Technology Manager in the Chemical Operations Department, responsible for developing next generation ultra high purity chemicals, and researching the impact of chemical quality on wafer manufacturing processes.

Marc Heyns received his MS degree in 1979 and his PhD in 1986, both from the Katholieke Universiteit Leuven. From 1979 to 1985 he held a fellowship from the National Fund for Scientific Research (NFWO) in the Laboratory for Physics and Electronics of Semiconductors of the K.U. Leuven, investigating the trapping and degradation of thermally grown SiO_2-layers during various forms of carrier injection and field stressing. In January 1986 he joined the Interuniversity MicroElectronics Center (IMEC) where he is now responsible for a research group working on the cleaning and physics of insulators. His current research topics include Si-surface characterization, wet and dry cleaning optimization, ultra-clean process technology, thermal oxide layer and deposited insulator characteristics, the degradation of insulating layers during charge injection, and breakdown and wearout of insulators.

Abstract

The metal removal and particle behavior of various dilutions of HCl at 20° and 70° C has been characterized. In a previous paper [1] it was reported that the lifetime of H_2O_2 in the standard (1:1:5) SC2 is exceedingly short at normal processing temperatures (80° to 85° C). This led to the investigation of metal removal without H_2O_2. It was found that removal was as efficient with the H_2O_2 as without, even in the case of metallic Cu on hydrophobic wafers. In this paper, it is reported that in addition to good metal removal, dilutions of HCl provide superior particle performance. The theoretical aspects of the improved particle performance will be discussed. Particle data from different temperatures and HCl concentrations will be presented which are in close agreement with recent models. It will be shown that under appropriate operating conditions, (temperature, concentration, and liquid particle level) a particle neutral metal removal process can be implemented.

Metal Removal

CZ, p-type, <100>, 1 to 30 Ωcm, wafers were intentionally contaminated with Fe, Ca, and Zn using both low quality and intentionally spiked SC1 solutions. This contamination technique leaves a metal contaminated oxide on the surface of the wafers. The amount of each metal that was

deposited from the different SC1 solutions is shown in Table 1. These contaminated wafers were then exposed to dilutions of HCl at 20° and 70° C. The exposure time was always 10 minutes, and, unless otherwise stated, the cleaning was performed in a quartz bath with no recirculation or filtration. Metal levels before and after each cleaning were measured using the Vapor Phase Decomposition Droplet Surface Etching (VPD-DSE) TXRF technique.

Table 1 *Range of initial metal surface concentration on wafers used in cleaning experiments.*

	(10^{10} at/cm^2)
Fe	44.8 - 143.5
Zn	36.3 - 83.8
Ca	9.3 - 60.6

The metal removal efficiencies of these different dilutions at 20° and at 70° C are shown in Figures 1a and 1b. At 20° C, there is a noticeable loss in metal removal as the concentration of HCl is decreased, most notably for Fe. At 70° C, however, the loss in metal removal due to lowering of the HCl concentration is offset by the higher temperature and so no net loss in metal removal is seen. (The high variation and low overall removal that is seen for Ca is the result of the lower initial levels on the wafers combined with inherent variability in the measurement process due to contamination from the environment.) This result is reasonable as pH and temperature would be expected to exert strong influences on the metal removal process. If the pH is low, the temperature is less critical whereas if the pH is high, the temperature becomes more critical.

It has been demonstrated by other researchers that it is easier to remove oxidized metals from a wafer surface than ones that are in the metallic state [2]. It was for this reason that metallic Cu removal was investigated. Cu was deposited onto wafers from a highly spiked HF solution, resulting in very high levels of Cu deposition (1 to 6 x 10^{14} atoms/cm^2). It is known that at this level the Cu is in a metallic state [3]. Experiments performed with two dilutions of HCl at 70° C show that the removal efficiency is very high (95.6 to 99.9%) as can be seen in Table 2. There is some loss of Cu removal with the more dilute HCl but it must be remembered that the challenge in this case was extremely high. With levels of the type that would normally be encountered in semiconductor processing (10^{10} to 10^{12} at/cm^2) the Cu would be reduced to near or below the detection limit of the VPD-DSE-TXRF technique.

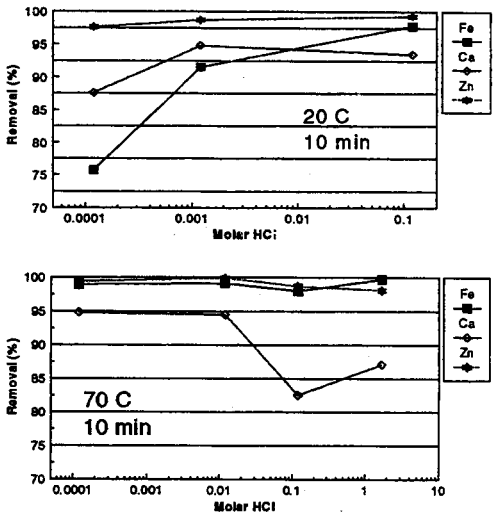

Figures 1a and 1b: Metal removal of dilute HCl solutions at 20°C (1a) and 70°C (1b).

Table 2: *Removal of metallic Cu from a silicon surface by dilute HCl.*

	Cu (10^{12} atoms/cm^2)	
Initial	646	102
post 10^{-1} M HCl	0.3	<0.1
post 10^{-4} M HCl	23.4	4.5

Further investigation of the metal (specifically Fe) removal efficiency of the dilute HCl solutions was performed. Fe was used as the target element due to the experimental observation that Ca and Zn were in general easily removed to levels near the detection limit of the VPD-DSE-TXRF technique and would thus make it difficult to measure any difference in removal. The purpose of the investigation was to better understand the interplay of temperature, bath dynamics, HCl molarity and immersion time, as control parameters for optimizing metal removal.

The exact influence of solution temperature is demonstrated in Figure 2 which shows the Fe removal achieved with a 0.00012 M HCl solution at 20°, 50°, and 70° C. It can be seen that very little thermal energy is necessary to remove the Fe as increasing the temperature to 50° C was enough to effect near total removal.

To investigate bath dynamics, molarity and immersion time, wafers with contamination levels as shown in Table 1 were cleaned in a continuous

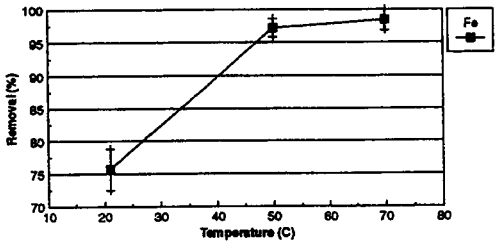

Figure 2: The effect of temperature on the metal removal efficiency of a 0.00012 M HCl solution.

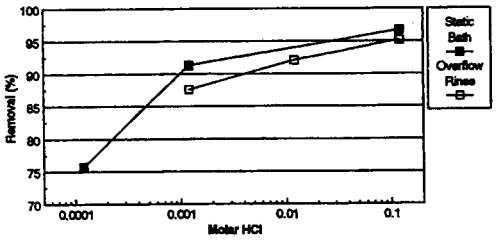

Figure 3: Fe removal as a function of bath dynamics.

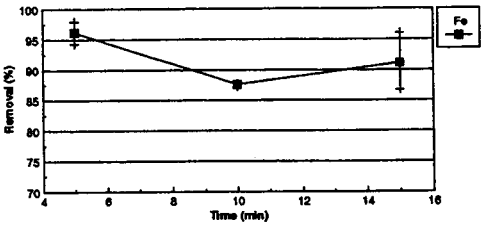

Figure 4: Fe removal as a function of time in 0.0012 M HCl.

overflow rinse bath which was spiked with different levels of HCl. This ensured that fresh HCl solution was always in contact with the wafers, thus reducing the influence of loading on the ultimate metal removal. The efficiency of Fe removal by 10 minute cleanings with different HCl concentrations in the rinse tank is shown in Figure 3. It can be seen that the metal removal in the rinse tank not only follows the exact trend as in the static tank but is also very close in absolute value. This points to the conclusion that the pH and temperature of the liquid solution are primarily responsible for the metal removal and not the bath dynamics. Further information is provided by the data in Figure 4 which shows the results of different cleaning times on metal removal with a 0.0012 M HCl solution at 20° C in the overflow rinse tank. The ultimate metal removal of this solution is reached in the first five minutes, following which, no measurable increase in metal removal is observed. The critical parameters to control are then, are the temperature and HCl concentration.

Particle Behavior

Riley and Carbonell have shown that particle deposition onto silicon wafers is greatly reduced at pH values above 2 - 2.5 [4]. This is due to the fact that the isoelectric point for silicon and silicon dioxide is between pH 2 and 2.5 [5]. At a pH above the isoelectric point, the wafer surface has a net negative charge, while below it, the wafer surface has a net positive charge. It has been reported that many of the particles in a liquid will be negatively charged as anions are usually more poorly hydrated than cations and so are more readily adsorbed onto the particle surface [5]. Thus, at pH's above 2 - 2.5 an electrostatic repulsion barrier between the particles in the solution and the surface is formed. This barrier impedes particle deposition from the solution onto the wafer surface during immersion. Below pH 2, the wafer surface is positively charged, while many of the particles remain negatively charged, removing the repulsion barrier and resulting in particle deposition while the wafers are submerged. This is why it is commonly observed that a standard SC2 solution is particle "dirty". The pH of that solution is below 0 and so the wafers will have a high positive charge. Recently, Riley and Carbonell have published a model of this phenomenon which predicts that particle deposition from a liquid solution should be sharply depressed above pH 2 to 3 depending on the particle size and the wafer and particle potentials [4].

The practical implication for diluted HCl chemistries is that at concentrations higher than 0.01 M (1:1000 dilution of 37% HCl), particle deposition should occur while the wafers are submerged , much as is the case with a standard SC2, while at concentrations below 0.01 M, particles will not deposit. To test this, 125 mm diameter wafers (averaging 50 particles >0.15 microns, 15 particles >0.2 microns, and 2 particles >0.4 microns per wafer) were processed for ten minutes in various dilutions of HCl at 20° and 70° C and then spin dried. The solutions were analyzed with a liquid particle counter and consistently had 40 - 60 particles per ml >0.5 microns. Particles were measured on the wafers before and after using a sensitive light scattering technique. Figures 5a and 5b show the results of these experiments, demonstrating that particle addition can be greatly reduced with these diluted acid cleans. In Figure 5b

a sharp drop-off in particle addition at pH 2.0 to 2.5 can be seen which is in remarkable agreement with the theoretical prediction of Riley and Carbonell.

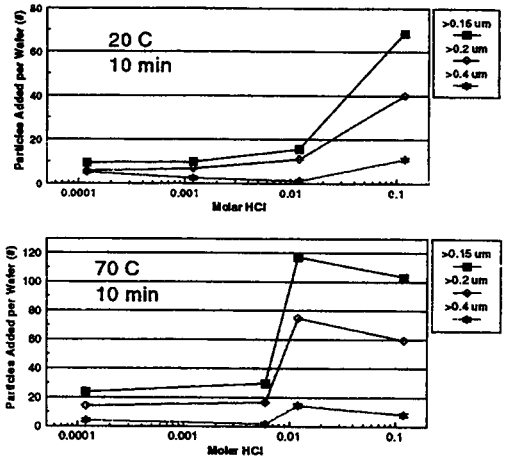

Figures 5a and 5b: Particle addition from dilute HCl solutions at 20°C (5a) and 70°C (5b).

In order to give a closer approximation of the absolute particle capability of these dilute HCl cleans, (which cannot be accomplished in a static quartz tank) clean wafers were processed in an overflow rinse bath that was continuously spiked with HCl. At 0.01 M, the particle level in the liquid was approximately the same as in the static tank experiments while at 0.1 M it was 10X higher and at 0.001 M it was 10X lower. (This is calculated from the particle level in the water and the particle addition caused by the injection of HCl into the rinse tank.). These results are shown in Figure 6 and demonstrate that with a cleaner liquid the particle addition from HCl can be driven to zero by controlling the concentration. At 0.0012 M the

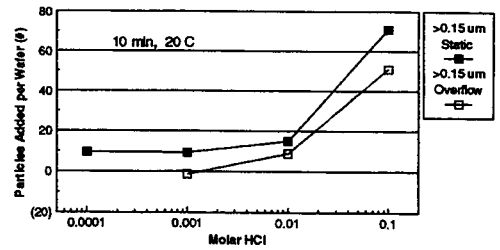

Figure 6: Effect of bath dynamics on particle deposition in dilute HCl solutions.

solution shows particle removal. Figure 7 further demonstrates that there is no particle addition from the bulk liquid as the length of time that the wafers were immersed in 0.0012 M HCl had no impact on how many particles were added or removed.

Close comparison of Figures 5a and 5b reveals that there is a slight influence of temperature on particle deposition, namely, at higher temperatures, more particles deposit. Figure 8 gives a temperature profile of particle deposition (similar to the metal removal profile in Figure 2) showing that between 50° and 70° C the particle deposition slightly, but significantly increases.

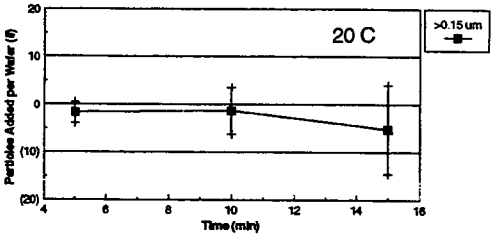

Figure 7: Particle deposition over time from 0.0012 M HCl.

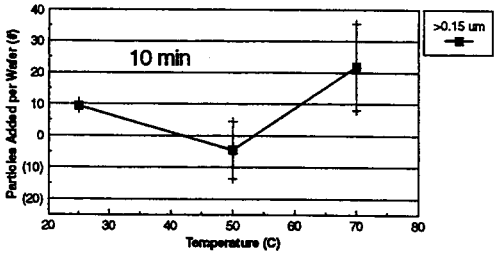

Figure 8: Effect of temperature on particle deposition from 0.00012 M HCl.

Optimized Metal and Particle Cleaning

Optimizing the metal and particle performance of the dilute HCl cleans revolves around controlling two main parameters: temperature and pH (HCl concentration). Higher temperature and lower pH are expected to improve the metal removal and overall robustness of the solution while lower temperature and higher pH have been seen to improve the particle behavior. In Figures 9a and 9b the process windows existing at 20° and 70° C that allow for maximum metal removal and minimum particle addition can be seen. At 20° C, metal removal is the limiting factor with metal removal dropping off quickly at concentrations below 0.0012 M. The optimum solutions lie between 0.012 and 0.0012 M HCl. While this is a good range for a process window (one order of magnitude) the situation can be improved dramatically by increasing

the temperature. Figure 9b shows that the metal removal situation is greatly improved by the higher temperature with no appreciable loss in metal removal even at concentrations down to 0.00012 M. If the data in Figures 2 and 8 is included in the analysis it becomes apparent that the optimum temperature and concentration should be at 50° C and 0.0012 M. Figure 4 adds the fact that the immersion time could be as short at 5 minutes. This process should give optimum metal removal and particle performance while still allowing one order of magnitude of variation in concentration and 10° to 20° C in temperature for tuning to a particular process flow.

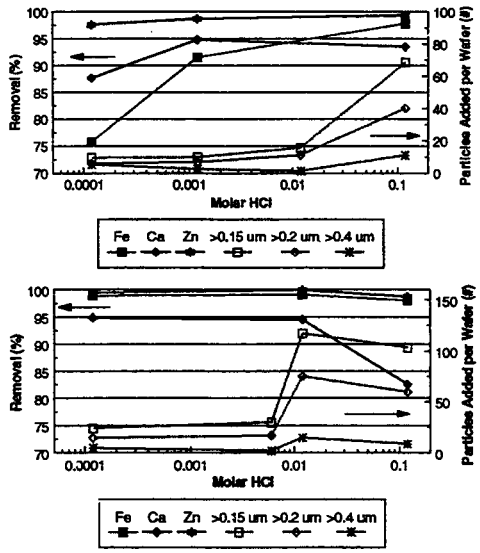

Figures 9a and 9b: Metal removal and particle addition behavior of dilute HCl at 20°C (9a) and 70° C (9b).

Conclusions

It has been demonstrated that dilutions of HCl can be used to effectively remove metals from the surface of hydrophilic wafers. This was also demonstrated for metallic Cu on the surface of hydrophobic wafers. By lowering the concentration below the critical threshold of 0.012 M, the metal removal process can be performed without paying the penalty of depositing particles. This particle behavior is in perfect agreement with theoretical models. An optimum temperature and concentration of 50° C and 0.0012 M was proposed. This allowed for one order of magnitude variation in concentration and 10° to 20° C variation in temperature without serious degradation in the metal and particle performance. It was also seen that the metal removal in these solutions reaches it maximum in 5 minutes or less which allows for a faster total cleaning cycle.

References

[1] T.Q. Hurd, P.W. Mertens, H.F. Schmidt, D. Ditter, L.H. Hali, M. Meuris, and M.M. Heyns, *IES 40th Annual Technical Meeting 1994 Proceedings* (IES, Mount Prospect Illinois, 1994) *to be published.*

[2] H. Park, C.R. Helms, D. Ko, M. Tran, and B.B. Triplett, *Mat. Res. Soc. Symp. Proc. Vol. 315*, (1993 Materials Research Society, Pittsburgh) p. 287.

[3] S. Bedge, B.S. Barron, and H.H. Lamb, *Mat. Res. Soc. Symp. Proc. Vol 315* (1993 Materials Research Society, Pittsburgh) p. 467.

[4] D.J. Riley and R. G. Carbonell, *J. of Coll. and Interface Sci.* **158**, 259 (1993).

[5] J-K Lee, B.Y.H. Liu, and K.L. Rubow, *IES 39th Annual Technical Meeting 1993 Proceedings Vol. 1* (IES, Mount Prospect, Illinois, 1993) p.209.

DIAGNOSTICS OF PROCESS-HYGIENE IN LARGE SCALE Si-MANUFACTURING USING TRACE-ANALYTICALTOOLS

L.Fabry, L. Köster, S. Pahlke, L. Kotz, J. Hage
Wacker-Chemitronic GmbH, D-84489 Burghausen, Germany

... everything is being a concordance and succession of causes and conditions, a thing itself does not exist, because it has a relative connection with causes and conditions...
[1]

1. PROCESS-HYGIENE, DIAGNOSTIC TOOLS AND CONTINUOUS IMPROVEMENT

Trace-analytical tools are the key both to recognizing the causes of sub-optimal process conditions and to confirming specified quality parameters. Generating systematic data on incoming materials, processes, production environment and products by contamination monitoring is the prerequisite of efficient diagnosis, problem solving and total quality management (TQM) in the semiconductor industry. Thus, contamination analysis systems are also primary tools of statistical process control (SPC) and failure mode & effects analysis (FMEA) [2-4], fundamental procedures of continuous improvement. International guidelines of ISO 9000-9004 regulate the application of analytical tools and process monitoring in the production process [5].

Large scale manufacturers of S- and S^2-ULSI integration density persistently pursue a narrowing range of fluctuations in the quality of both starting materials and consumables [6]. Therefore, diagnostics and problem solving in semiconductor research, development and industrial processes rely heavily on closed loop contamination monitoring and analysis systems, because monitoring is more cost-effective than casual, trouble-shooting diagnostics.

In this talk, we have focused on the role of analytical tools in the pursuit of TCS in the large scale manufacturing of silicon wafers. We review the basic rules of the efficient diagnostic use and the limitations of these analytical tools and describe them in several examples.

2. STATISTICAL AND PHYSICAL LIMITS OF TRACE-ANALYTICS

2.1 Sampling and probe volume

Engineering knowledge consists of a lucky mixture of facts, beliefs and creativity. Basically, analyses must provide the facts and, simultaneously, support and channel the right engineering beliefs and creativity. In the course of problem solving by trace-analyzes, sampling sets the physical boundaries to the information value of the results. Whenever possible, the analyst shall lean on statistical sampling tables in order to assure adequate and technologically relevant analytical results [7].

The ultimate limits to the performance of trace-analytical methods are set by the relative concentration of impurities, the probe volume and the probability of discovering a single contaminant atom due to a detectable event [8-11]. In an extreme setting, the probe volume contains only a few atoms of interest. Then,

the diminishing size of both the detection spot and the penetration depth limits the accuracy, precision and sensitivity of the trace-analytical technique as a whole.

2.2 Calibration and outliers

In order to quantify the extent of trace-contamination, detectors must be calibrated. During a measurement that calibration is supposed to remain accurate and stable at a level of cleanliness that is usually hardly attainable for commercial standards at sub-ppba / ppta levels. For ULSI-use, two basic calibration approaches were proposed to SEMI [12]. Both of them are based on Student statistics that outlines the confidence level of few (<30) results after random sampling. In order to provide reliable data, multielement analysis methods should operate with LOD at least one order of magnitude lower than the specified values to be controlled. Otherwise, there is a high probability of material fails due to statistical measurement uncertainties (Tab. 1, [12]).

Calibrations are regression calculations. As such, the error of any calibration function contains 4 error contributions: error in the independent variable (standard reference samples), error in the dependent variable (noise) and missing or inaccurate fit between the variables. Error in the variables and in the fit can be both of systematic and of random origin. Therefore, the continuous improvement of calibration will reduce all sorts of errors economically.

Provided that calibration and measurements are in a state of statistical control, outliers among analytical data can be distinguished from the relevant ones by simple statistical methods [13]. A particular process / product quality variation can be characterized by performing replicate analyses on a certain number of reference samples [14]. Thus, the analyst should obey the statistical guidelines for sampling, detection and instrumental functions. Moreover, analytical instruments are more subject to SPC than the processes monitored [15].

Concentration of specification % of LOQ	**Probability of simultaneously missing**		
	1 component present	**4 components present**	**10 compomnents present**
110 %	0.016 %	0.064 %	0.16 %
100% (LOQ)	0.14 %	0.52 %	1.3 %
83 %	2.3 %	8.8 %	21 %
67 %	16 %	50 %	82 %
60 %	27 %	72 %	96 %
50 % (LOD)	50 %	94 %	99.9 %

Table 1:

Risk of false accepts due to not detecting the contamination at the level of specification. Specification lies between LOD (background + 3σ) and 1.1*LOQ (LOD + 3σ), standard deviation of analytical method is not higher than that of the instrument.

Elements of quality							
Control			and Assessment				
Item		Cost	Test	Contribution to Accuracy	Precision	Intro-spec-tive	Inter-lab
certified standard reference	[16]	expensive	definitive measurements	high		X	X
internal reference	[16]	usually inexpensive	reference measurement replicate measurement	high		X	X
blank adequate calibration	[12,16]		[7, 11, 15, 17, 19, 20]		high	X	
standard solution	[16]	inexpensive	Round Robin [19, 20]	high			X
spiked sample	[16, 17]	usually inexpensive	spikes, recovery rate	high		X	
surrogate determinand	[16]	inexpensive	surrogates, matrix effects	high		X	
appropriate analytical technique dissolution, separation, preconcentration, instrumentation	[21]	expensive	cross-checking by means of comlementary methods [11,19,20]	high	high	X	X
suitable facilities lab-enviroment	[9]	expensive	audits [5]	high	high	X	
competent presonal (continning education)	[18]	expensive		high	high	X	
SPC statistical process control	[2 - 5, 13, 14]	inexpensive	control charts [2 - 5, 13]	high	high	X	
documentation (GLP, GMP, SOP, PSP)	[3, 4, 18]	usually expensive		high	high	X	

Table 2 :
Data quality assurance in semiconductor diagnostics and its relative costs

2.3 Accuracy, precision and SPC in the trace-analytical lab

Quality assurance (i.e. quality control and assessment of the diagnostics) requires a particular emphasis in the range of trace-contaminations. The principles of introspective and interlaboratory data quality controls are standardized (Tab. 2 [16-23]). However, trace-analysts have to find unconventional ways to assure high data quality in spite of peculiar issues such as micro-sampling in an inhomogeneous entity, the rare availability and stability of certified standard reference materials and a vague definition of the effective sample reference-volume and reference-surface (Tab. 3).

2.4 Statistical traps in diagnostics

Most statistical data treatments describe what and how to evaluate. However, the diagnostician must also be aware of the limits of statistical evaluation. Benevolent unawareness at this point can end in confusion and misleading conclusions. An incomplete list shows some of the usual pitfalls of large scale data evaluation.

- Memory effects in sampling, sample preparation and analysis
- Misuse of "<LOD" in a sense of "absent" and confusing zero and nothing
- Incomplete data on variability: Do the digits stand for maximum error, signal-to-signal error, one (or two) standard deviation(s) at a stated confidence level and by what kind of statistics?
- Equating statistical relevance with practical relevance
- Failing in proving a relevant difference should not imply the absence of any difference
- Overestimation of the relevance of a correlation coefficient of any non-zero value and assuming without statistical testing that correlation means causation
- Placebo effects or uncontrolled or unmentioned bias on the side of the experimenter / evaluator
- Ignoring that extreme data exist in the population and they are becoming more likely with increasing population size and elapsing time or
- Believing that isolated populations tend to converge toward the mean as time passes

3. CONTAMINATION MONITORING AND TRACE-ANALYSIS METHODS

In the semiconductor industry, analysts are expected to provide reliable, meaningful and real-time results even if trace-analysis techniques usually require a tedious sample preparation. The analyst has to invent / modify / apply novel techniques to detect traces of contaminations and their fluctuations in ever-improving process media and products. Accuracy, precision, limit of detection / quantification [12, 14, 17], sensitivity, analysis time, throughput and analytical expenses should always be fine-tuned to the particular case. Monitoring must rely on a specified precision of high confidence, whereas diagnostic investigations anticipate both high accuracy and precision.

Sources of Uncertainty Physical				Engineering Issues
Issue		Contribution to Accuracy	Precision	
sampling procedure	[7-11]	low	high	expert system [24]
physical sample preparation		high	high	
chemical dissolution separation, enrichment	[20]	high	high	real-time diagnostics
additional contamination		high	high	high local / environmental
blank calibration	[12, 15]	high	low	cleanliness
reference sample volume / surface	[12, 15]	high	low	minispot probe [8, 11] detection sensitivity
certified standard	[9, 16]	high	low	stabilization of sub-ppba /ppta contamination
instrumentation operator, lab enviroment	[18]	high	high	servicability, cost and reliability standardization due to good engineering practice (SEMI)
custom-taylored methodology	[24]	high		

Table 3:
Semiconductor ultra-trace-analytical challenges

The diagnostic work begins with the evaluation of the sampling and analytical feasibility, the costs and the technological relevance of the anticipated results [24]. The job must conclude in a conference on the consistency, completeness, validity and relevance of the results. Regarding process conditions that can affect distribution of the contaminats [25], the participants shall consider all effects of sample history.

In most device technologies, the final chip yield is limited by the bulk and surface metallic cleanliness and by the recombination / generation lifetime of minority carriers in / on bare semiconductor silicon wafers. Monitoring only these relevant quality indicators does not require the whole complexity of semiconductor diagnostics. A few sensitive analytical tools such as VPD/AAS, GF-AAS,

ICP-MS, TXRF μ-PCD and Elymat are necessary and sufficient for a thorough metallic contamination control.
Due to the limited space here, we discuss only the TXRF. Application of other diagnostic tools has been discussed earlier [26, 27].

4. Si-SURFACE ANALYSIS USING TXRF

Recently, TXRF has become generally accepted in monitoring surface contamination [28-37]. TXRF is popular because it works in-line ("class 100") without tedious preparation and provides real-time multielemental data on both as-polished and epi-wafers and clean process media droplets on surrogates for elements of $20<Z<35$ and $56<Z<83$ (P through the anode element, usually Mo, Cu or W; throughput: 20 min / spot). By means of a special arrangement light elements also can be analyzed [38]. The current instruments are throughout automated and sensitive down to the 10^{10} at.cm^{-2} range without chemical preparation / preconcentration. VPD preparation allows analyses down to the 10^{8} at.cm^{2} range (200 mm wafer) [39-41]. They run stably under SPC, irrespective of the chemical form of the elements of interest. The repeatability of a measurement is >> 95% [29, 31, 35, 42, 43]. The high degree of automation facilitates also a detailed mapping of contamination distribution. However, the simpler the mechanical construction of the TXRF instrument the higher its up-time rate. Fine-focused, sealed-tube machines usually have an up-time rate higher than 90 % in round-the-clock use.
Due to the applied VPD-treatment, soluble contamination from the native oxide layer of the wafer surface is collected. The corresponding LOD can be increased by 2 orders of magnitude. The measurement data on a VPD-droplet must be recorded only at the sites of integrated maximum contamination ("quick-search" [41]). Adding a suitable internal standard to the scanning solution makes the analysis virtually independent of the geometry of the spot. It is worth noting that the chemical form of the metallic contamination determines the yield of a given VPD treatment. Thus, recovery rates must be investigated on spin-coated or as-dipped, vapor-deposited and ion-implanted [44] wafer spikes using different solvents.
In order to accurately interpret the TXRF data, the user must be reminded of the assumptions in converting TXRF intensities into contamination data:

1. The background noise is a function of the optical quality (i.e. microroughness and flatness) of the reflective surface. Quantification assumes that they are of the same value on the reference and on the sample surface. The level of background noise depends on the crystallographic orientation when intense W-L_{β} beams are reflected e.g. from the (224) and (444) Si planes. That condition satisfies the Bragg incidence of <110> and the reflected intensity can excite contaminants also in the beam path [45].

2. The fluorescence yield is dependent upon the optical condition of contamination: Counts on plated films increase with rising incident angles, whereas, counts on particulate residues are independent of the incident angle up to the degree of relevant penetration.

3. Applying spin-coat or immersion calibration samples, homogeneous metal coverage can be achieved only in the range of 10^{11}-10^{13} at.cm^{-2}. After converting the calibrating fluorescence intensity into the surface concentration of the standard calibration reference sample, the surface concentration is assumed to be proportional to the fluorescence yield down to the LOD in the whole analytical range of interest. The precision of the calibration is dependent upon the precision of the independent method(s) used to determine the surface concentration of the standard reference sample!

4. The calculation of the LOD is according to

$$N_{LOD} = N_{ref}(3 * \frac{\sqrt{S_{bg}}}{S_{ref}})$$

N_{LOD}: lowest detectable counts/sec (cps) at LOD; N_{ref}: cps found on standard calibration reference sample (e.g. microdroplet on virgin epi-wafer or spiked as-polished wafer surface); S_{bg}: standard deviation for background measurement on virgin epi-wafer or HF-cleaned as-polished wafer surface; S_{ref}: standard deviation for standard calibration reference sample. Similarly, replacing N_{ref} cps data by the known number of atoms.cm^{-2} in reference to the spot size, N_{LOD} is converted into surface concentration units. Accurately, this LOD is valid only for one single element, usually Ni. Each additional contaminant increases the background noise, therefore, the multielement LOD (c.f. POD) must lie higher!

5. The TXRF data are spot checks on a few sites of limited dimension (diameter of 8 mm) and over an information depth of 2-10 nm. That information depth is depending on the incident angle [29, 34]. Contaminations below 10^{11} at.cm^{-2} are usually inhomogeneous, therefore, the spot-result does not necessarily characterize the whole surface (c.f. [7]).

6. In order to assure a level of sufficient accuracy, TXRF instruments must be calibrated by certified reference wafers. The type of standard reference specimen must be selected on the basis of the optical type of analytes and specimens. Thus, analyzing film-type contamination requires sputtered or spin-coated film-type samples. For analyzing particulate-type contamination, such as a VPD spot, the calibration must be carried out using particulate-type samples such as a microdroplet. Similarly, the analysis of ion implanted substrates for metals should be calibrated by ion implanted samples. Any simplification must be carefully investigated to ensure accuracy for the given application. Baseline-offset can be subtracted only under statistical control [23].

7. If the correlation cannot be referred to certified standards such as microdroplets of known Ni amount, the calibration standard samples must be introspectively cross-checked with RBS, SIMS and VPD/AAS [30, 31, 34, 35, 46] or with SEM/EDX [42]. The mandatory use of the complementary method contributes to the calibration errors. The errors in the determination of calibration

standard reference results propagate and add to the random TXRF error. Process-media measurements must be correlated with ICP-MS [36] and, occasionally, on quartz-plate surrogates [4]. For industrial monitoring purposes, the high precision must be tested daily under SPC conditions [2-6]. A regular interlaboratory testing of all methods is recommended [19].

Acknowledgment

This work has been partly supported by the Federal Department of Research and Technology of the FRG under contract No. M 2793 F. The authors alone are responsible for the contents. The authors thank Dr. Betty Coulman of Wacker Siltronic Corp. for her valuable comments.

Acronyms of analytical techniques and characteristica

AAS:	Atomic Absorption Spectroscopy
EDX	Energy Dispersive X-ray spectroscopy
Elymat:	Electrolytical Metal Tracer [47]
GFA:	Gas Fusion Analysis (=heat extraction, [69])
GLP:	Good Laboratory Practice (protocol defining general operations)
GF-AAS:	Graphite Furnace AAS
ICP-MS:	Inductively Coupled Plasma Mass Spectrometry
LOD or DL:	Limit Of Detection (2-3 σ of noise level, [14, 17])
LOQ or QL:	Limit Of Quantification (>6 σ of noise level, Fig. 2/3, [12, 14, 48]
MAD:	Mixed Acid Droplet (c.f. VPD)
MDL:	Method Detection Limit [12], c.f. POD
µ-PCD:	Microwave reflection Photo Conductive Decay, for application ref. [49])
POD:	Power Of Detection (LOD of in real sample matrices, c.f. MDL) [50]
RBS	Rutherford Backside Scattering
SEM	Scanning Electron Microscopy
SIMS	Secondary Ion Mass Spectroscopy
TXRF:	Total Reflection X-Ray Fluorescence
UPW:	Ultra-Pure Water
VPD:	Vapor Phase Decomposition (vapor phase reaction of HF with native Si-oxide and scanning the surface with a UPW or H_2O_2 solution droplet [34, 51, 52], c.f. MAD)

REFERENCES

[1] The Teaching of Buddha, p. 108, Bukkyo Dendo Kyokai, Kosaido Printing, Tokyo (1989)

[2] SPC und FMEA, Qualität bei Hoechst, K.-D. Ziehmann, Editor, Frankfurt am Main, Hoechst AG 1991

[3] C.J. Spanos, Proc.of the IEEE, 80(6) (1992) 819-30

[4] Hitoshi Kume: Statistical Methods for Quality Improvement, AOTS Tokyo (1992)

[5] Internat. Standards, ISO 9000-9004-87, Quality management and quality assurance standards, 1987

[6] R. McMahon, SEMATECH Standards, 3(2) (1991) 3-5

[7] Internat. Norm IEC 410, Intern. Electrotechn. Commission, Sampling procedures and tables for inspection by attributes, 1973

[8] T.J. Schaffner, in Contamination Control and Defect Reduction Semicond. Manuf.I/1992, D.N. Schmidt, Editor, PV 92-21, p.162-74, The Electrochem.Soc. Softbound Proc.Ser., Pennington, NJ, 1992

[9] T.J. Schaffner, in Semicond.Si/1990,
H.R. Huff, K.G. Barraclough and J. Chikawa, Editors,
PV 90-7, p. 891-911, The Electrochem.Soc. Softbound Proc.Ser., Pennington, NJ, 1990
[10] B. Kratochwil, D. Wallace and J.K. Taylor, Anal.Chem., 56(5) (1984) 113-29R
[11] R. Klockenkämper, Z.Anal.Chem., 285 (1977) 345-52
[12] SEMI Draft Document # 2190 (08/19/93) and T. Bzik, P. Bouis, SEMI Statistical Task Force Reports June, Sep and Oct 1992, and Chem.Reagents Committee, Attachments #6 to the September '92 Meeting Minutes, Sep, 1992
[13] S. Noack in Stat. Auswertung von Meß- und Versuchsdaten, pp. 373-82 (Nalimov-test), de Gryter, Berlin-New-York (1980)
[14] K.S. Booksh and B.R. Kowalski, Anal. Chem., 66(15) (1994) 782A-91A
[15] E. Mullins, Analyst, 119 (1994) 369-75
[16] Analytical Methods Committee, Royal Soc.of Chem., Analyst, 114 (Nov 1989) 1497-503
[17] Anal.Chem.Div., IUPAC, "Nomenclature, symbols, units and their usage", Spectrochim.Acta B, 33B (1978) 241-
[18] J.K. Taylor, J.of Res.Nat.Bureau of Standards, 93(3), (1988) 232-6
[19] Int. Standard ISO 5725, Int.Org.for Standardization, Precision of test methods, 1986
[20] G. Tölg, Naturwissenschaften, 63, 99-110 (1976)
[21] Z. Laczik, R. Falster and G.R. Booker, Sol State Phenomena, 19&20 (1991) 39-44
[22] G. Tölg, Fresenius Z.Anal.Chem, 331 (1988) 226-35
[23] E.V. Thomas, Anal. Chem., 66(15) (1994) 795A-804A
[24] D.E. Passoja, L.A. Casper and A.J. Scharman in ACS Symp.Ser. Vol. 295 (Microelectron.Process: Inorg.Mater.Characterization), pp.1-17, 1986
[25] L. Fabry, B. Hackl and K.-J. Range, Jpn J. Appl. Phys., 33(1B) (1994) 510-3
[26] L. Fabry, L. Köster, S. Pahlke, L. Kotz and J. Hage, Proc.-ECS in Cryst Defects, 1993, B.O. Kolbesen, C. Claeys, P. Stallhofer and Tardif, Editors, PV 93-15, pp. 193-221, The Electrochem. Soc. Softbound Proc. Ser., Pennington, NJ, 1993
[27] R. Takiguchi, Y. Monma and Y. Hirofuji, Ultra Clean Technol., 4(5/6) (1992) 25-40
[28] P. Eichinger, H.-J. Rath and H. Schwenke,
Semicond. Fabrication. Technol. and Metrology,
ASTM STP 990, D.C. Gupta, Editor, Amer.Soc. for Testing and Materials, 1989
[29] W. Berneike, Spectrochim.Acta 48B(2) (1993) 269-75
[30] R.S. Hockett in Defect Control in Semicond., K. Sumino, Editor, pp. 1547-52, Elsevier, North-Holland, 1990
[31] R.S. Hockett, in Semicond.Cleaning Technol./1989, PV 90-9,
J. Ruzyllo and R.E. White, Editors, pp. 227-42,
The Electrochem.Soc. Softbound Proc.Ser., Pennington, NJ, 1990
[32] A. Prange, Nachr.Chem.Tech.Lab., 41(1) (1993) 40-45
[33] U. Reus, A. Prange Spectroscopy Eur., 5(1) (1993) 26-33
[34] A.C. Diebold, P. Maillot, M. Gordon, J. Baylis J. Chacon, R. Witowski , H.F. Arlinghaus, J.A. Knapp and B.L. Doyle, J.Vac.Sci.Technol.A, 10(4) (1992) 2945-52
[35] L. Fabry, S. Pahlke, L. Kotz and G. Tölg, Fresenius J. Anal. Chem., 349 (1994) 260-71
[36] V. Penka and W. Hub, Fresenius Z.Anal.Chem, 333 (1989) 586-9
[37] B.A.R. Vrebos and G.T.J. Kuiperes, X-ray Spectrom. 20 (1991) 5-7
[38] P. Wobrauschek, P. Kregsamer, C. Streli and H. Aiginger, X-ray Spectrom., 20 (1991) 23-8
[39] R.S. Hockett, 2nd Intern. Symp. on Ultra Clean Processing of Si Surfaces, Brugge, 1994
[40] A. Huber, R.J. Rath, P. Eichinger, T. Bauer, L. Kotz and R. Staudigl in Proc. Symp. Diagn. Techn. Semicond Mater. Devices, PV 88-20, pp 109-12 The Electrochem. Soc. Softbound Proc. Ser., Pennington NJ, 1988
[41] L. Fabry, S. Pahlke, L. Kotz, E. Schemmel and W. Berneike, Proc.-ECS in Cryst. Defects 1993, B.O. Kolbesen, C. Claeys, P. Stallhofer and F. Tardif, Editors, PV 93-15, pp. 232-9, The Electrochem. Soc. Softbound Proc. Ser., Pennington, NJ, 1993

[42] H. Kondo, J. Ryuta, E. Morita, T. Yoshimi and Y. Shimanuki, Jpn.J.Appl.Phys, 31 (1992) L11-3
[43] K. Nishihagi, A. Kawabata, T. Taniguchi and S. Ikeda, in Semicond.Cleaning Technol./1989, PV 90-9, J. Ruzyllo and R.E. White, Editors, pp. 243-50, The Electrochem.Soc. Softbound Proc.Ser., Pennington, NJ, 1990
[44] D.C. Jacobson, J.M. Paate, G.S. Higashi, T. Boone, D.J. Eaglesham and R. Hockett, MRS Spring Meeting, San Francisco, Apr. 26-29, 1993
[45] K. Yakushiji, S. Ohkawa, A. Yoshinaga and J. Harada, Jpn. J. Appl. Phys., 33(2) (1994) 1130-5
[46] M. Meuris, M. Heyns, W. Küper, S. Verhaverbeke and A. Philipossian, in ULSI Sci.Technol./1991, PV 91-11, J. Andrews and G. Celler, Editors, pp. 454-63, The Electrochem.Soc. Softbound Proc.Ser., Pennington, NJ, 1991
[47] G. Ferenczi, D. Huber, T. Pavelka, P. Eichinger and G. Veszely, Defect Control Semicond.Proc.Int.Conf. Sci.Technol.Defect Control Semicond. 1989, K. Sumino, Editor, (Publ.1990), 2, pp. 1585-91, North-Holland, Amsterdam, 1990
[48] J.N. Miller, Spectroscopy Eur., 5(1) (1993) 22/24
[49] H. Shimizu, N. Honma and C. Munakata, Jpn.J.Appl.Phys., 28(5) (1989) 743-7
[50] G. Tölg, Fresenius Z.Anal.Chem., 329 (1988) 735-,
[51] A. Shimazaki, H. Hiratsuka, Y. Matsushita and S. Yoshii, Ext. Abs. 16th (1988) Int. Conf. on Solid State Device and Mater., p. 281, Kobe, 1984, Business Center for Acad. Soc. Jpn, Tokyo 1988
[52] A.Maeda, M. Kageyama, S. Yoshii and M. Ogino, U.S. Patent 4,990,459 (Feb 5, 1991)

###

Ultra-trace Metal Analysis of Si Wafer Surfaces using Synchrotron Radiation

A. Fischer-Colbrie, S.S. Laderman, Hewlett-Packard Co., Palo Alto CA, USA;
S. Brennan, N. Takaura, P. Pianetta, Stanford University, Stanford, CA, USA;
A. Shimazaki, K. Miyazaki, Toshiba Corp., Kawasaki, JAPAN;
J. Kortright, Lawrence Berkeley Laboratory, Berkeley, CA, USA;
D.C. Wherry, Fisons Instruments, San Carlos, CA, USA

We have used synchrotron radiation to extend the detection limits of the total reflection x-ray fluorescence technique to ~$5x10^8$ atoms/cm^2 for Fe and ~$3x10^8$ atoms/cm^2 for Ni. In exploring the capability of the technique, we have also uncovered some difficulties which include the need for experimental improvement. This paper discusses current status of the technique and application to nominally clean Si wafers.

1. INTRODUCTION

Lowering the levels of metallic impurities on wafer surfaces has been a persistent concern of VLSI manufacturers. Currently, our ability to prepare clean wafer surfaces exceeds our ability to reliably measure the impurities which remain. This situation makes it difficult to efficiently develop and test new processes or to control them. Current methods for chemically identifying and quantifying wafer surface impurities include total reflection x-ray fluorescence (TRXRF) using a rotating anode source. The strengths of this technique are that the measurement is non-destructive, reproducible, allows for mapping, and it is not necessary to remove the impurity from the surface, the difficulty and uncertainty of which depends on the element. However, this method has a typical detection limit of ~$5x10^9$ atoms/cm^2, which is not sufficient for imminent industry needs.

In this work, we have explored the possibility of using synchrotron radiation to extend TRXRF detection limits as well as understand the limits of the method. Advantages of the synchrotron source for TRXRF are a higher brightness and nearly complete linear polarization, both of which improve signal to background. An additional advantage is the tunability of the x-ray energy to extend the range of elements to most of the periodic table for which high sensitivity is obtained.

2. SYNCHROTRON RADIATION TRXRF EXPERIMENT

Benchmark experiments were carried out at the Stanford Synchrotron Radiation Laboratory at a focussed wiggler beamline (10-2) using a double-reflection multilayer monochromator.[1-3] The band-pass of the multilayer is approximately 200 eV. For the experimental configuration used in this work, a photon flux of 10^{13} photons/sec-100mA at 10.5 keV was obtained with a 2x2 mm^2 incident beam aperture. The detector used in this work was a Kevex Si(Li) solid

state detector with a Quantum™ window[4]. In front of the detector was a W collimator with an ultrapure Be foil and a 25μm teflon window. The purpose of the teflon was to reduce the Si signal because of count rate limitations by the detector.

3. APPLICATION TO STANDARDS OF KNOWN CONCENTRATION

The measurements for a sample intentionally contaminated with $10^{11}/cm^2$ Fe, Ni, and Zn are shown in Fig. 1. For comparison, the same sample measured on the Rigaku 3726 TRXRF system with a $W_{L\beta}$ target is also shown. In the synchrotron radiation TRXRF (SR-TRXRF) spectrum, there is a factor of 200 increase in the Fe, Ni, and Zn signals and correspondingly less noise. This difference is due primarily to the difference in photon flux onto the sample. In addition, an obvious difference in the two spectra are that the relative Si, S and Cl signal is smaller in the SR-TRXRF case due to the attenuation by the teflon. Another difference is that the energies of the elastically scattered peaks is different. For the SR-TRXRF case, we were able to tune the energy so that it would not interfere with the Zn peak. Finally, the overall shape of the background is different. A careful study of these backgrounds is currently underway. The Ca peak in the conventional TRXRF case was inadvertently added between the measurements.

Using straightforward data analysis methods appropriate to Gaussian signals on linear backgrounds[5], the minimum detection limits were calculated Fe and Ni for the synchrotron case. These detection limits are ~$5x10^8/cm^2$ for Fe and ~$3x10^8/cm^2$ for Ni.

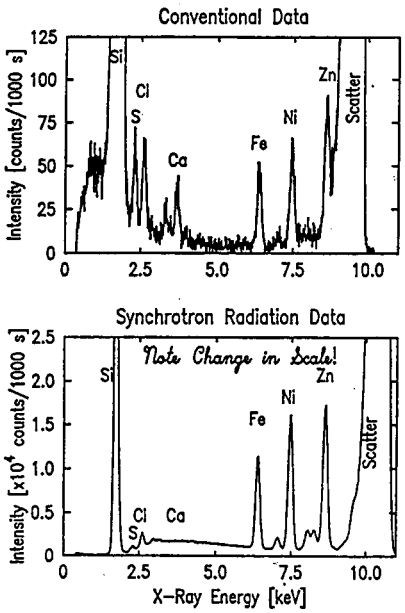

Fig. 1 SR-TRXRF vs. Conventional TRXRF for a sample with $1x10^{11}/cm^2$ Fe, Ni and Zn.

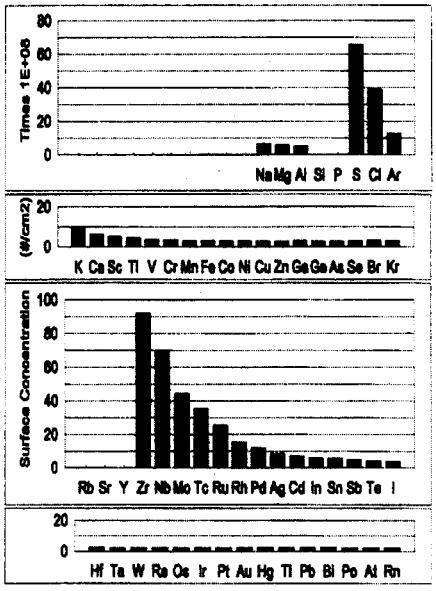

Fig. 2 Calculated SR-TRXRF Sensivities extrapolated from $3x10^8/cm2$ for Ni.

4. SENSITIVITY TO ELEMENTS IN PERIODIC TABLE

Calculations of the detection sensitivities for different elements were made and are shown in Fig. 2. By assuming a Ni detection limit of $3x10^8/cm^2$, a tunable x-ray source, scaling by the difference in absorption and fluorescence probabilities, and assuming attenuation through a teflon filter (for elements above Si in the periodic table), we see that the detection limit over much of the periodic table is extremely low, including elements such as Al. The calculation is for the K-edge for elements lighter than Kr and for the L-edge for heavier elements. The gap at Rb, Sr, Y and the jump at Zr are because we have assumed an energy cut-off of 15 keV. In principle, this technique should allow us to effectively measure most of the elements in the periodic table.

5. APPLICATION TO NOMINALLY CLEAN Si WAFERS

SR-TRXRF measurements of wafers which were as-received from different Si wafer vendors were made to explore both the limits of the technique as well as to see what contamination levels were associated with typical "clean" wafers. In this work, we discovered that for Fe, Ni, Cu and Zn, it was not possible to accurately measure levels at the detection limit. Rather, it became clear from a filtering study[1], that low levels of Fe, Ni, Cu and Zn fluorescence were being generated parasitically within the detector itself, the strength of which depended on the intensity of the x-rays elastically scattered into the detector. Thus, as the incident x-ray flux is increased, so do the apparent Fe, Ni, Cu, and Zn signals.

Using calibration standards of samples intentionally contaminated with $1x10^{12}/cm^2$, $1x10^{11}/cm^2$, and $1x10^{10}/cm^2$ Fe, Ni and Zn, we estimated the apparent concentration of Fe, Ni, Cu and Zn for clean wafers by scaling the elastically scattered signals and comparing them to the relative signals from the standards. The result of this calculation is shown in Fig. 3. The values for the cleanest wafer are: Fe $\sim 7x10^8/cm^2$, Ni$\sim 2x10^9/cm^2$, Cu$\sim 1x10^{10}/cm^2$, Zn$\sim 4x10^9/cm^2$. If these levels were actually present, the Cu and Zn could also be measured by conventional TRXRF. They were not observed for the cleanest wafer.

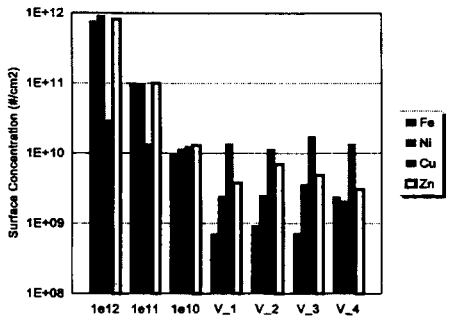

Fig. 3 Surface metal concentrations for various wafers. 1e12, 1e11, 1e10 are levels from known standards. V_1...V_4 are wafers from different vendors.

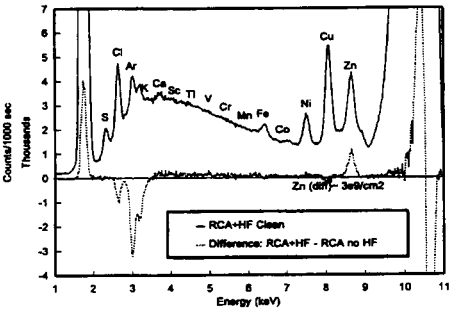

Fig. 4 Difference SR-TRXRF signal from a wafer cleaned by RCA+HF compared to one cleaned by RCA no HF.

Clearly, this increase in incident flux has pointed out a need for detector improvements in order to measure low levels of those metals.

For other elements, e.g. Sc through Mn and others, the existing detector does not have these limitations. Clean wafers show no detectable levels of these elements to very high precision. For example, in these measurements, the Mn level is less than ~ $6x10^8/cm^2$.

Even with the Fe, Ni, Cu, Zn parasitic contributions, we can compare data sets of samples measured under similar conditions to determine differences in between the amounts of real contamination. Two wafers which had two different cleans, RCA and HF versus RCA no HF, were measured, scaled by the elastic signal, and subtracted. This difference is shown in Fig. 4. It is clear from these data that the difference in Fe, Ni, and Cu signals from the two samples is essentially zero, but that there is a significant difference in Zn that can be estimated to be ~ $3x10^9/cm^2$. The ability to subtract the parasitic signals suggests that it is possible to still look at very low levels of Fe, Ni, Cu and Zn contamination.

6. CONCLUSIONS

This work points to several areas for potential improvement. These areas include detector modification for reduced parasitics as well as for higher count rate capability. Extremely careful wafer handling is also necessary. With the ability to measure these exceedingly trace amounts of material, mis-handling is easy to detect. In addition, we estimate that the use of a detector array should lower the detection limit by a factor of six to $5x10^7/cm^2$.

SR-TRXRF is not yet at its technical limit. The use of synchrotron radiation allows better sensitivities, the ability to measure more elements, as well as faster multi-point analysis. Because of its unique capabilities, synchrotron radiation-based metrology would be an extremely valuable tool for Si VLSI research and development, and possibly even manufacturing. While some practical and barriers exist to developing this tool, they are, in principle, surmountable.

ACKNOWLEDGEMENT

This research was performed at Stanford Synchrotron Radiation Laboratory which is operated by the Deparment of Energy, Office of Basic Energy Sciences.

REFERENCES

1. S.S. Laderman, Bull. Am. Phys. Soc. **39** 514 (1994).
2. S. Brennan, W. Tompkins, N. Takaura, P. Pianetta, S.S. Laderman, A. Fischer-Colbrie, J.B. Kortright, M.C. Madden and D.C. Wherry, Nucl. Instrum. Meth. **A 347** 417 (1994).
3. P. Pianetta, N. Takaura, S. Brennan, W. Tompkins, S.S. Laderman, A. Fischer-Colbrie, M. Madden, D.C. Wherry, J.B. Kortright, proc. of the 1994 SRI Intl. Conf., Stonybrook, NY, to be publ. Nucl. Instrum. Meth. (1995).
4. Fisons Instruments, San Carlos, CA.
5. P. Bertin, Principles and Practice of X-ray Analysis, Plenum Press, NY, NY, 1980.

QUANTITATIVE DEPTH ANALYSIS OF ULTRATRACE ELEMENTS IN SILICON WAFERS

M. Takenaka*, M. Hayashi*, H. Matsunaga*, Y. Honma*,
A. Kubota**, and Y. Matsushita**

* Research and Development Center, Toshiba Corporation, 1, Komukai Toshiba-cho, Saiwai-ku, Kawasaki 210, Kanagawa, Japan
** Semiconductor Materials Engineering Dept., Toshiba Corporation, 72, Horikawa-cho, Saiwai-ku, Kawasaki 210, Kanagawa, Japan

ABSTRACT - A new sensitive and quantitative depth analysis method , named SSA (step by step analysis), has been developed for the ultratrace metallic impurities in silicon bulk. Detection limits are found to be 2-3 orders of magnitude lower than that of obtained by SIMS. In this paper, we report the effect of H_2 annealing for DZ-IG formation and discuss the impurity depth profile.

1. INTRODUCTION

It is well known that the presence of ultratrace quantities of transition and alkaline metals on the surface of silicon substrate can have harmful effects on both device performance and process yields [1−3].

The study of a method with sufficient sensitivity to surface metal contamination at levels of 1 x 10^9 atoms/cm^2 has come to the development of TRXRF (total reflection X-ray fluorescenespectrometry (TRXRF) [4]. However, the SIMS (secondary ion mass spectrometry) and the RBS (Rutherford backscattering spectrometry) has been usually applied for the detection of trace metal impurities in silicon bulk not but on the surface. These methods have disadvantages such as insufficient sensitivity, difficulty for the full wafer analysis, and so on.

In this report, we have developed a new quantitative and sensitive analysis method, named SSA (step by step analysis), for the ultratrace impurities in silicon bulk, and discuss the relationship between oxygen concentration and metallic diffusion in silicon bulk.

2. EXPERIMENTAL

2.1. SSA Method

The outline of developed SSA is as follows. A silicon wafer sample is etched by a wet chemical technique in step by step of thin layer silicon wafer 0.01 to 10 μm thick can be dissolved by controlling the acidities of HF and HNO_3 in the etching solution. The thickness is calculated from Si concentration of the etching solution by ordinary spectrophotometry using the Molybdenum Blue method.

Silicon wafers are etched by 10ml of acid solutions containing appropriate

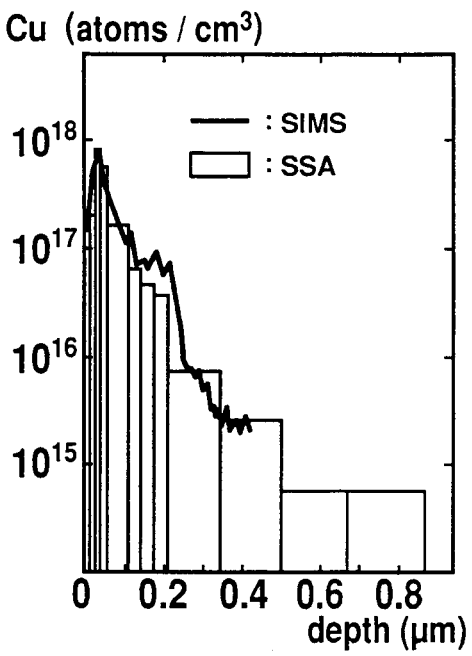

concentrations of HF and HNO_3. After the etching process, an aliquot of the solution is used for Si measurement. The rest was dried, dissolved in water and then subjected to elemental analysis by Graphite Furnace Atomic Absorption Spectrophotometry (Perkin Elmer Model 5100 ZL).

The accuracy of this method is proved by the analysis of a reference material. The depth profile is good agreement with that of obtained by SIMS as shown in *Figure 1.* The detection limits are found to be 2-3 orders of magnitude lower than that of SIMS [5].

Figure 1. Comparison of SSA and SIMS on Cu in-depth profiling.

2.2. Sample treatment

The sample wafers used in this experiment were prepared from 6-inches in diameter, (100) oriented, boron doped, 2-6 ohm-cm, grown by CZ and FZ methods. The wafers with the interstitial oxygen concentration about 4 x 10^{18} atoms/cm^3 were used for CZ (ASTM F121-80). Some sample wafers were annealed in H_2 atmosphere for 1 or 4 hours to form both a denuded zone (DZ) and an oxygen precipitated region. Then, all wafers were contaminated by spin coating of 1 x 10^{13} atoms/cm^2 Cu solution. After contaminated, wafers were annealed at 1000 °C for 60 min in N_2 atmosphere to promote diffusion. These wafers were cleaned by RCA cleans to remove initial contamination. After this cleaning, metallic impurities remaining on the surface of the wafers were confirmed to be less than 1 x 10^9 atoms/cm^2 by TRXRF. Then we measured the depth profiles of metallic impurity using SSA method.

3. RESULTS AND DISCUSSION

3.1. Oxygen depth profile

Figure 2 shows the oxygen depth profiles of each sample,

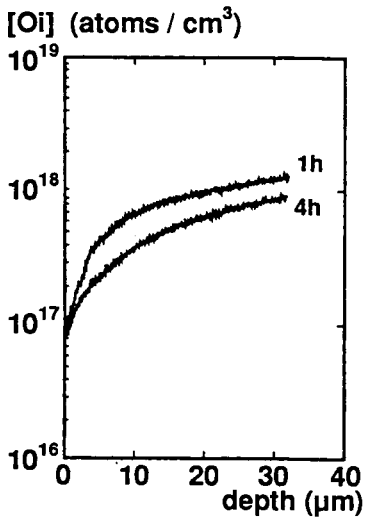

which were annealed for 1 or 4 hours in H_2 atmosphere at 1200 °C. After annealed, the oxygen concentration of the wafer annealed for 1 hour is 1 / 3 and for 4 hours is 1 / 50 that of the wafer with no annealed (4 x 10^{18} atoms / cm^3).

These results suggest that H_2 annealing is highly effective for outer oxygen diffusion, and to form DZ-IG zone.

Figure 2. Oxygen depth profiles of wafers annealed for 1 and 4 hours in H_2 atmosphere.

3.2. Metallic impurity depth profiles

To investigate the relationship between the oxygen concentration and metallic precipitates, the samples contaminated with Cu (1 x 10^{13} atoms / cm^2) were annealed at 1000 °C for 1 hour in N_2 atmosphere to promote metallic diffusion. *Figure 3* shows the Cu depth profiles of three wafer samples.

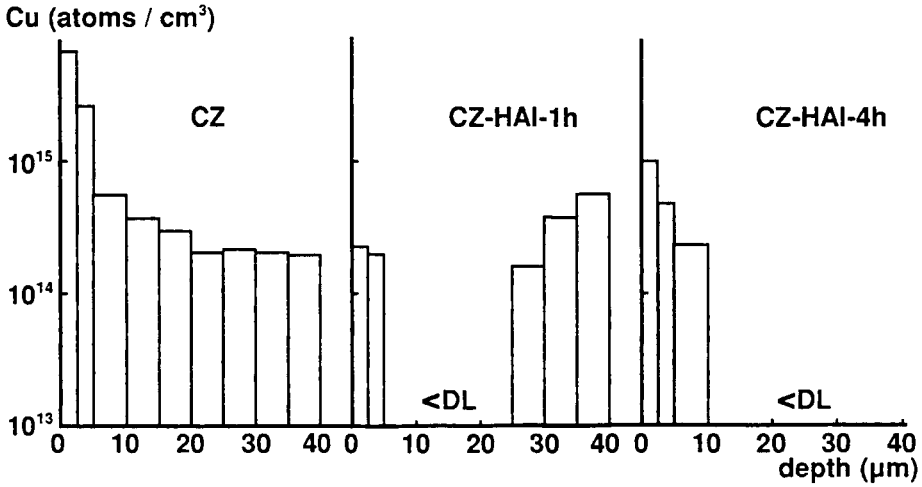

Figure 3. Cu depth profiles of CZ wafers for 0, 1, and 4 hours annealed in H_2 atmosphere. (Cu : intentional contaminated at 1 x 10^{13} atoms / cm^2 ; <DL : < 1 x 10^{12} atoms / cm^3 ; HAI: H_2 Annealed Insitrinstic)

Within a depth of 10 μm from the surface of the wafers, Cu impurity was observed in all wafers . This phenomenon is thought to be that metal atoms diffused into the bulk precipitate at the surface in supersaturation during cooling from high temperature.

However, within a depth of 10-25 μm, no impurity was observed in the wafers annealed in H2 atmosphere. Conversely, Cu impurity of 1 x 10^{14} atoms / cm^3 level existed in no annealed wafer. It is thought to be caused by the decrease of oxygen concentration in silicon bulk during H2 annealing process.

In addition, within a depth of 25-40 μm, Cu impurity increased again in the wafer annealed for 1 hour.

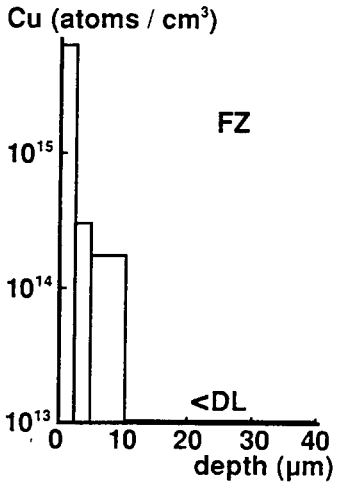

These tendency is considered as follows. The wafer annealed for 1 hour is less decomposition of oxygen than that of 4 hours. Therefore, the wafer could form the insitrinstic gettering site, and Cu impurity was gettered in silicon bulk. In contrast, the wafer annealed for 4 hours has less oxygen precipitates. As the result, metallic atoms precipitate at the surface of a silicon substrate.

To confirm the above idea, we investigated the depth profiles of FZ wafer. The result was shown in *Figure 4*. The depth profile was very similar to that of annealed for 4 hours.

From these results, it is shown that the H2 annealing process has highly effective to decrease oxygen concentration in silicon bulk.

Figure 4. Cu depth profile of FZ wafer.

4. CONCLUSION

A new sensitive and quantitative depth analysis method, named SSA has been developed. By using SSA, it was found that the effect of H2 annealing for DZ-IG formation. This method is thought to be effective in facilitating the measurement of impurity distribution in silicon bulk.

REFERENCES

1. H. J. Neuhaus, D. R. day, and S. D. Senturia, J. of Electr. Materials, 14 (1985) 379
2. E. Sacher, IEEE Trans. Electr. Insul., EI-18 (1983) 369
3. A. Ohsawa, K. Honda, and N. Toyokura, J. Electrochem. Soc., 131(1984)2964
4. Y. Matsushita and N. Tsuchiya, Proc. 6th Symp. Automated IC manufacturing (1991) 119
5. M. Takenaka, M. Tomita, A.Kubota, N.Tsuchiya, and H. Matsunaga, Bunseki Kagaku, 43 (1994) 173

CHARACTERISATION OF OXIDES AND THIN FILMS USING A NOVEL SCANNING KELVIN PROBE

Iain D. Baikie, Gerrit H. Bruggink and Sylvain Rival*

Department of Applied Physics, The Robert Gordon University, St. Andrew's Street, Aberdeen, United Kingdom, AB1 1HG.

1. INTRODUCTION

Using a new, high resolution, microscopic Scanning Kelvin Probe (SKP), work function topographies of metal, semiconductor and metal/semiconductor surfaces have been studied in both Ultra-High-Vacuum (UHV) and air environments.

The work function is a very sensitive indicator of surface and interface condition and has been previously utilised to examine preparation methods[1], surface roughness[2], adsorption processes[3], thin film monitoring[4] and residual surface contamination[2].

Extension of the basic method, via illumination of the semiconductor surface under the tip (Surface Photovoltage Spectroscopy), allows one to probe the local density of states (LDOS)[5]. Variation in LDOS can be used to monitor metal contamination, interface traps, bulk contamination[6], oxide imperfections, etc. This technique permits simultaneous monitoring of both surface state occupancy and barrier height throughout the adsorption process[5].

We have recently demonstrated the capability of the SKP in imaging the growth of very thin oxide films, charge retention on SiO_2 films and in monitoring the operation of pn junctions beneath the native oxide layer. Such topographies have major applications in quality control in all fields of semiconductor manufacturing including identification of wafer contamination both before and after cleaning, characterisation of oxides and interface traps.

The Kelvin method of measuring work function is non-contact and non-destructive, and can be applied to a wide range of environments ranging from UHV to air and at a wide range of temperatures.

2. BRIEF OUTLINE OF THE KELVIN METHOD

Consider fig. 1a which shows an electron energy diagram depicting two metals at separation 'd', having work function and fermi-level (Φ_1,ε_1) and (Φ_2,ε_2) respectively. Upon making electrical contact the fermi-levels equalise and the resulting flow of charge produces equal and opposite surface charges, see fig. 1b. The electrical potential arising V_c is related to the difference in work function, i.e., $-eV_c = \Phi_1 - \Phi_2$, where e is the electronic charge. Inclusion of an external,

---

*Department of Physics, CUST,Clermont-Ferrand, France. This work has been supported by the Science and Engineering Research Council, the Paul Instrument Fund and the Royal Society.

variable emf, V_b, see fig. 1c, permits nulling of the surface charges.

Differences in work function can be followed by making the two surfaces into a capacitor arrangement, vibrating one plate with respect to the other and determining the minimum output signal as a function of V_b.The Kelvin method is particularly suited to surface studies due to its high surface sensitivity (≤0.1 meV) and the fact that it operates in a null field mode[7].

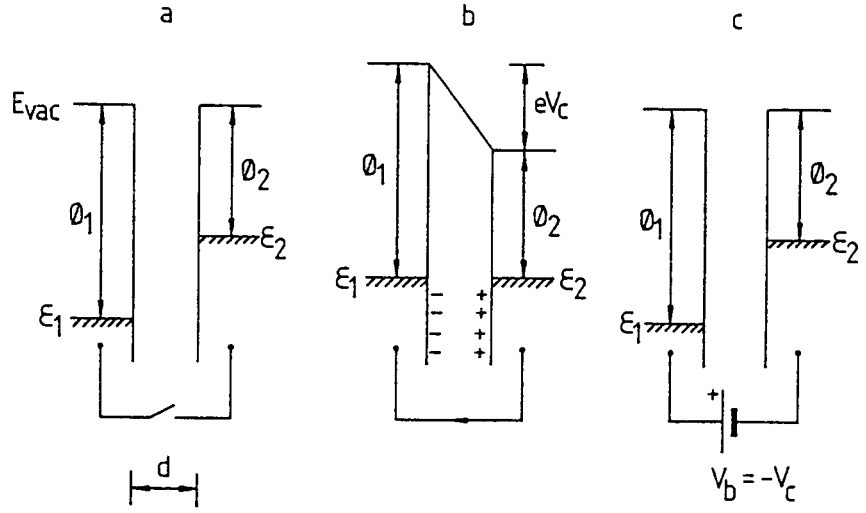

Figure. 1. Electron energy diagram illustrating Kelvin probe mode of operation.

3. THE SCANNING KELVIN PROBE (SKP)

The SKP is based upon a UHV compatible voice-coil driving element mounted using two stainless-steel diaphragm springs[8]. The suspension system offers a useable frequency range of 30 - 3000 Hz coupled to negligible off-axis displacement. Application of a dc-offset, via a 16-bit DAC, permits high accuracy (≤30 nm) probe positioning. High speed scanning is accomplished by a 2-axis piezo-scanner located above a 3-axis stepper micropositioner, this combination permits high resolution work function topographies to be performed at locations on the sample several cm apart. Signal detection is performed via a I/V convertor situated close to the tip (an etched Pt wire), an arrangement that has been shown to minimise the effects of parasitic capacity[9].

4 . APPLICATIONS TO SEMICONDUCTOR SURFACES

4.1 Initial Oxidation of Si

Molecular oxidation of Si(111) 7x7 has been performed at 300, 200 and 100 K under UHV conditions, see fig. 2. In all cases the initial work function change ($\Delta\Phi$) is linear with oxygen exposure indicating a constant sticking coefficient in this region, also indicated is the trend towards higher initial sticking coefficients

at lower temperatures. The increase in $\Delta\Phi$, due to the formation of an elementary dipole layer (negative end outwards), is subsequently followed by permeation of oxygen through the Si surface which tends to reduce the effective dipole[3].

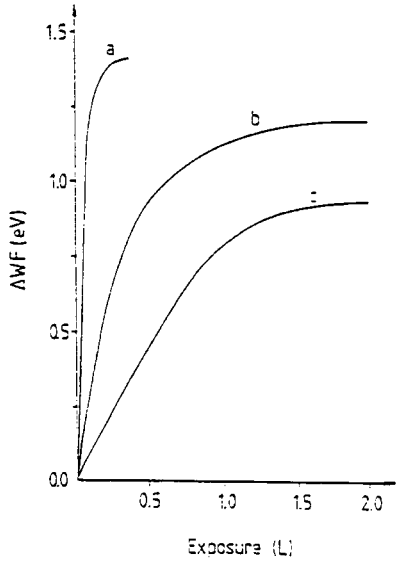

Figure. 2. The initial oxidation phase of Si(111): curves a, b and c refer to 100, 200 and 300 K respectively.

4.2 Surface Charge Imaging (SCI) on Si

Fig. 3. shows a SCI scan of a Si(100) sample terminated by a 100 nm thick SiO_2 layer grown using a new low temperature plasma enhanced evaporation process (sample provided by Baltzers, AG). In this scan the surface has been deliberately charged using the probe tip. The peak corresponds to negative charge, the troughs to positive charge. Such charges have a lifetime of several months and may affect the passage of charge carriers in the underlying device.

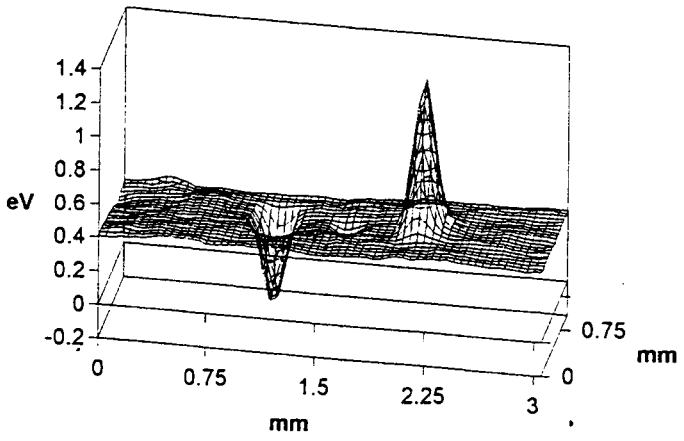

Figure. 3. SCI of a section of Si wafer: tip has been used to deposit charge.

4.3 Non-contact operation of PN Junction

The SKP has been used to scan the electronic structure beneath the native oxide layer of a pn junction, see fig. 4, in order to demonstrate its potential in imaging both operational and defective electronic devices. Here a base/emitter junction is shown under reverse biased conditions, before and after the maximum reverse bias has been exceeded. The changes in surface potential are clearly visible.

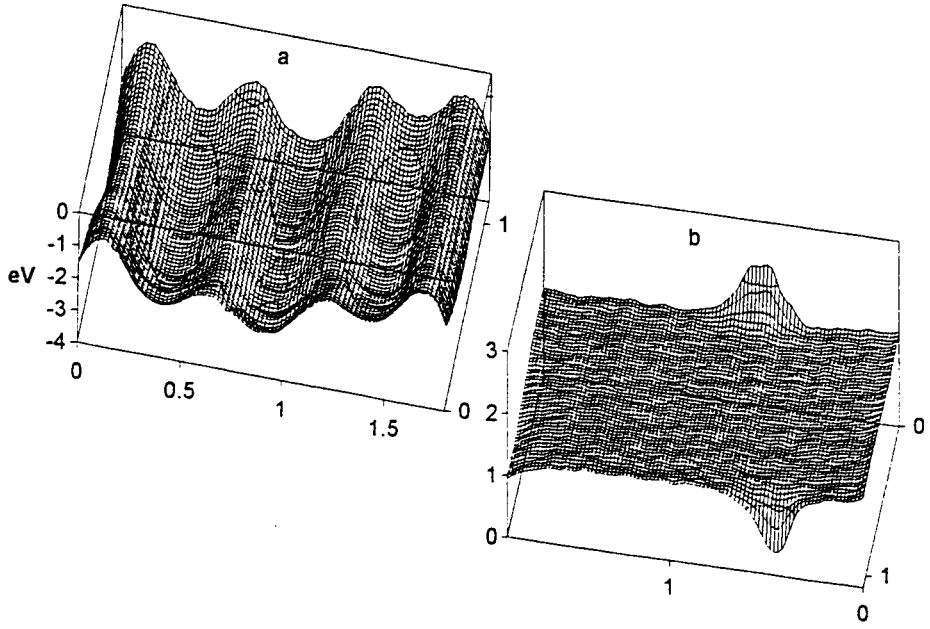

Figure 4. Work function topographies of a semiconductor pn junction, a) reverse biased: the peaks represent n-type material which is held some 1500 meV above the p-type regions (valleys). b) repeat scan, however the maximum reverse bias has been exceeded, no structure is visible. The trough in the foreground and the peak in the background are the edges of the contacts to the "n" and "p" type regions respectively. Scan dimensions are in mm.

REFERENCES

1. I.D. Baikie and G. Bruggink, Mat. Res. Soc. Proc., 306 (1993) 311.
2. I.D. Baikie, E. Venderbosch and B. Hall, Mat. Res. Soc. Proc., 261 (1992) 149.
3. I.D. Baikie, Mat. Res. Soc. Proc., 204 (1991) 363.
4. I.D. Baikie and G. Bruggink, Mat Res. Soc. Proc., 309 (1993) 35.
5. I. D. Baikie, Mat. Res. Soc. Proc., 259 (1992) 149.
6. J. Lagowski, P. Edelman and M. Dexter, Mat. Res. Soc. Proc., 261 (1992) 223.
7. I.D. Baikie, S. Mackenzie, P.J.Z. Estrup and J.A. Meyer, Rev. Sci. Instrum., 62 (1991) 1326.
8. I.D. Baikie, K.O. van der Werf, J. Broeze and A. van Silfhout, Rev. Sci. Instrum., 60 (1989) 930.
9. I.D. Baikie, E. Venderbosch, J.A. Meyer and P.J.Z. Estrup, Rev. Sci. Instrum., 62 (1991) 725.

REOXIDATION KINETICS OF HF-ETCHED Si(100), Si(110) AND Si(111) SURFACES IN AIR.

J. T. Beechinor, P.V. Kelly, G.M. O'Connor and G.M. Crean

National Microelectronics Research Centre, Prospect Row, Cork, Ireland.

ABSTRACT

The reoxidation kinetics of HF-etched silicon (100), (110) and (111) surfaces have been investigated using Spectroscopic Ellipsometry (SE) and Reflectance Anisotropy (RA) spectroscopy. A distinct difference in the SE and RA response was observed. The dependence of the surface layer thickness on etch conditions was studied. The topography of the post-etched silicon surfaces was studied using Variable Angle SE (VASE) and Atomic Force Microscopy (AFM).

1. INTRODUCTION

Optimisation of wet chemistry based silicon surface preparation prior to fabrication process steps, such as film growth or oxidation remains one of the most critical challenges for deep submicron metal oxide semiconductor (MOS) ULSI technology. Particular attention is focused on the resultant Si surface layer chemistry and topography. Characterisation of the native and chemical oxides, grown after different wet cleaning cycles, is an increasingly important consideration as these SiO_x ($x<2$) layers significantly impact the subsequent adsorption of metallic contaminants and electrical performance of MOS devices [1].

Recent work [2] comparing the kinetics of reoxidation of HydroFluoric acid (HF) etched Si(110) wafers measured by Spectroscopic Ellipsometry (SE) and Reflectance Anisotropy (RA) [3] showed that the kinetics of the post-etch RA and SE responses differed. This study investigates in detail the reoxidation kinetics measured by SE and RA for different HF etch treatments of principal Si surfaces.

2 EXPERIMENTAL

Single crystal CZ grown p-type Si(100), Si(110) and Si(111) wafers, with resistivities in the range 2-12 Ω.cm, were etched using 10:1 HF, 7:1 and 4:1 NH_4F-buffered HF (BHF), with and without pre-etch Caros (H_2O:H_2O_2:H_2SO_4 1:1:3) cleans. Cleaning and etching were performed in immersion baths.

Ellipsometric spectra were measured in reflectance in the photon energy range 2.0 - 4.5 eV at an interval of 0.02 eV using a phase modulated spectroscopic ellipsometer at an angle of incidence of 75°. A spot size of 2×5 mm was employed throughout. Variable angle SE was performed at angles of incidence of 70°, 75° and 80° on Si(100), Si(110) and Si(111) wafers after a 30 s 4:1 BHF etch. Atomic force micrographs over a 50 μm^2 surface area of these samples were recorded using a Topometrix 200 TMX atomic force microscope (AFM).

RA spectra were measured from Si(110) samples in the photon energy range 2.8 eV to 4.5 eV at an interval of 0.02 eV using a phase modulated RA spectrometer with a 12 mm diameter spot at normal incidence.

3 RESULTS AND DISCUSSION

The reoxidation kinetics of HF etched silicon surfaces in air were measured using a Levenberg-Marquardt nonlinear least-squares fit of an optically modelled

pseudo-dielectric function (ϵ) to the experimental SE data [2]. The surface layer was modelled as a thin layer of SiO_2. Reoxidation kinetics representative of the etch treatments and substrate orientations are shown in Figures 1-4. The corresponding reoxidation rates calculated by a linear regression fit to these data are detailed in Table 1.

Table 1. Average reoxidation rates of HF-etched Si over the first hour after etch

Substrate	Etch	Duration (s)	Reoxidation Rate (Å/min)
Si(100)	Caros/10:1 HF	30	0.022 ± 0.004
Si(100)	10:1 HF	30	0.024 ± 0.007
Si(100)	10:1 HF	60	0.027 ± 0.007
Si(100)	10:1 HF	90	0.032 ± 0.004
Si(110)	10:1 HF	30	0.028 ± 0.011
Si(111)	10:1 HF	60	0.042 ± 0.015
Si(111)	4:1 BHF	60	0.044 ± 0.015
Si(111)	7:1 BHF	60	0.035 ± 0.015
Si(111)	10:1 HF	30	0.065 ± 0.030
Si(111)	4:1 BHF	30	0.059 ± 0.019
Si(111)	7:1 BHF	30	0.059 ± 0.015
Si(110)	4:1 BHF	30	0.032 ± 0.010
Si(110)	4:1 BHF	60	0.028 ± 0.010
Si(110)	4:1 BHF	90	0.036 ± 0.010

A smaller post-etch effective oxide thickness was consistently extracted from SE spectra after 10:1 HF etching of Si(111) than on either BHF etched Si(111), Si(100) or Si(110) etched by any of the etchant solutions investigated. Furthermore, the *initial* post-etch effective oxide thickness on Si(111) was smaller for all etches performed for 30 s compared to the same etches performed for 60 s. The post-etch effective oxide thickness after 4:1 BHF etching of Si(110) was dependent on etch duration, as shown in Figure 3. The initial post-etch effective oxide thicknesses on Si(100) for the different 10:1 HF etch times differed by less than 1Å, as shown in Figure 1.

Performance of a Caros clean prior to the 30 s 10:1 HF etch lowered the effective oxide thickness on Si(100). The slowest reoxidation rate was measured on this surface. Marginally faster reoxidation rates were measured for Si(100) after longer duration 10:1 HF etches without a pre-etch Caros clean, and for Si(110) after different duration 4:1 BHF etches and after a 30 s 10:1 HF etch. These rates are all comparable to the reoxidation rates in air of 0.02 - 0.03 Å/min measured by XPS for reoxidation of wet or vapour HF-etched Si(100), averaged over the first hour after etching [4]. 4:1 BHF etching on both Si(110) and Si(111) resulted in an initially faster reoxidation rate than the average rate over the first hour. In the case of Si(111), significantly larger reoxidation rates of 0.07 Å/min were measured for 10:1 HF, 4:1 BHF and 7:1 BHF etches of 30 s duration compared to 0.04 Å/min for the same etches of 60 s duration. However, the shorter duration etches resulted in lower measurements for the initial post-etch effective oxide thickness. Figure 4 shows the comparison of reoxidation rates measured after 30 s 10:1 HF etching of Si(100), Si(110) and Si(111). A larger scatter in the effective oxide thickness data is evident for Si(111) compared to Si(110) and Si(100). A HF etch duration of 15 s is known to be sufficient to strip the native oxide from silicon. These results suggest that modification of the Si(111) surface occurs on longer exposure to HF etch solutions, which leads to a significantly modified surface and a slower

subsequent reoxidation rate as measured by SE. It is not possible using the SE model to distinguish the effects of surface roughness (modelled by void), film thickness,and surface film chemical termination due to parameter correlation issues present in the characterisation of ultrathin (<10 Å) films.

Figure 5 shows an AFM micrograph of a Si(111) sample one hour after a 30 s 4:1 BHF etch. Significant microroughness is generally evident over the surface, in addition to localised spikes. The average deviation from the profile mean, R_a, for similarly treated Si(100), Si(110) and Si(111) samples is shown in Table 2. VASE measurements were performed on Si(100), Si(110) and Si(111) samples one hour after a 30 s 4:1 buffered HF etch. A model of the surface layer as a homogeneous layer incorporating void in an effective medium approximation to represent roughness, using multiple angle fitting, was employed to determine the surface layer thickness data shown in table 2. This analysis is consistent with topographical data extracted from AFM micrographs. This surface roughness is larger than that measured for a Si(100) sample after RCA cleaning [5].

Table 2. Topographical data extracted from VASE data and AFM micrographs, for 4:1 BHF etched silicon wafers.

Silicon	(100)	(110)	(111)
Surface Layer Thickness (Å) (VASE)	20.4	44.0	18.5
Deviation from profile mean (R_a) (Å) (AFM)	22.2	51.0	22.2

Figure 6 shows RA (defined as {R(110)-R(001)}/R) spectra, measured before and after 10:1 HF etch treatments of Si(110). A sharp negative feature is observed at 3.2 eV in the RA spectra recorded from post-etched samples with no appreciable dependence on HF etch parameters [2,3]. This feature appears to arise from a bulk rather than a surface contribution [3]. The RA spectrum remained stable for over an hour after etching, and then recovered over the next four hours to the RA spectrum characteristic of the native oxidised surface prior to etching, in which the 3.2 eV bulk feature appears significant but small. In proposed models [3] the surface RA signal for Si(110) is of opposite sign to that of the bulk contribution. Differentiation of the RA spectra in Figure 6 showed that the point of inflection on the low-energy side of the E1 RA peak shifted 30 meV to the red between the newly-HF-etched and oxidised Si(110), while the E1 peak shifts negligibly. This is consistent with the broadening of the surface RA contribution associated with the E1 peak to partially cancel the bulk peak at 3.2 eV on reoxidation. SE reoxidation rates reveal an increase of approximately one monolayer in the effective oxide thickness before significant changes in the RA spectrum are noted. XPS studies of the reoxidation of HF etched Si in air also show a faster reoxidation kinetic appearing on a scale of hours after etching [6].

4. CONCLUSIONS

The reoxidation kinetics of Si(100) and Si(110) after different HF etch treatments measured using SE are generally similar as a function of etch duration and HF solution and agree with reoxidation kinetics measured by XPS. The SE-measured reoxidation kinetics of Si(111) are found to depend on etch duration, and are faster than expected. VASE and AFM reveal the presence of significant roughness in the surface topography of the principal Si surfaces after similar HF etches. A further study of the post-etch reoxidation kinetics and surface topography of HF-etched Si(111) as a function of etch time, using AFM and VASE, is under way. The RA spectrum of post-etched Si(110) only exhibits significant changes at

times longer than the typical time to monolayer reoxidation indicated by SE. The physical mechanism for this RA response is not understood at this time.

REFERENCES

1. S. Verhaverbeke, J. Alay, P. Mertens, M. Meuris, M. Heyns, W. Vanderhorst, M. Murrell and C. Sofield, Mat. Res. Soc. Symp. Proc. **259** (1992) 391
2. J.T. Beechinor, P.V. Kelly and G.M. Crean, Mat. Res. Soc. Symp. Proc. **324** (1994) 59
3. D.E. Aspnes, J. Vac. Sci. Technol. **B 3** (1985) 1498
4. P.A.M. van der Heide, H.W.L.Lindelauf and H.J. Ronde, Electrochem. Soc. Proc. **90-9** (1989) 321
5. R.K. Sampson, K.A. Conrad, H.Z. Mazood and E.A. Irene, J. Electrochem Soc., **141** (1994) 737
6. M. Grundner, P.O. Hahn, I. Lampert, A. Schnegg and H. Jacob, Electrochemical Soc. Proc. **90-9** (1989) 215

ACKNOWLEDGMENTS

This work was supported by the Commission of the European Communities DGXII under ESPRIT Basic Research Action no. 6878 EASI

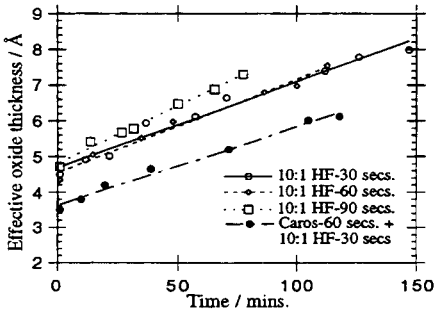

Figure 1. Reoxidation kinetics of 10:1 HF etched Si(100)

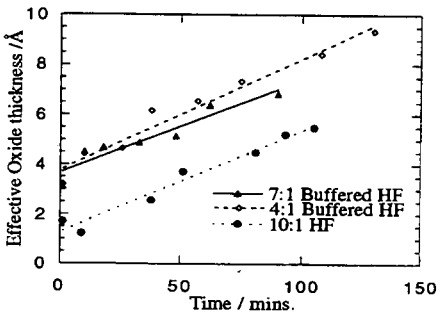

Figure 2. Reoxidation kinetics of 10:1 HF, 7:1 and 4:1 BHF etched Si(111)

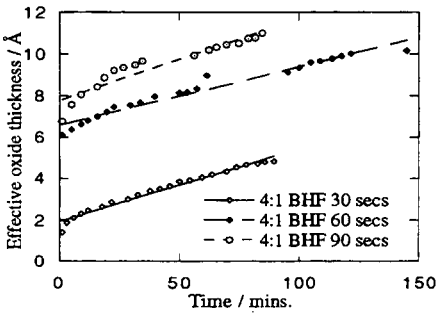

Figure 3. Reoxidation kinetics of 4:1 BHF etched Si(110)

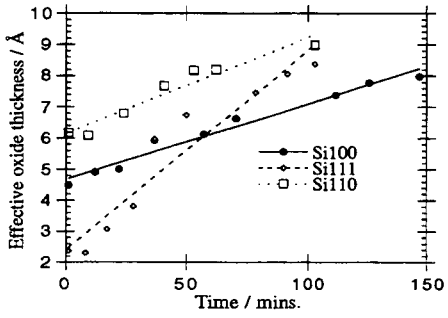

Figure 4. 30s 10:1 HF etched Si(100), Si(110) and Si(111): reoxidation kinetics

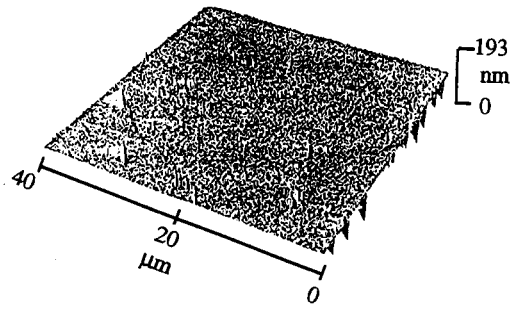

Figure 5. AFM micrograph of 4:1 buffered HF etched Si(111)

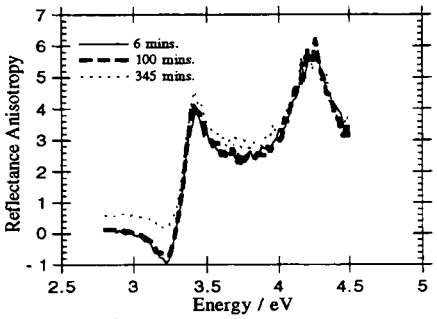

Figure 6. RA spectra of Si(110) after 10:1 HF etching

A COMPARATIVE STUDY OF MEASUREMENTS OF ROUGHNESS OF SILICON AND SiO_2 SURFACES AND INTERFACES USING SCANNING PROBE MICROSCOPY, NEUTRON AND X-RAY REFLECTIVITY.

A. Crossley*, C. J. Sofield, J. Goff[1], A. C. I. Lake[1], M. T. Hutchings, A. Menelle[2] and M. P. Murrell[3].

AEA Technology, 477 Harwell Laboratory, Oxon OX11 ORA, UK

1 University of Oxford, Department of Physics, Clarendon Laboratory. Oxford OX1 3PU, UK.
2 Laboratoire Leon Brillouin, CE Saclay, 91191 Gif sur Yvette, France.
3 East Coast Scientific, Cambridge, UK.

1. INTRODUCTION

As MOS devices scale down and thinner insulating oxide layers are used, the nature of the interfacial region between crystalline silicon and amorphous silicon dioxide acquires greater technological significance. Since rough silicon surfaces have been shown to degrade CMOS device yield and reliability[1,2], there is a requirement to minimise and control, and therefore measure, interfacial roughness on an atomic scale. Physical characteristics of the oxide closest to the silicon clearly need to be identified and understood if high quality, thin (<5nm) oxides are to be produced. Experimental and theoretical studies have not provided a precise picture of this region [3], although it differs from the bulk oxide.

Scanning probe microscopies (SPM), particularly the scanning tunnelling microscope (STM) and the atomic force microscope (AFM) have been used effectively [4] to measure silicon surface roughness. These techniques offer the required resolution but cannot be used to probe buried interfaces. In order to study Si / SiO_2 interfacial roughness after oxidation, the oxide must be removed by some means which does not damage the silicon substrate. This is usually achieved by dipping the wafer in hydrofluoric acid until the wafer is hydrophobic. It is important to determine how much this process perturbs the system under observation. Epitaxially grown silicon has been used in the present study to illustrate the effect of HF removal of oxide. Because of the characteristic growth pattern of this type of material, changes to the surface are easily visualised with SPM.

The neutron reflectivity technique is capable of probing the SiO_2 thickness and density, and the Si / SiO_2 interfacial roughness. However it is limited to oxides greater than 20 nm. This limit is set primarily by the source intensity. X-ray reflectivity gives complementary information on the electron density profile normal to the surface. The refractive index n is given by $n = 1 - (\lambda^2/2\pi)A$. For neutrons $A = b\rho_n$ where b is the mean scattering length and ρ_n is the number density, and for X-rays $A = r_e \rho_e$ where r_e is the classical electron radius and ρ_e is the electron density. Reflectivity as a function of wave vector transfer Q perpendicular to the surface is determined by the refractive index profile normal to the surface. This may be related to the layer thickness, density and roughness at the interfaces. The data is analysed using the recently developed Bayesian spectral analysis procedure of Sivia [5] which assumes the surface region can be split into a maximum of 20 slabs of varying thickness, density and roughness. Details of this will be presented elsewhere [6].

2. EXPERIMENTAL

Epitaxially grown silicon on a Si (100) substrate wafers were examined with an AFM before and after HF dipping, to monitor the effect of "native" oxide removal.

Si (100) (1.5-2.5 Ωcm) and Si (111) (6-9 Ωcm) 3" Cz wafers (supplied by Wacker-Chemitronic GmbH) were used for the reflectivity experiments. Prior to oxidation the native oxide was removed by HF etching. To obtain the smoothest silicon surfaces, 7:1 buffered HF (BHF) was used for Si (111) and 10:1 dilute HF (DHF) for Si (100) [4]. The silicon dioxide was grown in oxygen at 1173 K for 70 minutes. AFM roughness measurements were subsequently performed on these wafers following removal of the oxide with DHF. Wafers were prepared in a class 100 clean room. Contact mode AFM images were obtained using an ECS AFM (East Coast Scientific, Cambridge, UK) operating in a liquid cell containing 2-butoxy-ethanol.

The neutron reflectivity measurements were performed using the white beam time-of-flight reflectometer, EROS, on the Orphee reactor, Saclay. X-ray measurements were carried out using a triple-axis diffractometer at the Clarendon Laboratory, Oxford. Experimental details are reported elsewhere [6].

3. RESULTS AND DISCUSSION

AFM images of epitaxial silicon are shown in Figure 1. The effect of dipping the wafer in DHF and BHF to remove the native oxide is clearly seen. In both cases the fine structure observed on the "as received" wafer has degraded. BHF changes the surface more than DHF. The RMS roughness measurements given in Figure 1 indicate slight smoothing after DHF treatment and roughening following the BHF dip. This has also been observed on Si (100) Cz wafers [4] and has been attributed to preferential etching of Si (111) planes by higher pH HF solutions [7]. AFM RMS interface roughness measurements from the wafers used in the reflectivity experiments are 1.26±0.2 Å for Si (111) and 1.5 ± 0.1 Å for Si (100) taken from a 6 μm x 6 μm scan.

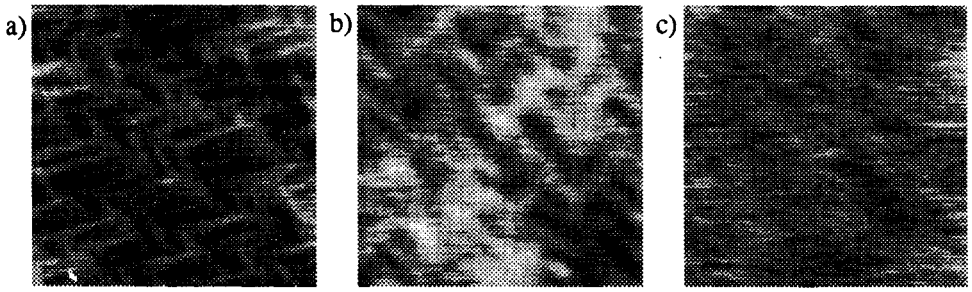

Figure 1. 1 μm x 1 μm AFM image from Epi-Si (100): a) "as received", RMS (Å) 1.14 b) after DHF dip, RMS (Å) 1.0 and c) after BHF dip, RMS (Å) 1.51.

Reflectivity profiles are shown in Figure 2. Because of the high contrast between the silicon and the silicon dioxide, a good fit to the neutron data is obtained using a single slab model. This allowed the thickness, density and interfacial roughness of the silicon dioxide layer to vary. The film density is found to be 2.17 g cm^{-3}, consistent with amorphous SiO_2 [8]. The overall layer thicknesses are estimated to be 356 Å and 205 Å for Si (111) and Si (100) respectively, compared with 357 Å and 214 Å obtained by ellipsometry. Contrast in electron density between silicon and silicon dioxide is low so it is not possible to obtain a single slab fit to the x-ray data. However because of this low contrast the x-rays are far more sensitive to the interface region.

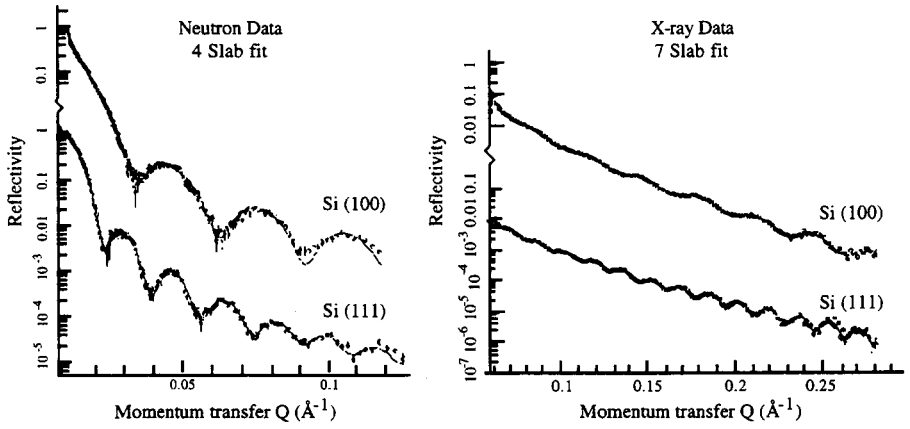

Figure 2. Reflectivity profiles for Si (100) and Si (111) with 20-30 nm oxide.

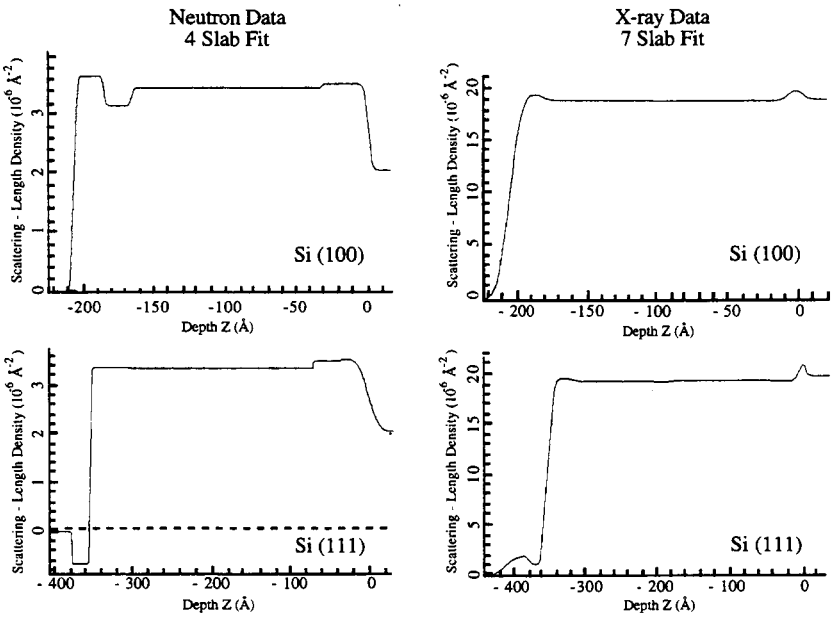

Figure 3. Density profiles for Si (100) and Si (111) with 20-30 nm oxide.

Density profiles were obtained using a multi-slab Bayesian approach, utilising parameters determined from the neutron data. These are shown in Figure 3. The Si (111) sample gives a negative neutron scattering length density at the outer surface, indicating possible hydrogenation at the oxide surface [6]. Both samples clearly show increased scattering length density at the interface. However it is difficult to obtain the actual density and width of the interfacial region since the profile changes depending on the number of slabs the model used to fit the data. Because of the presence of this interfacial layer, it is not possible to determine accurately the interfacial roughness but the results are consistent with the AFM data. The electron

density profile for the Si (111) also has a surface layer with low electron density, in agreement with the neutron data. More significantly, both samples show 5 - 10 Å interfacial layers with 10 - 20% increased electron density. The profiles obtained are independent of the number of slabs used in the model, giving confidence in the profiles shown and hence confirmation of the existence of a densified region at the Si / SiO_2 interface. This data, combined with previous XPS observations [9], suggests that this region contains more silicon than the rest of the oxide layer, ie. is a "reactive layer", rather than consisting of a densified SiO_2 network.

4. CONCLUSIONS

Scanning probe microscopy gives a visual image of the surface with accurate roughness measurements with sub-angstrom resolution. However removal of oxide chemically to expose a buried interface changes the interface under observation and care must be taken to minimise this perturbation. DHF causes less damage to the substrate than BHF.

Neutron reflectivity gives accurate information on the overall composition of the oxide surface layer and interfacial roughness. Higher intensity sources are required to obtain more accurate roughness measurements and examine thinner layers. X-ray reflectivity is most sensitive to the region between the silicon and the amorphous silicon dioxide.

Using a combination of the above techniques we have clearly identified the presence of a densified layer between the silicon and the amorphous silicon dioxide for both Si (111) and Si (100). The presence of this layer may explain observed deviations from the Deal - Grove model of oxidation [3] and is of enormous significance when attempting to grow very thin oxide films.

ACKNOWLEDGEMENTS

This work was funded by AEA Technology Corporate Research Programme and the CEC under the ESPRIT Basis Research Action 6108 (ASSIST). We would like to thank Dr. Paul Mertens from IMEC for providing us with the epitaxial silicon wafers. We would also like to thank Dr. A. M. Stoneham, AEA Technology, for helpful discussion.

REFERENCES

1. M. Heynes, M. Meuris, S. Verhaverbeke, P.W. Mertens, A. Philiposian, D. Graf and A.Schnegg, Ext. Abstracts of Int. Conf. on Solid State Devices and Materials, Tsukuba (1992) 187.
2. T. Ohmi, K. Kofani, A. Teramoto and M. Miyashita, IEEE Electron Device Lett, 12(12), (1991) 652.
3. C. J. Sofield and A. M. Stoneham, submitted to Semicond. Sci. and Technol.
4. A. Crossley, C. J. Sofield, J. Goff, A. C. I. Lake, M. T. Hutchings, and A. Menelle, in press : Journal of Non-Crystalline Solids : Proceedings of EMRS 1994 Spring Meeting, Strasbourg, France.
5. D. S. Sivia, W. A. Hamilton and G. S. Smith, Physica B 173, (1991) 121.
6. J. Goff, A. C. I. Lake, J. R. P. Webster, C. J. Sofield, M. T. Hutchings, A. Crossley, A. Menelle, to be submitted to J. Physics Condensed Matter.
7. S. Verhaverbeke, H. Bender, M. Meuris, P. W. Mertens, H. F. Schmidt and M. M. Heyns, Proc. Spring Meeting MRS, San Fransisco, CA, USA, 1993.
8. S. M. Sze, Semiconductor Devices, Physics and Technology, Wiley, NY, 1985.
9. J. R. Engstrom, O. J. Bone and T. Engel, Surf. Sci., 268, (1992) 2382.

IN SITU MONITORING OF THE EFFECT OF OXYGEN AND HYDROGEN PLASMAS ON THE PASSIVATION LEVEL OF SILICON SURFACES

H. Li, E. A. Ogryzlo, Department of Chemistry, University of British Columbia, Vancouver, B.C. Canada V6T 1Z1, **and J. G. Cook**, Institute for Microstructural Sciences, National Research Council of Canada, Ottawa, Ontario, Canada K1A 0R6.

ABSTRACT

We have developed a contactless method for monitoring carrier loss on surface states of silicon as it is being exposed to various reactive species from remote or in situ RF or microwave discharges. In this technique a remote RF probe is coupled to the silicon substrate, and the phase shift that results from the changing steady state carrier concentration in the silicon is used to monitor the carrier loss rate at its surface.

1. INTRODUCTION

The objective of our experiments has been the development of a remote, *in situ*, real time, sensor that would make it possible to detect changes in the surface carrier recombination rate on a silicon wafer while the surface is being processed. In earlier work[1], we described the technique in some detail, and presented some of the preliminary results obtained during the exposure of thermally oxidized wafer to a plasma. In the present work we briefly describe the method, and present results for the exposure of an HF-washed silicon wafer to various reactive species.

2. EXPERIMENTAL

The fast flow system used is shown in Fig 1. Upstream, a micro-

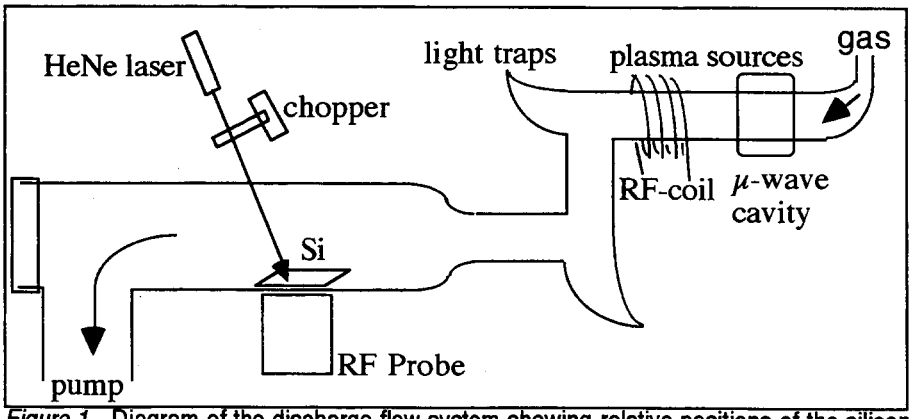

Figure 1. Diagram of the discharge-flow system showing relative positions of the silicon sample, RF probe, laser, chopper, and discharge sources.

wave source was used to create a confined discharge, exposing the downstream sample to either oxygen or hydrogen atoms but very few ions or electrons. Alternatively, a 50 W RF source was used to produce an in situ plasma, i.e. to expose the silicon sample to all the plasma products including atoms, ions, electrons, and radiation. In the following, O-plasma and H-plasma will be used to describe *in situ* plasmas in 5% O_2 in He and 5% H_2 in He mixtures respectively. In all cases the total gas pressure was kept at 0.3 Torr.

The RF probe, consisting of a coaxial resonator, was placed against the quartz vessel opposite the sample. The associated RF circuitry was described previousely[1]. The samples were <100> p-doped 12 Ω-cm Si, initially coated with 170Å of thermal oxide. The oxide on one side was removed and replaced with an H-passivated surface using 10%HF solution. A chopped 633 nm laser beam was used to excite the photocarriers. The probe detects the change in sheet conductivity of the sample which is determined by the silicon-surface recombination-rate.

3. RESULTS AND DISCUSSION

The steady state carrier concentration (which we will also refer to as the relative passivation level for that wafer) was found to be highest when a wafer was covered with a "thermal oxide". This passivation level was reduced to 25% when the "thermal oxide" is removed from a wafer surface with HF. All the silicon samples were cleaned with a 10% solution of HF before they were introduced into the discharge-flow system.

3.1 Exposure of an HF washed surface to to O-atoms or H-atoms

The exposure of an HF-washed silicon surface to O-atoms from a remote microwave O_2/He plasma instantly drops the passivation level by more than two orders of magnitude, from which there is no recovery when the exposure is continued for at least 40 minutes. The simplest explanation of this reduction in passivation level is that O-atoms can strip hydrogen atoms off the HF passivated surface, producing surface states that catalyze the carrier recombination. Since there is no recovery of the passivation level as the surface is oxidized, we conclude that oxides formed with a remote microwave discharge do not provide well passivated interfaces. This is consistent with earlier evidence[2]

A similar drop in passivation level occurred when a freshly HF-washed surface of Si was exposed to the H-atoms from a remote microwave discharge. Continued exposure to H-atoms did not lead to any recovery of the passivation level. The explanation of this observation may be that offered by Stathis and Cartier [3], i.e. in the presence of H-atoms the steady state density of "dangling bonds" on Si increases because it is determined by the reactions:

$$\text{Si-H} + \text{H} \rightarrow \text{Si} + \text{H}_2 \qquad (1)$$

$$\text{Si} + \text{H} \rightarrow \text{Si-H} \qquad (2)$$

3.2 Exposure of an HF washed surface to an O-plasma

As illustrated in Fig. 2, after the initial drop in the passivation level when the HF-washed surface is exposed to an O-plasma, continued exposure cause the passivation level to rise over a period of 15 minutes until it assumes a value which is very close to that of the freshly HF-washed sample.

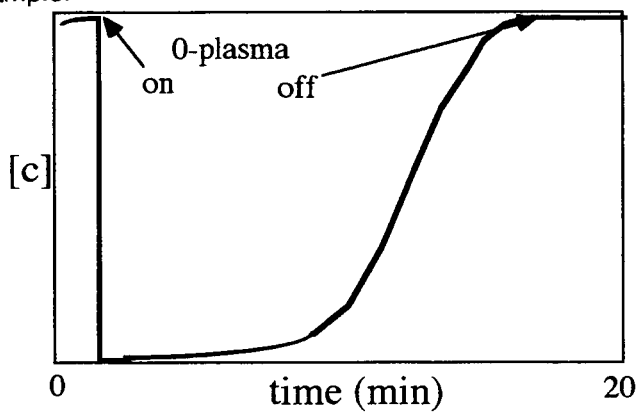

Figure 2. Effect of an O-plasma exposure on the steady-state carrier-concentration [c] of an HF-washed silicon sample.

3.3 Effect of an H-plasma on the O-plasma passivated surface

Once the Si surface has been treated with an O-plasma to maximize its passivation level, an H-plasma rapidly de-passivates the surface to less than 1% of its original value. Subsequently the original passivation level can be recovered by re-exposing the surface to an O-plasma for under a minute. This is illustrated in Fig. 3.

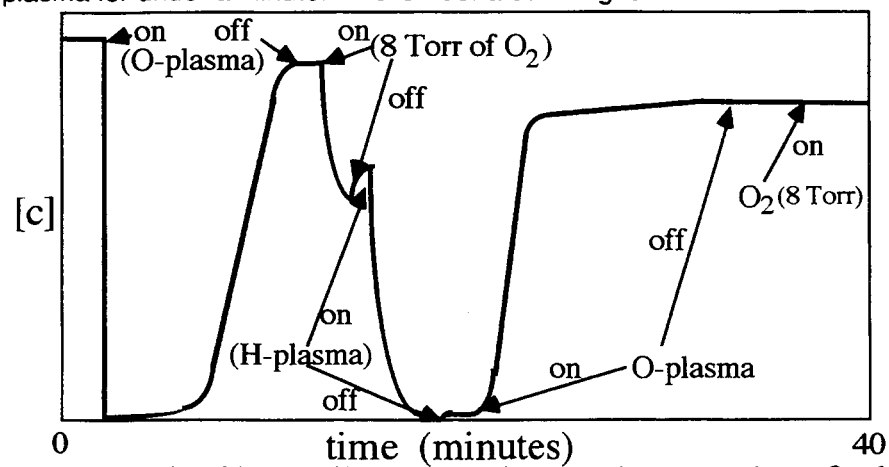

Figure 3 Illustration of the insensitivity of the steady state carrier concentrations to O_2 after long plasma exposures, and the effect of an H-plasma exposure on the re-passivation rate.

Also illustrated in this series of exposures is the fact that a quickly O-plasma passivated surface is easily depassivated by exposure to a few Torr of O_2, but after an H-plasma + O-plasma exposure the surface is stable in the presence of O_2.

3.4 XPS measurements of oxide thicknesses during plasma processing.

To establish the extent to which a surface oxide coating was present at the different passivation levels discussed above, the exposures were stopped at the points indicated on Fig. 4, and the thicknesses of the SiO_2 layers were measured with a Perkin Elmer XPS spectrometer. The remote microwave discharge (O-atoms) produced only 5Å of oxide in 40 minutes, whereas the *in situ* RF-plasma produced 42Å in 50 minutes. Furthermore, the H-plasma did not remove any of that oxide layer.

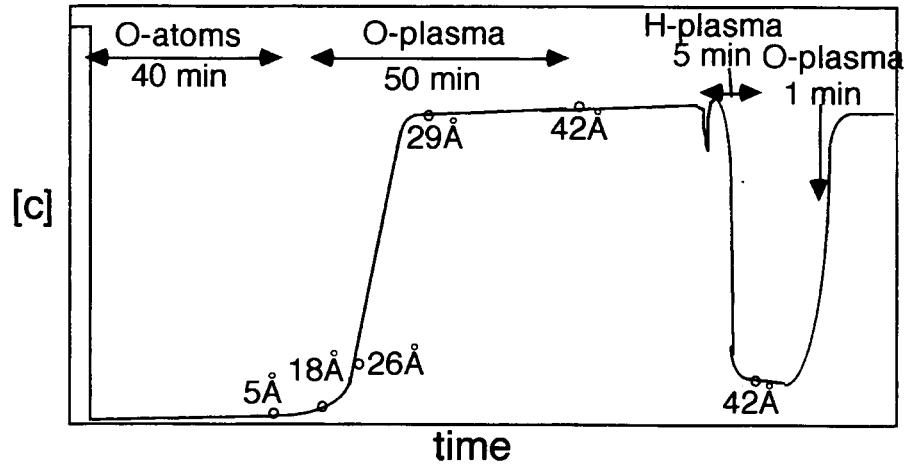

Figure 4. Somewhat schematic diagram of the passivation level, and film thickness, determined by XPS, at 6 stages in the processing of an HF-washed silicon surface.

4. CONCLUSIONS

At room temperature H-atoms and O-atoms instantly depassivate an HF washed Si surface. An O-plasma is effective at producing an oxide layer more than 40Å thick, but the presence of that oxide does not guarantee an effective passivation of that interface, when judged by its response to O_2, or an H-plasma. The complex behavior of such surfaces appears to be related to the effect of a plasma on both the SiO_2/Si interface and the exposed surface of the oxide[1].

REFERENCES

1. H. Li, E. A. Ogryzlo, T. Tiedje, and J. G. Cook, to be published in Proceedings of the 22nd International Conference on the Physics of Semiconductors, Vancouver, Canada, August 15-19, 1994.
2. J. Ruzyllo, A. Hoff, and G. Ruggles, J. Electron. Mater. 16 (1987) 373
3. J.H. Stathis and E. Cartier, Phys. Rev. Lett. 72 (1994) 2745

EFFECT OF DYNAMICAL PLASMA CLEANING ON Si-SiO_2 STRUCTURES

V.M. Maslovsky* and G.Ya. Pavlov**

The effect of surface cleaning by arc plasma jet on electrical parameters of Si-SiO_2 structures has been investigated. The relaxation time, charge stability, and breakdown voltage of MOS structures have been found to depend on arc plasma jet treatment mode. During the treatment, UV plasma irradiation deleteriously affects the structural parameters, which can be improved by athermal annealing of defects in the plasma impact area due to high-density flow of plasma-excited particles (10^{19} $cm^{-2}s^{-1}$) and hydrogen.

1. INTRODUCTION

One of new technologies which meets the requirements of ultra clean processing [1] is the arc plasma jet treatment (APJT) of surface at atmospheric pressure [2].

The APJT is conducted using a hydrodynamically continuous high-enthalpy (>10 J/g) low-temperature (< $2x10^4$ K) plasma jet which modifies the surface. Plasma jet provides the transport of charged and neutral excited particles to the surface by diffusion through the thin boundary layer of plasma. Thus, the extremely high flow density (10^{19} to 10^{21} $cm^{-2}s^{-1}$) of active particles with low kinetic energy (< 0.1 eV) can be obtained on the surface. The heat flow density is also very high (10^2 to 10^4 $W{\cdot}cm^{-2}$). The dose of near-UV irradiation during APJT is 10^{17} to 10^{18} $cm^{-2}s^{-1}$. The surface temperature during processing is controlled by the intersection velocity of wafer and plasma jet. APJT is a step forward in the development of plasma operating at atmospheric pressure. The aim of this work is to investigate the effect of APJT on the electrical parameters of Si-SiO_2 structures.

2. EXPERIMENTAL

The test Si-SiO_2-Si*-Al structures were prepared using thermal oxidation of *n*-Si(100) wafers. The Al electrode area on chips was 10^{-3} to 10^{-2} cm^2. The treatment was carried out using argon plasma (sometimes, with addition of NH_3) in two cleaning modes, i.e., soft and hard, which were determined by heat flow density. The soft mode corresponded to silicon surface cleaning from chemisorpbed layers (OH-group). The hard mode provided photoresist stripping at a rate of ~ 20 μs^{-1}. The total dose of Si-SiO_2 treatment was determined by the number of arc plasma jet impacts (n = 1, 4, or 10). The UV plasma irradiation dose

* Zelenograd Research Institute of Physical Problems, 103460 Moscow, Russia

** Centre for Analysis of Substances, 9, Elektrodnaya st., 111524 Moscow, Russia

was nearly uniform across the entire wafer surface. In order to make the effect of APJT more clear, the plasma jet trajectory on the surface passed at a certain distance from the wafer center. We measured relaxation time τ of high-frequency transient capacitors, distributions of charge stability Q, and C-V and I-V characteristics.

3. RESULTS

The distributions of the initial parameters of Si-SiO_2 structures were uniform across the wafer surfaces and were similar for all the wafers. The parameters were as follows: flat band voltage V_{fb} from -0.22 to -0.20 V; τ from 2 to 3 s; Q from 0.3 to 0.5 $C \cdot cm^{-2}$; breakdown voltage $V_{bd} \sim 20$ V; interface density of states in the middle of the silicon band gap $N_{ss} < 2.10^{10}$ $eV^{-1}cm^{-2}$; and leakage current I in the range $(2\text{-}4) \cdot 10^{-11}$ A at a voltage of 5 V.

After APJT of one wafer side the electrical parameters of the structures were nonuniform across the surface. However, under these conditions, the flat band voltage was slightly shifted: $\Delta V_{fb} = 0.03$ V. We showed that this APJT does not significantly change neither the C-V characteristics ($V_{fb} < 0.02$ V), nor the I-V characteristics, nor the interface density of states in the middle of the silicon band gap ($N_{ss} < 2x10^{10}$ $eV^{-1}cm^{-2}$). I also changed only slightly ($\sim (2\text{-}8) \cdot 10^{-11}$ A).

The most APJT-sensitive parameter of the silicon surface layers is generation time of minor charge carriers, which is proportional to τ [3]. The distribution of τ along the wafer diameter perpendicular to the plasma jet trajectory on the surface is shown in Fig. 1. The result suggests that beyond the plasma impact area τ drastically decreased due to defects generated by UV near the Si-SiO_2 interface.

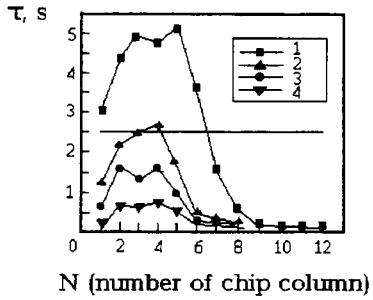

Figure 1. Distribution of relaxation time τ of MOS structures after hard APJT mode: (*1*) $n = 10$, with NH_3; (*2*) $n = 10$, (*3*) $n = 4$; and (*4*) $n = 1$. The horizontal line is the initial τ value. $n = 1$ to 6 corresponds to plasma impact area.

In the plasma impact area, τ substantially increased with dose as a result of hard APJT and with addition of NH_3 (curves *1-3*, Fig. 1). The two peaks in the curves (Fig. 1) probably appeared because APJT was conducted using two plasma jets. An increase of dose in soft treatment mode considerably changed the C-V

characteristics in the vicinity of the Si-SiO_2 interface (Fig. 2). After one plasma impact all the structures had similar *C-V* characteristics (curve *1*, Fig. 2).

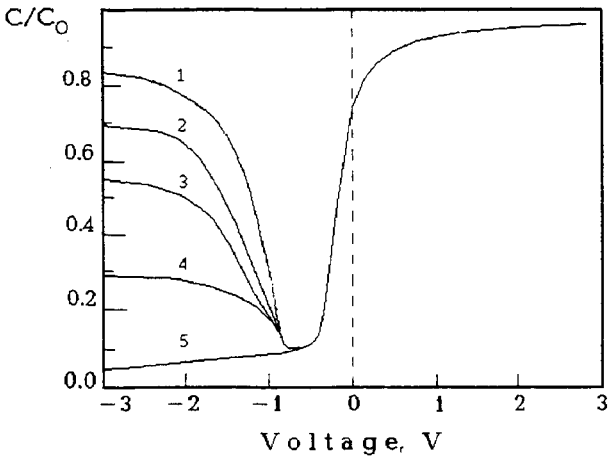

Figure 2. *C-V* characteristics of MOS structures (the frequency *f* is ~ 106 Hz) after soft APJT mode: (1) $n = 1$, $N = 1$ to 12; (2) $n = 4$, $N = 6$ to 12; (3) $n = 10$, $N = 9$ to 12; (4) before APJT, $N = 1$ to 12; and (5) for treated surface portion. *N* is chip column number.

For larger numbers of plasma impacts, the relaxation time τ increased (curve *5*, Fig. 2). Beyond the plasma impact area C/C_0 decreased. The distribution of charge stability of MOS structures after APJT (Fig. 3) was similar to the τ distribution (Fig. 1). Beyond the plasma impact area *Q* decreased for all the specimens,

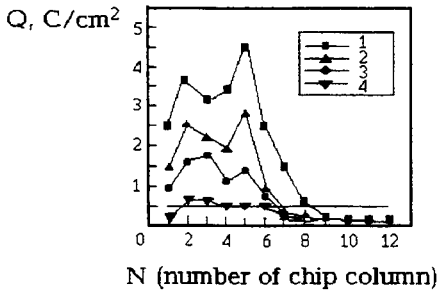

Figure 3. Distribution of charge stability *Q* of MOS structures after hard APJT mode: (1) $n = 10$, with NH_3; (2) $n = 10$; (3) $n = 4$; and (4) $n = 1$. The horizontal line is the initial *Q* value.

whereas in the plasma impact area the charge stability increased in hard mode and with addition of NH_3 (curves *1*, *2*, and *3*, Fig. 3). The breakdown voltages of Si-SiO_2 structures correlated with changes in τ and Q and could exceed the initial value by 50%. DLTS data did not indicate any significant shift of N_{ss}.

4. DISCUSSION

The correlation between τ and Q suggests the existence of two mechanisms whereby APJT affects the structures:

- UV impact affects defect-defect and defect-impurity reactions in Si [4] and, probably, in SiO_2. The effect of UV radiation on the defects in the vicinity of the Si-SiO_2 interface is analogous to changes produced by pulse magnetic field treatment [3];
- APJT provides transport of hydrogen and electron excitations (e.g., Forster mechanism) and athermal annealing of the defects in the plasma impact area due to the high density of electron excitations generated by the relaxation of plasma particles on the surface.

The latter process significantly accelerates the diffusion, causes athermal stress relaxation in the Si-SiO_2 system, and, hence, reduces the density of defect centers, including weakly bonded hydrogen [5].

5. CONCLUSIONS

APJT considerably changes some electrical parameters of MOS structures. The parameters could be improved in the plasma impact area, whereas beyond this area the parameters were deteriorated. The result is accounted for by the fact that UV irradiation deleteriously affects the MOS structures, whereas plasma annealing improves their quality due to defect-hydrogen interaction and relaxation of mechanical stresses.

REFERENCES

1. T. Ohmi, J. Microelectr. Eng., 10, 3/4 (1991) 163.
2. G.Ya. Pavlov and I.N. Knyazev, Book of Summaries "International Conference on Advanced and Laser Technologies", Moscow, Part 4 (1992) 118.
3. M.N. Levin and V.M. Maslovsky, Solid State Communs., 12 (1994) 813.
4. A.B. Danilin, Yu.N. Erokhin, and V.N. Mordkovich, Nucl. Instrum. and Meth. in Phys. Res., B59/60 (1991) 985.
5. P. Balk, V.V. Afanas'ev, and J.M.M. de Nijs, Physica of Semiconductor Devices, Narose Publishing House, New Delhi (1993) 219.

Adsorption and Desorption Studies of U-238 on Silicon Surfaces

G. Mainka, S. Metz, A. Fester, H. Ochs and B.O. Kolbesen
Institute of Inorg. Chemistry, Marie Curie Str. 11, D-60439 Frankfurt

Abstract

U and Th as α-particle emitters can cause soft-errors of dynamic random access memories (DRAMs) if they are contained in trace amounts in materials used in DRAM manufacturing. Here first studies regarding the adsorption and desorption behaviour of U-238 on silicon surfaces are presented. Radiochemical methods, TXRF (total reflection x-ray fluorescence analysis) and XPS (x-ray photoelectron spectroscopy) were applied to the characterization and quantitative analysis of U on the silicon surface. The concentration range of U in the solutions used for the contamination experiments was 1 - 100 ppm. U deposition on silicon surfaces is promoted in the neutral pH-regime, the pretreatment of the silicon wafers exhibits a distinct influence on the adsorption behaviour. HF treatment prevents U deposition on silicon surfaces out of acid solutions. By a complete RCA cleaning sequence U can effectively be removed. XPS measurements indicate that the chemical configuration of U on the silicon surface is UO_2-like. TXRF measurements confirmed the α-particle measurements in general. Differences observed on some wafers may be related to a non-uniform U distribution. Under similar experimental conditions no deposition of Th-232 could be observed.

Introduction

α-particle induced leakage current generation, so called soft-errors, is a well known failure mode and reliability problem of DRAMs (dynamic random access memories) [1]. The sources of α-particle emission are natural radionuclides like U, Th and their daughter products which are contained in trace amounts in packaging materials such as ceramics, insulating and conducting materials and thin films, e.g. plasma silicon nitride, tungsten and tungsten silicide and chemicals (e.g. H_3PO_4) fabricated or used in device manufacturing, respectively [2]. Up to now there is little information available in the literature about the behavior of these impurities regarding adsorption on and desorption from silicon surfaces. All radionuclides out of theU-238 and Th-232 decay chains [3] with a fairly long half-life (some days and more) are potential hazardous contaminants. The aim of this work was to get some first informations about adsorption and desorption behavior of natural U and Th on and from silicon wafers out of solutions with various concentrations and pH settings.

Engineers have developed various techniques, from process changes to new cell designs, to minimize the problem of α-particle induced soft errors. With increasing chip density detection of these contaminants is essential. We therefore made experiments to find out detection limits for those α-emitters.

Experiments

For all experiments 100mm silicon wafers (p-type Czochralski) with orientation (100) and a resistivity of 0,67-1,33 Ωcm were used. Before immersion in the contamination solution they were cut into quarters, subsequently RCA cleaned and

then rinsed with DI water and dried. The contamination solutions contained U-238 and Th-232 in the ppm range (1-100 ppm) and were prepared from $UO_2(NO_3)_2$ and $Th(NO_3)_3$. The pH-values of these solutions were set with NaOH or HCl in the range from 1-14.

α-particle detection was performed either with a low-level large area proportional counter FHT 700A from FRIESEKE & HÖPFNER or a 10-channel low-level system LB770 from BERTHOLD. Both systems are gas flow counters with the detector chamber separated from the sample by a thin Mylar film. As counting gas a P10 mixture with 10% methane and 90% argon was used. Front and backside of the wafers were measured separately. Calibration curves for U-238 and Th-232 were taken. The α- measurement background level is ≈ 0.0004 alphas/hr.

To check the reliability of the results of the alpha measurement TXRF spectra were taken with an ATOMIKA TXRF 8010 spectrometer. In order to get more information about the chemical configuration of the contaminants on the silicon surface XPS experiments were carried out with a KRATOS XSAM 800.

Results

In **Fig. 1** the dependence of wafer surface concentration in relation to various U concentrations is shown for wafers stored in air or under DI water before immersion into the contamination solution. In contrast to wafers stored under DI water a strong dependency of wafer surface concentration to solution concentration is found. No significant differences in the behavior of front and back side can be observed. **Fig. 2** illustrates how surface concentration varies at different pH settings of the contamination solution. Treatment of the contaminated wafers with aqueous solutions of pH 1-14 did not result in any significant U desorption while each step of RCA standard cleaning (NH_3/H_2O_2; HF; HCl/H_2O_2) reduced the surface U concentration distinctly. Application of the full RCA sequence pushed the U concentration below the actual detection limit of ≤ E13 cm^{-2}. Treatment of wafers with HF before contamination resulted in a prevention of U deposition on the surface. The XPS spectrum of a sample covered with

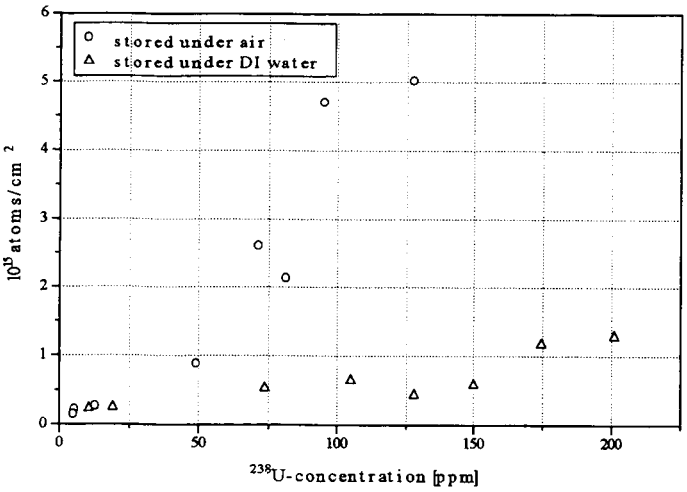

Fig. 1: ^{238}U concentration on wafer surface vs. ^{238}U-concentration in contamination solution in which wafer were immersed (pH 1,6)

5 x E14 atoms cm^{-2} U-238 is shown in **Fig. 3.** From the binding energy of the U $4f_{5/2}$ and U $4f_{7/2}$ peaks (381.4 eV and 391.9 eV, respectively) it can be concluded that the chemical configuration of U on the wafer surface is UO_2 **[4]**.

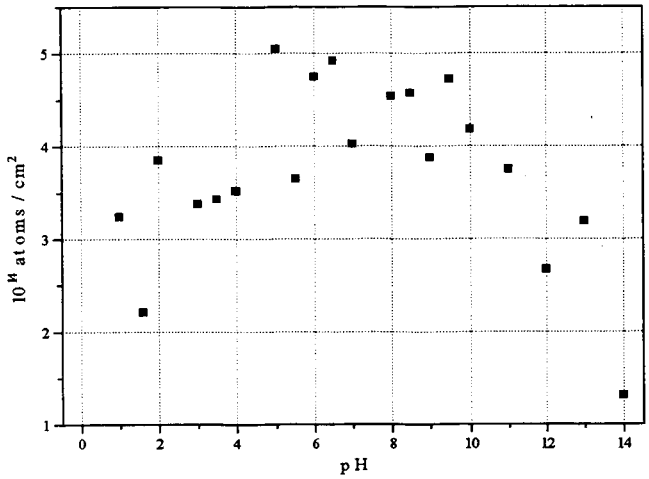

Fig.2: Dependence of the ^{238}U surface concentration on pH of the contamination solution (5 ppm)

TXRF measurements confirmed the results of the radioanalytical experiments in general. Differences in measured surface concentrations are closely related to an inhomogenous distribution of U on the silicon surface. However the TXRF values were systematically lower (up to a factor 10) than the α-measurement values.

Fig.4 shows the TXRF results for 13 measuring points on two 100 mm wafers. Both wafers were contaminated with U-238 in a parallel experiment (concentration of the solution 16.2 ppm, pH 1.6). Whereas the surface concentration on the wafer shown in b) is fairly uniform, it fluctuates up to a factor of 10 on the wafer in a).

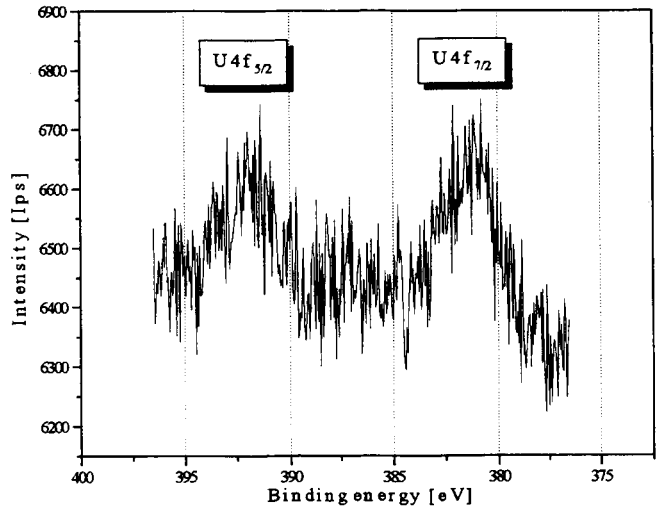

Fig.3: XPS spectrum of a sample covered with ^{238}U (5 ppm; pH 10)

Similiar experiments with Th solutions of 5 to 50 ppm did not show any deposition of Th on the silicon surface within the actual detection limits of radiochemical measurements, TXRF and XPS, which are of the same order of magnitude as found for U.

Discussion

In accordance with its chemical properties U deposits as oxide on silicon surfaces. Due to its amphoteric character the deposition is promoted in the neutral pH-regime (**Fig. 2**). As for many other metals a silicon surface passivated by hydrogen due to HF treatment is prohibitive for U deposition out of solution.

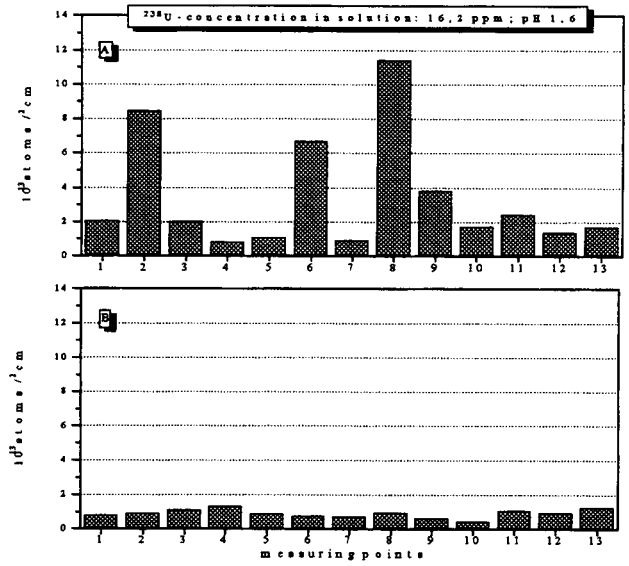

Fig.4: ^{238}U surface concentration determined by TXRF at differend measuring points of two 100 mm wafers contaminated in parallel experiment

The fact, that in contrast to complete RCA cleaning a treatment of the surfaces with acidic (HCl) or alkaline (NaOH) solutions shows no significant effect, again indicates how crucial is the dissolution of the silicon surface oxide during cleaning processes.

Even with average values measured over several points with TXRF, significant differences to the radiochemical results are observed. Up to now it is not clear if these differences are related to inhomogeneities of U depositon on the silicon surfaces. A reduction of the U concentration by absorption effects on the walls of our solution containers is no explanation because this effect affects both examination methods in the same way. Why Th did not deposit on silicon surfaces under similiar conditions as U is still not understood and is under further investigation.

References

[1] *T. C. May and M. H. Woods,* A new physical mechanism for soft-errors in dynamic memories, Proceedings, 16th Ann. International Reliability Physics Symposium, April 1978, p. 33

[2] *A. Ditali and Z. Hasnain,* Semicond. Int. June 1993, p. 136

[3] *K. H. Lieser,* Einführung in die Kernchemie, VCH-Verlagsgesellschaft Weinheim 1969

[4] *R. Schlögl and G. Inleghofer, P. Briggs and M. P. Seah,* Practical surface analysis by auger- and x-ray photoelectron spectroscopy, Perkin Elmer Corporation

Acknowlegements

The authors are grateful to Wacker Chemitronic/Burghausen for providing the silicon wafers and Fa. ATOMIKA/ München for performing the TXRF measurements

A UHV COMPATIBLE PLASMA CHEMICAL CLEANING PROCEDURE FOR LOW TEMPERATURE EPITAXIAL GROWTH ON PATTERNED SILICON SUBSTRATES

E. Beck, A. Dommann*, I. Eisele, W. Hansch**, N. Korner*, D. Krüger***, J. Ramm**

1. INTRODUCTION

Developing ultra clean technology, lowering the thermal budget of the wafer, and reducing the bombarding energy of particles involved in plasma processing are some of the challenges for the production of advanced semiconductor devices. Cleaning procedures which fit this concept are of particular importance. They could prove to play a decisive role in cleaning deep trenches and achieving low temperature epitaxial growth. Here, an ultra high vacuum (UHV) compatible plasma cleaning procedure is presented which prepares bare and patterned silicon wafers in a single step for low temperature epitaxial growth.

2. EXPERIMENTAL DETAILS AND RESULTS

An extensive description of the cleaning procedure and more details of the low energy Balzers plasma source are given in previous publications [1,2]. In the following, only some properties of the plasma cleaning process will be listed. For the cleaning of the silicon substrate, a hot filament DC discharge (in argon working gas) operating at a discharge voltage of about 30 V is established by the plasma source. It combines high electron currents (10 A to 100 A) with low electron and ion energies. For the cleaning, hydrogen is added to the discharge and activated. The energy of the ions impinging on the silicon wafer is low (typically 5 eV), thus avoiding sputtering of the substrate and the chamber walls. The silicon wafer is immersed in the discharge plasma for cleaning. The activated hydrogen forms volatile compounds with some of the contaminations on the wafer surface (oxides of silicon, carbon, boron). The potential of the substrate holder controls the nature of the cleaning process. The wafer is mainly bombarded by electrons if the substrate holder is grounded (this is the case for the experiments reported here). If the substrate holder is insulated from ground the bombardment with low energy ions is realized. The energy of these ions, however, is below the sputter threshold. In both cases a pure chemical cleaning (electron or ion stimulated) is realized. The bulk temperature of the wafer during cleaning is low and ranges from 100 °C to 400 °C depending on the plasma discharge power.

BALZERS AG; FL-9496 Balzers, *Neu-Technikum Buchs, CH-9470 Buchs, **Universität der Bundeswehr München, D-85579 Neubiberg, ***Institut für Halbleiterphysik, D-15230 Frankfurt(O)

In a next step, silicon layers are grown by molecular beam epitaxy (MBE) on the *in situ* plasma cleaned silicon substrates. Therefore, the wafers are transferred from the plasma cleaning module to the MBE chamber (both UHV). The layers are deposited by an electron beam evaporator with a deposition rate of about 0.1 nm/s, controlled by a quadrupole mass spectrometer. The substrate temperature during deposition is about 500°C. No high temperature desorption step for the native oxide removal is necessary for the whole process sequence. Homoepitaxial layers of good cristallinity can be achieved on the plasma cleaned substrates, indicating a damage free plasma procedure [3,4].

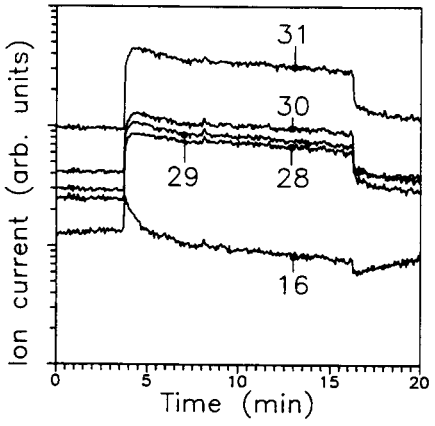

Figure 1. Multiple ion detection versus time during cleaning of a silicon wafer.

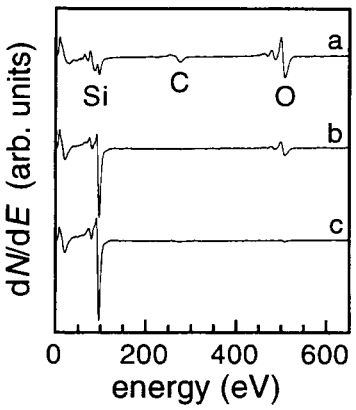

Figure 2. Auger spectra of the silicon wafer surface (untreated wafer (a), cleaning duration of 30 s (b) and 120 s (c), respectively.

2.1. *In situ* plasma monitoring

The Balzers plasma process monitor PPM 400 was utilized to investigate the plasma. Fig.1 depicts the ion currents for O^+, Si^+, SiH^+, SiH_2^+, and SiH_3^+ (m/e = 16, 28, 29, 30 and 31, respectively) as a function of time (discharge current 40 A, Ar:H_2 flow of 18:35 sccm). It reflects the process chemistry for the cleaning of silicon wafers without wet chemical pretreatment. At t = 4 min, the wafer is immersed in the plasma and the production of oxygen and the Si-H complexes can be clearly seen. About 1 min later, a distinct decrease in the oxygen production is seen, indicating that most of the oxygen has already been removed from the wafer surface. At t = 16 min, the wafer is taken out of the plasma. From this and other experiments [1] we can conclude that materials forming volatile compounds with hydrogen, *e.g.* silicon, oxygen, silicon oxide, carbon, hydrocarbons, boron, arsenic etc., are etched in the plasma.

2.2. Auger analysis

The question is how the results from monitoring the plasma during cleaning correlate with the chemical reactions at the silicon wafer surface. Therefore, an Auger spectrometer was attached to the process chamber which allowed to record spectra of the wafer surface without vacuum break. The results are given in Fig.2. (a) shows the spectrum of the silicon wafer before cleaning as delivered by the manufacturer. Oxygen and carbon peaks are found at the energies of 503 eV and 271 eV, respectively. Between 70 eV and 100 eV the peaks of Si and SiO can be recognized. Plasma cleaning for 30 s reduces the carbon and oxygen contamination at the wafer surface. The carbon concentration is below the noise limit of the measurement. Now the silicon peak (92 eV) is clearly developed. Additional 90 s cleaning are necessary to reduce also the oxygen to the noise limit. This is in accordance with the results obtained by plasma monitoring (Fig.2, m/e = 16) from which also a process time of about 2 can be deduced to remove most of the oxygen.

2.3. Secondary ion mass spectrometry analysis

In Fig.3, the secondary ion mass spectrometry (SIMS) depth profiles of a sample cleaned in the argon-hydrogen discharge are shown. The interface between the 200 nm thick epilayer and the silicon substrate is indicated by the increase in the oxygen signal. Integrating this signal at the interface, an areal concentration of about 7 x 10^{12} cm^{-2} can be deduced. For comparison, the silicon atomic density of the (100)

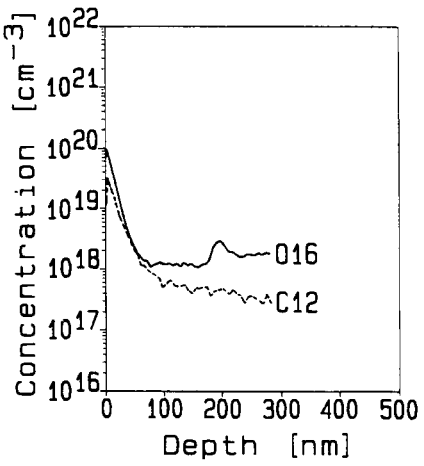

Figure 3. SIMS depth profile of ^{16}O and ^{12}C for low temperature epitaxial growth of a 200 nm thick epilayer on a plasma cleaned silicon substrate.

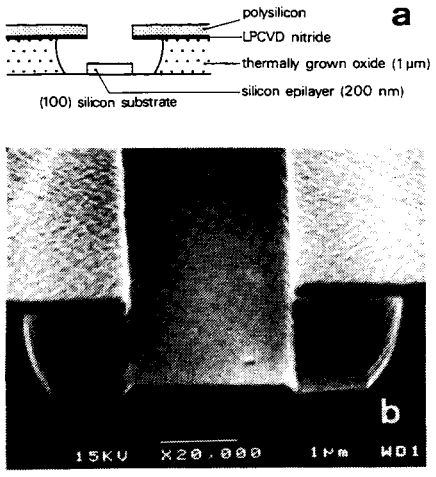

Figure 4. Schematic diagram of the patterned substrate after silicon deposition (a); SEM image of the actual substrate (b).

surface is 6.8 x 10^{14} cm^{-2}. It was observed that the oxygen in the interface decreased gradually down to the detection limit during a series of cleaning steps, suggesting a conditioning of the plasma cleaning chamber. In the case of the carbon signal no interface peak can be detected. Hence, an areal carbon concentration of less than 10^{-3} monolayers can be estimated.

2.4. Application of the cleaning procedure to patterned substrates

The cleaning procedure was also investigated for patterned silicon substrates. The substrates were (100) wafers with a 1 μm thick thermally grown silicon dioxide layer and 100 nm LPCVD grown silicon nitride layer on top. Micro shadow masks for local epitaxial growth were formed by patterning and underetching the silicon nitride [5]. Again, we used only the single plasma cleaning step for these patterned substrates. The discharge current was 30 A at a substrate temperature of about 200 °C. The wafer was exposed to the plasma for 5 min, much longer than necessary based on the data in Figures 1 and 2. Then 200 nm of silicon were deposited at 550 °C. The substrate after the 200 nm deposition is sketched schematically in Fig.4(a). Figure 4(b) shows the scanning electron microscopy (SEM) image of the sample fabricated in this process. It illustrates the good contrast between the rough polysilicon on top of the silicon nitride mask and the smooth surface of the epilayer on the silicon substrate.

3. CONCLUSIONS

The plasma cleaning procedure presented is compatible with *in situ* processing under UHV conditions and at low temperatures. Low interface contamination levels for carbon and oxygen were achieved by this single step cleaning procedure. It was shown that the cleaning procedure is also suited for preparing patterned substrates for low temperature local epitaxial growth.

REFERENCES

1. J. Ramm, E. Beck, A. Züger, A. Dommann and R.E. Pixley, Thin Solid Films, 222 (1992) 126.
2. J. Ramm, E. Beck, A. Dommann, I. Eisele and D. Krüger, Thin Solid Films, 246 (1994) 158.
3. J. Ramm, E. Beck and A. Züger, Mater. Res. Soc. Symp. Proc., 220 (1991) 15.
4. J. Ramm, E. Beck, F.-P. Steiner, R. E. Pixley and I. Eisele, Mater. Res. Soc. Symp. Proc., 259 (1992) 249.
5. E. Hammerl, F. Wittmann, J. Mesarosch, I. Eisele, V. Huber and H. Oppolzer, Mat. Res. Soc. Symp. Proc., 220 (1991) 27.

SOFT CLEANING BY IN VACUO ULTRAVIOLET RADIATION BEFORE MBE

G. Lippert* and H.J. Osten*

ABSTRACT

An UV/hydrogen procedure performed in vacuo is able to remove adsorbed hydrocarbons from a protective silicon oxide layer prior to its sublimation. The efficiency of UV/H_2-cleaning increases with increasing substrate temperature, with the time of treatment and with increasing partial pressure of hydrogen. At least three different mechanisms give rise to the observed removing of carbon-containing contaminants, namely (i) thermal desorption due to the higher substrate temperature, (ii) a direct interaction between the high energy UV photons and the adsorbed species (photochemical degradation), and (iii) a mechanism based on the presence of the activated hydrogen atoms. Each single process has its own temperature dependence. This moderate in situ procedure removes preferentially weakly bonded species. It can be successfully used to clean the protective layer prior to sublimation. All wet chemical treatments before introducing the wafer into the deposition equipment can be avoided and silicon substrates as-received from the producer can be used to growth high quality epitaxial layers, which seems to be a good alternative to high sophisticated wet chemical procedures, where you hardly can avoid recontamination's during wafer loading. Opposite to the UV/ozone process the thickness of the oxide layers will not be changed during an UV/hydrogen process.

1. Introduction

Impurities at a silicon surface are able to disturb the structural and electrical properties of MBE-grown films. A sophisticated *ex situ* cleaning procedure should remove most of these contaminants. Nevertheless, loading the substrate into the UHV-machine and all handling steps before deposition recontaminate the surface again. An *in situ* cleaning step immediately before molecular beam epitaxy (MBE) is also required if you wish to use epi-ready silicon substrates as received from the producer (covered by a recontaminated protective oxide layer).

In this paper a moderate *in situ* procedure based on UV-radiation only will be presented. Usually a wafer loaded into the MBE-equipment is covered with a protective layer (oxide, H-passivated). Impurities are mainly physisorbed at this protective layer; they can easily be detected with X-ray photoelectron spectroscopy (XPS) (Fig. 1). Most of these recontaminants will remain at the surface during the sublimation of the protective layer. Therefore, it would be useful to remove all impurities from the protective layer prior sublimation.

* Institute of Semiconductor Physics, PO 409, 15204 Frankfurt (O), Germany

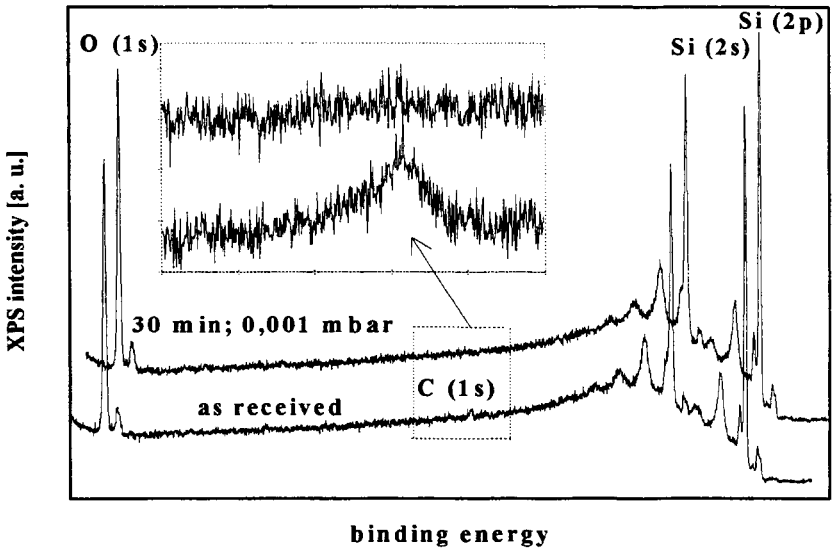

Figure 1. XPS-spectra of an untreated and with UV/H_2 treated silicon (100) sample (T_S = 300 °C)

The characterisation of the surface by XPS indicates the presence of physisorbed carbon (1s) at an as received Si wafer. After a treatment of this surfaces with UV-hydrogen (10^{-3} mbar) for 30 minutes no carbon signal could be detected.

2. Experimental

All experiments were performed in a three-chamber vacuum equipment with a basic pressure of 5 x 10^{-11} mbar. The oilfree vacuum system consists of dryvac pumps, turbomolecular pumps and titanium sublimation pumps with a liquid nitrogen cooled baffle. In our experiments we used Si(100) wafers produced by Wacker Chemitronic. As an UV light source we used a special designed low pressure mercury lamp mounted inside the chamber in a distance of 5 mm above the sample position. Molecular hydrogen was introduced into the chamber with a purity of 99.999 %, while simultaneously the pumping efficiency had been reduced. It could be varied from 1 mbar down to 10^{-8} mbar. Substrate temperatures up to 300 °C were used. Another chamber of the MBE-equipment contains the XPS tools. The emitted photoelectrons were recorded with a spherical analyzer and processed with an appropriated software (SPECS). The detection limit of this XPS configuration is below 10 % of a monoatomic layer *.

3. Results and discussion

Using intensive UV-radiation, a photochemical degradation of hydrocarbons from a clean as well as a covered silicon surface could be observed. The efficiency of this procedure in dependence on radiation time and substrate temperature is detected.

The addition of a gaseous component may support the UV cleaning efficiency. Using a higher partial pressure of oxygen ($p > 10^{-2}$ mbar) inside the UHV preparation chamber the UV-radiation activates oxygen to form ozone (UV/ozone cleaning [1]). The cleaning efficiency will be higher than using UV light only. This efficiency depends on the oxygen partial pressure and on the temperature of the silicon substrate. UV/ozone cleaning results in an oxidation of the organic impurities at the surface into volatile compounds and in an oxidation of the silicon (Fig. 2).

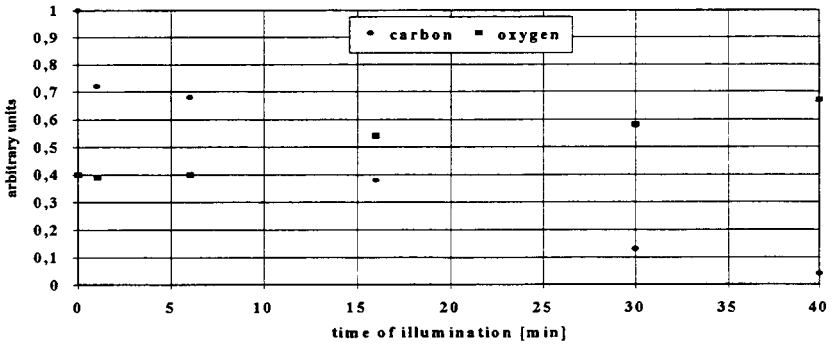

Figure 2. Coverage of an in situ cleaned silicon surface by UV/Ozone (p_{O2}= 0.1 mbar; XPS)

Using hydrogen instead of oxygen during the UV-illumination (UV/H_2 cleaning) organic compounds at the surface can also be removed rapidly, but no additional oxidation of the silicon surface takes place (Fig. 1). The efficiency of UV/H_2-cleaning increases with increasing substrate temperature, with the time of treatment and with increasing partial pressure of hydrogen (Fig. 3).

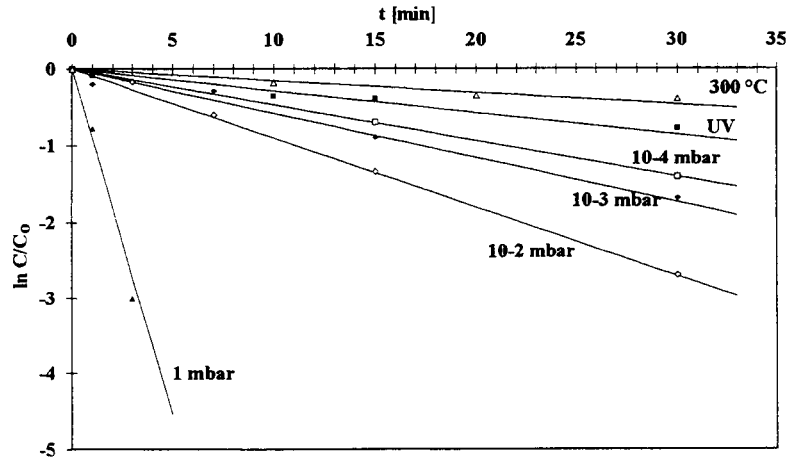

Figure 3. normalised intensities of the C(1s) XPS signal as a function of time at a substrate temperature of 300 °C. The individual conditions (only heating, heating and UV illumination with/without additonal hydrogen atmosphere) are indicated.

The drawn lines in Fig. 3 represent a fit of the experimental results to the following relation where:

$$C = C_0 \exp (- t / \tau)$$

C_0 is the initial coverage with carbon containing species;
τ is the time constant descrbing the efficiency of removal;

We demonstrate an UV/H_2-cleaning procedure with we consider a compromise between sufficient cleaning results and acceptable handling time (the bad pumping efficiency for hydrogen leads to long handling time). The whole cleaning process can be described by only one single time constant τ, indicating that other mechanism, as recontamination's (which should increase with time) can be neglected. As we could show [2] the efficiency of UV/H_2-cleaning increases with increasing substrate temperature, with the time of treatment and with increasing partial pressure of hydrogen. A significant reduction of carbon (a source for structural defects) is achieved. At least three different mechanisms give rise to the observed removing of carbon-containing contamination's, namely (i) thermal desorption due to the higher substrate temperature, (ii) a direct interaction between the high energy UV photons and the adsorbed species (photochemical degradation), and (iii) a mechanism based on the presence of the activated hydrogen atoms. Each of them has its own temperature dependence.This moderate *in situ* procedure removes preferentially weakly bonded species. It can be successfully used to clean the protective layer prior sublimation. Experiments to remove carbon deposited on fresh grown silicon surfaces (atomically clean) were not successful. With XPS we could detect the formation of silicon-carbide-like bonds immediately after the carbon deposition. A stronger treatment like H_2-plasma cleaning [3] is required for the removal of SiC-species.

Conclusion

We presented two useful in situ cleaning procedures based on UV radiation. Comparing the represented UV/hydrogen cleaning procedure with in situ UV/Ozone [4] we would state the following: Both methods are able to remove hydrocarbons from a protective oxide layer with nearly the same efficiency. But opposite to the UV/ozone process the thickness of the oxide layers will not be changed during an UV/hydrogen process (see also Fig. 2). It leads to lower temperature/time-treatment for the removal of this oxide prior Si-MBE.

References

* We used an elemental carbon source (with external calibrated flux density) to deposite a known amount of carbon submonolayer. In this way we were able to quantify our XPS signal intensities.

1. M. Tabe; Appl. Phys. Lett. **45** (1984), pp. 534
2. G. Lippert and H. J. Osten, Electrochem. Soc., in press;
3. J. Ramm, E. Beck, and A. Zueger; proc. MRS Symp. Vol. **220** (1991), pp. 15
4. G. Lippert, D. Krüger, H. P. Zeindl, J. Ramm, E. Bugiel, and H. J. Osten, Proc. MRS **315**, 85 (1993)

THE EFFECT OF VARIOUS PROCESSING AND HARDWARE PARAMETERS ON THE DECOMPOSITION OF H_2O_2 IN APM

A. Philipossian and R. Wilkinson
Intel Corporation, Santa Clara, CA 95052

1. INTRODUCTION AND OBJECTIVE

The decomposition rate of H_2O_2 in APM (mixture of $H_2O_2/NH_4OH/H_2O$ at a typical ratio of 1/1/5) has recently been the subject of numerous investigations [1,2]. The purpose of this study is to further explore the effect of key parameters such as temperature, individual and combined Fe and Cu content, megasonic energy, presence of wafers, convection and the shape factor of the processing tank on the decomposition kinetics of H_2O_2 in APM. This investigation is comprised of several independent studies as described below.

2. EFFECT OF TEMPERATURE, Fe CONTENT, CONVECTION AND SHAPE FACTOR

Table 1 summarizes the parameter space. The mixtures were kept in closed beakers in order to prevent NH_4OH from evaporating (this was verified experimentally). To determine the decomposition rate, samples were drawn periodically (i.e. 0, 0.5, 1, 1.5 and 2 hours after the mixture was made) and were titrated with ceric sulfate. Starting H_2O_2 and NH_4OH solutions had individual trace metal contents of less than 0.2 ppb. The shape factor was determined by taking the surface area to volume ratio of two differently configured containers. In one container, the 40 cc solution was in contact with 30 cm^2 of the container (shape factor of 0.75), while in another, the solution was in contact with 22 cm^2 (shape factor of 0.55). Convection was introduced in the system with a magnetic stirrer. Stirring rates for the 2 shape factors were normalized by visualizing the fluid dynamics of the bath using a tracer dye and equating the times needed to reach steady-state mixing. Linear regression was used to analyze the data.

Table 1: Factors investigated in the H_2O_2 decomposition experiment (16 runs).

Factor	Level 1	Level 2
Temperature (°C)	30.0	70.0
Fe Content (ppb)	0.2	10.0
Shape Factor (cm^{-1})	0.55	0.75
Convective Bath	No	Yes

With a regression coefficient of 0.89, the empirical model indicated the significant terms to be (in order of significance): Fe content, temperature, convection and the interactive effect between Fe content and temperature. As expected, higher Fe content and higher temperatures promoted decomposition. This was consistent with previously reported studies suggesting an Arrhenius relationship between decomposition rate and temperature [1,2]. Convection also increased the decomposition rate suggesting that the catalytic decomposition of H_2O_2 may be mass transport limited. The shape factor did not seem to effect decomposition rate indicating that decomposition was not driven by interactions with the wall. Figure 1 summarizes the relationship between the Fe content and temperature for stagnant and convective systems. In both cases, the shape factor is maintained at 0.75 cm^{-1}. It should be noted that even at 30 °C, H_2O_2 can decompose significantly given a high Fe content in APM. For instance, based on the convective system of Figure 1, H_2O_2 (in APM) at 30 °C and 10 ppb Fe decomposes just as rapidly as one at 70 °C and 1 ppb iron. The pronounced effect of convection on decomposition suggests that, in production wet benches with recirculating acid baths, the turnover ratio of the tank needs to be understood and optimized with respect to the desired lifetime of the bath

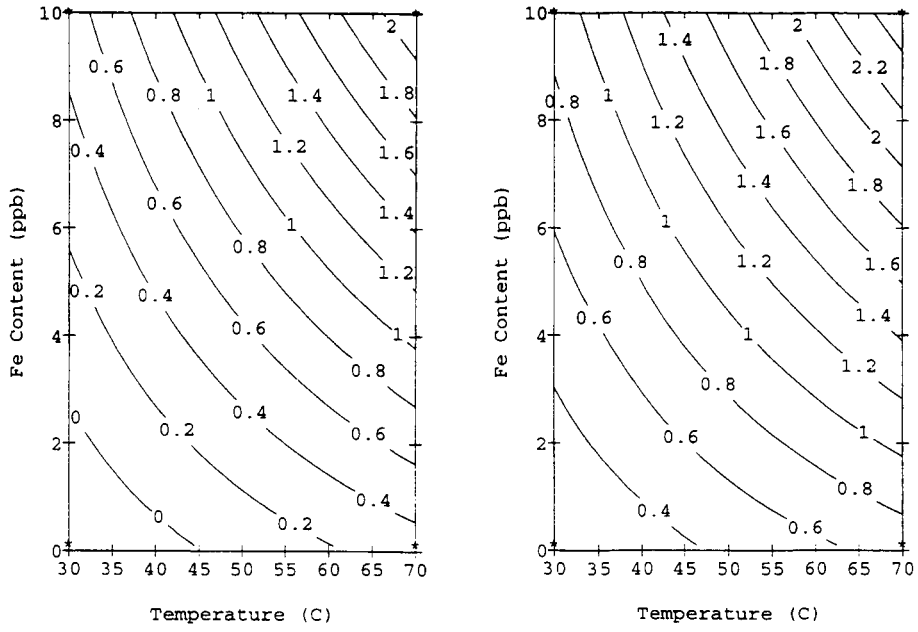

Figure 1: Contour plots representing the combined effect of Fe content and bath temperature on H_2O_2 decomposition rate for stagnant bath (left) and convective bath (right). The decomposition rate is highlighted on the contour lines in units of percent H_2O_2 (by volume in the APM) per hour. The shape factor is at 0.75 cm^{-1}.

3. EFFECT OF INDIVIDUAL AND COMBINED Fe AND Cu CONTENT

The factors investigated in this study were the total Fe and Cu content in APM (10, 100 and 1000 ppb), and the weight fraction, R, of Fe (0, 0.5 and 1) where R is defined as:

$$R = [Fe] \div \{ [Fe] + [Cu] \} \quad (1)$$

H_2O_2 decomposition rate was obtained through successive autotitrations for a period of 2 hours. As in the previous case, baths were kept in closed beakers at 30 °C. Starting H_2O_2 and NH_4OH solutions had individual trace metal contents of less than 0.2 ppm and the H_2O_2 decomposition rate for an unspiked APM was determined for reference. In all cases, the amount of H_2O_2 decomposed varied linearly with the age of the APM thus allowing a straight line fit to the decomposition data for determining the decomposition rate (i.e. absolute value of the slope). Typical run-to-run variability of the titration technique never exceeded 8 percent RSD. Figure 2 summarizes the effect of metal content in APM on H_2O_2 decomposition rate. The data point corresponding to the unspiked mixture is plotted as having a total Fe and Cu of 0.1 ppb (this was verified experimentally). Under the conditions of this experiment, at a given metal concentration, Fe catalyzes H_2O_2 decomposition 15 to 20 times faster than Cu. This is in contrast to a previous study at 70 °C indicating Cu to be more catalytic [2]. This suggests that the relative catalytic activity of Fe and Cu is a function of temperature. At Fe concentrations in excess of 100 ppb, the decomposition rate is not a function of Fe content, while up to Cu concentrations of 1000 ppb, the decomposition rate continues to strongly depend on Cu content.

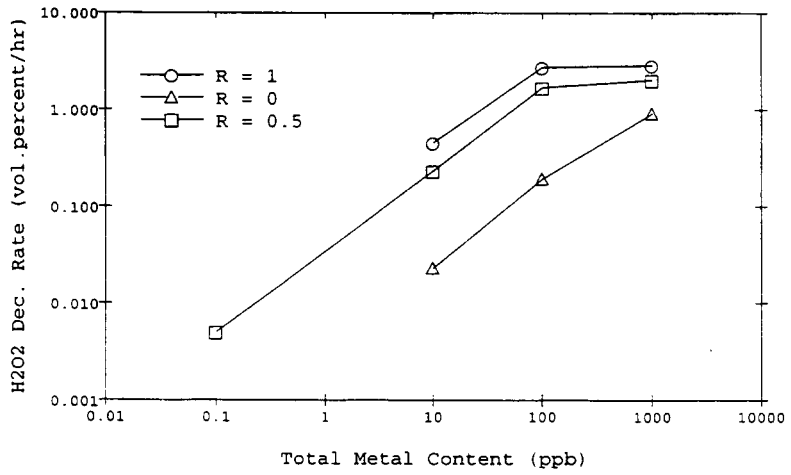

Figure 2. H_2O_2 decomposition rate as a function of total metal content and Fe weight fraction (R).

For mixtures of Fe and Cu (in equal amounts), the decomposition rate of peroxide is governed by Fe which is consistent with the rates observed for individual Fe and Cu contaminated cases.

4. EFFECT OF MEGASONICS AND WAFERS IN THE BATH

Table 2 summarizes the parameter space. All experiments were performed at ambient temperature in a recirculating bath of a research wet bench. In the experiments with megasonic cleaning, in order to simulate somewhat typical production conditions over long periods of time, megasonic power (set arbitrarily at 900 kHz and 150 W) was turned on for 10 minutes and then turned off for the next 10 minutes in repeating cycles for over 5 hours.

Table 2: Factors investigated in the wet bench H_2O_2 decomposition experiment (4 runs plus 4 replicates).

Factor	Level 1	Level 2
Megasonic energy	No	Yes
Wafers in the bath	No	Yes

With a regression coefficient of 0.90, the empirical model indicated a total lack of any significant main or interactive terms. The fact that presence of wafers did not affect decomposition rate was consistent with our earlier observation that the shape factor of the bath (and hence the surface area in contact with the fluid) was an insignificant parameter (see Section 2). The observation that megasonic energy did not affect H_2O_2 loss was interesting. Further studies are underway to understand this phenomenon.

7. ACKNOWLEDGMENTS

The authors would like to thank Dr. Baylor Triplett for many valuable discussions, and Mark Tran for performing the megasonics experiments.

REFERENCES

1. Sugihara, Y., S. Shimokawa and Y. Oshida, *Influence of metallic impurities on SC-1 cleaning,* Semiconductor Pure Water and Chemicals Conference, Santa Clara, CA (1993).
2. Schmidt, H. M. Meuris, P. Mertens, A. Rotondaro, M. Heyns, T. Hurd and Z. Hatcher, *Physico chemical aspects of H_2O_2 based silicon wafer cleaning solutions,* Ultra Clean Processing of Silicon Surfaces, Brugge, Belgium (1994).

SCA DETERMINATION OF CHARGES IN OXIDE AFTER METALLIC CONTAMINATION

K.BARLA
CNET, CENTRE COMMUN CNET SGS-THOMSON
F-38290 Crolles, FRANCE
F.TARDIF, D.WALZ, C.d'ASSENZA
LETI, MEL, CENG
F-38054 Grenoble, FRANCE

1-INTRODUCTION:

for the future technology gate oxide is so thin that monitoring metallic contamination is becoming more and more important. up to now the way to obtain precise information on the oxide quality after cleaning and oxidation is to perform c(v) measurements on thick oxide. this method is time consuming and its response time is very long. new methods are to-day available. they are based on the modification of the surface potentiel of the silicon under illumination. SCA (surface charge analyser) deduced, from this modification in function of the applied potentiel, charges in oxide, doping level and interface states.
in this contribution, we studied the capability of the SCA to detect charges induced by metallic contamination and we compared the results to c(v) measurement, in order to apply this new method to monitor cleaning and furnace in an industrial plant

1-EXPERIMENTAL

100 Si Wafers are contaminated by Aluminum, Calcium and Sodium by using the spin coating method, some wafers are also contaminated by Aluminum in SC1 solution. Then the wafers are oxidized in furnace in order to get 400A oxide. VPD-AAS measurements are made on Si wafer just after contamination, and after oxidation in order to determine contaminants in the oxide. SCA measurements on 10 points are made on oxide wafers and on some of them we also performed C(V) measurements after metallisation and photolithography and anneal in forming gas.

2-RESULTS

The VPD-AAS measurements are difficult with calcium, aluminium and sodium due to the presence of these elements everywhere. So, the dispersion in the measurements is very high. But it can be seen in Figure 1 (a) , (b) that aluminum and calcium which are deposited on the silicon remains after oxidation in the oxide and that this is not the case with sodiumb. All the sodium which is put on the silicon goes out of the oxide during the oxidation. So that we have not been able with this contamination method to get some sodium in the oxide to perform charges measurement with SCA and C(V).

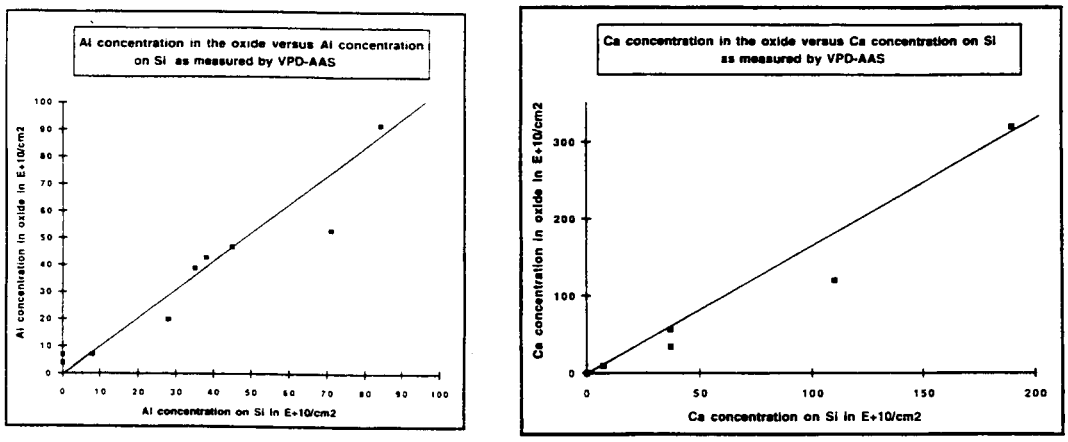

Figure 1: Contamination measurements by VPD-AAS
(a) Aluminum
(b) Calcium

Figure 2 (a) and (b) represents variation of charges that we obtain by decreasing the mean value of the charges measurement of tha contaminated sample by the mean value of the uncontaminated value. So the trends in the figure is only due to the contamination. it is clear from the figure2 (a) that C(V) is not capable to see any aluminum contamination, while SCA is sensitive to contamination less than 1E+11/cm2 in aluminum. Figure 2(b) shows that SCA and C(V) give the same answer for calcium, but that the sensitivity is very low, about 1E+12/cm2.

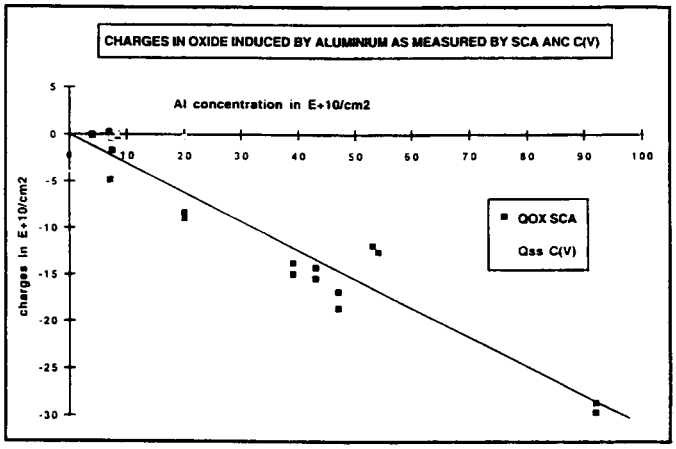

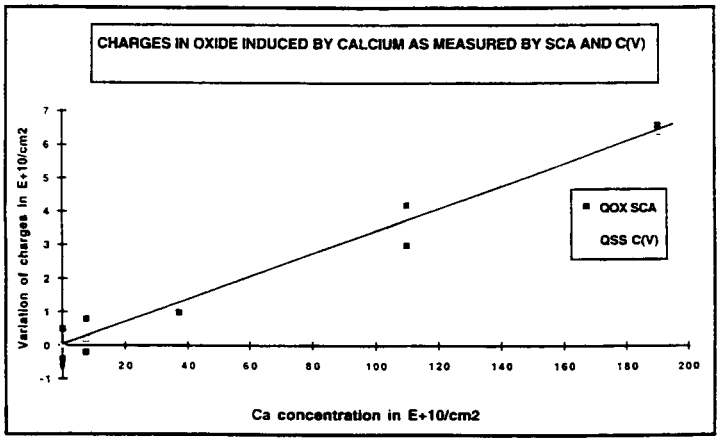

Figure 2: Charges measurements by SCA and C(V)

CONCLUSION:

We have demonstrated the capability of the SCA to determine contamination in oxide. The measurement of the SCA is the same as the C(V) for Calcium contamination, but the sensitivity is low, 2E+12 at /cm2 of Calcium are need to get 7E+10/cm2 charges. For Aluminum SCA is much more superior than C(V) because it is known that Al remains on the upper surface of oxide and so cannot be seen by C(V) measurements. The results show that about 1 / 3 Al atoms give a charge in SCA measurement. The response is more difficult for Sodium because we have not be able to put sodium in the oxide certainly due to its high volability . SCA is now used for monitoring cleaning and furnace in Crolles plant, with good results.

Calibration of TXRF Equipment

J. Knoth*, H.Schwenke* and P. Eichinger**

Total reflection X-ray fluorescence spectrometry (TXRF) is a new analytical X-ray fluorescence technique which is characterized by grazing incidence of the primary beam. Typically the technique operates at angles near a critical angle below which total reflection of X-rays occurs. Owing to its shallow information depth and its extreme sensitivity TXRF has proven to be a valuable tool for the determination of metallic contaminants in or on silicon wafer surfaces. The calibration of TXRF equipment, however, needs considerable attention. This is a consequence of the fact that in the total reflection regime the primary X-ray field is not homogeneous but forms standing waves immediately above the surface. Therefore, the fluorescence intensity in the total reflection mode depends strongly on parameters which are usually not of interest in X-ray fluorescence analysis, namely the position of the analyte atoms with respect to the interface (in terms of nanometers) and the incident angle of the exciting beam (in terms of millirad). The influence of both parameters on the TXRF signal has been early recognized and is used to be exemplified on two boundary cases of surface contamination [1, 2] which are shown in Fig. 1. The fluorescence signal vs. incident angle from a monolayer of Ni-atoms (film-type contamination) differs strongly from the signal from the same amount of atoms arranged as particles (particle-type contamination) on the silicon surface .

Fig.1

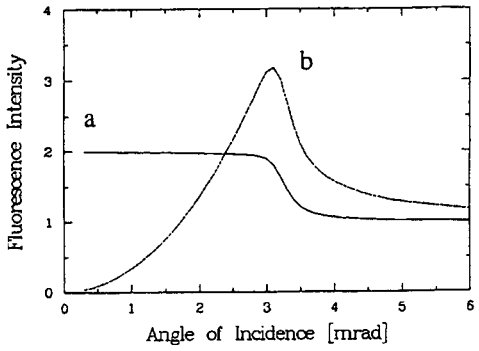

In this study we will show, that the standing waves character of TXRF, which is manifested by the different nature of both curves in Fig. 1 indicates the necessity for introducing reliable quantitation procedures and standards for quantitative analysis. First we will examine two calibration techniques which are already in use and subsequently we describe a new method which we believe to be the

* GKSS-Forschungszentrum, Max-Planck-Str., D-21502 Geesthacht
** GeMeTec, Geretsrieder Str. 10a, D-81379 München

most reliable solution for the quantitation problem in TXRF. We begin with the oldest technique here called "ng technique", which was already applied for wafer analysis in 1989 [2].

1. *The "ng" technique*

This procedure starts from a certain volume of a diluted aqueous metal salt solution, e.g. 5 µl of a 200 ppb Ni standard solution which exactly contains 1 ng Ni. Using a micro-pipette this volume is put on the surface of a cleaned silicon wafer and allowed to dry. With an annular diaphragm of e.g. 8 mm in front of the X-ray detector the amount of 1 ng Ni per detected area corresponds to 2.05 x 10^{13} atoms/cm^2 in this example. The calibration is easily carried out by relating the Ni counting rate from the detector to this value. Errors, which arise from pipetting, diluting and detection statistics can be kept within 5 %. Basically the ng-technique has proven successfully in intercomparisons test between 5 laboratories in Europe, USA and Japan.

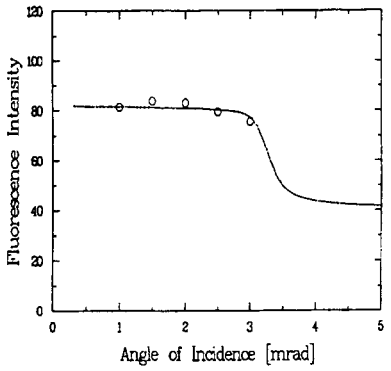

Fig.2a

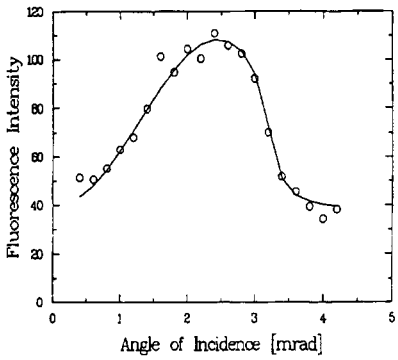

Fig.2b

There are, however, two risks associated with this calibration. A calibration wafer loaded with just 1ng metal must be carefully stored and is sensitive against additional contamination or even losses of microcrystals if it is used repeatedly. Even more serious, however, is a complication which is connected with the standing wave structure of the primary field.

During the evaporation of the water matrix of the sample it can not be excluded that tiny or flat microcrystals develop. The fluorescence radiation from those crystals show an angular distribution similar to curve (b) from Fig.1, in contrast to crystals whose diameters exceed at least 200 nm. Their fluorescence is described by curve (a) in Fig.1. Therefore, each calibration wafer must be examined, if its fluorescence signal shows a correct behavior . The term "correct" means, that the fluorescence intensity remains constant at incidence angles below the critical angle of total reflection, because otherwise the sample cannot be applied for calibration purposes. Fig. 2 displays the angular dependence of two ng-samples which are made for calbration. While one sample (Fig.2a) meets the requirements, the angular scan (Fig.2b) of another standard wafer sample reveals a frequently occurring anomaly associated with too small crystals.

2. the "spin-drying" technique

The second commercially available calibration method is done by the so called "spin-drying" technique [3]: a hydrophilic wafer surface is completely covered by a spiked solution which is allowed to interact chemically with the surface for about one minute. Thus chemical equilibrium is achieved between the metal atoms in the solution and those plated to the surface. One interesting feature of the method is the fact, that the electrochemical plated artificial contamination on the standard wafer simulates contamination from a realistic process, e.g. from wet chemical treatment. An additional advantage is the stability of the sample, which permits its repeated use for calibration.

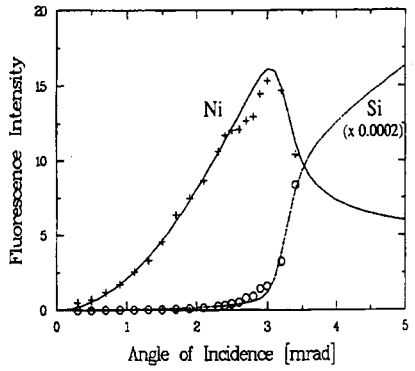

Fig. 3a

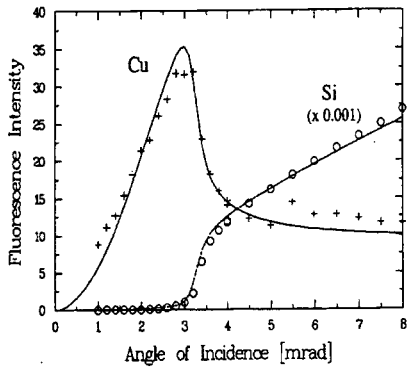

Fig. 3b

A shortcoming may be seen in the necessity to draw upon at least one further method for calibration in terms of absolute concentration such as N^+RBS or TXRF in connection with the ng-technique or VPD-AAS.

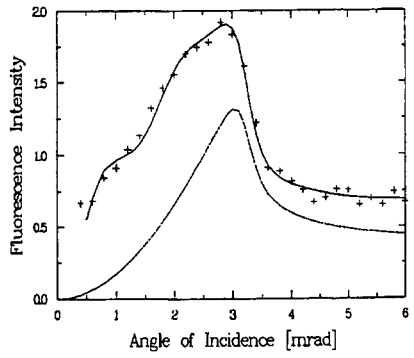

Fig.4

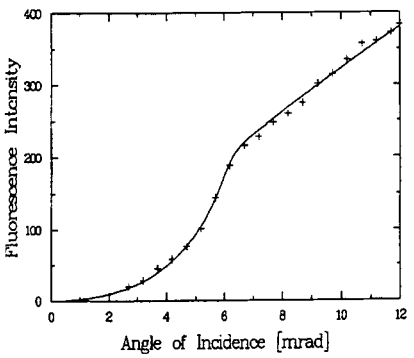

Fig.5

As part of this study commercial standard wafers, prepared after the spin-drying technique by two suppliers, were examined with respect to absolute area concentration (in atoms/cm^2). Additionally we checked their fluorescence intensity

as a function of the incident angle and compared the measured data with calculations based on the Fresnel theory [4,5] in order to detect potential deviations from the basic assumption that the metal atoms are electrochemically bound to the silicon surface. We looked at a Ni- (Fig. 3a) and a Cu-Wafer Fig 3b) specified with 1.1 x 10^{12} or 1.0 x 10^{13} atoms/cm^2 respectively from supplier A and we found 1.23 x 10^{12} or 1.0 4 x 10^{13} atoms/cm^2 respectively. In addition, it is shown in Fig. 3 a and b (symbols = measured data, solid lines = expected curve after model calculations) that the Fresnel equations for film-like contamination fit the measured data.

Less cause for satisfaction gave the examination of a further standard from supplier B which was specified with 5 x 10^{12} atoms/cm^2 . For this wafer we found 8.8 x 10^{12} atoms/cm^2 and an arrangement of the metal atoms which certainly is not film-like (Fig.4). The measured data were fitted by a model which is characterized by a particular mixture of distances of the analyte atoms to the interface. This result admit the conclusion, that the spin-drying procedure in this case was not correctly performed but lead to the development of isles of metal atoms on the silicon surface.

3. The "pure metal" technique

In view of the deficiencies of the "ng" as well as of the "spin drying" technique (instability and microcrystals for technique 1 and lack of absoluteness for technique 2) we favor a novel calibration method which is free of the above mentioned drawbacks. Due to the fact, that the Fresnel theory in combination with X-ray absorption and enhancement algorithm describes the fluorescence radiation from surfaces as a function of the incident angle perfectly it seems reasonable to measure an exactly defined surface, such as a polished 100%-metal surface and to compare the measured fluorescence count rates with the respective Fresnel calculation. In such a particular case of a pure metal surface all parameters (such as composition, density, depth profile) are well known.. The sensitivity of the used instrument is the only free parameter. Therefore the calibration factor can easily be obtained by a fit procedure. Fig.5 illustrates the pure metal calibration technique for Ni. The best fit to he measured fluorescence intensities yielded an instrumental calibration factor of 3.9 x 10^{-12} ((counts/s)/(atoms/cm^2)). Using the "ng-technique" (Fig.2a) the calibration factor was determined to be 4.1 x 10^{-12} ((counts/s)/(atoms/cm^2)) for the same instrument.

Conclusion

The "pure metal" - method was found to be the most reliable and robust absolute calibration technique for TXRF. Standard wafers which are obtained by the spin-drying technique remain useful as secondary standards but should be verified over the entire relevant angular range by the Fresnel model.

References

1 Iida, A.; Sakurai, K. and Gohshi, Y. Adv. X-Ray Anal. 31 (1988) 487

2 Eichinger, P.; Rath, H.J.; Schwenke, H. ASTM Spec. Tech. Publ. 990 (1989) 305

3 Hourai, M; Jap. J. Appl. Phys 27 (1988) 2361

4 de Boer, D.K.G. Phys. Rev. 44 B (1991) 498

5 Weisbrod, U.; Gutschke, R.; Knoth, J.; Schwenke, H. ; Appl. Phys. A53 (1991) 449

Transfer behavior of metallic contaminants from solutions to wafers

U. Keller, W. Aderhold and E.P. Burte

1. CLEANING PROCEDURES

Our investigations concerned with the transfer of trace metals in semiconductor-grade chemicals to wafer surfaces. The metals of interest were Na, Ca, Al, Cr, Fe, Co, Ni, Cu, Zn and Pb because their presence has a dramatic influence on DRAM yield in semiconductor manufacturing.
The extent of metal transmission was examined as a function of concentration in various chemicals. Thereby, also the influence of different matrices could be studied.
The cleaning solutions used were 1% HF, 4% choline with hydrogenperoxyde (cleaning performed at 70° C) and conc. sulfuric acid with hydrogenperoxyde (Caro acid, cleaning performed at 140° C).
At first all wafers were cleaned in Caro acid and rinsed in deionised water for 15 min.
The influence of the cleaning solutions with chemicals as delivered was studied by standard processing of the wafers. This means that they were immersed in choline at 70° C for 10 min and rinsed for 15 min in DI-water. Cleaning with HF lasted for 3 min, then again a 15 min rinse was performed. The procedure in Caro acid is the one mentioned above. After rinsing all wafers were dried in a spin-dryer at 600 r.p.m. for 3 min. The analysis of the wafer-surface was then carried out by VPD-ETV-ICP-MS. Not only the wafers but also the non-contaminated cleaning solutions were examined to get the true starting-point for our experiments.
The next step in our investigations was to add contaminants to the cleaning solutions so that the concentration of the above relevant elements was 4 ppb. Wafers were "cleaned" in these solutions. Furthermore, cleaning procedures were carried out with concentrations of 10, 25, 40 and 100 ppb of each metal in the cleaning solutions. For each experiment five wafers were used.

2. TRANSFER BEHAVIOR

With the help of the graphical diagrams the most critical elements are distinguished by two criterias. The first one is the intersection of the graph with the ordinate. This parameter is the gradient in linear scale and therefore describes the dimensions of metal transfer and sensitivity of wafers to metals. A high value means that even a small amount of concentration of this element in the solution causes a severe contamination of the wafer surface. The second criteria is the shape of the graph. In logarithmic scale straight lines with a gradient of 1 indicate a linear dependence of bath contamination and surface concentration of a contaminant. In this case, contamination of the wafer surface can much more easily be

reduced by using less contaminated chemicals than if the graph appears as a curve which shows saturation of a certain metal on the wafer surface. Saturation even at low metal concentrations in the cleaning solution means that the purity of the chemical has to be improved to a large extent to cause any decrease of contamination on the wafer surface at all.

2.1. Transfer of cationic contaminants in choline to the wafer surface

Due to this considerations the experiments with contaminated choline proof that up to 1 ppb metal concentration in the alkaline solution, the most critical elements are in this sequence Ni, Na, Fe, Ca, Cr and Co. In this low concentration range they all show a non-linear behavior with Ni at the top of the concentration levels. It has to be emphasized that these critical elements are those which can be removed by not-contaminated choline from the wafer surface to some extent. As mentioned above, even a dramatic reduction of those metals in the bath solution would cause only a small improvement of the wafer surface. Therefore the most successful way to diminish wafer contamination with respect to Ni, Na, Fe, Ca, Cr and Co is to develop a cleaning sequence which is processed before the choline procedure and which removes those metals more effectively than choline, so that the starting-point is more favorable to a cleaning process in choline solution.
At low metal concentrations in the bath solution the transfer behavior of Al, Zn and Pb is represented by a straight line with a gradient of 1, which indicates a linear dependence. Although the curves of Al and Zn show high concentrations on the wafer surface and high values of the interception with the ordinate at the starting-point, it should be easy to reduce these metals by use of purer chemicals. The graph for Pb is also a straight line and in addition to that the concentration at the beginning is low as well as the interception with the ordinate. Because of this behavior it is unlikely that Pb causes problems on a wafer surface. It should be mentioned that choline has no cleaning efficiency on Al, Zn and Pb, but tends to deposit these cations on the wafer surface.
In this low concentration range, the contamination values of Cu are below the detection limit (8.15×10^9 cm^{-2}).
Metal concentrations >1 ppb in the alkaline solution are no longer representative for a cleaning process in microelectronics, but a interesting subject of research on wafer surface reactivity.
The at first linear behavior of Al, Zn and Pb changes into a state of saturation where the gradient of the graph decreases and for Zn even a maximum of the curve can be seen between a bath concentration of 1 and 10 ppb. The phenomenon that the surface concentration of Zn decreases although the bath concentration increases has to be the result of a displacement mechanism. The same effect seems to take place with Na and Cr at bath concentrations >1 ppb whereat the concentration values on the surface go down until they are below the detection limits. On the other hand it is striking that the at first flat graphs of Co and Cu develop a linear dependence of metal concentration in the bath and on the wafer surface at higher concentration levels (1 respectively 33 ppb) in the bath. With Ni only a slight increase of the wafer surface concentration can be noticed until a

bath concentration of 100 ppb. Fe and Ca show a similar behavior so that the gradient of the flat curves at low bath concentration levels increases for metal contents >1 ppb but already changes into a saturation state for bath concentrations >10 ppb.
As a result it can be summarized that for a cleaning process in diluted choline it is most recommendable to reduce the starting concentration level of Ni, Na, Fe and Ca on the wafer surface by other cleaning procedures and to try to diminish the metal concentration of Al and Zn in the choline solution.
Our cation transfer studies at high metal concentrations in the choline bath show that the contaminants have a very different affinity to the wafer surface. Until bath concentrations of 10 ppb Al and Zn are obviously able to displace Na and Cr to a large extent on the wafer surface. On the other hand it seems as if Al and Zn were replaced at concetration levels exeeding 10 ppb by Co and Cu. Due to these mechanisms and the cleaning efficiency of choline, Fe and Ca are obviously hindered by this combination of elements in depositing on the wafer surface to a large extent.

2.2. Transfer of cationic contaminants in DHF to the wafer surface

The surface contamination levels for Ni were below the detection limit (Ni: $8x10^{10}$ cm^{-2}) for the whole concentration range.
At metal concentrations <1 ppb in DHF only the surface concentration values of Ca and Co were above the detection limits (Ca: $4,6x10^{10}$ cm^{-2}; Co: $1,1x10^{10}$ cm^{-2}). The graphs show a non-linear behavior in this concentration range, which means that the wafer surface is not very sensitive to the Ca and Co concentration levels of the solution. An improvement of the wafer surface was therefore only achievable by reducing Ca and Co by other cleaning procedures before the HF-dip.
The investigations at high metal concentrations in the DHF bath show straight lines with a gradient of 1 for Al, Co and Pb. Like the results of choline, a displacement mechanism obviously takes place. At bath concentrations > 33 ppb the surface concentration values for Na, Ca and Cr decrease until they are below the detection limits (Na: $1,3,6x10^{11}$ cm^{-2}; Cr: $5,75x10^{10}$ cm^{-2}). Fe, Cu and Zn show a small increase in surface concentration at metal levels >10 ppb in the solution, as if their deposition was hindered. Thus the behavior of this combination of contaminants in DHF is very similar to that in choline whereat the small differences should depend on the kind of solution used.
As a result one can say that the only problem in a DHF cleaning process is the starting point of the wafer contamination with respect to Ca and Co, which can hardly be influenced by the purity of HF.

2.3. Transfer of cationic contaminants in caro acid to the wafer surface

Independent on the volume concentration of the wet solution, the surface concentrations of Ca, Fe, Ni, Na and Cu were below the detection limits (Na: $1.4x10^{10}$ cm^{-2}; Ca: $2.3x10^{10}$ cm^{-2}). For solution concentration values lower than 4 ppb the surface concentration of Cr and Zn are also below the detection limits (Cr: $1,15x10^{11}$ cm^{-2}; Zn: $1,4x10^{10}$ cm^{-2}) as well as the values of the surface concentration of Co and Pb up to bath concentrations of 25 ppb (Co: $1,08x10^{10}$ cm^{-2}; Pb: $3,28x10^{8}$ cm^{-2}). Only Al, which has the highest concentration level over the whole concentration range is detectable on the wafer surface after a cleaning procedure in not-contaminated caro acid. A decrease of the surface contamination level after a caro acid cleaning process therefore aims at a reduction of the Al concentration. The use of a purer acid would not be very successful because of the shape of the graph at low bath concentrations. A flat line indicates, that the wafer surface is not very sensitive to the Al content of the caro acid and the only way to reduce the Al concentration on the surface is therefore another cleaning procedure before this process which effectively removes the Al contamination.
At concentration levels exeeding 10 ppb in the cleaning acid, the gradients of the flat lines increase and it can be supposed that they will reach the value 1 at higher metal concentration values in the acid. Thus a linear dependence of bath concentration and surface contamination probably develops at metal contents higher than 100 ppb in the solution.
The occurrence of a linear dependence only at high contamination levels in cleaning solutions was already noticed at the procedure with choline. This delayed contamination is due to the cleaning efficiency of the respective medium against the regarded elements.

3. DISCUSSION OF THE RESULTS

An explanation of the transfer behavior may be found if one looks on the experiments in an atomic scale.
In a diluted choline solution, there is an oxide layer present on the silicon surface. This layer with its partially negative and positive charged centers makes the surface polar and hydrophilic. The oxygen atoms which are more electronegative than the silicon atoms and, therefore, are slightly negative charged, tend to occupy positions where they have enough space, that means they are positioned mainly in direction to the wet solutions. Because of this spatial order, the whole wafer surface has a partially negative charge. This charged surface will attract cations according to their amount of charge following Coulomb´s law. Probably, this electrostatic attraction is much more effective with cations which do not form insoluble compounds, especially hydroxides, in alkaline, because these hydroxides are electrically neutral and, therefore, not sensitive to electromagnetic fields.
Because of these facts cations which do not form insoluble compounds should show a linear dependence of content in the solution and wafer surface concentration even at low concentration levels. In choline this is realized for Al^{3+}, Zn^{2+} and Pb^{2+}, whereat Al^{3+} as the highest charged cation has the most critical contamination level. All other investigated elements tend to build insoluble hydroxides

which are not strongly attracted by the wafer surface but precipitate on it if the volume concentration in the solution is high enough. The coherence of bath concentration and contamination level on the surface is not supposed to be a linear one. This effect is indicated in Fig.3.1.1 in the course of the graphs for Co, Ca and Fe. A further discussion of the displacement mechanism can be found in chapter 3.1.1. It should be emphasized that the cleaning efficiency of a medium depends on its ability of complexation, that means whether it precipitates ions or not. Not-contaminated choline is therefore a cleaning agent with respect to Na, Cr, Ni, Co, Cu, Ca, and Fe.

In diluted HF, the situation on the wafer surface changes. The oxide layer is removed and the bare silicon surface is no longer polar but hydrophobic. A small negative charge remains on the surface which provides a high concentration of protons in the closest neighborhood of the wafer. Obviuosly the highly mobile protons prevent metal cations to some extent to be adsorbed on the surface. This is revealed by the lower contamination levels of all investigated elements in comparison to choline. Furthermore, the removal of the oxide layer may be responsible for the improvement in cleanness to some extent. The most critical element in DHF was Ca. The surface contamination of which seems to saturate on the wafer surface if its volume concentration is about 10 - 40 ppb. This saturation phenomenon may be due to the precipitation of CaF_2. CaF_2 is suspected to precipitate on the wafer surface.

In Caro acid the situation on the wafer surface should be similar to that in the case of choline with the difference that in acid solutions protons are present, which are attracted by the partially negative charged polar surface. In our investigations, the measured values of the surface concentrations of the investigated elements are not influenced by cleaning or intentional contamination until a volume concentration of about 10 ppb in the solution is reached. Nevertheless, the only elements which could be detected on the wafer surface were those which do not form an insoluble sulphate in caro acid. This corresponds to the theory that cleaning efficiency is highest against elements which can be precipitated. At the present time it is not possible to draw final conclusions from these results, as several measured values are too close to the detection limits of the ETV-ICP-MS and the wafers used were not clean enough with respect to the initial Al surface contamination level.

REFERENCES

1. M. Olcer, H.J.Bühlmann, M. Ilegems, J. Electrochem. Soc. 133, (1986) 3.
2. R.J. Kriegler, Denki Kagaku 41, (1973), 466 ; R.S. Ronen and P. H. Robinson, J. Electrochem. Soc. 119.
3. K. Honda, T. Nakanishi, A. Ochsawa, N. Toyokura, Metal Impurities at the Si/SiO_2 Interface, Semicond. Mater. Conf. No. 78, Oxford (1987).
4. R. Takizawa, T. Nakanishi, A. Ohsawa, J. Appl. Phys. 62, (1987), 12.

LOW TEMPERATURE OXIDES DEPOSITED BY REMOTE PLASMA ENHANCED CVD

L-Å. Ragnarsson†, S. Bengtsson†, M.O. Andersson† and U. Södervall‡

A Remote Plasma Enhanced Chemical Vapor Deposition (RPECVD) process was used to prepare SiO_2/Si structures at ~300 °C. Best midgap interface trap densities, D_{itm}, as obtained by C-V techniques are for SiO_2/Si(100), 6 - $8 \cdot 10^{10}$ $cm^{-2}eV^{-1}$ and for SiO_2/Si(111) 2 - $3 \cdot 10^{11}$ $cm^{-2}eV^{-1}$.

1. INTRODUCTION

The continuing trend towards smaller thermal budgets call for alternatives to normal thermal oxidation of gate oxides. To achieve high quality thermal oxides, high temperatures (~900 °C) must be used. The RPECVD method has, during the last few years, been proven to be an important candidate for low temperature deposition of dielectrics. High quality SiO_2 has been deposited at temperatures below 300 °C. The process can also be used in plasma nitridation of oxides. A similar RPECVD process has been described by G. Lucovsky et. al. [1,2].

2. EXPERIMENT

2.1. Experimental setup

The system for RPECVD shown schematically in Figure 1, consists of a UHV deposition chamber with a separately pumped load-lock for convenient loading of 3" Si-wafers as well as small samples. The base pressure in the deposition chamber is approximately $3 \cdot 10^{-10}$ mbar after pumping and bakeout at 200 °C for 24 hours. During deposition a roots pump is used with a regulated gate valve, controlling the pressure. The plasma is excited at 13.56 MHz with the power adjustable within the range 10 to 600 W. Process gases used are high purity SiH_4 (2% in He), O_2, H_2, N_2, He, NH_3 and N_2O. To avoid cracking of the silane in the plasma it is injected through a gas ring positioned downstream between the sample holder and the plasma. The other gases are either fed through a similar second gas ring or the plasma tube. Installed equipment for in-situ analyses are a Reflection High Energy

†. Department of Solid State Electronics, Chalmers University of Technology
S - 412 96 Göteborg, Sweden, email: loke@ic.chalmers.se
‡. SIMS - Laboratory, Department of Physics, Chalmers University of Technology

Electron Diffraction (RHEED) unit which enables us to analyze the structure of the substrate surface and a Residual Gas Analyzer (RGA) to analyze chemical reactions and residual gases in the chamber before and during deposition.

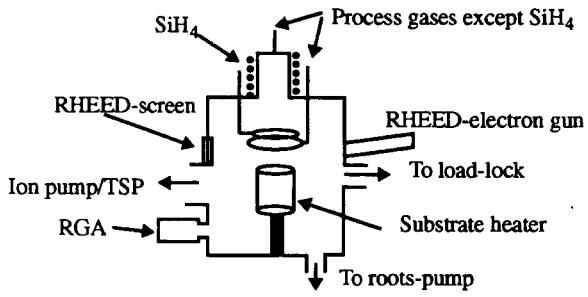

Figure 1. Schematic view of the RPECVD-system

2.2. Sample preparation

In this experiment we used <100> oriented 3" *n*-type silicon wafers with a substrate resistivity of 5.6 Ωcm. The wafer was cleaned using an RCA-clean with a final 30 s dip in diluted HF (1:50 HF:H_2O). After rinsing and drying, the wafer was loaded into the UHV-system. Considering that any surface contaminants would be incorporated *at* the interface, it is of great importance that they are removed before the oxide is deposited. This can be achieved by exposing the wafer to an oxygen plasma [2]. After the in-situ cleaning a SiO_2-film was deposited at ~300 °C at a pressure of 0.1 - 0.4 mbar. To form SiO_2, a mixture of He, O_2 and N_2 (flow ratio 15:1:1) with O_2 flow rate = 10 sccm was remotely excited with rf powers in the range 10 - 90 W. The SiH_4 (10 sccm of 2% SiH_4 in He) was injected downstream. For these conditions the deposition rate varies between 10 - 50 Å/minute. To form MOS-structures, aluminum gates were evaporated on the oxide and finally the samples were subjected to a PMA (Post Metalization Anneal) in N_2 at 425 °C for 15 min.

2.3. Measurements

2.3.1. Electrical characterization

A computerized system with a HP4284A LCR-meter was used to measure high-frequency (1 MHz) C-V curves. The quasi-static C-V curves were acquired using a setup with a Keithley 617 electrometer, a Keithley 220 current source and a HP3478 voltage meter. Measurements for two separate samples, RPMOS3#5 and RPMOS3#6 are shown in Figure 2 and Figure 3 together with extracted interface trap densities.

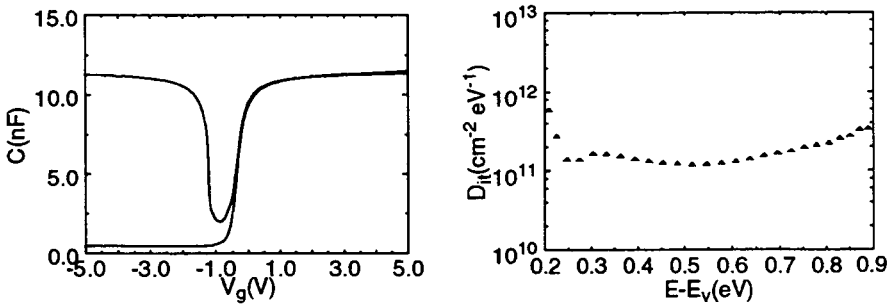

Figure 2. HF/QS-CV and extracted D_{it} for RPMOS3#5 (100)

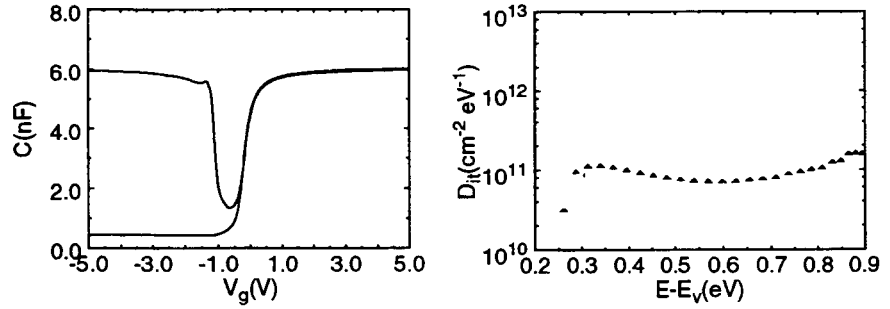

Figure 3. HF/QS-CV and extracted D_{it} for RPMOS3#6(100)

2.3.2. Ellipsometric characterization

Ellipsometry was used to measure the thickness and the refractive index of the samples. A Rudolph AutoEl-II was used at a wavelength of 632.8 nm. Thickness and refractive index are shown for the samples in Table 1.

Table 1. Thickness and refractive index of RPMOS3#5(100) and RPMOS3#6(100)

	n	t_{ox} (nm)
RPMOS3#5	1.475±0.045	13±1
RPMOS3#6	1.42±0.06	20±4

2.3.3. SIMS-analyses

A few of the samples were analysed using Secondary Ion Mass Spectroscopy (SIMS). The sample shown in Figure 4 was fabricated on <111> oriented *n*-type

silicon with a substrate resistivity of ~10 Ωcm. The midgap interface trap density extracted from the C-V measurements for this sample was $2 \cdot 10^{11}$ $cm^{-2}eV^{-1}$.

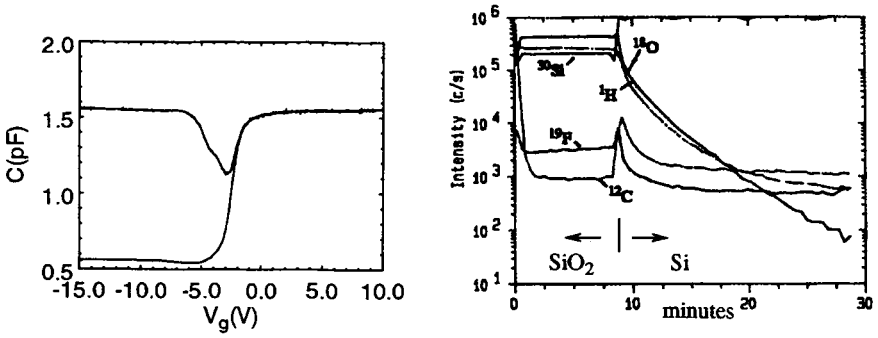

Figure 4. HF/QS C-V and SIMS-measurements for RPMOS2#6(111)

The SIMS depth profile show high concentrations of hydrogen in the as deposited oxides. There are strong indications [2], that the general quality can be improved by optimizing the process.

3. SUMMARY

We have used a Remote Plasma Enhanced CVD process to deposit SiO_2 with minimum D_{itm} in the range of 6 - $9 \cdot 10^{10}$ $cm^{-2}eV^{-1}$ and with physical parameters indicating it to be stoichiometric SiO_2. We find high concentrations of hydrogen in the as deposited oxides. The process needs to be further developed to produce films with enhanced quality.

4. ACKNOWLEDGEMENTS

This work was sponsored by a grant from the Swedish Research Council for Engineering Sciences, Teknikvetenskapliga Forskningsrådet (TFR) and from the National Board for Industrial and Technical Development, Närings och Teknikutvecklingsverket (NUTEK). We wish to thank G. Lucovsky, C. Björkman, G.G. Fountain, S. Banerjee and their groups for valuable discussions during the development of the system.

REFERENCES

1. G. Lucovsky, P.D Richard, D.V. Tsu, S.Y. Lin, and R.J. Markunas: J. Vac. Sci. Tehcnol. A4 (1986) 681

2. G. Lucovsky, Yi Ma, T. Yasuda, C. Silvestre and J.R. Hauser: Jpn. J. Appl. Phys. Part 1 No. 12B Vol. 31 (1992) 4387

H_2O MICROCONTAMINATION GENERATED BY REACTION BETWEEN ANHYDROUS HBr GAS AND TRANSITION METAL OXIDES

A. Boireau, H. Chevrel*, N. Uchida, K. Miyazaki, E. Ozawa, J.M. Friedt
Air Liquide Laboratories, 5-9-9 Tokodai, Tsukuba, Ibaraki 300-26 Japan

1. INTRODUCTION

HBr is an etchant of choice for semiconductor manufacturing technologies in the plasma etching of polysilicon. Due to its aggressive corrosive nature, it can react with the material of construction of the delivery system and generate contamination at the point of use. It has been widely accepted, that the degree of corrosion in metal tubing exposed to HBr is strongly related to the presence of moisture which forms an acidic solution with the gas and attacks the metallic surface. According to FTIR analysis in the gas phase, HBr contains only a very small amount of moisture (< 1 ppm)[1]. HBr gas itself does not introduce moisture into gas delivery system. The main moisture sources for corrosion will be insufficient initial dry down or improper cylinder exchange procedure[2]. The stainless steel surfaces are always covered by an oxide layer, mainly composed of Fe_2O_3, NiO, Cr_2O_3. Moisture might also be generated at temperatures above 200°C from the reactions between HBr and the metal oxide surfaces through the following mechanism: M_xO_y + zHBr -> M_xBr_z + nH_2O[3][4]. Several choices are available for the construction of an HBr gas line. Electropolished stainless steel SUS 316 L tubings are the more commonly used. For the critical parts, more corrosion resistant materials (i.e. hastelloy) have been incorporated. Recently, oxide base passivation has been proposed for usage in the gas distribution system for the wafer fab. e.g. for specific low moisture - surface interaction - oxide passivated (OP)[5] or improved corrosion resistance - chromium passivated (CrP)[6]-. Another source of contamination lies in the welding process where MnO_2 particles can be generated during welding and deposit around the welding bead. This MnO_2 layer is the most sensitive area to corrosion[7][8]. Modeling of the reactions between these surfaces and HBr was conducted by exposing HBr to oxide powders which were representative of the various surfaces, and unwelded or welded stainless steel tubes.

2. EXPERIMENTAL PROCEDURE

Pure or mixed metal oxides representative of the stainless steel surface composition were sintered in a furnace at 1100°C for 8 hours. The pellets were then shaped and set into removable Nupro stainless steel filters upstream the FTIR cell. Before exposure to HBr, the pellets were purged and dried in dry N_2 (1 slm), at 100°C for one night and were cooled down to room temperature. HBr was flown through the sample with a flow rate of 0.7 SLM and analyzed by FTIR for 2 hours. After the analysis, the whole system was purged with N_2 at 1 SLM and heated at 100 °C for 1 night. FTIR measurements were also performed for the first hour of the purge

*New address : Air Liquide Electronics Europe 164/166 Av. J. Kessel, 78960 Voisins le Bretonneux, France

procedure. 82 welds were performed on 4 m of two different kinds of 1/4" EP 316L stainless steel tubes: VOD-VAR (Mn: 2 wt%) and VIM-VAR (Mn: 0.05 wt%). Unwelded (OP and EP VOD-VAR) and the above welded tubes were set before the FTIR cell, dried down with N_2 (1 slm) at 80°C for 1 night and cooled down to room temperature. HBr was then sent into the tubes and kept for 5 days. After reconditioning of the surrounding lines, a continuous HBr flow was flown through the tubes and the resulting gas was analyzed by FTIR for 90 min. At the end, the tubes were purged with N_2 (1 slm) at 80°C for 1 night. Concerning the welded tubes, FTIR measurements were also performed for the first hour of the purge procedure. The reactivity of the metal oxides towards HBr was evaluated by different methods: difference of weight before and after HBr exposure, structure characterization by X-rays diffraction, bromine concentration after HBr exposure by EDAX and moisture generation during HBr exposure followed by FTIR.

3. RESULTS AND DISCUSSION

FTIR revealed no generation of moisture due to the exposure of Cr_2O_3 and NiO pellets to HBr even at 120°C for N_2 purge (Fig.1). No trace of reaction was detected with the different characterization methods.

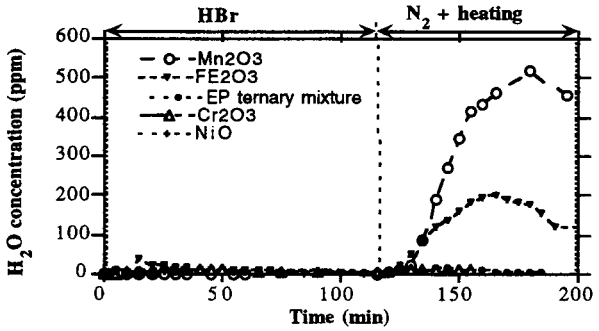

Figure 1: Moisture concentration in HBr gas phase during HBr exposure of metal oxide powder

Fe_2O_3 and Mn_2O_3 pellets reacted with HBr and generated H_2O (Fig.1). During the consecutive N_2 purge at 120°C the concentration of moisture increased up to 200 ppm and 500 ppm respectively. After one night of N_2 purge and opening of the cell, both pellets exhibited a color change before HBr exposure and after HBr exposure and a weight increase (Table I). MBr_2 (M = Fe, Mn) was observed at the

Table I: Mass gain and Br concentration in the pellets after exposure to HBr

Oxides	Fe_2O_3	Cr_2O_3	NiO	Fe-Cr-Ni-O (EP)	Mn_2O_3
Δm	+ 22%	0	0	0	+ 8%
EDAX (Br%)	66%	< D.L.	1.7 %	2.6 %	66 %

surface of the pellets by EDAX measurements. X-rays diffraction revealed after grinding of the pellets that Fe_2O_3 exhibited no change of structure of the bulk while

Mn_2O_3 changed to $MnBr_2,4H_2O$. The resulting powders were deliquescent. During N_2 purge at 120°C, a lot of moisture is released in the gas phase. During HBr exposure, MBr_2 is formed first and then (MBr_2,xH_2O (x=0-6)). The release of moisture during heating is attributed to the dehydration of the hydrate. An additional experiment was conducted with two pellets: HBr passing through them was bubbled in DI water during 30 min. A slight yellow coloration appeared in the solution was attributed to a generation of Br_2.

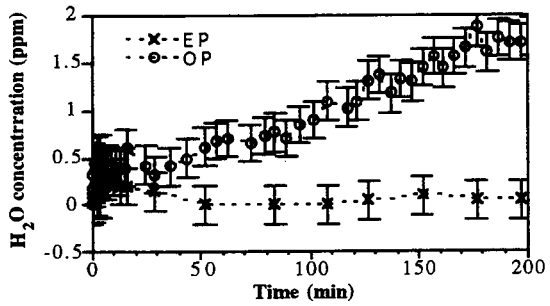

Figure 2: Moisture concentration in HBr gas passing through EP and OP tube

From the above results and in agreement with the literature[3], the reaction mechanism can be described as follows:

During HBr exposure: $M_2O_3 + 6\ HBr \rightarrow 2MBr_2 + 3H_2O + Br_2$

$MBr_2 + xH_2O \rightarrow MBr_2,xH_2O$

During drying down at 120°C under dry N_2:

$MBr_2,xH_2O \rightarrow MBr_2 + xH_2O$

The reaction between HBr and Mn_2O_3 is stronger than the one with Fe_2O_3 (higher generation of H_2O, stronger yellow coloration of DI solution, higher enthalpy of reaction (ΔH^o = -49 KCal/mol instead of -25 KCal/mol, total reaction). In order to obtain models of the tube's surface, Fe_2O_3, Cr_2O_3 and NiO were mixed at various ratios and sintered. Among the resulting phases Xray diffraction revealed $(Fe_{0.6}Cr_{0.4})_2O_3$ and NiO and $NiFe_2O_4$ at an impurity level. When exposed to HBr no reaction was observed (Fig. 3). Chromium may have a stabilizing effect in Fe_2O_3 structure. From these powder experiments, it can be assumed that EP hastelloy surface, composed of nickel and chromium oxides and CrP surface, composed of Cr_2O_3 will be inert toward HBr gas. Surfaces with Fe_2O_3 or Mn_2O_3 will react with HBr to generate moisture. Similarly to the Fe_2O_3 powder, the OP tubing which consists of a 225 Å thick iron oxide surface reacted with HBr and generated moisture (Fig. 2). For the EP 316 L stainless steel tubing, no moisture was detected during 2 hours exposure to HBr (Fig. 2). This is assigned to the high chromium content in the passivation layer. Only a limited quantity of H_2O is released during HBr exposure, by the welded VOD-VAR tube and the by the welded VIM-VAR tube (0.4 (1) and 0.26 (10) ppm repectively after 90 min). However, during the begining of the N_2 purge, no evolution of the moisture concentration was observed for the welded VIM-VAR tube when the temperature increased, whereas for the welded VOD-VAR tube, the moisture concentration increased (Fig. 3). This behavior is attributed to the reaction between HBr and the MnO_2 layer resulting from the welding of the VOD-VAR tubing.

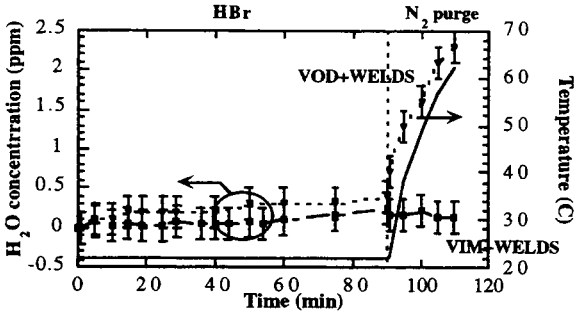

Figure 3: Comparison of the moisture generation between welded VIM-VAR and VOD-VAR tube exposed to HBr and then purged and heated with N_2.

The generated moisture forms locally an acidic solution with HBr which deteriorates the stainless steel surface. This phenomenon can explain the sensitization of the downstream of the welding bead in conventional stainless steel and thus the better properties of VIM-VAR.

4. CONCLUSION

Exposure of stainless steel surface to corrosive gas may result in moisture generation at room temperature depending on the surface oxide layer. NiO and Cr_2O_3 are resistant to HBr exposure while Fe_2O_3 and Mn_2O_3 react with HBr to generate moisture. For corrosive ESG gas distribution system, special attention should be taken on the material selection: the presence of Fe_2O_3 and Mn_2O_3 must be avoided or minimized. From an economical point of view, low Mn stainless steel and Chromium oxide rich EP tubings must be used. Otherwise, Both CrP and hastelloy are available.

REFERENCES

(1) K. Miyazaki and T. Kimura; Bull. Chem. Soc. Jpn. 66 n°1 (1993) 3508.
(2) M. George, D. Bohling, W. Bailey and T. Del Prado; Semiconductor International July (1993) 98.
(3) J.D. Christian and N.W. Gregory; The Journal of Physical Chemistry 71 n°6 (1967) 1583.
(4) Gmelin Handbook of Inorganic and Organometallic Chemistry: "Bromine" supplement; B1, (1990) 371.
(5) H. Tomari, H. Hamada, Y. Nakahara, K. Sugiyama and T. Ohmi; Solid state technology, February (1991).
(6) T. Kojima, S. Takahashi, S. Miyoshi and T. Ohmi; U.C.S. proceeding December (1993) 206.
(7) M. Morin, S. Miyoshi, K. Kawada and T. Ohmi; "Ultraclean Welding for High Grade Gas handling Technology.", in ElectroChem. Soc,. Meeting, Hawai (1993).
(8) T. Hattori, H. Takagi, H. Chevrel, E. Ozawa and J. M. Friedt; Japanese Journal of Applied Physics, To appear in April (1994).

U.V. ACTIVATED CLEANING USING NO, HCl AND NO/HCl

C.Elsmore *, R.Gluck, P.Carr #, M.Meuris, P.W.Mertens & M.M.Heyns.

IMEC, Kapeldreef 75, Leuven, Belgium.
* BOC Gases at IMEC.
# BOC Ltd., 10 Priestley Road, The Priestley Centre, Surrey Research Park, Guildford, Surrey, GU2 5XY. England.

ABSTRACT

This paper demonstrates a dry cleaning method for the removal of metallic contamination from Si <100> surfaces using U.V. activated HCl gas mixtures at reduced pressure and low temperature. The cluster tool compatible clean consists of a one minute exposure of gas to the wafer surface at 100 Torr and approximately 200°C and is shown to be sufficient at removing several metal contaminants at high efficiencies. The data also shows the benefits of increased temperature especially for the removal of high levels of contamination. High background levels of some metals present in the data illustrate the need for good vacuum practice and careful material selection for the system . Silicon roughening is shown not to be a problem and particle levels are manageable.

INTRODUCTION

The vapour phase cleaning of silicon has received increasing attention over the last decade due to heightened awareness of environmental concerns and the problems of using "wet" cleaning methods with cluster tools. As device size continues to shrink, gases may offer a solution to the low particle levels needed and decreased level of silicon surface contamination, without having the surface tension limitations of liquid processes. The goals of the IMEC dry cleaning program are to establish, wherever suitable, dry cleaning substitutes for wet process steps, with equal or improved efficiency. The SC-1 step (NH_4OH:H_2O_2:H_2O) can be replaced with gaseous U.V./Ozone treatment with the metals removal stage in the SC-2 step (HCl:H_2O_2:H_2O) being substituted by reactive gas chemistry. Removal of metallic contaminants by gaseous reagents (HCl, NO and NO/HCl) at relatively high temperatures and atmospheric pressure [1] was initially investigated, although high temperatures may induce diffusion into the bulk. More recent work has involved the use of Cl_2 [2-6] or HCl [7,8] at reduced pressure and/or temperature. The use of U.V.[2-6] or R.F. afterglow [8] to create excited gases which enhance surface cleaning has been reported. Apparatus specifically designed for vapour cleaning has been developed with the capability to interface with process modules in a cluster configuration [9,10].

1. DRY CLEANING APPARATUS

The SubMicron Systems (SMS) vapour phase cleaning tool (PRIMAXX) was used, with a schematic as shown in figure 1. The silicon wafer is suspended on alumina pins in an alumina reactor, and is rotated during processing using a magnetically levitated spindle. Sapphire diffuser plates ensure adequate gas distribution and a sapphire window above the wafer allows wafer heating with halogen lamps and U.V. activation of the gases from external sources. Irradiation is normal to the wafer surface while process ambient is directed parallel to the surface.

The system pressure, gas flows, wafer temperature, U.V. activation and process time are independently controlled using a dedicated computer and custom software. Stainless steel components, electropolished where possible and Ni-coated near the reactor, are used for the gas supplies and vacuum connections. Wafers are loaded and unloaded from the system using an evacuated load lock equipped with a wafer manipulator.

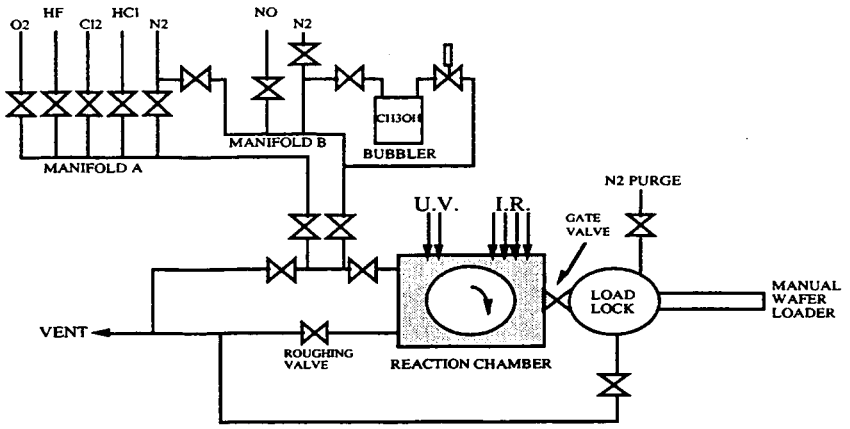

Figure 1 . Simplified Dry Cleaning Tool Schematic

2. EXPERIMENTAL TECHNIQUES

Experiments were carried out on <100> oriented wafers which were contaminated with metals ranging from $5x10^{11}$ to $3x10^{13}$ atoms/cm^2 by exposure to spiked SC-1 or HF dips. Samples contaminated by Fe evaporation and photo-resist ash were also evaluated. Elemental doping levels and cleaning efficiencies were characterised by Total-reflectance X-Ray Fluorescence measurements (TXRF - Atomika 8010), pre-treated by the HF vapour decomposition and droplet surface etch technique [11] (VPD-DSE). This method provides detection sensitivity to 10^9 atoms/cm^2. Particulate levels were monitored in the range 0.12-1.5 µm latex-sphere-equivalents using a CENSOR ANS100 light scattering particle counter. A standard cleaning sequence involved a pre-heat step, followed by a 60 second exposure of U.V. activated reactive gas mixture at 1 litre/min., 100 Torr and 200°C. A nitrogen purge completes the cycle.

3. RESULTS AND DISCUSSION

Table 1 shows the comparison of the three main gas processes evaluated at 200°C and it can be clearly seen from the poor removal efficiencies achieved, that the NO process alone is not suitable for metallic removal. All the processes showed changeable removal levels of Ca which was due to a background Ca contamination problem, in the order of 1 x 10^{11}-10^{12} atoms/cm^2, and possible environmental contamination. Overall removal of metallic contamination in the ionic and metallic form is excellent for both HCl processes. In all processes extremely low removal efficiencies were obtained when U.V. was not used (<5%). The high standard deviations (σ) can be explained by a number of factors. Large variations were seen in contamination levels due to the inherent characteristics of the spiking process, and back-diffusion of contamination from the vacuum system was also experienced along with possible o-ring degradation.

Table 1. Removal Efficiencies at 200°C (%)

		Max. Removal (%)	Min. Removal (%)	σ	**Average Removal (%)**
HCl	Ca++	67.5	-11.9	34.7	**17.7**
	Cu(m)	95.6	28.3	29.3	**70.0**
	Cu++	99.3	93.1	2.8	**97.3**
	Fe+++	99.0	72.4	13.6	**81.0**
	Fe(m)	87.2	72.4	8.0	**78.0**
NO/HCl	Ca++	73.5	-165.1	103.7	**18.4**
	Cu(m)	95.6	89.2	2.7	**91.8**
	Cu++	87.0	87.0	0.0	**87.0**
	Fe+++	99.0	99.0	0.0	**99.0**
	Fe(m)	17.0	-6.3	11.9	**6.6**
NO	Ca++	75.8	-28.0	40.8	**13.1**
	Cu(m)	77.3	17.8	42.1	**47.6**
	Cu++	-24.3	-142.4	61.0	**-76.5**
	Fe+++	-5.3	-13.5	4.4	**-9.6**

Figure 2 shows an increase in removal efficiency for HCl processes when the process temperature is increased to 240°C. Higher temperatures could not be tried due to system limitations. To gain an understanding on how the processes perform on a wider spectrum of contamination and to see the effects of a different contamination medium, ashed photo-resist (APR) samples were processed. Table 2 shows the levels of several well known contaminants found in APR before and after cleaning. Due to hardware problems NO/HCl could not be compared. The data shown, suggests that with further work, the HCl process can be used to remove contaminants in APR to acceptable levels. Furthermore, the data supports the conclusion that increased temperature enhances metallic removal.

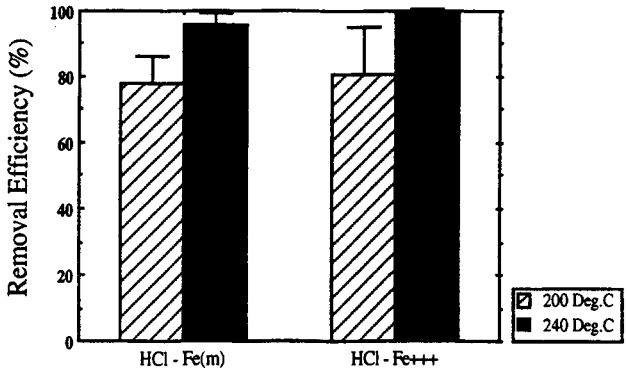

Figure 2. Removal efficiency at elevated temperature for HCl process

Table 2. HCl and NO Removal Efficiency Using Ashed Photo-Resist

	Ca	Fe	Ni	Cu	Zn	Cr	Pb
Initial Contamination (1)	5.8	31.4	1	121.7	123.3	76.7	5.4
Typical Background (1,2)	8.9	14.6	2.1	6.2	3.5	4.3	d/l
Removal with HCl @ 200C (%)	++	+	++	93.7	95.1	44.4	98.1
Removal with HCl @ 240C (%)	+	18.5	+	97	97.6	91.7	98.1
Removal with NO @ 200C (%)	++	++	++	28.8	23.9	+	69.1
Removal with NO @ 240C (%)	++	+	++	51.2	57.8	10.2	75.9

1) Contamination and background levels shown as atoms/cm^2 x 10^{10}
2) Background levels taken from RCA cleaned wafers treated with HCl, NO or NO/HCl process.
+ Indicates addition >1x10^{10}, ++ indicates addition >1x10^{11}

Although Ca and Fe removals were high in Table 1 at higher levels of initial contamination, at lower initial levels, additions are seen due to the high background levels of Ca, Fe and Ni. Despite the large noise levels, high removal efficiencies were obtained on Cu, Zn, Cr and Pb indicating that cleaning should not be a problem once the noise levels are controlled. We deduct that back-diffusion from the vacuum system and reactor background contamination levels are the causes of additions and we are currently investigating this problem.

Using standard processing conditions low haze and light particle defect (LPD) addition on blank monitor wafers indicate that silicon etching seems not to occur. Atomic Force Microscopy (AFM) data supports these findings; Spectral Power Density (RMS) values in Table 3 show no significant difference between processes. Particle data from all processes taken during the same period shows particle addition not to be a problem and removals are shown in a number of processes, namely APR. As a reference a Cl_2 standard process is also shown with the large increase of the haze and severe LPD additions in the range of 0.12-0.30 μm, indicating etching and roughening of the silicon surface for these process conditions. Particle additions to the reactor due to back-streaming from the vacuum line contaminants during load-lock pump downs were eliminated by closure of the roughing valve during wafer loading, and high-flow, gas line purges.

Table 3. Particle Conditions and Surface Roughening

Process	Haze Before (ppm)	Haze Inc. (ppm)	Spectral Power Density (nm)	Particle Removal 0.12 - 0.15μ (diameter (LSE))	0.15 - 0.30μ (diameter (LSE))	0.30 - 1.50μ (diameter (LSE))
HCl	0.100	0.001	0.088	-78 ± 163	-804 ± 308	-1267 ± 1345
NO	0.080	0.000	0.065	85 ± 167	-389 ± 688	-88 ± 999
NO/HCl	0.059	0.000	0.064	-21 ± 27	-29 ± 41	-1 ± 6
Cl_2	0.054	0.114	n/a	1252 ± 2191	69.25 ± 1053	-38.3 ± 127.8

4. CONCLUSIONS

It is expected that the halogen mixtures form metal chlorides which are sufficiently volatile, at the reduced pressures used in the system, to allow removal of the contaminants. The NO/HCl mixtures form nitrosyl compounds which have also been shown to be highly volatile [1].

Generally, HCl is emerging as an efficient process for removing major metal contaminants, with the benefit of being a single gas process. Higher temperature increases the removal efficiency with all the processes tested and cleaning efficiency should be improved further by increasing the temperature above the present system limit of 240°C. Since much of the ionic contamination lost was contained within chemical oxides as opposed to being on the wafer surface, this shows that the cleaning species can diffuse into these layers, react with the metallic cations and form volatile species which can be out-diffused.

The variable background levels evident in some of our data, and more prominently so in the APR, indicate the need for careful material selection and good vacuum practice. Where possible, Ni-coated pipework should be used, even in the vacuum system, to avoid back-diffusion of corrosion products, with all o-rings being metal and pigment free.

Low LPD counts indicate that particle contamination is manageable providing careful vacuum practice is observed. Silicon roughening is shown not to be a problem with the processes proposed in the paper.

References

1. R.M. Gluck, ECS Mtg. ext. abstract 510, Vol 91-2, 1991, p. 759
2. T. Ito et al, in Proceedings of the First International Symposium on Cleaning Technology in Semiconductor Device Manufacturing, Proceedings Volume 90-9, The Electrochemical Society Inc., Pennington, N.J. 1989, pp. 114-120
3. Y. Sato et al, Extended abstracts of the 22nd Conference on Solid State Devices and Materials, Sendai, 1990, pp. 1103-1106
4. S. Watanabe et al, Jap. J. of Applied Physics, Vol .28, No. 10, 1989, pp. 2167-2171
5. R. Sugino et al, ECS Mtg. ext. abstract 512, Vol. 91-2, 1991, p. 762
6. H. Fukuda, U.S. Patent 4,871,416, October 3, 1989
7. Y. Limb et al, ECS Mtg. ext. abstract 339, Vol. 93-2, 1993, p. 555
8. J. Ruzyllo et al, J. Electrochem. Soc. Vol. 136, 1989, pp. 1471-1476
9. R. Grant, U.S. Patent 5,228,206, July 20, 1993
10. B.E. Deal et al, in Proceedings of the First International Symposium on Cleaning Technology Semiconductor Device Manufacturing, Proceedings Volume 90-9, The Electrochemical Society Inc., Pennington, N.J., 1989 pp. 121-128
11. P. Eichinger, "Total reflection X-ray fluorescence analysis (TXRF) for contamination monitoring", in Proceedings of the Satellite Symposium to ESSERDIC (BERLIN), PV90-11, The Electrochemical Society Proceedings Series, 1991, pp. 227-237

Acknowledgements

The authors are grateful to Pieter Boelen, Karine Kenis and Geert Doumen for their experimental help and to Elie Andre and Frederick Chollet of CNET, Grenoble for their assistance with the AFM measurements.

THE INFLUENCE OF DIFFERENT SI (100) SURFACE CLEANING PROCEDURES ON RESIDUAL CONTAMINATION AND SOME ELECTRICAL PROPERTIES

K. Blum, G. Lippert, R. Sorge, D. Krüger and K. Höppner
Institut of Semiconductor Physics, PO 409, 15204 Frankfurt(Oder), Germany

1. INTRODUCTION

In spite of some accepted standard cleaning procedures (RCA, Shirarki, Pirania) every advanced silicon device technology requires a specific optimization of removing impurities at the surface. The RCA-cleaning procedure, for example, has been is optimized for application prior deposition of the cleaned wafer by chemical vapor deposition (CVD), oxidation and photolithography. Touchstones to judge the quality of cleaning are the density of particles at the surfaces, the content of contamination , the electrical properties of the oxid- semiconductor interface and the activ device regions and the silicon surface roughness. Different procedures comparing to our standard cleaning treatment (RCA/1/) were tested.

2. EXPERIMENTAL

The total organic content (TOC) of the used deionized water (DI) was lower than 5 ppb and the resistivity to p > 18,0 M Ωcm. In Fig. 1 you can see our TOC-reduction equipment for deionized water (DI). The equipment consists of two UV-lamps (254 nm and 185 nm), pure water mixed bad polisher with carbon filter and p.o.u. filtration.

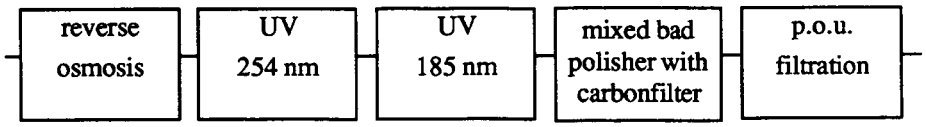

Fig. 1 : Design of TOC-reduction equipment

The SC1- step was assisted by megasonic (M), with a frequency at 750 kHz/1,25 MHz and a power at 300 W. Drying was done by rinse drying with DI-water and hot nitrogen.
Fluorine hydrid acid (HF)-treatments were placed in various sequences to standard clean (SC1, SC2).

2.1. DETERMINATION OF ELECTRICAL PROPERTIES

The determination of electrical properties of the semiconductor interface and active device region with the douple sweep HF-CV- technique is a process monitoring tool for MOS technologies (Fig. 2 a,b,c).

Non equilibrium HF CV curves recorded as a fast forward sweep (index f) from accumulation towards depletion and a slower backward sweep (index b) from deep depletion towards accumulation with a constand voltage ramp rate R enable the extraction of diverse MOS parameters. The data aquisition time is efficiently reduced in comparision with the separate application of the usual equlibrium single CV techniques. Corona charging protects from building up a permanent inversion edge layers when p-substrates are to be investigated. A mercury probe enables measurements directly after oxidation.

Extracted parameters:

- density of fixed oxide charge in midgap

$$N_f = \frac{C_{ox} \cdot (V_{mg} - \Phi_{MS/q})}{q}$$

- integral density of trapped interface charge between flatband and midgap

$$\overline{D}_{it} = \frac{C_{ox} \cdot \Delta V_g}{A \cdot q \cdot kT \cdot 1n(N/ni)}$$

- generation current

$$I_{gen} = C_{ox} \cdot \frac{1 - \frac{dC/dV_f}{dC/dV_b}}{\frac{1}{R_f} + \frac{1}{R_b} \cdot \frac{dC/dV_f}{dC/dV_b}}$$

generation lifetime from the slope of I_{gen} (X_g) curve surface generation velocity from extrapolated intercept at $X_g = 0$

- deep depletion CV slope in inversion region for doping profile determination

$$\frac{dC}{dV_d} = \frac{\frac{dC}{dV_b} + \frac{R_f}{R_b}\frac{dC}{dV_f}}{\frac{R_f}{R_b} + 1}$$

- slow term impact during the measurement

$$\overline{N}_{ot} = \frac{C_{ox} \cdot (V_f - V_b)}{q}$$

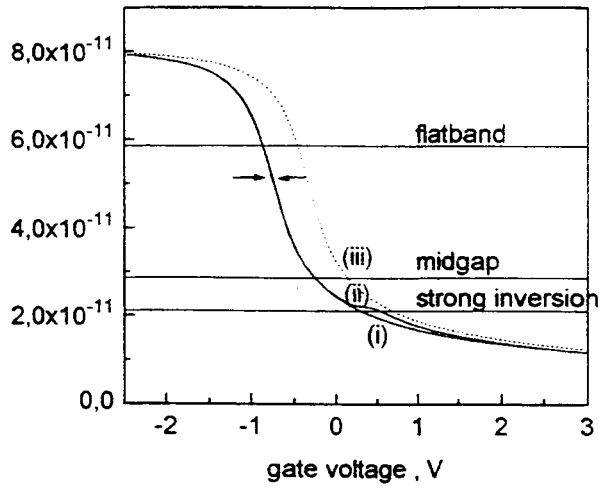

Fig. 2a: double sweep HF-CV-technique
(i) forward sweep
(ii) backward sweep
(iii) theoretical deep depletion curve

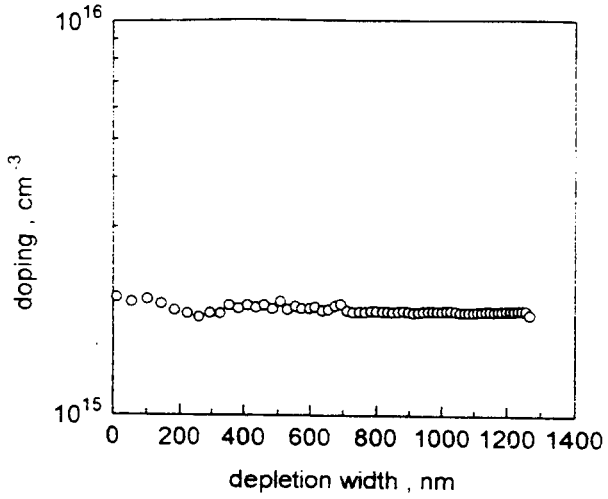

Fig. 2b: extracted doping profile with generation impact correction

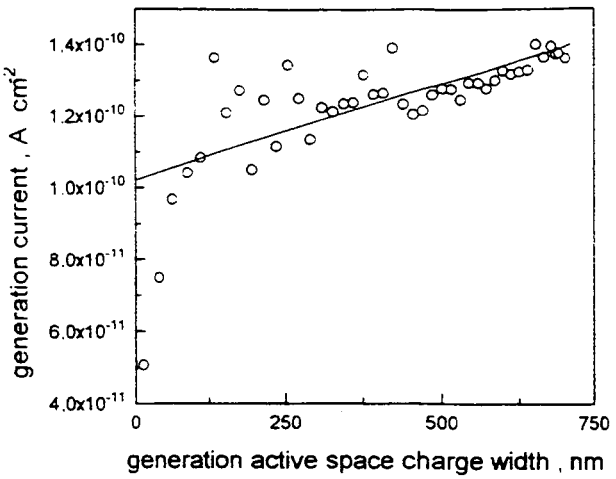

Fig. 2c: depth dependent generation current extracted from the forward and backward HF CV sweep in non equilibrium non steady state

2.2. AES AND SIMS MEASUREMENTS

AES and SIMS measurements were performed to characterize the contamination level. The SIMS experiments reported here were carried out with mass-filtered Cs^+- and O^--ions at 5 keV and 15 keV on encapsulated with amorphous silicon or silicon oxide samples. Oxygen, carbon and boron contaminations were measured quantitatively using reference samples with shallow implantations.

3. RESULTS

Figure 3 (dotted line) shows an unexpected majority carrier profile measured with HF-CV before optimization of the RCA cleaning procedure. A SIMS profile of boron concentration is also shown in Fig.3 (solid line).A good correlation between HF-CV profiling revealing high acceptor concentrations near the gate oxide-silicon interface and the SIMS boron depth profiling was obtained.

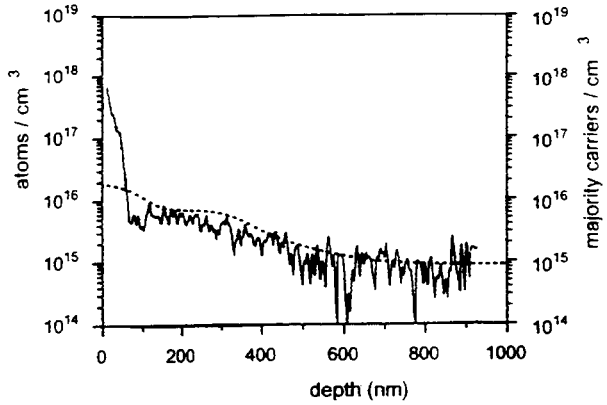

Fig. 3: Majority carrierer profile and boron SIMS profile after HCL-oxydation

Also we can see in Fig. 4 a SIMS profile of boron concentration with 10^{18} cm^{-3} in a Si-MBE probe after the cleaning steps SC1 and SC2 without fluorine hydrid acid treatments.
A reduction of boron at the surface of the treated wafer is achieved, if the HF-step is placed between SC1 and SC2. The result we see in Fig.5.The SIMS profile shows a boron concentration of 2 x 10^{17} cm^{-3}.

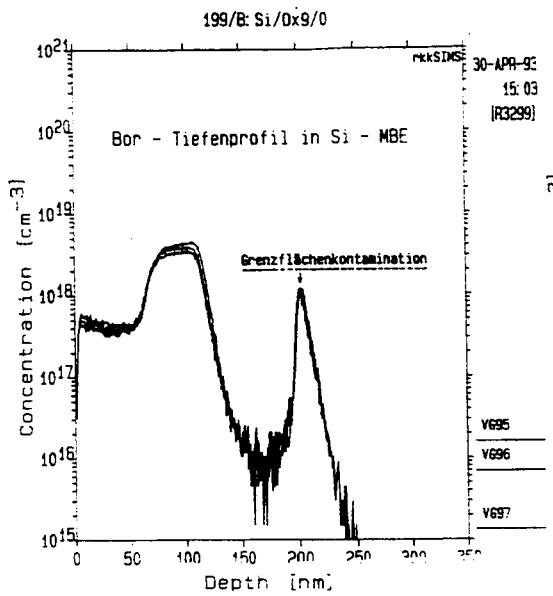

Fig.4: SIMS-profile of boron concentration

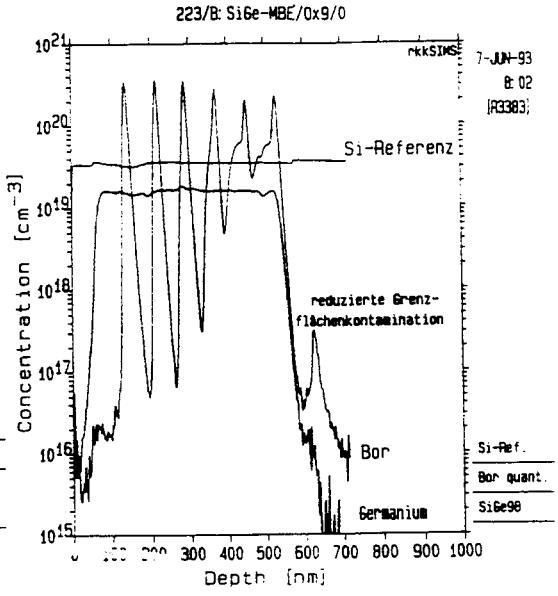

Fig. 5: SIMS-profil of boron concentration after optimisation of cleaning

Our modified RCA-procedure reduced significantly the surface density of boron but also of oxygen, chlorine, sodium and calcium. However an increased content of carbon and fluorine was detectable by SIMS.
The megasonic assistance (M) of the SC1-procedure decreased the density of particles at the surface of cleaned (100) Si-wafer and improved the interfaces of gateoxide regarding to the density of fixed oxidecharge per cm^2 (N_f), the density of interface trapped charge (D_{it}) and generation lifetime in the semiconductor bulk (τ) (Tab. 1).

Table 1: Properties of oxide interfaces after various cleaning procedures (electrical and SIMS measurements)

variant	particle density(>200nm)	Nf [10^{11}eVcm^{-2}]	Dit [10^{10}eVcm^{-2}]	τ [ms]	boron [10^{18}cm^{-3}]	carbon [10^{18}cm^{-3}]
SC1/SC2	34	3,1	8	1.100	7	1
SC1(M)/SC2	6	2,7	2,6	2.600	1	5
SC1(M)/SC2/HF		2,2	2,9	2.500	3	1,5
HF/SC1(M)/SC2	4	2	5	1.300	1	-
SC1(M)/HF/SC2	11	2,8	3,9	2.300	0,35	5

The characterisation of the Si-surface roughness after cleaning procedures were taken with Atomic Force Microscopy (AFM). Figure 6 shows the RMS-parameter (Standard deviation of the z-values). After SC1-cleaning we observe an increase of the Si-surface roughness with longer treatment. This results are the beginning of systematic research of roughness with AFM to make a contribution about the mechanism of Si-etching during RCA-cleaning.

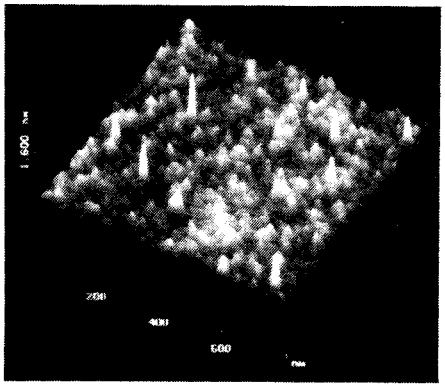

Fig. 6a: RMS = 0,07 nm of a non cleaned Si-wafer

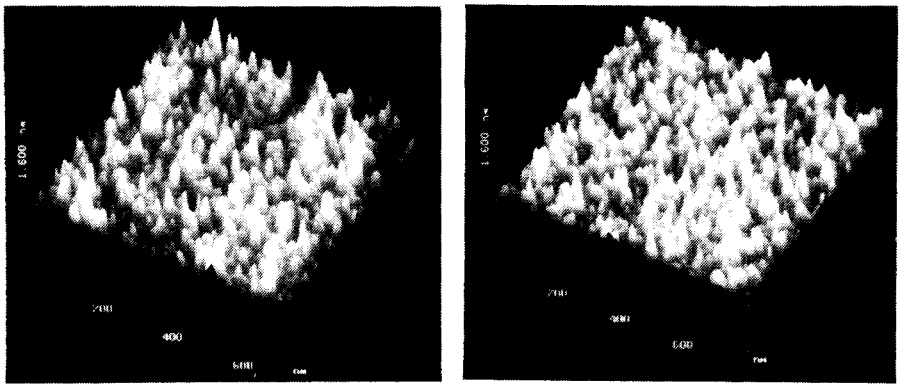

Fig. 6b: RMS = 0,14 nm of a SC1-cleaned Si-wafer 20 minutes-treatment
Fig. 6c: RMS = 0,11 nm of a SC1-cleaned Si-wafer 10 minutes-treatment

4. CONCLUSION

The best particle densities yield the SC1 cleaning with megasonics but the electrical properties will be better after SC1 and SC2 cleaning.
Flourine hydride acid treatment between SC1 and SC2 reduced boron and other impurities at the surface and is developed for sensitiv techniques as MBE-deposition /2/.
The HF-treatment , placed at the end of the procedure to minimize the thickness of the finished oxide is a variant for an application prior to the deposition of polycristalline silicon layers, thin oxides or metalliziation.

5. REFERENCES

/1/ W. Kern, J. Electrochem. Soc., 137 (1990), 6, pp. 1887
/2/ H.P. Zeindl, G. Lippert, J. Drews, R. Kurps and H.J. Osten; Solid State Phenomena Vol. 32-33 (1993), p. 11

MOS GENERATION LIFETIME FOR MEASURING METAL CONTAMINATION IN SILICON

D. Walz, J.P. Joly, F. Tardif

LETI DMEL (CEA Technologies Avancées) 17 Rue des Martyrs
F38054 Grenoble Cedex 9 France

ABSTRACT

The influence of iron and nickel contamination on MOS-generation lifetime has been studied. Ni has a strong tendency to precipitate on the wafer surface if no efficient internal gettering treatment has been done before contamination [1]. We found a good correlation between the gettering treatment on wafers intentionally contaminated with Ni and the MOS generation lifetime. We show further that sensitivity of MOS generation lifetime on deep levels associated with iron contamination can be completely screened by lateral surface generation. We propose a differential measurement method based on FeB decomposition [2] to enhance the sensitivity of MOS generation lifetime to iron contamination in p-type Si.

1. INTRODUCTION

The MOS generation rate is generally considered to be a useful indicator of metallic contamination such as Iron [3] and of defect formation in the Silicon device area. Nevertheless the process factors during device fabrication affecting the total generation rate of a MOS capacitor are poorly documented in the literature. The different contributions to the total generation rate which is measured is given according to [4] in figure 1. Among this contributions g_2 and g_3 depend on the space charge region width W whereas all other terms are independent of W.

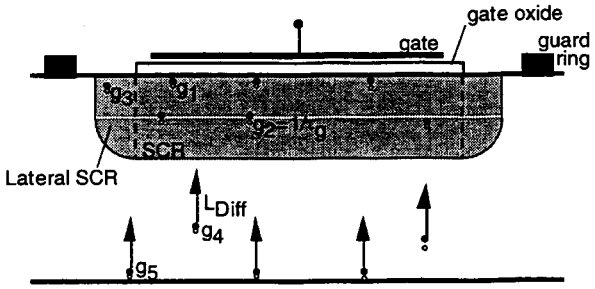

Figure 1: The contributions to the carrier generation in a simple MOS structure: surface space charge region (SCR) generation under the gate g1, the lateral surface SCR generation at the gate edge g3, the bulk SCR generation g2, the diffusion of carriers generated out of the SCR g4, back side surface generation g5.

2. EXPERIMENTAL

In order to better understand the different contributions, we have fabricated and measured MOS Al gate capacitors with guard rings on different kind of wafers (FZ, CZ) with and without intentional Fe or Ni contamination. The metal impurities were deposited in intentionally contaminated SC-1 and driven in the samples during the gate oxidation. The essential device parameters are given in table 1.

GENERAL PARAMETERS		GEOMETRY		
Gate material:	Al	Device 1:	200*200	μm^2
Distance guard ring to gate.	10 µm	Device 2:	500*500	μm^2
Thickness of gate oxide:	250 Å	Device 3:	1150*870	μm^2
Silicon resistivity p-type	15 Ωcm	Device 4:	2280*1140	μm^2

Table 1: Parameters of the MOS capacitors used in this work

The measurement was done using the constant capacitance technique introduced by Pierret [5]. On wafers contaminated with Ni at a level of about $2*10^{12}$ cm^{-2} without Internal Gettering, like FZ wafers or CZ wafers without oxygen precipitation, the generation rate is at the higher limit of the measurement capabilities and τ_g tends consequently to 0. On the other hand the generation is not affected on CZ wafers having a proper Internal gettering treatment and being contaminated with the same amount of Ni (see figure 2). According to this result MOS generation lifetime is very sensitive to the presence of metal precipitates in the active device region.

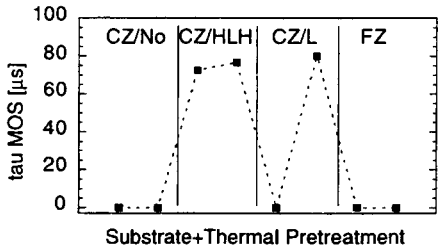

Figure2: Influence of internal gettering on lifetime for Ni contaminated samples. Intentional contamination was done after different SiO_2 precipitation annealings: HLH: complete high low high gettering cycle; L: only nucleation anneal

In order to determine the influence of the edge related generation compared with the generation rate from deep levels with different capacitor sizes have been measured on each site. This was done on high purity samples and on samples intentionally contaminated with different concentrations of iron. The iron concentration in the samples was measured by SPV after gate oxidation according to [1]. The edge generation rate was determined according to the method proposed by Schröder [4]:

$$\frac{dQ_n}{dt} = -\frac{qn_i W}{\tau_g} - \frac{qn_i s_g PW}{A_g} - g_3 - g_4 - g_5 \qquad (1)$$

dQ_n/dt represents the thermal generation components, q is the electronic charge, n_i the intrinsic carrier concentration, W the space charge layer width, τ_g the space charge generation rate, s_g the lateral surface generation rate, P is the gate perimeter and A_g is the gate area. It is the clear from equation (1) that a plot of the inverse total generation lifetime as a function of the gate perimeter to surface ratio permits to distinguish between the contribution of lateral generation and the other

generation terms. Results of this representation for samples with and without intentional contamination are given in figure 3.

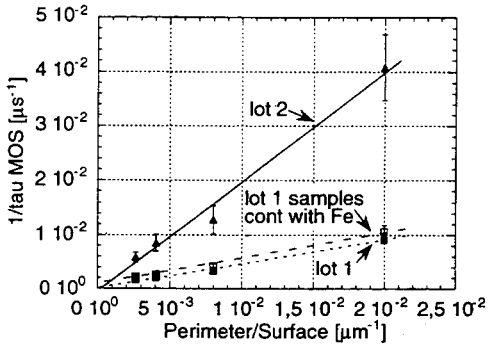

Figure 3: Influence of lateral generation on measured lifetime for two lots produced consecutively with the same process. Contaminated samples of lot 1 contain $10^{13}cm^{-3}$ Fe.

It is clear from figure 3 that the edge related generation rate is not reproducible from one lot to another and that its contribution to the overall generation is very high compared to all the other terms. Even on intentionally contaminated samples g_3 is the major contribution for the currently used capacitor sizes and for the MOS capacitor technology which has been used. The volume generation lifetime can be obtained on such a graph by extrapolating the curves to x=0 but several capacitor sizes must be used and the precision can be very poor as can be seen on the figure. The edge related generation rate given by the slope in the graph depends on the interface states at the edge of the capacitor and the extension of the lateral SCR. These parameters are often poorly controlled: they can be affected by the patterning technology or by contamination arising at the end of the process on the bare Silicon dioxide surface. Considering this point it is very difficult to rely on a simple measure to obtain a clear identification and precise quantification of metallic contamination. An example of this difficulty is seen on figure 4 which shows that the dynamic of the response of generation lifetime to Fe concentration can be very poor for a given lot. On the other hand benefit can be taken of the FeB pair decomposition in p-type material [2,6]. On the same samples as presented on figure 4 the MOS generation lifetime has been measured before and after Fe-B pair decomposition using low temperature anneal (220°C) + quench. As can be seen on figure 5 the difference between the inverse of the two lifetimes before and after the decomposition is proportional to the Fe concentration measured by the SPV technique [5] in parent wafers. This differential measurement permits to eliminate the large contribution of the edge and of any contribution other than Iron.

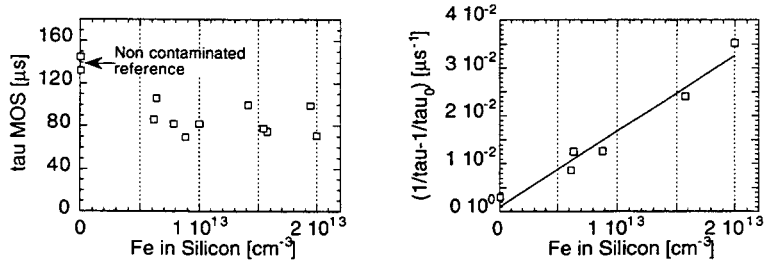

Figure 4: MOS generation lifetime as a function of Fe concentration (1 mm^2 capacitor)

Figure 5: Difference between $1/\tau$ before and after 250°C FeB dissociation anneal plus quench to room temperature (same samples as figure 4)

Just after this treatment the generation lifetime is significantly lower due to the higher generation efficiency of interstitial Fe, and it relaxes very slowly and in a reversible way to the initial value (see figures 6 and 7) in function of the FeB reassociation kinetics. As a further result figure 7 indicates that reliable measurement of the FeB contribution to generation lifetime can not be done before an ageing period of at least 1 day after the last thermal treatment due to incomplete formation of FeB pairs from interstitial Fe.

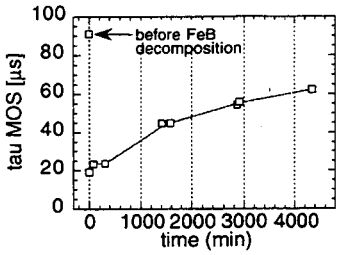

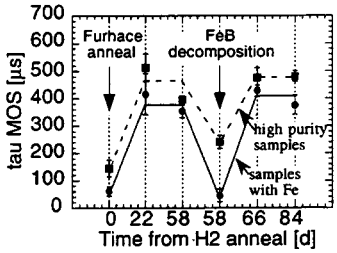

Figure 6: Relaxation of lifetime at room temperature after FeB decomposition for 1mm^2 capacitor (reformation of FeB from interstitial Fe^+ and B^-)
Figure 7: Influence of last furnace anneal on FeB formation and reversibility of FeB dissociation (1mm^2 capacitor)

In a recently published paper it has been shown that lateral space charge generation can be excluded if the capacitors are laterally isolated by Local oxidation of Silicon (LOCOS) [7]. This procedure is multiplying the device manufacturing cost at least by a factor 4 impeding a current application of this technique as a process control tool.

3. CONCLUSION

We show in this work a good sensitivity of MOS generation lifetime to Ni precipitation in the SCR. We demonstrate further that the sensitivity of MOS generation lifetime measurement on simple capacitor structures to Fe contamination can be significantly enhanced by doing differential measurement before and after FeB dissociation. This experimental validation opens a simple way of a quantitative measurement of bulk Fe concentration in Silicon within the depth of active devices on simple structures without necessity of an expensive and time consuming LOCOS step.

We are thankful to J.L. Di Maria (CEA-LETI) for the generation lifetime measurements, to K. Barla (CNET) for helping us in SPV measurements and to G. Kamarinos (LPCS-ENSERG) for many helpful discussions. D. Walz is "boursier de doctorat CEA-inducstrie (BDCI)" and is financially supported by MEMC Electronic Materials.

REFERENCES

1. R.FALSTER, W. BERGHOLZ, *J. Electrochem. Soc*, **137**, 1548 (1990)
2. G.ZOTH, W.BERGHOLZ, *J.Appl.Phys.*, **67**, 6764 (1990)
3. F.TARDIF et al. in "Crystalline defects and contamination..." *Electrochem. Soc. Proc.*, **93-15**, 114 (1993)
4. D.K SCHRÖDER, H.C.NATHANSON, *Sol.-St. Electron.*,**13**, 577 (1970)
5. R.F.PIERRET, *IEEE Trans.Electron. Dev.*, **ED19,7**, 869 (1972)
6. W.WIJARANAKULA, *J.Electrochem.Soc.*, **140**, 275 (1993)
7. L. FONSECA, F.CAMPABADAL, *Sol.-St. Electron.* **37**, 115 (1994)

EFFECT OF DIFFERENT CHLORINE SOURCES DURING GATE OXIDATION

B. Vermeire[a], P.W. Mertens[a], M.J. McGeary[b], K. Kenis[a], M.M. Heyns[a], M. Schaekers[a] and A. Lubbers[c]

[a] IMEC, Kapeldreef 75, B-3001 Leuven, Belgium
[b] Olin, 350 Knotter Drive, Cheshire, CT 06410-0586, U.S.A.
[c] OCG, Keetberglaan 1A, B-2070 Zwijndrecht, Belgium

1. Introduction

In this paper the removal of metal contamination when adding chlorine to the ambient during oxidation will be discussed. Three different chloro-organic substances were added as chlorine source using a bubbler: 1,1,1 trichloroethane (TCA), trans-dichloroethene (DCE) and oxalyl chloride (ESC-96^{TM}). The primary motivation is finding an ozone-friendly alternative for TCA. For each of these sources, the efficiency of chlorine to remove certain metals from the silicon surface will be demonstrated. Secondly, the diffusion of Fe into the bulk will be discussed. Lastly, gate oxide integrity (GOI) measurements comparing oxidations in a chlorinated ambient with dry oxidations are reported to show that no negative effects of low level chlorine addition can be seen.

2. Experimental

Different oxidation processes were studied. Wafers were ramped up to the oxidation temperature, 850°C, in 5% O_2 / 95% N_2 (no chlorine added). Wafers were then oxidized either in pure oxygen, or in oxygen containing 1% (for DCE and oxalyl chloride) or 0.167% (for TCA and oxalyl chloride) atomic-Cl equivalent using the different chlorinated chemicals as source to a thickness of 8 nm.

In order to study the metal removal, wafers were intentionally contaminated, before oxidation, with different metal solutions using the spin contamination technique [1] to a level of approximately 10^{12} atoms/cm^2. To measure the metal surface contamination oxide layers grown on p-type Cz wafers, were decomposed using vapour phase decomposition (VPD). The metal left behind on the surface is then concentrated using droplet surface etching (DSE). The droplet residue was measured by total-reflection X-ray fluoresence (TXRF). Using this procedure the total residual metal contamination on the silicon surface and in the oxide is obtained. To study the Fe bulk contamination the surface photo voltage (SPV) method was applied.

To look for possible negative effects of the different chlorine sources GOI test were performed on uncontaminated p-type FZ wafers (metal concentration < few x 10^{10} at./cm^2). Capacitors were fabricated by LPCVD poly-Si deposition, phosphorus solid-source doping and

standard wet lithography. Four wafers were evaluated for each oxidation condition. For different sets of experiments were performed and each time a dry oxidation was performed as a reference.

3. Results

3.1. Surface metal concentration

Cu and Ni (fig. 1) are never incorporated in the oxide. It was found (fig. 1) that K, Ca, Fe and W can be effecively removed from the silicon surface by any chlorinated oxidation. Ti is not removed save partially by oxalyl chloride oxidation.

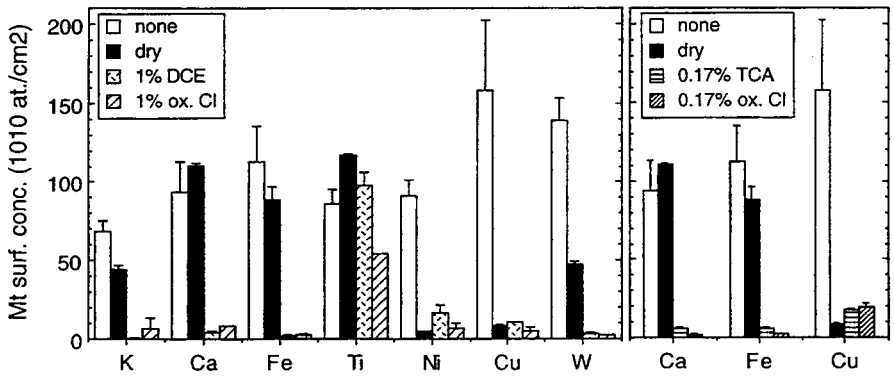

fig. 1: Concentration of metal in the oxide or on the surface prior to oxidation or after dry or chlorinated oxidation to 8 nm thickness, measured with VPD-DSE-TXRF. p-type Cz wafers were used. Concentrations refer to atomic Cl equivalent.

3.2. Bulk metal concentration

Fig. 2 represents the total Fe bulk concentration obtained by SPV. It was found that wafers with Fe contaminated surfaces always exhibit an increase in Fe bulk concentration. The increase is the same for the different oxidation conditions under study.

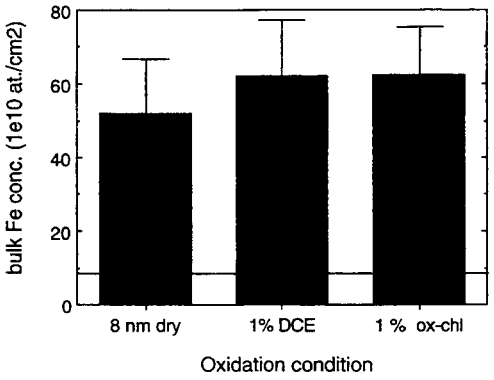

fig. 2: Integrated bulk Fe concentration after oxidation in different ambients on intentionally contaminated p-type Cz wafers (10^{12} Fe at./cm^2) measured by SPV. The solid line is the background level for uncontaminated wafers. Concentrations refer to atomic Cl equivalent.

3.3. Gate Oxide Integrity

The breakdown field (Ebd) was determined by a ramped voltage test for capacitors with an area ranging from 1.2 mm^2 to 15.8 mm^2. The defect density was determined according to the method described in [2]. Results are shown in fig. 3a. The constant current charge-to-breakdown (Qbd) value was determined for capacitors with an area of 0.126 mm^2 (fig. 3b). It was found (fig. 3a and fig. 3b) that the 1% at. chlorine addition does not significantly adversely effect the defect density or the Qbd value for any chlorine source used.

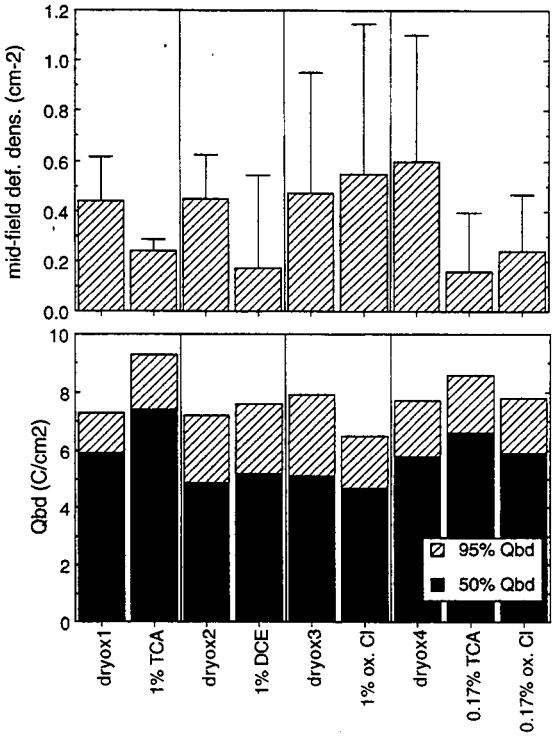

fig. 3a: Ebd MFBD defect density (2 MV/cm < Ebd < 12 MV/cm) for 8 nm oxides on p-type FZ wafers oxidized in different ambients. The defect density was fitted from the yields of capacitors with areas 1.2 mm^2, 3,8 mm^2 and 15.8 mm^2. Concentrations refer to atomic Cl equivalent.

fig. 3b: Qbd value for 8 nm oxides on p-type FZ wafers oxidized in different ambients. The current density was 200 mA/cm^2 and the capacitor area 0.126 mm^2. Concentrations refer to atomic Cl equivalent.

4. Discussion

When undergoing thermal oxidation, the initial surface metal contamination on a wafer may be redistributed [3].

Cu and Ni are nearly completely removed from the surface during an oxidation step (fig. 1). Since they have higher diffusion constants than does Fe [4, 5], it is reasonable to assume that they diffuse into the silicon bulk.

Fe-surface contamination can partially diffuse into the bulk before it is incorporated into the oxide layer. The fraction of Fe diffused into the bulk is not affected by the use of Cl-chemistry during the oxidation. Only the Fe incorporated into the oxide during the

ramp up is removed during subsequent oxidation in a Cl-containing ambient.

K, Ca, W, and Fe are removed by Cl if present in or on the oxide. During an oxidation in a chlorinated ambient, a metal can be removed if it forms a volatile metal chloride (K, Ca, Fe) or metal oxy-chloride (W) [6, 7]. Ti can not effectively be removed as its oxide is too stable.

It was found that, for Ca and Fe, TCA and oxalyl chloride have a high removal efficiency even at a Cl-equivalent concentration as low as 0.17%.

TCA and DCE introduce both HCl and Cl_2. Oxalyl chloride introduces only Cl_2. Therefore, as comparable removal of K, Ca, W and Fe, and better removal for Ti, has been observed using the three different Cl-sources, this study proves that Cl_2 removes metals at least equally well, if not better than does HCl. In contrast to TCA and DCE, oxalyl chloride offers the possibility to obtain a hydrogen-free oxidation ambient.

5. Conclusions

It was found that K, Ca, Fe and W contamination can be removed from the surface during an oxidation in a chlorinated ambient at Cl-concentrations as low as 0.17 %. Ti cannot effectively be removed. While any chlorine source will remove Fe from contaminated silicon surfaces, there is no significant influence of the oxidation ambient on the final bulk concentration of Fe. No significant negative effects of the chlorine addition on the gate oxide integrity were observed.

References:

1. M. Hourai, T. Naridomi, Y. Oka, K. Murakami, S. Sumita, N. Fujino and T. Shiraiwa, Jpn. J. Appl. Phys. 27, L2361 (1988).
2. P.W. Mertens, B. Vermeire, M. Depas, M. Meuris, M.M. Heyns and D. Gräf, in IES 40th Annual Technical Meeting 1994 Proceedings Vol. 1 (IES, Mount Prospect, Illinois, 1994) p. 350.
3. P.W. Mertens, T.Q. Hurd, D. Gräf, M. Meuris, H.F. Schmidt, L. Kwakman, M. Hendrickx, M. Kubota and M.M. Heyns, in Proceedings of Symposium on Contamination Control and Defect Reduction in Semiconductor Manufacturing III, PV 94-9, (The Electrochemical Society, Pennington, NJ, 1994) p. 241.
4. F. Wohlier, "Diffusion and Defect Data - Solid State Data", Trans Tech Publications, 1986.
5. "Properties of Silicon", (INSPEC, The Institute of Electrical Engineers, London, 1988).
6. W. Kneen, M. Rogers and P. Simpson, "Chemistry: Facts, Patterns and Principles", (Addison-Wesley, 1972).
7. M. Chase, C. Davies, J. Dawney, D. Frunip, R. McDonald and A. Syverud, "JANAF Thermochemical Tables", 1986.

Kinetics and Morphology of Copper Deposition on Hydrogen-Passivated Silicon Surfaces from Dilute HF Solutions

Jennifer A. Sees, Lindsey H. Hall
Chemical Operations Department, Texas Instruments, Inc., Dallas, TX 76265

Oliver M.R. Chyan, Jin-Jian Chen, Hsu Y. Chien
Department of Chemistry, University of North Texas, Denton, TX 76203

Silicon wafer cleaning has remained an integral part of semiconductor device fabrication since the 1950s, and in fact, is the most frequently applied processing step in the integrated circuit manufacturing sequence.[1,2] The importance of adequate cleaning cannot be underestimated in that contamination remaining on the substrate surface is known to degrade device performance, reliability, and yield. It has been estimated that over fifty percent of yield losses in IC manufacturing are caused by microcontamination.[1] Although the traditional RCA clean as introduced by Kern[3] uses H_2O_2, NH_4OH, and HCl for wafer cleaning, the etching capability of dilute HF is increasingly utilized in wafer surface preparation.

1. EXPERIMENTAL

The present investigation reveals the kinetics and morphology of copper deposition from dilute HF solutions onto silicon substrates. Copper was chosen because of its known deleterious effects to important device characteristics. One by one cm^2 sections of p-Si <100>, CZ grown, 1.6-2.2Ω cm wafers were hydrogen passivated by exposure to low particulate, electronic grade 4.9% HF for 60 seconds, followed by a rinse in DI water, R>18MΩ. Samples were prepared by exposure to 5.1 ppm Cu^{++} ($CuSO_4.5H_2O$, 99.999%, AESAR) in 4.9% HF solutions for varying deposition intervals. Experimental control samples consisted of substrate exposure to noncontaminated HF solution. Samples were then DI water rinsed and surface morphology of copper deposits was characterized by atomic force microscope (Nanoscope III, Digital Instruments). A sample capsule fabricated from perfluoroalkoxy polymer (PFA) was used to dissolve copper deposits from a known area of the polished silicon using double distilled 50% HNO_{3aq} (OPTIMA, Fisher). Copper deposition per surface area was measured by analyzing the copper collected in the HNO_3 by inductively coupled plasma-mass spectroscopy (ICP-MS, Fisons PQS model). Cleanliness of teflon labware was insured by rinsing in 10% HNO_3 (OPTIMA, Fisher). A final experiment was performed by exposing silicon wafers to varying concentrations (100 ppt to 5.1 ppm) of copper in dilute HF for 60 seconds, and analyzing by total reflection X-ray fluorescence (TXRF, Rigaku 3726).

2. RESULTS AND DISCUSSION

AFM analysis reveals the surface of hydrogen passivated silicon to be featureless (mean roughness < 0.2 nm). As exposure interval to 5.1 ppm Cu^{++} increases, increasing numbers of nanometer size copper nuclei deposits appear.[4] Topographical analysis further reveals the number of copper deposits increases with deposition time up to 60 seconds. Additionally, the average diameter of copper nuclei was measured at about 10 nm during the first 60 seconds of silicon exposure to contaminated HF, and then increased to about 18 nm after 80 seconds of exposure. The nucleation process dominates during the first 60 seconds exposure to contaminated solution, during which time no growth is observed. Copper deposits grow after all the silicon active sites are occupied.

Deposition kinetics were explored by measuring absolute mass of copper deposits from Cu^{++}/HF solution and plotting against exposure time. Copper mass (M_{Cu}) was determined by dissolution from the substrate surface with HNO_3 and quantified by ICP-MS. As can be seen by Figure 1, M_{Cu} is linearly proportional to $t^{1/2}$. This result is consistent with a diffusion-limited kinetic model. This result was confirmed by quantification of copper deposits by integration of the total volume during AFM analysis. This measurement was also found to plot linearly to $t^{1/2}$, Figure 2. The results of the TXRF experiment demonstrated that copper deposited is linearly proportional to the concentration of Cu^{++} in HF solution. Because the diffusion rate of Cu^{++} depends on the concentration gradient established between the solution and silicon interface, this result is consistent with a diffusion-controlled kinetic mechanism.

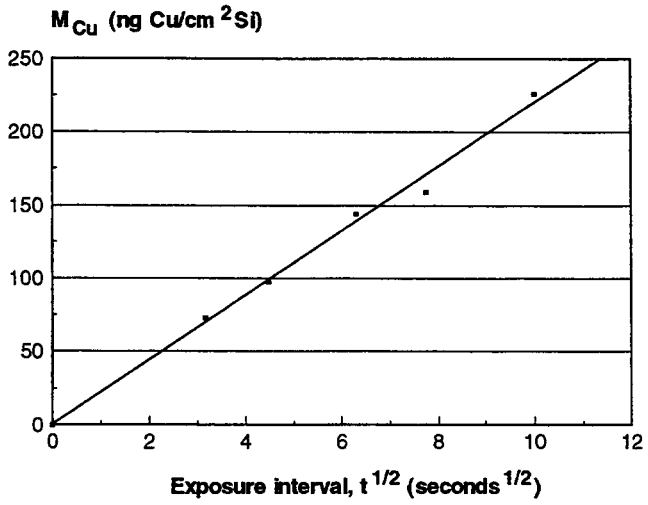

Figure 1. Copper deposit weight (M_{Cu}) v exposure interval ($t^{1/2}$)

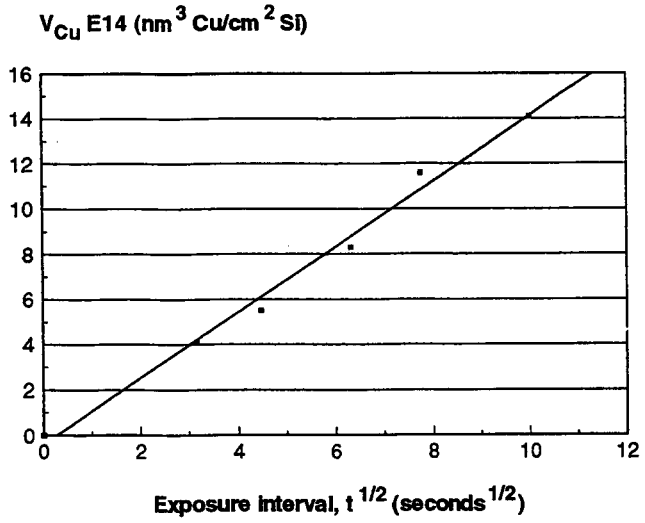

Figure 2. Copper deposit integrated volume (V_{Cu}) v exposure interval ($t^{1/2}$)

3. CONCLUSIONS

During the initial stages of silicon exposure to copper-contaminated dilute HF solution, the process of nucleation dominates. Also during this time, no growth of copper deposits is observed. Growth of copper deposits begins in the secondary stages of exposure to contaminated solution.

This study involved high concentrations of copper in dilute HF. Because of the presence of such a high concentration of impurity, a constant concentration of copper exists at the solution/boundary layer interface. Copper deposition onto substrate surfaces is therefore limited by the rate of diffusion of Cu^{++} across the boundary layer. This result was revealed by two methods: measurement of mass of copper deposits by ICP-MS, and by volume integration of the deposits during AFM analysis. Currently, work is underway to reveal diffusion kinetics of copper in dilute HF solutions at lower concentrations, specifically 5 ppt to 100 ppb.

ACKNOWLEDGMENTS

The authors acknowledge Lisa Lester and Bud Schmidt for valuable assistance and Leanne Mallini for ICP-MS analysis.

REFERENCES

1. W. Kern, "Overview and Evolution of Semiconductor Wafer Contamination and Cleaning Technology," in *Handbook of Semiconductor Wafer Cleaning Technology*, W. Kern, Editor, Noyes Publications, Chapter 1, 1993.

2. J. Ruzyllo, "Overview of Dry Wafer Cleaning Processes," in *Handbook of Semiconductor Wafer Cleaning Technology*, W. Kern, Editor, Noyes Publications, Chapter 5, 1993.

3. W. Kern, D. Poutinen, "Cleaning Solutions Based on Hydrogen Peroxide for Use in Silicon Semiconductor Technology," *RCA Review*, Vol. 31, pp 187-206, 1970.

4. O.M.R. Chyan, et. al., submitted to *Journal of Electrochemical Society*.

A New Wet Cleaning Strategy

Mike Jolley*

Summary
A new cleaning technique based around repetitive applications of SC1 and HF has been developed. To explain the high cleaning efficiencies of this process a new particle removal mechanism is proposed. Target applications are post polish cleans, monitor wafer re-claiming and as an improvement or replacement for traditional RCA cleans.

Repetitive Hydrophilic Cleaning Process Description
This new silicon cleaning method evolved out of an effort to develop a more effective method to clean wafers using spray techniques based on the principles of colloid physics. This process was designed to etch most of the chemical oxide with dilute HF and then re-grow the chemical oxide in an SC1 solution. The key aspect of the clean is the repeated partial strip of the chemical oxide and the re-growth of the oxide from the hydrophilic state.

The proposed cleaning mechanism is the rapid volume expansion of the very thin silicon layer that is consumed to form the layer of oxide in the SC1 step. During the growth step the particles embedded in the surface would be placed under stress by the oxide film growing around and underneath them.

The baseline clean consists of three SC1 treatments, with two HF treatments interspersed between water rinses. The SC1 application time is typically 5 minutes @ 80 deg °C in a 5:1:0.25 mixture of water, hydrogen peroxide and ammonium hydroxide. The HF mixture was 500:1 at 25 deg °C and the etch time was targeted to remove approximately 75% of the chemical oxide layer. The chemical processing and intermediate rinsing was done in an all Teflon spray acid tool. The final rinse and dry is done in a stainless steel spin/rinse dryer.

Experimental Procedure
All processing was performed with spray acid tools and spin/rinse dryers manufactured by Semitool. Particle counting was performed with a Tencor 5500. SEMI grade chemicals were used along with 17 Mega Ohm Resistivity DI water. The processing was done under Class 100 laminar floor hoods. Wafer size was 150 mm and all particle count data is 0.2 micron and greater.

* Semitool, Kalispell MT. USA

Results

The first application of this clean was the re-claiming of seven lots of used 150 mm particle count wafers. Chart One shows the lot average starting counts and final counts. In some cases the baseline clean was repeated up to four times. Table One contains the summary statistics for the whole lot measurements.

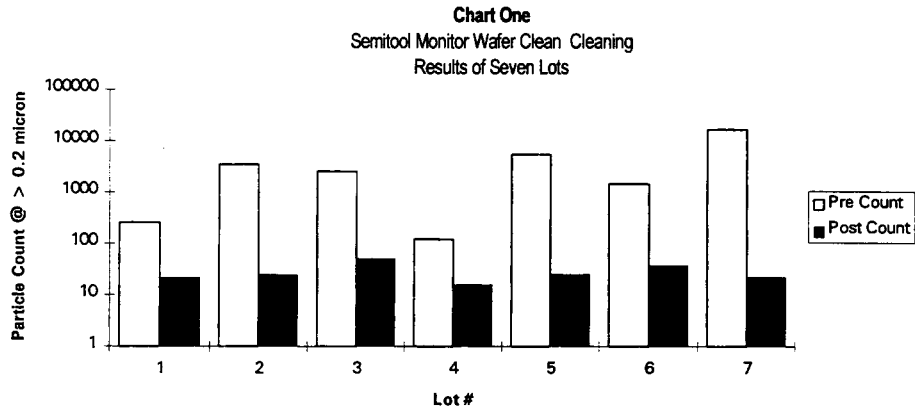

Table One

Lot #	Pre Count-Average	Pre Count STD DEV	Post Count Average	Post Count STD DEV	% Particle Removal	Lot Size
1	254.80	147.00	21.96	7.79	91.38	24
2	3428.00	1195.00	24.86	21.17	99.27	22
3	2481.00	239.00	50.80	17.70	97.95	21
4	121.80	230.60	15.80	11.00	87.03	25
5	5282.80	625.00	25.05	9.67	99.53	21
6	1438.60	3011.00	37.08	12.85	97.42	13
7	17029.00	5148.00	22.09	8.04	99.87	11

Screening Experiments

In an effort to further understand this process and to optimize it two screening experiments were performed using a more controlled type contamination. Clean wafers were stripped in HF and then rinsed and dried and then scanned for particles. The first screening experiment was meant to optimize the SC1 cleaning step. The factors looked at were time, temperature and concentration. A full factorial experiment was run and analyzed using the technique of multiple linear regression. Besides the three controlled factors, the wafer starting particle count was added into the model as a variable. The best results were with a 5:1:0.25 mixture at 80 deg °C. The effect of time was minimal.

The second experiment looked at number of SC1/HF repetitions, SC1 etch time and the HF etch time as a fraction of the time needed to strip a chemical oxide. This

experiment showed that increasing the number of repetitions and etching a larger percentage of the chemical oxide resulted in a higher percentage removal of particles.

First Screening Experiment

Regression Results on Fractional Particle Removal

Multiple R	0.786388		Level	Plus	Minus	
R Square	0.618405	Factor	SC1 Time	15 min	5 min	
Adjusted R Square	0.491207		SC1 Temp	80 °C	60 °C	
Standard Error	0.047998		SC1 Concentration	5:1:0.25	5:1:0.05	
Observations	17					
ANOVA						
	df	*SS*	*MS*	*F*	*Significance F*	
Regression	4	0.044801	0.0112	4.861748	0.014544	
Residual	12	0.027645	0.002304			
Total	16	0.072446				
	Coefficients	*Standard Error*	*t Stat*	*P-value*	*Lower 95%*	*Upper 95%*
Intercept	0.621612	0.08785	7.075875	1.29E-05	0.430205	0.81302
SC1 TIME	0.000756	0.002374	0.318586	0.755517	-0.00442	0.00593
SC1 TEMP	0.002089	0.001196	1.746106	0.106316	-0.00052	0.004695
SC1 CONC	0.354075	0.118625	2.984816	0.011383	0.095612	0.612537
PRE COUNT	9.56E-05	3.77E-05	2.536701	0.026096	1.35E-05	0.000178

Second Screening Experiment

Regression Results on Fractional Particle Removal

Regression Statistics			Level	Plus	Minus	Center Point
Multiple R	0.692756392	Factor	# of SC1/HF Cycles	5	1	3
R Square	0.479911418		Fraction of HF etch time to sheet	0.75	0.25	0.50
Adjusted R Square	0.396697245		SC1 Time (min)	5	1	3
Standard Error	0.196153795					
Observations	30					
ANOVA						
	df	*SS*	*MS*	*F*	*Significance F*	
Regression	4	0.887599813	0.2219	5.76718	0.00198	
Residual	25	0.961907782	0.03848			
Total	29	1.849507595				
	Coefficients	*Standard Error*	*t Stat*	*P-value*	*Lower 95%*	*Upper 95%*
Intercept	-0.054689189	0.169702261	-0.3223	0.74993	-0.4042	0.29482
# of Cycles	0.056619094	0.020306512	2.78822	0.00998	0.0148	0.09844
Fraction of HF Etch	0.496735903	0.164882436	3.01267	0.00586	0.15715	0.83632
SC1 Time	0.042620349	0.020571748	2.07179	0.04875	0.00025	0.08499
Pre Count	4.48706E-05	1.36441E-05	3.28865	0.00299	1.7E-05	7.3E-05

Clean Wafer Testing

A final verification of this new process was to evaluate its repeatability on clean starting material (< 40 particles @ .2 u). Two twenty-five wafer cassettes were run through the baseline clean five times. Wafers were particle counted before any processing and after each of the cleaning cycles. The results show the process to be particle neutral on clean wafers. Chart Two shows the lot average results.

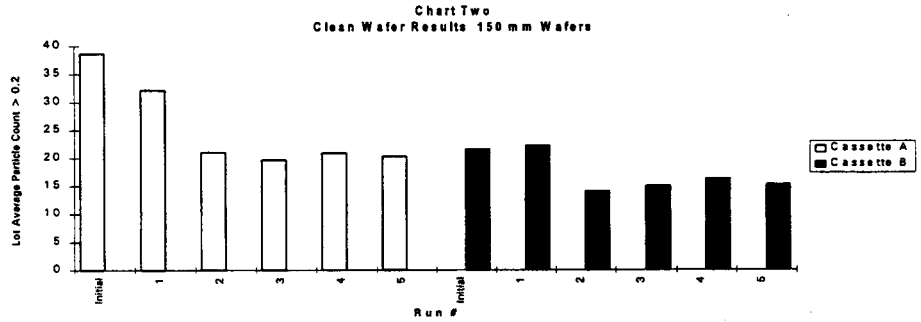

Discussion

This new technique takes advantage of the flexibility of spray processors to explore the effects of repetitive chemical cleans. It appears that the effectiveness of this clean is based upon the repetitive partial strip of the chemical oxide in a very dilute HF mixture and its re-growth in an SC1 mixture. This entire process is done with the wafer surface in the hydrophilic state, avoiding the challenges that hydrophobic surfaces pose during wet cleaning.

The current process has some limitations. The surface metallic levels are higher than traditional RCA cleans. This clean also appears to roughen the surface more than traditional RCA cleans. Probably the largest problem is the process time. The baseline clean described in the paper takes around forty minutes, excluding dry time.

None of these problems are insurmountable, however. The metallic levels could be reduced through use of higher purity grade chemicals or the use of a modified SC2 clean. The roughness issues could be influenced by the SC1 concentrations and temperatures used. Throughput could be maximized through reductions in intermediate rinse times and chemical application.

The most important ramification of this new process is the concept of manipulating the chemical oxide during the cleaning sequence. Differences in native oxide etch rates, densities and surface charge could all perhaps be capitalized on to develop an even more effective clean.

CHARACTERIZATION METHODS OF cSi/aSi INTERFACE FOR HETEROJUNCTION SOLAR CELLS

F. Roca, D. Della Sala, G. Fameli, P. Grillo, F. Pascarella

ENEA - Centro Ricerche Fotovoltaiche -
Via Vecchio Macello, 80055 Portici, ITALY

In the last 5 years, a remarkable progress has been observed in the development of low temperature process of solar cells, obtained growing an amorphous silicon emitter on a crystalline silicon base (aSi/cSi heterojunction).

We have investigated, ex-situ, by using a standard infrared Multiple Internal Reflection (MIR) setup, cSi surface cleaning and chemical bonding of ultrathin layers of amorphous silicon.

The technique is of general interest, infact we currently analyze also ultrathin layers of silicon nitride and chemical oxide on cSi, but at our knowledge, this is *the first application of MIR* to characterize chemical bonding of ultrathin layers of amorphous materials on cSi.

1. EXPERIMENTAL

The substrates used are 20x40mm platelets, cut from one-side mirror polished cSi wafers, (111) p-type 100 Ω cm FZ and (100) p-type 1 Ω cm FZ. The samples were degreased ultrasonically in IPA and cleaned with the standard RCA process.

The MIR setup consists of the MIR sample holder of the Perkin-Elmer 1720 FTIR spectrophotometer, including a Ge-prism (Fig. 1). We clamped the platelets beetween a simple rubber sheet and the Ge-prism.

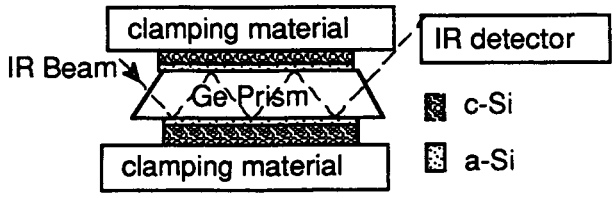

Fig 1. Sample arrangement in the MIR spectroscopy setup.

The IR beam enters the Ge-prism through the 45° bevel angle side, and after multiple reflections it gets a solid state IR detector. The setup provides up to 50 internal reflections by clamping two identical specimens against the prism. When the coating film has a refractive index larger than 2.1 (as

for aSi), the internal reflection is not total and a part of IR beam passes the whole substrate. We avoid the interference of the absorption bands of the organic molecules of rubber sheet, by wrapping it with Al-foil. Continuous nitrogen purging helps reducing the atmosferic CO_2 adsorption in the range 2300-2380 cm^{-1}. The maximum resolution available is 2 cm^{-1}.

2. INFRARED SPECTROSCOPY OF Si(111) and Si(100) SURFACE AFTER OXIDE REMOVAL

After RCA cleaning, an appropriate etching in HF (or BHF, NH_4F, etc.) removes the native oxide leaving a chemically stable, contamination free surface. Chabal and others, using a very powerful IR spectrophotometer (0.25 cm^{-1} resolution), investigated the nature of Si-H bonds on c-Si after HF etch, analyzing the several contributions from mono-, di- and tri-hydrides[3].

In order to test the sensitivity of our MIR setup, and to find the ideal way to remove native oxide, we analyzed, with spectra in unpolarized radiation, the cSi surface, with orientation (111) and (100), after etcning for 5 min. in 5% HF, or 7:1 BHF or 40% NH_4F (Fig. 2 (a), 2 (b)).

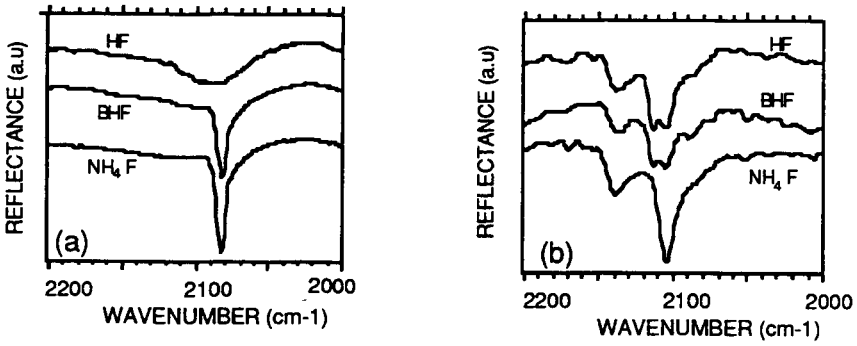

Fig 2 MIR spectra of p-type c-Si (111) (a) and p-type c-Si (100) (b), in the Si-H stretching region after native oxide removal.

According to the conclusions of Ref [1,2,3], a prominent narrow peak at 2084 cm^{-1} (Fig. 2) shows that etched Si (111) surface is atomically flat and terminated with monohydride bonds. This is obtained here using NH_4F and BHF etch. Conversely, the presence of minor peaks between 2060 and 2120 cm^{-1} implies the presence on surface of appreciable amounts of dihydrides and trihydrides that are associated to a microscopically rough surface [2,3]. This is the case of our HF etch, for which MIR spectrum reveals only a broad peak at 2080 cm^{-1} obtained as a sum of all contributes from mono-, di-, trihydrides peaks.

The spectrum of a ideally terminated Si (100) surface is dominated only from $Si-H_2$ groups vibrations, corresponding to a double peak at 2102.5

cm^{-1} and 2090 cm^{-1} [3]. From the analysis of Fig. 2(b), BHF and HF etch leave cSi surface terminated with SiH_2 and SiH_3 bonds, with the typical SiH_3 bonds peak at 2140 cm^{-1}, but with SiH_2 doublet shifted to 2113 and 2104 cm^{-1}. MIR spectrum of the 40% NH_4F etch shows only a peak at 2104 cm^{-1}. We think that the unusual aspect of spectra for Si-H_2 bonds at the c-Si surface for (100) orientation, is a consequence of disorder in Si-H_2 bonds induced from the our HF, BHF etch, and even more from the 40% NH_4F etch.

3. INFRARED SPECTROSCOPY OF aSi/cSi INTERFACE. CHARACTERIZATION OF ULTRATHIN aSi ON cSi.

We have grown aSi on cSi platelets by Plasma Enhanced Chemical Vapor Deposition (PECVD) by setting: pressure 195 mTorr, SiH_4 flow rate 30sccm, substrate temperature 240°C, RF power density 13 mW/cm^2, growth rate 1.4 Å/s.

IR transmittance is typically used to analyze Si-H bonds in thick aSi films (1μm) [4]. These data are often used to infer the characteristics of ultrathin layers of aSi (<100nm) grown in the same deposition conditions. This is erroneous; infact the structure of aSi at interface are strongly dependent on the stabilization of the plasma after ignition, the nucleation-coalescence process of film growth, the surface conditions (temperature, roughness), etc., and it is expected to be quite different from the bulk aSi, as shown by R. W. Collins using UV-Visible spectroscopic ellipsometry [5]. To support this issue, we use MIR spectroscopy as an alternative way to analyze Si-H bonds of aSi films on c-Si.

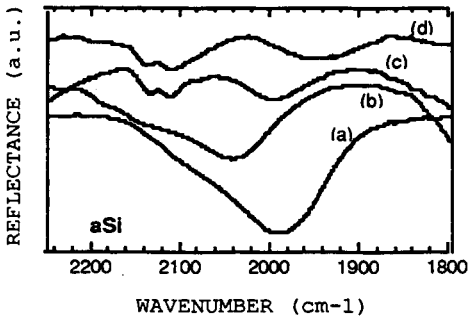

Fig. 3 MIR spectra of aSi layers on (111) cSi; film thickness is 600 nm (a), 30 nm (b), 10 nm(c) and 3 nm (d). The absorption bands in (b,c,d) are amplified by a factor 6.

The spectra of Fig.3, show that the structure of ultrathin aSi layers (<30 nm) are very different from thick layers with only a IR peak at 2000 cm^{-1}

(SiH groups) as for ideal aSi. Infact, the presence of peaks at 2120 cm^{-1} and 2140 cm^{-1}, in accordance with the band assignment of Ref. 5, can be attributed to SiH_2 and SiH_3 groups. As we have specifically verified [6], aSi film is not homogenous along the thickness and SiH_2, SiH_3 bonds are located near aSi/cSi surface.

4. CONCLUSIONS

MIR is a very powerful technique. Infact it shows that the choice of the most appropriate method of native oxide removal is not univocal and depends on the orientation of cSi.

It is possible also to study and optimize ultrathin aSi (up to 3 nm) as deposited on c-Si, and apply the technique to other thin film materials characterization (silicon nitride and chemical oxide) [7].

REFERENCES

1 M. Nishida et al., Appl. Surf. Sci. 79/80 (1994) 409.

2. G. S. Higashi, et al., Appl. Phys. Lett. 56 (7) (1990) 656.

3 Y. J. Chabal et al., J. Vac. Sci. Technol. A7 (3) (1989) 2104.

4 R. W. Collins, J. Non-Cryst. Solids 114 (1989) 160.

5 M. H. Brodsky et al., Phys. Rev. B 16 (1977) 3556.

6 G. Fameli, et al., submitted to J. Appl. Phys.

7 D. della Sala et al., Proc. 12th E. C. Photovoltaic Solar Energy Conference, Amsterdam (NL) (1994), to be published.

THE IMPACT OF CA, CU, ZN SILICON SURFACE CONTAMINATION ON THE YIELD OF A MOS DRAM TEST PROCESS

W.R. Aderhold, N. Streckfuss, E.P. Burte and U. Keller[1]

1. Introduction

Surface contaminations of Ca, Cu and Zn have a detrimental effect on GOI. Ca is found to be incorporated into the oxide structure [1], Cu can change the properties at the oxide interfaces [2]. In this report MOS devices were produced with various amounts of surface contamination of the elements Ca, Cu an Zn. To simulate the introduction of contamination by wet cleaning the wafers were dipped in solutions spiked with selected contamination. The electrical properties of the MOS structures were tested to get more insight in CMOS device relevant effects of surface contaminations introduced prior to thermal processes.

2. Experimental

The process is cut from a 4Mbit process using 20 nm gate oxide and n-doped poly for gate metallization. The wafers were 150mm CZ, <100>, p-type, 4-6 Ωcm. Prior to gate oxidation a scattering oxide and a sacrificial oxide were grown and removed. Before each of the furnace processes the wafers were cleaned and contamination in varied amounts was applied by dipping the wafers into spiked 0.07% HNO_3 followed by spin drying in a standard tool. Piranha cleaning (140°C) with DI water rinsing and spin drying formed a hydrophilic surface. All oxidations were carried out in thermal furnaces at a maximum temperature of 950°C in dry oxygen which was also flowing during temperature ramping. To minimize cross contamination low contaminated wafers were placed at the gas inlet side of the tube, the higher contaminated wafers at the door side. Between seperate runs for each contaminant the tube was purged with HCl. The polysilicon was structured by wet etching. The surface contamination was measured by TXRF and VPD-ICPMS prior to oxidation. After oxidation the Cu contaminated wafers were analyzed by angle resolved TXRF [3]. EBD tests were carried out on 0.02, 1 and 16 mm^2 devices, QBD tests on 0.02 mm^2 devices, always for both voltage polarities. For the 100 kHz C-V measurements 0.1 mm^2 devices were used. 100 devices per wafer were analyzed. EBD yield values of devices, which survived 10MV/cm and 12MV/cm field stress were labled C^{1+} and C^{2+}, respectively. QBD values were obtained by stressing the devices with 350mA/cm^2.

3. Results and discussion

Fig. 1 shows a EBD yield decrease for all elements. Ca contamination leads to a dramatic decline beyond 10^{11} cm^{-2} independent of gate polarity. Zn leads to decreasing yields significant for concentrations higher than 10^{13} cm^{-2}. Above 10^{12} cm^{-2} of Cu contamination the yield drops dramatically for negative ramping but to a lesser extend for positive ramping. At 10^{11} cm^{-2} of Cu contamination the yield

[1]work was part of the JESSI-Project E2A Ultrapure Chemicals and partly supported by E.Merck

is reduced independent of the gate polarity.

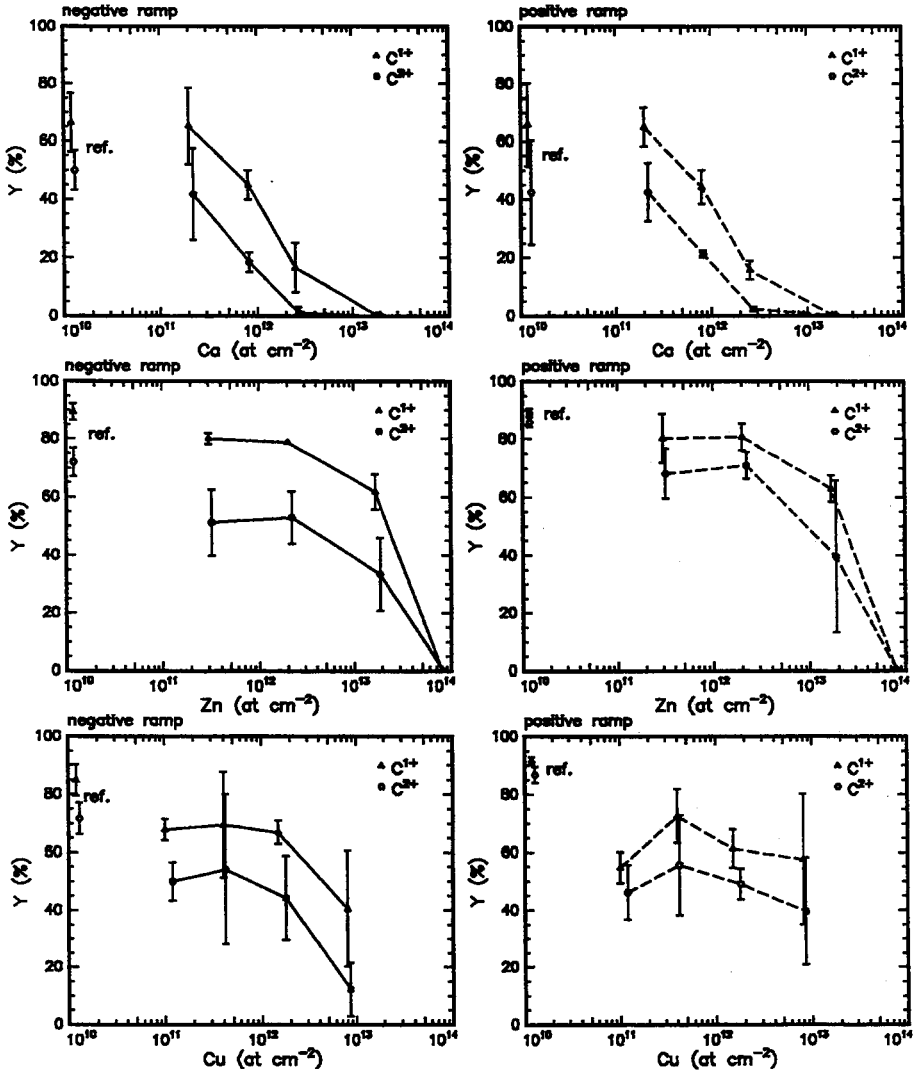

Fig.1 EBD yield C^{1+} and C^{2+} of MOS capacitors (area 1mm^2) processed with the given surface contamination prior to furnace processes. Error bars from 3 identically processed wafers. Uncontaminated reference samples left.

For Cu contamination a QBD value near 22C/cm^2 was found for positive and negative gate voltage, comparable to uncontaminated reference samples. With Zn contamination the QBD values increased from QBD >22C/cm^2 to >23.5C/cm^2 and from >25C/cm^2 to >26.5C/cm^2 for both negative and positive gate polarity, respectively. Due to the large portion of midfield breakdowns even at small contamination levels the QBD values for Ca contamination were for both gate polarities all below 10C/cm^2, dropping below 1C/cm^2 at contamination levels

above 10^{11} cm^{-2}. The uncontaminated samples processed parallelly showed a significant yield decrease for Ca contamination. This is a indication that Ca leads much stronger to cross contamination than the other elements investigated. The C-V measurements showed that the oxide thickness is independent of the contaminations. A significantly increased scattering and shift of flatband voltage is observed with Ca contamination (low Ca: U_{fb}= -1.18...-1.12 V , 2.10^{13} Ca: U_{fb}=-1.33...-1.18 V). For Cu and Zn U_{fb} was independent of contamination (U_{fb}=-.93V +- 0.005 V).

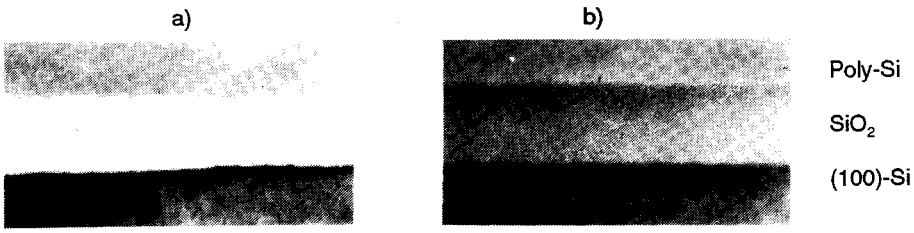

Fig. 2 HR-TEM fotograph of a) Ca contaminated and b) Zn contaminated sample

The breakdowns observed for Cu and Zn are related to spot like defects. This is evident as even with the highest contaminations a large number of the devices with the smallest gate area show intrinsic breakdown behaviour. The Ca contamination leads to a much larger defect density as the QBD and EBD results for small gate areas show. The yield decrease in the case of Zn contamination is mainly due to A-mode (0-1.5MV/cm) breakdowns. The density of A-mode defects is increasing from 0.1 cm^{-2} for the reference sample to more than 100 cm^{-2} at $8{\cdot}10^{13}cm^{-2}$ of Zn contamination. The HRTEM investigations showed a perfectly flat oxide everywhere, see Fig. 2b. This indicates that the defects are concentrated at a few single spots which are hard to find by TEM. It is significant that the intrinsic QBD and the EBD yield values of $0.02mm^2$ devices increase with Zn contamination which may be due to gettering effects at the defect sites reducing the defects elsewere. Ca and Cu contamination leads mainly to increased breakdowns in the mid and high field region. The reason for this is a shift of the I-V curves to lower fields. This shift is increasing with contamination. For Cu contamination above $10^{13}cm^{-2}$ the shift approached reproducable 4 to 5 MV/cm for all measured curves on a wafer. For Ca contamination the shift scattered from 0 to 6MV/cm. I-V shifts of that extend are reported [4] to occur due to i) the lowering of the barrier height for electrons, ii) a positive charge close to the injecting surface or iii) increased surface roughness at the injecting electrode. Similar contamination experiments with Ca conducted elsewhere led to comparable I-V curves and were attributed to Si/SiO_2 interface roughness [1]. Here for Ca contaminated samples roughness on *both* interfaces was found by HRTEM (Fig. 2a) which is correlated with the shift of both polarity I-V curves and the yield results. Cu contamination has a more sophisticated effect as only a shifting of the negative polarity I-V curves is observed. This is correlated to the yield difference for the both polarities. Significant surface roughness on Cu contaminated samples could not be found by HRTEM investigations. Although the I-V curves were shifted the devices could be stressed without breakdown to current densities

comparable to uncontaminated samples and much higher as for Ca contaminated samples where surface roughness was found. Cases i or ii are therefore more probable. In fact, it was revealed by AR-TXRF measurements [3] of oxidized Cu contaminated wafers that copper is found both on top of the oxide and at the interface to the substrate rather than in the bulk of the oxide. Fig. 3 shows the angular dependence of the resulting curves from three different spots on a wafer. The shape of the curves is typical for a combination of a surface layer and a buried layer. The method is averaging over the sampling area of 1 cm^2. TXRF measurements carried out prior to oxidation at the same spot show that 1/3 of the Cu remained at the interfaces. The electrical effects of a shift to lower electric fields for only the negative gate polarity I-V curves without any influence on C-V measurements can just be explained with *spotlike* Cu precipitates at the oxide/poly interface and a more regular concentration at the oxide/substrate interface. The effect of a spot like Cu distribution would be much stronger due to a higher concentration as the average value. For a test of this model Fowler-Nordheim curves were calculated [4] using a barrier height of 3.1 eV for 90% and arbitrary 2.5 eV barrier for 10% of the poly/oxide interface and 3.1 eV for 100% of the Si interface. The calculations fit perfectly to measured curves for positive and negative polarity. This model is also consistent with the C-V measurements because 10% of the surface with the lower barrier height would only change the U_{fb} value by less than 1%. Stressing the Cu devices with negative fields of 10MV/cm let the shift of I-V curves disappear. The C-V curves prior to and after stress were identical. High field stress of either polarity did not significantly change the shifted I-V curves of Ca contaminated wafers but led to breakdown.

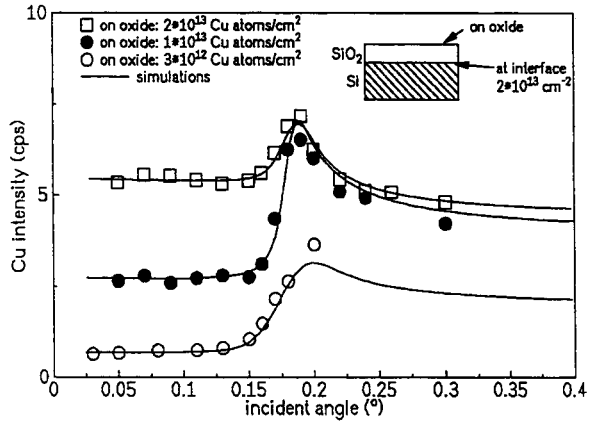

Fig.3 AR-TXRF results of oxidized (20nm) Cu-contaminated wafers. Simulations by inverse modeling. Fitting parameters show Cu layers at interfaces.

References

1. P.W.Mertens et.al., IES 38th Ann.Tech.Meet.Proc., Vol.1, (1992), 475
2. Honda et.al., Inst. Phys. Conf. Ser., No. 87, Sec. 6., (1987), 463
3. N.Streckfuss et.al., ECS Proc. Vol. 93-15, (1993), 83
4. D.J.DiMaria et.al., J.Appl.Phys., 51, (1980), 2722

UV/ozone Pre-treatment on Organic Contaminated Wafer for Complete Oxide Removal in HF Vapour Cleaning

L. Li* , J. Alay, P.W. Mertens, M. Meuris, W. Vandervorst, M.M. Heyns,
IMEC, Kapeldreef 75, B-3001 Leuven, Belgium
R. de Blank, and E. Schuivens
ASM International, Rembrandtlaan 9, 3727 BG Bilthoven. The Netherlands

1. Introduction

As the device dimensions continually shrink to the deep submicron region, the effect of organic contamination to wafer processing becomes more obvious. The organic impurities can prevent native oxide removal from wafer surface and other contamination cleaning. Therefore they must be removed first in the cleaning process.[1] An UV/O_2 procedure is found to remove effectively hydrocarbon contamination from the wafer surface.[2] For HF vapour process, a distinct improvement in oxide etch uniformity was observed for the ozone pre-treated wafers.[3] HF vapour etching on wafer stored for a long period leads to haze values as high as 499 ppb. Wafers from the same batch that were cleaned with SPM+HF+RCA had a haze value, after HF vapour etching, of only 160 ppb. In this experiment, the effect of surface organic contamination to the oxide removal during the HF vapour cleaning, and the improvement of oxide removal by an UV/ozone pre-treatment are investigated.

2. Experimental

The wafers used in this experiment were 125 mm (100) p-type Si-wafers. After a SPM+HF+RCA pre-clean, the wafers were contaminated by dipping into a solution of 20ml photoresist(PFRIX 500EL)/4500ml actone for 5 min before withdrawing and drying in the air. The UV/ozone treatment was performed by exposing the wafers to O_2 gas in the presence of UV light. The HF cleaning was done in a prototype HF vapour module built by ASM. The wafer surfaces were characterized by XPS measurement.

3. Results and Discussion

Figure 1 shows the C1s XPS spectrum from a SPM+HF+RCA cleaned sample. The exposure of the wafer surface to cleanroom atmosphere leads to a

---

* Present address: Micron Semiconductor, INC., Mail Stop 306, 2805 East Columbia Road. Boise, Idaho 83706-9698, USA

hydrocarbon absorption. For the resist contaminated sample, the XPS profile in Figure 2 shows one peak at higher binding energy, indicating the presence of the resist on the surface. After a treatment in UV/ozone for 20 and 40 min, the peak which corresponds to the resist contamination is disappeared in the XPS spectra in Figure 3. This means that the resist which was adsorbed on the wafer surface is removed. Besides, the total C1s signal is found slowly decreases with exposure time.

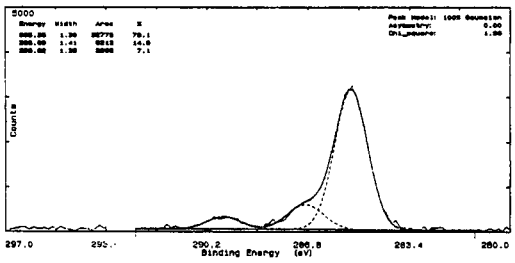

Figure 1. XPS C1s spectrum from SPM+HF+RCA cleaned wafer surface.

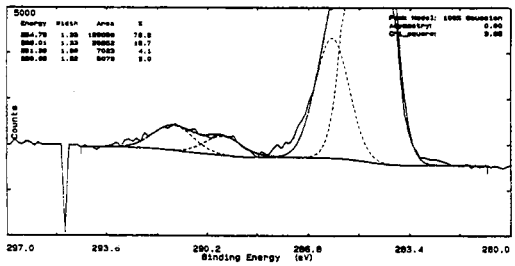

Figure 2. XPS C1s spectrum from photoresist contaminated wafer surface.

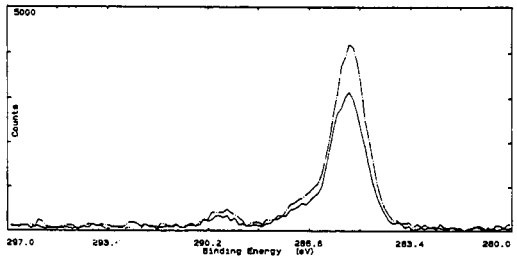

Figure 3. XPS C1s spectra from photoresist contaminated samples, after 20 min (broken line) or 40 min (solid line) UV/ozone exposure.

Figure 4-6 compare the C1s, O1s, and Si2p XPS spectra obtained on HF vapour cleaned wafers with or without UV/ozone pre-treatment. For HF vapour cleaning with 30 min UV/ozone pre-treatment, the surface SiO_2 is completely removed after the HF vapour step, and the C1s and O1s signals are found around the normal levels on HF cleaned wafer surface.[4] However, much higher C1s and O1s signals are observed after a cleaning without UV/ozone pre-treatment, and a clear SiO_2 signal is detected. The latter suggests the resist still remains on the surface even after HF vapour step, which shields the surface oxide to be removed. So, if the wafer surface is contaminated with big hydrocarbon molecules (i.e., photoresists or surfactants), it is difficult to achieve a complete oxide removal and surface cleaning with only the HF vapour process.

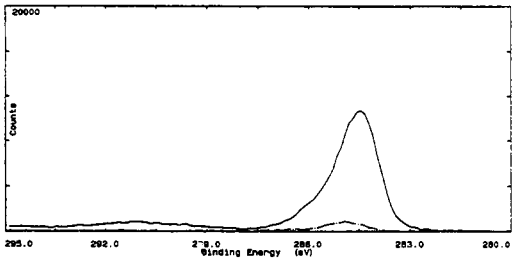

Figure 4. XPS C1s spectra from photoresist contaminated samples, after 10 min HF vapour (solid line) or 30 min UV/ozone+10 min HF vapour treatment.

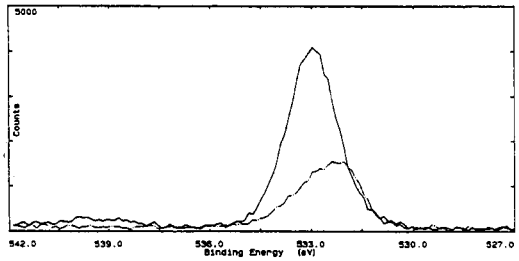

Figure 5. XPS O1s spectra from photoresist contaminated samples, after 10 min HF vapour (solid line) or 30 min UV/ozone+10 min HF vapour treatment.

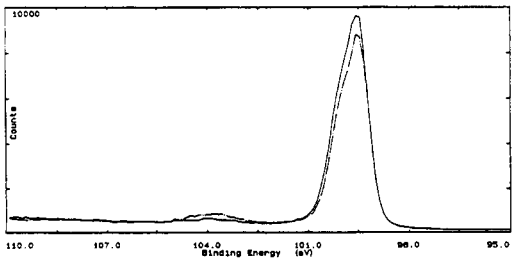

Figure 6. XPS Si2p spectra from photoresist contaminated samples, after 10 min HF vapour (solid line) or 30 min UV/ozone+10 min HF vapour treatment.

4. Conclusions

The photoresist residues remain on the wafer surface in HF vapour cleaning, then seriously influence the oxide removal efficiency. The UV/ozone treatment effectively remove the surface resist residues. Therefore, an UV/ozone exposure prior to HF vapour step provide a way to improve the cleaning efficiency.

References

[1] T. Ohmi, T. Isagawa, M. Kogure, and T. Imaoka, *J. Electrochem. Soc.*, **140**, 804 (1993).

[2] S.R. Kasi and M. Liehr, *J. Vac. Sci. Technol. A*, **10**, 795 (1992).

[3] B.E. Deal and C.R. Helms, "Handbook of Semiconductor Wafer Cleaning Technology" Ed. Werner Kern (1993).

[4] J. Alay, S. Verhaverbeke, W. Vandervorst, and M.M. Heyns, *Jpn. J. Appl. Phys.*, **32**, 385 (1993).

Improvement and Evaluation of Drying Techniques for HF-last Wafer Cleaning

L. Li* , G. Zou, H. Bender, P.W. Mertens, M. Meuris, H.F. Schmidt and M.M. Heyns,
IMEC, Kapeldreef 75, B-3001 Leuven, Belgium

1. Introduction

Wafer drying technique can play a critical role in HF-last cleaning where surface oxide is removed and bare silicon surface is exposed.[1] In this work, the hot water drying is improved and a controlled boiling water drying technique is developed. The integrity of gate oxide grown on Si surfaces dried with different techniques is evaluated, and the underlying influence factors are investigated.

2. Experimental

Si(100) wafers (125 mm, p-type, 16-24 Ωcm) were first SPM+HF+RCA cleaned. After a 6 min 0.5% HF dip to completely remove the surface oxide and a DI water rinse, the wafers were dried with boiling water, controlled boiling water(pH=2.5), Marangoni dryer(Steag/Pokorny), and Spin dryer(SemiTool).

3. Results and Discussion

Figure 1 shows the hot water immersion causes a fast reoxidation, while a prolonged boiling water treatment results in an oxide free Si surface. It is believed that the continuous H_2O gas bubbling can effectively drive the dissolved oxygen out of the boiling water.

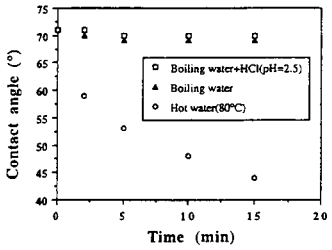

Figure 1. Contact angle (as an indication of surface oxidation state) as a function of treatment time.

---

* Present address: Micron Semiconductor, INC., Mail Stop 306, 2805 East Columbia Road. Boise, Idaho 83706-9698, USA

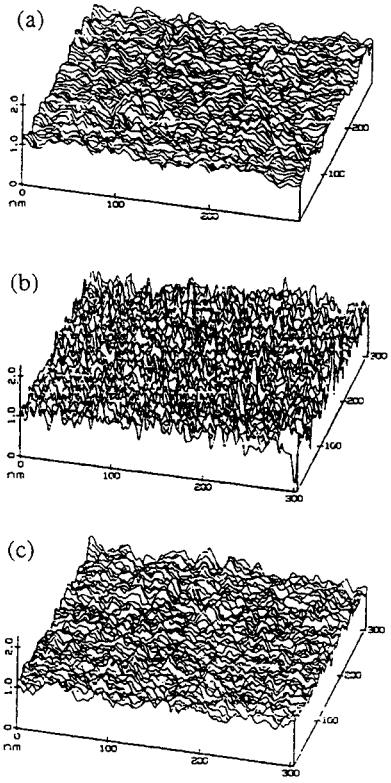

Figure 2. AFM profiles of an HF etched wafer surface after 10 min treatment in (a) RT water, (b) boiling water, (c) boiling water (pH=2.5).

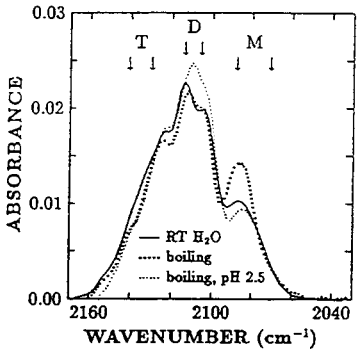

Figure 3. MIR-FTIR spectra after a 10 min treatment of an HF etched wafer in RT water, boiling water, and boiling water (pH=2.5). Mono- (M), di- (D), and tri- (T) hydrides can be distinguished.

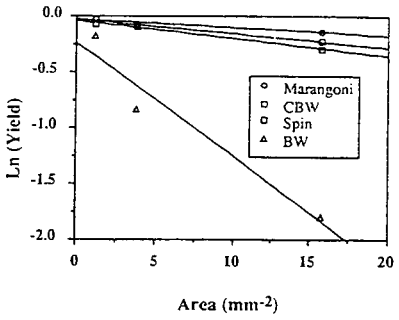

Figure 4. Intrinsic (Ebd > 12 MV/cm) electrical breakdown yield of capacitors (on 10 μm Epi wafers) as a function of gate area and drying techniques.

Comparing with the room temperature(RT) water rinsing(Figure 2a), AFM measurements revealed a significant increase of surface roughness after boiling water treatment(Figure 2b). Obviously an increase of the temperature enhances the anisotropic etching of the Si(100) surface. This enhancement can be partially attributed to the temperature dependence of the surface reaction rate.[2] But, another factor, which has been overlooked so far, is the strong temperature dependence of the self-ionisation of water. The negative logarithm of ionization constant of water, $-\log K_w$ (where $K_w=[H^+][OH^-]$), changes from 14.133 at 20°C to 12.265 at 100°C.[3] Assuming equal $[H^+]$ and $[OH^-]$ in pure water, the OH^- concentration is about one order of magnitude higher in boiling water than in RT water. Therefore, it might be that the higher OH^- concentration in the boiling water accelerates the anisotropic etching and leaves a rough Si(100) surface by (111) micro-facetting in our case and otherwise a smooth Si(111) surface.[2] The important role of OH^- is further confirmed by the experiments in the HCl spiked boiling water. By adjusting the pH level to 2.5, the surface roughening in boiling water is effectively suppressed(Figure 2c). These surface morphology changes were also studied by FTIR. As shown in Figure 3, a much higher monohydride peak is observed for boiling water treated sample; suggesting an increase of (111) microfacets resulted from an anisotropic etching of Si(100) surface by OH^-.

Figure 4 shows the impact of drying techniques to the gate oxide integrity(GOI). The BD-yield was measured on 100 capacitors fabricated on 15 nm thermal oxide(grown in Cl-free dry O_2 ambient). The particle and metallic contamination are illustrated in Figure 5 and Table 1 respectively.

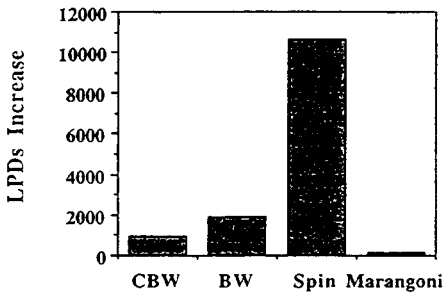

Figure 5. Increase of light point defects on 125 mm wafer surfaces (Censor ANS 100, ϕLSE 0.12 - 0.22 μm) during HF clean and drying process.

Table 1. Metallic contamination ($*10^{10}$ atoms/cm^2) after different drying techniques measured with VPD-DSE-TXRF.

	Element					
Dryer	K	Ca	Fe	Ni	Cu	Zn
CBW	-	0.82	0.16	-	-	0.19
BW	0.82	1.97	0.27	-	-	0.30
Spin	1.05	1.70	0.26	0.06	0.20	0.11
Marangoni	-	2.42	0.26	0.08	0.07	0.15

It is found that the Marangoni dry provides the highest yield and lowest particle contamination. The boiling water drying provides a very low yield. It can thus be concluded that the surface roughness plays a crucial role here. However, to control the surface roughening by adjusting pH=2.5, a big improvement for GOI is obtained by using this controlled boiling water dry. This technique also results in the lowest metallic contamination. The Spin dry leaves a large amount of particles on the wafer surface; but only causes limited GOI degradation, suggesting that this kind of particle contamination has no major influence on GOI.

4. Conclusions

The experimental results show the controlled boiling water and Marangoni drying are promising techniques for HF-last cleaning.

References

[1] J.H. Eisenberg, S.F. Shive, F. Stevie, G.S. Higashi, T. Boone, K. Hanson, J.B. Sapjeta, G.N. Dibello, K.L. Fulford, Mat. Res. Soc. Symp. Proc. Vol.315, 485 (1993).

[2] G.J. Pietsch, U. Kohler, and M. Henzler, Chem. Phys. Lett., **197**, 346 (1992).

[3] "CRC Handbook of Chemistry and Physics" 73rd Edition, Editor-in Chief. D.R. Lide, pp. 8-42 (1992-1993).

QUANTIFICATION ISSUES FOR VPD/TXRF

R. S. Hockett and J. M. Metz
Charles Evans & Associates, Redwood City, CA

Samantha Tan
Chemtrace, Inc., Hayward, CA

1. INTRODUCTION

Vapor Phase Decomposition followed by Total reflection X-Ray Fluorescence (VPD/TXRF) was first introduced by Huber et al [1] in 1988 as an analysis technique for surface metal contamination on silicon wafers. Further explanation of the technique was later reported by Neumann and Eichinger [2] in 1991. Results using this technique have been subsequently reported also by others [3-10]. SEMI Europe has recently proposed that this technique be used to characterize surface metal contamination from minienvironments [11]. The interest in this technique is primarily its detection limits, about $10^9(10^7)$ atoms/cm^2 using the oldest(latest) TXRF instruments and 200 mm diameter wafers, but also its automatic multi-element capability. This is in contrast to VPD/AAS which is single-element, and even VPD/ICP-MS where the elements of interest are pre-selected and the greater the number of elements, the higher the detection limit for any single element.

2. QUANTIFICATION ISSUES

The quantification of VPD/TXRF is influenced by two issues: (1) the chemistry of the VPD; and (2) the preparation of a suitable reference standard for the TXRF analysis of the VPD residue. The chemistry issues of the VPD have been reported elsewhere for surface copper [12] and surface nickel [13-14]; VPD collection of surface iron may also be an issue [15]. The issues for making reference standards for (non-VPD) TXRF analysis of contamination arising from cleaning have been reported recently by Hockett [16].

It has been believed that the preparation of appropriate reference materials for VPD/TXRF would be easier than for TXRF, because of the earlier experience of residue analysis in Europe using fixed-angle TXRF instruments [17]. However, some recent reports question this assumption. Yakushiji et al [18] present calculations and data showing the effect of the finite gap between the sample and the EDS detector on the TXRF detection of small residues as a function of residue diameter. Kondo et al [19] reveal that a diluted AAS droplet of several millimeters can dry with a segregation of Ni metal to less than 100 microns in

diameter, and this can lead to unexpected mass absorption effects [20] in the quantification of TXRF. Ohmi et al [21] have shown the lateral segregation of metals deposited from drying water droplets on silicon wafers, as a function of the ambient used in the drying. Mori and Shive [22] showed the crystallization behavior of metals in water drying is a function of the metal species. Verhaverbeke et al [8] have reported a correlation between different elements by TXRF of solution residues versus AAS where the TXRF reads low and in some cases has a change in slope at higher levels. Streckfuss et al [10] reported a bias for a similar correlation for Ni.

The essential problem is to dry a reference residue and a VPD "unknown" residue in a controlled manner so that the metals always distribute laterally in the same way, to have the residue mass density/flux ratio be small enough to avoid mass absorption effects, and to locate the center of the residue metals (not just visible organic material) under the center of the TXRF detector. We find in our VPD/TXRF procedure that a non-linearity arises for total metal atoms in the 10^{14} range, so that if a 200 mm diameter "unknown" wafer were to have 10^{12} metal atoms/cm^2, or more, then the resultant VPD residue would have enough metal atoms to cause non-linear mass absorption effects, and the analysis would "under-report" the amount of contamination. This suggests the need in some cases to pre-measure the surface with standard TXRF to determine if the surface is "too contaminated" for VPD/TXRF to be accurate. Implications are that if the drying process leaves the metals in areas with very small dimensions, on the order of 100 microns, then the total number of metals atoms on the wafer must be equal to or less than 10^{12} to minimize mass absorption effects. Otherwise, the problem of accuracy becomes even more severe. Neumann and Eichinger demonstrated they could maintain accurate VPD/TXRF quantification for surface Zn which reached about 10^{15} atoms in the residue, however, the lateral distribution of the metals in the residue was not reported [2]. In our studies we have found we can dry dilute (9×10^{11} atoms) vanadium residues and analyze them by TXRF (TECHNOS TREX 610T) with a resulting CV of 25% (N=22). In a test of nine unknown 150 mm diameter wafers taken from the same unopened cassette, we found resulting CVs for VPD/TXRF between 30 and 40% for Ni, Cu and Zn in the 10^{11} atom range in the residue. Assuming 100% collection by VPD (which is valid for metal-oxide bonds), this corresponds to surface metals in the 10^9 atoms/cm^2 range on these commercial wafers. Other elements, such as Mn, Cr, and Ti, were not found in the residue above 3×10^{10}; this corresponds to detection limits in the 10^8 atoms/cm^2 range for those elements.

CONCLUSIONS

1. VPD results in an "average" measurement over the wafer, and thus metal-containing particles contribute to the "average metal reading." A clean room and procedure is necessary to avoid adding metal-containing particles to the measurement.

2. VPD allows TXRF to reach detection limits of e8/cm2. this is the most sensitive VPD/... multi-element technique when state-of-the-art TXRF instrumentation is used. Tthis is the most sensitive surface analysis technique for metals.

3. VPD chemistry effects may bias the measurement in an unknown way, and under-report the level of surface metals. This is true for all VPD/(AAS, ICP-MS, TXRF) techniques, not just VPD/TXRF.

4. If the VPD residue is too concentrated, mass absorption effects result in under-reporting of the level of metals. it is recommended that TXRF measurements be made on the non-VPD wafer first to avoid highly concentrated VPD residues.

5. The real size of the metal residue may be less than the visible size of the residue, and the reference residue size needs to be the same as the unknown residue size; otherwise there will be a bias.

6. Reproducibility and repeatability should be demonstrated using commercial wafers without intentional contamination. it is highly recommended that round robin studies be completed for VPD/TXRF.

REFERENCES

1. A. Huber, H. J. Rath, and P. Eichinger, ECS Extended Abstracts Vol. 88-2, Abstract 422, pp. 619-620 (1988).

2. C. Neumann and P. Eichinger, Spectrochimica Acta 46B, 1369 (1991).

3. M. Meuris, M Heyns, S. Verhaverbeke, P. Mertens, and A. Philipossian, in Microcontamination 91, Canon Communications, pp. 658-665 (1991)

4. M. Meuris, M. Heyns, P. Mertens, S. Verhaverbeke, and A. Philipossian, in Cleaning Technology in Semiconductor Device Manufacturing, edited by J. Ruzyllo and R. E. Novak, ECS Proceedings Vol. 92-12, pp. 144-161 (1992)

5. S. Verhaverbeke, M. Meuris, P. Mertens, A. Kellher, M. M. Heyns, and R. F. De Keersmaecker, M. Murrell, and C. J. Sofield, Ibid. pp. 187-196.

6. P. W. Mertens, M. Meuris, H. F. Schmidt, S. Verhaverbeke, M. M. Heyns, P. Carr, D. Graf, A. Schnegg, M. Kubota, K. Dillenbeck, and R. de Blank, in Crystalline Defects and Contamination: Their Impact and Control in Device Manufacturing, edited by B. O. Kolbesen, C. Claeys, P. Stallhofer, and F. Tardiff, ECS Proceedings Vol. 93-15, pp. 87-102 (1993).

7. H. F. Schmidt, M. Meuris, P. W. Mertens, S. Verhaverbeke, M. M. Heyns, M Kubota, and K. Dillenbeck, in 1993 IES Proceedings, Las Vegas (1993), The Institute of Environmental Sciences, Mount Prospect, IL, pp. 238-244 (1993)

8. S. Verhaverbeke, C. Werkhoven, M. Meuris, H. F. Schmidt, K. Dillenbeck, P. Mertens, M. Heyns, and A. Philipossian, Ibid., pp. 423-431.

9. W. Hub and V. Penka, in Microcontamination 91, Canon Communications, Santa Monica, CA, pp. 266-279 (1991)

10. N. Streckfuss, T. Frey, G. Zielonka, F. Kroniger, C. Ryzlewicz, and H. Ryssel, Fresenius J. Anal. Chem. 343, 765 (1992).

11. "Test Method for the Determination of Inorganic Contamination from Minienvironments," SEMI Europe Doc. #2237, Yellow Ballot, 1/21/94.

12. A. Shimazaki, in Defects In Silicon II, edited by W. M. Bullis, U. Gosele, and F. Shimura, ECS Proceedings Vol. 91-9, pp. 47-56 (1991).

13. C. R. Helms and H-Soo Park, "Generalized Model of Metal Bonding and Cleaning from Wafer Surfaces, Spring'93 MRS Meeting, San Francisco, 1993.

14. R. S. Hockett, in 1993 IES Proceedings, Las Vegas (1993), The Institute of Environmental Sciences, Mount Prospect, IL, pp. 238-244 (1993).

15. S. Pirooz, L. W. Shive, D. I. Golland, "Metallic Contamination on the Surface of P+ and P- Wafers," Extended Abstract from First International Symposium on Ultra Clean Processing of Silicon Surfaces (UCPSS-92), Leuven, Belgium, September 17-19, 1992.

16. R. S. Hockett, "TXRF Reference Standards: A Discussion," Contamination Control and Defect Reduction in Semiconductor Manufacturing III, edited by D. N. Schmidt, D. R. Reedy, J. V. Martinez de Pinillos, and R. Guidi, ECS Proceedings Vol. 94-9, The Electrochemical Society, pp. 323-338 (1994).

17. Proceedings of the biannual TXRF workshops are published in Special Issues of Spectrochimica Acta Part B. See Vol. 44B, No. 5, 1989; Vol. 46B, No. 10, 1991; Vol. 48B, No. 2, 1993.

18. K. Yakushiji, S. Ohkawa, J. Takano, and M. Kogure, Advances in X-ray Chem. Anal. Japan 24, pp. 97-111 (1993).

19. H. Kondo, J. Ryuta, E. Morita, T. Yoshimi, and Y. Shimanuki, Jpn. J. Appl. Phys. 31, L11-L13 (1992).

20. R. Klockenkamper and A. von Bohlen, Spectrochimica Acta. 44B, 461 (1989).

21. T. Ohmi, Imaoka, I. Sugiyama, and T. Kezuka, J. Electrochem. Soc. 139, 3317 (1992).

22. E. J. Mori and L. W. Shive, in Contamination Control and Defect Reduction in Semiconductor Manufacturing I, edited by D. N. Schmidt, ECS Proceedings Vol. 92-21, pp. 155-161 (1992).

Elimination of HF-last Cleaning Related $CoSi_2$ Defects Formation

G. ZOU*[a], F. Jonckx*, R. Donaton*, W. Küper*, K. Maex*, P. W. Mertens*, M. Meuris*, M. M. Heyns*, K. Locke, M. Korac**, and R. Schild****

*IMEC, Kapeldreef 75, B-3001 Leuven, Belgium
**POKORNY, Huefinger Strasse 35, D-7710 Donaueschingen 17, Germany

ABSTRACT

The HF-last cleaning, commonly used to prepare the Si surface prior to the Co deposition, sometimes leads to the formation of $CoSi_2$ defects during the subsequent silicidation. In this work we have conducted several experiments to investigate the mechanism of this defect formation. Experimental results indicated that while the HF dipping time, the HF solution, and the DI water rinsing mode have no or very little influence on the $CoSi_2$ defects formation, the wafer drying technique is the key factor that determines the density and form of defects.

1. INTRODUCTION

Recently, $CoSi_2$ has been gaining more and more interest for deep sub micron applications [1]. Cobalt, however, does not reduce a native oxide layer like Titanium. As a consequence, the silicidation of Cobalt is more vulnerable than that of Ti with respect to the cleanliness of the interface [1]. Previous experimental results revealed that the HF-last cleaning, commonly used to prepare the Si surface prior to the Co deposition, sometimes leads to the formation of $CoSi_2$ defects during the subsequent silicidation [2,3] as indicated in Fig. 1. In this work we have conducted several experiments on the HF-last clean procedure to investigate the mechanism of this defect formation. Finally, a novel drying technique is demonstrated on patterned wafer resulting in defect-free silicides.

2. EXPERIMENTAL CONDITIONS

CZ grown p- and n-type Si <100> 5-inch wafers were used in our experiments. The wafers first received a full IMEC modified FSIb cleaning (SPM + DHF + RCA). The resulted surface chemical oxide was removed in an HF solution. Different etching times from 20 sec to 300 sec and different HF solutions (2 % or 0.5 % HF) with/without 0.4 or 0.1 % IPA were used. After the oxide etching, the wafers were rinsed in DI-water (overflow or quick-dump mode) and dried by one of the following techniques: (1) spin-dry (wafer placed vertically, top speed 1800 rpm), (2) spin dry (wafer placed horizontally, top speed 750 rpm), (3) N_2 gun dry and (4) Marangoni dry. Then, a 20 nm Co layer was sputter deposited onto the wafers. Finally, $CoSi_2$ was formed by a conventional two step silicidation process as indicated in Fig. 1. In order to simulate a real process, a similar experiment was performed on structured wafers (1cm x 1 cm squares in active area, surrounded by TEOS isolation deposited on CZ grown p-type 5-inch wafers). The wafers were dried either in the spin dryer (1) or in the Marangoni dryer (4). The effect of oxide thickness on the formation of $CoSi_2$ defects was also examined. The wafers were examined by microscope inspection with Nomarski contrast. Optical surface inspections were executed with the CENSOR ANS 100 in microview mode.

---

[a] Present Address: Applied Materials Asia Pacific Ltd., 2 Jurong East Street 21, #05-07 IMM Building, Singapore 2260.

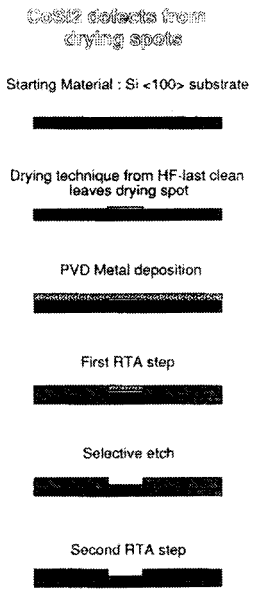

Figure 1: Overview of $CoSi_2$ defects formation mechanism due to drying spots.

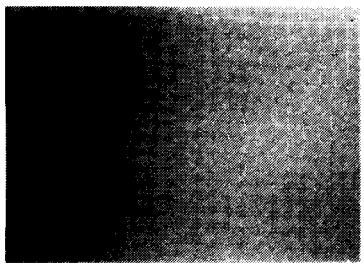

Figure 2: Microscope picture (x5, Nomarski) of silicide surface. N_2 dry (3) yields defect free surface.

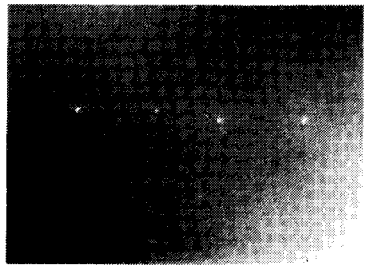

Figure 3: Microscope picture (x5, Nomarski) of silicide surface. Spin dry (2) leaves drying spots along a line on the surface.

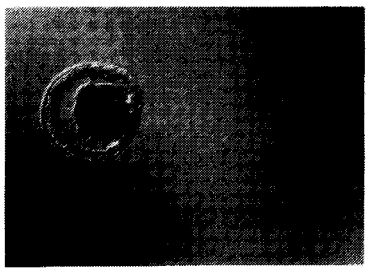

Figure 4: Microscope picture (x40, Nomarski) of silicide surface. Spin dry (2) leaves big droplets on the surface.

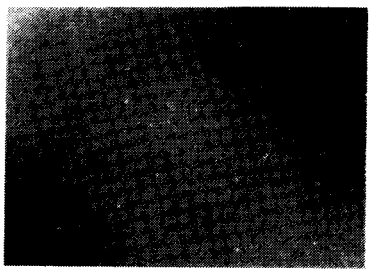

Figure 5: Microscope picture (x40, Nomarski) of silicide surface. Spin dry (1) leaves many small drying spots on the surface.

3. RESULTS AND DISCUSSION

Fig. 2 shows a microscope picture of a bare wafer that received a nitrogen gun dry after the quick-dump rinse and that shows no defects. One can observe some dark spots on the pictures, but those are caused by dirt on the lens. For the same conditions a spin dried wafer with technique (2) shows big drying spots along a line (Fig. 3), indicating that a droplet moved towards the wafer edge by the centrifugal force. Apparently, some parts of the droplet remained on the wafer surface along the path and could not be spinned off by the centrifugal force. The HF solution, HF etch time and DI rinse mode did not seem to affect the formation of these defects.

A comparison of different drying techniques is shown in Fig. 4 and 5. The shape of the big spots in spin dry (2) is illustrated in Fig. 4. Placing the wafers vertically in a spin dry tool and increasing the rotational speed to 1800 rpm (technique 1) leads to the formation of many small defects (Fig. 5). This result is believed to originate from water droplets scattering inside the spinning drum and redepositing on the wafer surface.
The defects can be avoided by a simple manual nitrogen gun dry but this method is unsuitable for high throughput manufacturing purposes. A novel drying technique, called the Marangoni dry, was used after some promising results obtained on patterned wafers [2]. No defects can be observed on the surface of those wafers.
A real process application with structured wafers including hydrophilic and hydrophobic surfaces was simulated. The patterns on the wafers included wide openings of 1cm x 1cm of active area. Inspections of the silicided surface in these areas were performed in microview mode on the CENSOR ANS 100 system. In this mode, a different lens is used to focus the laser beam to a 12 µm diameter spot on the surface. Surfaces up to 3.5 x 3.5 mm^2 can be inspected for haze with high resolution. Using a threshold on the haze value to reject the background haze of the sample, one can clearly distinguish the drying spots on the surface. Fig. 6 shows the result for a wafer which was dried with technique 1, resulting in about 130 drying spots in the inspected area. The same type of wafer is shown in Fig. 7, only this time a Marangoni dry was used yielding a defect free surface. In Table 1, all results on structured wafers are summarized showing that oxide thickness has only little influence on the defect formation. In addition, the sheet resistivity data measured on Van der Pauw structures (Table 2) show that the Marangoni dryer is suited for large scale VLSI manufacturing purposes.

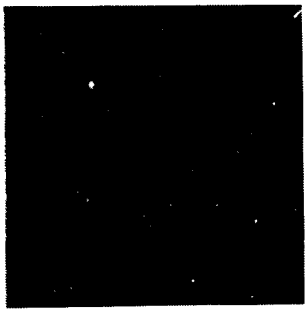

Figure 6: Microview inspection of silicide surface (3.5 x 3.5 mm^2). Spin dry (1) yields many defects.

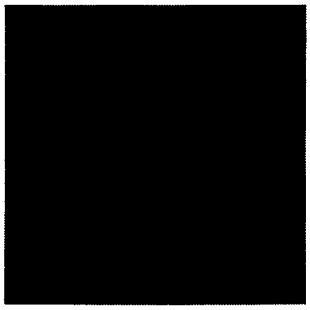

Figure 7: Microview inspection of silicide surface (3.5 x 3.5 mm^2). Marangoni dry (4) yields defect free surface.

Table 1 : Defect counts in 3.5 x 3.5 mm^2 areas by Microview inspection on structured wafers.

Wafer ID	Isolation thickness (nm)	Rinse	Dry	Defect count
1	200	Marangoni tank	Marangoni	1
7	400	Marangoni tank	Marangoni	2
19	600	Marangoni tank	Marangoni	0
2	200	Overflow	Technique 1	120
8	400	Overflow	Technique 1	140
20	600	Overflow	Technique 1	150

Table 2 : Sheet resistivity data measured on Van Der Pauw structures

Dryer	Wafer ID	R_{sh} (Ω/sq)	σ (Ω/sq)
Technique 1	T1	2.66	0.133
	T2	2.60	0.201
Marangoni dryer	T3	2.54	0.119
	T4	2.62	0.175

4. CONCLUSION

The HF-last clean prior to metal deposition sometimes leads to defects in a two step self-aligned $CoSi_2$ process. In this work, the defect formation has been identified to be caused by the drying step after the HF-last etch and DI water rinse. Conventional spin drying of wafers leaves some drying spots on the surface that impede subsequent silicidation. Manual spin drying overcomes these problems but can not be implemented in production. The Marangoni dry also avoids drying spots and offers a feasable manufacturing solution.

5. ACKNOWLEDGEMENTS

Part of this work is sponsored by the ESPRIT, Adequat project. G. ZOU would like to thank Applied Materials Asia Pacific Ltd. for financial support. K. M. is a research associate of the Belgian National Fund for Scientific Research.

REFERENCES

1. Karen Maex, Mat. Sc. and Eng., R1 (1993), p. 117.
2. Franky Jonckx et al., technical report IMEC.
3. K. Locke et al., UCPSS '94.

THE USE OF DEEP ULTRAVIOLET PHOTONS TO REMOVE SURFACE CONTAMINANTS

A.C. Engelsberg
Radiance Services Company
4405 East West Highway, Suite 512
Bethesda, Maryland 20814 USA

Abstract

Dry, chemical-free, laser-assisted removal of particles and films has inherent advantages for standalone and cluster tools. Other applications include the cleaning of non-coincidental surfaces for applications such as gas delivery pipes and tool interiors.

1. Introduction

The industry recognizes that alternative methods for the preparation of clean surfaces are required to maximize yield. Industry experts project approximately 300 cleaning steps will be required for sub-0.5 micron processing.(1) The process complexity makes cluster tools with in-situ cleaning modules and tool self-cleaning desirable. Wet chemical cleaning methods employed today do not lend themselves readily to clustering. A dry cleaning method using an integrated cluster module approach would reduce water and chemical usage along with hazardous waste production. Vapor-phase halogen and UV-initiated reactive species methods have been shown to be adaptable to the cluster module approach. For these methods, etch rate and reaction quenching are key process control problems since electrical parameters as well as the surface integrity can be affected.(2,3)

A new cleaning technique which uses a laser and flowing inert gas with no water or reactive chemicals is a viable and cost-effective approach for standalone cleaning and cleaning modules in cluster tools as well as for tool interiors that have non-coincidental surfaces.

2. Irradiation sources and the flowing, inert gas combination

Combining a chemically inert gas in the laminar flow regime with a photon flux directed to the surface produces a cleaning effect. A high energy irradiation source such as laser can deliver photons of sufficient energy to break bonds, causing the contaminant to rise from the surface through the boundary layer of the flowing gas, where it is entrained and swept out of the processing chamber.(4) Non-thermal bond-breaking occurs at the electronic level where electrons in the outer shell are "shifted" or "exchanged" to one side of the bond or the other to form a stable, neutral species. The precise mechanism of how this type of bond breaking

occurs is not well understood. Since energy exchange is not a perfect process, "simultaneous" multiple photon interactions are probably required.

For this process to be efficient, the choice of irradiation source is important. We have evaluated several UV sources. These include Hg/Xe lamps (500 W and 2400 W), argon ion lasers (single line at 365 nm and multi-line at (351 nm, 353 nm and 365 nm) and KrF excimer lasers (single wavelength at 248 nm). Experiments have shown that broadband Hg/Xe lamps or single or multi-line wavelength, near ultraviolet continuous sources do not provide the correct set of conditions for fast, efficient, bondbreaking. Krypton fluoride (KrF) excimer lasers are the best sources to date for this process.(5) We have determined the base requirements for a light source using this process: wavelength: 248 nm; output energy per pulse: 600 mJ; repetition rate: 30 Hz; duty cycle: 34 ns; and beam profile: flat top. Other excimer lasers such as XeCl (308 nm) or ArF (193 Nm) may be applicable for materials that have poor absorption bands at 248 nm. For all the materials that we have experimented with to date: silicon, gallium arsenide, chrome (bright and dark) on quartz photomasks, indium tin oxide (ITO) on quartz and thin glass, quartz, stainless steel, steel, industrial plastics, oxides from metals, and ceramics.

We have videotaped the removal of particles and thin films (oxides, paint, fingerprints) from surfaces. The contaminants penetrate the thin boundary layer which is located close to the surface through into the bulk gas flow. The bulk flow provides directional bias for the removal of contaminants away from the surface. Contaminant entrainment under the laminar flow regime can be enhanced by by thinning the boundary layer and increasing gas viscosity.

3. Process configuration

The basic process configuration consists of a irradiation source; beam aperture, turning optics (45 degrees) and a final focusing lens. A Lambda Physik LEXtra 200 KrF excimer laser is used. It has a maximum energy output of 600 mJ at 30 Hz with a duty cycle per pulse of 34 ns. Process monitoring is with a Sony C350 CCD camera which is C-mounted to an Infiniti-Var microscope. Stage control is through an Aerotech Unidex-12 controller or by a custom software program that is run from a Macintosh 512. Beam apertures are used to provide beam uniformity. Energy measurements are made with a Molectron JD-1000 joulemeter using a J-50 detector and JBQS diffuser head. Energy measurements between the joulemeter and the laser's internal energy meter are corroborated. Stainless steel gas lines have 0.003 μm point of use filters and an oxygen/moisture filter to 0.01 ppb to minimize contamination. Flow meters regulate gas flow.

4. Process Parameters

This process is "tunable" to the surface and the contaminants to optimize cleaning efficiency and throughput. The key control parameters for the laser are: wavelength, output energy per pulse, repetition rate, duty cycle (pulse duration) and

beam profile. Wavelength, duty cycle and beam profile are fixed conditions of the laser but can be optimized through choice of unit. As explained in section 2, 248 nm is a preferred wavelength probably because there is sufficient photon energy (5.01 eV) to the surface to break typical covalent bonds by the absorption of one or more photons. The choice of the flat top beam profile over the gaussian profile allows for more flexibility in shaping the beam uniformity as it passes through the optical train. Duty cycle refers the pulse duration as achieved by the laser. Duty cycle depends upon the laser's thyratron design. A duty cycle of 34 ns has worked well.

Repetition rate and output energy per pulse are user selectable. These parameters in conjunction with beam focus and scan rate can be adjusted to enhance cleaning efficiency and throughput. We have found that the maximum scan rate (stage velocity) is limited to approximately two-thirds of the maximum scan rate which allows full coverage of the surface without a gap between pulses. Scanning at two-thirds of the maximum rate allows for sufficient pulse overlap to provide good coverage. For the LEXtra 200, this value is 20 mm/s with a beam width of 1 mm.

Output energy of the system depends on the pulse energy leaving the laser and the losses as the pulse train travels along the optical path to the surface. The laser output energy, repetition rate, beam width, and scan rate can be selected to deliver a sufficient energy and power flux to the surface.

We have found that there is generally an energy and power flux window for efficient cleaning which varies by surface and contaminant. Figure 1 shows the window for the removal of thin films and particles from quartz. The optimum average power flux is between 0.1 -0.6 W/cm^2 and average energy flux is between 4-10 J/cm^2. Conditions outside this window are not as efficient. Suitable flux conditions can be achieved for the removal of several types of contaminants at one time. By optimizing the parameters that contribute to the flux values, cleaning efficacy and throughput are readily enhanced.

5. Conclusion

Particles and films can be removed from various substrates by using a dry, laser-assisted process. Throughput and cleaning efficiency are optimized by controlling energy and power fluxes and entrainment by a flowing inert gas removes contaminants from the processing chamber and the gas can be scrubbed and recycled. The absence of liquids and reactive chemicals minimize hazardous waste production from the cleaning process. A variety of materials and objects besides semiconductor wafers can be cleaned.

Figure 1: Average power and energy fluxes for the removal of thin films and particles from quartz.

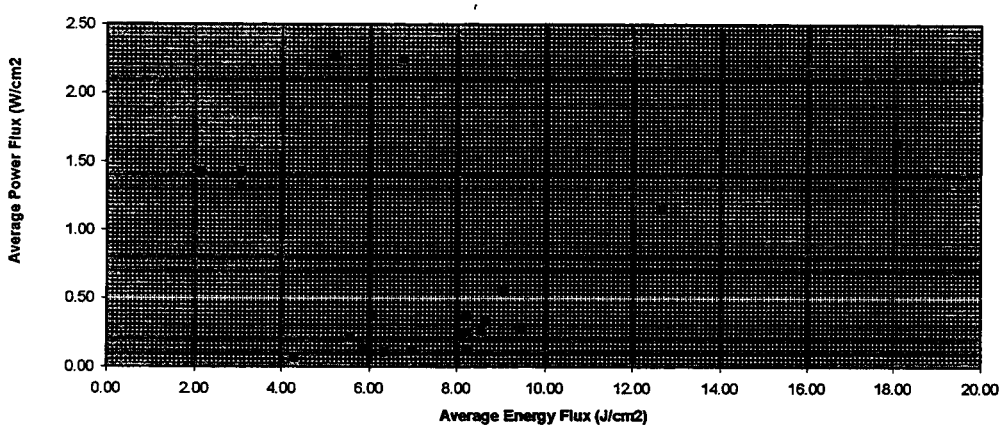

6. References

1. Microcontamination 92 - Ultraclean methods are key to success", January, 1993, p.14.
2. B. Van Eck, S. Bhat, and V. Menon, Proceedings, Microcontamination 92, (Santa Clara, CA, October 27-30, 1992), p.694.
3. C. Werkhoven, E. Granneman, L. Kwakma, M. Hwnseika, S. Verhaverbeke, M. Heyns, and H. Bender, in Proceedings of the Materials Research Society, vol. 315, (Pittsburgh, PA: Materials Research Society, G. S. Higashi, G. A. Irene, and T. Ohmi, eds.,1993,) p.211.
4. A. C. Engelsberg, U.S. Patents 5 024 968, 5 099 557 and patents issued and pending in the United States and foreign jurisdictions.
5. A. C. Engelsberg, in vol. 2361, Optical Contamination IV, (San Diego, CA, S.P.I.E., July 27-28, 1994), in press.

UV-ENHANCED ETCHING OF SILICON OXIDE BY CHLORINE TRIFLUORIDE

C. Fred Hiatt, Jeffery W. Butterbaugh and David C. Gray
FSI International, 322 Lake Hazeltine Drive, Chaska, MN 55318

1. INTRODUCTION

In semiconductor device processing, silicon oxides are used in many forms for many different applications. Dense thermally grown silicon oxide is used as the gate dielectric film in MOS transistors. Steam grown thermal silicon oxide is used as a field oxidation dielectric layer. Doped silicon oxides such as phosphosilicate glass (PSG) and borophosphosilicate glass (BPSG) are used as intermetal dielectrics because they can be easily planarized through reflow. During the processing of silicon based semiconductor devices, other types of silicon oxide films may be formed as the result of exposure of silicon surfaces to chemical processing step, or to the ambient environment. In many cases, these residual oxides are considered surface contaminants since they must be removed to allow the formation of a high quality electrical interface. Often, it is necessary to remove a chemical or native oxide, along with associated residues and contamination from a pattern feature bottom in the presence of one or more of the silicon oxides mentioned above. Oxide etching selectivity is of paramount importance in these cases since different oxides may be etched at drastically different rates.

A current trend in semiconductor wafer processing is towards using gas vapors or all dry gas processes in a cluster tool environment to remove residual oxides and contaminants. It has long been known that vapors of HF/water mixtures will etch various silicon oxide films, and this technology has been well studied [1,2] and commercialized. Etching of oxide films with anhydrous HF has also been well studied [3] and has been found to be affected by the quantity of residual water in the process environment and in the oxide film itself, such that the etching mechanisms appear to be similar to those for HF/water mixtures. A limitation encountered in the use of HF vapor phase etching of oxide films is the low etching rates for native and chemical silicon oxide films relative to doped silicon oxides

Wong et al. [1] have studied the selectivity of the HF vapor etching processes to many different types of oxide films. The results show that native, chemical, and thermal oxides are typically removed at rates up to 10 times slower than the removal rates of PSG and BPSG doped silicon oxides. This is problematic in several common processing circumstances. First of all, it is commonly necessary to clean native oxide and other contaminant from the bottom of contact holes through dielectric layers of BPSG. Using the current vapor phase processes, several hundred angstroms of the BPSG can be removed before the

silicon oxides and contamination in the contact hole are removed. Secondly, it is common to use sandwich structures of different types of silicon oxide films. For instance, a BPSG layer between two undoped oxide layers is sometimes used as the intermetal dielectric film in the above mentioned contact application. Cleaning of contact or other topographic features through this type of composite film with the current HF vapor technology causes enhanced lateral etching of the BPSG layer relative to the undoped oxide layers. This results in an undercut profile which is difficult to fill with subsequent films without forming voids

Here, we describe the application of photochemical (UV-enhanced) processes for the rapid etching of doped and undoped oxide films, and the removal of thin chemical oxide surface layers. Previous work with ClF_3 reported enhanced selectivity of native oxide over silicon under UV irradiation [4]. The processes reported here employ ClF_3 gas in a dry nitrogen carrier stream and simultaneous UV irradiation. Doped and undoped oxides are observed to be removed at nearly identical rates in a large process window (pat. pending).

2. EXPERIMENTAL

The full-wafer reactor used in these studies was an experimental single wafer vacuum cluster module capable of conducting photochemical processing of 100, 150, or 200 mm wafers. The module was attached to a vacuum cluster robotic handler. The reactor module was constructed of hardcoated 6061 aluminum. A dry rough pump was used to pump the vacuum reactor to a base pressure below 10 mtorr. High purity sapphire windows were used to allow UV light exposure of the wafer front side. Gases were introduced in a uniform radial laminar flow, to enhance the transport of etching products away from the wafer surface. High intensity (~200-300 mW/cm^2 at 200-400 nm), broad band UV irradiation was achieved with a commercially available 300 W/inch, medium pressure mercury arc discharge lamp. The wafer pre-process temperature was controlled using a proximity heater. During the period of UV exposure the wafer temperature was transient due to IR output from the UV lamps. However, the wafer temperature typically did not exceed 300°C during processing. Process pressure was monitored and controlled using a capacitance manometer in a feedback loop with a downstream throttle valve.

Substrates used in this study were 150-mm p<100> silicon wafers, 1-5 ohm-cm. Oxide films were prepared by growing 4000Å of silicon oxide in a steam oxidation process at 1000 °C. 5000Å BPSG (3% B, 3% P) films were deposited by CVD over 1000Å of thermal oxide. The gases used C.P. grade (99.0%) ClF_3 and VLSI grade (99.998%) Cl_2. Dry N_2 from a liquid N_2 vapor delivery system was used as a diluent gas.

Thermal oxide and BPSG removal rates were measured by comparing the film thickness, measured by spectroscopic reflectometry, before and after

processing. Silicon removal rates were measured by stylus profilometry on wafers partially covered by a patterned oxide layer.

3. RESULTS AND DISCUSSION

Rates for etching of thermal silicon oxide and BPSG in UV/ClF_3 processes are shown in Figure 1 for an initial wafer temperatures of 150°C as a function of ClF_3 concentration. Total flow was maintained at 1000 sccm using dry N_2 as a diluent, and total pressure was maintained at 100 Torr. Thermal oxide and BPSG were found to etch at similar rates with a selectivity of better than 1.5 (BPSG:thermal oxide).

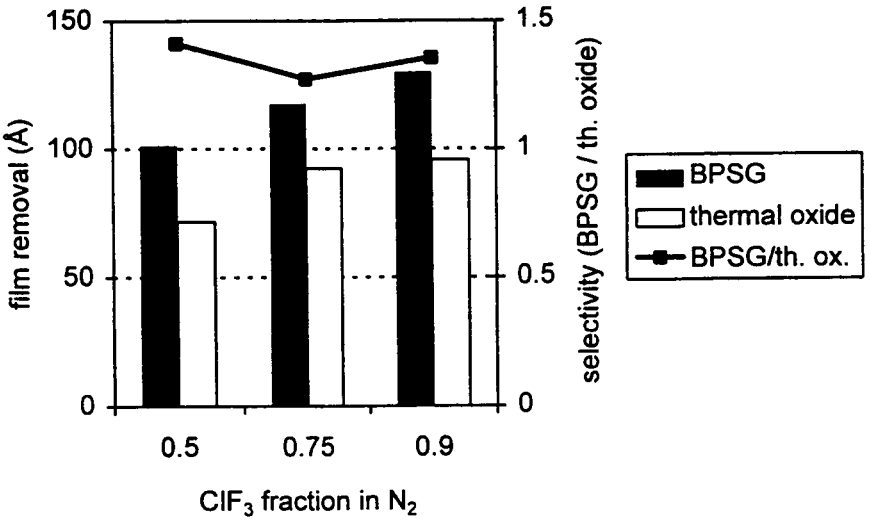

Figure 1. Removal rates of BPSG and thermal oxide during UV/ClF_3 processes at 150°C as a function of ClF_3 concentration.

The removal of 10-20Å chemical oxide layers using UV/ClF_3 and UV/(ClF_3+Cl_2) processes was also investigated. Oxide patterned p<100> wafers, comprising 1-5μm lines and vias, were subjected to an RCA-type wet chemical clean to produce the chemical oxide layer in the unpatterned regions. The wafers were then processed with UV/ClF_3 or UV/(ClF_3+Cl_2). The ClF_3 only process used 2.5 sccm ClF_3 with 997.5 sccm N_2. The ClF_3+Cl_2 process used 2.5 sccm ClF_3, 50 sccm Cl_2 and 947.5 sccm N_2. Both processes were run at 100 torr with an initial wafer temperature of 100°C. Several wafers were exposed to UV for time periods ranging from 0.5 minutes to 3 minutes. The oxide pattern mask was subsequently stripped, and the depth of etching into the silicon substrate was measured using a

stylus profilometer. The results of these experiments are summarized in Figure 2. Regression of the time series back to a zero (undetectable silicon etch depth) indicates that the chemical oxide was removed after approximately 30 seconds of UV exposure under the experimental conditions. Comparison of the silicon surface roughening after chemical oxide removal for the two processes revealed that the UV/ClF_3 process resulted in a visually rough surface, while the UV/(ClF_3+Cl_2) process left the silicon surface substantially smoother. This process is expected to be applicable as a dry contact clean.

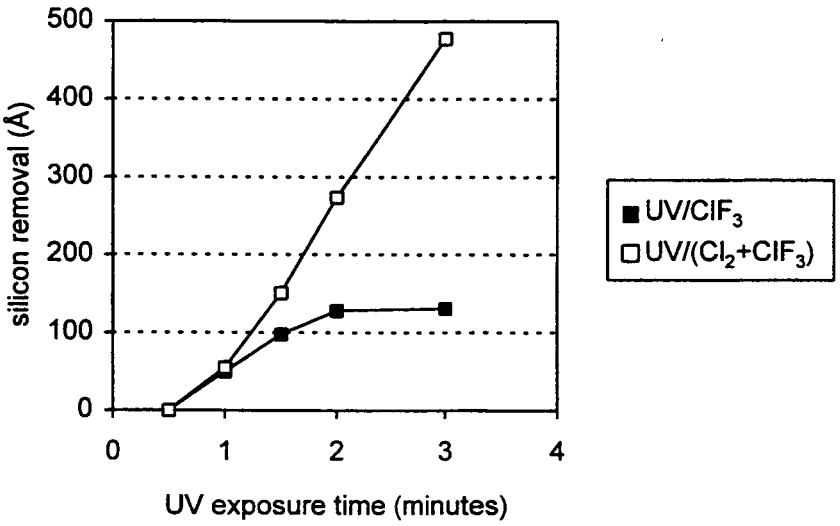

Figure 2. Silicon removal as a function of UV exposure time for UV/ClF3 and UV/(Cl2 + ClF3) processes indicating the time to remove 10-20Å of chemical oxide.

REFERENCES

1. M. Wong, M. Moslehi and D. Reed, *J. Electrochem. Soc.* **138**(6), 1799(1991).
2. M. Wong, M. Moslehi and R. Bowling, *J. Electrochem. Soc.* **140**(1), 205(1993)
3. C. Helms and B. Deal, *Journal of the IES*, 21(1992).
4. Y. Saito, O. Yamaoka, amd A. Yoshida, *Appl. Phys. Lett.* **56**(12), 1119(1990).

A NEW METHOD FOR IN-LINE, REAL-TIME MONITORING OF WAFER CLEANING OPERATIONS

E. Kamieniecki*, P. Roman, D. Hwang, and J. Ruzyllo

EMPRL, Dept. of Electrical Eng., Penn State Univ., University Park, PA 16802, USA
* QC Solutions, Inc., Woburn, MA 01801, USA

1. INTRODUCTION

Surface charge is very sensitive to the physical and chemical condition of the silicon surface. In particular, its sensitivity to the parameters of surface cleaning operations has been demonstrated using conventional surface charge measuring systems that required physical contact between the probe and the wafer [1,2]. The problem with this last technique is that while monitoring cleans the probe may transfer surface contaminants from one wafer to another. Also, as a result of frequent physical contacts with measured surfaces the condition of the probe head gradually degrades altering the results. In addition, these measurements require designated test wafers as once brought to contact with the measuring probe, the wafer cannot be returned to the production lot. As a result, such measurements are potentially suitable for diagnostic purposes, but are not useful for in-line process monitoring.

In this work, a novel commercial surface charge sensing apparatus [3], which does not require contact to the wafer and uses low intensity light excitation to measure surface charge, is introduced as a tool for monitoring wafer cleaning operations. The system works with either individually handled wafers, or with a wafer transfer system to provide real-time, in-line monitoring of the condition of the surface of the product wafer in motion. Consequently, each product wafer, not just selected test wafers, can be inspected in the truly non-invasive fashion and without any effect on the wafer transfer between processes.

2. EXPERIMENTAL

Figure 1 shows a block diagram of the system used in this study. The measurement, based on the photovoltaic effect, is accomplished by passing a wafer underneath the charge measuring probe equipped with an adequate light source. The distance between probe and the wafer was automatically adjusted to 0.1 mm. Both the distribution of surface charge along the diameter of the wafer and the average surface charge are determined, recorded, and displayed.

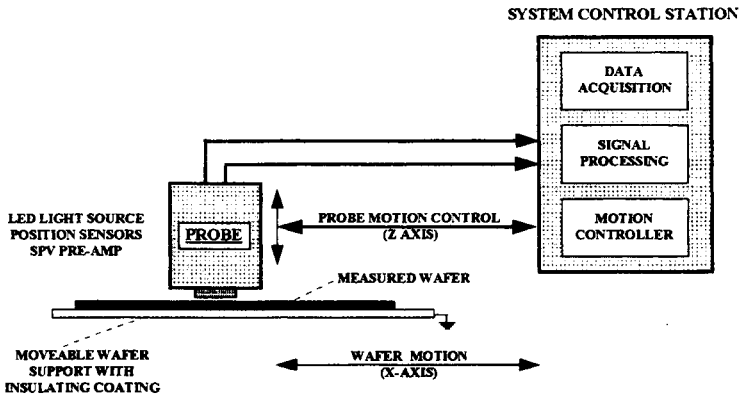

Figure 1 Schematic diagram of the surface charge profiler used in this study

In this study, the above system was used to monitor the performance of wet cleaning operations via remote sensing of surface charge. The standard cleaning sequence in this study involved the following steps: SC-1(5:1:1) / Rinse / HF:H_2O(1:100) / Rinse / SC-2 (5:1:1) / Rinse- Dry / Charge measurement.

3. RESULTS AND DISCUSSION

Each step in the cleaning sequence given above affects the surface in a different and distinct fashion that is reflected in the magnitude of the surface charge as shown in Fig. 2. It was observed that the surface charge for wafers directly out of the box varies depending on batch and supplier, but after the SC-1 step always turns negative. Subsequent HF

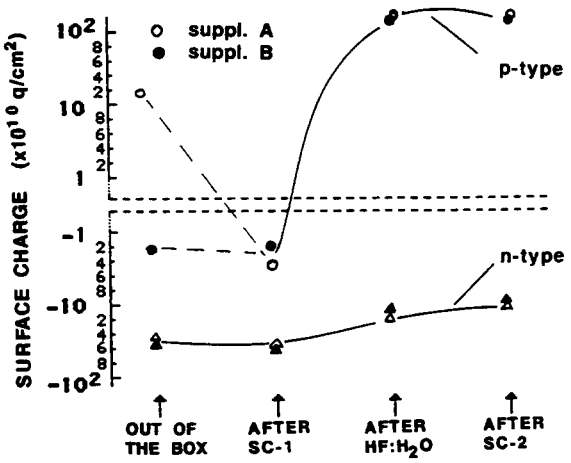

Figure 2 Surface charge at various stages of Si wafer cleaning process.

dip always renders surface substantially more positively charged and SC-2 step sustains this condition

Figure 3 demonstrates that changes in the cleaning recipe can be readily detected by the remote monitoring of surface charge after completion of the entire cleaning sequence.

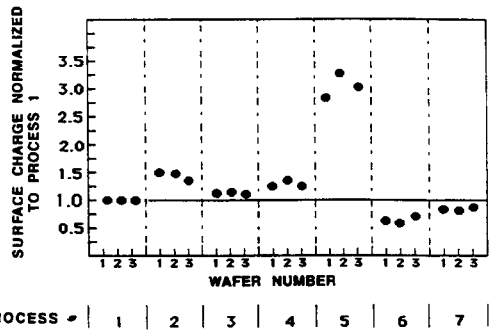

1 - SC-1(5:1:1, 80 °C) / Rinse / HF:H_2O (1:100) / Rinse / SC-2(5:1:1, 80 °C, 10 min.) / Rinse-Dry

2 - SC-1(5:1:0.25, 80 °C) / Rinse / HF:H_2O (1:100) / Rinse / SC-2(5:1:1, 80 °C, 10 min.) / Rinse-Dry

3 - SC-1(5:1:1, 60 °C) / Rinse / HF:H_2O (1:100) / Rinse / SC-2(5:1:1, 80 °C, 10 min.) / Rinse-Dry

4 - SC-1(5:1:1, 80 °C) / Rinse / HF:H_2O (1:100) / Rinse / SC-2(5:1:1, 80 °C, 1 min.) / Rinse-Dry

5 - SC-1(5:1:1, 80 °C) / Rinse / SC-2(5:1:1, 80 °C, 10 min.) / Rinse / HF:H_2O (1:100) / Rinse-Dry

6 - SC-1(5:1:1, 80 °C) / Rinse / SC-2(5:1:1, 80 °C, 10 min.) / Rinse-Dry

7 - SC-1(5:1:0.25, 80 °C) / Rinse / SC-2(5:1:1, 80 °C, 10 min.) / Rinse-Dry

Figure 3 Changes in the cleaning recipe cause changes in the value of surface charge measured after completion of cleaning

The sensitivity of the remote surface charge profiler used in this study to the condition of the silicon surface is further demonstrated in Fig. 4. This figure shows the distribution of surface charge along the diameter of the wafer which following SC-1/Rinse treatment was partially immersed in HF:H_2O solution. The shape of the distribution curve clearly distinguishes between part of the wafer that was exposed to SC-1 only (lower charge), and part that following SC-1 was exposed to HF:H_2O (higher charge).

A method introduced in this paper also allows non-invasive monitoring of the evolution of the surface charge following various treatments. Figure 5a demonstrates changes of the surface charge vs. time of exposure to ambient air following two cleaning sequences in which only difference was composition of SC-1 clean (H_2O(5):H_2O_2(1):NH_4OH(1) vs. 5:1:0.25). Figure 5b in turn illustrates evolution of surface charge following HF(1):H_2O(100) immersion with and without subsequent D.I. water rinse. Superior surface stability resulting from the latter treatment is established very clearly.

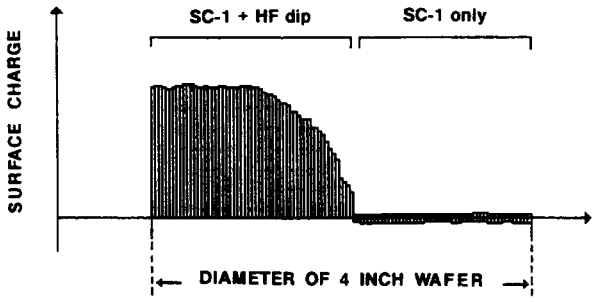

Figure 4 Profile of the surface charge on the 100 mm wafer which after SC-1 was partially immersed in HF/water solution.

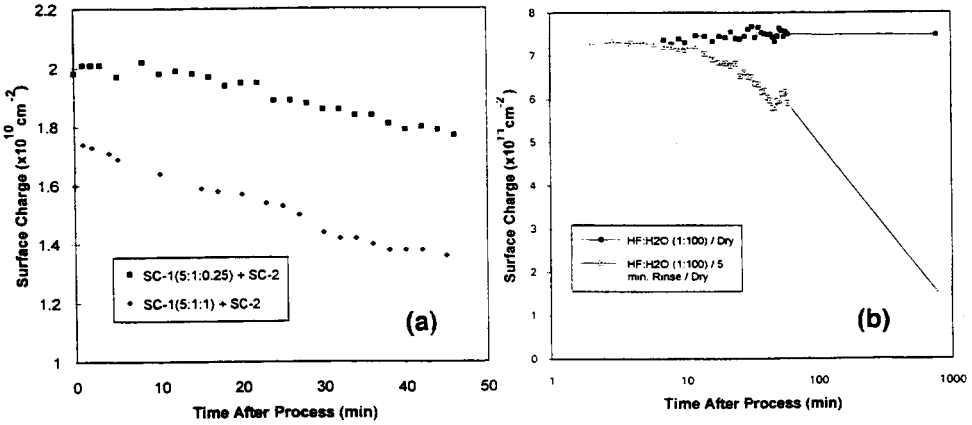

Figure 5 Evolution of surface charge after (a) SC-1 / SC-2 and (b) HF treatments as a function of time of exposure to ambient air.

4. CONCLUSIONS

A totally non-invasive remote surface charge profiler introduced in this paper was found to be a highly versatile and reliable in-line wafer cleaning monitoring tool. Preliminary results indicate also potential usefulness of this tool in the inspection of incoming wafers.

REFERENCES

1. E. Kamieniecki and G. Foggiato, in *Handbook of Semiconductor Wafer Cleaning Technology*, Ed. W. Kern, Noyes Publ., 1993.
2. C. Daffron, K. Torek, J. Ruzyllo, and E. Kamieniecki, Proc. Third. Intern. Symp. on Cleaning Technol. in Semicon. Dev. Manufact., Eds. J. Ruzyllo and R. Novak, The Electrochem. Soc., 1993, p.281
3. Surface Charge Profiler, SCP-110, QC Solutions, Inc., Woburn, MA.

Si surface charge imaging using a high resolution Scanning Kelvin probe

Gerrit H. Bruggink, Iain D. Baikie, The Robert Gordon University, St. Andrew's Street, Aberdeen, United Kingdom, AB1 1HG.

1. Introduction

Surface charge imaging (SCI) via work function topography was performed on a Si wafer supplied by Baltzers Ltd, using a new high resolution scanning Kelvin probe. The Si wafer was terminated by a 100 nm thick oxide layer produced by low temperature plasma evaporation. SCI was performed 1) on the wafer as received 2) after cleaning with ethanol 3) after depositing charge with the probe tip and 4) after depositing charge with a SEM. The study was performed to examine the effect of charged particles and SEM on the surface electrical properties. It was found that such layers are extremely susceptible to electrostatic charging and that once charged, the SiO_2 layer retained its charge over long periods. Initial studies were performed to ascertain the effectiveness of utilising the Kelvin probe to eliminate or reduce surface charging.

The measurement of the work function change, using the non-destructive and non-contact Kelvin probe, provides a simple method of monitoring the surface charge, further extension of the basic technique via illumination[1] can be used to detect surface trapping by defects and perform barrier height measurements.

The Kelvin method depends on the charge flow between two plates of a vibrating capacitor and is thus applicable to conducting and semiconducting materials. If the work function of the reference plate can be maintained constant, then changes in the work function of the sample can be determined absolutely. The scanning Kelvin probe permits both high resolution work function and sample height topographies under a variety of conditions ranging from ultra-high-vacuum (UHV) to ambient.[2 - 5]

2. The Kelvin method

The work function Φ is defined as the minimum energy required to remove an electron from the fermi level Ef to a position 'just outside' Ev. Figure 1a shows an electron diagram of two metals having different work function. In figure 1b the two plates are electrically connected, by closing SW1. The plates form a capacitor, so due to the work function difference, there will be a charge flow from plate two to plate one, charging the capacitor. Vibrating one plate with respect to the other will result in an ac current flow between the plates. By placing an adjustable battery in this circuit, figure 1c, and detecting when this ac current goes to zero, one can determine the work function difference Vc=-Vb, by adjusting the battery. In this way the Kelvin probe operates in the so called null field mode.

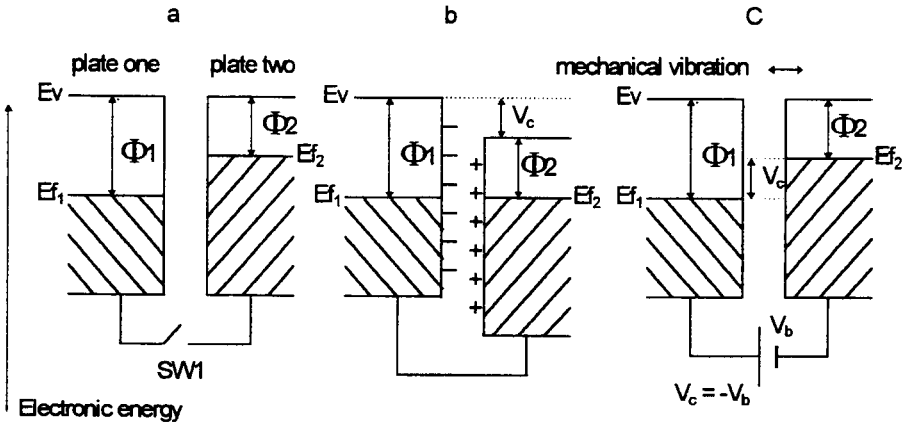

Figure 1 Energy diagram of principle of the Kelvin probe.

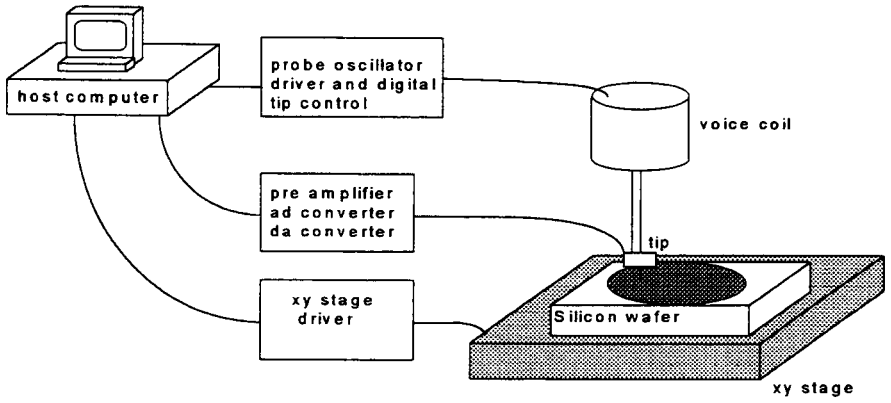

Figure 2 Schematic diagram of measuring equipment.

Figure 2 shows a schematic diagram of the measurement equipment. The xy stage is stepper motor driven for course positioning and with a piezo stack for the fine positioning. The voice coil is constructed using two diaphragm springs to minimize the off axis displacement[6]. An I/V converter is situated close to the tip (an etched Pt wire), an arrangement that has been shown to minimize the effects of parasitic capacity [7].

3. Surface charge imaging

In the following figures surface charge images of a silicon wafer having a 100 nm thick oxide layer grown using a new low temperature plasma deposition process (Baltzer).

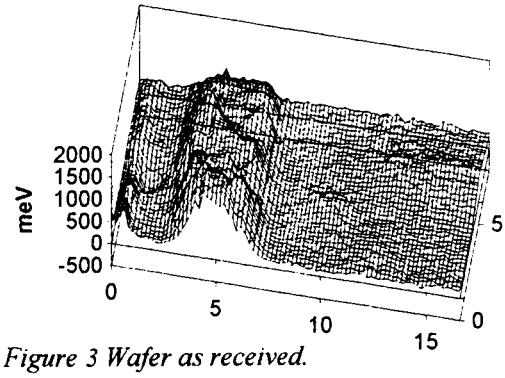

Figure 3 Wafer as received.

In figure 3 we see a scan of a part of a Si wafer as it was received. Differences in surface potential of up to 1500 meV are visible on the surface. This charge could have been deposited before or during shipment of the wafer.

After cleaning with ethanol a scan of the same area of the surface gives a variation in surface potential of 200 meV. See figure 4.

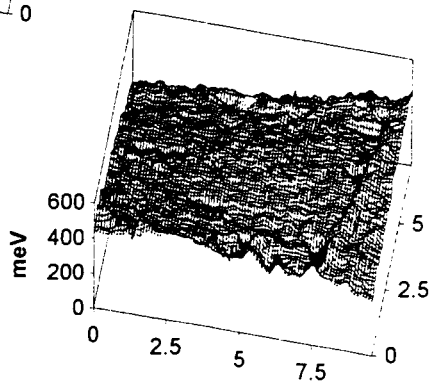

Figure 4 Wafer cleaning

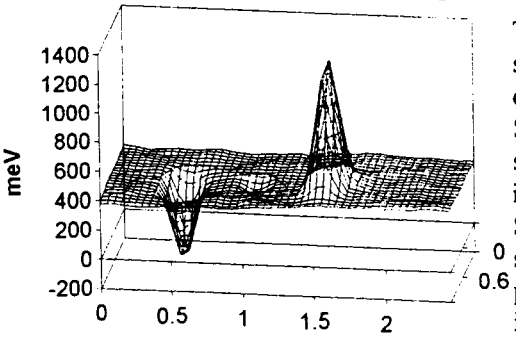

Figure 5 After charge deposited with SKP

To determine if this is charge situated at the surface, charge was deposited on the surface using the SKP, and a part of the surface was scanned, see figure 5. To determine if the charge was not trapped in SiO_x white light was shined on the surface and another scan was performed, there was no difference in the two scans.

To study if there was no physical damage on the surface the sample was examined in a SEM. This showed that there was no damage at the surface. After the SEM study a scan was performed what a SEM did to the charge at the surface. This results in high charges were the SEM was zoomed in. See figure 6.

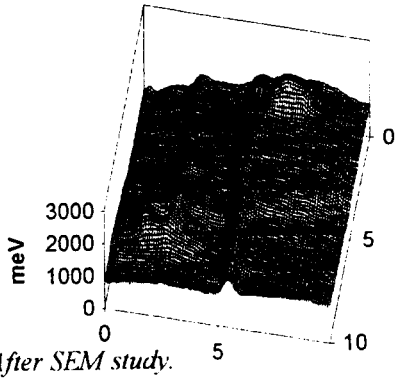

Figure 6 After SEM study.

4. Conclusion and future work

The scanning Kelvin probe (SKP) is a very useful instrument in mapping surface charges. Current resolution is < 100pC / cm ^{2} and spatial resolution is approximately 5μm.

The results for the Baltzers Si/SiO_2 sample shown above indicate that either before or during transportation large amount of charge was deposited on the outside of the oxide layer. Although ultrasonic cleaning in high parity ethanol appears to remove the surface charge we do not attribute this to a removal of charged dust particles or contamination, as charge deposited on the SiO_2 layer using SEM or polarized SKP tip can also be removed in this fashion.

Further investigations using SCI and DLTS surface photovoltage spectroscopy will be performed on Si wafers, supplied by IMEC, which have undergone various cleans and contain known amounts of Fe contamination.

The SKP has also been utilized to image internal, sub-surface, potentials of operational devices such as a transistor and operational-amplifier. Further work on such devices with tips of even higher spatial resolution is in progress.

Research support

This work has been supported by:
The Paul Instrument Fund
The Science and Engineering Research Council (SERC)
The Royal Society
The Engineering and Physical Sciences Research Council (EPSRC)

References

1. I.D. Baikie, Mat. Res. Soc. Proc., 259 (1992) 149.
2. I.D. Baikie and G.H. Bruggink, Mat, Res, Soc. Proc., 306 (1993) 311.
3. I.D. Baikie, E. Venderbosch and B.Hall, Mat. Res.Soc.Proc.,261 (1992) 149.
4. I.D. Baikie, Mat Res. Proc., 204 (1991) 363.
5. I.D. Baikie and G.H. Bruggink, Mat. Res. Proc., 309 (1993) 35.
6. I.D. Baikie, K.O. van der Werf, J.Broeze and A. van Silfhout, Rev. Sci. Instrum.,60 (1989) 930.
7. I.D. Baikie, E Venderbosch, J.A. Meyer and P.J.Z. Estrup, Rev. Sci. Instrum., 62 (1991) 725.

RECOMBINATION ACTIVITY OF IRON-RELATED COMPLEXES IN SILICON STUDIED WITH MICROWAVE AND LIGHT-INDUCED ABSORPTION TECHNIQUES

A.Kaniava, *A.L.P.Rotondaro, *J.Vanhellemont, *E.Simoen, E.Gaubas, J.Vaitkus, **T.Q.Hurd, *P.W.Mertens, *C.Claeys, ***D.Graf

Vilnius University, Vilnius, Lithuania
*IMEC, Leuven, Belgium
**assigned to IMEC from Texas Instruments, Dallas, TX, USA
***Wacker-Chemitronic, Burghausen, Germany

1. INTRODUCTION

The contamination of silicon wafers by transition metals during IC processing has a detrimental effect on crystal perfection and device performance. Iron is one of the most harmful impurities in Si and degrades the electrical characteristics of the devices even at low contamination levels of 10^{11} at/cm^3, which can be easily incorporated during processing [1]. Due to its high mobility, even at room temperature, iron can diffuse into the bulk of the wafer, and form complexes with other impurities, or precipitate [2]. Both dissolved and precipitated iron defects are electrically active. Therefore, a comprehensive control and monitoring of iron contamination is required to avoid deterioration of the device performance.

Methods based on the measurement of carrier lifetime have the potential to be a powerful tool for in-line process control as the carrier lifetime is quite sensitive to low levels of iron contamination [3]. Different measurement conditions are employed for various lifetime measurement techniques, demonstrating that a different behaviour of the recombination activity of the iron-related complexes can be expected depending on the carrier generation rate. In the present paper, recombination properties of Fe-related complexes in intentionally contaminated Si wafers are studied by microwave absorption (MWA) techniques both at low and moderate excitation levels and by a light-induced absorption (LIA) technique at high excitation levels.

2. EXPERIMENTAL

Silicon wafers, CZ, p-type, <100>, 24-36 Ωcm, 125 mm diameter, with medium oxygen content, received a uniform Fe contamination from Fe spiked (0.25:1:5) NH_4OH:H_2O_2:H_2O solutions. The resulting Fe surface concentration (N_S) was in the range of 10^9 at/cm^2 to 10^{13} at/cm^2. The surface contamination was driven into the bulk of the wafers by thermal treatments at 900 ºC for 30 min in dry O_2, wet H_2+O_2 and N_2 ambients. To allow the Fe-B pairing reaction to reach a steady state a one week delay was applied between drive-in and measurement. Low level (LL) injection lifetime was measured by MWA with a 22 GHz Phoenicon GmbH instrument. Surface photovoltage (SPV) and deep level transient spectroscopy (DLTS) were used to address the Fe content in the bulk and to identify the deep levels introduced by iron defects. Effective lifetime under a moderate level (ML) of injection (concentration of excess carriers ≈5×10^{15} carriers/cm^3) was measured by MWA using a 10 GHz microwave system in the microwave transmission mode. After polishing the back side of the samples, measurements of high level (HL) injection lifetime at the excitation level of 10^{17} at/cm^3 were carried out by the light-induced infrared absorption technique (LIA) [4]. The ML and HL techniques used a Q-switched Nd:YAG laser with a wavelength of 1.06 μm and a pulse duration of 10 ns to create excess carriers. The temperature dependence of the carrier lifetime was measured from 20 ºC to 180 ºC on selected samples to evaluate the activation energy of the recombination active defects in a contactless manner. It should be pointed out that all techniques measure the effective carrier lifetime (τ_{eff}) which is affected by the surface recombination to different degrees depending on the excitation levels.

3. RESULTS AND DISCUSSION

A strong influence of the surface passivation is observed for the samples with N_S lower than 10^{11} at/cm^2 (Fig. 1). Annealing in an oxidizing ambient (dry or wet) provides a good surface passivation due to the oxide layer, allowing the bulk lifetime to dominate the measured LL τ_{eff} values. On the other hand, the wafers annealed in nitrogen have a poor surface passivation and the lifetime in those samples is limited by the surface recombination velocity (S). The passivation has a reduced impact for the ML injection regime as S is also injection level dependent [5]. The passivating layers were removed completely when preparing the samples for the optical technique (LIA).

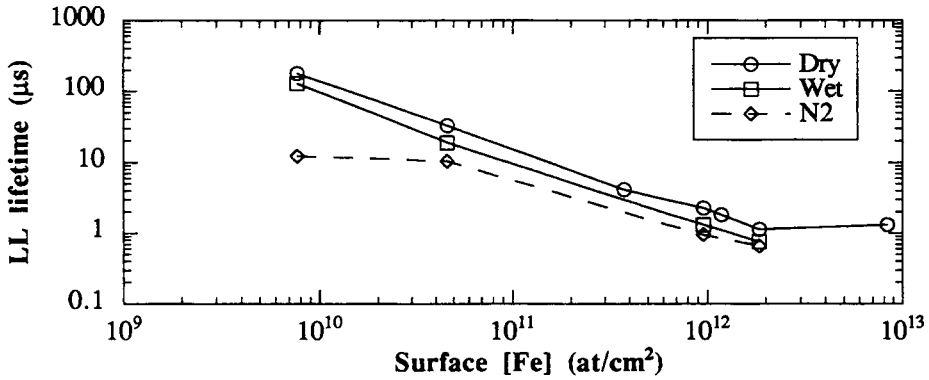

Figure 1: LL lifetime measured by MWA as a function of the Fe surface concentration for wafers annealed in different ambients at 900 °C for 30 min.

The dependencies of the measured ML and HL lifetime for different annealing ambients are presented in Table 1 as a function of Fe surface contamination prior to annealing. In both cases the lifetime decreases by an order of magnitude for wafers with N_S exceeding 10^{11} at/cm^2. The samples with N_S equal to 8.3×10^{12} at/cm^2 exhibit a somewhat increased lifetime values. This wafer was from a different vendor than the other ones and it has a higher as-grown lifetime. The lifetime of the wafers which were annealed in a wet oxidizing ambient is smaller than of those annealed in dry O_2. It was revealed from the Fe bulk concentration measurements based on the SPV algorithm that in a wet ambient more Fe is incorporated in the bulk than in dry O_2 [6]. A possible explanation for this phenomenon is that Fe might be mobile in wet oxides allowing the entire surface contamination to be driven into the bulk.

Table 1: ML and HL lifetime measured, respectively, by MWA and LIA as a function of the Fe surface concentration for wafers annealed in different ambients at 900 °C for 30 min.

Annealing Ambient	Surface [Fe] (at/cm^2)	ML (µs)	HL (µs)		Ratio
			T1 (Fe-B)	T2 (Fe_i)	T2/T1
Dry	7.7E9	43.3	29.3	-	-
Wet	7.7E9	59.1	25.6	-	-
Dry	4.6E10	27.1	21.8	-	-
Wet	4.6E10	24.4	25.0	-	-
N2	4.6E10	6.7	19.2	-	-
Dry	3.7E11	3.65	3.84	19.6	5.1
Dry	9.5E11	1.56	2.3	11.1	4.8
Wet	9.5E11	1.05	1.2	12.7	10.6
N2	9.5E11	0.83	2.5	6.6	2.6
Dry	1.8E12	0.88	0.69	11.3	16.4
Wet	1.8E12	0.64	0.38	3.82	10.1
Dry	8.3E12	1.4	1.0	13.2	12.8

Since both interstitial Fe (Fe_i) and Fe-B pairs introduce deep levels in the lower half of the Si bandgap, they can be detected by DLTS and used for the determination of the Fe content. DLTS measurements performed on the wafers annealed in dry O_2 indicate that all Fe is paired with B, even for the highly contaminated samples. The Fe-B pairs introduce a shallow donor level at Ev+0.10 eV. The density of this trap is in good agreement with the LL lifetime (Fig. 2).

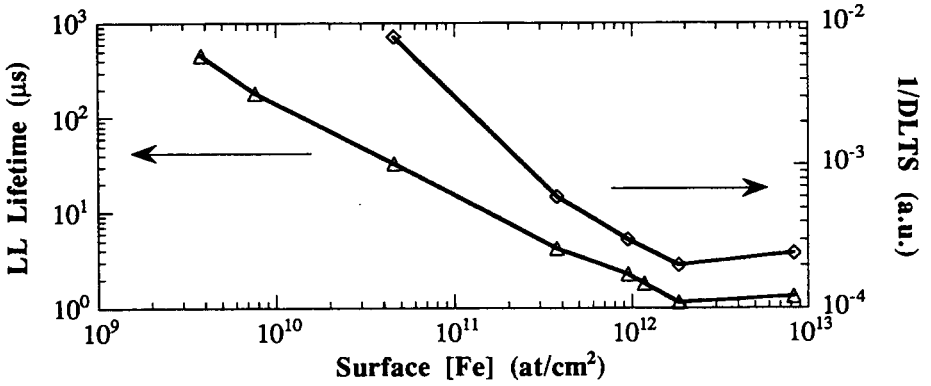

Figure 2: Correlation between the inverse of the DLTS peak and LL lifetime measured by MWA as a function of the Fe surface concentration for wafers annealed in dry O_2 ambient.

It is well known that Fe-B pairs dissociate under thermal treatment at 200 ºC or by illuminating the sample with intense light [7]. The photo-dissociation (PD) mechanism was effectively explored for the fast decomposition of Fe-B pairs to monitor Fe in the low concentration range by the SPV method [8]. The transformation of iron defects and the evolution of the HL lifetime due to the PD effect has been observed in the iron-contaminated samples under illumination by a series of laser pulses employed for the carrier generation in LIA measurements. The excitation level was increased up to 10^{18} carriers/cm^3 to accelerate the process. The PD could only be detected on the wafers with N_S larger than 10^{11} at/cm^2. The HL lifetime increases during the decomposition of Fe-B pairs and the ratio of the lifetime after and before the PD varies from 2.5 to 16.5 for different samples (Table 1). As reported by some of the authors [9] the same effect of the increase of the HL lifetime by an order of magnitude was observed previously in CZ and FZ Si wafers contaminated with Fe and high temperature (1200 ºC) furnace annealed. An activation energy of 0.49 eV was determined for the Fe-B pairing process from the HL lifetime recovering after the PD.

The influence of the Fe-B decomposition on the HL lifetime is opposite to what should be expected when the shallow level at Ev+0.10 eV (Fe-B pair) is transformed into the deep level at Ev+0.4 eV (Fe_i), which appears to be a 10 times stronger recombination center than the previous one for LL minority carrier lifetime [10]. For HL both the lifetime of minority and majority carriers contribute to the measured lifetime value. According to the ratio of the capture coefficients of Fe-B and Fe_i [10] for minority and majority carriers, the Fe-B decomposition should increase the HL lifetime about 10 times in agreement to what has been observed. A weak (10-20%) reduction of the ML lifetime has been observed due to the PD of the Fe-B pairs. Most probably, this is caused by the intermediate excitation level used for this technique.

The temperature dependence of the ML and HL lifetime measured on a sample with N_S=1.8x10^{12} at/cm^2 are different (Fig. 3). The HL lifetime increases with temperature and has two well defined slopes with estimated activation energy of E1=0.07±0.02 eV and E2=0.24±0.05 eV in low and high temperature regions, respectively. However, the curve for ML lifetime shows a valley in the interval 80-130 ºC and also has two slopes with E1=0.12±0.02 eV and E2=0.27±0.04 eV in the same temperature regions as the HL. Although the temperature analysis of carrier lifetime yields information on the defect energy level it does not reveal whether this level should be attributed to the conduction or valence band. However, according to the published data on the energy levels of iron-related defects in Si [11,12], one

can conclude that both levels are associated with Fe-B pairs with the bandgap positions Ev+0.10 eV and Ec-0.29 eV, respectively. This explains the recombination-enhanced behaviour of the Fe-B pairs via level Ec-0.29 eV that was observed for the HL lifetime as it is a more effective recombination center than the hole trap at Ev+0.10eV.

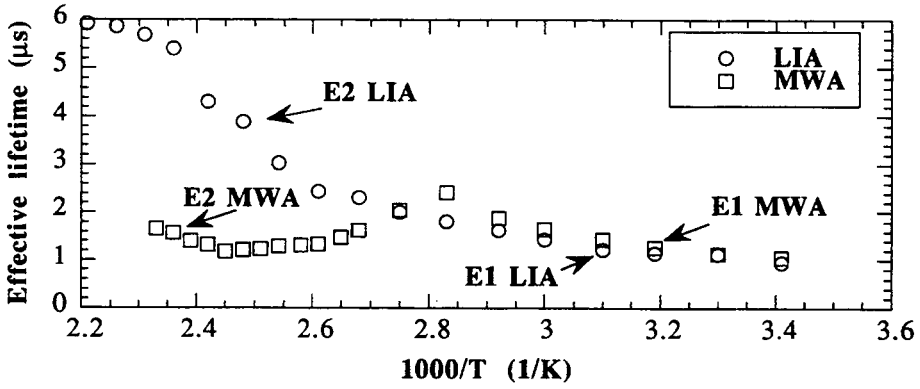

Figure 3: Temperature dependence of ML (MWA) and HL (LIA) lifetime in a sample with surface Fe concentration of 1.8×10^{12} at/cm^2 that has been annealed in dry O_2.

4. CONCLUSIONS

The recombination activity of iron-related complexes in silicon has been studied at low, moderate and high level of excitation. The LL lifetime correlates with the inverse density of Fe-B traps for a range of 10^{11}-10^{13} at/cm^2 of Fe surface concentration before annealing. The photo-dissociation effect of the Fe-B pairs in wafers with surface contamination levels exceeding 10^{11} at/cm^2 has been established at high excitation level, confirming that Fe-B pairs are about 10 times more effective as recombination sites than the interstitial Fe at those injection levels. The temperature dependence of the lifetime, for the temperature range of 20-180 ºC, is governed by the thermal dissociation of Fe-B pairs. Two levels derived from this dependence originate from the recombination behaviour of the Fe-B complex.

5. ACKNOWLEDGEMENTS

A.L.P.Rotondaro would like to acknowledge CNPq (Conselho Nacional de Desenvolvimento Científico e Tecnológico) Brazil, for financial support.

6. REFERENCES

1. L.Jastrzebski et al., Solid State Technol., **35**, pp.27 (1992).
2. K.Graff, Mater. Sci. Engineer., **B4**, pp.63 (1989).
3. L.Jastrzebski et al., J. Electrochem. Soc., **140**, pp.1152 (1993).
4. J.Vaitkus et al., Lith. J. Phys., **32**, pp.1 (1992).
5. D.K.Schroder, Semiconductor material and device characterization, New York, 1990.
6. A.L.P.Rotondaro et al., Extended Abstracts of 186th ECS Meet., pp.625 (1994).
7. K.Graff and H.Pieper, J. Electrochem. Soc., **128**, pp.669 (1981).
8. J.Lagowski et al., Inst. Phys. Conf. Ser. No 135, pp.271 (1993).
9. V.Amstibovskis et al., Sov. Phys. Collect., **28**, pp.80 (1988).
10. G.Zoth and W.Bergholz, J. Appl. Phys., **67**, pp.6764 (1990).
11. Y.Hayamizu et al., J. Appl. Phys., **69**, pp.3077 (1991).
12. S.D.Brotherton et al., J. Appl. Phys., **57**, pp.1941 (1985).

Improved rinsing efficiency after SPM (H_2SO_4/H_2O_2) by adding HF

S. Verhaverbeke[1)], R. Messoussi[1)2)] and T. Ohmi[1)]

[1)]Department of Electronic Engineering, Faculty of Engineering, Tohoku University, Aza-Aoba, Aramaki, Aoba-ku, Sendai 980, Japan
[2)]Research Institute of Electrical Communication, Tohoku University, Katahira 2-1-1, Aoba-ku, Sendai 980, Japan

1. INTRODUCTION

In Manufacturing processes of submicron and deepsubmicrometer ULSI's, the surface microroughness and surface cleanliness of the silicon substrates are becoming crucial for device performance and reliability [1,2].
For the cleaning of silicon substrates, a mixture of an oxidizing and an etching agent is often used. One of the first succesful mixtures (1965) is the well known APM or SC-1 cleaning ($NH_4OH/H_2O_2/H_2O$) [3]. Since then, other mixtures (oxidizing agent/etching agent) such as HNO_3/HF [4], H_2O_2/HF [5] were developed. For the cleaning of silicon substrates, a mixture of an oxidizing agent and an etching agent always results in good particle performance, since the Si under the particles is continuously oxidized and etched simultaneously [4,5].
From all the solutions used in the cleaning technology, one of the best chemical oxides is formed in the H_2SO_4/H_2O_2 mixture. AFM measurements showed that this oxide is the thickest chemical oxide obtained [6]. It also exhibits the slowest etching rate in HF solutions [7]. Moreover, this chemical oxide is one of the best oxides to be used as a preoxide [8] to protect the surface from organic contamination before gate oxidation. However, because of the viscous character of the sulfuric acid, sulfur is difficult to remove completely from the surface even after the standard 10 minutes rinse in deionized water. Recently, an etching study and an electrical evaluation study were performed using an H_2SO_4/H_2O_2/HF mixture by T. Ohnishi et al. [9]. Therefore, we have investigated this mixture that we call SPFM from Sulfuric acid Peroxide hydrogen Fluoride Mixture according to the terminology used by T. Ohnishi et al. [9].

2. RESULTS AND DISCUSSION

At first we investigated the hydrophobicity/hydrophilicity after the cleaning and before the DI water rinsing. Unlike the conventional SPM cleaning after which the treated surfaces are hydrophilic, the SPFM cleaning leads to hydrophobic surfaces as shown by contact angle measurements for various HF concentrations in fig. 1 and 2 on bare Si and on oxide surfaces after the cleaning itself. The SPFM treatment time was held constant at 1 min. If longer processing times are used, then the curves shift even to the left, i.e. higher contact angles for lower HF concentrations. After the following DI water rinse, the surfaces become hydrophilic again (fig. 1 and fig. 2). After the SPFM treatment, there is still a chemical oxide on top of the Si wafer. This is shown in fig. 3 as a function of the HF concentration. In this figure the thickness of the native oxide as after SPFM and followed by a DI water rinse is shown as a function of HF concentration. The SPM treatment without HF yielded an oxide thickness of 0.9 nm. Up to a concentration of 0.01 vol % of HF the same thickness is obtained. Only for higher HF concentrations, the obtained oxide thickness is thinner. XPS measurements show that the surface is F passivated after SPFM, but the F passivation is removed by rinsing in DI water. In fig. 4 the F1s peak is shown after SPFM treatments for different HF concentrations and before DI water rinsing. After DI water rinsing the surface is completely hydrophilic again as can be seen from fig. 1 and fig. 2. Fluorine cannot be detected any more after DI water rinsing. This shows that the fluorine is being replaced during rinsing and thus, after rinsing the same surface is obtained as for a SPM treatment where no HF is present. Since the surface after SPFM is hydrophobic however, both the bare Si and the oxide parts of the wafer, there is no chemical

carry-over in the DI water bath and rinsing is performed much faster. The DI water rinsing efficiency after the cleaning in various SPFM solutions (different HF concentrations) compared to the standard SPM solution was investigated by measuring the time dependence of overflow rinse DI water resistivity as is shown in fig. 5. The resistivity of the DI water reaches 18 MΩ.cm much faster in the case of the SPFM solutions. In this experiment, the flow was maintained at a very low flow of 250 cc/min. In the case of the conventional SPM treatment, often, as in this case is shown, the resistivity shows an irregular behaviour. Of course, this is not always reproducible, but this behaviour can be observed regularly after SPM treatments. This is due to a randomly removal of sulfuric acid contamination.
Whenever an etching agent is mixed with an oxidizing agent, a possibility for surface roughening exists. Therefore, we investigated the surface roughening as a function of HF concentration. The result is shown in fig. 6. The roughness was measured on epi-wafers by Atomic Force Microscopy. The chemical oxide is first removed before the AFM scanning in a 0.5% HF solution. So, every cycle consists of an SPFM treatment followed by an 0.5% HF treatment. The maximum number of iterations was 6. From these measurements it can be seen that the roughness does not increase even after 6 cleaning cycles for HF concentrations of up to 0.01 vol. %. For a concentration of 0.02 %, we can detect a small increase in roughness after the 6th iteration. For a concentration of 0.1%, we can detect an increase in roughness already after the first SPFM treatment. However, after 3 iterations, the roughness is not increased with respect to only 1 SPFM treatment.

3. CONCLUSIONS

We have shown that SPFM solutions result in hydrophobic surfaces, as well oxide as bare Si surfaces. This is most probably due to the fluorine termination after SPFM. In spite of the possible etching character of the SPFM solutions, chemical oxide still remains on top of treated bare Si surfaces. For the useful HF concentrations, the same chemical oxide thickness is obtained after SPFM as after the conventional SPM solution. This suggests that the HF, at the concentrations used, is only changing the termination of the surface of the oxide, but is not etching the oxide. This fluorine passivation results in better sulfur removal and shorter rinsing times, in addition to the power of particle removal reported by T. Ohnishi et al. [9]. Concurrently a chemical oxide still can be formed on the treated surfaces and the fluorine passivation layer is removed during the DI water rinsing. Furthermore, the surface microroughness is not affected by this cleaning for the HF concentrations which are useful for establishing this fluorine passivation.

REFERENCES

1. T. Ohmi , IEDM tech. dig. 1989, p. 49.
2. J.A. Amick, Solid State Technology, 1976, p.47.
3. W. A. Kern and D.A. Puotinen, RCA Rev., 31, p. 187 (1970).
4. A. Ohsawa, K. Honda, R. Takizawa, T. Nakanishi, M. Aoki and N. Toyokura, in *Semiconductor Silicon 1990* (The Electrochemical Society, Pennington, N.J., 1990), H.R. Huff, K.G. Barraclough and J. Chikawa eds., p. 601.
5. T. Shimono and M. Tsuji, Abstract 200, p. 278, The Electrochemical Society Extended Abstracts, Vol. 91-1, Washington DC, May 5-10, 1991.
6. S. Aoyama, Y. Nakagawa and T. Ohmi, in *Extended Abstracts of the 1992 International Conference on Soid State Devices and Materials* (Japan Society of Applied Physics, Tokyo, Japan, 1992), Tsukuba, 1992, p. 126.
7. K. Nakamura, T. Futatsuki, K. Makihara and T. Ohmi, Abstract no. 343, p. 563, The Electrochemical Society Extended Abstracts, Vol. 93-2, New Orleans, LA, October 10-15, 1993.
8. K. Ohmi, K. Nakamura, T. Futatsuki and T. Ohmi, 1994 Symposium on VLSI Technology, p. 109.
9. T. Ohnishi et al., SSDM 1993, Ext. Abst. p. 627, Makuhari, Japan.

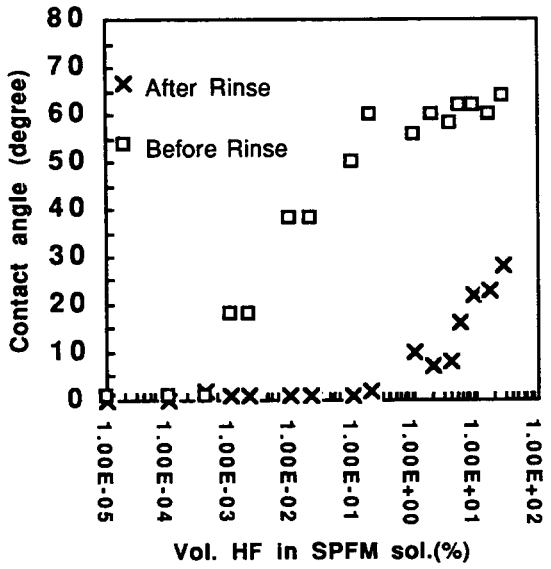

Figure 1. Evolution of the contact angle, before and after rins, on bare Si surface with the HF concentration varied in different SPFM solutions.

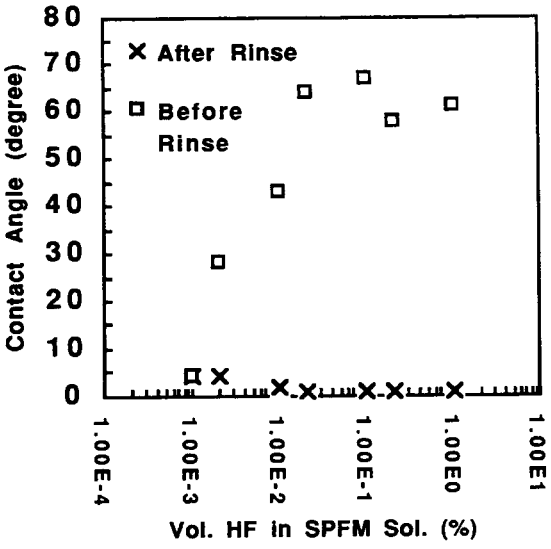

Figure 2. Evolution of the contact angle, before and after rinse on thermal oxide with the HF concentration varied in different SPFM solutions.

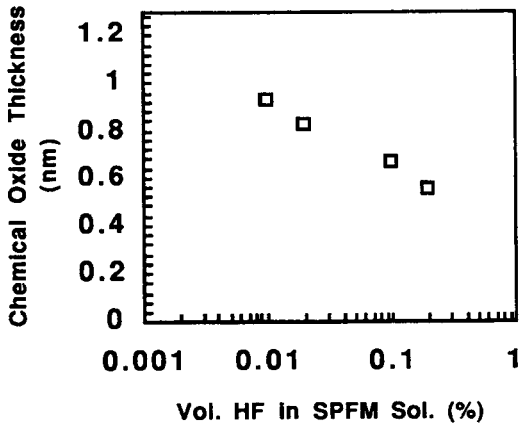

Figure 3. Evolution of the chemical oxide thickness after a 10 min rinse and following an SPFM treatment with different HF concentrations.

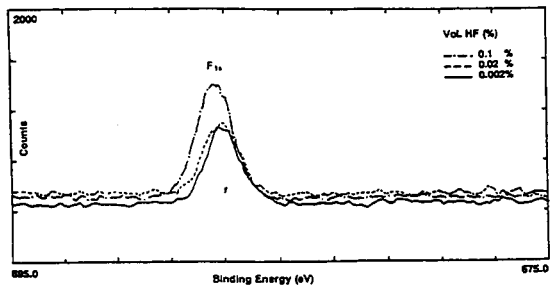

Figure 4 . F1s XPS spectra of Fluorine coverage after various SPFM treatments.

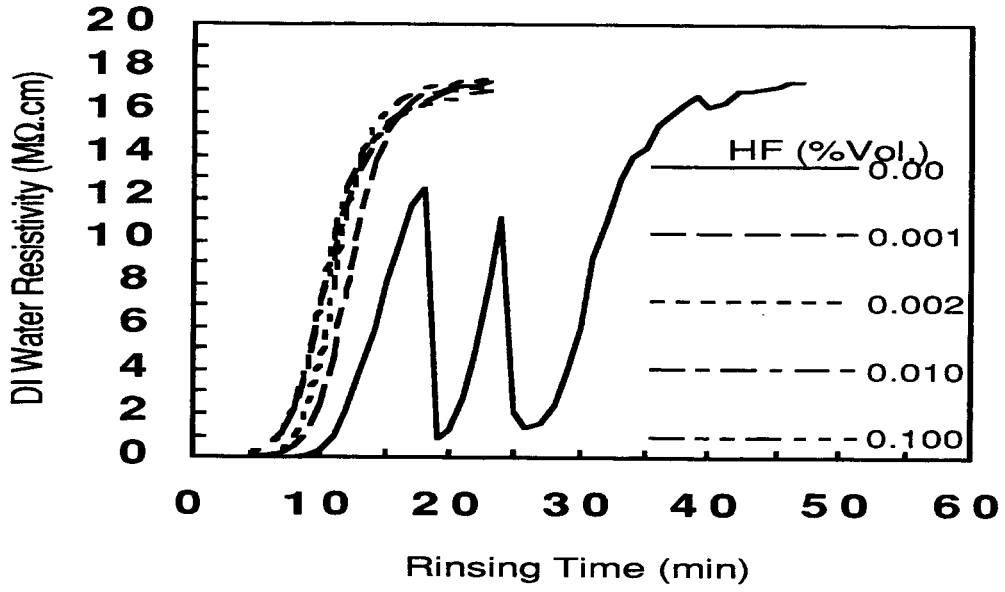

Figure 5. Variation of rinsing DI water resistivity as a function of rinsing time for various SPFM solutions and compared to the conventional SPM solution.

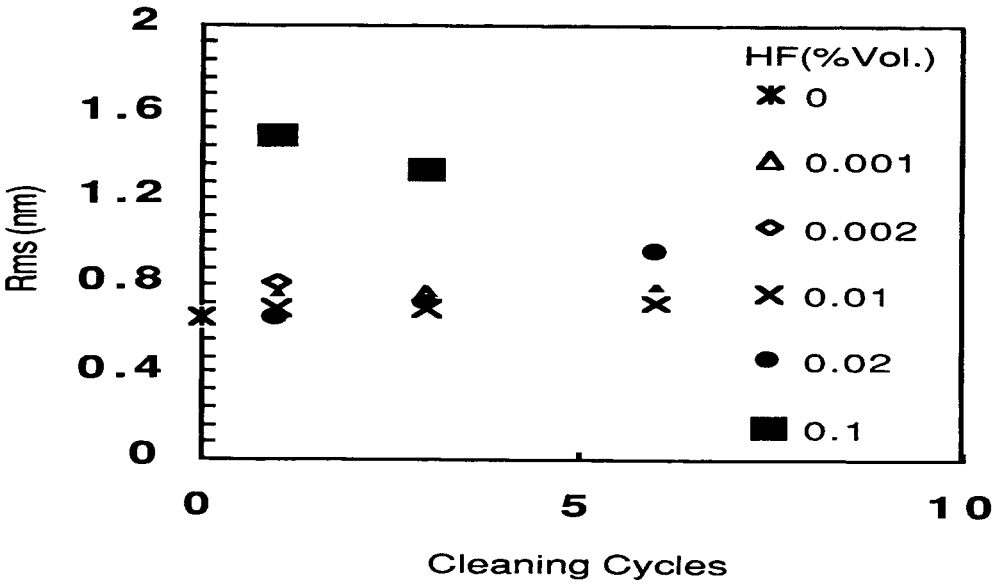

Figure 6. Evolution of the roughness as expressed in the Rms value in different SPFM solutions evalutated by AFM.

FUNDAMENTAL METALLIC ISSUES FOR ULTRACLEAN WAFER SURFACES FROM AQUEOUS SOLUTIONS*

C. R. Helms, H.-S. Park**, S. Dhanda***
Stanford University, Stanford CA
P. Gupta, M. Tran
Intel Corporation, Santa Clara CA

1. INTRODUCTION

The Preparation of wafer surfaces with ultra-low metal concentrations just prior to gate oxide growth is required to provide high yields with respect to low field breakdown defects. The current state of the industry provides for 10^{10} to 10^{11} cm^{-2} levels of metallics leading to 0.1 to 1 defects/cm^2 for 10 nm gate oxides. Future requirements not only lead to thinner gate oxides which are more sensitive to smaller defects and metallics, but yield/die-size/wafer-size considerations requiring lower defect densities. Defect densities down to 0.01 defects/cm^2 will be required for devices appearing shortly after the turn of the century with gate oxides (or equivalent) thinner than 5 nm! The translation of these requirements into allowable levels of surface metallics in the region of the gate oxide and its interface to the substrate are shown for Fe in the lower curve of Fig. 1 , plotted both as a function of year of first production and approximate equivalent oxide thickness. Not all metals on the surface prior to gate insulator formation end up in an active device region, since the properties of the wafer (p-/p+ epi) , the process sequence (add Cl), and gettering (time/temperature/partial pressure sequence) used will mitigate the presence of metals on the surface prior to gate oxidation. A best estimate of the current state of the art gives a tolerance to Fe of about a factor of 1000, which is shown as the upper curve in the figure. Whichever line or region between the lines we choose to target, metal levels consistently in the 10^9 cm^{-2} range will be needed prior to gate oxide growth.

The cleaning of metals to achieve these requirements is complicated by a number of factors: the nature of the bonding and chemistry of the metallics on or in the wafer, the delivery of reactants to the surface, the surface reactions taking place, not only with the metals but with the Si as well as other residues, and the desorption of the reaction products from the surface. In very simple terms the removal of metals from the Si surface can be described by the following "reaction" representing the steps discussed above:

$$(\text{Metal})_{\text{adsorbed}}+\text{Reactants}\Leftrightarrow(\text{Metal})_{\text{dissolved}}+\text{Reaction Products}+\text{Surface Residue}$$

The chemistry of the metal adsorbed on the Si surface is determined by its bonding to the surface region. It can be in the form of the element, its oxide, hydroxide, other salts, silicides, silicates, or organometallic compounds and carbides. Few metals can be expected to occur in the pure metal form due to the stability of their oxides and the fact that any real surface is exposed to oxygen and water. However in aqueous solutions some metals (Au, Cu, & Ni, for example) have large regions of stability compared to their oxides [1,2].

The goal of an aqueous cleaning process is to convert the adsorbed metal into its soluble form. High solubilities are found only for oxidized forms of

* Work at Stanford supported by The SRC and Santa Clara Plastics
** Present Address: Samsung Electronics
*** Additional support from Intel Corporation

metals, typically as the metal ions, hydroxylated ions ($HFeO_2^-$, $Fe(OH)_2^+$), and complexes ($Cu(NH_3)_4^{+2}$, AlF_6^{-3}) [1,2]. Therefore a major role of the reactant must be to oxidize the metal or provide an environment to keep it in an oxidized, soluble form. This is in competition with the equilibrium between the elemental metals themselves, insoluble oxides, and other insoluble forms. Thus low pH solutions (high oxide solubility) coupled with oxidizing agents (H_2O_2, HNO_3) are commonly employed for metal removal.

The kinetics of a given chemical process is also critical. If a metal is buried in or under a native oxide, favorable thermodynamics, although necessary, may be unimportant; the effectiveness of the cleaning chemistry may be determined by the kinetics of the leaching of the metal through the oxide or the removal of the oxide entirely. This is the reason that HF containing chemistries have been demonstrated to be effective for metal removal [3-5]. On the one hand HF can provide a low pH environment leading to high metal ion solubility and on the other it provides a mechanism to dissolve the native oxide that may be passivating not only the Si but absorbed metal.

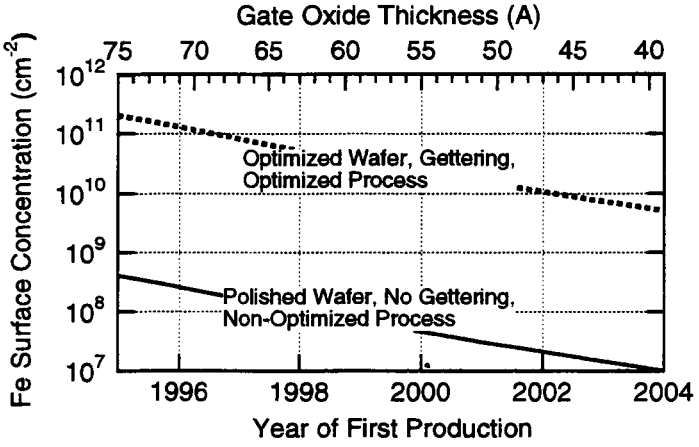

Figure 1. Projections of required Fe concentrations in the gate oxide region as a function of time and gate oxide thickness to meet gate oxide defect specifications (lower curve), and the ability of current state of the art to mitigate these effects, leading to a surface metal specification (upper curve).

2. NATURE OF THE ADSORBED METAL

The model we have developed is based on the assumption that the heats of adsorption of metallics are closely related to the heats of formation of similar bulk compounds [6-8]. We include not only Si and the metal but also oxygen as well. The thermodynamics of the Si/oxygen/metal system is understood with the aid of the ternary phase diagram for the system. The phase diagrams have been catalogued for numerous systems and have been used to understand the thermodynamics and kinetics of silicide formation and oxidation [9]. In addition they have also been used extensively for prediction of compound semiconductor properties, including metallization and passivation [10-12].

The phase diagrams to be constructed are by their nature equilibrium properties of the system at a fixed temperature. For many systems the diagrams are relative insensitive to temperature so it is possible to consider a particular diagram as representative of a system independent of temperature over a

considerable range. Equilibrium implies equilibrium with the vapor phase as well as with the solid phases present. Therefore, it is important to keep the partial pressures in mind, especially since we are considering oxygen as one of the system components.

Si/O/M systems can be categorized by four basic types of ternary phase diagrams[6-8]. One major distinction between two of the types relates to the existence of a stable silicide, a distinction between two other types is the relative stability of the metal oxide. The latter can be evaluated by considering the reaction:

$$\frac{1}{x}M + \frac{1}{2}SiO_2 \Leftrightarrow \frac{1}{x}MO_x + \frac{1}{2}Si$$

If the Gibbs free energy for the reaction is negative, it will be driven to the right (metal oxide more stable than SiO_2); if positive, to the left. Al, Ca, Na, K, and Li, all have oxides (or silicates) that are more stable than the M/SiO_2 couple. We call this a type 1 system with phase diagram as shown in Fig. 2 for Ca.

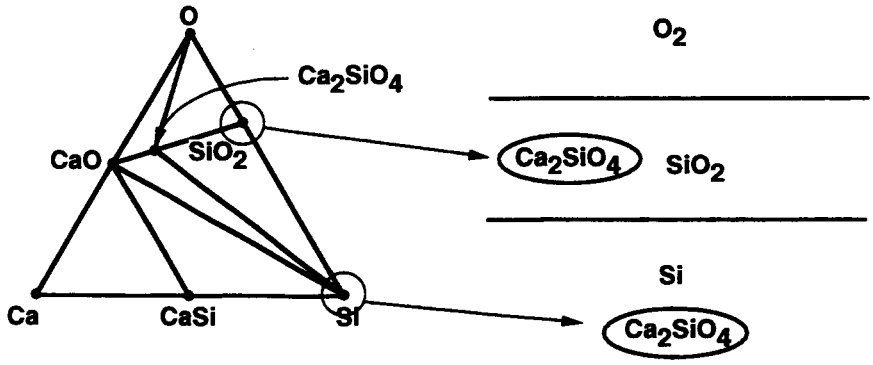

Figure 2. Ca/Si/O Phase diagram (left region) and application to Si/SiO2 system (right region) for gettering and cleaning.

Metals with relatively unstable oxides (Au, and Ag for example) exhibit type 2 diagrams. Cr, Cu, Fe, Ni, and W, with relatively unstable oxides, but stable silicides exhibit type 3 diagrams, whereas Ti with a stable oxide and silicide exhibits a type 4 diagram. They type 3 metals can be particularly difficult to remove for the general case since silicide type bonding may be dominant [6-8].

The region to the right of the phase diagram illustrates its application to surface bonding as well as gettering issues (a similar analysis has been applied to Fe [8]). The application requires a further understanding of the phase diagrams with respect to concentration issues, as the position in the phase diagram is determined by the overall system composition through an inverse level rule. In bulk Si we have a situation of very low oxygen and metal concentration; thus we are dealing with the region of the phase diagram near the Si corner. In CZ Si the oxygen concentration would always be greater than the metal placing the system above and to the right of a line drawn from the Si corner to the CaO position (1:1 Ca:0). The stable phases present would be those at the corners of the triangle enclosing this region of the phase diagram: Si, SiO_2, and Ca_2SiO_4 (in equilibrium with the dissolved species). We would therefore predict that Ca would be gettered in the bulk in SiO_2 precipitates containing some of the calcium silicate phase. As

we move into the Si/SiO2 interface and into the SiO_2 we move up the line between Si and SiO_2 in the phase diagram. The Ca_2SiO_4 phase is still the most stable as indicated. This has 2 implications. First Ca present at or near the interface after gate oxidation will likely be incorporated into the SiO2 matrix as a silicide-like bonded species, and second, the removal of Ca by a chemical clean must have the ability to dissolve the silicate form (it must therefor contain HF, which leads to CaF_2 precipitation to be discussed below).

Unfortunately these phase diagrams have seen little use in evaluating cleaning issues outside the Stanford group. It is interesting therefore to evaluate some other approaches. All approaches are a subset of the general considerations leading to the construction of the phase diagrams. One is based on the metal oxides' heat of formation compared to SiO_2. As we can see from the above reaction, however, such a consideration must be based on the number of oxygen atoms per oxide molecular unit (we must balance the reaction). A ranking on metal oxide stability based on this approach is shown in Table 1. below, showing that Al, Ca, Na, & K (not shown) all have oxides or silicates more stable than SiO_2, whereas all the others listed have oxides that are less stable. Previous rankings based only on the free energies listed Cr and Fe as having more stable oxides than Si and Ca and Na as having less stable oxides [13, 14]. Water has been listed as well to indicate that lacking a suitable oxidizing agent (such as oxygen gas) all the oxides listed below water are relatively unstable and will tend toward their metallic (or silicide) forms.

Table 1. Oxide (Silicate) Stability Ranking Based On Balanced Reaction

ΔH per Oxygen*	Metal Oxide (Silicate)
-169	Ca_2SiO_4
-152	CaO
-144	Al_2SiO_5
-142	Na_4SiO_4
-133	Al_2O_3
-109	SiO_2
-99	Na_2O
-90	Cr_2O_3
-68	H_2O
-65	Fe_2O_3
-58	NiO
-37	Cu0

*The silicates contribution from SiO_2 has been subtracted

2. NATURE OF THE DISSOLVED METAL

For effective cleaning as well as assuring that metals present in cleaning solutions don't deposit on surfaces, the heat of solution of the dissolved form must be greater than the heat of adsorption. This is complicated by the variation of the free energy with the concentration of the species through the entropy term. There is considerable confusion here since the electrochemical literature uses electrical potentials to assess these factors where the thermochemical literature uses an equivalence to enthalpy. An additional complication arises from the need to consider all species that are present. An example is shown in Table 2 where the half cell potentials for selected species are shown along with the corresponding Gibbs free energy (these values correspond to conditions of atmospheric pressure and 1 mole/liter of the appropriate species).

The outlined reaction involving hydrogen is defined as having a potential of 0 volts assuming that we are in equilibrium with 1 atmosphere of H_2 and there is one mole of H^+ per liter (pH = 0). Given this case all reactions above this position in the table are favorable by the free energy given and would proceed to the right. For other conditions of pH and/or equivalent H_2 pressure the effectiveness of the H^+ in oxidizing the metals must be recalculated. Given this information (as well as the information on the stable solid species), the equilibrium can be determined via a reaction such as the one below for Ca:

$$Ca(OH)_2 + 2H^+ \Leftrightarrow Ca^{+2} + 2H_2O$$

The next task is to display the information in a convenient way. One such method is to construct a Pourbaix diagram which maps out the stability of the various phases as a function of pH and potential (see other papers in the volume plus[2]). Another way is to plot the concentration of the soluble species as a function of the concentrations of the other species present. This is a plot of the solubility of the metal; if the concentration in the aqueous phase is less than this value the metal will tend to dissolve, if its is more the metal will tend to precipitate. Such a construction is shown in Fig. 3 for Al, Ca, Fe, and Cu at room temperature as a function of pH (assuming equilibrium with H_2 and no other species present in the solution!). In acid solutions the solubilities are all quite high so we would expect that at pH < 3 effective metal removal should be possible.

Table 2. Half Cell Potentials (per e^-) and corresponding Gibbs Free Energy

Reaction	$-\Delta G$	Potential
$Ca \leftrightarrow Ca^{+2} + 2e^-$	66 kcal/Mole	2.9 eV
$Fe \leftrightarrow Fe^{+2} + 2e^-$	9 kcal/Mole	0.4 eV
$e^- + H^+ \leftrightarrow 1/2H_2$	0 kcal/Mole	0 eV
$Cu \leftrightarrow Cu^{+2} + 2e^-$	-8 kcal/Mole	-0.35 eV
$Fe^{+2} \leftrightarrow Fe^{+3} + e^-$	-17.5 kcal/Mole	-0.75 eV
$H_2O \leftrightarrow 1/2H_2O_2 + H^+ + e^-$	-41 kcal/Mole	-1.75 eV
$CaF_2 + 2e^- \leftrightarrow Ca + 2F^-$	-73 kcal/Mole	-3.15 eV

Unfortunately the situation of Fig. 3 is considerably over simplified. For Cu we have neglected the fact that it is not easily oxidized so the equilibrium between Cu^{+2} and its oxidized form is not appropriate. If ammonium ion is present Cu-ammonia complexes are favored. Except for HF, all solutions of interest contain oxidizing agents (H_2O_2 or HNO_3). This also effects the equilibrium considerably. For the HF case itself, the CaF_2 reaction must also be considered as it is much more stable than $Ca(OH)_2$. Finally the possibility of the formation of silicates by reaction with dissolved silica or surface reactions between the metal ions and silicon surface must also be considered. Some consequences of these effects related to Si cleaning are shown in Fig. 4 where the solubilities have been recomputed for cases of interest. The presence of peroxide will effectively drive Cu to the plus 2 state and the effect of NH_4 complexing on the solubility at high pH's is also evident (in weak acids, especially HF, Cu reduction may be favored leading to metallic Cu deposition as is observed experimentally). For the Ca the effect of 1 ppm F^- ion is indicated; in addition the increased stability of the calcium silicate over $Ca(OH)_2$ will lead to a lower solubility in non fluoride containing solutions. Finally if we consider Fe, the +3 state is more stable in solutions containing even minute amounts of oxidizing agents. It has a

exceedingly low solubility at high pH, but is quite soluble at low pH (<2), especially in the presence of Cl ion.

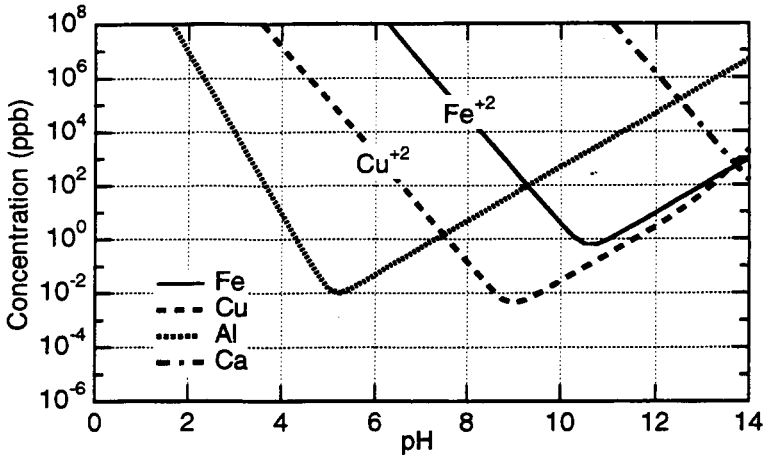

Figure 3. The solubilities of common metals as a function of pH

3. PUTTING IT ALL TOGETHER

The above analysis gives strong evidence that metallic issues in Si can be understood if an overall systematic approach is adopted. Fe deposition from SC1 solutions is driven by precipitation of insoluble Fe^{+3} [7, 15] (mitigated by the etching taking place) whereas the deposition of Al and Ca are driven by the stability of their respective silicates (and CaF_2 if fluoride ion is present). The effectiveness of HF in removing many metals is related to its ability to dissolve many silicates and metal oxides. It's enhanced effectiveness for removing Cu and Ni if employed with an oxidizing agent such as H_2O_2 is due to the ability of the peroxide to keep these metals oxidized; the use of more dilute HF with another stronger acid can dissolve Ca due to its enhanced solubility at low pH.

Although there is clearly more work to be done, a description of the framework of the fundamentals of aqueous cleaning of metallics based on the details of solid phase thermochemistry (through the phase diagrams) and aqueous electro and/or thermochemistry is well in hand. Based on these concepts, for example, it has been possible to construct a mini-CAD tool for prediction of Fe deposition from SC1 solutions, which can be applied to the development of chemical specifications as well as overall process integration and trouble-shooting. Additions to this simulation package for Al and Ca from SC1 solutions is underway [15].

4. SOME NEXT STEPS

There are a number of "incremental" improvements that can be implemented in today's cleaning technology. These improvements can best be developed using a more integrated view than has been applied in the past. For example, the discrepancy between the two lines of Fig. 1 is due to metallic contamination interactions all the way from cleaning through sacrificial oxidations, gettering, and the choice of wafer type.

With regard to metal removal the classification scheme described here presently requires at least 2 steps if we can guarantee that noble metal (Au, Cu, Ni) contamination is not an issues and at least 3 steps if these metals are of concern.

These are typically a sulfuric peroxide (SPM or equivalent) first step followed by an HF-based second step. Unfortunately such a 2 step sequence has an additional drawback related to particle deposition, especially for patterned wafers; in addition some Ca can be left on the surface depending on the Ca level in the HF solution (or solution loading). This has lead to the continued use of SC1 and/or SC2 solutions following the HF step, the former to remove particles and the latter to reduce the metal contamination associated with the SC1. In addition other HF steps may be employed to strip the native oxides formed during the SC1 or SC2 treatments.

A number of papers in this volume speak to possible recommendations for improvements in the chemistries most commonly used. We will summarize some of these here as well as others for comparison purposes.

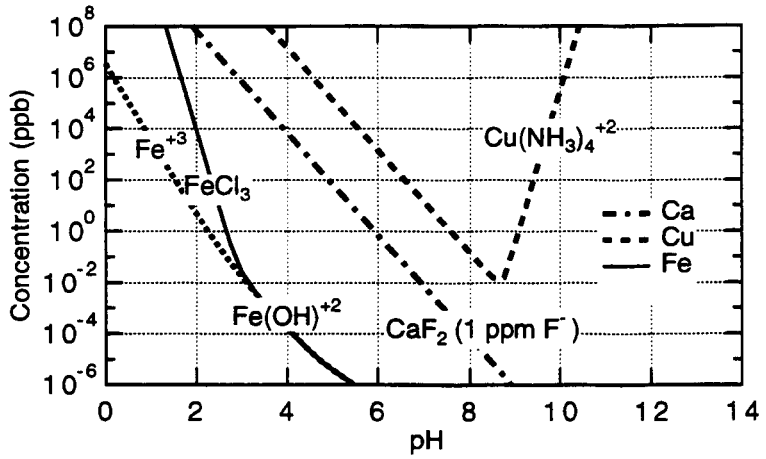

Figure 4. The solubilities of common metals as a function of pH including common additions to the solutions.

4.1 SC1

SC1 is probably the most important chemistry we utilize due to its ability to remove particles. Although we know it leads to the deposition of Fe, Al, Ca, it is still employed as a last cleaning step in numerous places in the industry. Work reported in this volume indicates that at the very least lower chemical concentrations in the SC1 solution are possible along with lower temperatures. Conservatively, ratios of 0.5:1:10 NH_4OH:H_2O_2:H_2O can probably be implemented today at temperatures as low as 50 C. The major problem for SC1-last still relates to the deposition of Fe, Al, and Ca. The latter can be controlled by assuring that the fluoride concentration (as well as total Ca) is kept low. The issues with Al and Fe are best dealt with using extremely pure solutions. From our modeling, we estimate that NH_4OH and H_2O_2 with < 10 ppt Fe and Al will be necessary to meet future metal specifications, even if metal mitigation through wafer choice and process design are practiced. The use of chlorinated species in an oxidation or preoxidation pyroclean can help provide additional process margin for this problem.

4.2 HF

The major issues with HF relates to particle deposition, especially for patterned wafers and the sensitivity of the surface to subsequent contamination; in addition since HF is normally used without an added oxidizing agent, noble metal

plate-back can be a problem and will be very sensitive to dissolved oxygen concentration. Additions of an oxidizing agent (minute amounts of H_2O_2 are sufficient) or a stronger acid with complexing ability lead to HF-based solutions very effective for metal removal, even though the particle problem is still an issue.

4.3 SC2

This is probably the most common pre-gate oxidation-last clean, leading to low metal levels as well as relatively low particle levels if following an SC1 clean. Reducing particle deposition from SC1 cleans can best accomplished by using dilute chemistries to raise the pH and thus modify the zeta potential. The reduced chemistries also lead to effective metal removal as well. From Fig. 4 (consistent with the experimental literature [16]) pH's as high as 2 (at room temperature) should be adequate. On the conservative side chemical ratios of 1:1:50 $HCl:H_2O_2:H_2O$ at a temperature of 50C should be adequate. The presence of the peroxide is necessary to mitigate against solution loading and to assist in removing and keeping the noble metals Au, Cu, and Ni in solution.

REFERENCES

1. W. M. Latimer, The Oxidation States of the Elements and their Potentials in Aqueous Solutions, Prentice-Hall, New York (1952).
2. M. Pourbaix, Atlas of Electrochemical Equilibria in Aqueous Solutions, Pergamon Press, Oxford (1966).
3. D. S. Becker, W. R. Schmidt, C. A. Peterson, and D. C. Burkman, in Microelectronics Processing: Inorganic Materials Characterization, L. A. Casper Ed., p. 366, American Chem. Soc. Symposium Series **295** (1986).
4. W. Kern, J. Electrochem. Soc. 137: p. 1887 (1990), and references therein.
5. M. L. Kniffin, T. E. Beerling, and C. R. Helms, J. Electrochem. Soc., **139**, 1195 (1992).
6. C. R. Helms, in Microcontamination '92 Proceedings, p. 555 (1992).
7. C. R. Helms & H.-S. Park, in Surface Chemical Cleaning and Passivation for Semiconductor Processing, G. Higashi, ed., MRS **315**, p. 287 (1993).
8. C. R. Helms & H.-S. Park, in Cleaning Technology in Semiconductor Device Manufacturing, J. Ruzyllo, ed., ECS **394-7**, p. 26 (1994).
9. R. Beyers, J. Appl. Phys., **56**, p. 147 (1984).
10. R. Beyers, K. B. Kim, and R. Sinclair, J. Appl. Phys., **61**, p. 2195 (1987).
11. C. R. Helms, J. Vac. Sci. Tech., A8, p.1178 (1990), and references therein.
12. C. R. Helms and V. Krishnamurthy, J. Vac. Sci. Tech., B10, p.1525 (1992), and references therein.
13. M. Takiyama, S. Ohtsuka, S.-I. Hayashi, and M. Tachimori, in Proceedings of the 19th Workshop on ULSI Ultra Clean Technology (1992).
14. T. Ohmi, T. Imaoka, I. Sugyiama, and T. Kezuka, J. Electrochem. Soc., **139**, p. 3317 (1992).
15. C. R. Helms, S. Dhanda, H. G. Parks, Sematech Report, to be published.
16. P. M. Mertens, T. Q. Hurd, D. Graf, M. Meuris, H. F. Schmidt, M. M. Heyns, in Contamination Control in Semiconductor Manufacturing III, D. Schmidt ed., ECS **94-9**, p. 241 (1994), and references therein.

ACKNOWLEDGMENTS

The Stanford authors would like to thank Baylor Triplett for his support and making the facilities on Intel's Component's Research Laboratory available for past studies. Additional support from and discussions with researchers at Texas Instruments, Sematech, Hewlett Packard, Motorola, and Santa Clara Plastics are gratefully acknowledged.

ELECTROCHEMICAL ASPECTS OF NOBLE METALS RELATED TO SILICON WAFER CLEANING

Oliver M.R. Chyan, Jin-Jian Chen and Hsu Y. Chien,
Department of Chemistry, University of North Texas,
Denton, TX 76203, USA

Lindsey Hall and Jennifer Sees
Chemical Operations Department, Texas Instruments,
Dallas, TX 75265, USA

1. INTRODUCTION

The presence of trace quantities of metal contaminants on silicon substrates is well known to have catastrophic effects on both device performance and process yield. For example, at 10^{11} - 10^{13} atoms/cm^2 level, degradation of the gate oxide integrity as well as crystal defects has been observed. Minority carrier lifetime has also been found to be reduced by metal contaminants as low as 10^{10} atoms/cm^2. As the microelectronic fabrication technologies gear toward submicron dimensions, there is a pressing need to reduce the sources of the possible surface metal contaminants on wafers, especially from wet chemical processing. In the past, efforts have been mainly directed on reducing the metallic levels across the board in process chemicals and wafer handling components. However, this method may not be cost effective due to the fact that not all the chemicals behave in the same fashion. For instance, with the same level of the metallic impurities, it may be acceptable in one chemical system but for another chemical systems it can have detrimental effects on device performance and yield. Therefore, understanding the deposition mechanisms of various metal contaminants and their interplays with silicon substrate surface properties at specific chemical environments have received a lot of research attention lately.

Heavy noble metals such as Cu, Ag, Au, Pd have been shown to plate out, at various degree, in the form of metallic deposits from many HF related wafer cleaning chemical systems. It is commonly accepted that the out-plating of noble metals is the results of a displacement electrochemical reaction between metal ions and the silicon surface. While several studies on the metal deposition of HF-treated surfaces have been reported[1-3], relatively little quantitative information is available on the electrochemical influences on the deposition kinetics and morphology, especially at the early stage of metal out-plating process. In this paper, we present an initial time dependent study of the interaction between Cu^{2+} metal ions and the

HF-treated silicon surfaces using atomic force microscope (AFM). The Cu out-plating kinetics was found to be consistent with the diffusion-control electrochemical reactions which are frequently encountered in large-amplitude potential step chronocoulometry experiments.

2. INTERFACIAL CHARACTERIZATION ON Cu/HF-TREATED SI

The experiments were carried out with polished *p*-Si(100) prime CZ-wafers (boron doped, 7 x 10^{15} atom/cm^2, ρ = 1.6-2.2 Ω cm, Texas Instruments). The HF pre-treated Si samples were placed into 5.10 ppm Cu^{+2} ($CuSO_4.5H_2O$, 99.999% , AESAR)/4.9% HF solution for various deposition times. After ultra-pure water rinses and air dry, the Cu^{+2}/HF treated silicon samples were characterized by the AFM. Our AFM results[4] demonstrated that the HF-treated silicon surface is smooth (mean roughness < 0.2 nm) and featureless. However, the subsequent dipping into Cu^{2+}/HF solution produces rougher terrains which are covered by the mostly segregated, nanometer size Cu nuclei deposits. The detailed topographical analyses reveal, as illustrated in *Figure 1*, that the number of Cu nuclei first increases with the deposition time up to 60 seconds and then it reaches a constant plateau at about 1.1 x 10^{10} nuclei/cm^2 level afterward.

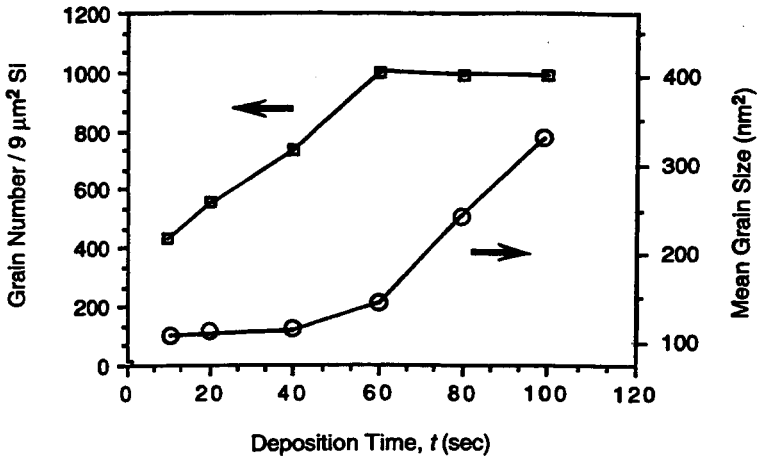

Figure 1. Nucleation vs. growth of Cu deposits on HF-treated Si.

Concurrently, the average grain size of Cu nuclei was found to be capped at about 110 nm^2 for the first 40 seconds period of Cu

deposition and then increases rapidly to ca. 340 nm^2 at the end of 100 seconds deposition. These results indicate the nucleation process dominates the initial stage (< 60 seconds) of Cu deposition, and the nucleation preferentially originates from a finite number of the active sites which depend on intrinsic surface properties of the silicon substrate. Consequently, the growth of the existing Cu nuclei is suppressed for the initial nucleation period until all the active sites are consumed. It is well documented that surface defects like dislocations, stacking faults and oxygen precipitates in CZ-grown silicon can be designated as the nucleation sites for the purpose of scavenging metal impurities[5]. However, similar information of linking metal deposition from wet chemical solutions to specific defect sites on silicon substrates is relatively scarce.

Scanning probe microscopic techniques, like AFM, have a unique imaging advantage of surveying three-dimensional topographical features on the sample surface. In the case of Cu^{2+} interaction with H-passivated silicon, the acquired three-dimensional AFM images of Cu deposits can be integrated to provide the total volume of Cu nuclei situated above the silicon background surface. Consequently, the deposition kinetics for the Cu^{2+}/H-passivated silicon system can be delineated from the relationship of Cu integrated volumes with respect to deposition times. *Table 1* lists the measured Cu deposits integrated volumes per cm^2 on the silicon substrate (V_{Cu}) with respect to deposition times (t).

Table 1. Total volume of Cu deposit vs. deposition time

Deposition time, t (sec)	10	20	40	60	80	100
Cu(s) volume, V_{Cu} (10^{14} nm^3)	4.1	5.5	8.3	11.6	12.8	14.1

3. ELECTROCHEMICAL ASPECTS OF THE OUT-PLATING PROCESS

The total integrated volume of Cu deposit (V_{Cu}) is found to be linearly proportional to the $t^{1/2}$. The $t^{1/2}$ dependence of deposition kinetics is consistent with the diffusion-control electrochemical reactions which are frequently encountered in a large-amplitude potential step chronocoulometry experiment. This well known "Cottrell condition" begins with a quiescent, homogeneous solution of redox species in which the planar working electrode is suddenly subjected to a large-amplitude potential step to initiate the heterogeneously electron

transfer reactions. The highly energized working electrode surface is very active and reacts instantaneously with the redox species upon contact. Therefore, the surface concentration of redox species is effectively zero and the overall reaction rate is limited by diffusion of the redox species across the stationary diffusion layer. As shown in equation 1, the resulting diffusion-limited cumulative charge (Q_d) is proportional to $t^{1/2}$.

$$Q_d(t) = 2nFAD^{1/2} C \pi^{-1/2} t^{1/2} \quad (1)$$

n is the number of electrons per molecule oxidized or reduced. F is the Faraday constant. A is the area of electrode. D and C are the diffusion coefficient and the bulk concentration of the redox species, respectively.

In the present case, a heterogeneous electron transfer reaction takes place at the interface between the H-passivated Si surface and Cu^{2+} ions from the HF solution. The extent of Cu out-plating is controlled not only by the reduction-oxidation potential differences between Cu^{2+} ions and the silicon surface, but also by the means of mass transport to supply Cu^{2+} ions to and remove oxidized products from the silicon surface. We will present some of our preliminary results on the potentiometric measurements in the various Cu^{2+}/HF related solutions. The results will be discussed in the context of metal deposition mechanisms and metal contaminant controls.

ACKNOWLEDGEMENTS: Texas Instrument is greatly acknowledged for financial support. O.M-R Chyan gratefully acknowledges the Faculty Research Grant from the University of North Texas. We thank Lisa Lester and Bud Schmidt for the technical assistance.

REFERENCES

1. L. A. Nagahara, T. Ohmori, K. Hashimoto and A. Fujishima, J. Vac. Sci. Technol., A11(4), (1993) 763.
2. E. Hsu, H. G. parks, R. Graigin, S. tomooka, J. S. ramberg and R. K. lowry, J. Electrochem Soc., 139, (1992) 3659.
3. T. Ohmi, T. Imaoka, I. Sugiyama and T. Kesuka, J. Electrochem. Soc., 139, (1992) 3317.
4. O.M.R. Chyan, J.J. Chen, H.Y. Chien, J. Sees and L. Hall , submitted for publication in J. Electrochem. Soc..
5. D.Graf, M. Grundner, R. Schulz and L. Muhlhoff, J. Appl. Phys., 68, (1990) 5155.

METALLIC PARTICLE GROWTH AND METAL INDUCED PITTING (MIP) ON SILICON SURFACES IN WET PROCESSING AND ITS PREVENTION

H.MORINAGA, M.SUYAMA, M.NOSE, S.VERHAVERBEKE
and T.OHMI
Department of Electronics, Faculty of Engineering
TOHOKU UNIVERSITY, Sendai 980, Japan

1. INTRODUCTION

In order to establish the advanced wet chemical processing, it is important to understand the mechanism of contamination adhesion and removal on Si surface. It is well-known that noble metallic contaminants such as Cu are likely to adhere onto the Si surface in wet chemical processing (especially, in HF etching processes) and can severely deteriorate device performance (1,2,3). The main purpose of this paper is to reveal the mechanism of noble metal adhesion and removal onto the Si surface in wet processing, and to establish the advanced wet chemical processing which can achieve the Si wafer surface free from noble metallic contamination.

2. RESULTS AND DISCUSSION

2. 1. Mechanism of noble metal deposition on Si surfaces in wet processes

In an attempt to understand the adhesion mechanism of noble metals in wet processes, the behavior of Cu^{2+} adhesion onto Si surfaces in various chemical solutions was investigated (4,5). It was found that Cu^{2+} ions deposit onto the bare Si surface in the form of particles (Figure 1). The result of XPS measurement revealed that the Cu particle features the metallic state. It has also been found that Cu deposition in HF solutions causes pits (Metal Induced Pits) being formed on the Si surface (Figure 2). The number and the diameter of the pits are almost the same as those of the Cu particles. In addition, in the case of the patterned

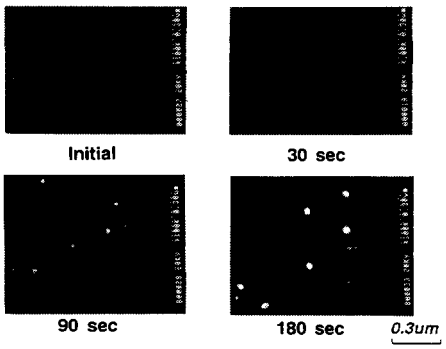

Figure 1. SEM images of the Cu particle growth process on the Si surface in a diluted HF (0.5%) solution [with Cu : 1ppm (using $CuCl_2$)].

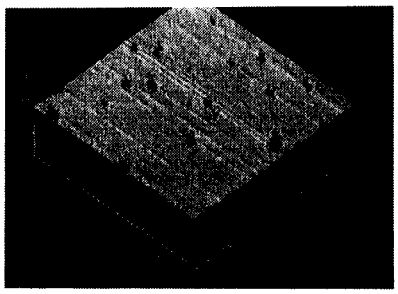

Figure 2. AFM image of the Si surface after Cu particles are removed by SPM cleaning (10 min). Cu was deposited in a diluted HF (0.5%) solution [with Cu : 1ppm].

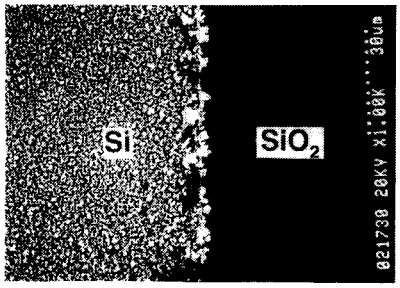

Figure 3. SEM images of the selective Cu deposition onto surfaces with poly-Si and SiO_2 surface from a diluted HF (0.5%) solution [with Cu : 100ppm]. The dipping time is 60 min.

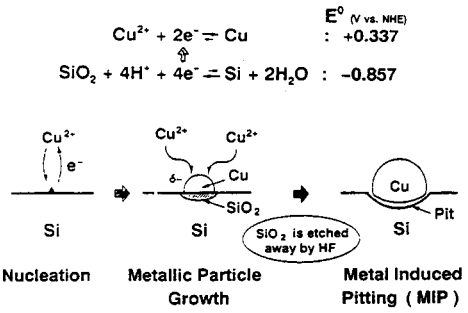

Figure 4. Mechanism of the Cu deposition onto Si surfaces in solutions.

wafer on which the Si surface and the SiO_2 surface coexist, selective Cu deposition onto the Si surface was observed (Figure 3). The experimental results reveal the Cu deposition mechanism shown in Figure 4 which is induced by the oxidation-reduction reaction between Si and Cu^{2+} ions. This metal deposition mechanism is considered to apply also to other metals such as Au or Ag, which have higher redox potential than Cu.

2. 2. Technology for preventing noble metal deposition in solutions

In order to establish a technology for preventing noble metal deposition, we have investigated the Cu deposition onto bare Si surfaces from various

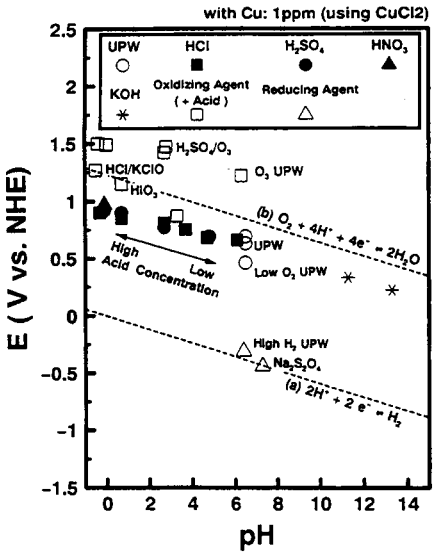

Figure 5. The pH and redox potential of various solutions (measured value).

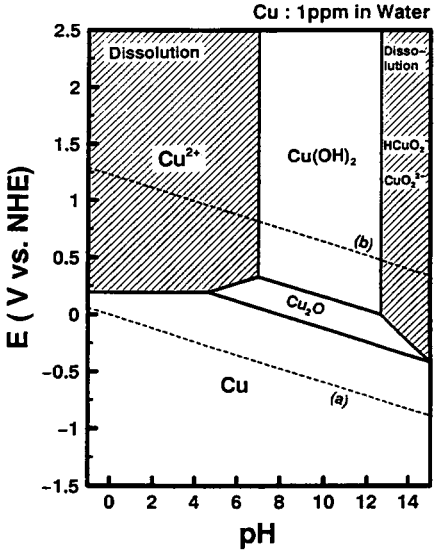

Figure 6. Potential-pH diagram for the Cu-Water system calculated from the equilibrium constant at 25°C (6).

solutions with different anions, pH and redox potential. Figure 5 shows the pH level and redox potential of various solutions measured by a pH and redox potential meter (PHL-10, DKK Corporation, Japan). Redox potential measurement were performed with a Pt electrode with an Ag/AgCl reference corrected to the normal hydrogen electrode (NHE). It is clear from this figure that the redox potential increases for lower pH, i.e. for a higher acidity of the solution. Moreover, the redox potential can be controlled by injecting such oxidizing agents as O_2, O_3, HCl/KClO (HClO), and HIO_3 and such reducing agents as H_2 and $Na_2S_2O_4$. Figure 6 presents the potential-pH diagram for the Cu-Water system calculated from the equilibrium constants at 25°C (6). As shown in this figure, Cu of 1ppm can dissolve in the solution which features a redox potential higher than 0.2 V and a pH lower than 7. However, it should be noted that this figure does not take into account the existence of the Si. Figure 7 shows the effect of pH and redox potential of solutions on the Cu deposition examined by testing various solutions shown in Figure 5. The amount of deposited Cu was measured with TRXRF. Cu deposition is found to be suppressed in the solutions which feature a redox potential higher than 0.75 V and a pH lower than 7. This is believed to be because the existence of the Si, which is strong reducing agent, raises the Cu/Cu^{2+} boundary line.

2. 3. Wet cleaning technology for noble metallic contamination

Figure 8 shows the effect of pH and redox potential of solutions on the Cu removal. Before the cleaning experiment, the n-type bare Si wafers were dipped in pure water with Cu of 1ppm added (using $CuCl_2$) for 3min (the wafer surfaces

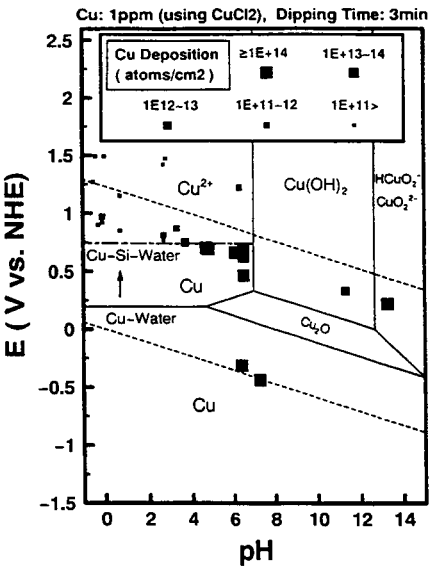

Figure 7. The effect of pH and redox potential of the solutions (ultrapure water with various chemicals added) on the Cu deposition.

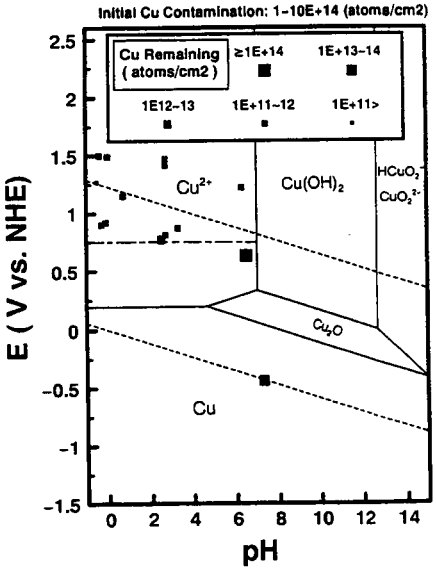

Figure 8. The effect of pH and redox potential of the solutions (ultrapure water with various chemicals added) on the Cu removal.

were contaminated with Cu at the level of 10^{14} to 10^{15} atoms/cm^2). Similar to the Cu deposition experiment, the solutions which feature a redox potential higher than 0.75 V and a pH lower than 7 are effective for removing Cu contamination. It was found that aqueous solutions with such acids as HCl and H_2SO_4, or such oxidizing agent as ozonized ultrapure water, H_2SO_4/O_3, and HCl/KClO (HClO) can remove Cu contamination to levels lower than 10^{12} atoms/cm^2 level. However, in general, these solutions could not remove the Cu contamination perfectly (as low as the blank level: lower than 10^{11} atoms/cm^2). The experimental results reveal that this is because Cu is partly included into the native oxide film when a native oxide is formed on the Si surface. The Cu remaining in the oxide film can be removed by HF/H_2O_2 etching.

3. CONCLUSION

The experimental results reveal that noble metals deposit as a result of oxidation–reduction reactions on the Si surface. It was found that Cu^{2+} deposition can be prevented by setting a redox potential of the solution at higher than 0.75 V (vs. NHE). For preventing noble metal deposition on Si surfaces, it is necessary not only to keep noble metals in the solution (i.e. to dissolve noble metals) but also to prevent reduction with a high redox potential. For removing noble metals, the same conditions are found to be necessary. Moreover, in the case of metals included in oxide films, etching is additionally needed for removing noble metals completely.

REFERENCES

1. T.Ohmi, T.Imaoka, I.Sugiyama, and T.Kezuka, *Journal of Electrochemical Society*, **139**, 3317, (1992).
2. F.W.Kern Jr, M.Itano, I.Kawanabe, M.Miyashita, R.W.Rosenberg and T.Ohmi, in *Proceedings of 11th workshop on ULSI Ultra Clean Technology,* p.23 (1991).
3. M.Hourai, T.Naridomi, Y.Oka, K.Murakami, S.Sumita and N.Fujino, *Jpn. J. Appl. Phys.* **27**, L2361 (1988).
4. H.Morinaga, M.Suyama and T.Ohmi, "Mechanism of Metallic Particle Growth and Metal Induced Pitting (MIP) on Si Wafer Surface in Wet Chemical Processing," *Journal of Electrocemical Society*, to be published.
5. H.Morinaga, M.Suyama, M.Nose, S.Verhaverbeke and T.Ohmi, in *Proceedings of 40th Meeting of Institute of Environmental Sciences,* Vol.1, p.332 (1994).
6. M.Pourbaix, "Atlas of Electrochemical Equilibria in Aqueous Solutions," Pergamon Press, London (1966).

Metal Adsorption on Silicon Surfaces from Wet Wafer Cleaning Solutions

Gerd J. Norga, K. Alexis Black, Hichem M'saad, Jurgen Michel
and Lionel C. Kimerling
Department of Materials Science and Engineering
Massachusetts Institute of Technology
Cambridge, MA 02139

1 Introduction

The steady decrease in the minimum feature size of silicon IC's has tightened the wafer cleanliness standards needed to achieve satisfactory device yields. While wet cleaning cycles continue to be used because of their excellent ability to remove particles and native oxides, the deposition of trace amounts of metals from contaminated solutions is a growing concern. Hence, the development of more effective cleaning chemistries will remain a priority in the foreseeable future. For this purpose, we propose the use of E-pH diagrams, which provide the thermodynamic basis for understanding metallic contamination in wet systems. Meanwhile, successful implementation of advanced cleaning chemistries in the fabline depends critically on in line monitoring of cleaning effectiveness. To this end, we have developed a radio-frequency photoconductance decay apparatus for the monitoring of copper deposition from dilute HF in real time.

2 E-pH diagrams of metals in cleaning solutions

E-pH diagrams [1] map the stable phase (metal, oxide or ion) as a function of pH and redox potential, E, of the solution. Figure 1a shows the E-pH diagram for Fe at 75°C, showing the stability regions for the various solids (Fe, Fe_2O_3, Fe_3O_4) and ionic species (Fe^{++} and Fe^{+++}).
In oxidizing cleaning solutions, the redox potential is essentially fixed by the concentration of oxidant present. The relationship between oxidant content and redox potential can be derived by applying Nernst's Law to the reduction reaction of the oxidant. For example, for hydrogen peroxide, the reduction reaction can be written as :

$$H_2O_2 + 2H^+ + 2e^- \longrightarrow 2H_2O \qquad (1)$$

This work was supported by NREL (Golden, Colorado) and the MIT Leader For Manufacturing (LFM) Program. Technical support from SEH America, Ibis Technology Corporation and Ashland Chemical is gratefully acknowledged.

Yielding a redox potential E :

$$E = 1.776 - \frac{RT}{F}pH + \frac{RT}{2F}ln([H_2O_2]) \quad (2)$$

Analogous relationships can be derived for other oxidizing cleaning mixtures based on nitric acid (e.g., HCl/HNO_3 and HF/HNO_3) or ozone (e.g., H_2O/O_3). Approximate (E, pH) values of some standard wafer cleaning mixtures are shown on an E-pH map in Figure 1b. Since the cleaning solution SC–1 falls in the stability region of a solid oxide phase (Fe_2O_3) in the Fe E-pH diagram, trace amounts of Fe ions present in the cleaning solution can lower their free energy by forming Fe_2O_3 on the wafer surface. This explains the strong contamination tendency of Fe in SC–1. Conversely, effective contaminant removal will occur when a cleaning solution lies in the stability region of a metal ion, as in the case of Fe in SC–2. In a similar fashion, the E-pH diagram of Cr explains the low contamination tendency of Cr in SC–1 ; and based on the Ca diagram, we predict that decreasing the pH of SC–1 will decrease Ca contamination levels, whereas changing the oxidation potential, E, will have no effect [2].

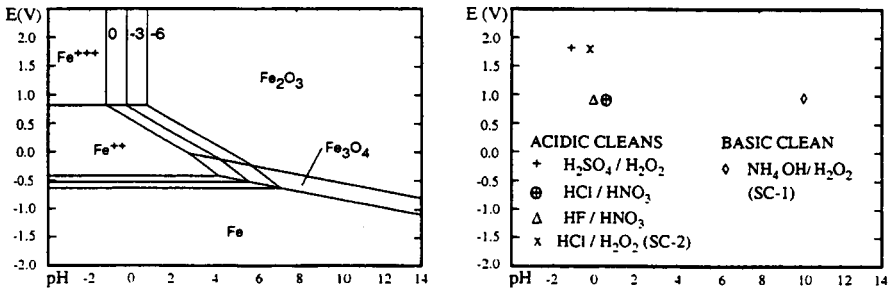

Figure 1. The E-pH diagram for Fe at 75°C, showing phase boundaries for 10^{-6}, 10^{-3} and 1 molal concentration in solution (a), and the (E,pH) values of some standard cleaning solutions (b).

3 *In situ* monitoring of copper deposition from dilute HF using RFPCD

3.1 Measurement principle

We have developed a high-sensitivity apparatus for the contactless measurement of minority carrier lifetime by Radio Frequency Photoconductance Decay (RFPCD) (Figure 2). When measuring on wafers with sufficiently high bulk lifetimes, the measured lifetime depends on the surface recombination velocity (SRV) [3]. In HF solutions, SRV is small because of the effective passivation of surface states by hydrogen.

Deposition of Cu atoms on silicon from HF solutions is thought to occur by

electrochemical outplating, where the electrons are provided by the dissolution reaction of the silicon. The deposition of Cu atoms on the silicon surface causes SRV to increase, giving rise to a decrease in the measured minority carrier lifetime.

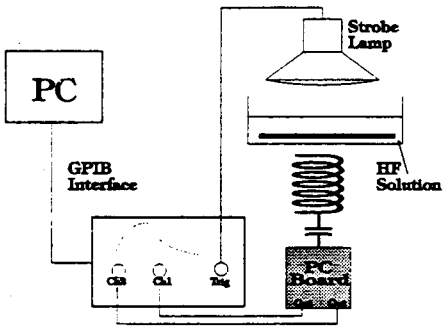

Figure 2. The radio frequency photoconductance decay system.

3.2 Experimental

High bulk lifetime (5-10 ms) single side polished CZ Si wafers were used for the *in situ* deposition experiments. The wafers (125 mm diameter, 625 μm thick, n-type, 11-25 Ωcm) received an initial clean consisting of 4 minutes 4:1 H_2SO_4/H_2O_2 at 90° (JT Baker CMOS grade chemicals), followed by a DI rinse and 2 minutes in 0.5% HF (Ashland Gigabit^{TM} grade). After the cleaning, the wafers were immersed in 0.5% HF for the RFPCD measurement. The measured minority carrier lifetime (τ_{meas}) was recorded as a function of immersion time in 0.5% HF (Figure 3a). After 5 minutes immersion, Cu (1000 ppm in 1% HNO_3, Atomic Absorption Standard) was added so as to obtain a Cu concentration of 10 ppb in the measurement solution.

3.3 Results and discussion

Figure 3a shows the measured RFPCD lifetime vs immersion time. After about 2 minutes immersion, τ_{meas} saturates to a value of 1050 μs. After Cu is added to the solution at t = 5 minutes, the measured lifetime starts to decrease. Assuming that bulk recombination can be neglected, the surface recombination velocity, s, depends on the measured lifetime, τ_{meas}, by the relationship [4]:

$$s = \sqrt{D_p/\tau_{meas}} tan(d/2\sqrt{\tau_{meas} D_p}) \quad (3)$$

where d is the wafer thickness and D_p is the diffusivity of minority carriers in n-type material. Since recombination is expected to occur predominantly at surface copper atoms, s can be related to the surface copper concentration, N_{Cu}, by [5] :

$$s = \sigma_p(Cu) N_{Cu} v_{th} \quad (4)$$

where $\sigma_p(Cu)$ is the cross section for surface recombination of minority carriers at a copper atom in n-type silicon, and v_{th} is the thermal velocity of the minority carriers. By correlating our results with TXRF, we have previously determined $\sigma_p(Cu)$ to be approximately 2.10^{-17} cm^2 [2], this is about 50 times smaller than typical cross sections for recombination at bulk defects [5]. Combination of equations (3) and (4) allows then to calculate N_{Cu} from τ_{meas}. The surface copper concentration vs time thus calculated is shown in Figure 3b.

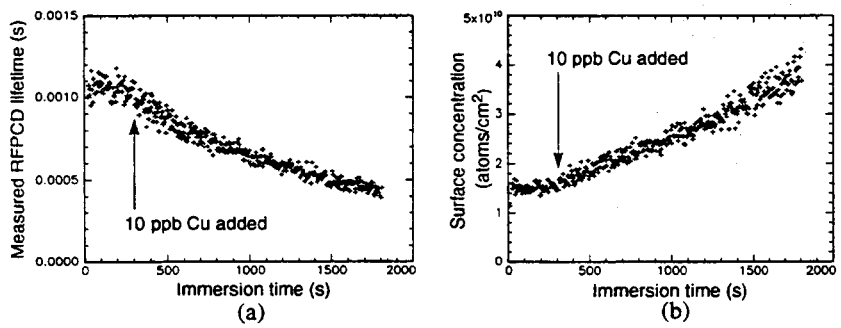

Figure 3. The measured RFPCD lifetime as a function of immersion time for the copper deposition experiment (a), and the calculated surface concentration of copper vs time (b).

3.4 Conclusions

We have demonstrated the use of RFPCD for in situ monitoring of Cu deposition from dilute HF solutions. Our tool is sensitive, compact, and noninvasive, and can be integrated in a wet station for monitoring cleaning effectiveness in real time.

References

[1] M. Pourbaix, "Atlas of Electrochemical Equilibria in Aqueous Solutions", Pergamon, Oxford (1966)

[2] G. J. Norga, L. C. Kimerling, submitted to J. Electr. Mat.

[3] H. M'saad, G. J. Norga, J. Michel, L. C. Kimerling, "Defect Monitoring and Control for Crystalline Silicon Processing", To be published in Proc. Photovoltaics R&D Meeting, Golden, CO (October 1993)

[4] H. M'saad, Jurgen Michel, J. J. Lappe, and L. C. Kimerling, J. Electr. Mat., 23, 5, 487 (1994)

[5] E. Yablonovitch, D. L. Allara, C. C. Chang, T. Gmitter, T. B. Bright, Phys. Rev Lett., 57, 249 (1986)

A NOVEL APPROACH FOR STUDYING THE IRON ADSORPTION AND DESORPTION MECHANISMS ON SILICON SURFACES DURING WET CHEMICAL TREATMENTS

H. Schäfer*, K. Budde**, SIEMENS AG, Research Laboratories, 81730 Munich, Germany

Abstract

Todays semiconductor manufacturing requires fast, ultra-sensitive and cost effective metrology methods for incoming inspection, process development and process monitoring. For the determination of the detrimental species of iron in liquid chemicals we developed a technique called simulation analysis (SA).
By SA the effects of all process parameters towards the adsorption/desorption of iron can be evaluated. The parameters include the chemical composition and concentration of process media as well as temperature, time, pH-value, spraying or dipping, etc. The LLD for monitoring the precipitation of iron is 10^9 atoms/cm². The concentration of adsorbable iron in ultrapure DI water was found to range from 0.7 to 2 ppt.

1. INTRODUCTION

Among the metallic impurities that disturb the processing in semiconductor industry, iron is known to be one of the most detrimental/1/. At the actual levels of metallic impurities that are tolerated in process media, income testing and process control of iron concentration becomes highly time and money consuming. Furthermore, the most frequently used methods like atomic absorption spectroscopy, e.g., often show doubtful results.
Table 1 shows the iron contents in H_2O_2 from three different vendors (A,B,C), each tested from several lots (1-4) by atomic absorption spectroscopy (AAS), ion chromatography (IC) and voltammetry (VA), respectively. While cleanings containing A or B resulted in good or sufficient DRAM yields, the use of C led to catastrophic results although the total iron concentration of C was much lower than that of B.

Our previous experiments showed, that the same contaminant: iron often simultaneously occured in a variety of different species within the same commercial chemical, like H_2O_2. Following species were detected:

$$\Sigma\,Fe = [Fe(H_2O)_x]^{3+} + [Fe(OH)_n(H_2O)_m]^{(3-n)+} + Fe(OH)_3 + \quad (1)$$

$$[Fe(L_x)_n]^{(3-x)+} + Fe(L_y)_m]^{y-} + [Fe(L_z)_p]^{z-} + Fe \text{ (particle bound)}$$

L_i : complexing agent i

---

* present address: METROHM AG, Herisau, Switzerland
** correspondence to K. Budde

Table 1 clearly indicates that not all of the iron is leading to defects. In order to identify the particular detrimental species, the details of the adsorption/desorption mechanisms of iron onto silicon have to be explored by metrology methods that are capable to distinguish between the species listed in (1). From these species usually only one is responsible for creating defects, e.g. by being adsorbed to the silicon surface.

Table 1 : Iron content in samples of a cleaning solution

Sample	iron concentration (ppb		
	AAS	IC (SA)	VA
A-1	<1	0.2	0.2
A-2	<1	0.08	<0.2
A-3	<1	0.08	<0.2
B-1	30	0.6	0.7
B-2	4	0.9	1.1
B-3	8	0.1	<0.2
B-4	16	0.4	0.5
C-1	3	2.6	---
C-2	2	1.8	---
C-3	3	3.2	---

(vendors : A, B, C; lots: 1, 2, 3, 4)
measured by Atomic Absorption Spectroscopy (AAS), Simulation Analysis (SA) with Ion Chromatography (IC), and voltammetry (VA)

2. EXPERIMENTAL

Fig.1 shows the general experimental setup. The simulation part (left) contains the various chemicals to be tested and the adsorption device. This is either a silicon wafer or a chromatographic column filled with crushed silicon of defined grain size. The temperature in the simulation part is adjustable in the range from 20°C to 80°C. By rinsing the silicon with the different chemicals - either solely or already mixed - at appropriate temperatures for defined periods of time, all wet treatments can be simulated. In the same way, new bath compositions or the use of additives can be tested. Having passed the silicon surface, the liquids are pumped through the preconcentration column (RSO_3H, bottom right).
The detection part (right) consists of two independently operating ion chromatographs, each equipped with an UV/VIS-detector. After switching of valve 2, the adsorbed iron is washed from the silicon by the use of a special eluent. Furthermore, this eluent requires no post column reaction for the detection of iron. The simulation is stopped by switching valves 2 and 3 in order to transfer the iron into the ion chromatographs. By this procedure the system distinguishes between the amount that was adsorbed to the silicon („active iron", detected in the upper part, cf. fig. 1), and the non-adsorbed fraction („non-active", detected in the bottom part, see fig. 1).

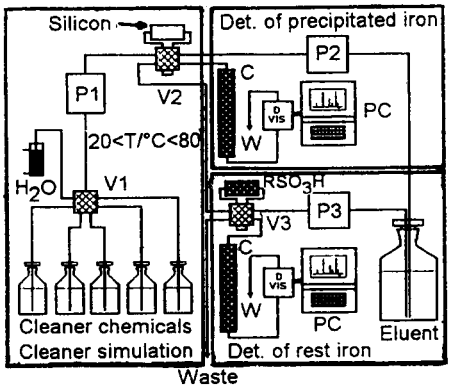

Fig.1: Instrumental setup for the detection of adsorbed iron by Ion Chromatography under the conditions of industrial cleaning processes
(Abbreviations: C - column, P - pump, PC - computer, V - valve, W - waste)

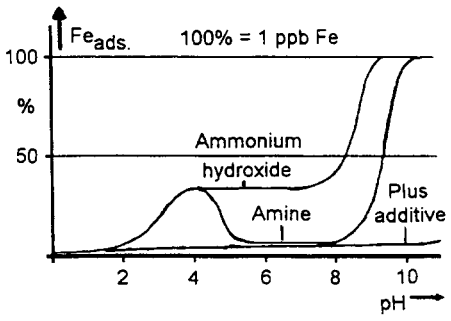

Fig.2: pH-dependence of the iron adsorption onto the silicon surface

3. RESULTS

Fig. 2 shows the dependence of the iron adsorption on the pH-value of a cleaning solution containing hydrogen peroxide. A concentration of 1 ppb iron was installed in all solutions. The pH value was adjusted either by ammonia or amines (for pH-values larger than 3) or by nitric acid (pH < 3). From fig. 2 it can be deduced that only 30 % of the iron is adsorbed in the pH range, where iron hydroxide is formed. Between pH = 5 and pH = 8, both, ammonia and amine containing cleaners have constant adsorption rates, but the ammonia based is much higher. At high pH values, all iron (1 ppb = 100%) is adsorbed, if the precipitation is not prohibited by an additive.

Fig. 3 shows the iron adsorption from a solution containing alkaline hydrogen peroxide (NC 2) for different concentrations of iron as a function of the concentration of an added complexing agent. The effect of the additive is not linear: while 0.05 mg complexing agent per liter NC 2 are required to cover iron concentrations up to 0.6 ppb , already 0.1 mg/l is sufficient to prohibit precipitation from an 3.3 ppb iron solution.

Fig. 4 shows the iron adsorption from solutions containing hydrogen peroxide for batches from different vendors as a function of the time the wafers remain in the cleaning solution. Only two of the curves (B,E) show no time dependence. B is the only solution without additive to prevent iron precipitation. So the iron adsorption

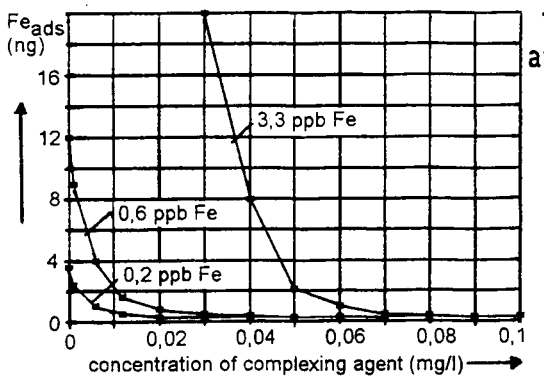

Fig.3: Adsorption of iron as a function of the concentration of a complexing agent in an alkaline hydrogen peroxide solution containing iron

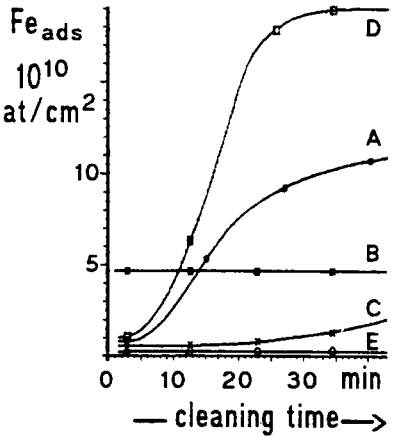

Fig.4: Time dependence of iron adsorption for different cleaner compositions containing hydrogen peroxide

here is quite high. Nevertheless, its constant value indicates that there has been established a chemical equilibrium between adsorption and desorption. E is the most favourite case for processing. This is because the additive in E is stable under the process parameters chosen. Curves A, C and D, respectively, respond to the presence of different additives that all show only poor stability in the process - there is a high risc of iron contamination if the process is not stopped in time.

4. RESUMEE

The newly developed „simulation analysis" shows several advantages when compared to the actually used metrology methods: i) the detrimental amount of iron (on the silicon surface) can be detected separately; ii) the iron determination is faster and more cost effective than by AAS or by TXRF; iii) by the use of specific eluents the determination can be extended to the iron content within thin layers of oxide /2/ - here the in-situ measurement by SA is much faster than the hitherto used VPD/AAS; iv) the system allows to check the impact of high levels of contamination without poisioning any process line; v) the effect of every relevant process parameter can be checked separately; vi) transport phenomena and any environmental impact are eliminated; vii) SA can be extended to determine a great variety of different ions.

REFERENCES

/1/ M.L. Kniffin and C.R. Helms, Int. Conf. Solid State Devices and Materials, Yokohama, 1991, pp 493-495

/2/ H. Schäfer and K. Budde, Int. Ion Chromat. Symp., 1992, Linz, doc. 49

RECENT RESULTS OF ULTRAVIOLET-INITIATED PROCESSES FOR CLEANING AND ETCHING OF SILICON

Jeffery W. Butterbaugh, David C. Gray, and C. Fred Hiatt
FSI International, 322 Lake Hazeltine Drive, Chaska, MN 55318
Herbert H. Sawin and A. Scott Lawing
Chem. Eng., MIT, 77 Massachusetts Avenue, Cambridge, MA 02139

1. INTRODUCTION

Photochemical Cl_2 etching of silicon with broad band UV lamps as well as UV lasers has been studied for several years. Applications for pattern delineation [1,2] and more recently for surface cleaning [3-9] have been reported. UV/Cl_2 processes have been shown to be effective in removing Fe, Ni, Cu, and Cr [3] as well as other metal contaminants [4,5]. It has been suggested that UV/Cl_2 can remove metal contaminants from the silicon surface through a native oxide layer [4]. Photochemical cleaning with NF_3 [6], F_2 [7,8], and ClF_3 [9] has also been reported. Studies with fluorine chemistry have concentrated on native oxide removal and silicon surface termination effects. Recent work with UV/ClF_3 [10] has led to the discovery of processes which provide nearly equal removal of doped and undoped oxides (pat. pending) which will be very useful for contact cleaning. In the future, photochemical dry processes will be an important part of cluster tool systems and will play a major role in cluster tool applications such as pre-gate oxidation cleaning, contact cleaning, pre-epitaxial deposition cleaning and post-resist ash cleaning.

Several UV-initiated processes are currently under investigation at FSI International for cleaning the surface of silicon wafers and etching thin films in the vacuum environment. Studies have been carried out in a full wafer 200-mm dry, vacuum cleaning system as well as in a small research vacuum chamber to determine silicon etching rates, surface roughening and metals removal due to ultraviolet-initiated chlorine (UV/Cl_2) and chlorine trifluoride (UV/ClF_3) processes. The effectiveness of these processes in removing metallic contamination from the surface of silicon and silicon dioxide was investigated and compared to HF/alcohol processes.

2. EXPERIMENTAL

A small quartz research apparatus was used to carry out parameter studies on the UV/Cl_2 silicon etching process. The base pressure of the apparatus was $\sim 5 \times 10^{-7}$ torr and the sample was illuminated through the quartz chamber walls with a 1000 W xenon short arc discharge lamp. The etch depth and surface roughness on a partially masked 1 cm square n(100) silicon pieces was measured as a function of chlorine pressure and initial silicon temperature by atomic force microscopy.

The full-wafer reactor used in these studies was an experimental single wafer vacuum cluster module capable of conducting photochemical processing of 100, 150, or 200 mm wafers. The module was attached to a vacuum cluster robotic handler. The reactor module was constructed of hardcoated 6061 aluminum. A dry rough pump was used to pump the vacuum reactor to a base pressure below 10 mtorr. High purity sapphire windows were used to allow UV light exposure of the wafer front side. Gases were introduced in a uniform radial laminar flow, to enhance the transport of etching products away from the wafer surface. High intensity (~200-300 mW/cm^2 at 200-400 nm), broad band UV irradiation was achieved with a commercially available 300 W/inch, medium pressure mercury arc discharge lamp. The wafer pre-process temperature was controlled using an in-vacuo heater plate. During the period of UV exposure the wafer temperature was transient due to IR output from the UV lamps. However, the wafer temperature typically did not increase by more than 10 °C during processing. Process pressure was monitored and controlled using a capacitance manometer in a feedback loop with a downstream throttle valve.

Substrates used for metals removal tests were 150-mm prime grade p(100), 1-5 ohm-cm, silicon wafers. Oxide surfaces were prepared by growing ~800 Å of silicon oxide in a dry oxidation process at 1000 °C. Gases used were electronic grade (99.9%) HF, C.P. grade (99.0%) ClF_3 and VLSI grade (99.998%) Cl_2. N_2 was used as a diluent gas in all processes.

Processes were defined for 150-mm wafers with the goal of removing 50-100 Å of surface material (silicon or silicon oxide) during the cleaning process. Oxide removal rates were measured by comparing the oxide film thickness measured by spectroscopic reflectometry before and after processing. Silicon removal rates were measured by stylus profilometry on wafers partially covered by a patterned oxide layer. Metals removal efficiency was determined by contaminating or "challenging" the wafers. Wafer were challenged by applying a 1-μm thick positive photoresist layer and then removing it with an oxygen plasma ash. TXRF analysis was used to compare the metals levels on cleaned wafers with that on unprocessed challenge wafers. Surface roughness was measured by AFM.

3. RESULTS AND DISCUSSION

The results of UV/Cl_2 process parameter examination in the small research apparatus are summarized in Figure 1. The pressure (1-100 torr) and initial temperature (70-260 °C) was varied while the process time was held constant at 90 seconds. In general, n(100) silicon surface roughness increased with etch depth under UV/Cl_2 processing. It is apparent from Figure 1 that removing 50-100 Å while maintaining a surface roughness of better than 5 Å RMS is achievable.

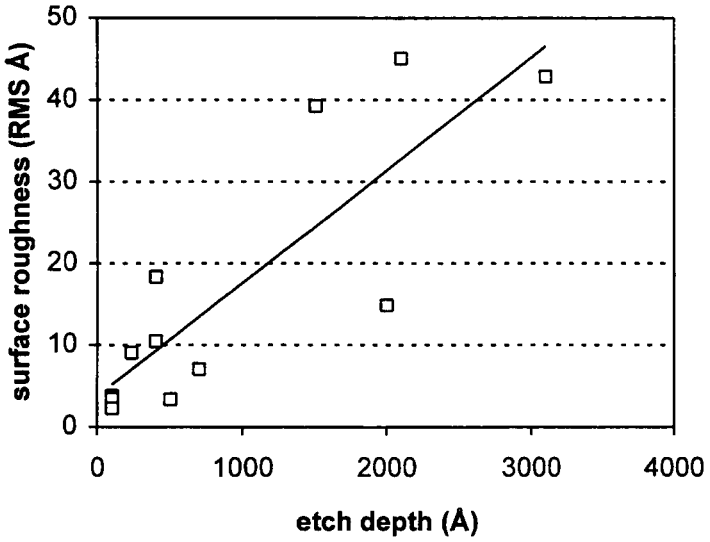

Figure 1. Relationship between surface roughness and etch depth on n(100) silicon during UV/Cl_2 processing.

Table 1 lists the processes and measurement results for an examination of metals removal efficiency and silicon surface roughness for several processes on 150-mm wafers. The HF/IPA process was run at 100 torr, 100 °C, 60% HF and ~2% IPA for 5 minutes. The UV/ClF_3 process was run at 100 torr, 100 °C and 0.8% ClF_3 for 30 seconds of UV exposure. The HF/IPA + UV/Cl_2 combination involved the above HF/IPA process at 50 torr for 120 seconds followed by a UV/Cl_2 process at 50 torr, 100 °C and 9% Cl_2 for 60 seconds of UV exposure. TXRF measurements were made at five points on each wafer and AFM measurements were made at two points. Even though the UV/Cl_2 and UV/ClF_3 processes both removed about 100 Å of silicon, the UV/Cl_2 process was much more effective at removing metallics. This can be attributed to the generally higher volatility of metal chlorides compared to metal fluorides. Cr and Fe appear to be most difficult to remove which is consistent with the work of deLarios and co-workers [3]. However, our data indicates complete removal of Ca contamination (not shown) in contrast to deLarios.

While the HF/IPA process left the silicon surface only about 1 Å rougher than a prime wafer, the UV/ClF_3 and UV/Cl_2 processes increase surface roughness by 2-5 Å. Further work is needed to determine if the extremely high roughness value for the UV/ClF_3 process at the center of the wafer is anomalous or actually due to the cleaning process.

Table 1. Cleaning results on bare silicon, p(100). TXRF results are expressed in units of 10^{10} atoms/cm^2 and are the average of five measurements. Surface roughness results (RMS) are given for both the center and mid-radius of the wafer.

surface/process	Si etched (Å)	Ti	Cr	Fe	Ni	Cu	RMS (Å)
clean (control)	n/a	<5	<5	<2	4	<3.5	0.9, 0.7
challenge (control)	n/a	53	1410	1030	22	176	5.1, 34
chal.+ HF/IPA	0	<5	296	153	21	13	1.5, 1.7
chal.+ UV/ClF_3	~100-300	9	420	169	6	31	97, 3.8
chal.+HF/IPA+UV/Cl_2	~100-300	<5	9	12	4	5	3.3, 5.2

Table 2 lists the processes and results for an examination of metals removal from a silicon oxide surface on 150-mm substrates. For the oxide substrates the process were somewhat different in order to achieve removal of 50-100 Å of oxide. The HF/IPA process was run at 200 torr, 70 °C, 50% HF and ~2% IPA for 60 seconds. The UV/ClF_3 process was run at 50 torr, 150 °C and 50% ClF_3 for 60 seconds of UV exposure. The HF/IPA + UV/Cl_2 combination involved the same HF/IPA process followed by a UV/Cl_2 process at 50 torr, 70 °C and 9% Cl_2 for 60 seconds of UV exposure. TXRF measurements were made at two points on each wafer. These results are similar to the results for bare silicon. However, while deLarios [3] found extreme difficulty in removing Fe or Ca from an oxide surface, our data indicates that Fe is significantly reduced by the HF/IPA + UV/Cl_2 process.

Table 2. Cleaning results on dry oxidized silicon. TXRF results are expressed in units of 10^{10} atoms/cm^2 and are the average of two measurements.

surface/process	SiO_2 etched (Å)	Ti	Cr	Fe	Ni	Cu
clean (control)	n/a	4	16	1	2	2
challenge (control)	n/a	100	15600	44600	3320	144
chal.+ HF/IPA	~100	13	84	9	2	5
chal.+ UV/ClF_3	~50-100	5	16	87	12	3
chal.+HF/IPA+UV/Cl_2	~100	6	11	5	3	2

REFERENCES

1. D. Ehrlich, R. Osgood and T. Deutsch, *Appl. Phys. Lett.* **38**(12), 1018(1981).
2. M. Sekine, H. Okano and Y. Horiike, *Jpn. J. Appl. Phys.* **25**(12), 1944(1986).
3. J. deLarios, W. Krusell, D. McKean, G. Smolinsky, S. Bhat, B. Doris and M. Gordon, *1992 Microcontamination Conference Proceedings*, 706(1992).
4. T. Ito, R. Sugino, T. Yamazaki, S. Watanabe, and Y. Nara, *Proceedings of the Symposium on Dtry Processes*, Electrochemical Proceedings Vol. 88-7, 287(1988).
5. C. Daffron, K. Torek, and J. Ruzyllo, *Proceedings of the Third International Symposium on Cleaning Technology in Semiconductor Device Manufacturing*, Electrochemical Society Proceedings Vol. 94-7, 281(1994).
6. K. Torek and J. Ruzyllo, *Proceedings of the Second International Symposium on Cleaning Technology in Semiconductor Device Manufacturing*, Electrochemical Society Proceedings Vol. 92-12, 80(1992).
7. T. Ito, R. Sugino, Y. Sato, M. Okuno, A. Osawa, T. Aoyama, T. Yamazaki, and Y. Arimoto, *Mat. Res. Soc. Symp. Proc.* Vol. 259, 195(1992).
8. T. Aoyama, T. Yamazaki and T. Ito, *J. Electrochem. Soc.* **140**(6), 1704(1993).
9. Y. Saito, O. Yamaoka, amd A. Yoshida, *Appl. Phys. Lett.* **56**(12), 1119(1990).
10. C.F. Hiatt, J.W. Butterbaugh, and D.C. Gray (presented at UCPSS '94 late submittal poster session).

CLEANING PERFORMANCE OF A CRYOGENIC AEROSOL SYSTEM

P. Sferlazzo, A. Dart, B.K. Libby, P. H. Rose, W. Scheer, and R.G. van der Heide
Krytek Corporation, Danvers, Massachusetts, USA

In recent years cryogenic jet spray cleaning of surfaces has emerged as one of the most promising techniques for the dry (anhydrous) removal of particulate contamination.[1-6] A broad range of applications has been explored, including cleaning semiconductor wafers, optical mirrors for space based telescopes, and magnetic disk drives. A new Cryogenic Aerosol Cleaning (CAC) system was recently developed and built at Krytek Corporation. The system is fully automated and is capable of cleaning up to 8"(200mm) Si wafers with a throughput of 60 wafers/hour using high purity Ar and N_2 sub-micron aerosols. A number of analytical tools including a Tencor 6200 surface scanner, a TXRF system, and an AFM were used to analyze the surface of the wafers before and after exposure to the aerosol. We found almost 100% removal efficiency for test particles of various compositions and with diameters ranging from 0.1-50 μm.

1. CRYOGENIC AEROSOL CLEANING

In cryogenic aerosol cleaning, a gas, liquid or supercritical gas, which may be pure or some mixture of substances, is expanded through a nozzle. Depending on the initial phase and details of the nozzle design, various different processes, such as nucleation and growth, vapor flashing, or standard liquid atomization, can take place, yielding a jet of frozen particles traveling at subsonic or supersonic speeds[1-6]. The dimensions of the particles vary greatly with thermodynamic conditions: pressure, temperature, flow, and particle formation mechanism. The efficiency in removing contaminants from a surface is closely related to these particle parameters. A number of gases can be used for cryogenic cleaning. Originally the technology was developed for use with CO_2, but for very demanding applications, such as semiconductor wafer cleaning, it was found that CO_2 would leave unacceptable amounts of organic contaminants due to the difficulty in filtering CO_2 to a high level of purity. Despite the complications involved in reaching lower cryogenic temperatures, Argon appears to be a better choice.

The cleaning mechanisms are still not fully understood. Direct momentum transfer has been the most common explanation.[6] There is, however, some evidence that other physical mechanisms, such as thermophoresis and shear stress from the rapidly evaporating aerosols,[7] may contribute. In air, the main adhesive force binding a particle to a surface is van der Waals force. Other forces, such as the electrostatic force or, in the presence of humidity, the surface tension of the liquid film trapped between the particle and the surface, need also to be taken into account under certain conditions. Coincidentally, most of these forces are linear functions of the particle diameter, a result which is confirmed by a wide variety of

experimental work. A useful expression that is often used for the adhesion force, F_{adh}, in dynes is:[8]

$$F_{adh} = 150\ d\ (0.5 + 0.0045\ \%RH) \quad (1)$$

where d is the particle diameter in cm and %RH is the per cent relative humidity. Under vacuum conditions or 0% humidity, equation (1) can be calculated from the van der Waals theory

$$F_{adh} = \frac{ad}{z^2} \quad (2)$$

where z is the average distance between the particle and the surface. Typically the value of z is chosen between 0.4 and 1 nm. Equations (1) and (2), for spherical particles coincide for z = 0.4 nm. The constant, a, depends on the Hamaker constant and on the physical shape of the particle. The total energy, W, required to dislodge a particle from a surface is calculated by integrating equation (1) from z to infinity.

$$W = F_{adh}\, z \quad (3)$$

Similar expressions can be obtained for particles of other simple shapes such as cylinders and those with flat surfaces.

Although a detailed solution to the physics of particle removal by momentum transfer is rather complicated and must take into account the elastic properties of the two impacting bodies and of the surface, we can obtain some insight into the process by applying simple conservation of energy. It follows that for single particle collisions the minimum velocity, Vmin, to detach for a projectile particle of mass M is

$$V_{min} = \left(\frac{2W}{M}\right)^{\frac{1}{2}} \quad (4)$$

where M is projectile particle mass. In figure 1, V_{min} is plotted versus the particle characteristic dimensions using a frozen aerosol diameter of 0.5 μm and various types of particle shapes.

The required range of velocities is quite broad and clearly is a strong function of the nature of the particle. Nevertheless we note that velocities of the order of a 1000 cm/sec should be sufficient to dislodge a great majority of the particles. This is consistent with the experimental evidence. Most importantly, these results also illustrate a fundamental characteristic of this technique in that the cleaning efficiency does not appear to decrease with particle size and therefore cryogenic aerosols can be used effectively in ULSI applications where controlling sub-

micron particles is of primary importance. So far we have neglected multiple collisions. Indeed more rigorous preliminary estimates, which take into account the aerosol densities, indicate that these can be quite important for larger particles. Effective control of aerosol size and velocity are clearly the two important parameters which give this technique its flexibility and a wide range of applications which are just beginning to be explored.

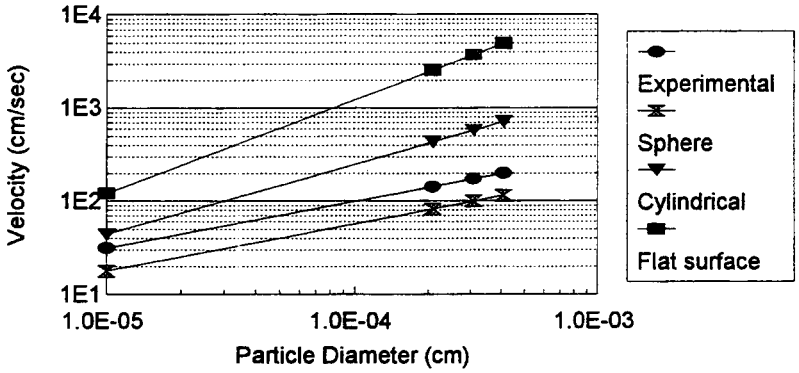

Figure 1. Minimum velocity to detach particles with a 0.5μ projectile

2. SYSTEM DESCRIPTION

A schematic diagram of Krytek's commercial cleaning system is shown in figure 2. High purity Ar and N_2 are mixed in proportions chosen by an operator controlled recipe and filtered using a 0.01 micron ceramic filter before entering a heat exchanger. In the present model, the heat exchanger consists of a pressurized liquid nitrogen tank where an appropriate length of the Ar/N_2 line coils in the bottom of the tank. The temperature in the heat exchanger is controlled by keeping a constant pressure in the tank (20 to 200 PSIG) and is selected to partially liquefy the Ar gas. This partially liquid mixture is then introduced into the process chamber where the aerosol is formed through a nozzle composed of a plenum, partially filled with liquid Ar, and a linear array of orifices spaced 0.5 cm apart. The dimensions of the holes determine the flow requirements, which are selected to achieve good cleaning performance and throughput, while minimizing consumption.

Due to the pressure drop between the plenum and the process chamber, the pressurized Ar liquid passing through the orifices is adiabatically cooled and atomized into a fine (sub micron) liquid aerosol. If he pressure in the process chamber is maintained below the triple point of Ar (0.68 ATM) a solid aerosol is formed. Cleaning is achieved by translating a wafer under the aerosol. A single pass of about 1 to 3 cm/sec is usually sufficient to remove loosely adhering particulates. Although it is only a sub-atmospheric process, the system is designed to be vacuum compatible to prevent moisture and other contaminants from

condensing on wafers or on some of the cold components of the aerosol delivery system. For the same reasons wafers are fed into the cleaning module through a cassette load lock (Brooks automation). Two standard configurations are available: a stand-alone tool and a cluster tool module equipped with a standard MESC interface.

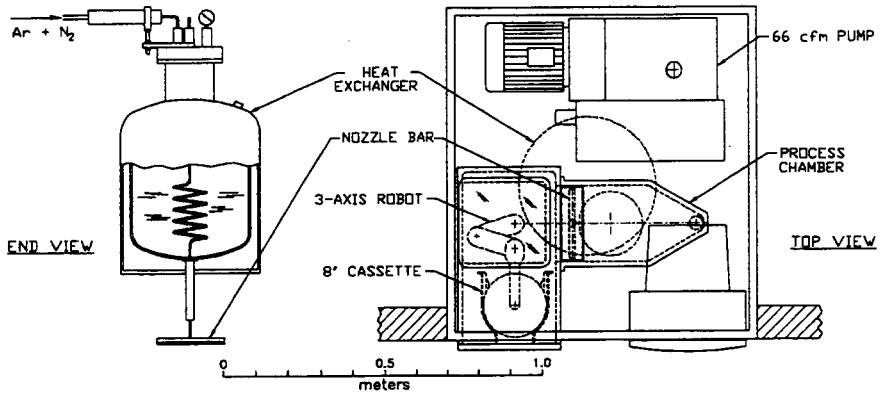

Figure 2. Schematic of a cryogenic aerosol cleaning system

3. RESULTS AND DISCUSSION

A Tencor 6200 scan of a contaminated wafer before and after exposure to the aerosol is shown in figure 3. A clean 100 mm wafer with 69 particles above 0.15μm was contaminated with about 4000 0.2 μm polystyrene particles and exposed to the aerosol for about 10 sec. The particle count after exposure went down to 53, below the original count on the clean wafer. This example illustrates well the high removal efficiency, and the low number of adders attributable to the system itself (typically below 5 particles above 0.2 μm). Similar results were obtained with particles ranging in size from 0.15 to 20 μm made of polystyrene, SiN_3 (these were particle of odd shapes not simple spheres), SiO_2 and other materials. In addition to pure Si substrates, SiO_2, nitrites and resist substrates were tried and gave similar positive results (>98% removal efficiency).

We estimate that the velocity of the aerosol for this process is relatively low, around 1000 cm/sec, because of this we found no evidence of damage on resist patterned wafers and, on bare wafers, no change in the surface roughness.

In order to extend the range of applications Krytek has developed a new technology which accelerates the aerosol to close to sonic, and perhaps even supersonic, velocities. Preliminary data have shown that with this technique it is possible to remove resist and aluminum films, finger prints and other contamination that was impossible to remove with the standard low velocity process. Whether

this new technology is viable for a broader range of applications, which may include for example post metal etch or post resist ashing cleans needs to be investigated. Some important questions such as damage, selectivity and throughput capability need to be carefully addressed. However, it is clear that CAC, in its low or high velocity forms, or both, in conjunction with other dry cleaning processes may constitute an exciting new alternative capable of replacing full wet cleaning steps in semiconductor manufacturing.

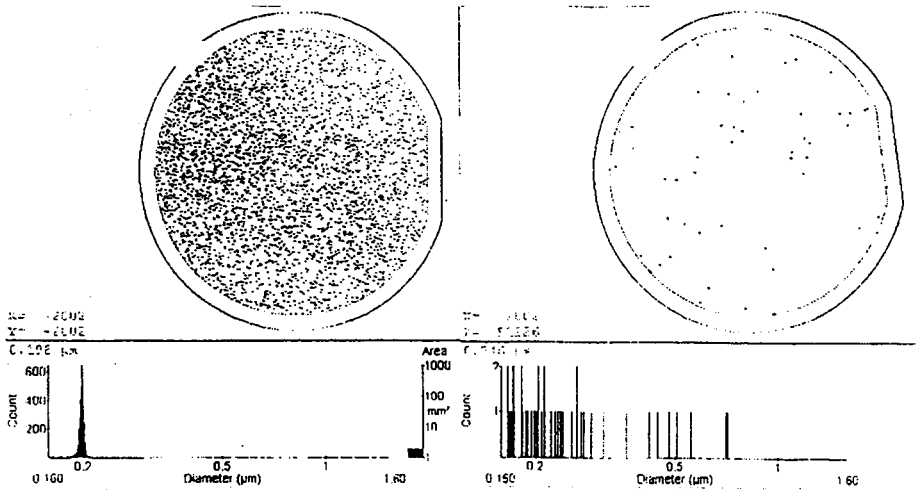

Figure 3 Contaminated wafer before and after cleaning by Krytek-100

REFERENCES

1. S. A. Hoenig, Compressive Air Magazine, Aug. 1986, p. 22
2. T. Ohmori, T. Fukumoto and T. Kato, Semiconductor International, Nov. 1989, p.16.
3. R. Sherman and W. Whitlock, J. Vac. Sci. Technol. B8, 563 (1990).
4. L. Layden and D. Wadlow, J. Vac. Sci. Technol. A8, 3881 (1990).
5. R. V. Peterson and C. W. Bowers, SPIE 1329, 72 (1990)
6. W. T. McDermott, R. C. Ockovic, J. J. Wu, and R. J. Miller, Microcontamination Oct. 1991, p.33.
7. E. A. Hill, Precision Cleaning Magazine, Feb. 1994, p.36.
8 W. C. Hinds, Aerosol Technology, John Wiley & Sons, 1982, p 129.

THE RESURGENCE OF MECHANICAL BRUSH SCRUBBING

W. C. Krusell* and J. Pollick*

Physical cleaning of the wafer surface is utilized as an alternative to conventional wet bench batch wafer cleaning methods. Mechanical brush scrubbing employs both the physical and chemical removal of surface contamination. The use of double-sided wafer scrubbers, for the simultaneous cleaning of both sides of the wafer's surface, is in production for prime, reclaim, epi, post-CVD device layer specific, and post-Chemical Mechanical Planarization (CMP) cleaning. Introduction of process chemistries in addition to deionized (DI) water-only scrubbing further reduces defect densities for LPD (Light Point Defect) levels @ ≥ 0.13 μm. Preliminary data indicates use of Megasonic spray just prior to wafer drying enhances particle removal on topographic and Tungsten surfaces.

Acceptance of mechanical brush scrubbing has been driven by the need for repeatable wafer-to-wafer process control. Single wafer cleaning using a double-sided wafer scrubber fulfills this requirement, as demonstrated by the stability of prime wafer data for particles ≥ 0.17 μm (Figure 1) and ≥ 0.20 μm (Figure 2).

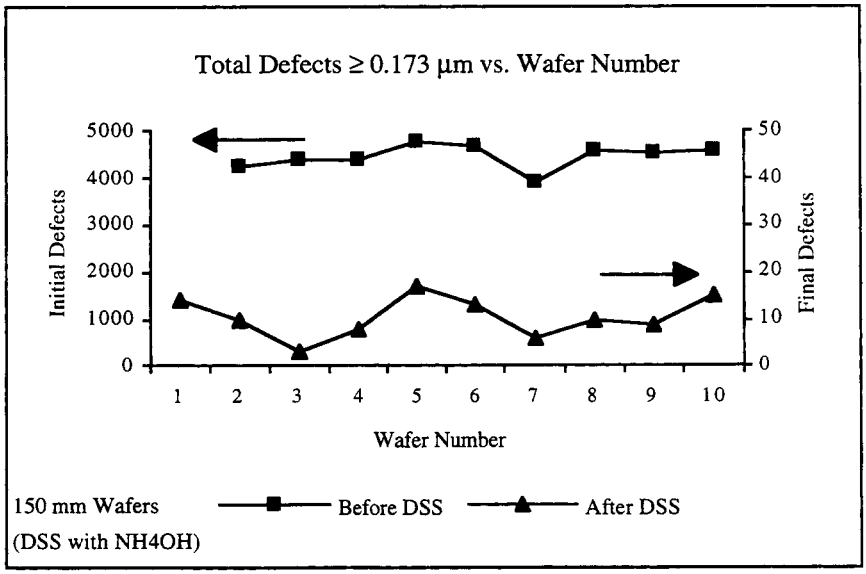

Figure 1. Prime wafers, 150 mm, DSS with NH_4OH.

* OnTrak Systems, Inc., Milpitas, CA

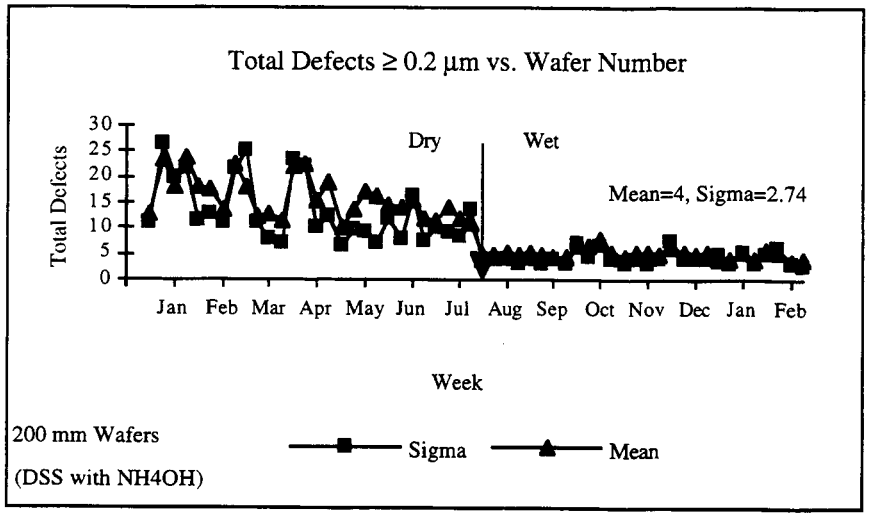

Figure 2. Prime wafers, 200 mm, DSS with NH_4OH.

Particle removal @ ≥ 0.13 µm is shown for epi (Figure 3), illustrating the capability of the standard Polyvinyl Alcohol (PVA) brush with a DI water-only process at small particle size.

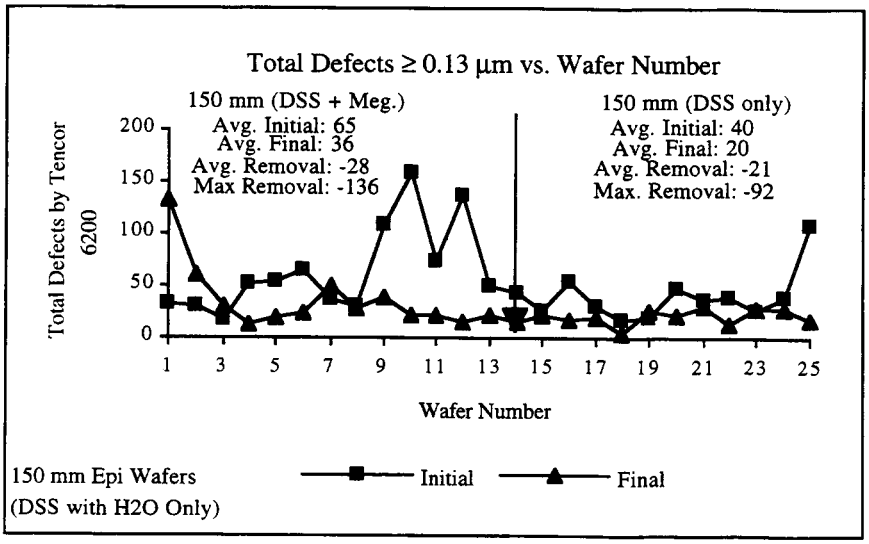

Figure 3. Epitaxial silicon, 150 mm, DSS with H_2O only.

Mechanical brush scrubbing has taken wet bench rejected PECVD wafers and returned them to product worthiness, achieving a greater than 98% LPD reduction in otherwise scrapped wafers (Table 1). Significant results are also found on post thermal oxidation cleaning (Figure 4).

	Typical Wet Bench Rejects Dry ≥ 0.2 μm	Same Wafers Post DSS Total LPD's ≥ 0.2 μm	Notes
	2847	37	
	2115	109	
	4402	55	
	1388	48	
	1113	86	
	3094	41	
	4953	38	
	3122	31	
Avg	2879.25	55.63	98% Reduction: 95% occurs in 0.2-1.0 μm Bin
Std Dev	1344.45	27.54	

Table 1. PECVD, wet bench rejects, DSS with H_2O only.

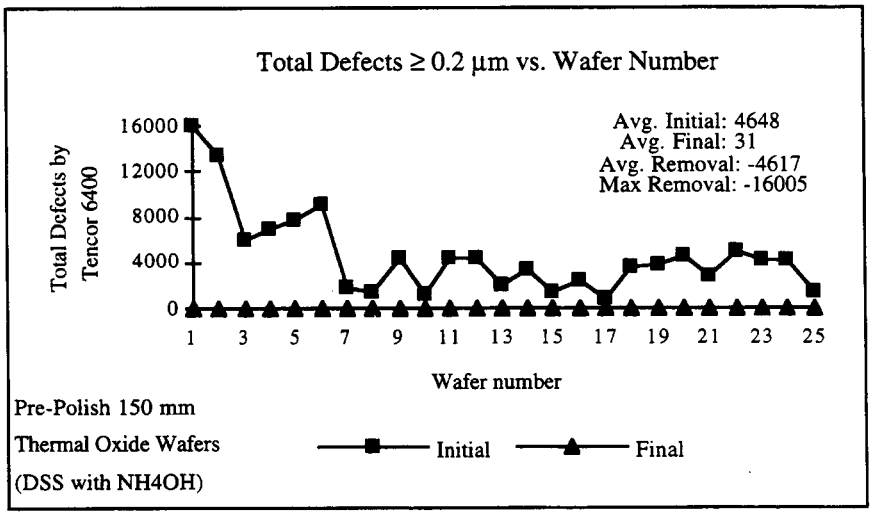

Figure 4. Thermal oxide, 150 mm, DSS with NH_4OH.

A key driver in the development of wafer scrubbing is post-Chemical Mechanical Planarization (CMP) cleaning. CMP is identified as an enabling technology in the fabrication of multi-level, ≤ 0.35 μm devices. Removal of post-CMP residues from both sides of the wafer is critical to subsequent processing. Performing a "slurry dip test" (pre-count, immerse in slurry, light rinse, scrub, post-count) demonstrates brush scrubbing's ability to not only remove slurry residue, but to reduce defect density existing "Pre Slurry Dip" (Figure 5).

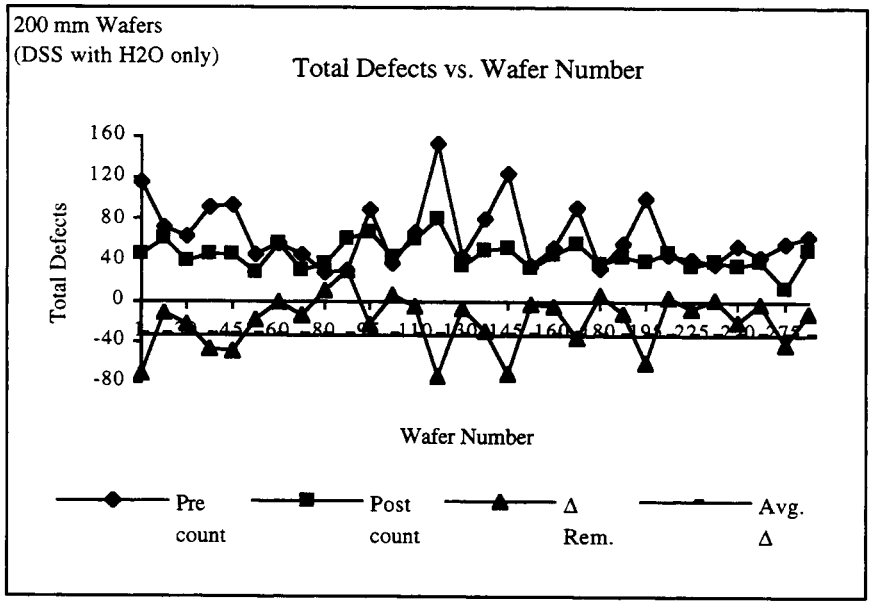

Figure 5. Post-CMP oxide "Slurry Dip Test," 200 mm, DSS with H_2O only.

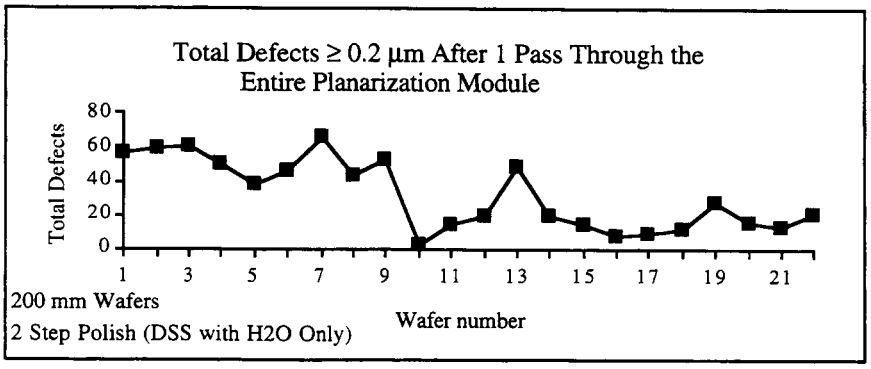

Figure 6. Post-CMP Oxide, 200 mm, DSS with H_2O only.

DI water-only scrubbing is utilized in the majority of the above wafer cleaning applications (Figure 6). However, cleaning of post-CMP processes has also embraced a 2.0 wt % (weight percent) Ammonium Hydroxide (NH_4OH) solution. It is speculated that this process solution, sprayed onto the brush surface before contact with the wafer, aids in 1) removal of particles from the wafer surface, and 2) flushing of the pores in the PVA brush to prevent build-up of removed material. In contrast, a 0.6 wt % solution was used to obtain the results given in Figure 1 for prime wafers. Additional experimentation is on-going in the use of "hot" DI (to 40°C), TMAH, Na and KOH, surfactants, Citric Acid, and other non-hazardous chemicals in the pH range of 2 to 12.

Mechanical brush scrubbing is a proven technique for the removal of contamination from specific wafer surfaces. The simplicity of modern double-sided wafer scrubbers contributes to their low Cost Of Ownership (COO). High reliability, small footprint, and low consumption of non-hazardous chemicals will facilitate additional research on their application into general wafer cleaning.

IN-SITU RINSE HF-LAST FOR PRE-EPITAXY CLEANING

Paul PATRUNO, Alain FLEURY
SGS-THOMSON Microelectronics, 38921 CROLLES, FRANCE
Elie ANDRE
CNET, France Telecom Laboratory, ZIRST, 38143 MEYLAN, FRANCE
François TARDIF
LETI-CEA, Avenue des Martyrs, 38041 GRENOBLE, FRANCE

ABSTRACT

A dilute HF mixture is increasingly being used as a final step, often referred to as "HF-last",providing an hydrogen passivated surface and removing metals that are still present. In this work, the effect of a wet chemical cleaning process used as HF-last cleaning in an automated wet bench is investigated, using a special tank design incorporating the capability of *in-situ* displacement of an extremely diluted HF solution by DI water. The performance of this tank (called *in-situ* rinse tank) is compared to that obtained on a conventional acid tank with its dedicated rinse tank to which the wafers are transferred. In such a case with conventional acid tank (called *standard* rinse tank) the transfer from the acid tank to the rinse tank causes hydrophobic wafers to be exposed to a liquid(acid)/air interface and to an air/liquid(water) interface.

1 INTRODUCTION

In this work, the effect of a wet chemical cleaning process used as HF-last cleaning in an automated wet bench is investigated, using a special tank design incorporating the capability of *in-situ* displacement of an extremely diluted HF solution. The performance of this tank (*called in-situ rinse HF-last tank*) is compared to that obtained on a conventional acid tank and its dedicated rinse tank to which the wafers are transferred. In such a case, with conventional acid tank (*called standard rinsetank*) the transfer from the acid tank to the rinse tank causes hydrophobic wafers to be exposed to a liquid(acid)/air interface and to an air/liquid(water) interface.

Particle contamination occurs from hydrophobic wafers being inserted in a liquid. Repeated experiments have shown that, in a single HF process-batch, fresh wafers (hydrophilic) will exhibit particle removal, while wafers that have been exposed to HF (hydrophobic) exhibit considerable particle addition. This has been attributed to immersion of hydrophobic wafers; as the wafers are inserted into the DI rinse water, particles on the liquid surface are transferred from the liquid and stay attached to the wafers. [2]

We can expect to reduce all forms of contamination with a special tank design, in which dilute HF step is performed for a certain amount of time, then some valves are switched such that the HF solution in the tank is displaced out, from the bottom of the tank with a DI water upflow. After the rinse step, the wafers are transferred through a final rinse tank and finally to the IPA dryer.

The benefits obtained from this *in-situ* rinse HF-last process are evaluated when

a silicon epitaxy layer is grown on BiCMOS technology wafers.

Epitaxy layer has the following specifications; epitaxy thickness is equal to 3.2 $\pm$ 0.1 micron and epitaxy resistivity is equal to 1.0 $\pm$ 0.10 ohm-cm

The epitaxy layer is grown in our production Epsilon One epitaxy reactor, made by ASM, at a reduced pressure of 60 torr, according our standard epitaxy deposition process which has a preclean step at 1100 degree for 1.5mn under hydrogen ambient gas and a deposition step at 1050 degree for 4.6mn, at a deposition rate of 0.7 micron/minute, with dichlorosilane ambient gas and arsine dopant gas.

Before and after epitaxy, surface microroughness is measured with a non-contact Atomic Force Microscope (AFM), after epitaxy cleaning chemical contamination is measured on the wafer using TXRF. Particle contamination is monitored using a patterned wafer defect laser particle counter and epitaxy defects are observed, identified and classified using an automated defect review station linked to the patterned wafer defect monitor.

The comparison of the conventional cleaning process to this new cleaning HF *in-situ* process is done on several split lots of BiCMOS production wafers.

Parametric test results significant of the bulk silicon interface with the epitaxy layer are compared and yield data are provided on a number of split lots.

The complete study has been done using 200 mm wafers.

2 EXPERIMENT

2.1 IPA dry particle contamination

Before starting the experiments, our drying process was referenced for 0.2 um particle size and above such that it would not lead to misinterpretation of contamination tests. Drying, as the last step is very critical, and the characterization of the level of performance of our IPA dryer, model FEL 281 supplied by S&K was felt as an absolute necessity.

These tests have shown an extremely good neutral behavior in terms of particle contamination from the total cleaning, rinsing and drying process, demonstrating the effectiveness, for this smaller particle size, of the drying technique and of the actual setup of the IPA dryer.

2.2 Particle contamination and hydrogen surface passivation

HF process time of 5 minutes was chosen for the HF step. This condition has been found elsewhere to exceed the minimum time in order to reach a stable and significantly high contact angle.[1] Rinse after HF process time of 5 minutes was chosen as well for both kinds of rinsing, standard rinse and *in-situ* rinse.

A reduction on particle contamination was observed when *in-situ* rinse is used. With higher HF temperature a quite significant effect is observed in particle contamination reduction. Contact angle of the wafers resulting from the same experimental conditions was also measured. High contact angle means that the surface is well passivated. This technique is a very good measure of the degree of completeness of native oxide removal and has been found to be well correlated to XPS measurement. The maximum value one can get on a perfect silicon surface is 78.9 degree. Contact angles very closed to this value have been obtained on the HF

in-situ rinse tests.

The DI water used during all these experiments is key to the extremely good results achieved. Production data from the DI water plant indicates that TOC (Total organic Content) and Dissolved Oxygen are well controlled and far below our specifications. In Particular, dissolved oxygen level achieved, 1 ppb range, gave us the best conditions possible in order to reach such a low particle contamination level and such a high and stable contact angle when using our *in-situ* rinse tank technique.

Surface preparation was done in our Crolles fab, while epitaxy deposition was done in our Grenoble fab and wafers transported after this critical cleaning step to the epitaxy deposition.

A waiting time ranging from 12 to 36 hours after pre-epitaxy cleaning have been used without any problem as reported below. This demonstrates the robustness and the insensitiveness to some delay between cleaning and deposition, of the cleaning processes used.

2.3 Epitaxy defect characterization

In this set of experiments, we have used a TENCOR 7600 patterned wafer defect monitor for defect characterization.

Contamination is measured before epitaxy and after epitaxy. Two levels of buried layers are present on the bare wafers, defects down to 0.15 um sensitivity are easily distinguishable from the IC patterns.

Each processed lot were split with 2 wafers out of 25 wafers, run through our new HF in-situ rinse process compared to RCA last standard process. These final cleaning processes before epitaxy being done after a complete oxide removal and native oxide formation with SC1 solution is performed in a previous step.

Defects obtained were classified by intensity level and grouped in 5 different classes for the sake of comparison with optical review by defect size. The classification used, is based upon 5 different size classes which are respectively, SM for small, SM/MD for small/medium, MD for medium, MD/LG for medium/large and LG for large size defects.

Other result are from a visual classification of the defects size under a microscope, after each defect is detected and located by X-Y coordinates on the monitor wafers and reviewed on the automatic defect review station, which automatically search the defects for review. Artefacts and scratches as well as double counted defects can be eliminated, resulting in an accurate comparison by actual defect size.

The defect densities achieved after epitaxy deposition are such that the total defects count (specially larger defects count) is reduced on the wafers that went through our new HF-last in-situ rinse process, compared to conventional RCA type pre-epitaxy clean process. This result has been repeatedly achieved on all test wafers.

2.4 Surface characterization

Surface microroughness has been measured using a non-contact or "tapping" mode, Atomic Force Microscope from Digital Instruments. RMS value instead of Ra value which is often used, and peak-to-valley (6 sigma) value from the AFM measurement are measured. RMS value is usually higher than Ra value.

Measurements are done on 2 different wafer regions. Steps and terraces are clearly visible on all regions, even though the epitaxy conditions are not favorable. We report from these measurements about equally low surface microroughness values on both cleaning processes. Typical values are 0.09nm RMS and 0.9nm peak to valley before epitaxy, and 0.06nm RMS and 0.6nm peak to valley after epitaxy.

Interesting effects of the epitaxy shift phenomenon are observed.

2.5 Electrical characterization and yield results

We have tested at parametric test level, the wafers from the split lots processed. These tests have shown no significant variation (less than 10%) on parameters such as epitaxy resistance, parasitic PNP gain and bulk PNP gain. Electrical yield did not show any significant difference on the split lots as well. We can state from these electrical results that our modified process can be implemented and fully tested through standard process qualification procedure.

3 CONCLUSIONS

Both standard and *HF in-situ* rinse processes have been studied. The two techniques have been compared and characterized for 200 mm wafers processed in a state-of-the-art class 1 fab environment using advanced automated wet benches with an established IPA drying process. Very good results have been obtained for various concentrations and temperatures. AFM measurement has shown very low surface roughness and typical steps and terraces patterns. The defect densities achieved after epitaxy deposition are such that the total defects count (specially larger defects count) is reduced on the wafers that went through our new HF-last in-situ rinse process, compared to conventional RCA type pre-epitaxy clean process. The *in-situ* rinse process is relatively easy to implement. The very low concentration of HF required makes it inexpensive when using very small and precise quantities of 50% HF mixed up with DI water, even though some of the HF solution is lost for every batch of wafers. A number of advanced tank designs are under evaluation for significant improvement in process time and process control, able to achieve even better cost ratio figure, by reducing waste treatment cost as well.

ACKNOWLEDGEMENTS

The authors would like to thank Frédéric CHOLLET from CNET, FRANCE TELECOM Laboratory in Meylan, FRANCE, for their support in carrying out measurements and for valuable discussions about the results. This paper would have not been achieved without this support.

Wafers have been borrowed out of the standard production flow with the help of the BiCMOS device engineering, and special thanks to Marie-Thérèse REYNAUD should be extended.

BIBLIOGRAPHY

1. Christopher F. McConnell, UCPSS 92, Sept. 1992.
2. Steven Verhaverbeke et Al, IEDM 92, page 637-640. Dec. 1992.
3. Paul PATRUNO, ECS 93, Oct. 1993.

ETCHING OF SiO_2 WITH ANHYDROUS HF AND ORGANIC SOLVENT VAPORS

Kevin Torek, Jerzy Ruzyllo, and Robert Grant*

Electronic Mat. and Proc. Research Lab, Penn State Univ., University Park, PA 16802, USA
* SubMicron Systems, Inc., Allentown, PA 18106, USA

1. INTRODUCTION

A gas phase process using anhydrous HF (AHF) and CH_3OH originally proposed for SiO_2 etching at atmospheric pressure [1] has been applied to cleaning applications in cluster tools [2]. It was established that when CH_3OH was substituted for H_2O as the AHF solvent, reasonable SiO_2 etch rates were achieved with lower particle counts after the etch. In the modified chemistry, CH_3OH scavenges H_2O from the reaction. The removal of H_2O from the etcher reduces the rate of the reverse reaction, thereby reducing the solid byproduct formation which is associated with higher particle counts resulting from some AHF/H_2O vapor processes.

Methanol vapor is not the only reasonable choice of organic solvent for silicon oxide etching [3, 4]. Other solvents should therefore be studied in order to optimize the etch. The ideal AHF solvent for gas phase oxide etching in a cluster tool should satisfy at least three requirements: (i) the AHF solvent should allow an etch process cycle time that is compatible with the cluster, (ii) the AHF solvent should enable a reaction that leaves the exposed surface completely free from oxide and the wafer totally free from solid residues that could compromise yield or reliability, and (iii) the AHF solvent should uniformly and repeatably remove only the desired amount of only the desired oxide.

In this work, we characterize the etch rates which are obtained using the vapors of methanol, ethanol-water azeotrope (EWA), 2-propanol, acetone, and water as AHF solvents for gas phase etching of thermal SiO_2 at reduced pressure and increased temperature. Ethanol with 4.4 w/o H_2O was used, rather than pure ethanol, in order to investigate the effect of adding a small amount of H_2O to the feed gas mixture.

2. EXPERIMENTAL

This experiment was carried out using a prototype of a commercial, cluster compatible module. The reaction chamber is constructed of alumina and designed for gas phase cleaning [5]. Wafers with dry thermal SiO_2 of 1000 Å initial thickness were used as starting samples. An ellipsometer was used to measure oxide thicknesses. A minimum of five runs was performed per etch condition. The AHF solvent is delivered by bubbling purified N_2 through the liquid solvent, which was contained in a temperature-controlled vessel. The bubbler temperature was adjusted for each solvent in order to produce 40 Torr vapor pressure in the bubbler head.

3. RESULTS AND DISCUSSION

In order to satisfy the above mentioned requirement (i) for removing native and sacrificial oxides, thermal SiO_2 etch rates ranging up to 200 Å/min should be readily achievable. Figure 1 shows the average overall thermal SiO_2 etch rates for methanol, EWA, 2-propanol, acetone, and water at 300 Torr. For the organic vapors, the overall average etch rate increases with decreasing solvent vapor pressure.

However, due to the nonlinear time dependence of SiO_2 etch depth, the overall average thermal SiO_2 etch rate is determined by the abscissa (initiation time) and slope (linear rate) of the etch depth versus etch time curve. In order to separate the effects of initiation time and linear rate on the overall average etch rate, the time dependent etch depth was characterized for these solvents; the results of this characterization are summarized in Fig. 2. Figure 2 shows that 2-propanol exhibits the fastest initiation time and the greatest linear rate, while water exhibits the slowest initiation time and the lowest linear rate.

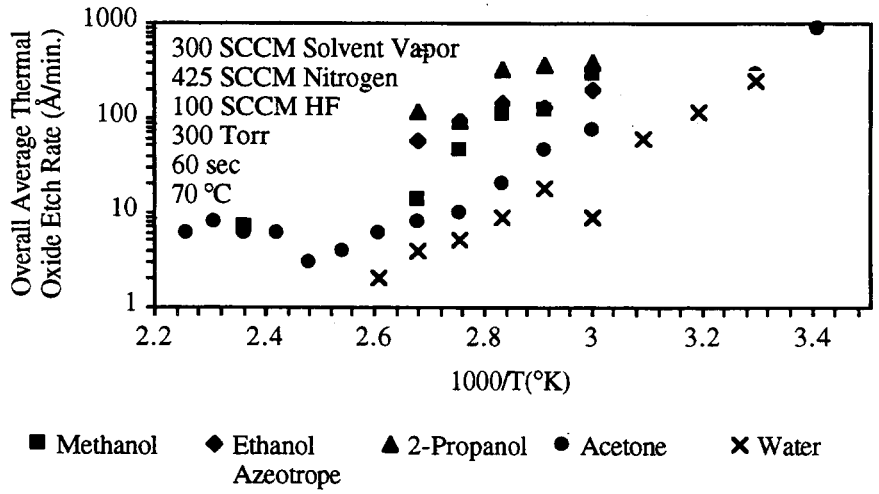

Figure 1. Thermal Oxide Etch Rates.

The differences in the etch rates for the different alcohols are out of proportion with the differences in their vapor pressures. In particular, we suggest that the use of EWA rather than pure ethanol is the cause of the lower than expected etch rate for EWA based its relative vapor pressure (where we assume that the difference between the vapor pressues of EWA and pure ethanol is negligible). Because EWA contains 4.4 weight % water, the lower than expected etch rate may be a symptom of different reaction rate constants, depending on the nature of the AHF solvent. Assuming that the mechanistic aspects of the overall etch reaction are identical for the organic solvents and for H_2O, then from LeChatelier's principle we expect that solvents that efficiently remove water will result in faster etching. The scavanging of H_2O by the organic solvents in Fig. 1 may be expected to contribute towards the higher SiO_2 etch rates observed when the organic solvents are used.

While the etch rates achieved by any of these organic solvents satisfy the throughput requirement (i) for gas phase native/chemical oxide etching in cluster

tools, lower etch rates are obtained when solvents having higher vapor pressures are used. Therefore, a means was sought to increase the etch rate for these solvents.

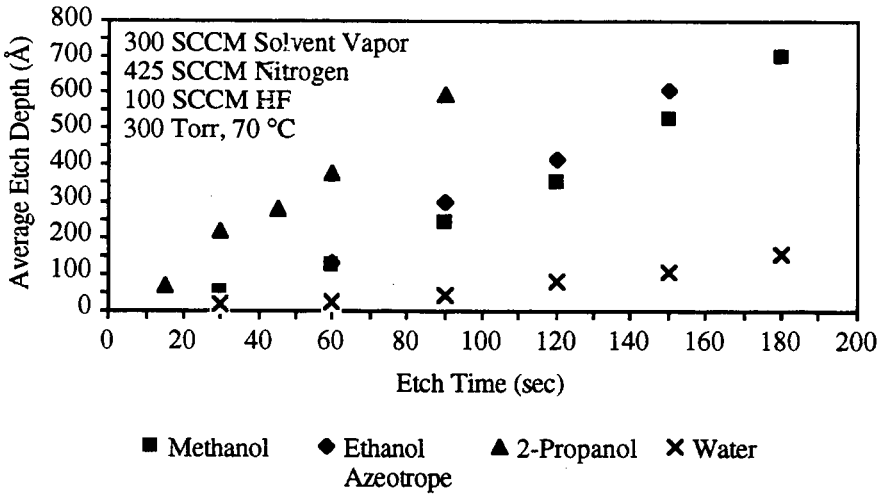

Figure 2. Thermal Oxide Etch Depth vs. Etch Time.

Figure 3 shows that the SiO_2 etch rate is a monotonically increasing function of AHF partial pressure for both methanol and acetone. The methanol runs were performed at a wafer temperature of 70 °C while the acetone runs were carried out at 20 °C. Although the temperature difference overcompensated for the difference in the vapor pressures of acetone and methanol, Fig. 3 nevertheless indicates that the adjustment of AHF partial pressure allows the desired etch rate to be achieved for the given solvent under otherwise fixed parameters.

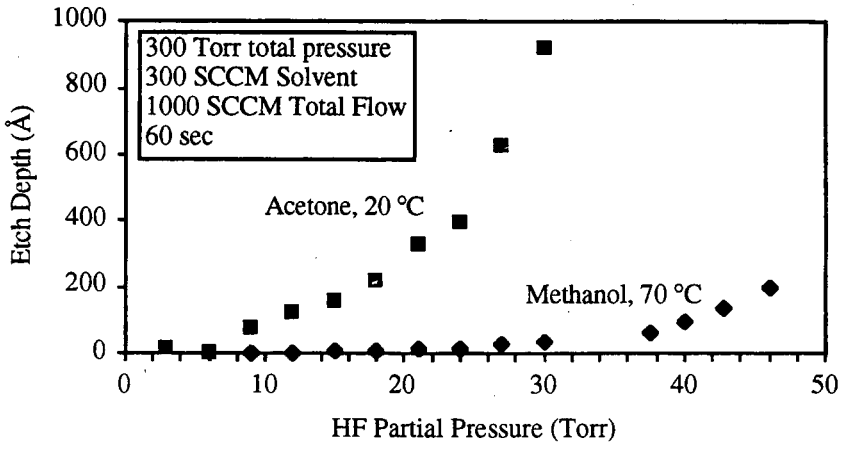

Figure 3. Effect of AHF Partial Pressure on Etch Depth.

4. CONCLUSIONS

Combinations of alcohol vapors with AHF etched SiO_2 faster than the combinations of either H_2O or acetone vapors with AHF. The solvent vapor pressures and drying efficiency control the SiO_2 etch initiation time and overall average etch rate. Silicon dioxide etch rates appropriate for gas phase cleaning applications may be achieved with the vapors of methanol, ethanol-water azeotrope, or IPA by adjusting the AHF partial pressure, but when either H_2O or acetone vapors are used, the SiO_2 etch rate is lower. In addition, when H_2O vapor was used for the AHF solvent in the same reactor and the mixture was allowed to condense on the wafer, large numbers of small (0.2-0.3 micron) particles [6] were counted on the wafer's surface following the SiO_2 etch.

Methanol is the most suitable alcoholic AHF solvent vapor for native/chemical oxide etching at reduced pressure. There are both technical and chemical motivations for choosing methanol vapor. The technical reasons are, due to the lower vapor pressure of methanol, vapor delivery was simplified and pump down times were shorter than when vapors of the other alcohols were used, while reasonable rates are achieved for etching thin SiO_2 films. The chemical reasons for choosing methanol are related to particle formation. The higher vapor pressure of methanol reduces its residence time, and thereby the residence time of associated water byproduct and backwards reaction tendency. Also, because methanol has no azeotrope with water, it does not retain water in the enhanced adsorption layer, therefor particle formation can be effectively suppressed.

When high SiO_2 etch rates are required, then other organic vapors such as IPA should be considered. A solid comparison of residue and selectivity are required for a more complete evaluation.

5. ACKNOWLEDGMENTS

Sponsorship of this project by the Semiconductor Research Corporation is gratefully acknowledged. We also wish to acknowledge the continuous support of this research by SubMicron Systems, Inc. The authors are grateful to Motorola, Inc. and Digital Equipment Corporation for supplying the wafers that were used in these experiments.

REFERENCES

1. A. Izumi, T. Matsuka, T. Takeuchi, and A. T. Yamano, in Second Intern. Symp. on Cleaning Technol. in Semicon. Dev. Manufactur. J. Ruzyllo and R. E. Novak, Editors, PV 92-12, pp. 260-266, The Electrochem. Soc., 1992.
2. J. Ruzyllo, K. Torek, C. Daffron, R. Grant, and R. Novak, J. Electrochem Soc., **10**, 4, pp. 164-166 (1993).
3. J. W. Butterbaugh, C. F. Hiatt, and D. C, Gray, in Third Intern. Symp. on Cleaning Technol. in Semicon. Dev. Manufactur. J. Ruzyllo and R. E. Novak, Editors, PV 94-7, pp. 374-383, The Electrochem. Soc., 1994.
4. J. M. de Larios and J. O. Borland, *ibid.*, pp. 347-354.
5. SubMicron Systems, Inc. Primaxx.
6. K. Torek, K. Settlemyer, and J. Ruzyllo, to be published.

IN SITU REMOTE HYDROGEN PLASMA CLEANED Si(100) FOR GATE OXIDE FORMATION: CORRELATION OF SURFACE AND DEVICE PROPERTIES*

J.S. Montgomery, J.P. Barnak, H. Ying, J.R. Hauser, and R.J. Nemanich
Center for Advanced Electronic Materials Processing
North Carolina State University
Raleigh, NC 27695-8202

This study of the H-plasma treatment prior to gate oxidation has demonstrated a region of operation (> 450°C) which does not produce any observable defects. We have shown the ability to use the H-plasma without increasing morphological damage or subsurface damage while reducing interfacial C and O. Devices fabricated following a high temperature H-plasma exposure have a threshold voltage at or near the theoretical value of 0.85 V, a peak mobility of ≈ 388 cm^2/V-s, the best observed surface roughness coefficients, and lowest values of interface scattering. The strongest correlation of surface properties and device performance is that of rms roughness and interface scattering.

1. INTRODUCTION

The motivation for this work is the evaluation of remote hydrogen-plasma treatment of silicon prior to gate oxidation in the fabrication of metal-oxide-semiconductor field effect transistors (MOSFET). As the feasibility of cluster-based process increases, there is a corresponding demand for *in situ* cleaning contained in a separate module or integrated into a multi-purpose etch/clean module. The criteria for the cleaning process is that surface impurities are removed and the surface is not roughened. Previous studies have shown that hydrogen plasma processing is a candidate for the *in situ* clean with the ability to remove hydrocarbons as demonstrated by AES and result in a well-ordered surface as shown by LEED and RHEED.(1-6) Preliminary results by this group have also shown that in the low temperature regime, the H-plasma clean causes surface etching which leads to an increase in surface roughness.(7) The previous studies have characterized the post-plasma silicon surfaces but have not addressed the impact of the hydrogen plasma treatment on fully fabricated devices. In this study we will compare surface roughness following the H-plasma cleaning step and the implications in the operation of MOSFET's .

2. EXPERIMENT

The wafers used in this study were 100mm p-type boron doped silicon with a nominal resistivity of 0.05 Ω·cm. Treatment of each sample was a combination of wet chemistry (SC1/SC2/HF last) and *in situ* processing subjecting the wafer to a remote H-plasma exposure with duration's from 120 to 600 seconds at substrate temperatures ranging from 200 to 700°C. The *in situ* processing was carried out in a cluster tool constructed *in house* which allowed for total *in situ* manipulation of each wafer through each step in the processing including 1) H-plasma treatment, gate oxide deposition, and polysilicon deposition or 2) H-plasma treatment and

* This work has been partially supported by the National Science Foundation Engineering Research Centers Program through the Center for Advanced Electronic Materials Processing (Grant CDR 8721505).

then either a polysilicon capping layer or low temperature oxide capping layer in preparation for SIMS analysis. SIMS analysis was performed by Charles Evans & Associates, Inc. and Evans East, Inc. The elements detected in the SIMS were H or deuterium, C, O, and F.

Following treatment in the remote H-plasma cleaning module, gate oxidation and polysilicon deposition was performed with an RTCVD module adjacent to the cleaning module on a four station cluster-type system which also includes a RPECVD module and a entry/exit module. The target gate oxide thickness was 100 Å on gate areas of $(100\ \mu m)^2$, $(300\ \mu m)^2$, and $(500\ \mu m)^2$. Following polysilicon deposition the wafers were removed from the cluster tool, and the final steps were executed for the completion of MOSFET's. C-V measurements were used to determine the oxide thickness for each chip on each wafer. The extrapolated threshold voltage as defined by Tsividis was obtained from the experimental I-V data.(8) The I-V data was also analyzed to determine the peak mobility as calculated from the peak in the transconductance as a function of drain voltage. The oxide thickness, threshold voltage and doping of the wafer were then used as input for a model proposed by Shin, et. al.(9) to extract a value for interface scattering and a roughness scattering coefficient. Each of these operational parameters are then evaluated on the basis of H-plasma treatment conditions, particularly temperature.

3. RESULTS

3.1 Surface Analysis

There is a strong dependence of the surface morphology on variations in substrate temperature during H-plasma processing. The regions of interest can be divided into a low temperature region (≤ 400°C) and a high temperature region (450 to 700°C). Treatments at and above 450°C result in a surface state similar to the starting surface following *ex situ* wet-chemistry, that is with an rms roughness of 1-5 Å. With decreasing substrate temperature during H-plasma exposure, the surface roughness increases. At 150°C the rms roughness was ≈ 18 Å.

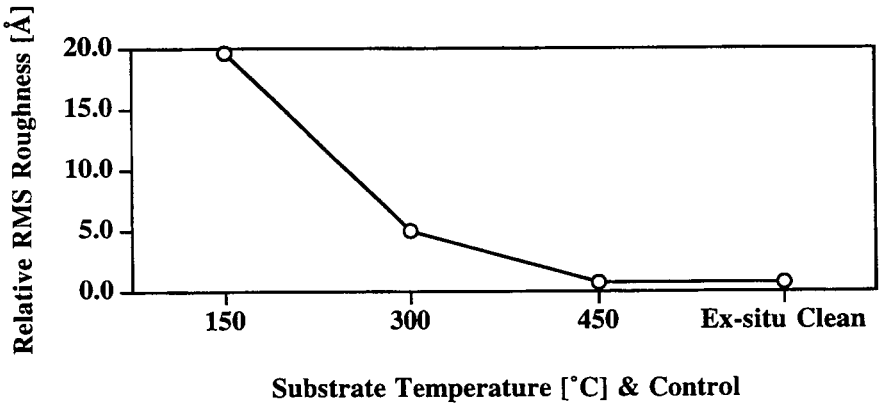

Figure 1. Relative rms roughness of Si(100) vs. substrate temperature during H-plasma exposure. Also included is the rms roughness of the silicon after only the *ex situ* cleaning.

SIMS analysis of C and O at the interface treated with a hydrogen plasma show only gradual trends as a function of substrate temperature. Areal density of C following H-plasma treatment was $5.5x10^{13}$ atoms/cm^2 while that of O was $1.3x10^{15}$ atoms/cm^2. Therefore changes in the morphology of the surface are primarily due to variations in substrate temperature.

3.2 Device Analysis

Shown in figure 2 is the dependence of threshold voltage on H-plasma processing temperature. The devices processed at 500°C for 120 s have a threshold voltage very close to the theoretical value for this device of 0.85 V. The peak mobility showed trends which were similar to the threshold voltage, with the processing at 500°C and for 120 s having the highest mobility at 388 cm^2/V-s. Devices with treatments below 450°C or for longer duration's show significant degradation of the peak mobility with values as low as ≈ 100 cm^2/V-s.

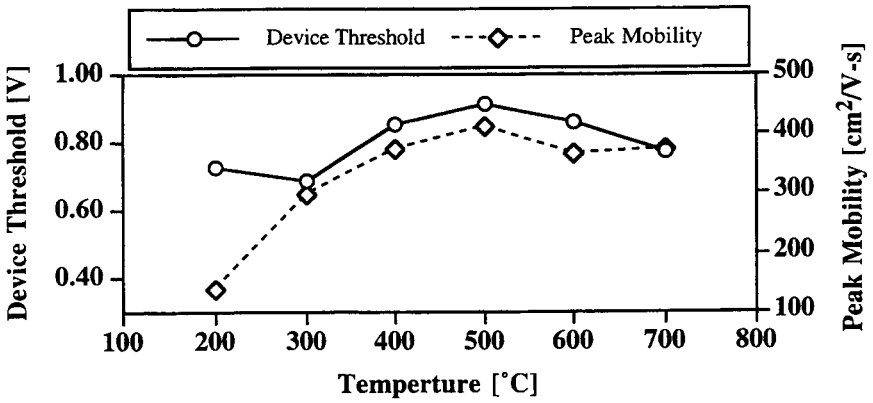

Figure 2. Threshold voltage and peak mobility of MOSFET's as a function of substrate temperature during H-plasma exposure.

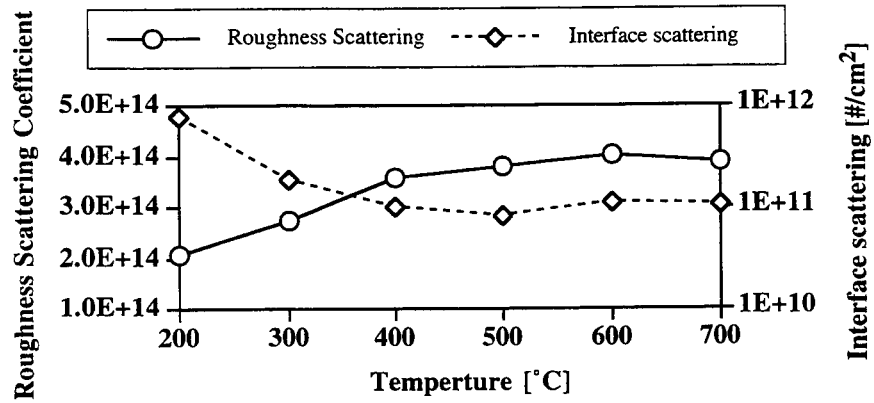

Figure 3. Roughness scattering and interface scattering as a function of substrate temperature during H-plasma exposure.

Using the threshold voltage, we then compute a roughness scattering coefficient and a value for interface scattering as outlined by Shin, et. al.(9) Again, the scattering mechanisms are highly dependent on H-plasma processing temperature (Figure 3). In this model the roughness scattering coefficient is derived from the slope of the high field fall-off of the mobility. Both the roughness scattering coefficient and the interface scattering indicate improved performance for surfaces treated at temperatures of 450°C and above.

4. DISCUSSION

The effects of the H-plasma treatment vary primarily according to the substrate temperature during processing. In the low temperature regime AFM shows physical evidence of increased roughness. Since the SIMS analysis showed virtually no change in interfacial contaminants for the various cleaning configurations in this study, we conclude that trends in the threshold voltage, peak mobility, the surface roughness coefficient, and interface scattering are due to changes in the surface morphology. Even with the interfacial C and O, the threshold voltage is at the expected level of 0.85 V for wafers treated in the high temperature regime (500°C). Likewise, the peak mobility reaches a value of 388 cm^2/V-s as compared to the reported empirical value of 450 cm^2/V-s according to the collection of data presented by Shin, et. al.(9) Comparing the trends in the AFM analysis with the derived values of the interface scattering and the roughness scattering coefficient, one can see that following a low temperature treatment of an H-plasma, the rms roughness increases. This roughness is manifested in the device performance as an increase in scattering due to interfacial roughness for temperatures of 400°C and lower. Interface scattering which combines the roughness scattering and ionized impurity scattering shows a similar correlation. There is a reduction of surface roughness for temperatures > 450°C and the lowest values of interface scattering for the same temperature range.

5. REFERENCES

1. J.R. Hauser, N.A. Masnari, and M.A. Littlejohn, Mat. Res. Soc. Symp. Proc. **146**, 15-26 (1989).
2. P. Singer, Semi. Int. **16**, 46-51 (1993).
3. B. Anthony, T. Hsu, L. Breaux, R. Qian, S. Banerjee, and A. Tasch, J. Elec. Mat. **19**(10), 1027 (1990).
4. S. Banerjee, A. Tasch, T. Hsu, R. Qian, K. Kinosky, J. Irby, A. Mahajan, and S. Thomas, Mat. Res. Soc. Symp. Proc. **259**, 43 (1992).
5. T. Hsu, B. Anthony, R. Qian, J. Irby, S. Banerjee, A. Tasch, S. Lin, H. Marcus, and C. Magee, J. Elec. Mat. **20**, 279 (1990).
6. T.P. Schneider, J.S. Montgomery, H. Ying, J.P. Barnak, Y.L. Chen, D.M. Maher, and R.J. Nemanich, in Third International Symposium on Cleaning Technology in Semiconductor Device Manufacturing. 1993, J. Ruzyllo and R. Novak ,Editors, p. 329-338, Electrochemical Society, NJ
7. J.S. Montgomery, J.P. Barnak, A. Bayoumi, J.R. Hauser, and R.J. Nemanich, in Third International Symposium on Cleaning Technology in Semiconductor Device Manufacturing. 1993, J. Ruzyllo and R. Novak ,Editors, p. 296-306, Electrochemical Society, NJ
8. Y.P. Tsividis, Operation and Modeling of the MOS Transistor. p. McGraw-Hill, New York (1987).
9. H. Shin, G.M. Yeric, A.F. Tasch, and C.M. Mazair, Solid-State Electron. **34**(6), 545-552 (1991).

Physico Chemical Aspects of Hydrogen Peroxide Based Silicon Wafer Cleaning Solutions

H.F. Schmidt[1], M. Meuris[1], P.W. Mertens[1], A.L.P. Rotondaro[1], M.M. Heyns[1], T.Q. Hurd[2] and Z. Hatcher[3]

[1]IMEC, Kapeldreef 75, B-3001 Leuven, Belgium
[2]Texas Instruments, Dallas, TX, U.S.A., presently at IMEC
[3]Ashland Chemical, Columbus, OH, U.S.A.

Abstract
This paper reports on some important aspects of hydrogen peroxide based chemical mixtures, used to clean up silicon surfaces before they enter the device fabrication process and also after nearly each further processing step. In particular mechanisms for metallic contamination and silicon surface roughening are discussed and illustrated with some experimental results which reveal a direct correlation between silicon surface roughening and gate oxide integrity. Also a brief description of a measurement tool will be given, which has been developed in order to investigate the stability of H_2O_2 in different mixtures as function of temperature and metal contamination.

1. Introduction

The standard wet cleaning chemistry for wafer processing operations is mainly based on the mixing of hydrogen peroxide with ammonium hydroxide (SC1 mixture) and hydrochloric acid (SC2 mixture). Several additional cleaning steps, which are under investigation or are already in use to improve the cleaning efficiency contain also H_2O_2 as one active component, e.g. sulphuric acid/hydrogen peroxide (SPM) and hydrofluoric acid/hydrogen peroxide [1,2]. This preference for H_2O_2 is based upon its unique properties, as it is a very strong oxidising agent (E^o=1.776), has no by-products except water (through desired reactions) and oxygen (through non-desired reactions), and is of itself very stable if critical impurities are kept low. Once H_2O_2 is mixed with other reagents and is exposed to certain metallic and non-metallic impurities, even in the low ppb range, its stability can suffer dramatically and the reliability of the cleaning bath goes down [3]. In the following, the different cleaning mixtures will be discussed in order of their appearance in the so called "standard wafer cleaning process": SPM/dilute HF/SC1/SC2.

2. The SPM mixture (H_2SO_4/H_2O_2)

This mixture is mainly used to remove organic contamination from the silicon surface because of its very strong oxidising power (in situ formation of Caro's acid, H_2SO_5. An other advantage is the good capability of this mixture to form a thick native SiO_2 on the silicon surface, imbedding all surface contaminations (metallics and particles), which can be striped of afterwards together with this wet oxide layer by applying an HF dip [4]. This results in a "new" surface where the metal contamination is as low as the intrinsic contamination of the bulk silicon material allows. Disadvantages of this mixture are based on its high viscosity, which results in difficulties to remove the residual boundary layer by normal DI water rinsing, and on the so called "time dependent haze", where it was found that while storing SPM-last wafers in clean room air, needle shaped, sulphur containing crystals are formed on the surface [5]. Another problem of this mixture is the instability of H_2O_2, which results in a pretty fast loss of oxidising power (Fig. 1). For a very clean SPM mixture with metals < 0.2 ppb the half-life of the H_2O_2 was found to be around 4 hours.

while the half-life decreases to 20 min, when the mixture was spiked with 100 ppb Cu^{2+} standard solution. The half-life (Tau/2) was defined by graphical extrapolation and corresponds to the time needed to decrease the concentration to half of its initial value.

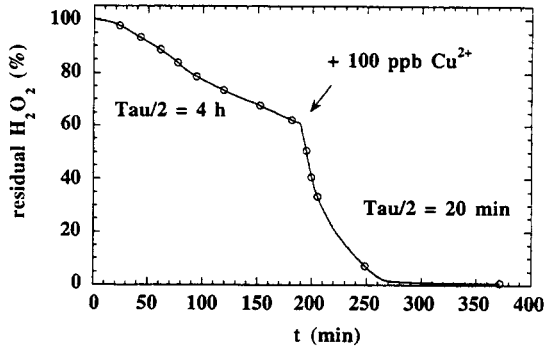

Fig. 1: Change of the H_2O_2 concentration in an ultra clean SPM mixture with time (metals < 0.2 ppb, H_2SO_4/H_2O_2 = 4:1, 90°C). At 190 min the solution was spiked with 100 ppb $Cu(NO_3)_2$ solution.

3. The SC1 mixture (NH_4OH/H_2O_2)

The SC1 cleaning step is applied in order to remove particles from the wafer surface by an under etch and lift off mechanism [4]. To achieve this, two processes are going on in this mixture at the same time. H_2O_2 is oxidising the silicon surface very fast, while the OH^- is catalysing the slow dissolution of the SiO_2 by H_2O to form $Si(OH)_4$ [6]. This so called molecular soluble silica has a very low solubility below an pH of 11. So in the SC1 environment (pH 10) it starts to coagulate to form negatively charged colloids or precipitates which can re-deposit onto the silica surface of the wafer. In the same environment Fe forms an iso-polybase shown in Fig. 2, which is positively charged and which is also absorbing and/or precipitating onto the wafer surface.

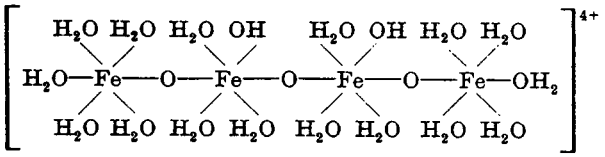

Fig. 2: Fe (III) hydroxide polymerisation to form positively charged colloids and precipitates.

This results in one of the problems the SC1 cleaning step is causing, metal contamination. Another species which can be found in high concentrations on the wafer surface is Al, if the applied chemicals are of low purity. Al^{3+} forms an aluminosilicat ion which co-precipitates with silica.
Another problem of the SC1 cleaning mixture is the evaporation of NH_3, which is lowering the pH, so that the dissolution of silica becomes slower resulting in a reduced particle removal efficiency. In sensitive light scattering measurements, particles show up as LPD's (light point defects) together with other surface irregularities. Under certain conditions a large increase in small LPD's is observed after SC1 cleanings. In some work it has been shown, that such an increase in small LPD's can be due to the formation of COP's (Crystal Originated Pits) [7]. Other publications discussed the possibility of surface roughening due to the increased etching by NH_4OH, because of the decrease in the H_2O_2 concentration [8]. In

our work we have found that these LPD's and their formation mechanism are mainly related to the oxygen gas bubbles created by the decomposition of H_2O_2. By applying atomic force and scanning electron microscopy, these LPD's could be identified as small silicon spikes, which were caused by small oxygen gas bubbles blocking the wafer surface from the etching action of the SC1 chemistry [3]. This micro-roughening effect may only occur on wafers which are hydrophobic before being immersed into the SC1 solution [3,9]. By monitoring the rate by which oxygen gas is released in real time with a gasometric technique (Fig. 11), it is possible to correlate the "oxygen evolution rate" of an SC1 mixture with the addition of LPD's on a wafer surface. This is shown in Fig. 3. LPD's below 0.16 µm show a strong correlation with the initial oxygen evolution rate, while LPD's between 0.16 and 0.30 µm are only slightly affected. No influence could be found for LPD's above 0.3 µm.

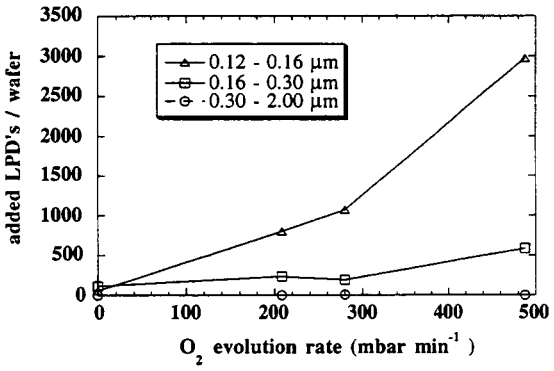

Fig. 3: Correlation between oxygen evolution rate of an SC1 bath and LPD addition on hydrophobic wafers.

The decomposition behaviour of an SC1 mixture with ~1ppb of metallic contamination in total solution is shown as a function of time in Fig. 4.

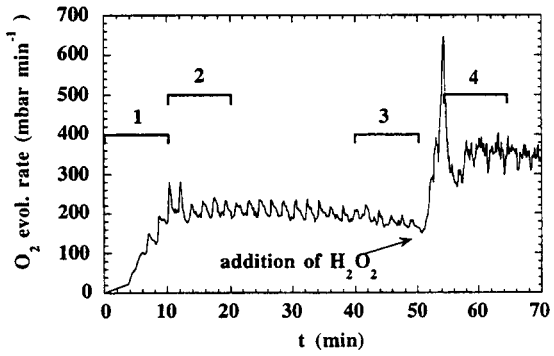

Fig. 4: Typical decomposition behaviour of an SC1 mixture at 70°C with an impurity level of ~1 ppb of metallic contamination in total SC1. The oscillating behaviour of the decomposition reaction is clearly to see (the H_2O_2 contains a stabiliser).

Four cassettes with pre-cleaned, metallic contamination free, hydrophobic wafers were immersed one after another in this bath for 10 minutes. Each cassette contained different types of silicon substrates: CZ (n, p) and EPI (p/p^+). The immersion times are marked in Fig. 4 with numbered horizontal bars. Between the third and the fourth cassette, the SC1 mixture was re-spiked with H_2O_2 to obtain the initial mixing ratio. As a result of the addition of H_2O_2 the oxygen evolution rate increased very strongly, which also yielded a

much higher number of LPD's added on wafers immersed at this point. The sensitive light scattering maps of representative wafers from the four cassettes of this experiment are shown in Fig. 5.

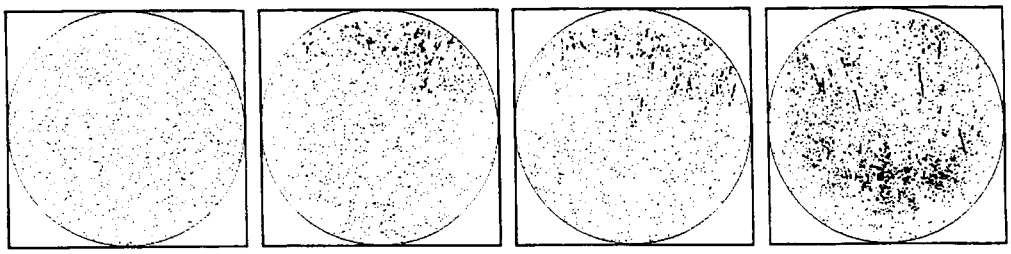

1 2 3 4

Fig. 5: Typical decomposition patterns from 4 consecutively cleaned cassettes of hydrophobic wafers (labelled from 1 to 4 in Fig. 3).

Fig. 6 and Fig. 7 are showing LPD maps of wafers with typical decomposition patterns, measured after cleaning and gate oxidation, and the corresponding analogue E_{bd} wafer mappings after build up of Al/poly-gate capacitors on the same wafers. This significant impact on GOI was found on p-type CZ and EPI substrates with 6.5 nm and 15 nm oxides (n-type has not been tested).

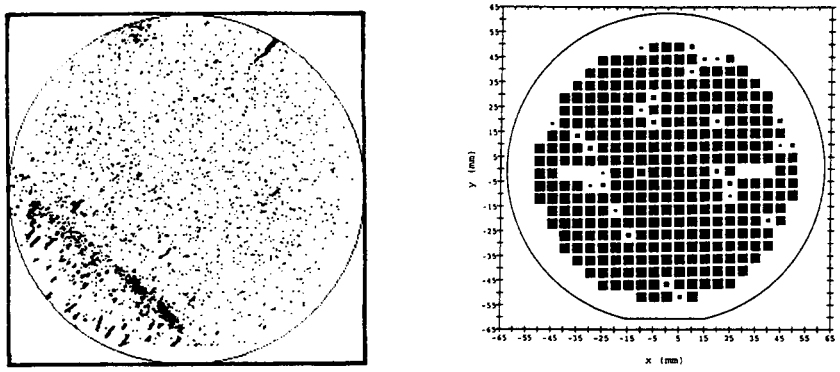

(a) (b)

Fig. 6: Correlation between decomposition patterns (a) and the resulting 0 - 18MV/cm analogue E_{bd} - yield plot (b). The largest black squares are symbolising good capacitors while the smallest ones are symbolising early break down events (capacitor area = 15.8 mm^2, 6.5 nm gate oxide, p-CZ substrate).

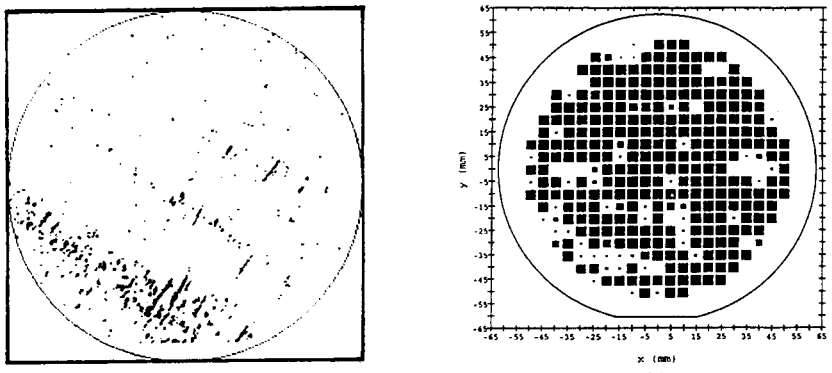

(a) (b)

Fig. 7: Correlation between decomposition patterns (a) and the resulting analogue E_{bd} - yield plot (b) on p/p$^+$ EPI substrate (capacitor area = 15.8 mm^2, 15 nm gate oxide).

The stability of H_2O_2 is influenced by both metallic and non-metallic contaminants, the temperature and the pH of the solution [10]. Fig. 8 shows the impact of the temperature on the stability of H_2O_2 in a very clean SC1 mixture which is following the Arrhenius equation (metal contamination < 0.2 ppb). The half-life (Tau/2), which is the time until 50% of the initial H_2O_2 decomposes, increases from 19.4 hours to 38.7 days by reducing the temperature from 80°C to 50°C.

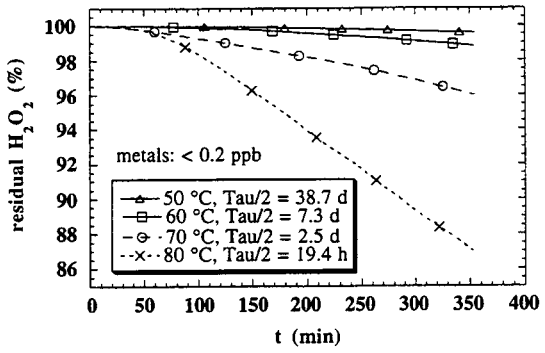

Fig. 8: Decrease of the H_2O_2 concentration in a very pure SC1 mixture with time as a function of the bath temperature (metal contamination < 0.2 ppb).

In Fig. 9, the impact of metallic impurities on the decomposition rate of an SC1 mixture is shown. The half-life decreases from 6.8 days to 1.7 hours with increasing metal contamination in the sub-ppb range. Especially Fe^{3+} was found to be very effective in de-stabilising an SC1 mixture while Cu^{2+} shows a lower catalytic activity. If both are mixed together the decomposition reaction shows a very strong oscillating behaviour (Fig. 10).

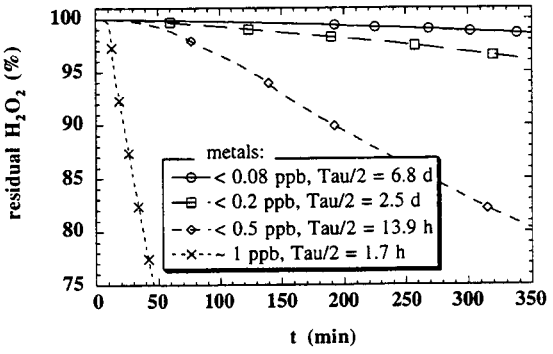

Fig. 9: Decrease of the H_2O_2 concentration as a function of the metal contamination level in the SC1 mixture at 70°C.

As mentioned above, a gasometric technique was used to monitor the decomposition behaviour of H_2O_2 in real time. Fig. 11 shows a schematic drawing of the tool, which has been developed at IMEC over the last 3 years. With this apparatus, the O_2 evolution rate as a function of time is measured by monitoring the pressure change over a certain range with a highly sensitive pressure sensor. Using the ideal gas equation and taking the ratio H_2O_2/O_2 = 2/1 into account, it is possible to determine the decomposition rate constant in (min^{-1}) as (dn/dt)/n and the residual amount of H_2O_2 in (%) as (n_o-n). The accuracy of that measurement method was cross checked by titration which resulted in a very good agreement of both techniques (Fig. 12).

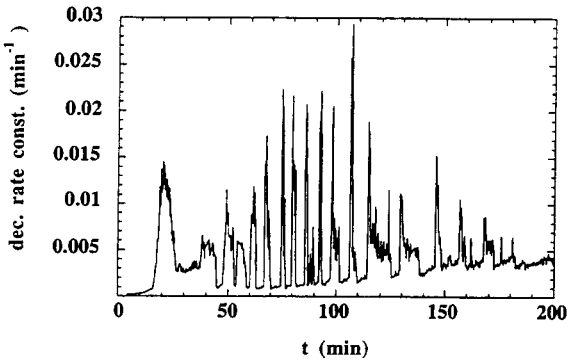

Fig. 10: Oscillating behaviour of an ultra pure SC1 mixture (intrinsic metals < 0.08 ppb) when spiked with 0.5 ppb Fe^{3+} and 0.5 ppb Cu^{2+} (as nitrates).

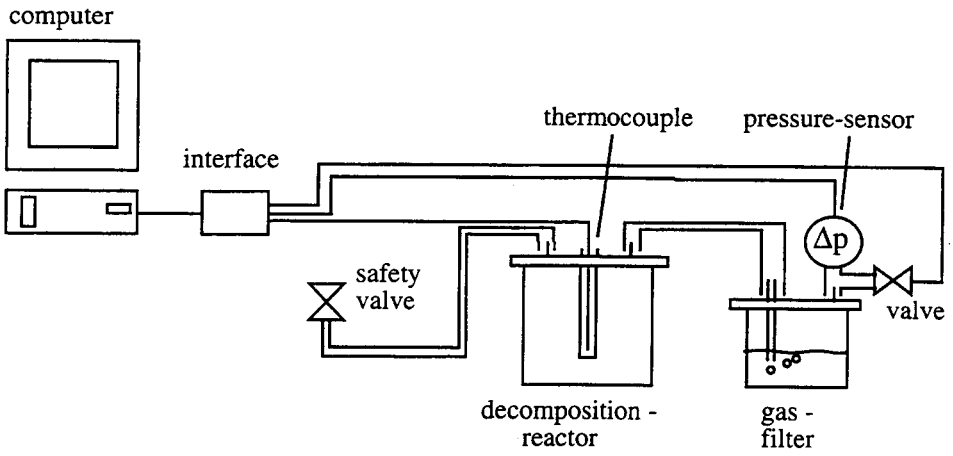

Fig. 11: Hydrogen Peroxide decomposition tester (schematic drawing).

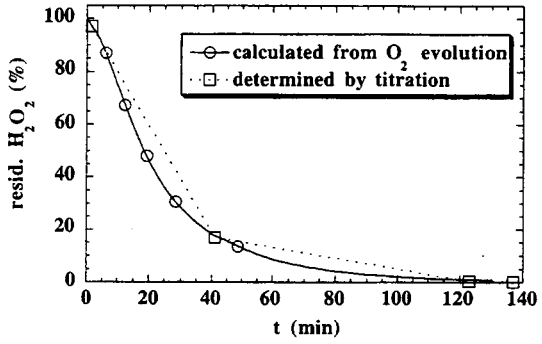

Fig. 12: Correlation between gasometric and conventional titration technique to determine the decomposition rate of H_2O_2 in an SC2 mixture.

4. The SC2 mixture (HCl/H_2O_2)

This solution is applied to the silicon surface in order to remove metallic contamination which are often originating from the previous SC1 cleaning step. The negative aspects of this solution are however the re-contamination with particles and again the instability of H_2O_2. But conversely to an SC1 mixture the SC2 mixture shows nearly no reaction to Fe^{3+} contamination (we spiked up to 100 ppb with Fe-nitrate), but it is very sensitive to the Cl^- concentration and also the pH (Fig. 13) [11]. Reducing the HCl concentration by a factor of 10 results in a half-life of around 19 hours, while in a standard SC2 mixture the half-life of the H_2O_2 is around 20 minutes. The reason for this is the activity of Cl^- as a decomposition catalyst, the presence of Br^- in the HCl, which is also known as a catalyst for the decomposition of H_2O_2 [12] and the pH of the solution. Addition of Cl^- to an SC1 mixture did not show any effect in enhancing the decomposition rate of H_2O_2.

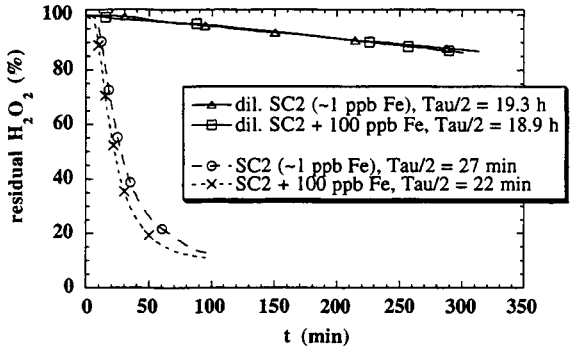

Fig. 13: Influence of the HCl and Fe^{3+} concentration on the stability of an SC2 mixture at 75°C (standard mixture $HCl/H_2O_2/H_2O$= 1/1/5 and dil. = 0.1/1/5.6).

The last graph (Fig. 14) represents the temperature dependence of the stability of H_2O_2 in an SC2 mixture.

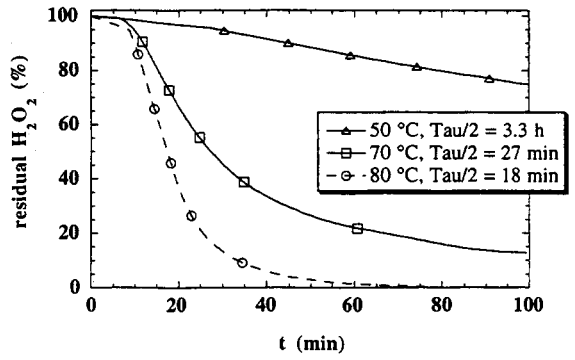

Fig. 14: Influence of the temperature on the stability of H_2O_2 in an SC2 mixture (1/1/5, metal contamination ~ 1 ppb).

5. Other mixtures with H_2O_2

Alternative cleaning methods to the above mentioned ones are under investigation (e.g. H_2O_2/HF) or already since a certain time in use (e.g. low temperature SC1 with megasonic agitation). In the H_2O_2/HF mixture again two processes are going on at the same time like in the SC1 mixture. Just here we have a slow oxidation of the silicon surface by H_2O_2 and a fast dissolution/etching of the formed silica by HF. But like the commonly used mixtures also the new chemistries are not very well understood and still some research has to be performed to optimise them.

6. Conclusion

In this paper we have discussed some critical aspects of hydrogen peroxide containing cleaning solutions. Beside all problems of metallic and particulate re-contamination, it has been shown, that the decomposition of H_2O_2 can cause severe problems. Especially the stability of H_2O_2 in the commonly used SC1 cleaning bath was investigated and found to have a direct impact on silicon surface roughness and with this on the integrity of thin gate oxides. A micro-masking effect through small oxygen bubbles, sticking on the initially hydrophobic silicon surface is believed to be responsible for this roughening. With real time observations of the decomposition behaviour of H_2O_2 we found that respiking of an SC1 mixture with H_2O_2 keeps the oxygen evolution rate high, which yields in higher surface roughening. Also Fe^{3+} and Cu^{2+} were found to be very effective catalysts for the decomposition reaction in a caustic environment especially when they are mixed together. In this case strong oscillations were obtained. In an acid medium, like the SC2 mixture represents, Fe^{3+} does not effect the stability but Cl^- does.

Acknowledgement: The technical and scientific support by Karine Kenis, Ann Opbebeeck, Peter Boelen, Geert Doumen and Peter Kruse is greatly acknowledged.

6. References

1) W. Kern: J. Electrochem. Soc. **137** (1990) 1887.
2) T. Ohmi et al.: J. Electrochem. Soc. **140** (1993) 811.
3) H.F. Schmidt et al.: Proc. 3rd Int. Symp. Cleaning Technology in Semiconductor Device Manufacturing, 1993 (The Electrochem. Soc., Pennington, NJ, 1994) p. 102.
4) M.Meuris et al.: Jpn. J. Appl. Phys. **31** (1992) L 1514.
5) A.L.P. Rotondaro et al.: this proceedings
6) R.K. Iler: The Chemistry of Silica, (John Wiley & Sons, New York, 1979)
7) J. Ryuta et al.: Jpn. J. Appl. Phys. **29** (1990) L 1947.
8) Y. Oshida et al.: Chemical Proc. 1992 Semiconductor Pure Water and Chemicals Conference, ed. M.K. Balazs (Balazs Analytical Laboratory, Sunnyvale, 1992) p. 63.
9) L.I. Vasilenko, Russ. J. Phys. Chem. **55** (1981) No. 2
10) H.F. Schmidt et al.: .Extend. Abstracts Int. Conf. Solid State Devices and Materials, 1994 (Business Center for Academic Societies Japan, Tokyo, 1994) p. 419.
11) T.Q Hurd et al.: Proc. 40th Annual Technical Meeting, 1994 (Institute of Environmental Sciences, Mount Prospect, Illinois, 1994) p. 218.
12) W.C. Schumb et al.: Hydrogen Peroxide, (Reinhold Publishing Corporation, New York, 1955) pp. 467 - 514.

AN HF-O_3 AQUEOUS SOLUTION FOR SILICON WAFER CLEANING

Y. Fukazawa*, K. Sanpei*, T. Nakajima*, K. Takase*, K. Miyazaki*

1. INTRODUCTION

The RCA clean developed by W. Kern, et al.(1), based on hydrogen peroxide (H_2O_2), is very effective in removing impurities on Si wafers and has long been used in manufacturing processes. Both HF and HCl/H_2O_2 (SC-2) solutions are effective in removing some metallic contaminants from Si surfaces. However, a metal contaminant such as Cu, which has a lower ionization tendency than Si and easily adheres to Si surfaces, is difficult to remove by HF or SC-2 solutions only. Furthermore, it has been shown that Cu contaminants can significantly degrade device performance(2)(3). Recently, a mixture of dilute HF and H_2O_2 has been suggested as a replacement for the SC-2 solution to remove metallic contaminants on Si surfaces(4)(5).

In this study, the authors examine a new cleaning treatment using a mixture of HF and O_3 water(HF/O_3 solution) to remove Cu contaminants on Si surfaces.

2. EXPERIMENTAL

P(100) Si wafers with a diameter of 150mm were used in this study. The removal efficiency of Cu adhered to Si surfaces in BHF was examined. Wafers were immersed in BHF that was spiked with a known Cu concentration to fabricate intentionally contaminated wafers. Cu levels of the contaminated wafers were evaluated by total reflection X-ray fluorescence spectroscopy(TRXRF). Clean ozone gas was dissolved into deionized water (DIW) to get 2ppm and 10ppm of dissolved O_3. After mixing the O_3, water, and HF solution, wafers were immersed into this mixture and the Cu removal effectiveness by HF/O_3 solution was measured. Hydrogen peroxide-based cleans including HCl/H_2O_2, H_2SO_4/H_2O_2, and HF/H_2O_2 were also investigated for comparison.

3. RESULTS AND DISCUSSION

3.1. Cu removal by hydrogen peroxide-based solution.

Figure 1 shows the Cu concentration on Si surfaces measured by TRXRF before and after cleaning by HCl/H_2O_2, H_2SO_4/H_2O_2 and HF/H_2O_2 solutions,

*Integrated Circuit Manufacturing Engineering Department
Toshiba Corporation 1, Komukai Toshiba-cho, Saiwai-ku, Kawasaki 210, Japan

respectively. The Cu contaminants were removed effectively by the HF/H_2O_2 solution, but not by HCl/H_2O_2 or H_2SO_4/H_2O_2 solutions alone. However, an additional HF step with HCl/H_2O_2 and H_2SO_4/H_2O_2 solutions considerably enhances the Cu removal efficiency. Moreover, under the cleaning sequence of HF followed by HCl/H_2O_2 solution, the Cu removal efficiency is dependent on the native oxide grown during rinsing after HF treatment as shown in Figure 2. These results indicate that native oxide grown before cleaning influences Cu removal. The HF/H_2O_2 solution is believed to dissolve the Cu contaminants and the native oxide simultaneously, resulting in a high efficiency of Cu removal.

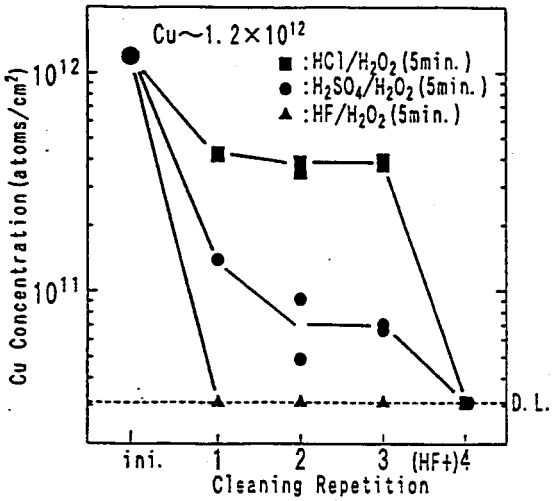

Fig. 1 Cu removal by hydrogen peroxide-base cleaning

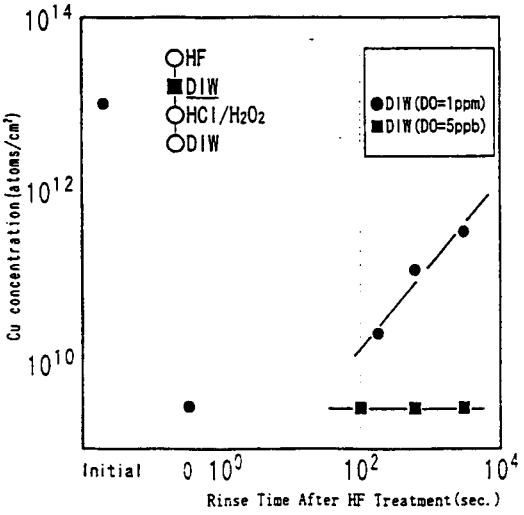

Fig. 2 Impact of DO in DIW on Cu removal by HF followed by SC-2 cleaning

3.2. Cu removal by HF/O_3 solution.

Similar to the HF/H_2O_2 solution, the HF/O_3 solution can be expected to remove the Cu contaminants because this solution can also dissolve the native oxide and Cu contaminants simultaneously. Figure 3 shows the Cu concentration on the Si surfaces before and after cleaning by an HF/O_3 solution at room temperature for 3 minutes. The Cu contaminants were effectively removed by the HF/O_3 solution, and the removal efficiency was dependent on the ozone content. The HF/O_3 solution with higher ozone concentration (10ppm) was most effective in removing Cu. Figure 4 shows the TRXRF spectra of the wafers after cleaning by the HF/O_3 solution.

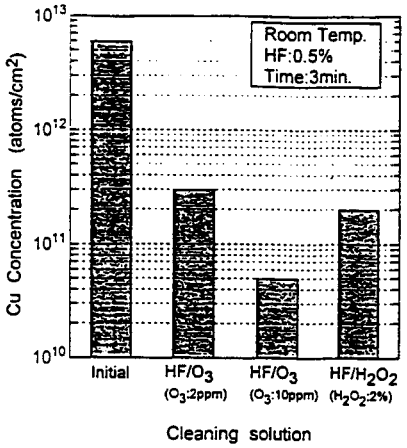

Fig. 3 Cu removal by HF/O_3 solution and HF/H_2O_2 solution

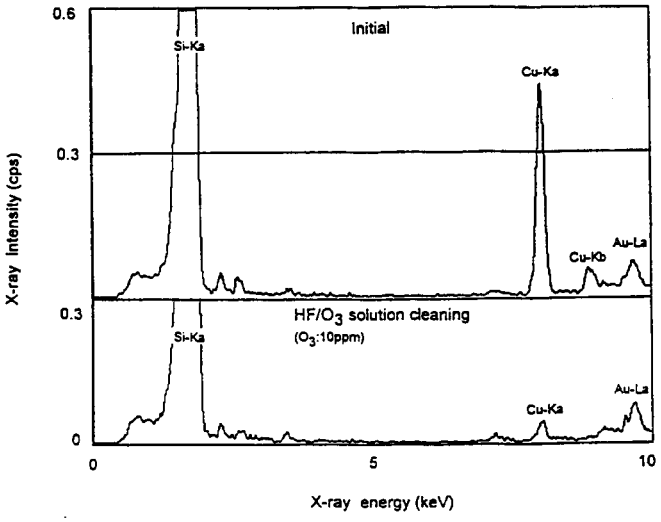

Fig. 4 TRXRF spectra of Cu before and after cleaning by HF/O_3 solution

4. CONCLUSIONS

An hydrogen peroxide-free, O_3 water based cleaning solution for Si wafers has been developed. A mixed solution of HF and O_3 water greatly enhances the removal efficiency of Cu contaminants adhered to Si surfaces, which are difficult to remove by HF, HCl/H_2O_2 or H_2SO_4/H_2O_2 solutions alone. The HF/O_3 solution can replace the SC-2 clean for metallic contamination removal in semiconductor manufacturing.

REFERENCES

1. W. Kern and D. A. Poutien, RCA Review, 31 ,187(1970)
2. K. Honda, A. Ohsawa and N. Toyokura, Jpn. J. Appl. Phys. 27(12)(1984)
3. K. Hiramoto, et al, Jpn, J. Appl. Phys. 28(12)(1989)
4.T. Shimono and T. Tsuji, 1st Workshop on VLSI Ultra Clean Technology(1989)
5. T. Ohmi, T. Imaoka, I. Sugiyama and T. Kezuka, J. Electrochem. Soc. Vol.139(1992)

METAL ADDITION OF THE RCA-1 CHEMISTRY AS A FUNCTION OF BLEND RATIO AND TEMPERATURE

K. K. Christenson* , Shelley Smith* and Dennis Werho**

1. INTRODUCTION

The RCA-1 or APM standard clean (NH_4OH:H_2O_2:H_2O), as published by Kern in 1970, has been the primary means of removing particles, trace organics and some metals in pre diffusion cleans for over 20 years.[1, 2] One negative effect of the APM solution is the deposition of metallics, particularly Al, Fe and Zn.[3, 4, 5] These metals are presumably located on the surface of the oxide, which grows from the Si/SiO_2 interface, and are easily accessible to the succeeding HPM (RCA-2) solution. Some of these metals are on the surface in a "molecular" form and some are aggregated into micro particles. However, it is possible that a metallic added by the APM and then removed by HPM might leave a local degradation to the oxide surface. There is also a hope of eliminating the need for an HPM step through improvements in the cleanliness of the APM. It is therefore desirable to reduce the quantity of metals left by the APM solution. This work measured the deposition of Al, Fe, Ni, Cu and Zn from APM as a function of blend ratio and temperature. The solutions were "unspiked"; no contaminants were deliberately added to the solution.

2. EXPERIMENT

N type, <100>, 150 mm CZ wafers were initially cleaned to near background levels in the MERCURY® MP spray acid processor with a B Clean chemistry sequence (SPM-DHF-APM-HPM). Two wafers were run in each of the 27 treatments with a 195 second APM dispense. Treatments consisted of a 3x3x3 full factorial matrix of H_2O_2 and NH_4OH concentrations and temperatures (27 treatments). Flow rates of 23, 92 and 320 cc/min were chosen to give two, approximately 4x changes in concentration and a blend ratio range of n:m:5 with n and m ranging from to 0.06 to 1.45.

Ashland SEMI grade H_2O_2 and NH_4OH were dispensed from the spray processor's chemical canisters through flow control systems with a nominal dynamic range of 100 to 300 cc/min. DI water was added to the blend to bring the total flow to a constant rate of 1760 cc/min. For instance, 1350 cc/min of DI water would be added to 320 cc/min of NH_4OH and 90 cc/min of H_2O_2 to produce an effective blend ratio of 1.2:0.3:5. Due to a 90 cc/min practical lower limit on the flow systems, the H_2O_2 and NH_4OH were diluted 3:1 in the canister to achieve effective flow rates of 23 cc/min when required. Fixing the total flow rate, along with the limited dynamic range of the flow control systems, resulted in blend ratios that were not simple fractions of the traditional 1:1:5 ratios.

* FSI International, Chaska, Minnesota USA.
** Motorola, Inc., Materials Characterization Laboratory, Mesa, Arizona USA

The in-line temperature of the APM before being sprayed on the wafers was varied over 20, 60 and 95 °C. For the runs at elevated temperatures, the in-line temperature was maintained at 60 or 95 °C by an in-line infrared chemical heater.[6] Heat loss through processes such as evaporation limited the on-wafer temperature from 60 and 95 °C to approximately 40 and 60 °C respectively for 195 second APM dispenses. A constant total APM flow rate of 1760 cc/min was used for all treatments so that the transient and steady state on-wafer temperatures were consistent. The results of chemical assays performed on the H_2O_2 and NH_4OH by ICP-MS at Balazs Laboratories (Sunnyvale California) are listed below:

	H_2O_2	NH_4OH	Det. Lim.
Al	24 ppb	1	.1
Cr	4.2	<.1	.1
Cu	0.1	<.1	.1
Fe	2.5	<2.0	2.0
Ni	<.1	.8	.1
Zn	5.0	<.5	.5

One wafer from each of the 27 treatments received metals analysis by Total Reflection X-ray Fluorescence (TXRF). TXRF was performed on a Technos TREX 610S. Each wafer was analyzed at three points located on a line with one point at the center and the other two points roughly equidistant from the center to the edge. An approximately one cm in diameter area at each location was analyzed for 1,000 seconds at an analyzing angle of 0.09°. A second wafer from 19 of the treatments was sent for metals analysis by VPD-ICP-MS at Balazs Laboratories in Sunnyvale, California.

3.RESULTS AND DISCUSSION

Al showed a strong tendency to deposit that was independent of temperature but scaled with the H_2O_2 concentration (Figure 1). The Al deposition appears to be a linear function of the Al concentration in the APM which is dominated by the Al in the H_2O_2 (Figure 2). That is, the chemistry or kinetics of the process does not change with blend ratio, only the amount of Al available in the solution to deposit. Al deposition can be reduced dramatically by the use of dilute chemistries.

Unlike Al, the deposition of Fe increased with the flows of either H_2O_2, NH_4OH or temperature. The data is consistent with Fe deposition being linear with solution concentration. But the noise in the experiment and the Fe levels in the NH_4OH being below the detection limit do not allow this theory to be confirmed. The deposition rate does double between 20 and 95 °C (20 and 60 °C on-wafer) indicating a small energy barrier to deposition. Fe deposition can be reduced dramatically by the use of dilute, cold chemistries.

Ni and Cu were between 1 and 2 x 10^{10} for all treatments. They showed little trend save a slight increase in Ni deposition with higher temperatures and Cu

with the combination of high H_2O_2, NH_4OH and temperature. Due to the extremely low concentrations of Ni and Cu in the solutions in these experiments (<0.1 ppb), it should not be assumed that these metals cannot deposit from the solution when present in higher quantities. Chromium levels were below the detection limit of $1.2x10^{10}$ on all of the samples.

Zn had the most complex behavior, initially rising with H_2O_2, NH_4OH and temperature. But at the highest NH_4OH concentrations, the Zn deposition was reduced dramatically. The increase with H_2O_2 is reasonable since H_2O_2 is the dominant source of Zn in the solution. But there is not enough Zn in the NH_4OH to account for the change in deposition on the basis of changing Zn concentrations in the solution. Apparently the chemistry or kinetics of deposition is affected by the NH_4OH concentration, perhaps via a change in pH. Regardless of the mechanisms, Zn deposition can be reduced dramatically by the use of dilute, cold chemistries.

It should be noted that all of these results refer to deposition on wafers with an initial chemically grown "native" oxide. It is possible that the deposition kinetics may be significantly different on hydrogen terminated silicon (fresh from an HF exposure) or a bulk oxide. The hydrogen terminated case is of the greatest interest as this is the state of the gate area entering the APM step after the sacrificial oxide is stripped by HF in the pre gate clean.

In summary, there is a strong general trend that metals deposition from APM solutions can be reduced dramatically by the use of dilute chemistries, particularly at reduced temperatures.

4. ACKNOWLEDGMENTS

We would like to acknowledge the generosity of the Motorola Corporation whose support made this work possible. In particular, we thank Robert Duffin and Kathy McCormack for their involvement in the FSI IRONMAN program.

5. REFERENCES

1. W. Kern and D. Puotinen, "Cleaning Solutions Based on Hydrogen Peroxide for Use in Silicon Semiconductor Technology", RCA Review (31) pp 187-206, 1970.
2. W. Kern, "The Evolution of Wafer Cleaning Technology", Proc. of the First Intl. Symp. on Cleaning Tech. in Semiconductor Device Mfg., ECS, Pennington, NJ, 90-9, pp 3-19.
3. J. Glick, "Characterization of Deposition and Removal of Metallic Impurities of the RCA Standard Clean", 1993 SPWCC, Santa Clara, M. Balazs ed., p 93.
4. Y. Sugihara, S. Shimokawa, Y. Oshida, "Influence of Metallic Impurities on SC-1 Cleaning", 1993 SPWCC, Santa Clara, M. Balazs ed., p 66.
5. P. Gupta, M. Van Horn and M. Frost, "Metal Contamination of Silicon Surfaces: Correlation of Chemical Purity to Silicon Surface Contamination", 1992 SPWCC, Santa Clara, M. Balazs ed., p 191.
6. K. K. Christenson, "The Effects of Increased Chemical Temperature in a Centrifugal Spray Processor," Proc. of the Third Intl. Symp. on Cleaning Tech. in Semiconductor Device Mfg,, ECS, Pennington, NJ, 94-7, pp 474-483.

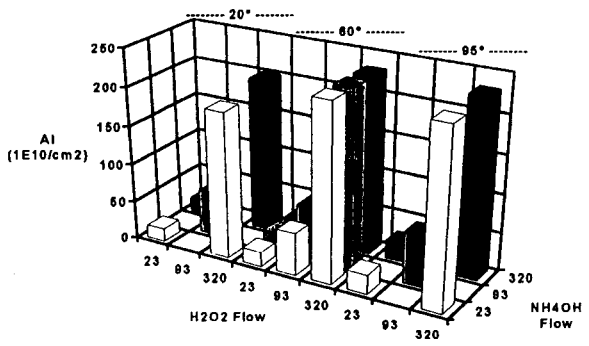

Figure 1. Aluminum added in APM solution.

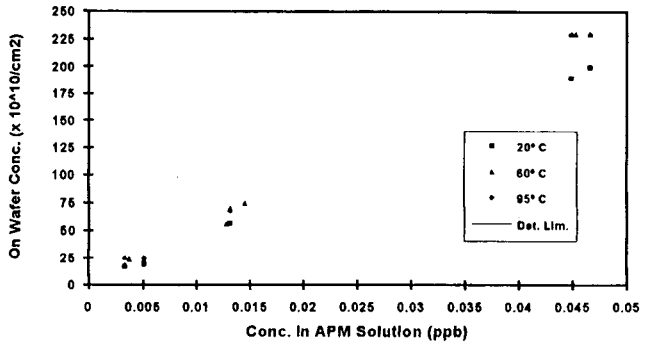

Figure 2. Al added to wafer vs Al in the APM solution.

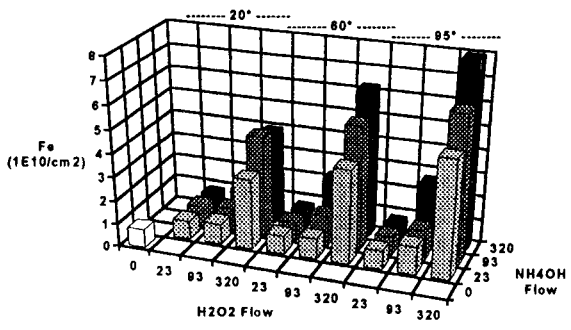

Figure 3. Iron added in APM solution.

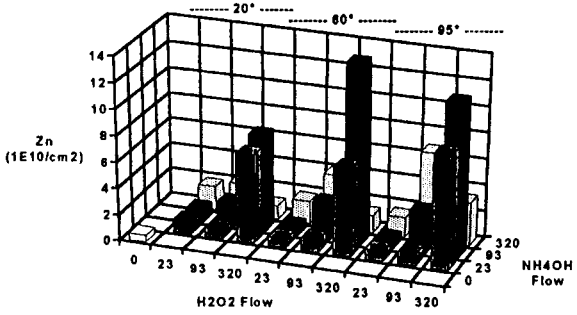

Figure 4. Zinc added in APM solution.

TiN ETCH RATE AND H_2O_2 DECOMPOSITION STUDIES IN THE $H_2O_2/NH_4OH/H_2O$ SYSTEM

A. Philipossian and J. Magana
Intel Corporation, Santa Clara, CA 95052

1. INTRODUCTION

The $NH_4OH/H_2O_2/H_2O$ mixture (a.k.a. APM) is used for a variety of purposes in ULSI manufacturing such as wafer cleaning and TiN removal. This mixture has been studied extensively in wafer cleaning applications. However, its effectiveness in TiN etching, and its stability over time are relatively less understood, and are the subject of this study.

2. EXPERIMENTAL

Tables 1 and 2 summarize the parameter space used for determining the effect of H_2O_2, NH_4OH and Ti concentration in the bath, on TiN etch rate and H_2O_2 decomposition rate. Full-factorial designs were adopted in both sets of experiments where the etch baths were prepared in 100 cc ultra-clean plastic beakers presoaked in a mixture of HNO_3 and HCl. Starting H_2O_2 and NH_4OH solutions had individual trace metal contents of less than 0.2 ppb. A spectrometric standard containing 10,000 ppm Ti in 10 percent HNO_3 and 2 percent HF was used as the Ti source. It was assumed that trace amounts of acids present in the etch baths did not affect TiN etch rate.

After mixing, the baths were left for one hour at room temperature to equilibrate. TiN films were etched for 2 minutes, rinsed in DI water, and nitrogen-dried. TiN etch rate was determined indirectly by measuring the sheet resistance of each 3 cm × 3 cm piece of wafer before and after the etch. Given the inverse relationship between sheet resistance and film thickness, and knowing the initial film thickness, the final film thickness and the etch rate was calculated. As for the decomposition experiments, the baths were kept in tightly closed beakers for five days and periodically titrated to determine the concentration of H_2O_2 (samples taken after 1, 48, and 96 hours). It was verified that the NH_4OH concentration remained constant.

Statistical linear regression was used to analyze the experimental data and establish empirical models for characterizing the chemical processes occurring in the etch bath (Section 3). Moreover, in order to test the validity of these models in a production environment, a time-dependent characterization of a state-of-the-art TiN etch bath was performed during which a total of 600, 200 mm TiN-deposited test wafers were processed through the bath. The production bath was monitored for TiN etch rate as well as H_2O_2, NH_4OH, and Ti concentration for a period of 5 days.

Table 1: Factors investigated in the TiN etch rate experiment (32 runs plus 7 replicates).

Factor	Level 1	Level 2	Level
H_2O_2 (% by volume)	25.0	50.0	62.5
NH_4OH (% by volume)	12.5	25.0	37.5
Ti (ppm)	0.0	62.5	250.0

Table 2: Factors investigated in the H_2O_2 decomposition experiment (8 runs plus 2 replicates).

Factor	Level 1	Level 2
H_2O_2 (% by volume)	25.0	62.5
NH_4OH (% by volume)	12.5	37.5
Ti (ppm)	0.0	250.0

3. RESULTS AND DISCUSSION

With a regression coefficient of 0.89, the TiN etch rate model indicated the H_2O_2 concentration to be the dominant factor. The NH_4OH concentration and its interaction with H_2O_2 were significant to lesser degrees, while the Ti content of the bath had no effect on etch rate. 3-factors interactions were assumed to be negligible.

Assuming that TiN etching proceeds via a 2-step mechanism whereby titanium is first oxidized by H_2O_2 and the product is then dissolved in the alkaline solution, the observed strong dependence on H_2O_2 concentration indicated the oxidation of Ti with H_2O_2 to be the rate limiting step, rather than the dissolution rate of titanium oxide. The latter is supported by the fact that NH_4OH concentration had a minor effect on TiN etch rate. The results are summarized in Figure 1 in the form of a contour plot. As an example, at a constant NH_4OH concentration of 25 percent, a 2-fold increase in H_2O_2 concentration (30 to 60 percent) corresponds to a 4-fold increase in TiN etch rate (30 to 120 Å/min).

With a regression coefficient of 0.89, the H_2O_2 decomposition model identified the two major factors to be H_2O_2 and Ti concentrations. The model assumed that H_2O_2 concentration varied linearly with time, and 3-factor interactions were negligible. The former assumption was based on in-house data as well as previous validations with Fe and Cu-contaminated H_2O_2 [1,2].

Based on this model, elevated H_2O_2 and Ti levels increase the H_2O_2 decomposition rate (Figure 2). NH_4OH concentration has no effect on H_2O_2 decomposition rate. The catalytic activity of titanium is believed to be due to the presence of titanium in hydroxide form in the alkaline solution. This is similar to the catalytic activity of iron and copper in APM.

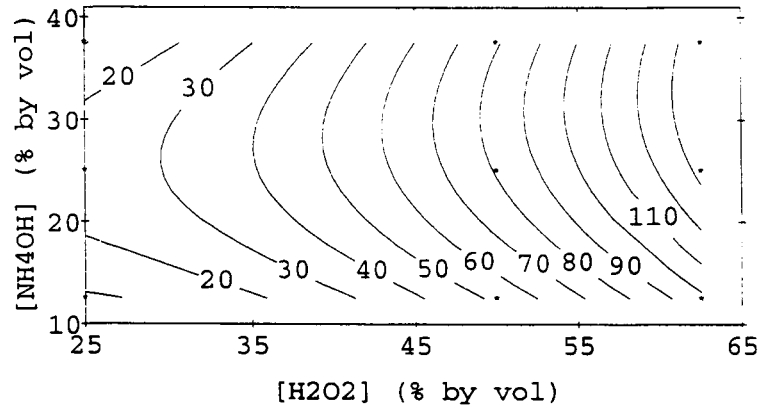

Figure 1. The effect of H_2O_2 and NH_4OH concentrations on TiN etch rate (highlighted on the contour lines in units of Å/min). Ti concentration is maintained constant at 62.5 ppm.

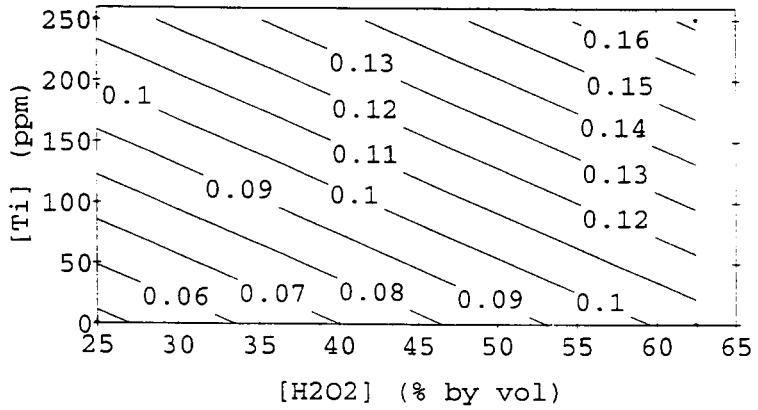

Figure 2. The effect of H_2O_2 and Ti concentrations on H_2O_2 decomposition rate (highlighted on the contour lines in units of percent by volume in the bath per hour). NH_4OH concentration is maintained constant at 25 percent.

Figure 3 (next page) summarizes the results of monitoring an automated production wet bench etch bath for H_2O_2, NH_4OH, and Ti concentrations as well as TiN etch rate. Over the 5-day period, roughly 22 and 55 percent of the H_2O_2 and NH_4OH were lost due to decomposition and evaporation, respectively, resulting in a 59 percent reduction in TiN etch rate. The etch rate model (discussed

above) was then used to obtain the theoretical etch rate based on the actual individual species concentrations in the production bath. Figure 4 indicates that a reasonably good correlation exists between TiN etch rate measured in the actual product environment, and statistical models based on laboratory-scale experiments.

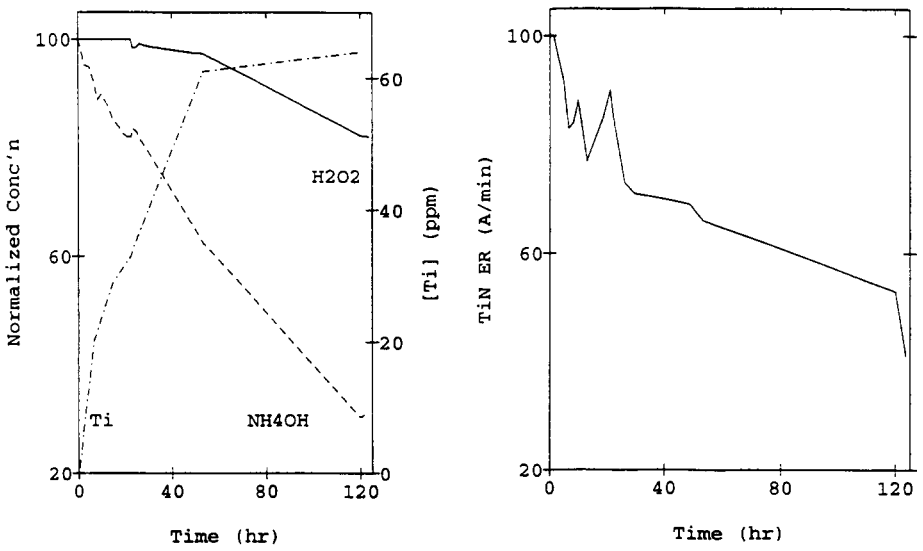

Figure 3. Changes in H_2O_2, NH_4OH, and Ti concentrations as well as TiN etch rate as a function of time in a production etch bath.

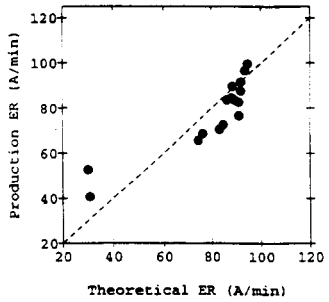

Figure 4. Correlation between actual (based on data from the production environment) and theoretical (based on the statistical model) TiN etch rate.

REFERENCES

1. Schmidt, H. M. Meuris, P. Mertens, A. Rotondaro, M. Heyns, T. Hurd and Z. Hatcher, *Physico chemical aspects of H_2O_2 based silicon wafer cleaning solutions,* Ultra Clean Processing of Silicon Surfaces, Brugge, Belgium (1994).
2. Sugihara, Y., S. Shimokawa and Y. Oshida, *Influence of metallic impurities on SC-1 cleaning,* Semiconductor Pure Water and Chemicals Conference, Santa Clara, CA (1993).

REACTION LIMITED CONTROLLED ETCH IN DILUTED HF AQUEOUS SOLUTION WITH HNO_3

G. Seo*, H. Kim*, S. Kang*, D. Kim*, K. Ryoo** and P.Hong***

Surface contamination, smoothness and native oxide free Si have been recognized for the top issues of ultraclean wafer technology. Reaction Limited Controlled Etch(RLCE) solution of $0.1HNO_3$: 1HF : $100H_2O$ ratio is able to remove Fe contamination to 2E10 atoms/cm^2. Because of very small concentration of HF, the rate of Si removal would be rate-dependent on the arrival of HF at the SiO_2 surface which contains the metallic contaminants and oxide complex formed by the reaction of HNO_3 and Si surface. AFM and XPS spectra show that both RLCE and diluted HF cleanings provide for the very identical Si surfaces.

I. INTRODUCTION

Surface contamination, smoothness and native oxide free Si have been recognized for the top issues of ultraclean wafer preparation technology. The technology is focused on reducing the major metallic contaminant of Fe and surface microroughness, and being free from native oxide after wet cleaning. The importance of wet cleaning technology for metallic contamination has to be still considered to improve the semiconductor manufacturing yield and reliability of the next generation devices. For wet cleaning evaluation, Reaction Limited Controlled Etch(RLCE) method based on HNO_3 : HF : H_2O was investigated intensively. This method differ from the conventional cleaning process which is simply removing the contaminants on Si surface. Because of very small concentration of HF in diluted HF/HNO_3 solution, the rate of Si removal would be rate-dependent on the arrival of HF at the SiO_2 surface which contains the metallic contaminants and oxide complex formed by the reaction of HNO_3 and Si surface[1-2].

II. EXPERIMENTAL

Silicon wafers of 5 inch, p-type, (100) were used for cleaning. All the

* Researcher, Semiconductor Research Team, Research Institute of Industrial Science & Technology P.O. Box 135. POHANG, 790-600, KOREA
** General Manager, Semiconductor Research Team, Research Institute of Industrial Science & Technology
*** Team Leader, Application Engineering, POSCO HULS Co., Chonan, Korea

wafers were treated by sulfuric solution at 120℃ for 15 minutes. And then, the wafers were contaminated by contacting wafer surfaces to 0.6% hydrochloric solution containing Fe impurities for 2 minutes[3]. Finally, the wafers were treated with RLCE solutions. The wafers were measured with Total Reflection X-Ray Fluorescent Analyzer(TRXFA) at 30kV, 400mA and 0.1 degree of reflection for 500sec for Fe contamination variations, with Atomic Force Microscope(AFM) for smoothness variations, with X-ray Photoelectron spectroscopy(XPS) for native oxide existence.

Ⅲ. RESULTS AND DISCUSSION

All starting wafers treated with the sulfuric solution are contaminated with Fe, followed by TRXFA measurements before cleaning to obtain contamination baselines. It takes 2 minutes for Fe contamination to be saturated as shown in Fig.1. Hence 2 minutes is determined for Fe contamination. Then wafers cleaned using RLCE solutions are measured by TRXFA again to observe the cleaning effects as shown in Fig. 2. RLCE solution treatment with the condition of $0.1HNO_3$: 1HF : $100H_2O$ during 3 minutes seems to be able to remove Fe contamination to 2E10 atoms/cm^2. There is no difference observed for the cleaning time dependence on removing Fe contamination and hence 3 minutes is determined for convenience.

The AFM images have revealed that the smoothness of the Si surface is not deteriorated with HF concentration changes. Especially the surfaces of RLCE cleaned wafers show very low surface microroughness, and therefore the RLCE with HNO_3 is proven to be one of the effective ways for Si surface smoothness control. XPS spectra shown in Fig. 3 reveals only Si_{2p} peak for both RLCE and diluted HF cleaned wafers, which is quite distinguishable from the bare wafers with SiO_2 peak. Hence it can be concluded that RLCE provides for the bare surface without native oxide for a while.

Ⅳ. CONCLUSIONS

RLCE solution of $0.1HNO_3$: 1HF : $100H_2O$ during 3 minutes is able to remove Fe contamination to 2E10 atoms/cm^2, and there is no difference for the cleaning time dependence on removing Fe contamination. The surface image of RLCE cleaned wafers shows very low surface microroughness, and therefore RLCE with HNO_3 is proven to one of the effective ways for Si surface smoothness control. XPS spectra of both RLCE and diluted HF

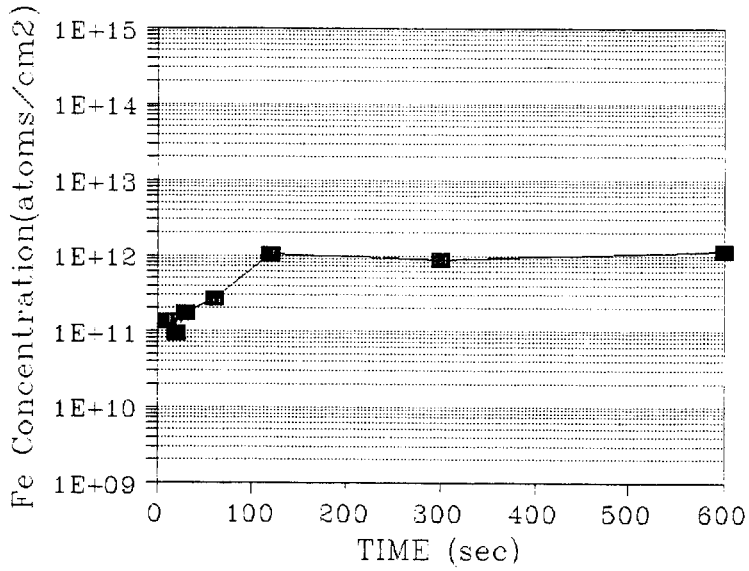

Figure 1. Fe concentration changes according to contamination times

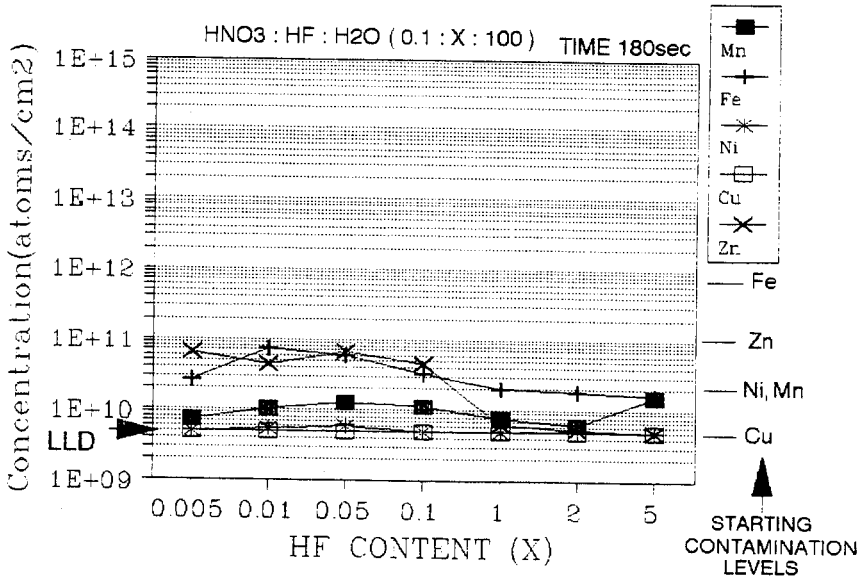

Figure 2. Fe concentration changes according to the HF ratios of RLCE solutions

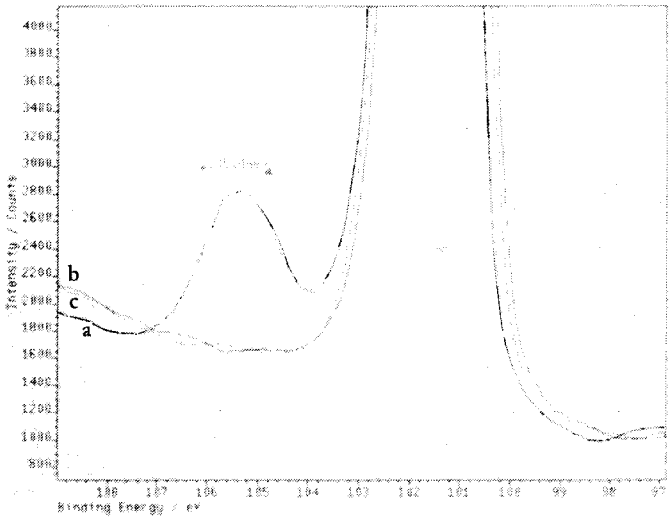

Figure 3. XPS spectra of Bare wafer (a), diluted HF (b) and RLCE (c) treated wafers

treated wafers show no native oxide formation on Si surface.

Changing HNO_3 concentrations from 0.1 to 5 maintains Fe concentration levels of 1-2E10 atoms/cm^2. Namely, the wide range changes of HNO_3 concentrations from $0.1HNO_3$ do not seem to affect cleaning behaviors. Hence it is recommended that wafer makers may use $5HNO_3$: 1HF : $100H_2O$ ratio because of its fast reactivity degradation due to heavy contamination from wafering processes. While device makers may use $0.1HNO_3$: 1HF : $100H_2O$ ratio because of relatively clean environment in device processes.

V. REFERENCES

1. D.L.Klein and D.J.D'Stefan, J. Electrochem. Soc., Vol.109, No. 1, p37-42 (1962)
2. Ritsuo Takizawa, Toshiro Nakanishi, J. J. Appl., Phys., Vol.27, No. 11, pL2210-L2212 (1988)
3. B.Hanckl and K.J.Range, J. Electrochem. Soc., Vol.139, No.5, p1495-1498 (1992)

THE CONTRASTIVE BEHAVIOR OF COP / FP AND SEP DEFECTS IN CZ SILICON CRYSTALS

Takao Abe*

1. INTRODUCTION

Since current ULSI device quality CZ crystals are grown with tightly controlled oxygen concentration, carbon under the limit of detection (0.05 ppma) and extremely low concentration of heavy metals [1] ($<10^{10}$ / cm^3), it has been believed that any as grown defects such as, of course, dislocations, oxygen precipitates and other microdefects have been eliminated. Recently, Tachimori *et al.* [2] reported that in the center area of CZ crystals grown with high growth rate thin gate oxide integrities (GOI) are degraded. Successively, Ryuta *et al.* and Yamagishi *et al.* found the so - called COP (crystal originated particle) [3] revealed by NH_4OH / H_2O_2 (a part of so - called RCA cleaning) detected by a particle counter and FP (flow pattern) [4] defects by Secco etching for 30 min. in the area corresponding to GOI degradation as shown in Fig. 1 of a micrograph respectively. COP and FP defects are regarded to have the same origin associated with secondary defects due to point defects. Takeno *et al.* found evidence by TEM observation that secondary defects [5] consist of clusters of interstitial type dislocation loops in CZ crystals.

The purpose of this paper is to show the relationships between the COP and FP defects both recently found, the behavior of FP defects and SEP defects (Secco Etch Pit) which do not accompany the flow pattern as shown in Fig. 1, the GOI degradations by these defects and to discuss the prevention of these defects during crystal growth.

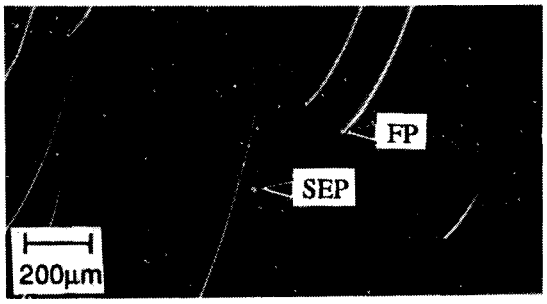

Figure 1. Optical micrograph of the FP and SEP defects

* Isobe, Annaka, Gunma 379-01, Shin-Etsu Handotai

2. *IN - SITU* ANNEALING

2.1. FP and SEP defects

By rapidly lowering the growth rate temporarily, the variations of the actual distributions of point defects can be observed as *in - situ* annealing. In fact, it is reported that not only the prior but also the post grown area are affected concerning secondary defect formation [6].

Figure 2 (a) is an x - ray topograph of AOP (anomalous oxygen precipitation) annealed (1000 C, 16hrs in oxygen) crystals which are grown with the high growth rate of 1.8 mm / min and then a low growth rate of 0.2 mm / min. Generally there is no contrast in the case of as grown crystals but after AOP annealing the growth interface, in other word a growth striation induced by the oxygen precipitation is observed as the white contrast shown in the schematic of Fig. 2 (b). Due to the lower growth rate for 30 minutes, the shape of the striation is changing from concave to convex, and then after taking the high growth rate again, it is requires the 10 ~ 15 minutes to obtain the concave striation. The occurrence of remelting is seen in the periphery at the initial interface of the low growth rate L region. The AOP region distributes as sidewise v shape which is symmetrical to the L region.

Figure 2 (c) and (d) are the distribution of the FP and SEP defects measured along the growth direction on center and 20 mm from edge lines in Fig. 2 (a). The density of the FP defects has its lowest value at the L region and distributes symmetrically to both the prior and post grown area of the L region. On the other hand, the density of SEP defects is the same as that of FP defects in the high growth rate area but largely increases in both prior and post grown area.

2.2. COP

The COP defects are only detected by the so - called particle counter because they are too small and rare to observe by an optical microscope and an electron microscope, respectively. Figure 2 (e) shows the COP map measured by the LS - 6000 (Hitachi) of the as grown crystal. The COP is revealed by NH_4OH / H_2O_2 solution for 20 minutes. The particle size counted is in the range of 0.1μm ~ 0.13μm.

The density of the COP is very low in the L region, the sidewise v region and the periphery of the crystal. On the other hand, as described in the previous section, the density of the SEP defects at both the sides of the L region is very high as seen in Fig. 2 (c) and (d). It is concluded that the COP defects probably are related to the FP defects but not the SEP defects.

3. GOI AND GROWTH CONDITIONS

Figure 3 are the breakdown voltage maps of the gate oxides fabricated on the longitudinal cut as grown wafers corresponding to Fig. 2. The gate oxide

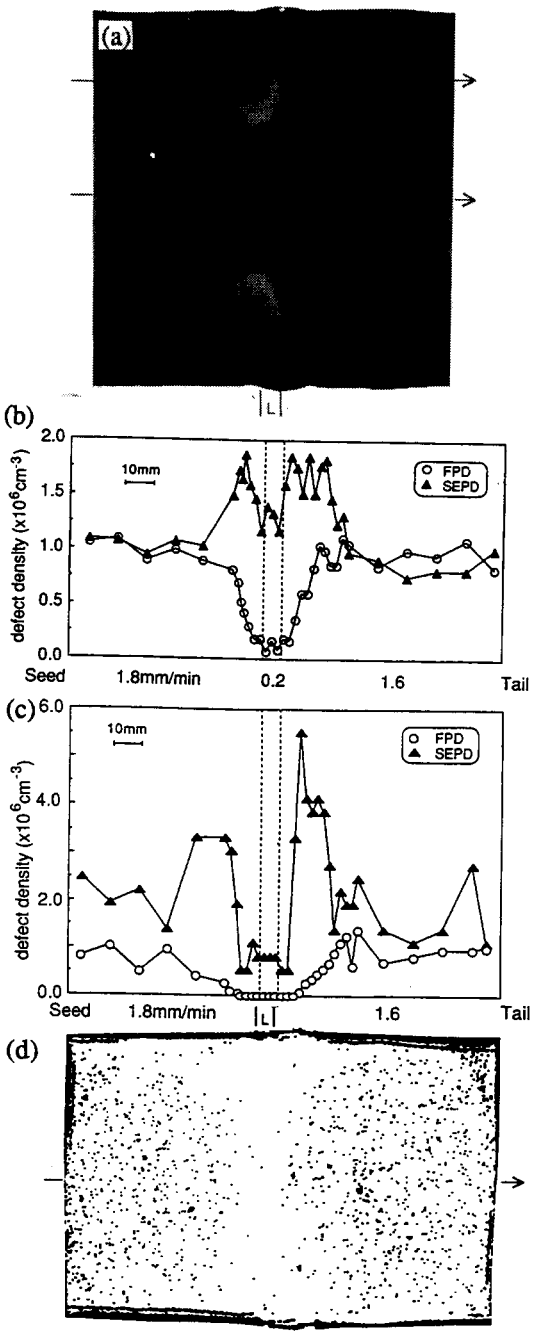

Figure 2. x - ray topograph of the *in - situ* annealed crystal (a), FP and SEP defects of the as grown crystal along center line (b) and 20 mm from edge (c). COP distribution of the as grown surface measured by LS - 6000 (d).

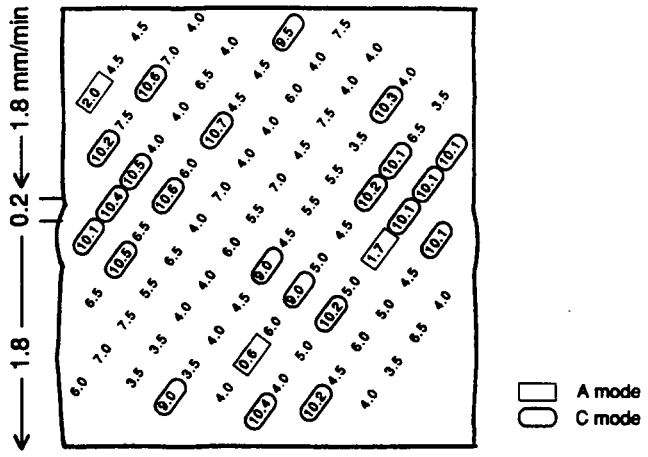

Figure 3. Oxide breakdown map the in - situ annealed crystal of Fig. 2.

thickness grown with a dry oxygen ambient is 300 A. The polysilicon gate voltage is negative voltage and the gate area is 8×10^{-2} cm^2. The definition of the breakdown mode, i. e., A mode, B mode and C mode is < 3 MV / cm, 3 ~ 8 MV / cm and> 8 MV / cm, respectively.

The SEP defect region are covered with the C mode in Fig. 3. This indicates that the SEP defects do not severely affect the GOI degradation. From the Fig. 3, the gate oxides with the C mode congregate in the both sides of the L region sidewise v shape and also exist in the L region where there are SEP defects in a high density.

4. DISCUSSIONS

From the correlation experiment between the NH_4OH / H_2O_2 etching and the Secco etching, it is confirmed that the COP distribution coincides with that of the FP defects, but not that of the SEP defects on the (100) wafer cut parallel to the growth direction using the *in situ* annealed crystal. Based on optical microscope observations, both the etch pits of the FP and SEP defects have comparable sizes and round shape delineated by Secco etching. So it is expected that the NH_4OH / H_2O_2 solution only reacts with the FP defects to reveal the COP.

The features of the FP defects are as follows : 1. mainly distributed in the center of crystal 2. dependence on growth rate 3. annihilation by in situ annealing 4. associated with GOI degradation [4] 5. growth relatively low temperature [7] 6. close relation to the FP defects which are induced by vacancies in FZ crystals [7]. On the other hand, the features of the SEP defects are as follows : 1. main distribution at the periphery 2. density depending on high thermal gradient 3. growth during cooling 4. no relationship with GOI 5. due to the similarity with the symmetric distribution of R-OSF, generation by excess interstitial silicon [6].

Moreover, the features of both types of defects are clarified by detaching experiments, i. e., the growth of these defects do not occur in the AOP region. Memory effects associated with lowering the growth rate are observed in the case of *in situ* annealing. The bulk life time is affected by an extremely high density of SEP defects.

Our result represents a new confirmation that the degradation of the GOI is not influenced by the SEP defects but by the FP defects. This fact agrees with the degradation of GOI by the D defects but not the A defects in FZ crystals. In addition to this, it has been reported by many authors that both the COP and FP defects degrade the GOI in CZ crystals.

From the above discussions the FP defects may be the aggregates of vacancies generated at equilibrium concentration in the vicinity of the growth interface. On the other hand, the SEP defects probably consist of oxides which are made by excess interstitial silicon atoms reacted with excess oxygen atoms and grow during the cooling process. It is known that the R-OSF nuclei are made by oxides [9]. A similar process on the nucleation of both R-OSF and SEP defects is to be considered based on the two facts : one is the symmetrical and enhanced distributions to the low growth rate region and another is the oxide as a nucleation which may induces interstitial type dislocation loops. During the growth with a low growth rate, an increase of the thermal gradient leads to an increase of excess interstitial silicon [10]. The origins of the SEP defects and FP defects in CZ crystals correspond to the D defects and the A defects in FZ crystals, as classified in Table 1.

Table 1. Proposed classification of as grown and annealed defects.

FZ	CZ		Point Defect Species
A defects (striation)	SEP defects	R - OSF (striation)	silicon interstitial
D defects (homogeneous)	COP / FP defects	AOP (region)	vacancy

In order to suppress FP defect generation, it is known that low growth rate is effective. We propose not only low growth rate but also small thermal gradient near the growth interface to keep up the recombination with excess interstitial silicon and the up - hill diffusion to the growth interface. Especially, it is important that the generation of excess interstitial silicon is controlled by selecting the thermal gradient near the growth interface.

5. CONCLUSION

FP and SEP defects are generated in CZ crystals. COP defects are identified as to be the same as FP defects based on the agreement of their respective

distributions. The FP defects may probably be attributed to the aggregation of excess vacancies procreated at melting point. On the contrary, the SEP defects are related to the oxides which are generated by the reaction between excess interstitial silicon and oxygen. From the GOI tests of as grown crystals, the GOI degradation is not depended on the SEP defects but the FP defects. In order to prevent the FP defects, a low growth rate and a high thermal gradient in the relatively low temperature range (<1300 C) are essential. On the other hand, the SEP defects can be minimized by the minimization of the thermal gradient near the growth interface.

ACKNOWLEDGEMENTS

The author thanks Professor U. Gosele, Duke University for his critical discussions and gratefully acknowledge Mr. A. Tamura (SEH Takefu Plant) for crystal growth.

REFERENCES

1. T. Abe, T. Itoh, Y. Hayamizu, K. Sunagawa, S. Yokota and H. Yamagishi, *Defect Control in Semiconductors* edited by K. Sumino (North Holland, Yokohama 1989) p. 297.
2. K. Tachimori, T. Sakon and T. Kaneko, 7th Symposium of Crystal Engineering, Jpn. Soc. Appl. Phys., Catalog No. AP 902217 p. 27 (1990) in Japanese.
3. J. Ryuta, E. Morita, T. Tanaka and Y. Shimanuki, Jpn. J. Appl. Phys 29 (1990) L 1947.
4. H. Yamagishi, I. Fusegawa, N. Fujimaki and M. Katayama, Semicond. Sci. Technol. 7 (1992) A 135.
5. H. Takeno, S. Ushio and T. Takenaka, *Defect Engineering in Semiconductor Growth, Processing and Device Technology*, eds. S. Ashok *et al.* MRS Symp. Proc. Vol. 262 (1962) p. 51.
6. H. Harada, T. Abe and J. Chikawa, *Semiconductor Silicon 1986* eds. H. R. Huff *et al.* (Electrochem. Soc. Pennington, 1986) p. 76.
7. T. Abe and M. Kimura, *Semiconductor Silicon 1990* eds. H. R. Huff *et al.* (Electrochem. Soc. Pennington, 1990) p. 105.
8. T. Abe, H. Harada, N. Ozawa and K. Adomi, *Oxygen, carbon, Hydrogen and Nitrogen in Crystalline Silicon*, eds. J. C. Mikkelsen *et al.* MRS Symp. Proc. 59 (1985) p. 537.
9. S. Shinoyama, M. Hasebe and T. Yamauchi, Oyo Buturi (J. Appl. Phys in Japanese) 60 (1991) 766.
10. T. Abe, H. Harada and J. Chikawa, Physica 116B (1989) 139.

Roughening during wet processing studied by AFM of stepped surfaces

S. Verhaverbeke[1)], R. Messoussi[1)2)] and T. Ohmi[1)]

[1)]Department of Electronic Engineering, Faculty of Engineering, Tohoku University, Aza-Aoba, Aramaki, Aoba-ku, Sendai 980, Japan
[2)]Research Institute of Electrical Communication, Tohoku University, Katahira 2-1-1, Aoba-ku, Sendai 980, Japan

1. INTRODUCTION

In manufacturing processes of submicrometer and deep-submicrometer ULSI's, the surface microstructure and surface cleanliness of the Si substrates are becoming crucial for device performance and reliability. Device characteristics such as gate oxide dielectric breakdown can be influenced substantially by the underlying Si substrate. In particular. the use of Cz versus Epi wafers can change the properties of the dielectric breakdown substantially. Recently, it has been shown that H_2 annealing of Cz wafers can improve the gate oxide breakdown properties of SiO_2 films grown on these annealed surfaces. In this work, at first the surface topography of Cz and epi-wafers was investigated. Then, the effect of H_2 annealing of Cz surfaces was studied. Finally, these surfaces are used to study the effect of wet chemical cleaning on the surface topography.

2. RESULTS AND DISCUSSION

2.1 Chemical solutions

The roughening during wet chemical cleaning can be characterized by the Rms roughness of the surface. However, this has some severe limitations for characterizing very smooth Si surfaces. At first, the Rms value only characterizes the roughness in the z-direction. In order to characterize the lateral scale roughness, the power spectrum can be used. However, in many cases this method is not sensitive enough to investigate the roughening during wet chemical cleaning. Secondly, the Rms roughness value was found to depend on the cantilever which is being used when measuring very smooth surfaces. This introduces systematic errors. Recently, Y. Yanase et al. reported that the stepped surface was formed after H_2 annealing at temperatures of 1100 °C [1]. The surface after epitaxial Si deposition looks similar to the surface after H_2 annealing. Therefore, we now can use the stepped surfaces to investigate the roughening during wet chemical cleaning merely by monitoring the attack of the steps and terraces during wet chemical cleaning. We used epi-wafer surfaces and H_2 annealed Cz wafers, which both have the steps and terraces structures, to study the effect fo H_2SO_4/H_2O_2 (SPM), dilute HF, $NH_4OH/H_2O_2/H_2O$ (APM) and Ozonized Ultrapure Water (Ozonized UPW) on the Si wafer surface. The APM solution was optimized to minimize the roughening [2]. The roughening can now be characterized as the amount in which the surface steps and terraces are attacked or dissapear by treatment in the chemical solutions.
In order to investigate the roughening due to SPM and APM, the SPM and APM were followed by HF to remove the grown chemical oxide and to measure the roughness of the Si substrate. This was repeated several times for Cz wafers with and without H_2 annealing. The result for the SPM is shown in fig. 1 for the Rms roughness. On the AFM image, we can not detect any attack at the step edge or on top of the terrace. Thus, we can conclude that there is no surface roughening even after 5 cycles. This shows that there is no surface roughening during the SPM treatment and during the HF etching of the chemical oxide and the formation of the hydrogen passivation. The same procedure was followed for the APM cleaning. The results are shown in fig. 2 for the Rms roughness. In this case, we could clearly see that the steps gradually

disappear and that the terraces become attacked by the cleaning solution. After 10 cycles, there is no more difference between the H_2 annealed Cz wafers and the non-annealed Cz wafers.
Wet chemical solutions can be divided into 2 groups. The first group are those cleaning solutions which dissolve or decompose only contaminations on the silicon surface and the second group are those cleaning solutions which etch silicon wafers. APM and HF are solutions which etch, H_2SO_4/H_2O_2 and O_3/H_2O are solutions which grow an oxide without etching. We have shown that those solutions which do not etch, do not increase the roughness, since they preserve the steps and terraces. From the solutions which etch, only the APM solution destroys the steps and terraces. The HF solution preserves the steps and terraces, since the etch rate of Si is extremely slow [3].

2.2 Hot ultrapure water

In the conventional RCA cleaning cycle, hot ultrapure water rinsing has been conducted after APM cleaning to remove residual NH_4OH which adheres on the plastic wafer carriers. More recently, hot water rinsing has been used even at the end of the cleaning cylce to aid in the drying of the wafers. Hot water has certainly a higher cleaning capability. One of the problems to be solved today in wet chemical cleaning technology is the occurence of watermarks. The origin of watermarks is not always clear, but insufficient rinsing of chemicals and contamination is certainly leading to watermarks. As a result, adequate rinsing is very important. The use of hot ultrapure water for rinsing will certainly increase the rinsing efficiency and therefore, it will probably also reduce the watermarks and other residues left on the surface. Also, for reducing the carry-over of chemicals when using cassettes, hot water rinsing of cassettes and wafers is necessary. Finally, for single wafer processing, such as spin cleaning [4], fast processing is very important. The use of hot ultrapure water is very efficient in reducing the rinsing time. We have investigated the effect of hot ultrapure water on hydrogen passivted silicon surfaces, i.e. after HF etching. Studies by Watanabe et al. [5] show that Si (111) facets can be produced by hot water immersion. This, in turn, implies that hot water etches silicon with an anisotropic etch rate. Recently, the etch rate of hot water on Si (100) was measured [6]. In this work, we investigated the effect of hot water exposure of hydrogen passivated surfaces as a function of hot water immersion time. We used ultrapure water with a dissolved oxygen concentration of 5 ppm, since it was reported that the etching of Si (100) increased with higher dissolved oxygen concentration [6] and the temperature was kept at 80 °C. The effect of hot ultrapure water exposure with a dissolved oxygen content of 5 ppm i shown in fig. 3 in top view and in solid model. After 1 min , the steps and terraces are still vaguely visible, but already after 2 min, the steps completely dissappear. After 10 min, the roughness is increased quite dramatically.

2.3 Oxide protection

In order to avoid the roughening in hot ultrapure water, we investigated the use of a protecting oxide. At first, the effect of hot ultrapure water as a function of time on top of an SPM chemically grown oxide was investigated. Even after 6 hours of exposure, the steps and terraces are still clearly visible and there is no detectable roughening. Then, we investigated the use of ozonized ultrapure water. The use of ozonized ultrapure water is very attractive, since it can be performed in the rinse tank itself, no separate bath is required and there is no chemical waste treatment necessary. The ozonized ultrapure water is electrolyzed by using a lead oxide catalyst and a solid electrolyte to generate clean O_3 gas. This gas is fed into a gas permeation membrane (PTFE hollow fiber membrane) to get the O_3 filtrated and to get the O_3 dissolved into the ultrapure water. The advantage of this technique is that this ozonized ultrapure water features almost the same impurity concentrations as ultrapure water. Moreover, with this technique O_3 gas can be produced at high pressures leading to high ozone concentration levels in O_3/H_2O. We used 10 ppm of dissolved ozone which is close to the solubility limit. In the case when ozone is generated by the silent discharge technique, a high concentration of ozone in the ultrapure water is difficult to obtain an it is difficult to avoid metallic contamination from the electrodes. We investigated oxidation times in the ozonized ultrapure water ranging from 1 min up to 20 min. It was reported earlier that 20 min of immersion are necessary to grow a thick chemical oxide of 1.2 nm in ozonized ultrapure water at roomtemperature [7]. Since ozone

selfdecomposition occurs very rapidly at higher temperatures, only room temperature processing can be used for O_3/H_2O processing. However, T. Ohmi et al. [7] also reported that initially the oxidation rate in O_3/H_2O is very high and that in less than 1 min already an oxide of about 0.6 nm is grown. After growing oxides in O_3/H_2O for times ranging from 1 minute to 20 minutes, these surfaces were exposed to hot ultrapure water at 80 °C and with a dissolved oxygen content of 5 ppm. Times of exposure ranged from 1 minute up to 2 hours. Even when the surface was only protected with an oxide grown in O_3/H_2O for only 1 mijnute, the surface was resistant to hot ultrapure water even for exposures of 2 hours : the steps and terraces are still present on the surface. No roughening has occured.

3. CONCLUSIONS

H_2 annealed Cz wafers were used to study the effect of wet chemical cleaning on these stepped surfaces. The H_2SO_4/H_2O_2, ozonized ultrapure water and HF cleaning do not attack the stepped surface. In a $NH_4OH/H_2O_2/H_2O$ solution, the stepped su rface is completely destroyed. Hot ultrapure water exposure, with 5 ppm of dissolved oxygen, of hydrogen passivated surfaces destroys the steps as well and leads to very high roughness levels. If the surface is passivated with an oxide no roughening occurs in hot ultrapure water. Finally, in order to protect the surface in hot ultrapure water, 1 min of ozonized ultrapure water treatment is sufficient.

REFERENCES

1. Y. Yanase, H. Horie, Y. Oka, M. Sano, S. Sumita and T. Shigematsu, Extended Abstracts ECS Fall Meeting, New Orleans, LA, October 10-15 1993, Vol. 93-2, Abstr. No. 296.
2. T. Ohmi, M. Miyasita, M. Itano, T. Imaoka and I. Kawanabe, IEEE Trans. El. Dev., Vol. 39, No. 3, march 1992, pp. 537-545.
3. S. Verhaverbeke, M. Meuris, P. Mertens, H. Schmidt and M. Heyns, in *Proceedings of third International Symposium on Cleaning Technology in Semiconductor Device Manufacturing* (ECS, Pennington, NJ, 1994), **94-7**, 176 (1994).
4. F. Kunimoto, F.W. Kern, Jr. and T. Ohmi, Proceedings of IES 38th Annual Technical Meeting, May 1992.
5. S. Watanabe, N. Nakayama and T. Ito, Appl. Phys. Lett. 59, 1458 (1991).
6. J.H. Eisenberg, S.F. Shive, F. Stevie, G.S. Higashi, T. Boone, K. Hanson, J.B. Sapjeta, G.N. Dibello and K.L. Fulford, in Surface Chemical Cleaning and Passivation for Semiconductor Processing (MRS, Pittsburgh, Pennsylvania, 1993), MRS Symp. Proc. Vol. 315, p. 485, 1993.
7. T. Ohmi, T. Isagawa, M. Kogure and T. Imaoka, J. Electrochem. Soc. Vol 140, No. 3, March 1993, p. 804.

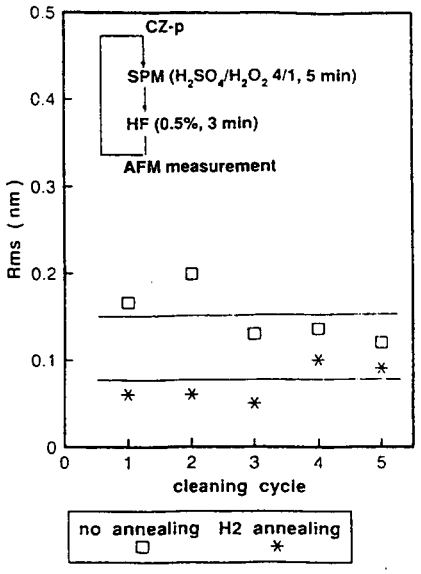

Figure 1.Rms roughness as after SPM + HF cycles for H_2 annealed and non-annealed Cz wafers.

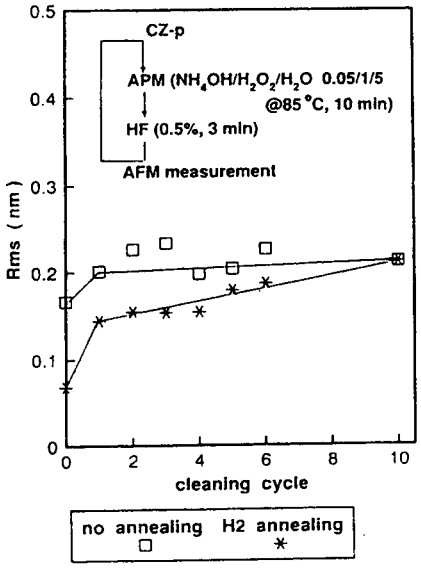

Figure 2.Rms roughness after APM +HF cycles.

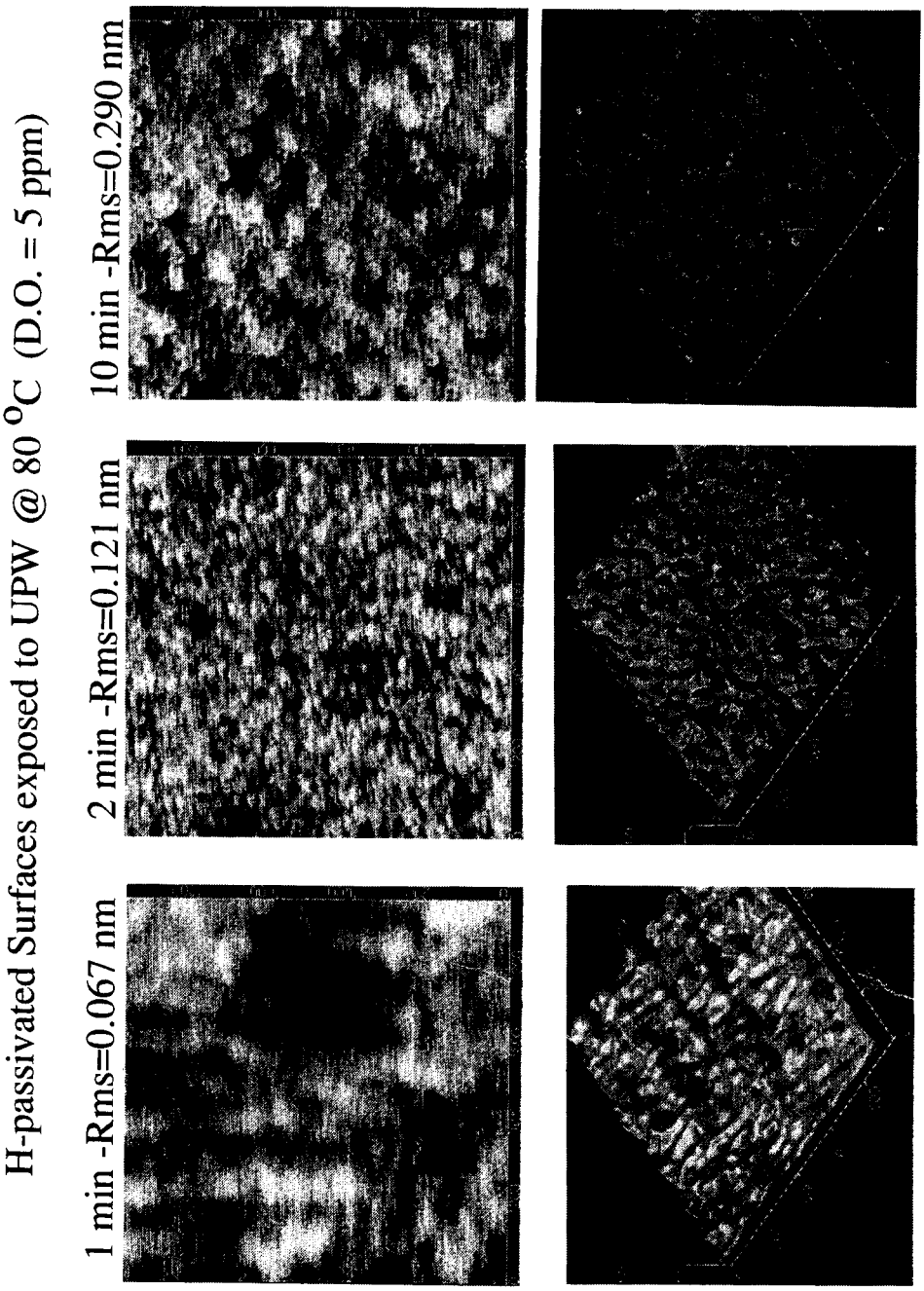

Figure 3. Top view and solid model of an epi-wafer surface as a function of hot ultrapure water exposure (80 °C).

PITTING ON WAFERS BY AG TRACE IN DILUTED HF

D.Lévy and P.Patruno,
Centre Commun CNET/SGS-Thomson, 850 rue Jean Monnet, BP16 F38921 Crolles Cedex
L.Mouche and F.Tardif
LETI, MEL, CENG, 17 rue des Martyrs, F38054

Abstract.

Si attack has been observed on the P^+ doped zones of 200 mm manufacturing lots after immersion of the Si wafers in ULSI grade 2.5% HF . Sutface and chemicals analysis have shown that the "pitting" effect came from a contaminated HF batch. This contamination was found to be desastrous for submicron CMOS technology, but with no impact on 1.2 micron BICMOS technology. The presence of 12 ppb Ag found in the suspicious HF lot is suspected to be the only cause of the contamination of the wafers. Only 0.06 ppb was found in a non-contaminated HF batch . The contamination of Ag found in the bottled ULSI grade HF came from insufficient rinse of the filling line at the chemicals supplier plant. The attack of Si wafers by Ag can be easily explained by elementary electrochemistry : for all metals which have positive oxido-reduction potential with respect to the standard hydrogen electrode i.e only the noble metals, the metallic ions in solution react with Si to form SiF_6^{2-} (which causes pitting) and to give metal deposition on top of the wafers.

1. EXPERIMENTAL

1.1. Problem description

Anormalous lighting points found on manufacturing lots were first identified as an attack of the Si itself by using optical microscope in the dark field and SEM measurement. The "pitting"effect was then reproduced on bare Si wafers using the same chemicals, same process conditions and quantified by the haze measurement on a standard particle measurement tool (Tencor 5500). On pitted wafers, haze values such as 50ppm and 99% surface were found, whereas typical values on non contaminated wafer are 2-6 ppm, 0%. After different trials where we have changed the Si wafers, the bench and its environment, the chemical delivery mode, the process time, the chemical, we have clearly identified a 2.5% HF batch as the only cause of the pitting.

1.2. Electrical results

The impact of the pitting on manufacturing lots processed in the new 200 mm Crolles plant is summarized in Table 1.The electrical results of this contamination were found to degrade the gate oxide integrity for submicron CMOS technologies but had no impact on 1.2 micron BICMOS technology. On CMOS 0.8 micron technology, 0% yield was found on seven consecutive lots which have been

manufactured using the incriminated HF batch.

Table 1 : Impact of the pitting on devices characteristics

	Technology		
	Bicmos	Cmos	Cmos
Minimum feature size	1.2 mic	0.8 mic	0.5 mic
Gate oxide thickness	22 nm	17 nm	12 nm
Parametric results	Not tested	B.v.s (*)	B.v.s. (*)
Functional results	Good yield, no impact	0% yield	Not tested

B.v.s (*) : Breakdown voltage shift

1.3 Surface and chemicals analysis

TXRF spectrometry measurements were done on a reference Si wafer i.e which has received the same process but using HF coming from an other batch and on a "pitted" wafer. Anomalous peaks at 3.02 Kev and 3.19 Kev energy have been observed on the "pitted" wafer and attribuated either to Pd or Ag. The discrimination between the two metals was done with the help of intentionally contaminated wafer with Pd and Ag. The presence of Ag was confirmed by this test.

Quantitative measurements of Ag in the two 2.5% HF have been obtained using GFAAS technique. 0.06 ppb and 12 ppb were found respectively in the "clean" HF batch and "contaminated" one. This 12 ppb value in the suspicious 2.5 HF lot is out of specification which is 10 ppb. A factor of 200 in Ag level was found between the suspicious lot and the "good" lot.

1.4 Verification.

In order to confirm if the presence of 12 ppb of Ag in 2.5% HF can create pitting when Si wafers are immersed in it for a long time (45 minutes to one hour), Ag was intentionally added to 2.5% HF and an etch performed. Inspection on a visual microscope showed the presence of pitting on the wafer dipped in contaminated HF, whereas no defect was observed when the wafer is immersed in non polluted HF. This last experiment is the proof that the presence of Ag in 2.5% HF at a level of 11 ppb creates pitting on Si.

1.5 Ag contamination in HF at the chemicals supplier's plant

After discussions with the chemical supplier, the presence of Ag was admitted. Trace of silver has been found by the supplier's analysts due to an incomplete rinsing of the filling line : this particular filling line is not dedicated to this grade but common with an other grade where gazeous HF is cooled down in a cooler made from silver...This type of contamination is claimed by the chemicals supplier not to be possible when ULSI/SLSI grade HF is deliver in drums : a dedicated line for each grade is used when ULSI and SLSI grade HF is filled in drums, which is not the case for bottles.

2. DISCUSSION

In the literature, Kern et al [1] and Torcheux [2] have shown that if Si wafers are immersed in diluted HF where impurities (Ag, Cr, Cu, Fe, Ni, Zn) have been intentionally added at a level of between 0.1 ppm and 1 ppm, only Ag and Cu is deposited on the surface of the wafer. In these two publications, this result is explained using elementary electrochemistry.The equilibrium :
Oxyd.1 + Red.2 <--> Oxyd.2 + Red.1 is displaced to the right if the oxido-reduction potential of the couple 1 is greater than the couple number two. The metallic ions M^{n+} are reduced following the half-cell reaction : $M^{n+} + 4\ e^- \rightarrow M_o$
We have reported below the oxido-reduction potential [3] of most of the metallic impurities which can be found in the electronic industry.

$Au^+ + 1\ e^- \rightarrow Au^\circ$	$E_o = +1.68$ V
$Pt^{2+} + 2\ e^- \rightarrow Pt^\circ$	$E_o = +1.20$ V
$Ag^+ + 1\ e^- \rightarrow Ag^0$	$E_0 = +0.80$ V
$Cu^{2+} + 2\ e^- \rightarrow Cu^0$	$E_0 = +0.34$ V
$2H^+ + 1\ e^- \rightarrow H_2$ (g)	$E_0 = +0.00$ V
$Fe^{3+} + 3\ e^- \rightarrow Fe^\circ$	$E_o = -0.04$ V
$Ni^{2+} + 2\ e^- \rightarrow Ni^0$	$E_0 = -0.23$ V
$Fe^{2+} + 2\ e^- \rightarrow Fe^0$	$E_0 = -0.44$ V
$Cr^{2+} + 2\ e^- \rightarrow Cr^0$	$E_0 = -0.56$ V
$Cr^{3+} + 3\ e^- \rightarrow Cr^0$	$E_0 = -0.74$ V
$Zn^{2+} + 2\ e^- \rightarrow Zn^0$	$E_0 = -0.76$ V
$Mn^{2+} + 2\ e^- \rightarrow Mn_o$	$E_o = -1.03$ V

When exposed to HF, bare silicon is oxidized by the half-cell reaction :
$SiF_6^{2-} + 4\ e^- \rightarrow Si_o + 6\ F^-$ $E_o = -1.2$ V
This potential is very low. It means that for all the metals listed above, the reaction:
$Me^{n+} + Si <-> SiF_6^{2-} + Me^\circ$ will be displaced to the right.
However, Kern explains in his paper that the presence of hydrogen acts to keep the metals, whose oxidation half-cell potentials (the negative of the above list) are positive relative to hydrogen, in solution. For reference, the H_2 reduction half-cell is shown below :
$2H^+ + 1\ e^- \rightarrow H_2$ (g) $E_0 = +0.00$ V
It means that for all metals which have negative oxidation half-cell potentials, the following half- reactions have to be considered :
$2H^+ + 1\ e^- \rightarrow H_2$ (g) $E_0 = +0.00$ V
$M^{n+} + n e^- \rightarrow M^\circ$ $E_0 < 0.00$V
Consequently, the reaction which takes place is : $2\ H^+ + M^\circ \rightarrow M^{n+} + H_2$
The metallic impurities stay in solution. Si does not react with HF.
For all metals which have a positive oxidation half-cell potential, the following half-reactions have to be considered :
$M^{n+} + n e^- \rightarrow M^\circ$ $E_o > 0.00$V
$SiF_6^{2-} + 4\ e^- \rightarrow Si_o + 6\ F^-$ $E_o = -1.2$ V
Consequently, the reaction which takes place is : $Me^{n+} + Si \rightarrow SiF_6^{2-} + Me^\circ$
The metal is deposited on the Si wafer and the Si is attacked by HF to form SiF_6^{2-}.
The conclusion of Kern's paper is that only noble metals are susceptible to deposition when bare Si is exposed to HF solution (Ag^-, Au^+, Cu^-, Hg^{2+}, Pd^{2+}, Pt^{2+}, Re^{3+}, Te^{4+}).

The electrochemical corrosion mechanism described above fits qualitatively with the experiments performed by Kern [1] and Torcheux [2]. Quantitative results have been also reported in the two publications. The metallic deposited concentration observed by Kern is four orders of magnitude lower than predicted by the Nerst equation. This is because the Nerst equation predicts equilibrium concentration and does not take into account the effects of reaction kinetics or transport properties / diffusion. Torcheux has shown that the time of immersion of the wafers in contaminated HF and the concentration of the impurity play an active role in the quantity of Cu deposited on top of the Si. AFM investigations have shown that Cu is deposited in the form of small "islands" on very few "active sites" on the Si surface. These islands are found to be associated with holes in Si (pitting) and are interpreted as an electrochemical corrosion of the Si in a microcell formed by the Si as the anode and the noble metal as the cathode.
More extensive work is being performed in our laboratories using TXRF and AFM measurements in order to characterize more deeply the metal electro-deposition and Si etching mechanisms. The Fe^{3+}/Fe^{2+} (E_0 = 0.77V) and Fe^{2+}/Fe^{O} (E_0 = -045V) will be especially studied. Indeed, the preliminary results show that Fe contamination in HF could attack Si without deposition. These results have to be confirmed.

3. CONCLUSION

The presence of 12 ppb of Ag in diluted HF, a value only slightly higher than the specification, which is 10 ppb, is the source of the pitting observed on Si wafers observable with an optical microscope with the dark field and quatified by the haze using a conventional particle counter. This attack of Si by metallic ions is responsible for major device failure in submicron technologies : a drastically degraded gate oxide integrity explains 0% yield obtained on consecutive manufacturing lots processed before the problem was identified. It is interesting to note that the pitting has no influence on 1.2 micron Bicmos technology. An insufficient rinsing line of the 2.5 litres bottle filling line at the chemicals supplier plant was the cause of the Ag contamination.The silicon attack by Ag can be explained using conventional electrochemistry concepts.From a practical point of view, this problem has driven us to introduce an incoming test which consists of immerging Si wafers in HF followed by a rinse and dry after each change of HF batch and qualify and other source of HF in bottle.
The next step is to determine the specification limit of Ag in diluted HF. For this purpose, known values of Ag in HF will be prepared. The pitting will be characterized using AFM (Atomic Force Microscopy) technique correlated with haze measurement with Tencor 6200 or equivalent after dipping the wafers in contaminated HF.

This work was supported by JESSI T15, WP5.

REFERENCES :
1. F.W.Kern et al., 37th IES meeting, San Diego, CA, May 1991
2. L.Torcheux, Ph.D thesis, to be published.
3. Handbook of chemistry and physics, 63rd edition

AFM CHARACTERIZATION OF THERMAL OXIDES FORMED ON ATOMICALLY FLAT Si(111) SURFACES

M. Fukuda, C.H. Bjorkman*, T. Yamazaki, S. Miyazaki, M. Hirose

Department of Electrical Engineering, *Research Center for Integrated Systems,
Hiroshima University, Higashi-Hiroshima 724, Japan

Changes in the surface morphology of flat H-terminated Si(111) surfaces during oxidation and subsequent chemical etching have been investigated using Atomic Force Microscopy (AFM). It is found that the morphologies of the SiO_2 surface and at the SiO_2/Si interface are essentially similar to those of the initial Si surface. Also, it is shown that the thermal oxide is uniformly etched by dilute HF and the initial surface morphology is preserved at each step of etching.

1. INTRODUCTION

Atomic scale control and characterization of the Si surface microroughness and the SiO_2 thickness fluctuation are crucial for the continued scale down of MOS devices. The structure of the SiO_2/Si interface has so far been investigated by XPS [1,2] and FT-IR [3,4]. AFM (Atomic Force Microscopy) is a powerful tool for the investigation of ultra-thin oxide surfaces as well as Si surfaces obtained by stripping off the oxide. In order to get better information about oxide surfaces through AFM measurements, well defined surfaces which show atomic steps and terraces should be used as initial surfaces. In fact, AFM images of UHV-cleaned Si surfaces and oxidized surfaces have been compared and the preservation of the initial atomic step structure on the oxide surface has been demonstrated [5]. Since dilute HF or buffered-HF treatment is used before the thermal oxidation of Si, we have in this paper systematically studied the surface morphology changes before and after thermal oxidation of chemically cleaned, H-terminated Si surfaces by AFM.

2. EXPERIMENTAL

The wafers used in this study were cz, p-type Si(111) with a resistivity of about $10\,\Omega \cdot$ cm and a misorientation angle of 0.1° or less. Since control of the misorientation angle within 0.1° is very difficult, we have in this study chosen wafers exhibiting wide terraces and no corrugation. After RCA cleaning followed by 4.5%HF dipping, the wafers were treated in a 40%NH_4F solution for 10 min at room temperature in order to obtain atomically flat surfaces. This initial surface was oxidized at 1000°C in a 2%O_2 + N_2 gas mixture. Changes in surface morphologies before and after etching the oxide layer in 4.5%HF or 0.5%HF were investigated by AFM. The AFM employed in this study was a SPA300/SPI3700 from Seiko Instruments Inc. A force of less than $1x10^{-9}$ N was applied to the Au-coated silicon nitride tip.

3. RESULTS AND DISCUSSION

Si is anisotropically etched in solutions containing OH^- ions, such as KOH or NH_4F or pure water, in which atomically flat Si(111) surfaces spontaneously emerge because of the slowest etch rate in the <111> direction. Especially a 40%NH_4F (pH=7~8) solution makes the Si(111) surface atomically flat with wide terraces and ideal biatomic steps with a height of 0.31 nm. An AFM image and a model structure of this initial Si(111) surface are illustrated in Fig.1. The step edge configuration is composed of triangular etch pits with a depth of a biatomic layer. Three straight edges of triangular etch pits parallel to the $<\bar{1}10>$, $<0\bar{1}1>$, and $<10\bar{1}>$ directions are observed, reflecting the threefold symmetry of the (111) planes. The maximum triangular etch pit size depends on the solution because the difference of etching rate between <111> and the other directions limit the size. Changes in the misorientation angle influence the terrace width. Also, a change in the misorientation direction influences the step edge configuration from straight to zigzagged as shown in Fig.1(b). When the terrace is wider than the maximum etch pit size, we can observe triangular islands and triangular pits.

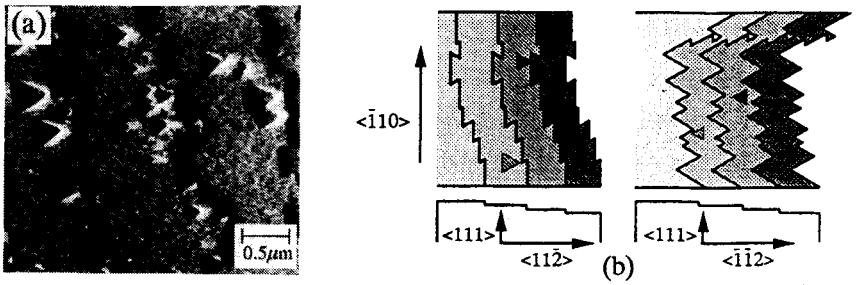

Figure 1. AFM image of an atomically flat Si(111) surface (a) and a model structure of Si(111) surface with biatomic steps (b).

Figure 2 represents AFM images of a Si(111) surface covered with a 2nm thick thermal oxide (a) and that after the removal of the oxide in 4.5%HF (b). The step structure is observable in both of the images although they are somewhat faded compared to the initial surface (Fig.1(a)). Therefore, the initial Si surface morphology is well preserved not only on the thin SiO_2 surface but also at the SiO_2/Si interface. This implies that the thermal oxidation basically proceeds through a layer-by-layer mechanism [2,6] and that the thermal oxide has excellent thickness uniformity over a device scale range.

Figure 3(a) represents the AFM image of a Si(111) surface covered with a 4nm thick thermal oxide. The initial atomic step structure of the surface is still clearly observable. The step structure on the SiO_2 surface is preserved even after etching 1.5nm (Fig.3(b)) and 3nm (Fig.3(c)) of the oxide. The oxide layer thickness was determined by ATR signal intensity of the Si-O-Si stretching vibration at $1080cm^{-1}$ [4]. This result indicates that dilute HF etching of the thermal oxide proceeds uniformly on an atomic scale by preserving the atomic step morphology as schematically shown in Fig.4 which illustrates layer-by-layer etching of SiO_2. Although the structure of the ultra thin SiO_2 layer is amorphous, a kind of residual order induced by the Si substrate might remain in the oxide network, thereby preserving the step structure.

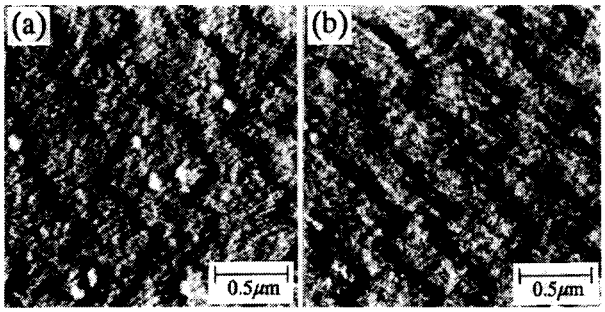

Figure 2. AFM images of (a) thermally oxidized Si(111) surface (2 nm thick) and (b) after stripping the oxide in 4.5%HF.

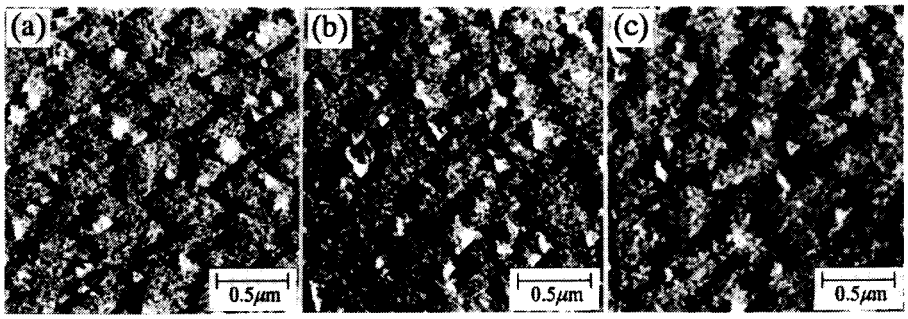

Figure 3. AFM images of (a) 4 nm of thermal oxide grown on atomically flat Si(111), (b) after etching 1.5 nm oxide and (c) 3 nm oxide removal in 0.5%HF.

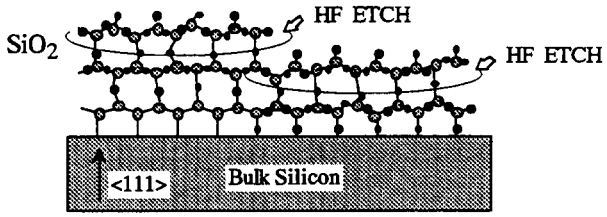

Figure 4. A possible model of layer-by-layer oxide etching in dilute HF solution.

The spectra in Fig.5 illustrates different H-terminations on Si(111) surfaces measured by FT-IR-ATR before and after oxidation. As demonstrated by Higashi et al.[7], a NH_4F treatment yields a dominant mono-hydride termination. Moreover, if this treatment is followed by a 1 min dip in 4.5% HF, there is only a slight increase in the number of di- and tri-hydrides, showing that this treatment does not alter the surface morphology significantly. However, if the 2nm thermal oxide grown on a NH_4F treated surface is removed during a 1 min dip in 4.5% HF, the spectrum shows a sharp decrease in the number of mono-hydride terminated Si bonds at the surface, and increases in the density of di- and tri-hydride termination, indicating that the oxidation process induces an atomic scale microroughness. This was surprising since the AFM image in Fig.2(b) shows that the initial step structure still remains after oxide removal in 4.5% HF. Combining these two results shows that the

oxidation process induces an atomic scale microroughness of less than a biatomic step height (<0.31nm). This roughness is most likely atom trenches whose sizes are smaller than the horizontal resolution (~4nm) of the AFM probe head with a radius of ~30nm.

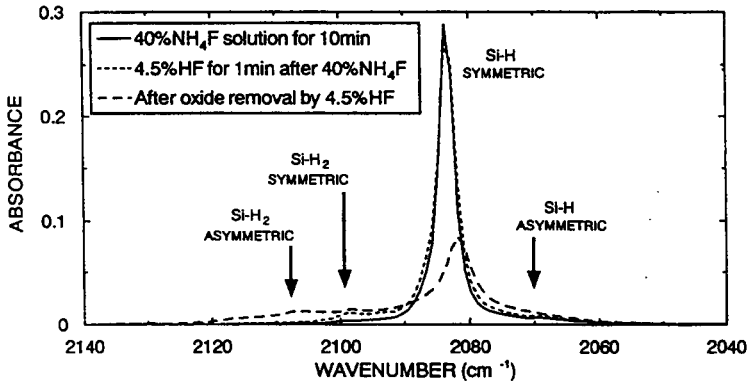

Figure 5. ATR spectra of different H-terminations on Si(111) surfaces before and after oxidation.

4. CONCLUSION

We have shown that the initial atomic step structure produced by 40%NH_4F is preserved during oxidation. The step structure was observed on the oxide surface and at the SiO_2/Si interface, in agreement with the layer-by-layer oxidation model. However, the oxidation induces local monoatomic roughness at the interface which was confirmed by FT-IR-ATR measurement after removing the oxide. This microroughness cannot be clearly resolved by AFM, showing that AFM and ATR must be used together in order to characterize such surfaces. Moreover the etching of thermal oxide by dilute HF solution occurs uniformly on an atomic scale, since the step structure was maintained during etching.

REFERENCES

1. F. J. Himpsel, F. R. McFeely, A. Taleb-Ibrahimi, J. A. Yarmoff and G. Hollinger, Phys. Rev. B 38 (1988) 6084.
2. K. Ohishi and T. Hattori, Jpn. J. Appl. Phys. Vol. 33 (1994) L 675.
3. G. Lucovsky, J. T. Fitch, E. Kobeda and E. A. Irene, "The Physics and Chemistry of SiO_2 and the Si-SiO_2 interface" ed. by C. R. Helms and B. E. Deal (Plenum Press, New York, 1988) p.139.
4. T. Yamazaki, S. Miyazaki, C. H. Bjorkman, M. Fukuda and M. Hirose, Mat. Res. Soc. Symp. Proc. Vol. 318 (1994) 419.
5. Y. Homma, M. Suzuki and N. Yabumoto, J. Vac. Sci. Technol. A10 (1993) 2055.
6. T. Yasaka, M. Takakura, S. Miyazaki and M. Hirose, Mat. Res. Soc. Symp. Proc. 22 (1991) 225.
7. G. S. Higashi, R. S. Becker, Y. J. Chabal and A. J. Becker, Appl. Phys. Lett. 58 (1991) 1656.

INTERACTION OF THE SULPHURIC ACID HYDROGEN PEROXIDE MIXTURE WITH SILICON SURFACES

A.L.P. Rotondaro, H.F. Schmidt, M. Meuris, M.M. Heyns, C. Claeys and J. Mulready*

IMEC, Kapeldreef 75, B-3001 Leuven, Belgium.
*INTEL, Santa Clara CA, USA

1. INTRODUCTION

The sulphuric acid hydrogen peroxide mixture (SPM), with its high oxidizing power, has been widely used as an organic removal agent, especially as a first step in modified RCA cleans [1], as well as a chemical oxide growth step in the proposed IMEC clean [2]. However, due to its high viscosity SPM is hard to rinse and a high number of Light Point Defects (LPDs) is observed after this step when the wafers receive a non-optimised rinsing. Moreover, a time dependent increase in the LPD count is observed on wafers during storage in clean room ambient, which is a major concern for SPM last cleanings. The HF addition at the ppb level to the SPM has been proposed [3] to minimize both the rinsing problem and the time dependent increase in the LPD count, but the disposal of a H_2SO_4:HF mixture may be very costly which is a drawback of this approach. In this paper, the SPM rinsing problem is addressed and conditions for achieving zero LPD addition are proposed, the time dependent LPD issue is investigated and a simple solution for avoiding such an effect is given without the need of mixing additives to the SPM.

2. EXPERIMENTAL

Silicon wafers, CZ, <100>, p-type, with resistivity between 1 to 30 Ωcm were treated in SPM's with ratios of (4:1) and (6:1) H_2SO_4:H_2O_2, at temperatures ranging from 55 °C to 130 °C for 10 min in a stagnant quartz tank. The wafers were rinsed in DI water for 10 up to 60 min in an overflow tank and spun dry. The added LPDs were evaluated with a Censor ANS-100 light-scattering equipment immediately after drying. Some wafers were stored in clean room ambient (class 1) and remeasured after different time intervals (up to one month) to analyse the time dependent LPD problem.

3. RESULTS AND DISCUSSION

The effect of the DI water rinsing time after the SPM treatment on the number of added LPDs is shown in Figure 1. The longer the rinsing cycle, the fewer the added LPDs on the wafers. This can be explained by the fact that during overflow rinsing a boundary layer is formed on top of the wafer surface [4] and the contaminants must diffuse through it in order to be removed by the water flow. Also, a strong effect of the SPM processing temperature is observed, with the lowest LPD addition being achieved for treatments at lower SPM temperatures. Varying the mixture ratio from 4:1 to 6:1 has a negligible effect on the LPD addition.

When a 5 min dip in an isopropyl alcohol (IPA) stagnant bath is performed between the SPM treatment and the DI water rinse a strong decrease on the number of added LPDs is observed for all SPM temperatures (Figure 2). In this case the amount of added LPDs becomes independent of the rinsing time and even for short rinse cycles low LPD counts are obtained. The IPA mainly acts as a surfactant on the SPM carry-over layer that is present on the wafer surface. It reduces the surface tension between the DI water and the SPM film making it easier to be rinsed. The beneficial effect of the IPA dip between the SPM treatment and the DI water rinse can also be observed on the resistivity values of the rinse water at the outlet of the overflow tank (Figure 3). However, the water

resistivity is not a good end-point indicator for the rinse process as it saturates after 5 min rinsing at 16 MΩ, whereas the added LPD data shows that contamination is still being removed from the wafer surface after 30 min rinsing.

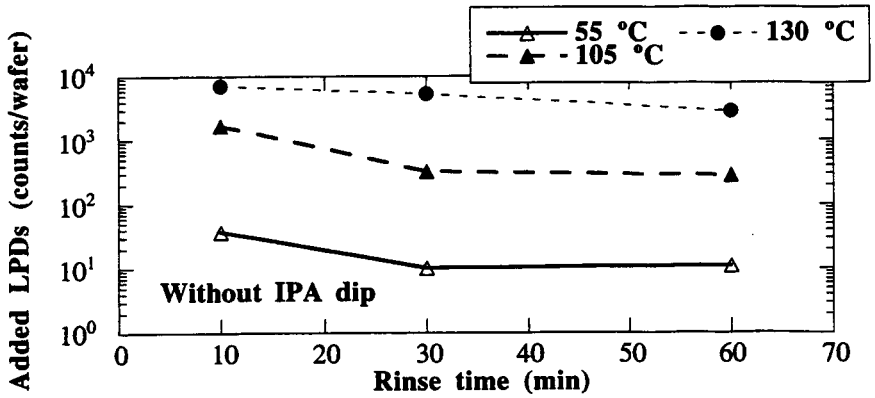

Figure 1: Added LPDs > 0.30 μm LSE as a function of the rinse time in overflow DI water. The wafers were treated in (4:1) SPM at different temperatures.

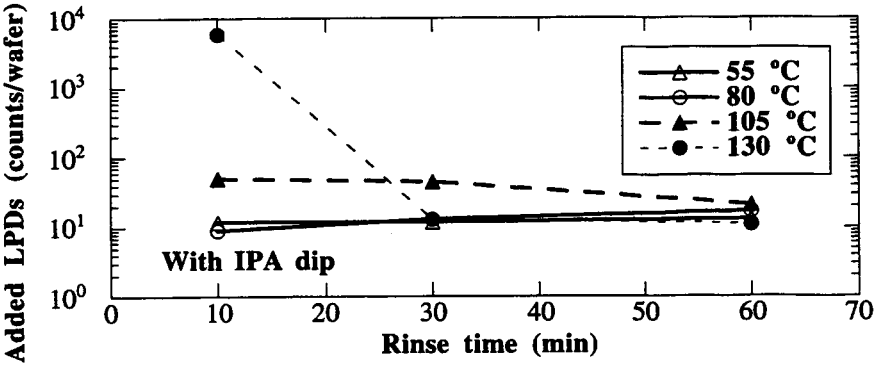

Figure 2: Added LPDs > 0.30 μm LSE as a function of the rinse time in overflow DI water. The wafers were treated in (4:1) SPM at different temperatures and received a 5 min IPA dip before the rinse cycle.

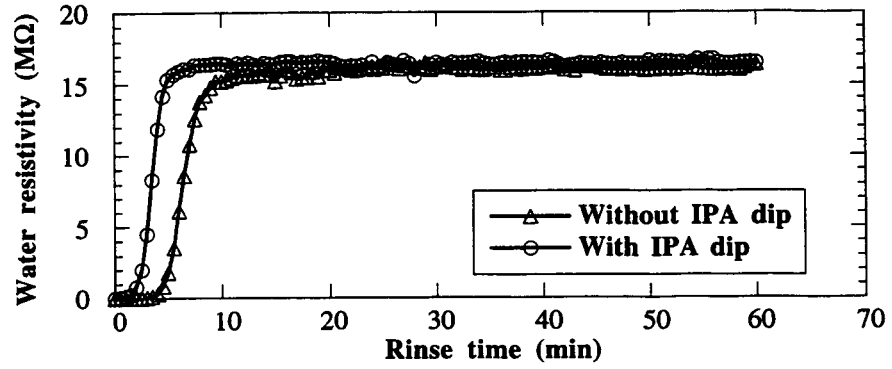

Figure 3: Typical water resistivity values measured at the outlet of the overflow rinse tank for a rinsing cycle of 60 min after treatments in (4:1) SPM at 55 °C.

Independent of the SPM and rinsing conditions a time dependent increase of the LPD count is observed on wafers stored in a class 1 ambient (Figure 4). Scanning Electron Microscope (SEM) inspection of those wafers showed that needle shaped crystals (Figure 5) had formed on top of the SPM chemical oxide during storage. These crystals can be easily rinsed in DI water and will not regrow even after 2 month storage. These results point to the fact that contamination, which was trapped in the SPM chemical oxide, diffused to the wafer surface and coalesced, forming micro-crystals during storage. After several weeks storage, most of the contamination has already diffused to the surface and a simple rinse step can remove it, preventing further crystal formation. Electron Probe Micro Analysis (EPMA) and Auger inspection of those crystals could only detect sulphur. More investigations are being performed to determine their exact structure.

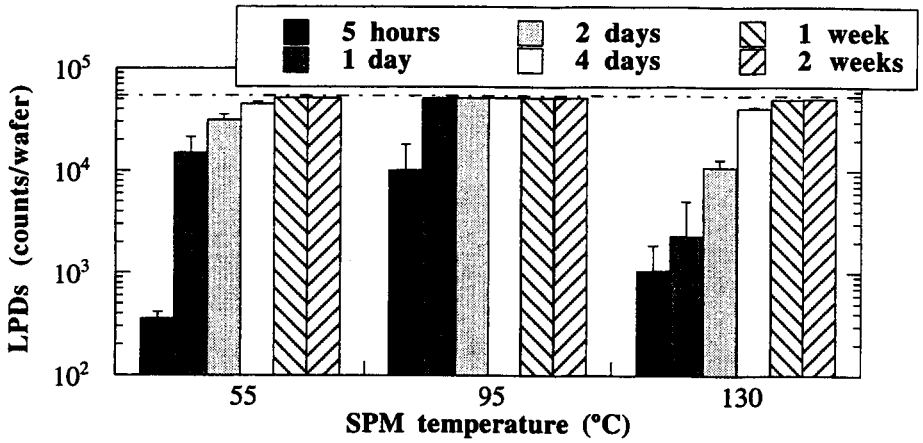

Figure 4: Time evolution of the number of LPDs > 0.15 µm LSE on wafers stored in class 1 ambient after (4:1) SPM treatments. The dashed line indicate the saturation level of the measurement technique.

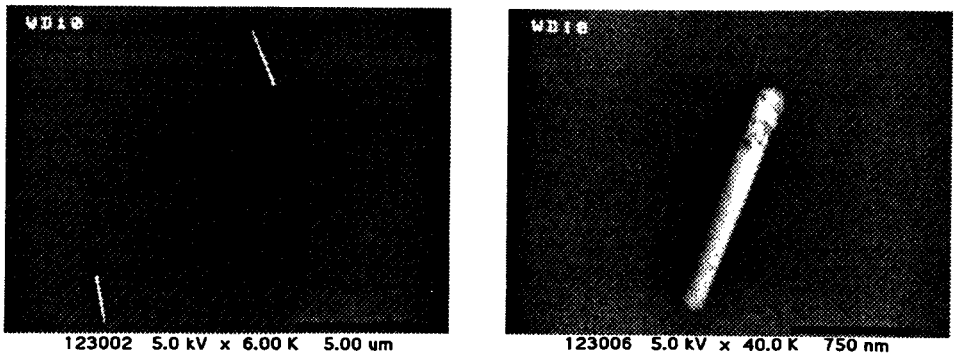

Figure 5: Typical Scanning Electron Microscope (SEM) pictures of the needle shape crystals observed on the stored SPM wafers.

A possible solution for the time evolution LPD problem is to accelerate the crystallisation process, by driving the contamination to the surface and then removing it with a DI water rinse. To investigate this possibility, different treatments were applied to wafers that had received an SPM cycle, which included an IPA dip, 30 min DI rinse and spin dry (Figure 6). If a second DI rinse is performed after the SPM cycle (SPM+DI2)

the number of LPDs only starts to increase after 2 weeks of storage. This indicates that the first spin dry process drives part of the contamination to the surface allowing the second DI rinse to remove it. When the wafers are heated by a 20 min infrared exposure after the SPM cycle (SPM+IR) a sharp increase on the LPD count is observed after a short storage time, indicating that this step can force the crystallisation to occur, by driving the contamination out of the chemical oxide. When the above mentioned steps are combined, meaning that the wafers are heated by an IR step and receive a subsequent DI rinse after the SPM cycle (SPM+IR+DI) no increase in the number of LPDs is observed even after 1 month storage. This shows that the SPM+IR+DI treatment leaves a clean chemical oxide passivation on the wafer surface.

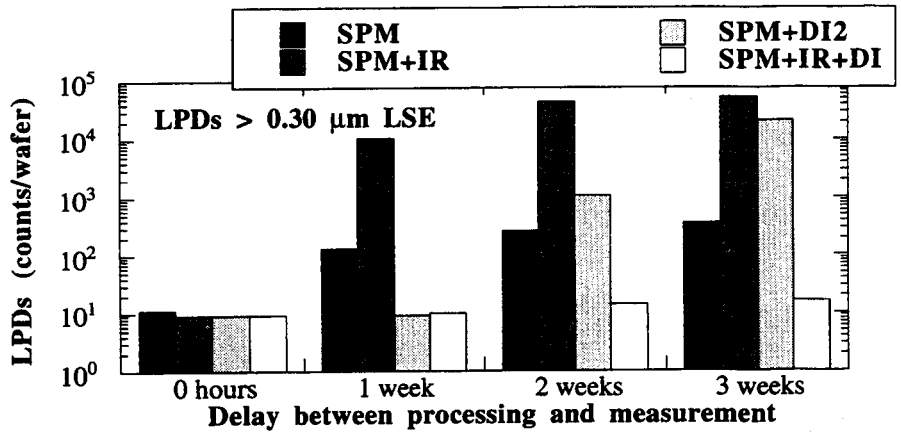

Figure 6: Effect of post-SPM treatments on the time evolution of LPDs > 0.30 μm LSE on wafers stored in class 1 ambient.

4. CONCLUSIONS

An in depth analysis of the interaction of the SPM with the silicon wafer surface has been carried out providing key information about this cleaning step. An IPA dip between the SPM treatment and the rinsing cycle strongly reduces the number of added LPDs. The time dependent LPDs observed after SPM are sulphur based and appear to grow out of the chemical oxide. An infrared treatment followed by a DI rinse can prevent the SPM induced time dependent LPDs, resulting in a clean surface.

5. ACKNOWLEDGEMENTS

A.L.P. Rotondaro would like to thank CNPq (Conselho Nacional de Desenvolvimento Científico e Tecnológico) Brazil, for financial support. Part of this work has been supported by the European Union (Contract # ESPRIT 8003).

6. REFERENCES

1. M. Itano et al; IEEE Trans. on Semicond. Manufact., **6** (3), pp.258-267 (1993).
2. M. Meuris et al; Softbound Proc. Electrochem. Soc., PV94-7, pp.15-25 (1994).
3. M.J. Fleming Jr. et al., European Patent Application # EP 91112984.9 (1992).
4. A. Tonti; Softbound Proc. Electrochem. Soc., PV92-12, pp. (1991).

DIFFERENT REACTION OF O_2 AND OXYGEN RADICALS WITH Si UNDER CRITICAL CONDITIONS FOR GROWTH OF SiO_2

K. Hayama[1], T. Tougun, M. Ishida and T. Nakamura[2]

The oxidation process of Si surface is studied as a function of different oxygen sources. The Si surface was oxidized and/or etched by exposure of O_2 and oxygen radicals. At the substrate temperature of 800 °C and O_2 pressure of 1.3×10^{-3} Pa, the morphology was a rough Si surface with occasional growth of SiO_2. In the case of oxygen radicals instead of O_2 gas, the surface was flatly oxidized and was covered with thin SiO_2 layer. At the substrate temperature of 900 °C with O_2 gas, the Si surface was etched and was damaged. Using oxygen radicals at 900 °C, the surface was extremely degraded.

1. INTRODUCTION

Heteroepitaxial growth of various insulator films on Si have many applications to fabricate Si on insulator devices, quantum well devices and other novel devices. We have already reported epitaxial Al_2O_3 films on Si as an insulator material by metalorganic molecular beam epitaxy. In this growth method, O_2, oxygen radicals excited with rf plasma and $Al(CH_3)_3$(TMA) were used as source gases[1]. For novel device applications using very thin (<10 nm) Al_2O_3 film, it is required to form high quality Al_2O_3 film and abrupt Al_2O_3/Si interface. However, satisfying those requirements is difficult due to nonuniform oxidation of Si surface in the initial growth stage of Al_2O_3 film. It is desired to clear the reaction of O_2 and oxygen radicals with Si surface under the growth conditions of Al_2O_3[2].

The Si oxidation process using O_2 gas has been investigated by many researchers [3,4]. The oxidation using excited species such as ozone, oxygen radicals and oxygen plasma environment are also examined[5-7]. However, these studies using excited O species were generally examined with relatively low temperatures of several hundred degree centigrade and the pressures from atmospheric to 10^{-1} Pa. At relatively higher temperatures and lower pressures, the study of Si oxidation using excited oxygen species was insufficient because of the poor quality of the oxide film with those oxidation conditions.

In the present study, we investigated the Si oxidation process using the different oxygen source to clear the influence of Si surface condition on the grown Al_2O_3 crystallinity in the initial growth stage of Al_2O_3. The O_2 and oxygen radicals were used as oxygen sources. The oxidation was carried out under different substrate temperatures, O_2 pressure and rf excitation power of O_2 gas. The Si surface was oxidized and/or etched by exposure of O_2 and oxygen radicals with the same oxidation conditions as the typical conditions of Al_2O_3 growth.

2. EXPERIMENTAL

Figure 1 shows the diagram of experimental apparatus which is metalorganic molecular beam epitaxy system for fabrication of Al_2O_3/Si stacked structure. The

[1] Department of Telecommunication, Kumamoto National Collage of Technology, 2659-2,Nishigoshi-cho Kikuchi-gun, Kumamoto 861-11, Japan

[2] Department of Electric & Electronic Engineering, Toyohashi University of Technology, 1-1, Tempaku-cho, Toyohashi, Aichi 441, Japan

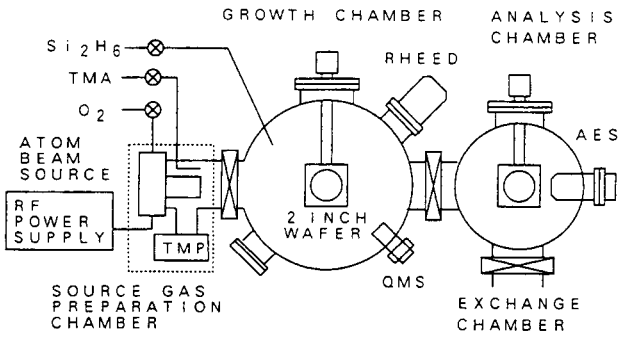

Fig. 1. Diagram of experimental apparatus

pressure of a growth chamber was maintained at ultrahigh vacuum of $3x10^{-8}$ Pa. The Si2H6, TMA and O2 gas (purity 99.995%) can be introduced to the growth chamber. The source gas preparation chamber was attached with an atom beam source (Oxford Applied Research) which is operated by means of electrical discharge created from inductively coupled rf excitation at 13.56 MHz. The oxygen radicals were generated from the O2 gas by the atom beam source. This apparatus were also equipped with an *in situ* reflection high-energy electron diffraction and an Auger electron analyzer.

The n-type (3-6Ωcm) Si(100) CZ wafers with a misorientation of 0.4° toward [110] were used in this experiment. The wafers were chemically cleaned with 2.5% HF solution and were covered with thin protective oxide layer. The experiment was carried out after resistive-heating at 900 °C in the growth chamber. The O2 and oxygen radicals were exposed to the heated wafer at the various conditions of substrate temperatures and pressures of oxygen sources. Though the amount of oxygen radicals could not be measured, these were estimated by the pressure of O2 gas. The rf excitation power was 0 and 400 W. The oxidation time was 1 hour.

3. RESULTS AND DISCUSSION

Figure 2(a) shows the replica TEM image of oxidized Si surface at the substrate temperature of 800 °C and O2 pressure of $1.3x10^{-3}$ Pa. The morphology indicates a rough surface with occasional unevenness. The surface was analyzed by Auger electron spectroscopy (AES) measurement as shown in Fig. 3(a). The split SiLVV peaks and OKLL peaks were observed. The SiLVV peak of 92 eV was from bulk Si. The chemically shifted SiLVV peaks around 80 eV results from the oxidation of the Si surface. It is found that the substrate surface consists of occasional growth of SiO2 and degraded Si surface. The rough surface may be caused by the etching in order to expose of O2 gas. F.W.Smith *et al.* reported the critical conditions for growth of SiO2 with Si(100) and Si(111)[3]. The Si surface reacts with O2 and desorpted out as SiO molecules in the etching region. In the oxidation region, the Si surface was oxidized by exposure to O2 gas. In our results, the oxidation and etching were observed at the same time. These oxidation conditions can be considered the critical conditions.

Figure 2(b) shows the surface oxidized with oxygen radicals at the rf excitation power of 400 W. Flat surface was observed compared with that of Fig. 2(a). The decreasing of bulk SiLVV peak and the increasing of chemically shifted SiLVV peaks from SiO2 and OKLL peaks were also shown in Fig. 3(b). It is inferred that the surface is evenly covered with thin SiO2 layer. The morphology of the surface was

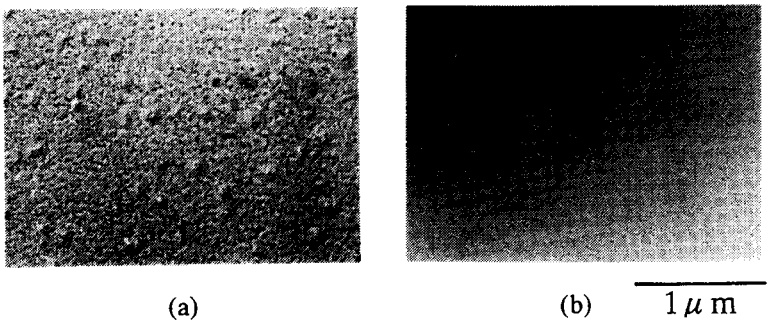

Fig. 2. Replica TEM images of oxidized Si surface with different oxygen sources using O_2 (a) and oxygen radicals (b) as source gases. The substrate temperature and the pressure of oxygen sources are 800 °C and 1.3×10^{-3} Pa, respectively.

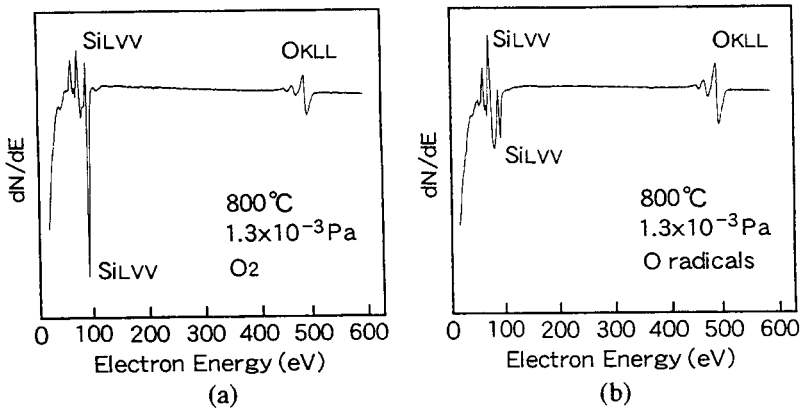

Fig. 3. Auger spectra from the surfaces using O_2 (a) and using oxygen radicals (b) at 800 °C and 1.3×10^{-3} Pa.

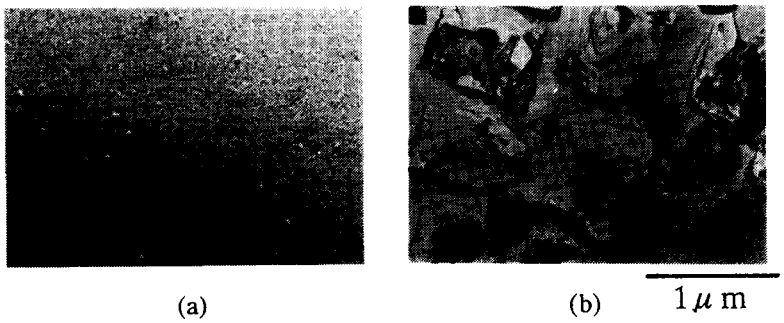

Fig. 4. The surface degraded with O_2 (a) and oxygen radicals (b) at 900 °C and 1.3×10^{-3} Pa.

improved, because using oxygen radicals instead of O_2 gas is effective to oxidize the Si surface.

At the substrate temperature of 900 °C with exposure of O_2 gas, the Si surface

Table 1. Different reaction of oxidation and etching with O_2 and oxygen radicals.

	800°C		900°C	
O_2 pressure	O_2	O radicals	O_2	O radicals
1.3×10^{-3} Pa	SiO_2 island	oxidation	etching	etching
4.0×10^{-3} Pa	oxidation	oxidation	etching	oxidation

was etched and the morphology was degraded [Fig. 4(a)]. The Si_{LVV} peak of 92 eV from bulk Si was only observed by AES measurement. Therefore, the surface was not oxidized. In the case using oxygen radicals instead of O_2 gas at 900 °C, the surface was extremely degraded as shown in Fig. 4(b). Auger spectra indicates only Si_{LVV} peak of 92 eV from bulk Si, so that the Si surface was not oxidized and was etched by exposure of oxygen radicals. The morphology shown in Fig. 4(b) have specific patterns which were based on the square like patterns. These patterns may depend on the crystallographic direction of the Si surface.

Table 1 shows the different reaction of oxygen sources with Si surface at various conditions of substrate temperature and O_2 pressure. The boundary between oxidation and etching is at the O_2 pressure of 1.3×10^{-3} Pa and the substrate temperature of 800°C in our study. The reaction moves toward oxidation by increasing the O_2 pressure. In contrary, the reaction moves toward etching by increasing the substrate temperature. Compared the effect of O_2 and oxygen radicals with Si surface, the results shown in table 1 indicate that the boundary conditions move toward oxidation using oxygen radicals instead of O_2 gas.

4. CONCLUSIONS

The reaction of O_2 and oxygen radicals with Si surface was studied at various conditions. The surface was oxidized and/or etched by exposure of these oxygen sources. The boundary between oxidation and etching moved toward oxidation using oxygen radicals instead of O_2 gas. The control of the reaction of oxygen sources with Si surface is important for epitaxial growth of Al_2O_3 on Si.

ACKNOWLEDGMENTS

The authors wish to express their thanks to Mr. N. Kaneda for his experimental support. This work was partially supported by Grant-in-Aid for Encouragement of Young Scientists (No.06750318) from the Ministry of Education, Science and Culture of Japan.

REFERENCES

1. K.Hayama, M.Ishida and T.Nakamura, Jpn.J.Appl.Phys.,33,(1994)496.
2. K.Hayama, M.Ishida and T.Nakamura, Control of Semiconductor Interfaces, (Elsevier Science Publishers B.V., Netherlands,1994)289.
3. F.W.Smith and G.Ghidini, J. Electrochem. Soc., 129(6), (1982)1300.
4. T.Horie, Y.Takakuwa and N.Miyamoto, Extended Abst. of the 1993 Int. Conf. on Solid State Devices and Materials(1993)599.
5. S.Kiyama, et al.,J.Appl.Phys. 63(9),(1988)4655.
6. G.G.Fountain, et al., J.Appl.Phys.63(9),(1988)4744.
7. S.K. Ray, C.K.Maiti and N.B.Chakraborti,J. Mater. Sci. 25,(1990)2344.

PERFORMANCES OF USUAL WET CLEANINGS AND STUDY OF THEIR COUPLING WITH 7 nm GATE OXIDATION PARAMETERS

F. Tardif, T. Lardin, C. Paillet, D. Bremond, J.P. Joly, F. Martin, P. Mur, L. Mouche *
P. Patruno, A. Tonti, D. Levy, K. Barla **
W. Sievert ***

1. INTRODUCTION

Usual wet cleaning performances achieved with 1 ppb grade chemicals are established here during 3 successive runs on wafers initially contaminated in the 10^{11} to 10^{12} at/cm^2 range and roughened in a 10' spiked (1,1,5) SC1, in order to simulate the actual Silicon state during the process steps. The parameters studied are therefore the ability of these cleanings to really remove metallic contaminants such as Ca, Cu, Fe, Ni, Zn (and not the residual contamination left on initially clean wafers) and their surface smoothing capacity. The coupling between these cleanings and 7 nm gate oxidation gaseous ambiences are then studied on Ptype CZ(100) 14-22 Ω.cm substrates.

2. PERFORMANCES OF USUAL CLEANINGS IN TERMS OF METALLIC REMOVAL AND ROUGHNESS

Different usual cleanings sequences are performed after a contaminated (1,1,5) 70°C, 10' SC1[(1)]. One ppb level grade chemicals are used for the different recipes described above except for nitric and BOE (VLSI grade).
- Contamination levels are measured by VPD-TXRF except for Copper (TXRF) and averaged on 3 runs (see table 1).

	Polluted wafer	BOE	HF	HF+ CHOL	HF+ SC1	HF+ SC2	HF+ RCA	HF+ CARO	HF+ HNO3	CHOL	SC1	SC2	RCA	CARO	HNO3
Fe	9.0	0.76	0.54	89	94	0.24	0.78	0.85	0.79	73	83	1.19	1.23	1.51	.87
Zn	102	31	1.85	28.7	50.0	1.50	1.50	0.62	0.54	41	61	1.8	1.6	.68	.53
Cu	25	15	6.4	1.4	1.5	1.2	1.4	1.3	1.7	1.8	1.6	1.5	1.4	3.6	1.5
Ni	14	0.26	0.24	0.16	0.16	0.08	0.52	0.73	0.60	0.63	0.55	0.88	0.84	1.13	.95
Ca	76	1.25	0.86	0.82	0.81	1.8?	0.7	0.61	1.08	1.00	1.18	1.09	1.56	1.27	1.16
Cl	22	4.8	1.5	21	20	1.5	1.5	17	25	23	20	20	22	16	24
S	4.7	25	60	22	18	17	13	750	40	27	20	39	31	560	49

Table 1 : Residual contamination after different cleanings on initially contaminated wafers (x 1E10 at/cm^2).

Copper is still present after HF and BOE as predicted by electrochemical potential. Without the presence of high oxidant species in appreciable amounts (H_2O_2, ...), the same phenomenon is assumed to occur for Ag, Au, and other couples with a potential greater than H^+/H_2 potential.

---

* LETI (CEA - Technologies avancées), MEL-CEN/G-17 rue des Martyrs-F-38054 Grenoble
** SGS/Thomson Centre Commun, F-38290 Crolles
*** Riedel-de Haën AG, D-3076 Seelze

In terms of residual Iron contamination, figure 1 shows that the best results are obtained with Chlorinated Chemistries : RCA, or even better SC2 only, probably due to the very high solubility of metals in Chlorides (better than in Fluorides for example). Nitric acid could also be a good candidate.
The necessity of eliminating a contaminated chemical oxide with an HF pre-treatment is also clearly demonstrated.
As previously published[2], we can verify on the same curve that MOS generation lifetime of minority carriers is, in practice, mainly correlated with Iron contamination. The *HF+SC2* as a final cleaning step seems to be the most interesting in terms of minority carriers lifetime and therefore particularly well suited to *Bipolar*, *CCD* and *DRAM* technologies.

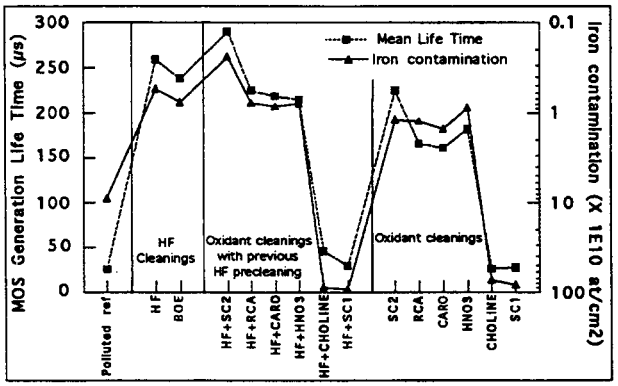

Figure 1 : Residual Iron contamination after different cleanings and associated MOS generation lifetimes

Optimisation of Kern's (1,1,5) SC2 mixture by decreasing the Hydrochlorhydric ratio is very tempting but excess dilution seems to be dangerous when ultimate Silicon purity is required. These results are correlated with Elymat lifetime (Iron aspect) : when SC2 is more diluted, the recipe is not able to remove all the Iron ; if it is more concentrated, the final Iron concentration is higher due to the higher bath contamination. Results of figure 2 are obtained with 1 ppb level grade chemicals by VPD-TXRF for Iron and VPD-AAS for Aluminium and Sodium. Wafers were initially contaminated in a spiked conventional SC1 .

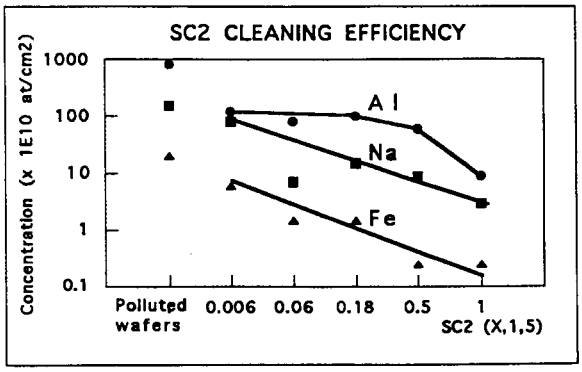

Figure 2 : Residual contamination after different diluted SC2

- RMS roughness results obtained by contact AFM (figure 3) highlight the advantage of using a highly oxidant chemistry such as CARO's acid. The chemical oxidation of the surface peaks smoothes the surface, as thermal oxidation does.
Two different correlations between mean breakdown fields at low ramp rate and final RMS roughness seem to be obtained for each studied case : with and without HF precleaning. Roughness measured by contact AFM is therefore, as previously demonstrated[4], one of the main factors to obtain high intrinsic gate oxide integrity. A very oxidant cleaning step such as *CARO* in the final acid phase of the whole cleaning process is from this point of view very well suited before the gate oxide step in *MOS* technology. Nevertheless, particle addition has to be drastically reduced in this case using a filtered bath.
It can also be verified that as predicted by electrochemical potentials, a 1% HF precleaning during 1' increases the Silicon roughness by protonic oxidation (E H^+/H_2 > E SiF_6^{2-}/Si). This effect could also be due to the presence of metals for which the electrochemical potential is greater than the corrosion potential of Silicon by protons (- 0.11 V), but a high impurity concentration (>100 ppb) or a long time treatment is necessary (>30')[3].

A more simple oxidant treatment consists in using *ozonisated Di water* at 20 °C. A 10' bath in 1.5 ppm of Ozone yields even better results in terms of 7 nm dry oxide integrity especially in the case of an initially relative rough surface as after a conventional SC1 (1,1,5), 70°C, 10' treatment (figure 4). But at this neutral PH, this cleaning sequence is not able to remove all the metals efficiently. An acidic treatment has to be previously performed.

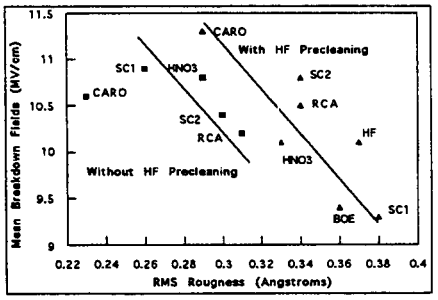

Figure 3 : AFM RMS roughness after different cleanings and consequences on 25 nm dry gate oxide integrity (1 mm^2 capacitors)

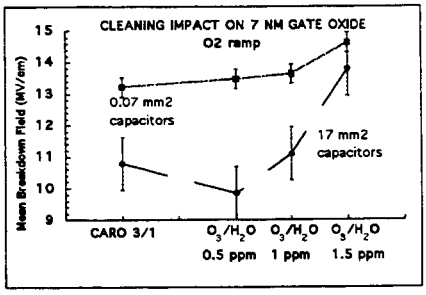

Figure 4 : Ozone/H_2O cleaning performances on 7 nm dry gate oxide. Wafers initially roughened in SC1 10', 70°C.

3. PERFORMANCES OF USUAL CLEANINGS FOR PARTICLE REMOVAL

Different alkaline cleanings optimised according to the "2 nm thermal oxide etch" criterion[5] : SC1, Choline/Peroxide and TMAH/Peroxide are compared with the 2 steps cleanings : CARO+HF/IPA (so called IMEC clean)[6] and CARO + diluted HF. (The latter treatment was designed to control the chemical oxide etching in order to still leave a hydrophilic surface). Three hundred $\pm$ 50 particles of different natures are deposited on both hydrophilic (after CARO) and hydrophobic (after HF) 100 mm wafers by dipping them in baths contaminated with Silicon nitride particles, Silicon oxide particles, in a non-filtered HF bath and in tap water. Figures 5 and 6 indicate that the removal efficiency is higher on hydrophilic surfaces.

The best performances are obtained with *SC1* for particles after HF bath, and *CARO+HF/IPA*, especially for nitride particles. Ozonisated water+HF/IPA do not give as good results as CARO+HF/IPA.

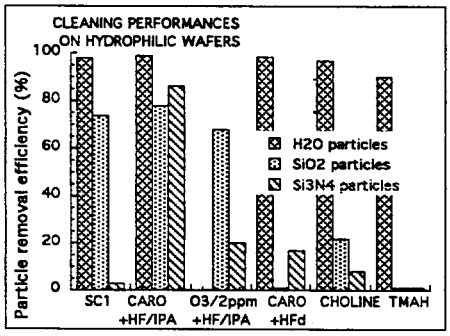

Figure 5 : Cleaning efficiency on 100 mm hydrophilic wafers initially contaminated with about 300 particles

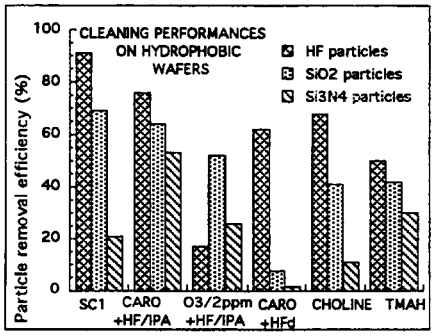

Figure 6 : Cleaning efficiency on 100 mm hydrophobic wafers initially contaminated with about 300 particles

4. IMPACT OF CLEANINGS/THERMAL PROCESS PARAMETERS IN THE CASE OF 7nm GATE OXIDE

For critical process steps, as the chemical state of the Silicon surface intimately interacts with the following thermal process conditions, cleaning processes are difficult to develop and optimise for general purposes : they have to be perfectly adapted to their associated thermal process parameters. Some examples are given here concerning 7 nm gate oxide.

After a 1% HF to remove a simulated sacrificial oxide, different pre-gate cleanings are performed.
In the case of HFlast cleanings, non oxidant steps during thermal ramping and wafer loading degrade the oxide integrity drastically. As demonstrated in figure 7, even in the case of a traditional open furnace, wafer loading under 100% oxygen appreciably improves the mean breakdown fields of 7 nm dry oxides. In these gaseous oxidant conditions, HF cleanings can be used as the final step of the cleaning sequence instead of the classical RCA but the best cleaning is still smoothing CARO.

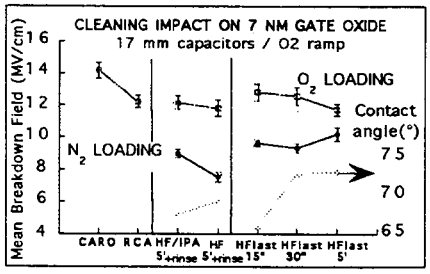

Figure 7 : Impact of cleanings and wafer loading under 100% Oxygen on 7 nm gate oxide integrity

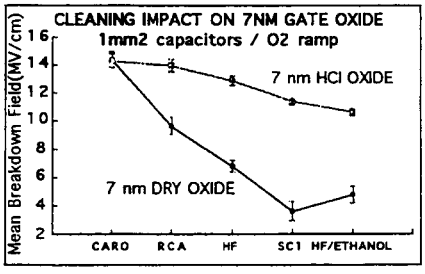

Figure 8 : Impact of cleanings and Chlorinated ambience on 7 nm gate oxide integrity (N_2 loading)

During 900°C oxidation, a Chlorinated ambience (3% HCl or TCA) enabled better mean breakdown fields to be obtained than for dry oxide, as seen in figure 8. In these conditions, the RCA cleaning process gives as good results as CARO's acid. Nevertheless, we detected that the use of HCl can sometimes induce infant QBD breakdown even if HCl is introduced after Oxygen. A micro-pitting phenomenon is suspected here and could be the limitation of the method.

5. CONCLUSION

With today's high chemical grades, the metallic removal performances on initially dirty wafers by conventional cleanings show that chlorinated chemistry such as HF+SC2 is the most efficient.
Highly oxidant cleanings such as CARO's acid smooth the Silicon Surface and give better intrinsic oxide properties at least up to a thickness of 7 nm.
The two-step particle removal cleaning : CARO+HF can, for major particle natures, advantageously replace the polluting alkaline recipes.
A non oxidant ambience even during wafer loading in the furnaces is damaging for thin gate oxide achieved after HFlast cleaning processes.
In a Chlorinated gaseous ambience, the best 7 nm gate oxide is obtained with the RCA and again the CARO cleaning process.

CLEANING RECIPE, USED :

BOE 7/1	20 °C, 1'	SC2	(1, 1, 5), 70 °C, 10'	SC1	(0.25, 1, 5), 70°C, 10'
HF	1%, 20 °C, 5'	Nitric	70%, 70°C, 10'	Choline 5%	(1.5, 1, 5), 70°C, 30'
HFd	0.05%, 20 °C, 3'	CARO	(3, 1), 140 °C, 10'	TMAH 2.8%	(4.5, 1, 5), 70 °C, 30'
HF/IPA	(0.5%/0.1%), 20°C, 2'			$CARO_{(HF/IPA)}$	(4, 1), 100°C, 10'
$O3_{(HF/IPA)}$	2 ppm, 20°C, 10'			HF/ETHANOL	(1%, 99%), 20°C, 3'

Delay between HF and furnace loading < 20'.

REFERENCES

(1)- W Kern "Cleaning Solution based on Hydrogen Peroxide for use in Silicon Semiconductor Technology", RCA revue, vol. 2 1970
(2)- F Tardif et al. "Impact Study of the use of ULSI, VLSI and MOS grade Chemicals in the RCA cleaning process on MOS and Bipolar devices", The Electrochemical Society, Grenoble Symposium, September 1993
(3)- L Mouche "Etude des mécanismes de contamination particulaire et métallique des substrats de Silicium en Solution", ST/LETI thesis - September 1994
(4)- M Miyashita et al. "Optimizing NH_4OH/H_2O_2 Cleaning Process for Ultra-Clean Wafer Surface Preparation", The Electrochemical Society, vol. 91-1, Spring meeting, May 1991
(5)- M Heyns "Advanced wet Cleaning Technology for Highly Reliable Thin Oxides", The Electrochemical Society, vol. 93-1, Spring meeting, May 1993
(6)- M Meuris et al. "A New Cleaning Concept for Particle and Metal Removal on Si Surface", The Electrochemical Society, vol. 93-2, Fall meeting, October 1993

This work was performed within the framework of the E2A JESSI project.
Special thanks to Mr Fabre from CNRS/LAAS laboratory
for performing the high sensitivity AFM measurements.

THE IMPACT OF LOCOS FORMATION ON THE GATE OXIDE INTEGRITY

M. Dohmen, R. Wijburg and R. Girisch

Philips Semiconductors, Gerstweg 2, 6534 AE Nijmegen, The Netherlands

Wafer cleaning is seen as an important processing step with respect to the gate oxide integrity. However, other processing steps prior to the gate formation can have an impact on the gate oxide quality. This paper shows a significant difference between structured and non-structured wafers which cannot be attributed to the bird's beak. The experimental results suggest an interaction between the buffered oxide etch step and the succeeding APM-clean especially for the structured wafers.

1. INTRODUCTION

Wet chemical processing has increased in importance as semiconductor industry is moving to submicron structures. Especially, understanding and improvements of wafer cleaning have made considerable progress [1,2]. However, many papers discuss results obtained from plane (i.e. non-structured) wafers, see for instance [3,4]. This paper describes some aspects relating to the LOCOS formation in a submicron CMOS process which can have a serious impact on the gate oxide integrity.

2. EXPERIMENTAL SETUP

The samples were made using a conventional LOCOS scheme using padoxide and silicon nitride. The structured and non-structured wafers were identically processed except for the lithographic step that defines the active areas. After silicon nitride etching, this resulted in local silicon nitride for the structured wafers, whereas the non-structured wafers were completely covered by silicon nitride. After the wet oxidation at 1050 °C and silicon nitride removal, the wafers were subjected to a BOE 20:1 in order to remove the padoxide and to etch partly the LOCOS oxide. This etch time is referred to as the LOCOS Etch-Back (LEB) time. After the LEB, the wafers were cleaned in a wet-bench before growing of the sacrifical oxide. The standard clean consisted of an APM-step 1:1:8 at 65 °C for 10 min., followed by an HF-step. We found the interaction between the APM-step of the pre-sacox-clean and the preceeding LEB to be essential for the gate oxide deterioration. After sacrificial oxidation, and oxide stripping, the wafers were subjected to the standard wet-bench clean before loading into the gate oxide furnace. Gate oxide thicknesses were 15 or 25 nm. However, the wafer treatment before gate formation rather than the gate oxide thickness itself turned out to be the key to the effect, described

below. Then polysilicon was deposited and patterned, followed by the electrical measurements. The gate oxide integrity was evaluated in terms of Qbd with electron injection from the gate. From the Qbd-values, a yield-figure was derived as the percentage of devices having intrinsic Qbd-values.

3. EXPERIMENTAL RESULTS AND DISCUSSION

Fig. 1 illustrates the influence of the APM-temperatures of the pre-sacox-clean on the device yield. The LEB time was fixed in all cases at 8 min. The difference between the structured (LOCOS) and non-structured (no LOCOS) wafers is striking. Both types of wafers were identically processed except for the active area mask definition.

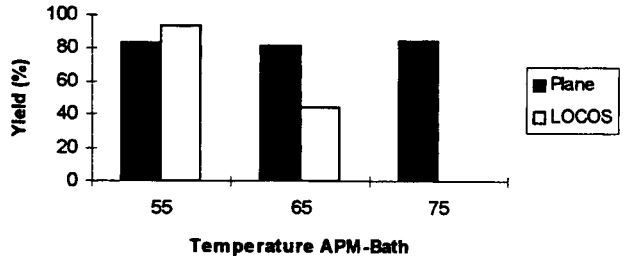

Fig.1. Influence of APM-temperature on device yield.

This effect cannot be attributed to the bird's beak as demonstrated by photo-emission measurements. The photograph, see Fig. 2, shows that the injection of carriers does not preferably take place at the bird's beak. Notice, however, that the electron flow is not homogeneous over the active area. The high injection area, lightly coloured, is in the lower-left corner of the active area window. The upper-right corner, darkly coloured, hardly reveals any injection.

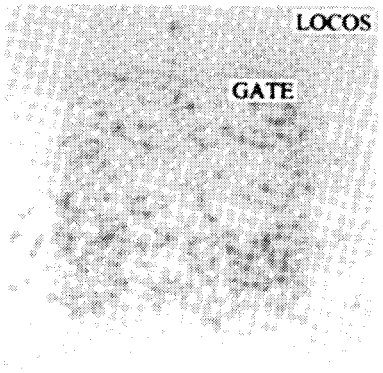

Fig.2. Photo-emission measurement of the active area window.

In Fig. 3, the AFM-results of the structured (left) and non-structured (right) wafers are compared. The APM-temperature of the pre-sacox-clean was 55 °C in both cases. The structured wafers show a higher surface roughness (Ra = 0.45 nm) than the non-structured wafers (Ra = 0.25 nm). Within an active area window of the structured wafers, a difference in surface roughness between, for instance, the lower-left and upper-right corner could not be detected by our AFM (Nanoscope III).

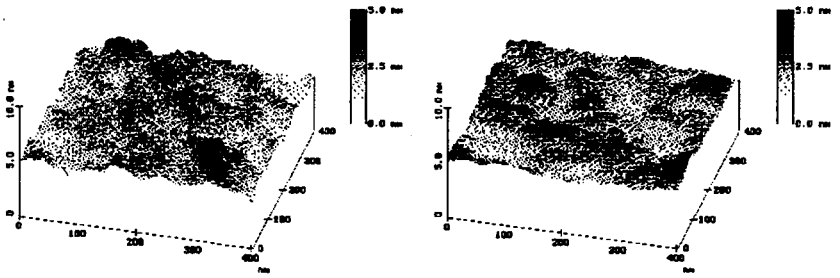

Fig.3. AFM measurements of structured (left) and non-structured (right) wafers.

The influence of the LEB time was studied too. The experiments were carried out with standard APM-cleaning. The results for the structured wafers are shown in Fig. 4. The device yield decreases with a prolonged etch-time. No influence on the device yield was found for the non-structured wafers despite the long time bare silicon was exposed to the buffered oxide etch.

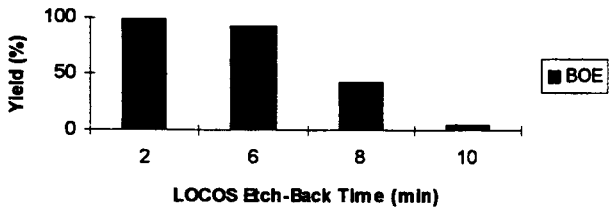

Fig.4. Influence LEB time on device yield.

By replacing the buffered oxide etch by a diluted HF-solution or a mixture of HF/H2O2, the detrimental influence of the LOCOS etch-back step on the gate oxide integrity can be eliminated, as is shown in Fig. 5. In all cases, the standard APM-temperature of 65 °C was used and a LEB time of 8 min.. Thus the HF- and HF/H2O2-mixtures were chosen such that the etch rate was equal to that of the BOE.

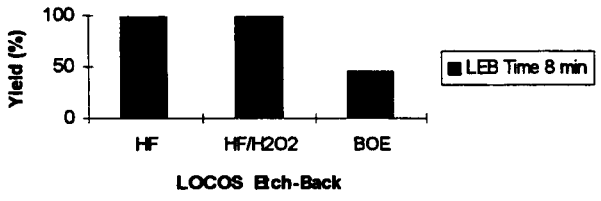

Fig.5. Influence HF, HF/H2O2 and BOE 20:1 at the LEB step.

From the results, described above, it can be concluded that structured and non-structured wafers, although identically processed, may have a significant difference in gate oxide quality. This cannot be attributed to the bird's beak. The AFM data indicate that this may be due to a difference in surface roughness. However, it is not clear why the structured wafers reveal a higher surface roughness than the non-structured wafers. Besides, it could not be explained why the injection of carriers is not homogeneous over the active area window of the structured wafers. Our results indicate an interaction between the LOCOS etch-back step in BOE and the succeeding clean before the sacrificial oxidation. Both a longer LEB time and a higher APM-temperature may cause a higher surface roughness. Therefore, we suggest that surface roughness, as caused by the LEB, is enhanced by the succeeding APM-step.

4. CONCLUSION

A significant difference in gate oxide quality between structured and non-structured wafers is reported. The sequence of the LOCOS etch-back step in BOE and the APM-step prior to sac-oxidation deteriorates the gate oxide quality of the structured wafers. AFM data indicate a relation with respect to surface roughness. However, the cause of the difference in surface roughness between structured and non-structured wafers is not clear yet.

REFERENCES

1. T. Ohmi, "Impact of wafer surface cleaning technology on device performance and reliability", proceedings of 1992 IEEE, Nashville, pp.287-296.
2. W. Bergholz, "Metallic impurities in Si-processing", Proceedings of the Electrochem.Soc.Fall Meeting.
3. T. Ohmi, M. Miyashita, M. Itano, T. Imaoka and I. Kawanabe, IEEE Trans. on El. Dev., vol. 39, No.3, March 1992, p.537.
4. M. Meuris, M.M. Heyns, P.W. Mertens, S. Verhaverbeke and A. Philipossian, Microcontamination Magazine, May 1992, p.31.

DEFECT DENSITY OF ULTRA-THIN GATE OXIDES GROWN BY CONVENTIONAL OXIDATION PROCESSES

M. Depas, B. Vermeire, P.W. Mertens, M. Schaekers, M. Meuris and M.M Heyns

IMEC, Kapeldreef 75, B-3001 Leuven, Belgium

ABSTRACT: In this work the extrinsic defect density of ultra-thin (3 to 6 nm) gate oxides grown by conventional dry and wet oxidation is examined. It is shown that for the presently used wet cleaning and conventional oxidation processes the gate oxide thickness scaling is limited to 4-5 nm.

1. INTRODUCTION

High quality ultra-thin gate oxide layers will become required for future CMOS generations. For a 0.18 µm CMOS process, the gate oxide thickness will have to decrease to only 4 nm because of scaling requirements. The economic feasibility of this process will be determined by the defect density of these ultra-thin gate oxides. The larger chip area and the more severe manufacturer's goal for the yield of these devices will demand a defect density less than 0.1 defects/cm^2 [1].

2. EXPERIMENTAL

The fabrication of MOS capacitors was done in a class 1 cleanroom. Silicon 125 mm wafers were chemically cleaned with a modified RCA followed with a dip in 0.5% HF + 0.1% IPA + 0.1% chloro-acetic acid for 5 minutes to obtain a hydrogen passivated surface with a low metal and particle density [2]. The ultra-thin oxide layers were grown in a conventional ASM (DFS 250) furnace with a fully automated loader for particle reduction. The oxide thickness was determined by spectroscopic ellipsometry and is given in Table 1 as a function of the oxidation process. No Cl addition was applied.

Table 1. Thickness d_{ox} of ultra-thin oxide layers grown by dry and wet oxidation, T_{ox} and t_{ox} are the oxidation temperature and period.

ambient	T_{ox} (°C)	t_{ox} (min)	d_{ox} (nm)
10% O_2/N_2	850	10	2.8
10% O_2/N_2	850	30	3.6
10% O_2/N_2	850	60	4.7
5% O_2/N_2	900	70	6.2
1:1.33 O_2/H_2	650	33	3.1
1:1.33 O_2/H_2	700	53	6.5

The metal contamination as determined by VPD-DSE-TXRF after the wet cleaning and oxidation was below 10^{10} atoms/cm^2. A poly-Si film was deposited in a LPCVD system at 625°C and subsequent phosporus doping was performed by solid source diffusion at 900°C. Aluminum-capped poly-Si gate capacitors were made using standard wet lithography. Finally, wafers were annealed for 30 min at 435°C in forming gas.

3. RESULTS AND DISCUSSION

The gate oxide integrity was determined with breakdown measurements (E_{BD}) using a ramped voltage test. On each wafer, 100 capacitors with an area from 1.12 mm^2 to 15.84 mm^2 were tested. As shown in the breakdown histogram of Fig.1, the mid-field breakdowns disappear for ultra-thin oxide layers, only low-field (short modes) and high-field breakdowns occur. The disappearance of the mid-field breakdowns for oxide layers thinner than 6 nm has also been demonstrated in [3] and [4]. The large electrical field values above 12 MV/cm in Fig.1 are obtained when the 0.3 A/cm^2 current compliance of the measurement system is reached without detecting a breakdown of the oxide layer.

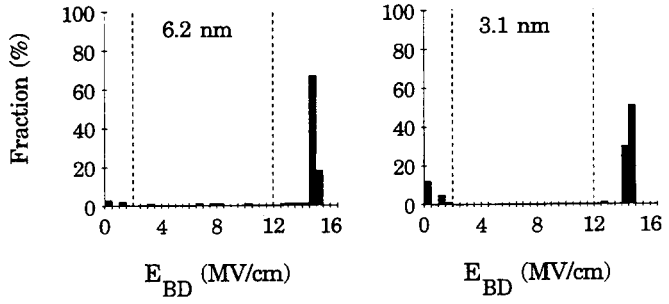

Figure 1. Breakdown histogram of a 6.2 and a 3.1 nm gate oxide (see table 1) as determined with a ramped voltage test (15.84 mm^2 area).

The presence of a short mode in the gate oxide can be seen from the current-voltage characteristic of the MOS capacitor, as illustrated in Fig.2 for a 3.1 nm oxide. If no extrinsic defects are present in the oxide layer, the measured current density can be explained by direct tunnelling of electrons through the oxide barrier [5].

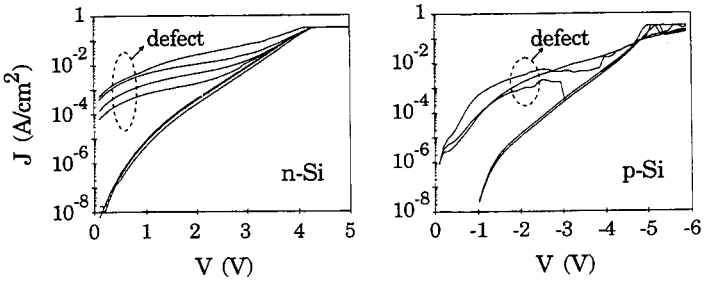

Figure 2. Measured J-V characteristics for MOS capacitors with an area of 15.84 mm^2 and a 3.1 nm gate oxide grown on a n-Cz or p-Cz Si substrate.

A very uniform distribution of this tunnel current was obtained over the Si wafer, independent of the capacitor area, as shown in Fig.3. The observed distribution is caused by the small (< 0.1 nm) oxide thickness variation over the wafer area. In contrast with this an anomalous high current is measured when pinholes occur in the ultra-thin oxide layer. These extrinsic defects are randomly spread over the wafer and are probably caused by particle contamination.

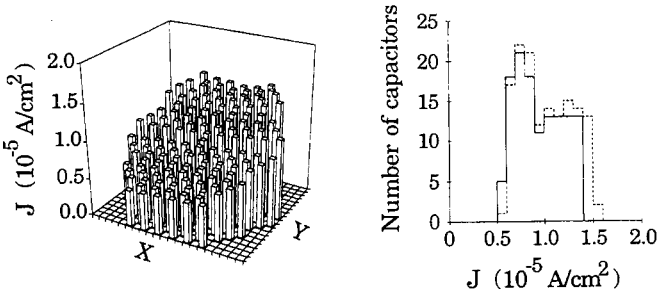

Figure 3. Distribution of the intrinsic tunnel current measured at a 1.2 V gate bias for a 3.1 nm oxide: a) wafer mapping, b) histogram (full lines: 3.84 mm^2 area, broken lines: 0.03 mm^2 area).

The yield of pinhole free capacitors is shown in Fig.4. No reproducible difference was observed for different substrates (n-type vs p-type or epi vs Cz grown). This demonstrates the decreasing importance of defects in the silicon substrate like oxygen precipitates for these ultra-thin oxide layers. The yield results for dry ultra-thin gate oxides are presented in Fig.5 as a function of the capacitor area and the oxide thickness. Each condition represents the mean of at least 4 wafers. An exponential decrease with the capacitor area is observed, as expected from a random distribution of point defects [6]. The defect density as obtained from the slope of these straight lines is shown in Fig.6. The very low defect density of the order of 0.1 defects/cm^2 that is observed for oxide layers thicker than 4-5 nm, shows an important increase for thinner oxides. This is explained by the increasing importance of gross imperfections like particles or metal clusters on the initial silicon surface oxidation.

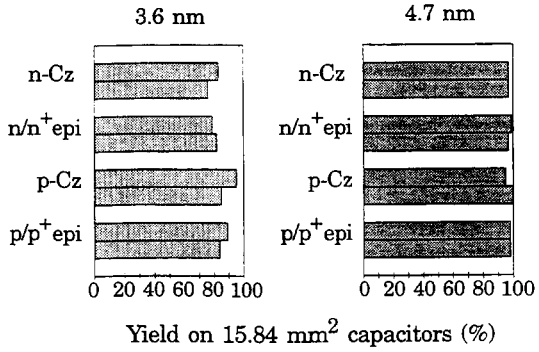

Figure 4. Si substrate dependence of the yield on large area MOS capacitors with an ultra-thin 3.6 nm and 4.7 nm oxide layer.

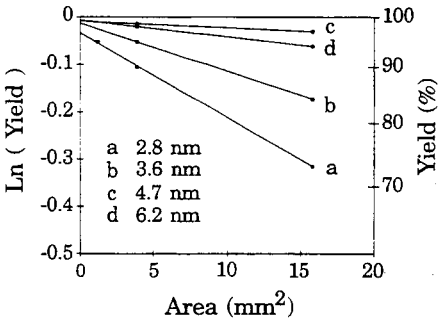

Figure 5. Yield of ultra-thin dry gate oxides as a function of the gate area and oxide thickness.

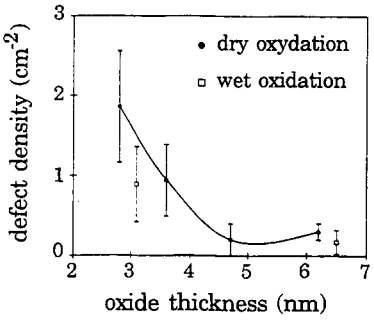

Figure 6. Defect density of ultra-thin gate oxides grown by conventional oxidation.

As was already demonstrated by Triplett [4], the relation between the defect density and the ultra-thin gate oxide thickness depends on the state of the cleaning technology. The influence of the oxidation technology on the density of short modes is shown in Fig.6. A reduction of the defect density for a 3 nm gate oxide was obtained by using wet oxidation.
Although the obtained defect densities are low, additional improvements in contamination control will be required to reduce this value further to below 0.1 defects/cm^2. The application of ultra-clean rooms and cluster tools may be necessary to reduce the defect density for oxide layers thinner than 4-5 nm.

4. CONCLUSIONS

The defect density of ultra-thin (3 to 6 nm) conventional dry and wet gate oxides was examined. It is shown that only short modes and no weak spots occur. Wet oxidation is shown to be an effective low temperature oxidation process to obtain defect densities at least as low as for dry oxidation. The important increase of the defect density for thinner oxide layers grown by these conventional processes, limits the gate oxide thickness scaling for CMOS technology to 4-5 nm.

Acknowledgements
Karine Kenis, Ann Opdebeeck, Hilde van de Plas, Sofie Mertens, Patricia Van Marcke and Luc Pauwels are greatly acknowledged for their technical support.

REFERENCES

1. SIA Semiconductor Technology-Workshop Working Group Reports, (Irving, Texas, Nov. 17-19, 1993).
2. S. Verhaverbeke *et al*, Semicon/Japan, (Chiba, Japan, Dec. 1-3, 1993).
3. T. Kusaka, Y. Ohji and K. Mukai, Ext. Abstracts of the 18th SSDM, (JSAP, 1986), pp 463-466.
4. B.B. Triplett, 7th Int. Symp. on Silicon Mat. Science and Technol., (Electrochem. Soc., NJ, 1994), pp 333-345.
5. M. Depas *et al*, Proc. of the 1994 VLSI Symp., (IEEE, NJ, 1994), p 23-24.
6. P.W. Mertens *et al*, IES 40th Annual Technical Meeting 1994 Proc.

ADSORPTION BEHAVIOR OF NONIONIC SURFACTANTS ONTO SILICON

Joong S. Jeon and Srini Raghavan

Department of Materials Science & Engineering
University of Arizona
Tucson, AZ 85721, USA

1. Introduction

Ionic as well as nonionic surfactants are increasingly considered for use in wet cleaning chemicals to improve wettability of silicon,[1,2] to suppress microroughness[3] and to reduce particulate contamination.[4] Although the properties of nonionic surfactants have been widely studied, there are relatively few reported investigations[5] aimed at elucidating their adsorption and desorption behaviors on silicon and their effect on the surface roughness of silicon. In this paper, the adsorption/desorption behavior of a series of octylphenol polyethylene oxide surfactants onto Si using an ATR FT-IR technique is reported. In addition, the effect of surfactant structure in modulating the wettability and the surface roughness of silicon is discussed. The passivation behavior of silicon in surfactant solutions is also reported.

2. Experimental Materials and Methods

Materials: Octylphenol polyethylene oxide (OPEO) nonionic surfactants of different ethylene oxide (EO) chain lengths were used in this investigation. Specifically, surfactants represented by the chemical structure, C_8H_{17}-C_6H_4-$(OCH_2CH_2)_n$-OH (n=5, 9.5, 16 and 30) were used.

For wettability and surface roughness measurements, n(100) Si wafers were cut into 13 mm × 19 mm samples. For the electrochemical passivation study, back side Au-coated p(100) Si wafers were used. All these samples were cleaned in BOE prior to use. The surfactant solutions were prepared in electronic grade DI water and the pH of solutions was adjusted to 9.5 ± 0.1 with NH_4OH. For the ATR FT-IR analysis of adsorption/desorption of surfactants, a flat shaped n(100) Si IRE (internal reflection element) was used. Since water exhibits strong absorbance in the aliphatic IR vibration range of alkyl surfactants, D_2O was used in the preparation of surfactant solutions.

Experimental Methods: The surface tension of surfactant solutions and the wettability of silicon in these solutions were measured using a dynamic contact angle analyzer (Cahn DCA-312) at an immersion/emersion rate of 64 μm/sec. The adsorption density of surfactants was measured using an ATR liquid flow

cell coupled with a FT-IR spectrophotometer (Perkin-Elmer 1725X). For the calculation of adsorption density, the IR spectra of aliphatic region (2800~3050 cm^{-1}) was monitored and the integrated spectral absorbance was determined. At the end of the adsorption experiments, fresh D_2O was pumped through the cell to investigate the desorption behavior of adsorbed surfactants. The extent of adsorption/desorption of surfactant (mole/cm^2) was calculated from the measured spectral absorbance using an equation based on a step-type adsorption profile.[5,6]

Atomic force microscopy (Digital Nanoscope II) was used to measure the root-mean-square surface roughness (R_{rms}) of silicon samples conditioned in alkaline solutions (pH=9.5±0.1) with and without the addition of OPEO surfactants. For the electrochemical investigations of the passivation of silicon, potentiodynamic polarization experiments were performed using an EG&G Potentiostat/Galvanostat (Model 273A) at a scan rate of 0.5 mV/sec.

3. Results and Discussion

The properties of OPEO nonionic surfactants used in this work were first characterized by the measurement of surface tension of their solutions at a pH of 9.5, and the results are shown in Fig. 1. Surface tension and CMC (critical micelle concentration) were affected by the length of polyethylene oxide chain. As the length of the hydrophilic EO chain in the surfactant molecule increased, the adsorption at the air/solution interface decreased and the CMC shifted to higher values.

Contact angles of OPEO surfactant solutions on silicon were measured to evaluate the change in wettability of silicon. As the solution concentration of surfactant increased, the wettability of silicon increased as shown in Fig. 2. This indicates that the EO groups are oriented toward the aqueous phase upon adsorption of the surfactants onto the hydrophobic silicon surface. Silicon was completely wettable in solutions of short EO chain (n=5 and 9.5) surfactants. Long EO chain (n=16 and 30) surfactant solutions exhibited finite contact angles even at CMC.

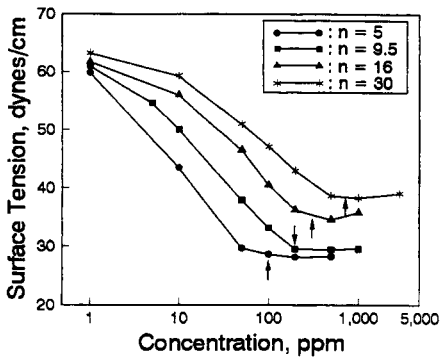

Fig. 1, Surface tension of OPEO surfactants (pH=9.5).

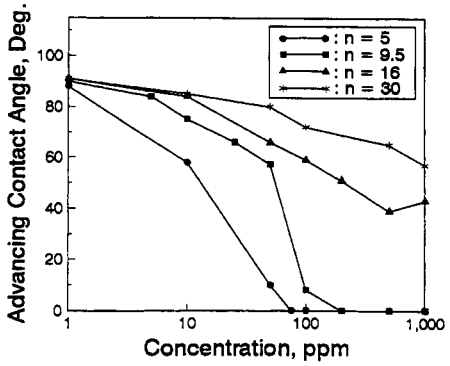

Fig. 2, Wettability of Si in OPEO surfactant solutions (pH=9.5).

In Fig. 3, adsorption isotherms for OPEO surfactants on silicon are plotted. It may be seen that the highest adsorption of different surfactants occurred around their CMC values. An increase in the EO chain length resulted in a decrease in adsorption density. It thus appears that adsorption of nonionic surfactants is mainly controlled by hydrophobic attractions between the alkyl chain and the silicon surface.

In the wet processing of silicon, the surfactant that adsorbs from a cleaning or etching solution should be easily desorbable in the subsequent rinsing step. The amount of OPEO surfactants that remained on silicon was measured as a function of washing time, and the results are shown in Fig. 4. It was found that OPEO surfactants were generally desorbable from the silicon surface. In the case of the long chain OPEO (n=30) surfactant, almost complete desorption took place in about 30 min. In contrast, short chain OPEO surfactants exhibited incomplete removal in the same time period.

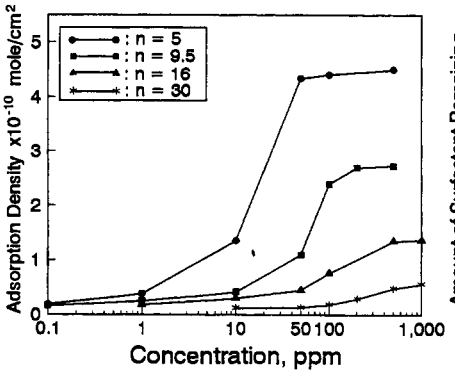

Fig. 3, Adsorption isotherms of OPEO surfactants onto silicon.

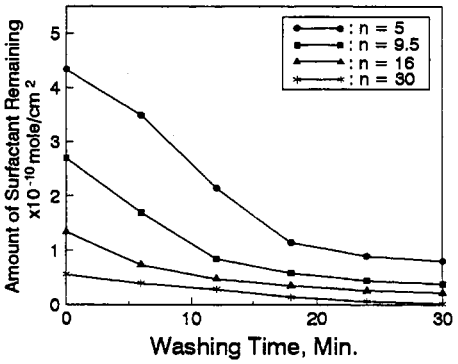

Fig. 4, Amount of surfactant remaining on Si as a function of washing time

Fig. 5 shows the surface roughness of silicon samples which were first conditioned in a series of OPEO surfactant solutions (pH=9.5, 30 min, CMC), and then cleaned in piranha followed by BOE and DI water to remove residual surfactant. The addition of surfactant to alkaline solutions suppressed surface roughness of silicon; however the degree of surface roughness was influenced by the structure of surfactants. A surfactant which had a longer EO chain (lower adsorption) was less effective in preventing microroughness.

Anodic polarization of silicon in surfactant solutions maintained at a pH of 9.5 yielded polarization curves which are typical for materials that undergo passivation. Fig. 6 shows the effect of surfactant (OPEO, n=9.5) concentration on the critical current density for passivation (i_{crit}) and passive current density (i_{pass}) of silicon at a solution of pH of 9.5. The critical current density for passivation decreased as the surfactant concentration was increased, and the passive current density was insensitive to the surfactant concentration. The magnitude of the passive current density was similar to that measured by Allonque et. al.[7] Thus, it appears that Si may be more

easily passivated in alkaline solutions by the addition of surfactants.

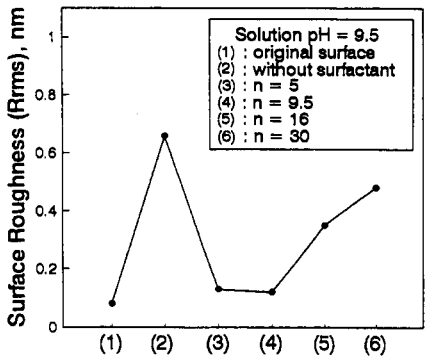

Fig. 5, Effect of surfactant structure on the surface roughness of silicon.

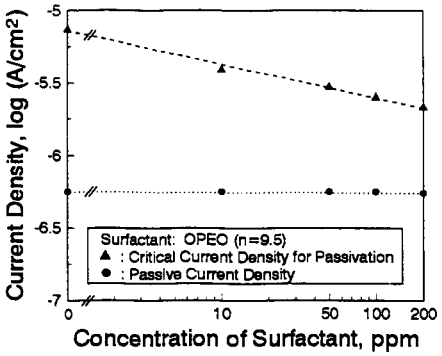

Fig. 6, Effect of the concentration of surfactant on the critical and passive current densities of silicon.

4. Conclusions

The adsorption/desorption behavior of OPEO surfactants were affected by the length of EO group. Short EO chain OPEO (n=5 and 9.5) surfactants were very effective in preventing surface roughness and improving the wettability of Si, but the desorption of these surfactants was slow. While the long chain OPEO surfactant (n=30) exhibited almost complete removal, it was not effective in preventing the formation of a rough surface.

Acknowledgment: The authors wish to acknowledge the Center for Microcontamination Control at the University of Arizona for the financial support to carry out this work.

References

1. H. Kikuyama, N. Miki, K. Saka, J. Takano, I. Kawanabe, M. Miyashita, and T. Ohmi, IEEE Trans. Semicon. Manuf., 3 (1990) 99.
2. J. S. Jeon and S. Raghavan, Proceed. of the 39th Annual Meeting of IES (1993) 268.
3. M. Miyamoto, N. Kita, S. Ishida, and T. Tatsuno, Electrochem. Soc. Extended Abs., 93-2 (1993) 283.
4. T. Kezuka, M. Ishii, T. Umemoto, M. Itano, M. Kubo, and T. Ohmi, Proceed. of the 40th Annual Meeting of IES (1994) 283.
5. J. S. Jeon, S. Raghavan, and R. P. Sperline, submitted to J. Electrochem. Soc., (1994).
6. R. P. Sperline, S. Muralidharan, and H. Freiser, Langmuir, 3 (1987) 198.
7. P. Allongue, V. Bertagna, V. Kieling, and H. Gerischer, J. Vac. Sci. Techol. B, 12 (1994) 1539.

PERFECT CLEANING TECHNOLOGY AND ANALYSIS FOR ORGANIC CONTAMINANTS ON Si WAFER SURFACE

Naomichi YONEKAWA, Sinichi YASUI and Tadahiro OHMI
Department of Electronics, Faculty of Engineering, Tohoku University
Aza Aoba, Aramaki, Aoba-ku, Sendai, Japan, 980

1. INTRODUCTION

It is very difficult to analyze the hydrocarbons on the Si wafer surface [1-2]. We have used the FT-IR-ATR which can directly detect the hydrocarbons on the Si wafer surfaces. However, there was not a calibration method for the FT-IR-ATR. Therefore, we have conceived the calibration method using the Langmuir-Blodgett-monolayer.

When the Si wafer is exposed to the ambience, the growth of native oxide is generally known [3]. Moreover, the organic impurities easily adhere onto the Si wafer surfaces. The Si wafer, therefore, must not be exposed to the ambience. For that reason, the advanced N_2 sealed wet station is required for the future semiconductor manufacturing.

2. SYSTEM DESCRIPTION

The ozonized ultrapure water has been used for the removal of hydrocarbons. Using ozone is advantageous for the environment, the air condition of the cleanroom and the damage for the Si wafers. This is because it is not necessary for the recovery of the waste, moreover, it is a low temperature process [4]. We have used the Dynamic-Spin-Cleaning method with the ozonized ultrapure water [5]. Figure 1 shows the structure of the Dynamic-Spin-Cleaning System. The wafer is mounted onto a special chuck in the cleaning chamber. The cleaning chemicals, the ozonized ultrapure water and the ultrapure water are introduced onto the Si wafer surface through a mobile nozzle while the wafer is being rotated. Inside of the chamber is constantly purged with high purity N_2 gas in order to prevent the contamination from the ambience.

For the analysis of the organic contaminants on the wafer surfaces, we have used the FT-IR-ATR method (Fig. 2). Generally, the method of the using both-side-polished wafers as the ATR-prism is used. However, the background spectrum in this method contains the remained hydrocarbon peaks. This is because the background spectrum is influenced by the Si wafer itself. Accordingly, this method can not confirm a very small amount of the hydrocarbons. This problem is solved by using an ATR-prism made from the other materials, like as germanium. Using other materials as the ATR-prism can correct the exact background spectrum which does not include the remained hydrocarbon peaks. Therefore, a very small amount of the organic impurities can be detected.

3. CALIBRATION METHOD FOR FT-IR-ATR

At present, the FT-IR-ATR method could not be calibrated. Therefore,

it is difficult to estimate the amount of the hydrocarbons on the wafer surfaces.

We have conceived the calibration method which is the measurement of the Langmuir-Blodgett-monolayer. The Langmuir-Blodgett-monolayer has adhered onto some kind of areas on the calibration samples, such as the complete area, the 1/2 area, the 1/4 area and the 1/8 area. The complete area is called the monolayer, the 1/2 area is called the 1/2 layer, similarly the 1/4 layer, the 1/8 layer (Fig. 3). These molecule-films have a good reproducibility. It is possible, therefore, for the calibration to use the Langmuir-Blodgett-monolayer.

Figure 4 shows the FT-IR spectrum of the monolayer, the 1/2 layer, the 1/4 layer and the 1/8 layer. The calibration curves for the FT-IR-ATR of the each polarization are shown in figure 5. The linearity of the absorbance of the each layer is confirmed by these figures. These results demonstrate that the calibration of the FT-IR-ATR has been established. The amount of the hydrocarbons on the wafer surfaces, therefore, can be estimated.

4. THE REMOVAL OF ORGANIC IMPURITIES

The FT-IR spectrums of the unintentionally contaminated wafers are shown in figure 6. The as-received wafer was not treated. The other wafers were treated by the each cleaning methods and the agents. This figure demonstrates that as-received wafer is contaminated by the unknown hydrocarbons. Moreover, the organic contaminants can not be completely removed in the case of the conventional dipping cleaning, because the hydrocarbon remains on the wafer surface. However, the combination of the Dynamic-Spin-Cleaning with the ozonized ultrapure water can perfectly remove the hydrocarbons from the wafer surface.

Figure 7 shows the spectrums of the intentionally contaminated wafers and the spectrums of the after cleaned wafers. For the experiment of the cleaning efficiency, the intentionally contaminated wafers with the each surfactant as the organic contaminants were used. This result demonstrates that the SPM solution and the ozonized ultrapure water can not perfectly remove the organic impurities in the dipping mode. However, the organic impurities can be completely removed by a combination of the Dynamic-Spin-Cleaning method with the ozonized ultrapure water. This is because the Dynamic-Spin-Cleaning system is constantly purged high-purity N_2 gas, therefore, the cross-contamination and the readhesion are not occurred. And the chemical mixing and the chemical flow speed are accelerated by the centrifugal force, the reaction products are quickly formed, and they are immediately removed from the wafer surface. Therefore, Dynamic-Spin-Cleaning method is more effective than the conventional dipping cleaning.

Table 1 demonstrates the contaminated level of the each wafers which can be estimated from the calibration curves. The each wafers were contaminated by the unknown hydrocarbons which is estimated as the arachidic acid.

5. CONCLUSIONS

The FT-IR-ATR can directly detect a very small amount of hydrocarbons on the wafer surfaces. The calibration method for the FT-IR-ATR could be established by using of the Langmuir-Blodgett-monolayer. It is possible, therefore, to confirm the contamination level of the hydrocarbons on the Si wafer surfaces.

The organic contamination free Si wafer surface can be realized by the combination of the Dynamic-Spin-Cleaning-System with the ozonized ultrapure water. And it is essential to realize the advanced cleaning process to make the ultraclean wafer surface. Following the results have been obtained by a simulation test ;

1. The analysis method for a very small amount of hydrocarbons on the Si wafer surfaces has been established by the FT-IR-ATR with the calibration method. The hydrocarbons on the Si wafer surfaces can be inferred from the calibration curves as the molecule layer.
2. The combination the Dynamic-Cleaning-System with the ozonized ultrapure water can effectively remove the organic contaminants which are difficult to remove by the conventional dipping cleaning. Moreover, it is not necessary recover the waste and it is environmental friendly.

The Dynamic-Cleaning method has the excellent characteristic for the removal of the organic impurities. The analysis of the hydrocarbons has become possible. Therefore, the efficiency of the Dynamic-Spin-Cleaning method can be confirmed.

6. REFERENCES

1. N.Yonekawa, S.Yasui, F.Kunimoto, F.W.Kern,Jr. and T.Ohmi, Proc. of ECS Soc., Vol.94-7, pp.94-101, 1993.
2. H.Bender, S.Verhaverbeke and M.M.Heyns, Proc. of ECS Soc., Vol.94-7, pp.186-194, 1993.
3. T.Ohmi, T.Isagawa, M.Kogure and T.Imaoka, Journal of ECS, Vol.140, No.3, March 1993.
4. M.Kogure, T.Isagawa, T.Futatsuki, N.Yonekawa and T.Ohmi, 1993 Proc., 39th Annual Technical Meeting, IES, Vol.1, pp.282-287,
5. N.Yonekawa, S.Yasui and T.Ohmi, 1994 Proc. Vol. 1, pp.419-424, 40th Annual Technical Meeting, IES.

Table 1. Comparison of hydrocarbon adhesion

Treatment	As-R.	SPM	O_3	SPIN
Number of layer [-]	0.16	0.04	0.03	0
Number of molecules [$x10^{15}$]	0.93	0.24	0.17	0
Number of CH_2-CH_2 [$x10^{15}$]	31	7.9	5.8	0

As-R : As-received wafer
SPM : H_2SO_4/H_2O_2 dipping cleaning
O_3 : O_3 UPW dipping cleaning
SPIN : O_3 UPW dynamic cleaning

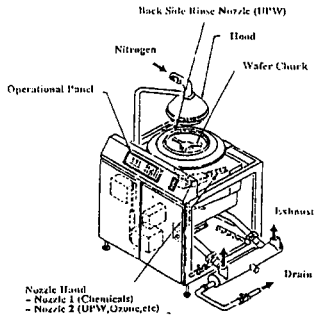

Fig. 1 Dynamic Cleaning System

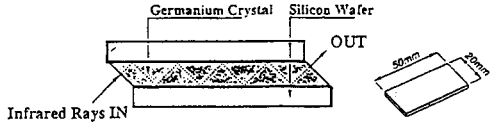

Silicon Wafer = Sample , Germanium Crystal = Prism

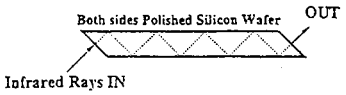

Silicon Wafer = Sample = Prism

Fig. 2 FT-IR-ATR method

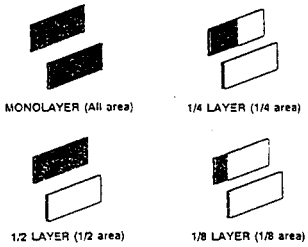

Fig. 3 LB monolayer adhesion area

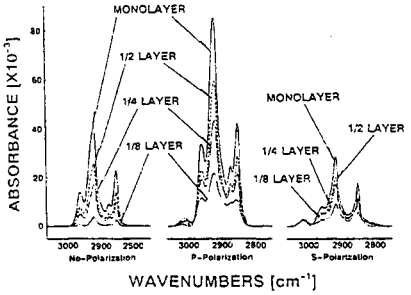

Fig. 4 FT-IR spectrum of LB monolayer (1/8, 1/4, 1/2, mono)

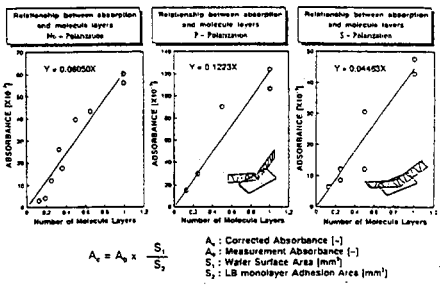

Fig. 5 The calibration curves for FT-IR-ATR by LB monolayer

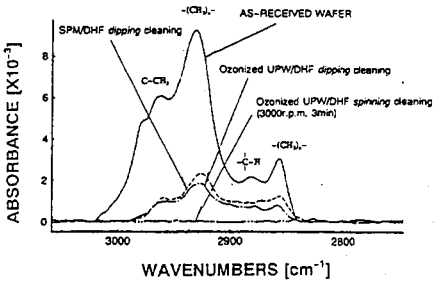

Fig. 6 Cleaning efficiency of each cleaning method for unintentionally contaminated wafer

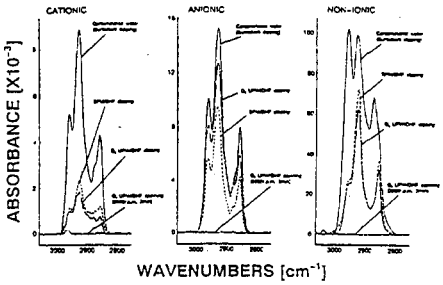

Fig. 7 Cleaning efficiency of various cleaning method for intentionally contaminated wafer

ASHING WITHOUT ACID: AN ASSESSMENT OF MODERN PHOTORESIST STRIPPERS

Lee M. Loewenstein & George Brown, Semiconductor Process and Device Center, Texas Instruments Incorporated, Dallas, Texas 75265, U.S.A.

1. INTRODUCTION

Cleanup processes will need to change to meet the demands facing them. Current processes need liquid reagents to clean well. Ever smaller device features will increasingly challenge liquid cleaning methods. Chemical purity, particle levels, operator safety, chemical disposal, equipment cost, cycle time and tool footprint will become increasingly important. These factors require us to consider alternative cleaning approaches. In this paper, we will consider different ways for removing photoresist, without using any liquid acids or oxidants, such as the commonly used piranha chemistries of H_2SO_4 and H_2O_2. While a completely dry process is desirable, photoresists contain substances such as sodium that are hard to volatilize. As a consequence, acceptable resist ashing processes will need to use water rinsing for the time being.

2. EXPERIMENTAL

We tested the following ashing methods: remote microwave plasma (μW), remote microwave/reactive ion etching (μW/RIE), high pressure triode (HPT), ozone and laser ablation (LA). All work, excluding LA, was done on commercially available tools. A post-ash rinse followed processing. The techniques can be described briefly:

- *μW*: The plasma region is far from the wafer, preventing direct bombardment of the wafer by ions or photons. Process chemistry is O_2 with another gas such as H_2, N_2 or N_2O added to increase the ashing rate. NF_3 or CF_4 may be used with O_2.
- *μW/RIE*: RIE is used to remove surface residues such as an implantation crust. The μW part is the same as above. Process chemistry includes O_2, H_2 and CF_4 in several process steps.
- HPT: The discharge region is above the wafer; however, the plasma is largely confined by grids. Process chemistry includes O_2 and C_2F_6.
- *Ozone*: O_3 is produced remotely in a high pressure corona discharge. The O_3/O_2 mixture passes over heated wafers, sometimes with UV radiation.
- *LA*: A beam from an excimer or other laser sweeps the wafer surface. The wafer is typically in O_2.

Successfully removing photoresist depends on accounting for the processing that that photoresist has experienced. Removing the photoresist is fairly easy: the difficult part lies in removing the contaminants dispersed in the photoresist. We thus processed wafers under different conditions to test the ability of each process tool to remove the photoresist and all residues. Photoresist was PFI26A - 1.3-1.6 μm - with UV hard baking. Table 1 summarizes the processes of the study.

Table 1. Wafer processing before photoresist ashing.

Process	*Conditions*
Ion implantation	Implanted P, 70 KeV, $3x10^{15}$ ions/cm^2 using Varian E220 implanter.
Polysilicon gate etch	Etched P-doped polysilicon: 3500 Å poly-Si using Cl_2/HBr in a Applied Materials 5000 reactor.
Si_3N_4 isolation etch	Etched 2500 Å Si_3N_4 on SiO_2 using CHF_3/CF_4/Ar in a Texas Instruments Advanced Vacuum Processor .[1]
SiO_2 via etch	Etched 10,000 Å PETEOS on TiN/Al/TiN stack using CHF_3/O_2 in a Lam Rainbow 4500 reactor.

3. RESULTS

Table 2 summarizes the ashing results that we observed by SEM. We ran splits to determine whether our processes left residues after standard ashing. They did. We also ran splits that followed the ashing with wet cleanup. For most material, the wet cleanup consisted of an acid resist strip and rinse. For the wafers with via etch, cleanup was a solvent clean. These procedures were successful in removing residues.

Table 2. Amount of residue remaining observed by SEM. Microwave processing was tested with (μW-F) and without (μW-No F) fluorine chemistries.

Process	*LA**	*Ozone*	*μW-No F*	*μW-F*	*HPT*	*μW/RIE*
Implant	Incomplete	Slight	Slight	Slight	Clear	Clear
Poly etch	Incomplete	Slight	Slight	Clear	Clear	Clear/Res.†
Nitride etch	Incomplete	Residue	Slight	Slight	Clear	Clear
Via etch	Incomplete	Slight	Residue	Slight	Clear‡	n.a.

*Observation by optical microscope only. Photoresist removal was incomplete. †Some areas were clear, and some still had residues. ‡Possible undercutting of oxide layer occurred.

The HPT and μW/RIE strippers result in the cleanest appearing wafers. But at what cost? The HPT and μW/RIE processes achieve their clean surfaces by bringing plasma near the wafer. This may cause electrical damage to the remaining films. Through additional investigations using μW processing, we found that the chemistry chosen has a significant effect on surface cleanliness. As the mechanism for obtaining cleaner surfaces seems to involve addition of a

fluorine-bearing agent (CF_4, C_2F_6, NF_3) which etches small amounts of SiO_2, we must question the neutrality of the cleanup on the eventual electrical properties of constructed devices. The role of F cannot be emphasized too strongly. The improvements shown by adding F to the μW process were the result of only preliminary work. With additional time, there is no reason to believe that the μW approach could not be as good as the HPT and μW/RIE processes.

We tested *n* and *p*-type Si (100) wafers for electrical damage. We ashed wafers after patterned silicon nitride etching. We processed the wafers after ashing to make MOS capacitors. The wafers undergoing nitride etch made wafers with field oxide isolated test areas. The patterned nitride etch defined these areas. Polysilicon gates were formed on all wafers.

Electrical results are shown in Table 3. S_{FN} chronicles the capacitor breakdown events that resulted from nondestructive Fowler-Nordheim tunneling. The breakdown voltage (*BV*) gives the median breakdown voltage. Mobile ion levels (Q_{mi}) are calculated from bias-stress tests. T_{geff} is the recombination lifetime and S_O the recombination velocity. Q_f is the fixed charge density. The control values result from two witness wafers which traveled along with test wafers to each manufacturer. One witness wafer was stripped prior to shipment using a μW-based ash followed by Nanostrip. The other wafer went out to the vendor with photoresist on it, and was stripped on its return. All wafers were then merged into one lot for the remaining MOS capacitor formation steps.

S_{FN} and *BV* are clearly equivalent to the controls. All of the measured Q_{mi} are essentially at the background level for the measurement so no meaningful distinction between them can be made. Due to the time-consuming nature of Q_{mi}

Table 3. Electrical characteristics of MOS capacitors formed after silicon nitride etch. Values are for *p*-type Si substrates unless noted.

Process	*Ozone*	*μW-No F*	*HPT*	*μW/RIE*	*Control*
S_{FN} *(%)*	97.5	97.5	97.2	98.0	97.5
BV (MV/cm)	8.4	8.4	8.4	8.4	8.4
Q_{mi} $(10^9\ cm^{-2})$	-2.27*	-0.50*	2.63	0.18	2.3†
T_{geff} *(μsec)*	259±33	891±218	412±192	365±191	281±117
T_{geff}‡	291	138	234	266	282
S_O *(cm/sec)*	1.33	0.867	1.06	1.05	0.667
S_O‡	1.05	0.916	0.857	0.784	0.737
Q_f/q $(10^9\ cm^{-2})$	130±14	135±7	125±7	66.5±75.7	123±15
$Q_{f/a}$‡	180	80	78	80	n.a.

*Negative values represent unmeasurably small charges and result from slight miscalibration of equipment. †The control value for Q_{mi} includes one small negative value. Rather than artificially depressing the control value, this value represents the average of the absolute values of measured Q_{mi}s. ‡Value for n-Si.

measurements, we did them only for *p*-Si wafers. For T_{geff}, where larger is better, all of the dry ash techniques performed as well or better than the control. The *μW-No F* may be superior to the control, however the *n*-Si results do not support this. Similar comments apply to the related quantity, S_O. Values for Q_f are comparable to the controls for all ashers. The difference for the *μW/RIE* asher is not statistically significant.

4. DISCUSSION

Huynh and Mitchener have compared ozone and μW-based ashing,[2] including post-ash wet strips of H_2SO_4/HNO_3 and H_2SO_4/H_2O_2. They found ozone to give better *Qmi* than μW at process temperatures above 200 °C. In our own study, *at fixed temperature*, we were not able to make this distinction. Other work has found lower flatband voltage shifts for μW than RF ashers.[3,4] In the system we tested closest to RF - HPT - we saw a slightly larger value for Q_{mi}, but this value is still comparable to the control.

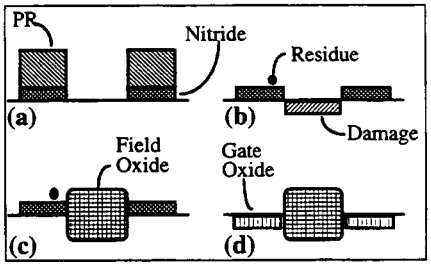

Fig. 1. (a) Nitride with photoresist (PR) after etching, (b) possible residue on nitride and damage to Si, (c) field oxide grown in regions defined by nitride mask, and (d) gate oxide grown after nitride stripping.

Each dry ash may be as good as the standard wet clean. Or we simply may not have done the right tests to show contamination and damage. We ashed after the nitride strip because it was a step which could very naturally be included in a standard MOS capacitor flow. The rest of the flow was unperturbed. This included the prefurnace cleans prior to field and gate oxidation. These cleans could remove any contamination. Moreover, the nitride layer is stripped during the process flow, and any residues on it presumably are removed at the same time. Substrate damage is most likely to occur where the field oxide is grown. The growth of this oxide could consume any regions of damaged Si. The gate oxides formed where the nitride mask once lay, will likely show only little sensitivity to any remaining damage. After isolation nitride patterning, post-ash residue cleans may be unnecessary.

References

[1]G.G. Barna, L.M. Loewenstein, R. Robbins, S. O'Brien, A. Lane, D.D. White, M. Hanratty, J. Hosch, G.B. Shinn, K. Taylor and K. Brankner, *IEEE Trans. Semicond. Manuf.* **7**, 149 (1994).
[2]C.K. Huynh and J.C. Mitchener, *J. Vac. Sci. Technol. B* **9**, 353 (1994).
[3]P.I. Mikulan, O.O. Awadelkarim, S.J. Fonash, T. Ta and Y.D. Chan, *Electrochem. Soc. Ext. Abstr.* **93-1**, 417 (1993).
[4]T. Ta, *Electrochem. Soc. Ext. Abstr.* **93-1**, 417 (1993).

CHARACTERIZATION OF THE REMOVAL OF HMDS MONOLAYERS

N. Porfiris[†], J. Newby, [‡], A.M.Gundlach[†], R. Pethrick[‡], S.Affrossman[‡], A. Tannahill[††]

1. INTRODUCTION

Surface primers are used in semiconductor manufacturing prior to the resist coating to promote adhesion and to reduce lift off of resist during development and undercut or lift off during subsequent process steps[1]. In-line, vapour phase HMDS (hexamethyldisilazane) coating is the most efficient way to convert the polar hydroxyl groups of the silicon substrate into non-polar trimethylsilyl (TMS) groups [2, 3, 4]. Conventional solvent systems are not efficient in breaking the bonds between the TMS groups and the substrate. Incomplete removal of HMDS, adversely affects device yield due to the attraction of contamination to residues [5], resulting in micromasking and poor metal contacts with degraded electrical properties.

2. EXPERIMENTAL PROCEDURES

The purpose of the study is to investigate which type of wet chemistry is most effective in the complete removal of the HMDS monolayer. This task is accomplished by the parallel use of a variety of characterization techniques to investigate the presence and removal of the TMS groups.

2.1. Materials.

For the silicon substrate study, p-type (Boron, 14-20 Ohm cm), (100), 3" silicon wafers have been used. Silicon dioxide film is thermally grown at a thickness of 1000Å by a dry oxidation of the Si wafers at 1100 °C. The silicon nitride film of 500 Å, is deposited by use of LPCVD. The reactive gases used are SiH_2Cl_2 and NH_3 at 800 °C. The substrates are subsequently coated with either HMDS on its own or HMDS and photoresist. A dehydration bake at 100°C is used immediately prior to the HMDS coating. Two slightly different novolak-based photoresists have been employed; the OCG-6512, g-line resist by Olin Hunt and the OFPR-800, high temperature, g-line resist by OHKA.

2.2. Stripper chemistries.

All the substrates have been treated under a variety of processing conditions by a range of conventional solvent resist strippers; pure NMP(N-Methyl-Pyrrolidone), DGA, Posistrip-830 (EKC) and Posistrip-854 (EKC). The control wafers in Figure 1 are *unprimed substrates* that undergo the same chemical treatment as the primed wafers. A reactive stripper, the hydroxylamine-based chemistry

† EMF, Electrical Engineering Dept, University of Edinburgh, UK.
‡ Dept of Pure and Applied Chemistry, Strathclyde University, UK.
†† EKC Technology Ltd, East Kilbride, UK.

EKC 265 [1], has been also evaluated. Fuming nitric acid, at room temperature, has been used as a benchmark test.

2.3. Characterization techniques.

The surfaces of the samples have been characterized by use of contact angle measurements, static SIMS and particle count measurements by use of a SURFSCAN. Contact angle measurements were employed to investigate the wettability of the resulting surfaces. Based on previous gas adsorption studies [6] triply distilled DI water was used to minimize the error due to factors related to water quality. The droplets shape (by taking the average measurement from five droplets) and droplets volume (by use of a microsyringe for accurate droplet volume of $10\mu L$) were also controlled. In order to avoid the error associated with droplet evaporation, the contact angle was recorded every 15s, 30s, 45s and 60s after the droplet was placed on the wafer. Particle count measurements (SURFSCAN) were used as a measure of the TMS residues on the wafer surface, while static Secondary Ion Mass Spectroscopy (SIMS) was used to quantitatively assess the surface coverage by the TMS group both prior to and after the various cleaning treatments.

3. RESULTS AND DISCUSSION

3.1 Contact angle measurements.

The 20° contact angle of the hydrophilic Si surface is increased to 52° and 55° after the 30s and 60s HMDS priming respectively. This increase is due to the ability of the TMS group to partially hydrophobe the Si surface. From Figure 1 it is obvious that fuming nitric acid removes the TMS group and lowers the contact angle value to the clean Si level. The contact angle data comparison for Si substrates in Figure 1, indicates that Posistrip-830, Posistrip-854, DGA and NMP are inefficient in removing the TMS groups that are present after the priming. Posistrip-830 partially removes the TMS groups and slightly reduces the contact angle measured on the Si surface. Increased stripping temperature, from 90°C to 120°C, further reduces the angle by only 4°. Increased stripping time does not make the surface more hydrophilic. The reduction in contact angle obtained by the Posi-830 treatment is due to its DGA component, since immersion of the primed wafer in NMP does not significantly affect the measured contact angle. The results for Posistrip-854 prove its inefficiency in removing the TMS layer. The treatment in the EKC-265 hydroxylamine-based chemistry at temperatures above 67°C for 10 min, removes completely the hydrophobic TMS monolayer and restores the contact angle value to the clean Si level. Contact angle measurements performed on the silicon dioxide and silicon nitride substrates, also indicate that the EKC-265 chemistry is the most suitable in reducing the contact angle of each substrate to the levels prior to the HMDS priming.

3.2 Correlation between static SIMS and contact angle measurements.

The contact angle measured on the substrate can be correlated to the TMS surface coverage [2, 4, 7]. It has been shown that the cosine value of the contact angle [8] is a linear function of the surface coverage of the TMS groups [9, 10]. Since the surface coverage is related to the chemical treatment of the surface, a quantitative assessment of the efficiency of each chemistry can be established. The relative surface coverage for TMS groups on Si versus the cosine of the contact angle is plotted in Figure 2. The TMS surface coverage has been estimated from the ratio $^{73}(CH_3)_3Si^+/[^{73}(CH_3)_3Si^+ + {}^{28}Si^+]$ of the integrated signal intensity peaks, as measured by static SIMS on a range of samples exposed to HMDS vapour for various times. The fitted line of Figure 2 can be used to qualitatively assess the

[1] US patent number 5334332 for EKC Technology Ltd; Foreign patent pending.

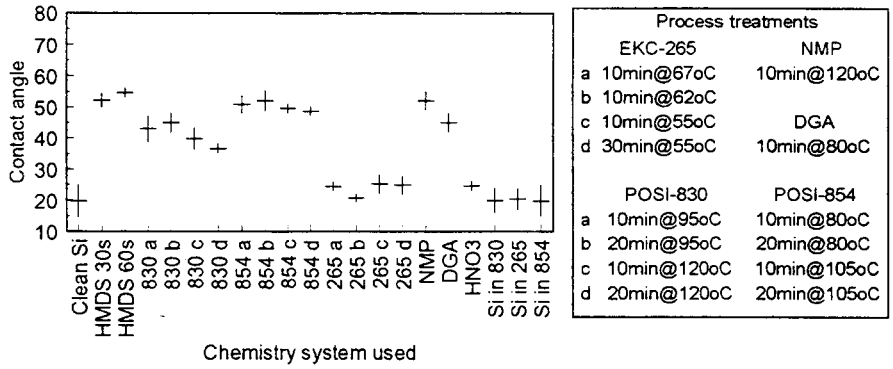

Figure 1. The contact angle measurements on Si substrate under various chemistries and process conditions.

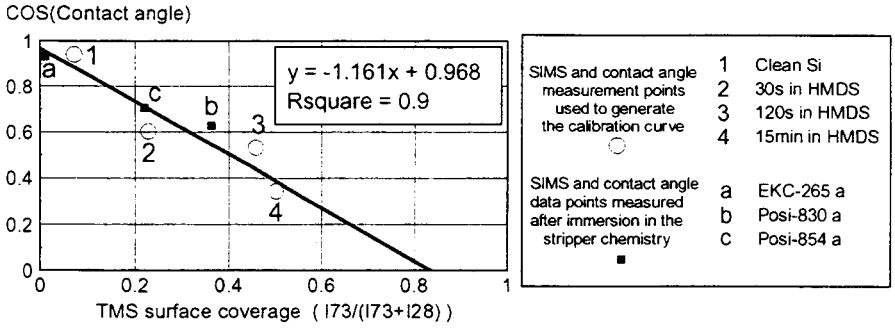

Figure 2. The SIMS-contact angle calibration curve is created by data points 1 to 4. Post stripping measurements (data points a to c) indicate the effectiveness of TMS removal for each chemistry.

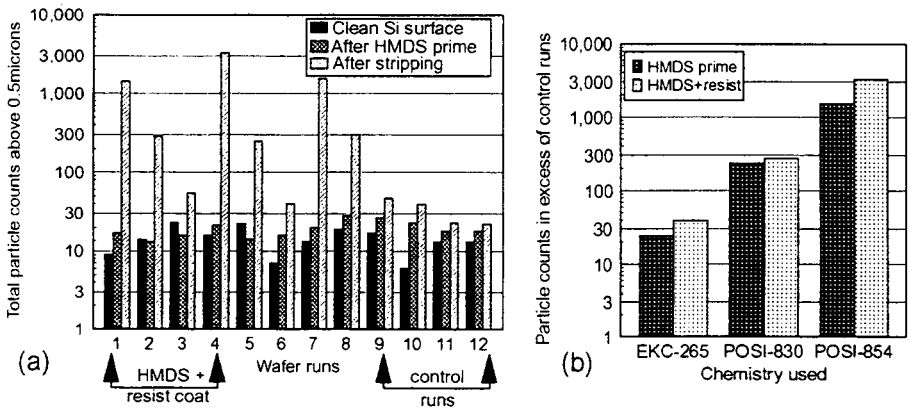

Figure 3. **(a)** The SURFSCAN particle counts for the various chemistries.
(b) The particle counts in excess of the control runs for each chemistry, on both HMDS and HMDS+resist coated wafers, indicate an eggectiveTMS group removal only by EKC-265 (least excess particles counts).

effectiveness of EKC-265 and the inability of conventional strippers, such as Posi-830 and Posi-854, to remove the HMDS monolayer.

3.3 Correlation betweeen particle measurements and TMS removal.

The total particle counts of the silicon surfaces measured prior to any processing, after the HMDS priming and after the priming and stripping steps are shown in Figure 3a. The control runs 10, 11 and 12 are used to monitor any increase in particle counts on the unprimed Si wafers, due to processing in the 854, 830 and 265 baths. Runs 1 to 4 include the wafers that are coated with resist on top of the HMDS, while the rest of the runs include only HMDS primed wafers. The particle counts on the control runs indicate an addition of a small number of particles on the Si surface after the chemical treatments. In contrast, the remaining runs with the exception of runs 3, 6 and 9, indicate an increase by at least two orders of magnitude in particle counts. The particle count increase in excess of the one observed in the control runs for each chemistry, can only be explained by the assumption that *TMS groups have been partially removed.* The excess particle counts for each chemistry are plotted in Figure 3b and agree with the contact angle and SIMS results. Runs 4 and 7, which were processed in Posi-854, indicate the largest particle count increase. Stripping in EKC-265, in runs 3 and 6, proves to be the most efficient method in removing TMS groups from the surface since the increase in particle counts is of the same order as the results of the control run, run 12. Posi-830 particle counts in runs 2 and 5 indicate that only a partial removal of the TMS group is achieved.

4. CONCLUSIONS

Hydroxylamine-based chemistry, due to its reactive nature, proves more efficient than conventional solvent chemistries in removing the HMDS coating from Si, SiO_2 and Si_3N_4 wafer surfaces. Therefore, it can be used in a single process step, to remove both HMDS and photoresist layer. It also complies with much tighter safety rules when compared to the hazardness of fuming nitric acid and sulfuric acid or the higher operating temperatures required for common organic solvents.

References

[1] K. L. Mittal. *Solid State Technology*, 22(5):89, 1979.

[2] M.C.B.A. Michielsen, V. B. Marriott, J.J. Ponjee, H. van der Wel, F.J. Touwslager, and J.A.H.M Moonen. *Microelectronic Engineer*, (11):475–480, 1990.

[3] B. Mohondro. Resist Adhesion Promoter Application. *European Semiconductor*, (11):14–15, 1991.

[4] J.J. Ponjee, V.B. Marriott, M.C.B.A. Michielsen, F.J. Touwslager, P.N.T. van Velzen, and H. van der Wel. *Journal of Vacuum Science and Technology B*, 8(3):475–480, 1990.

[5] M. A. Logan, D. L. O'Meara, and J. R. Monkowfski. In *Proceedings of the Microcontamination Conference and Exposition*, pages 111–122. Canon Communications, Santa Monica, CA, 1986.

[6] Y. Suzuki, T. Kajima, S. Nishiate, and T. Sekiguchi. Gas Adsorption on Wafers. *Microelectronics Manufacturing Technology*, (12):38–41, 1991.

[7] P.N.T. van Velzen, , J.J. Ponjee, and A. Benninghoven. *Appl. Surf. Science*, 37:147, 1989.

[8] A. B. Cassie. *Discuss. Faraday Soc.*, 3:14, 1948.

[9] R. Crawford, L.K.Koopal, and J. Ralston. *Colloids Surf.*, 27:57, 1987.

[10] M.A. Meshcheryakov, Y.G. Frolov, and V.S. Bannikov. *Colloid J. USSR*, 48:862, 1986.

EFFECT OF CHLORINE CONTAMINATED ORGANIC SOLVENT PHOTORESIST STRIPPER ON POST-METAL ETCH CORROSION

A. Philipossian* , J. Fadden, L. Roe and E. Krosche
Intel Corporation, Rio Rancho, NM 87124

1. INTRODUCTION

This study shows the collaboration between Intel and a supplier of an organic solvent photoresist stripper in identifying and resolving a post-metal etch corrosion incident characterized by severe pitting of aluminum lines. To satisfy the supplier's request for anonymity, the organic solvent stripper is referred to as OSS. In-line electrical data from the factory where the incident took place, clearly indicated that lots processed through the problematic batch (referred here as batch "B") had relatively less current flowing through metal lines due to metal thinning and/or disfiguration caused by corrosion.

2. CHEMICAL NON-CONFORMANCE

The problem was hypothesized to be due to abnormal pH and/or elevated amounts of chloride [1-3]. This was based on the fact that most metals corrode in the presence of acids, and some metals and metal oxides such as $Al(OH)_3$ are amphoteric and can also dissolve in basic solutions. Moreover, the passivation layer on metals can be disrupted by the presence of chloride, creating a localized micro-environment that supports metal corrosion (pitting).

The supplier's Certificate of Analysis (CoA) for Batch "B" reported it to be in total conformance in terms of all parametrics including pH and chloride content. In order to verify the supplier's CoA, 3 samples of Batch "B", along with 2 known good batches, were analyzed in-house. An in-house ion chromatographic (IC) technique was developed exclusively for analyzing chloride in the OSS (DL of 100 ppb/w). The results confirmed that all samples had acceptable values of pH. However, samples from Batch "B" had, on the average, 100 times more chloride compared to the control samples and were beyond the 5 ppm/w specification. As a result, all OSS batches at Intel sites, warehouses and *en route* were quarantined. The supplier was asked to re-evaluate their analytical technique while Intel took the responsibility of performing 100 % in-house analysis of OSS batches on a 24-hour turn-around basis.

3. CHLORIDE ANALYSIS

To resolve the difference between the supplier and Intel, the supplier tested spiked samples and found its SEMI-based method did not completely detect the spike.

---

* Intel Corporation, Santa Clara, CA 95052

They refined their turbidimetric method (DL of 1 ppm/w for chloride) and demonstrated consistency with Intel's results in correctly measuring the spiked sample. Several NaCl-spiked OSS samples were prepared and analyzed in triplicates for correlation. In addition, several production batches were also analyzed (including Batch "B"). RSD for both techniques were calculated to be no more than 10 percent. With a coefficient of correlation of 0.99, the above process resulted in the establishment of two independent, fully validated analytical procedures for chloride in the OSS and allowed the transfer of QC analysis back to the supplier.

4. SOURCE OF CHLORIDE

Considering the high levels of chloride in Batch "B", and that this was the only out-of-specification parameter, the team focused exclusively on finding the source. An internal baseline was established to ensure that chloride does not build up inside the stripping tools as a result of the chlorine-based dry etch by-products.

Given that 100 product lots could be processed through the tool in between re-pours, samples were drawn from the drain immediately following OSS batch pour, mid-way through the use of the batch (i.e. after processing 49 product lots), and near the end of the OSS batch (i.e. after processing 92 product lots). Results indicated the chloride level to be 0.9 ppm/w regardless of when the samples were drawn, thus indicating that chloride does not build-up in stripping tools as a function of wafer processing.

In parallel, once chloride was found in Batch "B", the supplier began investigating all possible sources of chloride contamination. A high purity grade of methylene chloride (CH_2Cl_2) was being produced in the facility. The supplier was able to detect roughly 15 ppm/w of CH_2Cl_2 in Batch "B". The production lines for the 2 products were completely dedicated, however both lines employed flexible transfer lines at certain places. The contamination is believed to have occurred when a OSS flexible transfer line was accidentally connected to the CH_2Cl_2 system during a routine re-routing step.

With CH_2Cl_2 identified as a potential source of chloride, the supplier next had to prove it was the source of the inorganic chloride detected in the OSS by undertaking a kinetics study of the reaction of methylene chloride in the stripper. Assuming the rate of loss of CH_2Cl_2 is linear with respect to its concentration, solving the appropriate first order differential equation results in the following expression:

$$C / C_0 = e^{-k \cdot t} \qquad (1)$$

where C and C_0 are the actual and initial CH_2Cl_2 concentration in ppm/w, respectively, k is the rate constant in day^{-1} and t represents time in days.

To test the validity of the kinetics model, OSS samples where spiked with 100 and 10 ppm/w of CH_2Cl_2 and left to age for 49 days while periodically measuring their CH_2Cl_2 content. The samples were stored at room temperature to simulate normal storage conditions (Figure 1). CH_2Cl_2 loss does indeed follow first order kinetics [4] with the best fit for k at 0.014 and 0.019 day^{-1} for 100 and 10 ppm/w initial CH_2Cl_2 concentrations, respectively. Coefficients of correlation were 0.98 and 0.99 for 100 and 10 ppm/w cases, respectively. Methylene chloride seems to have a half-life of 45 to 50 days. Figure 1 also shows the rate of chloride formation in the OSS corresponding to the initial methylene chloride levels. At 100 ppm/w, results indicate that roughly all of the decomposed CH_2Cl_2 yields chloride ions. As for the 10 ppm/w case, due to the lower initial concentration, the process seems to rapidly reach equilibrium. It should be noted that the precision of the analytical techniques employed here for both chloride and methylene chloride is 1 ppm/w, thus making it difficult to accurately interpret the data for the 10 ppm/w initial contamination case. Nevertheless, based on the current 5 ppm/w specification for chloride, results indicate that the concentration of methylene chloride in the OSS should not exceed 10 ppm/w.

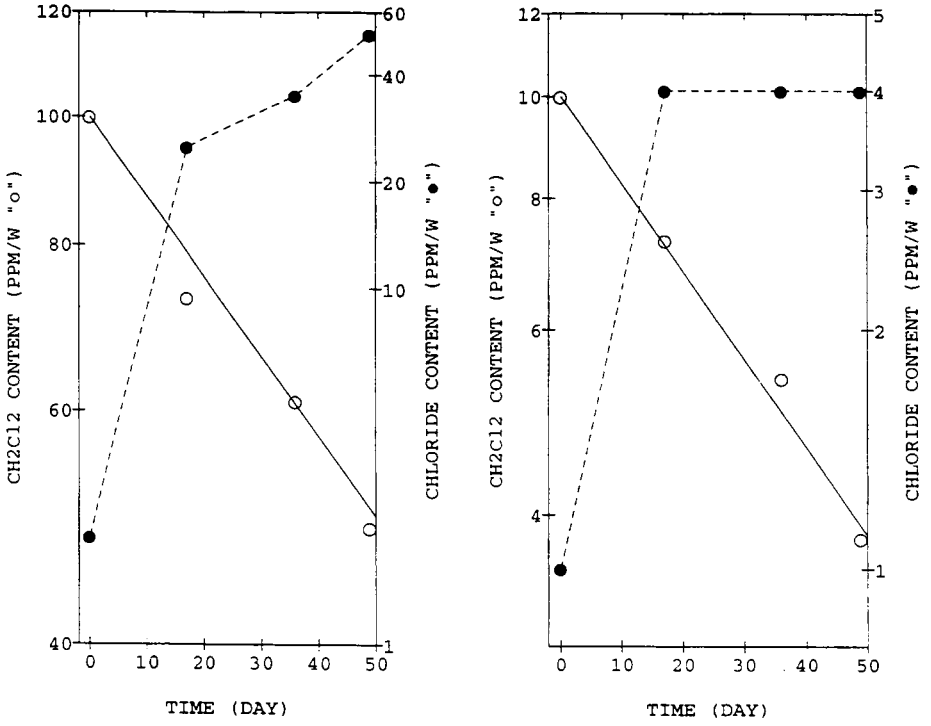

Figure 1. Decomposition of CH_2Cl_2 (o experimental, — theoretical) in OSS at room temperature and formation of chloride (- - • - - experimental) for initial CH_2Cl_2 concentration of 100 ppm/w (left) and 10 ppm/w (right).

5. FUNCTIONAL TESTING

In order to determine whether a correlation existed between the level of chloride contamination in the OSS and the extent of metal corrosion, a series of functional tests were conducted at Intel by processing product wafers using several Cl-spiked OSS solutions. Of the 8 OSS samples, 5 were spiked with HCl and 3 with NaCl to determine whether the chloride source had an effect on the extent of corrosion. Following processing, wafers were cleaned in an oxygen plasma (to remove photoresist residues from metal surface) and the extent of metal corrosion was quantified using Scanning Electron Microscopy.

The resulting micrographs (not shown here) showed 2 types of corrosion defects: voids (or pitting) and protrusions (or corrosion reaction by-products). The extent of corrosion on each sample was quantified by counting the corrosion related defects in the same defined area. The results indicated the number of protrusions to be relatively insensitive to changes in the chloride level or the chloride source (13 ± 5 defects per defined area). On the other hand, a general upward trend in the number of voids was observed as the chloride content in the OSS increased. This was consistent with previously published data on the effect of chloride on aluminum corrosion [1-3, 5, 6]. Furthermore, samples spiked with HCl showed a marked increase in corrosion as compared to those spiked with NaCl. HCl levels were not large enough to cause a significant pH shift in the OSS. However, HCl may have yielded more available chloride in the organic solvent, whereas NaCl may have had less due to ion association.

Figure 2 represents the total corrosion defect level as a function of chloride concentration. While there was not enough data to fully characterize the onset of heavy corrosion (especially in the case of NaCl-spiked samples), results indicated that the 5 ppm/w chloride specification was at best marginal. Further studies are required in order to better understand the mechanism of metal corrosion in the OSS.

6. CONTINUOUS IMPROVEMENT

In response to Intel's corrective action request, several on-line and off-line QC measures were taken at the supplier (2 subsequent audits of the facility by the Intel team verified that the corrective actions were performed satisfactorily): (a) CH_2Cl_2 production line was permanently piped, thus eliminating the opportunity to accidentally interconnect the line to the OSS production line. (b) A new design was developed for the OSS production line which eliminated as many of the flexible lines as possible and minimized the need for re-routing transfer lines during production. (c) An accurate quality control procedure was developed to ensure that Intel and the supplier's chloride specification was always met at the time of manufacture. (d) It was required of the supplier, and incorporated into Intel's specification, that all future batches of OSS be tested for CH_2Cl_2 to ensure that it never exceeds 10 ppm/w. This was based on accurate determination of the kinetics of chloride generation from CH_2Cl_2. Furthermore, the QC procedure at

the supplier was modified such that any detectable amount of methylene chloride in the OSS would flag that batch for further analysis and prevent its automatic shipment to Intel. (e) All QC technicians at the supplier underwent rigorous training by the supplier's analytical group to ensure that the new procedures for chloride and methylene chloride analysis were followed exactly. Future plans call for reducing the chloride specification in the OSS to 3 ppm/w or possibly lower.

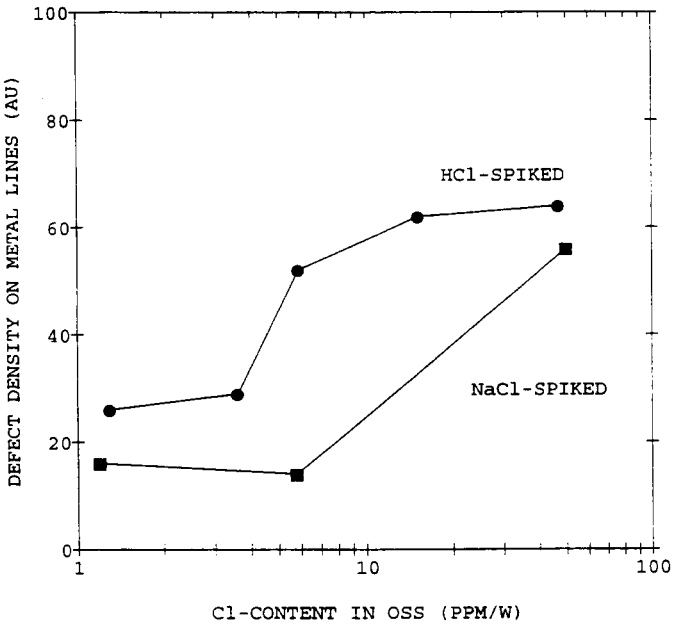

Figure 2. Effect of chloride in OSS on total number of metal line defects.

REFERENCES

1. Fontana, G. M. , *Corrosion Engineering*, McGraw-Hill Inc. (1986).
2. Brusic, V., G. S. Frankel, C. K. Hu, M. M. Plechaty, and G. C. Schwartz, IBM J. Res. and Dev., Vol. 37, 173 (1993).
3. Malik, F., Thin Solid Films, Vol. 206, 345 (1991).
4. Mills, J. E., C. A. Maryanoff, D. F. McComsey, R. C. Stanzione and L. Scott, J. Org. Chem., Vol. 52, 1857 (1987).
5. Foroules, Z. A. and M. J. Thubrikhar, *On the Kinetics of the Breakdown of Passivity of Pre-Anodized Aluminum by Chloride Ions*, J. Electrochem. Soc., Vol. 122 (1975).
6. Paulson, W. M. and R. P. Lorrigan, *The Effect of Impurities on the Corrosion of Aluminum Metallization*, in Proceedings of the 14th annual Rel. Phys. Symp., p.42 (1976).

REMOVAL OF POLYMER FOLLOWING REACTIVE ION ETCHING

D.K. Hwang, B.P. Luther, J. Ruzyllo, and D. Mount*

EMPRL, Department. Electrical Engineering, PennState University, University Park, PA 16802, USA
*SubMicron Systems, Inc., Allentown, PA 18106, USA

1. INTRODUCTION

During the Reactive Ion Etching (RIE) of oxide films on silicon a layer of polymer is formed on the silicon surface to assure adequate etch selectivity [1]. Prior to subsequent processing, notably prior to subsequent contact deposition, the polymer has to be removed.

In this experiment, two different polymer removal procedures followed by a gas-phase oxide etching are evaluated for potential inclusion into an integrated gas-phase cleaning process. These procedures involve UV/ozone and afterglow plasma generated oxidizing ambient with various gaseous additives [2]. An anhydrous HF etch was used to remove the thin oxide formed during the oxidizing procedure [3].

2. EXPERIMENTAL PROCEDURE

Starting wafers were prepared by reactive ion etching of a 200 nm thick layer of SiO_2 using CHF_3 at 75 mTorr and 400 watt power. These etch conditions resulted in a polymer layer approximately 95 nm thick. Polymer ashing was implemented using either an afterglow oxygen plasma or a UV/Ozone chemistry. The plasma was generated using microwave excitation at 2.46GHz with a gas mixture of argon and oxygen. Small amounts of NF_3 was also added to the input gas stream for some of the runs. The UV/Ozone process chamber has an ozone generator connected to the chamber and a high pressure xenon lamp that irradiates the reaction chamber through a sapphire window [4]. Gas flow of either oxygen or oxygen with methanol were used in the various runs. Both the afterglow plasma and the UV/ozone cleaning process leave a thin oxide on the sample surface. This oxide was removed using an anhydrous HF etch.

3. RESULTS AND DISCUSSION

Among issues of main interest in this study was the rate of polymer oxidation using various oxidizing chemistries generated in the tools capable of the subsequent in situ etching of the resulting ultra-thin oxide. Effective removal of the RIE deposited polymer is possible with either the remote oxygen plasma process or the UV/Ozone process.

The plasma system used in this investigation required a mixture of oxygen with argon to sustain a plasma. Figure 1 shows that as the amount of argon is increased in the input gas stream the polymer is removed at a faster rate. This may be due to the greater ionization of oxygen with increasing argon concentration. It may also be that more atomic oxygen is reaching the sample due to the higher total process gas flow. The addition of a small amount of NF_3 to the gas stream was

found to greatly accelerate the polymer removal rate. The presence of NF_3 in the plasma is most likely forming atomic fluorine, an aggressive oxidizing agent, which can enhances the oxidizing cleaning process [5]. The greater oxidizing potential resulting from the addition of NF_3 is also indicated by the relatively rapid thickening of the oxide after the polymer has been removed.

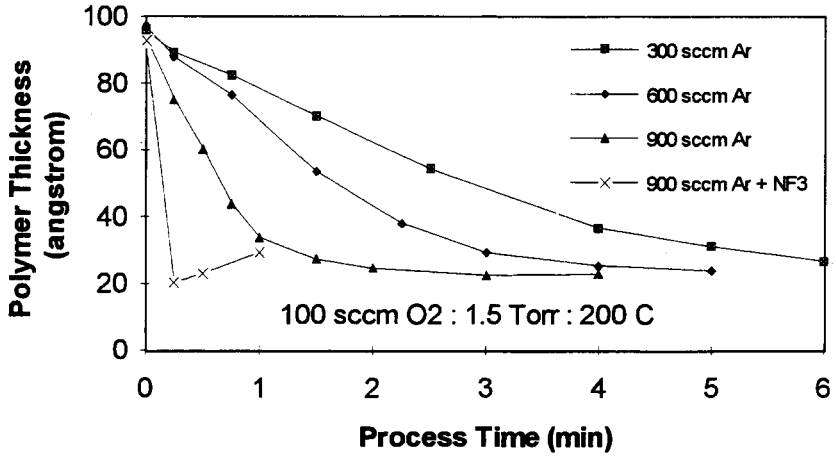

Figure 1 Effect of argon and NF_3 on the afterglow oxygen plasma removal of polymer.

Figure 2 shows that temperature is an important parameter in the polymer removal process using an afterglow plasma. As the temperature is increased the removal rate also increases. The results indicate that some thermal energy is required to activate the oxidation of the polymer in the presence of atomic oxygen. Pressure is also an factor that can affect the removal rate of the polymer. Our results show that the removal rate increases as the process pressure is decreased.

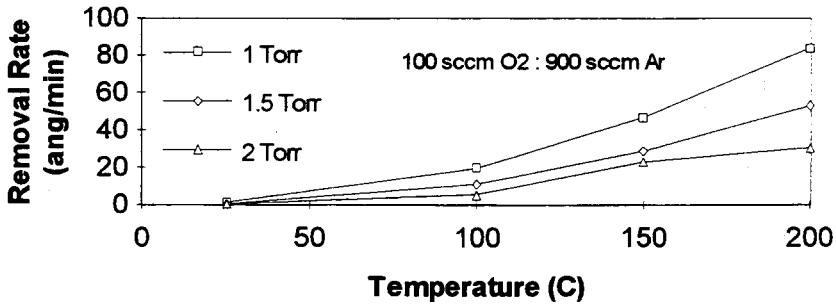

Figure 2 Effect of temperature and pressure on the removal rate of polymer in the afterglow oxygen plasma.

UV/ozone is another method that can be used to generate an oxidizing ambient capable of removing the polymer deposited by RIE [6]. Figure 3 shows that ozone produced from an electrical discharge combined with UV irradiation of the sample in the reaction chamber can effectively reduce the polymer thickness on

the sample surface. When methanol is added to the process chamber in the presence of ozone the removal of polymer is enhanced. It is likely that the addition of methanol to the process chamber is resulting in the formation of OH radicals which helps to oxidize the polymer [7]. The formation is of the OH radical is probably due to a reaction with some of the atomic oxygen since it was found that if a larger amount of methanol is added to the process the polymer removal rate starts to decrease, indicating the overall number of oxidizing species in the process ambient is decreasing.

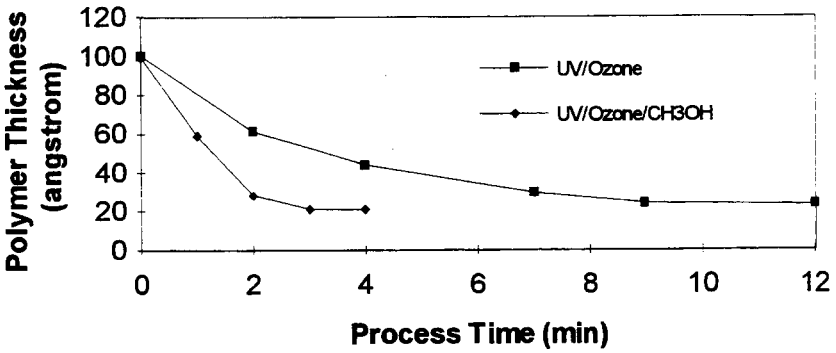

Figure 3 Polymer removal using UV/ozone and the enhancement of the removal by the addition of methanol.

Process temperature was also found to be an important parameter in the UV/ozone polymer removal process. Figure 4 shows that as the process temperature is increased from 75C to 150C the removal rate of the polymer is greatly increased.

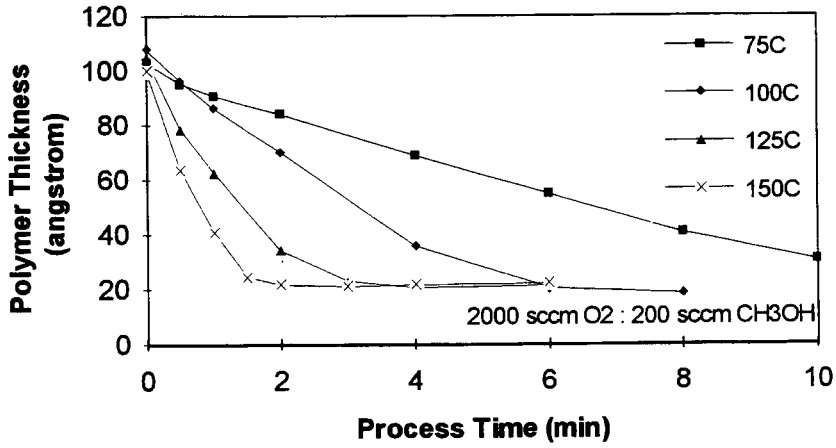

Figure 4 Temperature dependence of the UV/ozone polymer removal process.

4. SUMMARY

Afterglow oxygen plasma and UV/ozone were evaluated for feasibility of use as cleaning processes for post-RIE polymer removal. Both processes were found to effectively remove the polymer on the sample surface. The addition of a small amount of NF_3 to the afterglow plasma stream was found to greatly accelerate the removal of the polymer. Likewise the use of methanol in the UV/ozone process also showed an enhancement of the polymer removal process.

5. ACKNOWLEDGMENTS

Sponsorship of the Semiconductor Research Corporation of this project is gratefully acknowledged. Also, we would like to acknowledge the continuous support of this research by SubMicron Systems, Inc.

REFERENCES

1. F. K. Moghadam, X. C. Mu, IEEE Trans. Electron Dev. 36, 1602, 1989.
2. J. R. Vig, J. Vac. Sci. Technol. A3(3), 1027, 1985.
3. J. Ruzyllo, K. Torek, C. Daffron, R. Grant, R. Novak, J. Electrochem. Soc. 140, L6, 1993.
4. SubMicron Systems, Inc., Primaxx
5. A. M. Hoff, J. Ruzyllo, The Physics and Chemistry of SiO2 and the SiO2 Interface, C. R. Helms and B. E. Deal, Editors, p. 111, Plenum Publishing Corp., 1988.
6. D. K. Hwang, J. Ruzyllo, E. Kamieniecki, Proc. Third Intern. Symp. on Cleaning Technol. in Semicond. Dev. Manufactur., J. Ruzyllo and R.E. Novak, Editors, PV94-7, pp. 401-408, The Electrochem. Soc., 1994
7. S. Bedge, J. McFadyen, H. H. Lamb, MRS Symp. Proc. vol. 259.

INITIAL STAGE OF OXIDATION OF HYDROGEN-TERMINATED SILICON SURFACES

Takeo Hattori

Department of Electrical and Electronic Engineering,
Musashi Institute of Technology
Tamazutsumi, Setagaya-ku, Tokyo 158, Japan

1. INTRODUCTION

The control of oxide formation in atomic scale must be important for the formation of high quality SiO_2/Si interface for future metal-oxide-semiconductor (MOS) technology. Because the formation of native oxide can be suppressed by terminating silicon surface with hydrogen,[1] the hydrogen-terminated silicon, which is abbreviated in the following as H-Si, surface must be used instead of a clean silicon surface for the control of oxide formation in atomic scale. It is the purpose of present paper to clarify the possibility of realizing atomically flat interface by oxidizing atomically flat H-Si surfaces.

2. INITIAL STAGE OF SiO_2/Si(111) INTERFACE FORMATION

Atomically flat H-Si(111)-1 × 1 surfaces, whose surface structures were confirmed by performing FT-IR-ATR study and low-energy electron diffraction, were prepared by the treatment in 40% NH_4F solution.[2] The oxidation of these surface was performed at 300°C in dry oxygen with a pressure of 1 Torr up to the thickness of nearly 0.5 nm. The oxides thus obtained are called preoxide and can stabilize silicon surfaces at high temperatures.[3] The oxidation induced structural changes were investigated by measuring Si 2p and O 1s photoelectron spectra after each oxidation-treatment. These photoelectron spectra were measured at photoelectron take-off-angle of 15, 30 and 90 degrees using an ESCA-300 manufactured by Scienta instruments AB.[4] Other experimental details were described elsewhere.[5] After removing background signal based on Tougaard's method[6] from the observed Si 2p photoelectron spectrum, the spectrum is decomposed into the Si $2p_{1/2}$ and Si $2p_{3/2}$ spin-orbit partner lines. In this decomposition it is assumed that the spin-orbit splitting of Si 2p photoelectron spectrum is 0.60 eVand the Si $2p_{1/2}$ to Si $2p_{3/2}$ intensity ratio is 0.5.[7] The oxidation induced Si 2p and Si $2p_{3/2}$ photoelectron spectral changes for n-type surface measured at photoelectron take-off angle of 15 degrees are shown in Fig. 1. It can be seen from this figure that with the progress of oxidation Si^{1+},

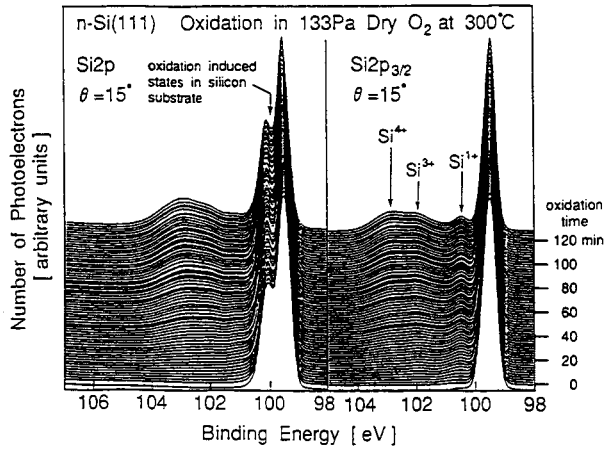

Figure 1. Oxidation induced change in Si 2p and Si $2p_{3/2}$ of NH_4F treated n-Si(111) surface.

Si^{3+} and Si^{4+} spectral intensities increase. Here, Si^{1+}, Si^{3+} and Si^{4+} denote the silicon atom bonded to three silicon atoms and one oxygen atom, the silicon atom bonded to one silicon atom and three oxygen atoms and the silicon atom bonded to four oxygen atoms, respectively.

The oxidation process thus measured is simulated using three dimensional silicon lattice consisting of 40 atoms × 40 atoms in each layer along (111) plane.

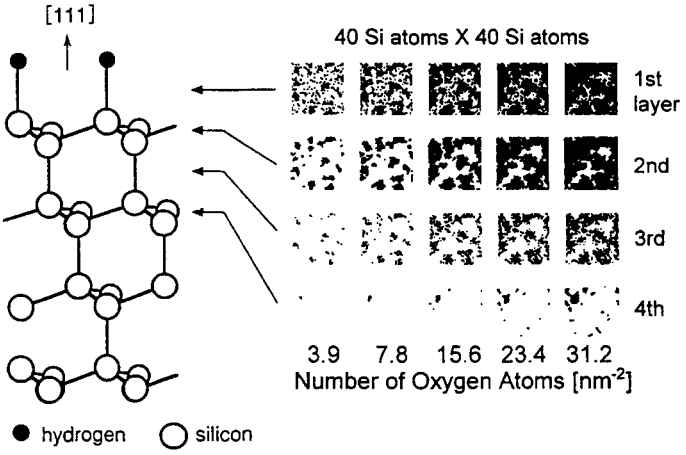

Figure 2. Distribution of oxygen atoms at and near the H-Si surface obtained from the simulation of oxidation process in Fig. 1.

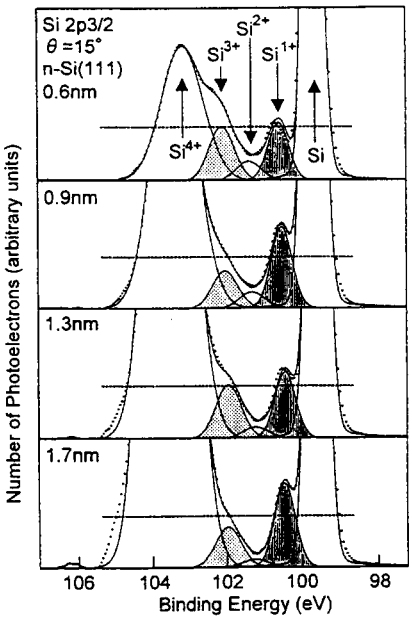

Figure 3. Oxidation induced changes in Si $2p_{3/2}$ photoelectron spectra obtained for photoelectron take-off-angle of 15 degrees with oxide film thickness as a parameter. The dashed line on each figure shows the average of the amounts of Si^{1+} and Si^{3+} in the thickness range from 0.6 to 1.7 nm.

The bonding probability of silicon atom with oxygen atom is adjusted until the simulated results are almost close to the experimental results. Then, it is infered that silicon atom bonded with oxygen atom has higher bonding probability with oxygen atom as compared with other non-oxidized silicon atoms. The distribution of bridging oxygen atoms on each silicon layer thus obtained is shown in Fig. 2. From top to the bottom of this figure the topmost layer, the second layer from the top, the third layer and so on are shown in this order. From the left to the right the amount of bridging oxygen atoms increase. This figure indicates that once the isolated bridging oxygen atoms are produced the oxidation proceeds in lateral direction around these oxygen atoms. In other words, the oxidation proceeds layer by layer in an atomic scale.

3. LAYER-BY-LAYER OXIDATION REACTION AT SiO_2/Si(111) INTERFACE

Through the preoxide thus formed, the oxidation was first performed at 600°C up to the thickness of nearly 1.0 nm, then at 800°C up to the thickness of nearly 1.7 nm, and finally at 900°C up to the thickness of nearly 2.0 nm in the same oxidation atomosphere.

Figure 3 shows the oxidation induced changes in Si $2p_{3/2}$ photoelectron spectra.[10]

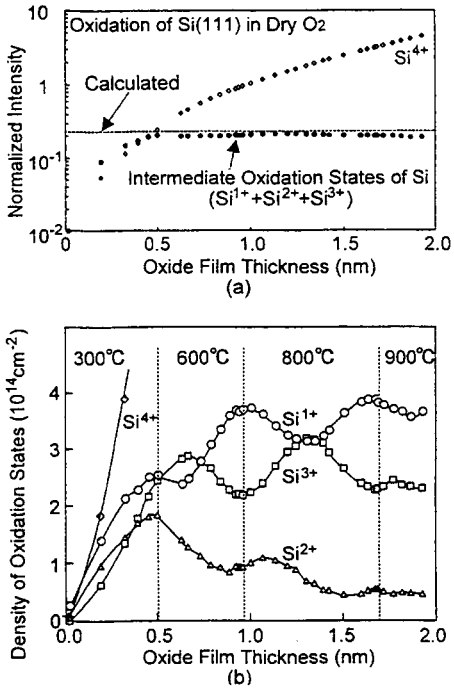

Figure 4. (a) Normalized spectral intensity of Si^{4+} and suboxides are shown as a function of oxide film thickness. The dashed line shows the normalized spectral intensity of suboxides calculated for abrupt interface. (b) Dependence of areal densities of Si^{1+}, Si^{2+}, Si^{3+}, and Si^{4+} on oxide film thickness.

Here, the spectral intensities of silicon substrate are adjusted to be equal to each other so that it is possible to see the oxidation induced structural changes at the interface. According to this figure, the amounts of Si^{1+} and Si^{3+} are almost the same for two thicknesses of 0.9 and 1.7 nm. This implies that the periodic changes in the interface structures appears with the progress of oxidation.

Figure 4(a) shows the spectral intensity of Si^{4+} and suboxides normalized by the spectral intensity of silicon substrate as a function of oxide film thickness.[10] According to Fig. 4(a), the spectral intensity of suboxides saturates at the oxide film thickness of nearly 0.5 nm, while the spectral intensity of Si^{4+} does not saturate at this thickness. Furthermore, the saturated value of spectral intensity of suboxides is in fairly good agreement with the areal density of 7.8 [nm^{-2}] calculated for abrupt interface. Therefore, this implies that after the interfacial layer becomes continuous the thickness of silicon dioxide only increases with further oxidation. Figure 4(b) shows the areal density of Si^{4+} and that of three kinds of suboxide as a function of oxide film thickness.[10] According to this figure, the areal density of Si^{1+} and that of Si^{3+} repeat increase and decrease. Furthermore, the areal density of Si^{1+} changes in opposite phase with the areal density of Si^{3+}. These clearly demonstrate that the interface structure changes periodically with the progress of oxidation. In other words, the oxidation reaction at the interface occurs layer-by-layer. This can be

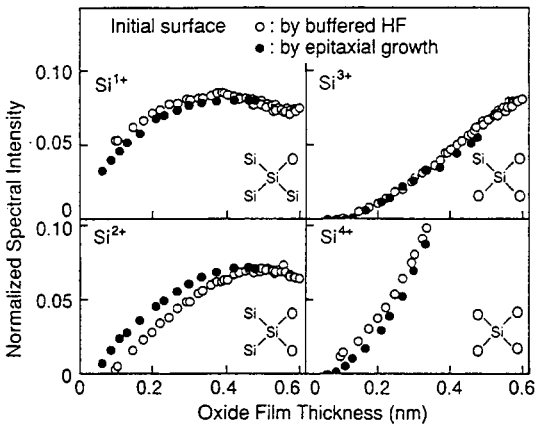

Figure 5. Foramtion of suboxides and Si^{4+} at the initial stage of oxidation for two kinds of initial surface.

correlated with layer by layer growth of oxide on Si(111) surface produced by the exposure at room temperature to 2.5×10^{-7} Torr H_2O. [11]

For atomically flat interfaces the minimum amounts of Si^{1+} and Si^{3+} must be zero and the amount of Si^{2+} must be close to zero at every stages of oxidation. However, this is not the case. In order to explain the coexistence of Si^{1+} and Si^{3+} in Fig. 4(b), it is necessary to consider the existence of atomic steps on silicon surface at every stages of oxidation. The decrease in the areal density of Si^{2+} with the the progress of oxidation in Fig. 4(b) implies that the microroughness at the interface decreases with the progress of oxidation.

4. OXIDATION REACTION AT SiO_2/Si(100) INTERFACE

In order to clarify the effect of initial surface morphology on SiO_2/Si(100) interface structure, the oxidation of two kinds of H-Si(100) surface was performed at 300°C in dry oxygen with a pressure of 1 Torr and subsequently at 600 and 800°C in the same oxidation atomosphere.[12] According to the measurement of vibrational spectra in the Si-H stretching bands excited by p- and s-polarized infrared, the silicon surface treated in buffered HF solution was found not to be covered only with monohydrides or dihydrides, but covered with mono-, di-, and tri-hydrides and is not atomically flat, while the silicon surface prepared by the epitaxial growth of silicon in hydrogen atomosphere at 1100°C was found to be covered only with pairs of monohydride, each of which is coupled with a Si dimer and can be considered as an atomically flat H-Si(100)-2 × 1 surface.[13] The chemical structural changes produced by the oxidation of these two kinds of initial surface at 300°C in dry oxygen with a pressure of 1 Torr were studied by measuring Si 2p photoelectron spectra at photoelectron take-off-angle of 15 degrees. The spectral intensities of Si^{1+}, Si^{2+}, Si^{3+} and Si^{4+} obtained from the analysis of these Si 2p spectra are shown in Fig. 5 as a

function of oxide film thickness. This figure indicates that for two kinds of initial surface there is a slight difference in the amount of Si^{2+} at the early stage of oxidation, but there is no distinct difference at the final stage. This implies that an atomically flat interface consisting only of Si^{2+} can not be realized even by the oxidation of an atomically flat H-Si surface.

By oxidizing these two kinds of surfaces further in the same oxidizing atomosphere at 600 and 800°C, the deviation from an atomically flat interface increase with the progress of oxidation and at the final stage of oxidation the contribution of Si^{2+} to the interface structure is only 25%. In other words, in this case the oxidation reaction does not occur layer-by-layer at the interface. However, the composition of suboxides at the interface can be roughly explained by the existence of surface microroughness on the order of one atomic layer.

5. SUMMARY

It was found from the measurent of structural changes in interface structures produced by the initial stage of oxidation of atomically flat H-Si(111)-1 × 1 surfaces in dry oxygen with a pressure of 1 Torr that the oxidation reaction occurs layer-by-layer at 800°C, once the interface layer becomes continuous. On the other hand, the oxidation reaction does not occur layer-by-layer on Si(100) surface and the deviation from atomically flat interface increases with the increase in oxide film thickness, even if the oxidation is performed on atomically flat H-Si(100)-2 × 1 surface.

REFERENCES

1) T. Takahagi, I. Nagai, A. Ishitani, H. Kuroda, and Y. Nagasawa: J. Appl. Phys. **64** (1989) 3516.
2) G. S. Higashi, R. S. Becker, Y. J. Chabal, and A. J. Becker: Appl. Phys. Lett. **58** (1991) 1656.
3) T. Ohmi, M. Morita, A. Teramoto, K. Makihara, and K. S. Tseng: Appl. Phys. Lett. **60** (1992) 2126.
4) U. Gelius, B. Wannberg, P. Baltzer, H. Fellner-Feldegg, G. Carlsson, C. -G. Johansson, J. Larsson, P. Munger, and G. Vegerfos: J. Electron Spectrosc. Relat. Phenom. **52** (1990) 327.
5) H. Nohira, Y. Tamura, H. Ogawa and T. Hattori: IEICE Trans. Electron. E-75-C (1992) 757.
6) S.Touggard: Surf. Sci. **216** (1989) 343.
7) F. J. Himpsel, F. R. McFeely, A. Talev-Ibrahimi, J. A. Yarmoff, and G. Hollinger: Phys. Rev. **B38** (1988) 6084.
8) Y. Tamura, K. Ohishi, H. Nohira, and T. Hattori: Ext. Abstr. Int. Conf. Solid State Devices and Materials, Tsukuba, 1992, p.111.
9) K. Ohishi, H. Nohira, Y. Shimizu, and T. Hattori: Ext. Abstr. Int. Conf. Solid State Devices and Materials, Makuhari, 1993, p.603.
10) K. Ohishi and T. Hattori: Jpn. J. Appl. Phys. **33** (1994) L675.
11) F. M. Ross and J. M. Gibson: Phys. Rev. Lett. **68** (1992) 1782.
12) T. Aiba, K. Yamauchi, Y. Shimizu, N. Tate, M. Katayama, and T. Hattori: IEICE, SDM 94-3 (1992) 13.
13) Y. J. Chabal and K. Ranghavachari: Phys. Rev. Lett. **53** (1984) 282.

COMPARISON OF THE STABILITY OF THE SURFACE STRUCTURE AND H-TERMINATION OF H_2 ANNEALED AND HF-LAST CLEANED (100) SILICON

H. Bender, L. Li, P. Mertens, M. Caymax and M.M. Heyns
IMEC, Kapeldreef 75, B-3001 Leuven, Belgium

1. INTRODUCTION

HF-last treatments of (100) silicon give rise to micro-rough H-terminated surfaces [1,2]. It has recently been shown that H_2 annealing of (100) silicon results in large flat terraces which have a 2x1 surface reconstruction with monohydride termination of the silicon dimers [3,4].

In this paper the stability of the surface structure and of the H-termination is compared for both types of surfaces during different subsequent treatments. The samples are analyzed by multiple internal reflection infrared spectroscopy (MIR) with polarized light. The SiH_x stretch vibration modes are studied as a measure of the surface passivation and micro-roughness.

2. EXPERIMENTS

MIR samples are prepared by KOH etching of nitride patterned (100) silicon as discussed in ref. [2]. After removal of the nitride, the samples are first wet chemically oxidized in a $NH_4OH/H_2O_2/H_2O$ (0.25/1/5) bath at 70°C. Subsequently one set of samples is only etched in 0.5% HF for 5 min, while a second set of samples is after this etch also annealed in a H_2 ambient at 1180°C for 10 min at atmospheric pressure. Both sets of samples then received different kinds of subsequent treatments, i.e. :

- storage of the samples in cleanroom air for different periods
- dipping of the samples in diluted HF
- rinsing with DI water
- immersion in pure DI water (no water flow)
- immersion in DI water with HCl added (pH 2.5)
- boiling in pure DI water
- boiling in DI water with HCl added (pH 2.5)

3. RESULTS AND DISCUSSION

The H-passivation of HF-last cleaned surfaces decreases slowly over several weeks during *storage in air* [2], whereas the H_2 annealed wafers, although the

initial stability of the 2x1 reconstruction, loose the major part of their passivation within a few days [3]. Hence the reconstructed surfaces oxidize more quickly than the rough surfaces. This can be related to a quick destabilization of the whole terrace once oxidation is started somewhere, probably at the edge, on the terrace. The terrace structure, however, can still be observed by AFM after the oxidation of the surface [4]. The fast oxidation of the terraces is consistent with the layer-by-layer oxidation previously reported [5,6].

Dipping the H_2 annealed samples in *diluted HF* immediately destroys the reconstructed surface and results in a spectrum as typical for the rough surfaces obtained after normal HF-last cleanings, i.e., the dimers are broken and some etching occurs such that the flat terraces are destroyed.

Rinsing in DI water increases the H-passivation in case of HF-last cleanings with high HF concentration due to etching of F-terminated sites or has only little effect for low HF concentrations [2]. For H_2 annealed wafers the rinse quickly destroys the surface reconstruction and leaves a low H-passivation with mono-, di- and trihydrides after 5 min rinsing (Fig. 1). Also some O-SiH bonds are present on the surface, indicating the on-set of oxidation. I.e. the silicon dimers of the reconstructed surface are broken in the DI water and during this process the silicon back-bonds are easily oxidized.

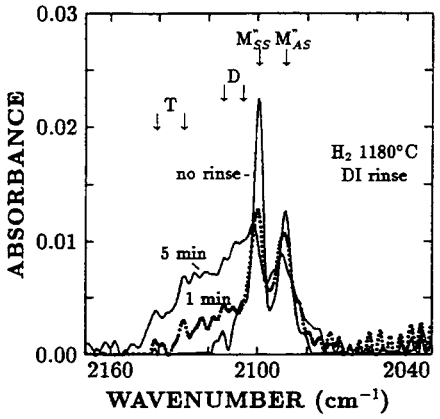

Fig. 1 : p-polarized MIR spectra as a function of DI rinse time of H_2 annealed (100) silicon. The initial spectrum with two sharp M" peaks at 2099.5 and 2088.5 cm^{-1} is typical for the reconstructed surface.

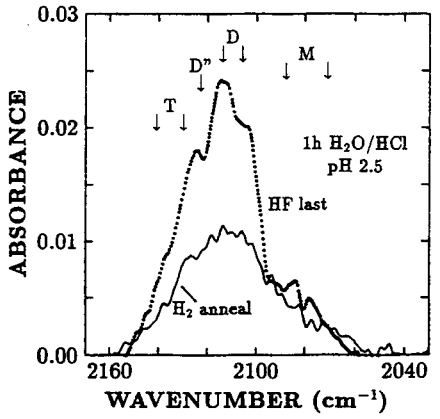

Fig. 2 : The SiH_x peaks after 1 h immersion in H_2O/HCl (pH 2.5) of H_2 annealed and HF-last treated surfaces (p-polarized).

Immersion in pure DI water without flow for longer periods (1-24 h) decreases the H-passivation more for H_2 annealed than for HF-last cleaned wafers. In the first case the reconstruction is fully broken-up and a broad structureless Si-H peak and a strong O-SiH signal are observed. After 21 h almost no Si-H

bonds are left and the surface is strongly hydrophillic. Hence, also in water the flat terraces oxidize more quickly than the micro-rough surfaces. With *HCl added to the water (pH 2.5)* (Fig. 2) the decrease of the H-passivation and the increase of the O-SiH are reduced compared to the immersion in pure DI water, indicating the importance of the OH^- concentration in the solution for the oxidation process.

Boiling the HF-last treated samples in pure H_2O results in an increase of the monohydride vibration mode compared to the spectrum of the 0.5% HF treated sample with a standard DI water rinse [7]. In both cases the monohydride modes consist of broad peaks (20 cm^{-1}) at 2084 and ~2070 cm^{-1}. *Adding HCl to the boiling water* has no effect on the monohydrides compared with the standard DI rinse, but increases the dihydride peak intensity. These observations can be interpreted as an etching effect in boiling pure water such that the step density increases and as a planarization and/or lower residual O content on the surface in the case that HCl is added to the water.

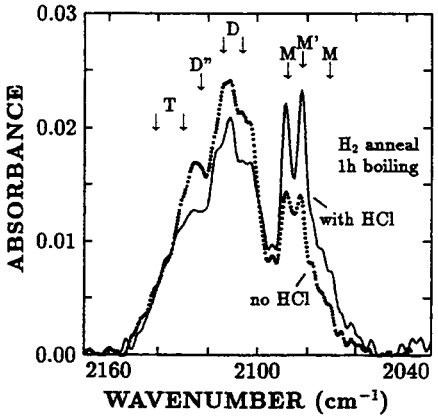

Fig. 3 : The SiH_x spectra after 1 h boiling with and without HCl of H_2 annealed surfaces (p-polarized).

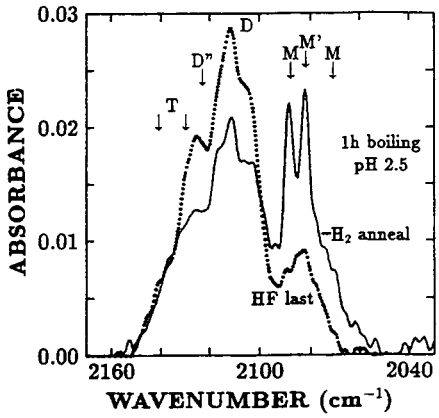

Fig. 4 : p-polarized MIR spectra of H_2 annealed and HF-last cleaned surfaces after boiling in water with HCl added (pH 2.5).

The effect of boiling water on the H_2 annealed samples is different. Treatment of the H_2 annealed surfaces *in boiling H_2O* results in the presence of mono-, di- and trihydrides (Fig. 3), i.e. the reconstructed surface is immediately destroyed. With increasing boiling time, two strong and sharp (FWHM = 6 cm^{-1}) monohydride peaks develop at 2088.5 and 2082.5 cm^{-1} respectively and a weaker shoulder peak can be distinguished at ~2070 cm^{-1}. The strength of the peak at 2082.5 cm^{-1} is almost independent of the polarization, i.e., corresponds to inclined monohydrides. The peak at 2088.5 cm^{-1} shows an important polarization normal to the surface, while the peak at 2070 cm^{-1} is mainly polarized parallel with the surface. The peaks can be related to two

different types of monohydride configurations on the surface, i.e., the symmetric and asymmetric coupled monohydride modes M (2088.5 and 2070 cm^{-1}) which occur on step edges and the 'ideal' monohydride M' on {111} microfacets. The narrow peak widths indicate a well organized surface structure, i.e., the M' terminated facets are relatively large and the coupled M probably occur in some regular structure. These sharp monohydride peaks are more pronounced when *HCl is added to the boiling water* (pH 2.5, Fig. 3) but are absent for the HF-last treated surfaces (Fig. 4). No O-SiH bonds can be observed, i.e. the surfaces are not oxidizing during the boiling treatments. It is also important to notice that the increase of the monohydride peak intensity is not connected with an important decrease of the di- and trihydride intensity as has e.g. been observed for buffered HF etchings [2]. This effective increase of the H-passivation has to be related to a stronger removal of the residual F and O during the boiling process.

CONCLUSION

The surface reconstruction of the H_2 annealed surfaces is quickly destroyed in all aqueous environments and after a few days in air. These surfaces show micro-facetting in boiling water, which is not the case for the HF-last treated samples.

The different behaviour of the H_2 annealed and the HF-last cleaned surfaces during subsequent treatments is related to the different surface microroughnesses. Once oxidation is started on the larger flat terraces of the H_2 annealed surfaces it will proceed quickly over the whole terrace so that the passivation is lost faster.

REFERENCES

1. Y.J. Chabal, Mat. Res. Soc. Symp. Proc. **259**, 349 (1992).
2. H. Bender, S. Verhaverbeke and M.M. Heyns, J. Electrochem. Soc. (1994), in press.
3. H. Bender, S. Verhaverbeke, M. Caymax, O. Vatel and M.M. Heyns, J. Appl. Phys. **75**, 1207 (1994).
4. O. Vatel, S. Verhaverbeke, H. Bender, M. Caymax, F. Chollet, B. Vermeire, P.W. Mertens, E. André and M.M. Heyns, Jpn. J. Appl. Phys. **32**, L1489 (1993).
5. M. Hirose, T. Yasaka, M. Takakura and S. Miyazaki, Solid State Techn. **34**, 43 (1991).
6. M. Morita, T. Ohmi, E. Hasegawa, M. Kawakami and M. Ohwada, J. Appl. Phys. **68**, 1272 (1990).
7. L. Li, G. Zou, H. Bender, P.W. Mertens, M. Meuris, H.F. Schmidt and M.M. Heyns, this conference.

THERMAL DESORPTION FROM AND CHEMICAL STABILITY OF HYDROGEN-TERMINATED Si SURFACES STUDIED BY HREELS

H. Nishimura, T. Yamazaki, S. Miyazaki and M. Hirose

Department of Electrical Engineering, Hiroshima University, Higashi-Hiroshima 724, Japan

Hydrogen-terminated Si(111) and (100) surfaces heated in UHV have been systematically characterized by using in-situ HREELS (High Resolution Electron Energy Loss Spectroscopy) and ex-situ FT-IR-ATR (Attenuated Total Reflection). Monohydride bonds on an atomically flat Si(111) surface fully disappear by heating at 465°C in UHV. On the other hand, SiH_x (x=2,3) termination on a Si(100) surface is converted to SiH termination of Si-Si dimer bonds by annealing at 320°C. This monohydride-terminated surface is chemically stable and hardly oxidized in air.

1. INTRODUCTION

Semiconductor memories beyond gigabit integration require gate oxides thinner than 5nm. Therefore, chemical composition and bonding features of Si wafer surfaces prior to thermal oxidation will affect the electronic properties of the oxide. Wafer cleaning by SC-1 followed by dilute HF treatment yields hydrogen-terminated Si surfaces [1,2]. Detailed knowledge of thermal stability of this surface is crucial for understanding Si surface conditions during wafer loading into an oxidation furnace.

It is known that hydrogen-terminated Si surfaces are chemically stable at room temperature [3] and hardly oxidized in air for a period between a few tens min and more than several hrs, depending on the surface orientation and extent of the flatness. Particularly pH-controlled BHF or 40%NH_4F treated Si(111) surfaces exhibit a sharp SiH absorption peak as observed by FT-IR-ATR [2], and a biatomic step structure as observed by STM (Scanning Tunneling Microscopy) [4] and AFM (Atomic Force Microscopy) [5,6]. This atomically flat surface is not oxidized for many hours [7]. In this study, we have systematically characterized 40%NH_4F treated Si(111) and 4.5%HF treated Si(100) surfaces by heating them in UHV and investigated hydrogen desorption and resulting changes in hydrogen bonding features by using in-situ HREELS and ex-situ FT-IR-ATR.

2. EXPERIMENTAL

P-type, cz Si(111) and (100) (10Ω·cm) wafers were used in this study. After SC-1 cleaning, Si(111) wafers were treated by 40%NH_4F and Si(100) by 4.5%HF to obtain hydrogen-terminated surfaces. The wafers were loaded into a UHV chamber ($<5x10^{-10}$ Torr) within 5min. The hydrogen bonding features were monitored by in-situ HREELS after each 1min annealing step. For testing the chemical stability of such surfaces in clean room air, the wafer was taken out from the UHV chamber, exposed to air for the ATR measurements, and again returned to the chamber for HREELS measurements. The electron energy loss spectra were measured using the

specular reflection condition. The spectral resolution was ~90cm^{-1} and the primary electron energy was 6.75eV. ATR spectra with a resolution of 2cm^{-1} were obtained by placing the wafer on a 60° cut Ge prism for p- and s-polarization. Note that the ion gauge was turned off during the HREELS measurements in order to avoid generation of atomic hydrogen by the tungsten filament.

3. RESULTS AND DISCUSSION

HREELS spectra of Si(111) and (100) surfaces are compared in Fig.1. A 40%NH_4F treated Si(111) surface exhibits only the SiH deformation (632cm^{-1}) and stretching (2088cm^{-1}) vibrational loss peaks [8], indicating monohydride termination and atomic scale flatness. In contrast, a 4.5%HF treated Si(111) surface shows SiOH deformation (785cm^{-1}) and stretching (3640cm^{-1}) vibrational loss peaks [9] in addition to the peaks of the 40%NH_4F treated Si(111) surface. This reflects that a Si(111) surface treated in 4.5%HF is atomically rough and therefore slightly oxidized in clean room air. However, the extent of oxidation is not significant since the Si-O-Si stretching vibrational loss peak at 1069cm^{-1} is not clearly observable. In the case of an HF treated Si(100) surface, the SiH_x stretching vibrational loss peak at 2130cm^{-1} is shifted towards higher wavenumber relative to the (111) surface peak because of existence of SiH_2 (2110cm^{-1}) and SiH_3 (2140cm^{-1}) bonds. Also, two peaks at lower wavenumbers are assigned as SiH_x deformation (655cm^{-1}) and bending (915cm^{-1}) modes [8-10]. Since this surface is also atomically rough and more reactive with clean room air, small OH stretching (3700cm^{-1}) and CH_x (2970cm^{-1}) vibrational loss peaks are observable. We have also found that a 4.5%HF treated Si(100) surface stored in clean room air is progressively contaminated with CH_x as the exposure time increases.

Thermal desorption of hydrogen from an atomically flat Si(111) surface occurs at temperatures above 380°C and SiH bonds disappear completely at 465°C as illustrated in Fig.2. Changes in the SiH_x peaks for a Si(100) surface are shown in Fig.3. When heated to 320°C, the bending mode at 915cm^{-1}, that

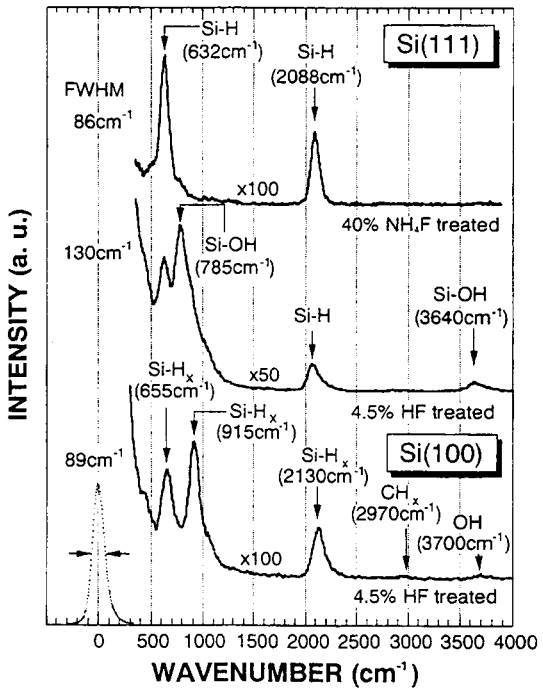

Figure 1. HREELS spectra of 40%NH_4F or 4.5%HF treated Si(111) and 4.5%HF treated (100) surfaces.

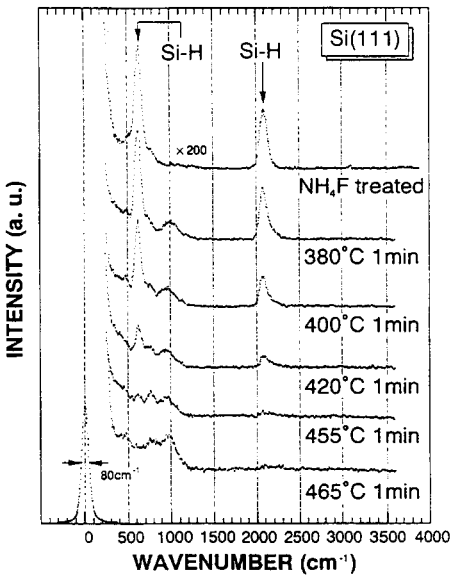

Figure 2. Thermal desorption of SiH from a 40%NH_4F treated Si(111) surface.

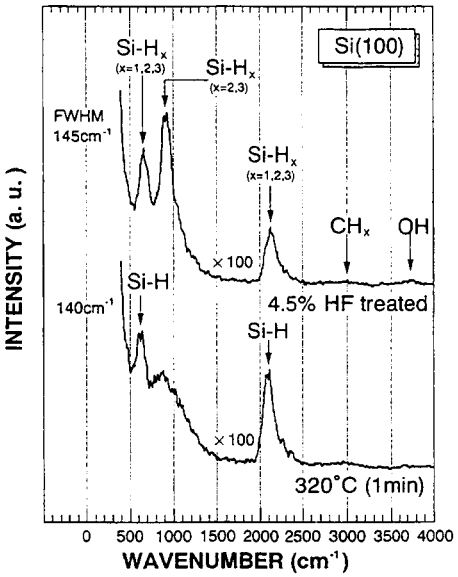

Figure 3. Thermal decomposition of SiH_x (x=2,3) on a 4.5%HF treated Si(100) surface.

indicates existence of SiH_2 and SiH_3, almost vanishes. At the same time, the SiH_x stretching vibrational loss peak increases significantly and exhibits a red-shift from 2130cm^{-1} to 2096cm^{-1}. This indicates that hydrogen desorption from SiH_2 and SiH_3 bonds at 320°C results in monohydride termination of the surface. Namely, surface reconstruction appears to occur through desorption of H_2 molecules from neighboring SiH_x

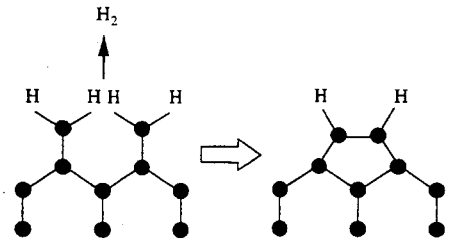

Figure 4. Schematic model for H_2 desorption from 4.5%HF treated Si(100) surface during heating at 320℃.

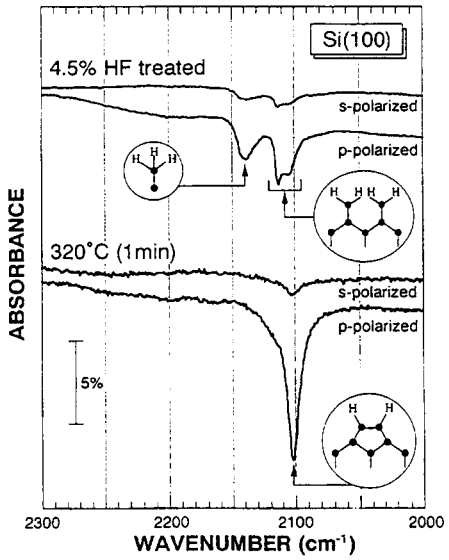

Figure 5. ATR spectra for Si(100) after 4.5%HF treatment and after subsequent heating at 320℃.

(x=2,3) bonds, and monohydride termination of Si-Si dimers is formed as schematically shown in Fig.4. In order to investigate the stability of this monohydride-terminated Si(100) surface, it was exposed to clean room air for 1min after which the HREELS measurements were repeated and showed that the spectrum remained unchanged. The ATR spectra, as shown in Fig.5, for an HF treated Si(100) surface indicates that SiH_2 and SiH_3 are the predominant bonding configurations. After heating to 320°C, a strong SiH absorption peak emerges at 2102cm^{-1} in the p-polarized spectrum although there is still SiH_2 on the surface. This also supports the proposed model of Fig.4. In fact, the monohydride-terminated surface is not oxidized in air. This phenomenon is helpful for maintaining stable Si wafer surfaces during temperature ramp-up for furnace oxidation. Additionally, change in Si(100) surface morphology by heating to 320°C could be explained by selective desorption of SiH_3 from the surface through reaction such as $SiH_3+H \rightarrow SiH_4$. It was recently reported that Si(100) surface turns into monohydride terminated and atomically flat when it is heated above 600°C in a low pressure (24 Torr) H_2 atmosphere [11], in consistency with the present result.

4. CONCLUSIONS

Monohydride bonds on atomically flat Si(111) surface fully disappear at 465°C as determined by HREELS. On the other hand, SiH_x termination on Si(100) surface is converted to SiH termination of Si-Si dimer bonds by a 320°C annealing in UHV and this monohydride-terminated surface is chemically stable.

REFERENCES

[1] T. Takahagi, I. Nagai, A. Ishitani, H. Kuroda and Y. Nagasawa: J. Appl. Phys. 64 (1988) 3516.

[2] G. S. Higashi, Y. J. Chabal, G. W. Trucks and K. Raghavachari: Appl. Phy. Lett. 56 (1990) 656.

[3] T. Takahagi, A. Ishitani, H. Kuroda, Y. Nagasawa, H. Ito and S. Wakao: J. Appl. Phys. 68 (1990) 2187.

[4] H. Tokumoto, Y. Morita and K. Miki: Mat. Res. Soc. Symp. Proc. 259 (1992) 409.

[5] M. Kageshima, H. Yamada, Y. Morita, H. Tokumoto, K. Nakayama and A. Kawazu: Jpn. J. Appl. Phys. 32 (1993) L1321.

[6] M. Fukuda, T. Yamazaki, S. Miyazaki and M. Hirose: Proc. of Advanced Microelectronic Devices and Processing (Sendai, Japan, 1994) p.355.

[7] T. Yasaka, K. Kanda, K. Sawara, S. Miyazaki and M. Hirose: Jpn. J. Appl. Phys. 30 (1991) 3567.

[8] D. Graf, S. Bauer-Mayer and A. Schnegg: J. Vac. Sci. Technol. A 11 (1993) 940.

[9] H. Ibach, H. Wagner and D. Bruchman: Solid State Commun. 42 (1982) 457.

[10] F. Stucki, J. A. Schaefer, J. R. Anderson, G. J. Lapeyre and W. Gopel: Solid State Commun. 47 (1983) 795.

[11] T. Ito: Extended Abstracts of 1994 Intern. Conf. on Semiconductor Manufacturing (Tokyo, 1994) p.103.

Electronic Properties of HF-Treated Si(111) Surfaces During Native Oxide Growth

H. Angermann, Th. Dittrich, H. Flietner
Hahn-Meitner-Institut, Abt. Photovoltaik, Rudower Chaussee 5, 12489 Berlin

1. Introduction

Native oxide films are one of the major contaminants on silicon surfaces after wet chemical treatments. The high integration in microelectronic technologies requires defect- and contamination-free Si surfaces as starting point for the preparation of thin oxide, epitaxial and passivation layers. Various chemical treatments have been developed aimed at atomically flat and hydrogen-terminated Si surfaces [1-2]. The control of native oxide growth has received an increasing attention in recent years. Oxidation in air and in ultrapure water was extensively investigated on hydrogen-terminated Si surfaces [3-4].
While a variety of spectroscopical and structural methods has been applied to study the morphology and the chemical structure of these surfaces, we report on investigations of the electronic properties. Surface potential and surface state distribution of differently HF-treated Si(111) surfaces are investigated immediately after treatment and during the native oxide growth in air by the large-signal field-modulated surface photovoltage technique (SPV) without any contact preparation [5-6]. The surface state distribution consisting of intrinsic and extrinsic Si dangling bond defects is directly related to the state of oxidation of the Si surface (*Fig. 1*) [7-9].

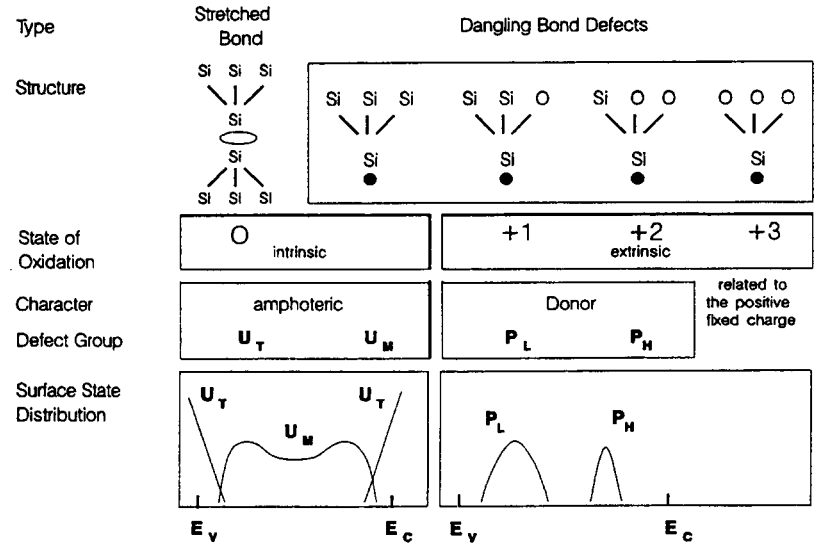

Fig. 1: Defect structure of the Si/SiO_2 interface

2. Experimental

We used polished Si(111) n- (70 Ωcm) and p-type (270 Ωcm) samples. Different methods of sample preparation were applied. The samples of the first series were chemically cleaned by conventional RCA process and subsequently dipped into HF(48%) for 30, 60, 180, 300 or 600 s. Those of the other series start from thermally oxidized samples. After RCA cleaning the thermal oxide was removed in a solution of NH_4F:HF (7:1). The samples were chemically reoxidized using a boiling solution of H_2SO_4 : H_2O_2 = 1 : 1 for 10 min, rinsed and placed into the etching solution, using HF(48%) for 30 s and NH_4F(40%) pH=7.8 for 6.5 min. After a short pure water rinse (5 s) and drying in pure nitrogen the surfaces were characterised by SPV immediately after preparation and repeatedly during native oxide growth in clean-room air (25°C, humidity about 50%) with exposure times ranging from 10 min to 15 months. We compared the same preparations carried out under two different conditions: chemical laboratory (using laminar flow boxes) and clean-room condition (particle class 100). The SPV measurements were performed in dry N_2 using a mica foil dielectric spacer in the same experimental configuration as described by Heilig [5]. A laser diode was used as light source (150 ns, wavelength 902 nm). From a large signal photovoltage pulse recorded with a Tectronics transient recorder (time resolution 5 ns) the surface potential was obtained as described in [6]. The minimal value of density of interface states in the gap $D_{it,\,min}$ is determined from a series of photovoltage pulses measured with different field voltages between electrode and wafer.

3. Results

The surface state distributions presented in *Fig. 2* were obtained on n- and p-Si surfaces after RCA cleaning and various treatment times in HF. The curves measured on n-Si (111) surfaces (a) show a superposition of different groups of states: intrinsic states forming the background spectrum combined with extrinsic states of the P_L-group forming a Gaussian distribution. A longer HF treatment was found to increase the concentration of these typical HF-induced extrinsic states below midgap [10]. Only on p-Si samples utilizing a short HF dip for 60 s (b) it was possible to prepare Si(111) surfaces without extrinsic states in the forbidden gap. Surface state distributions measured after various preparations, which started from thermally oxidized n- and p-type samples, are presented in *Fig. 3*. The conventional RCA process in all cases results in a high surface state density $D_{i,min} > 10^{13} eV^{-1}cm^{-2}$. Using HF treatment on n-type Si(111) surfaces a high concentration of extrinsic

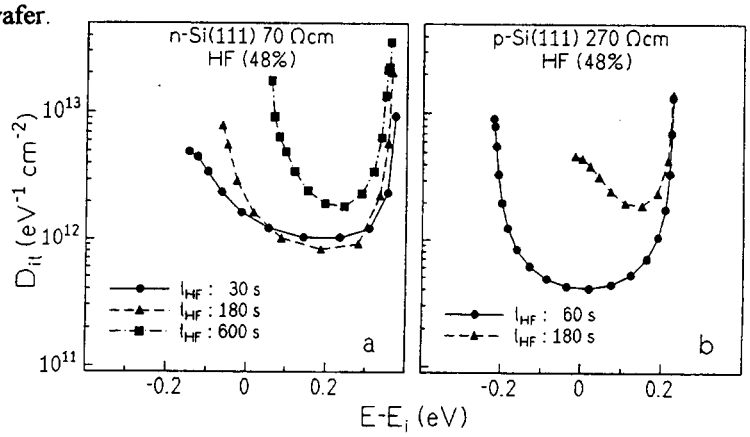

Fig. 2: D_{it} after HF treatment for different times

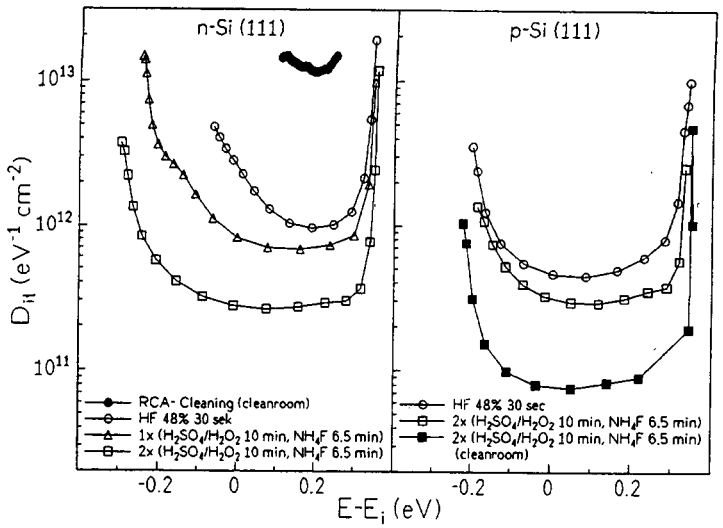

Fig. 3: D_{it} for differently treated Si(111) surfaces

defects with a lower state of oxidation (P_L) was observed. The concentration of these typical HF induced defects was significantly reduced by using NH_4F as the final etching solution. A nearly symmetric U-shaped distribution of states dominated by the intrinsic defects was observed when the chemical oxidation and the NH_4F treatment was repeated. Extrinsic defects can only be avoided on p-type Si(111) surfaces using a short HF dip or NH_4F treatment as final etching solution. The minimal surface state density of H-terminated surfaces prepared without clean-room conditions was nearly $2*10^{11}eV^{-1}cm^{-2}$. The same preparation carried out under clean-room conditions results in smaller surface state density $D_{it,min} < 7*10^{10}eV^{-1}cm^{-2}$.

During the oxidation process three typical phases were observed each characterised by specific defect structures (*Fig. 4*) [11]. After an initial phase (a) a group of extrinsic states additionally appeared in the midgap region reaching their maximum concentration after a few days (b) followed by a slow decrease during the further storage in air (c).

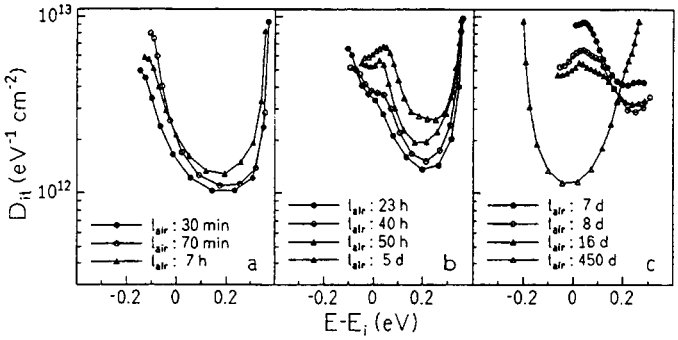

Fig. 4: Evaluation of D_{it} during native oxide growth in air

In *Fig. 5* the surface state density at midgap (a) and surface Fermi level position (b) of the HF-treated n-Si(111) surface is given as monitored during storage in air. We found the sequence of appearance and decrease of extrinsic surface states during native oxide growth to be independent of the kind of HF treatment. Otherwise, the duration of the initial phase was the shorter the higher the concentration of extrinsic defects after HF treatment was *(Fig 6)*.

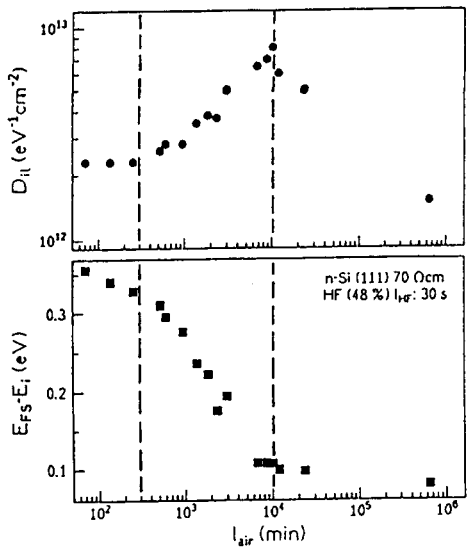

Fig. 5: $D_{it,min}$ and surface Fermi level during storage in air

4. Discussion

The surface state density of H-terminated surfaces was found to be directly influenced by the clean-room conditions.

The absence of O backbonded Si dangling bond defects indicates the successful preparation of H-terminated surfaces, characterised by an intrinsic surface state distribution. It was shown that the kind of HF treatment, namely the composition of the HF solution and the duration of the HF treatment, strongly influences the concentration of extrinsic defects with a lower state of oxidation. The competition between reactions of various nucleophilic components of the HF solution we regard to be responsible for different surface configurations after this treatment.

As recently reported we found the duration of the initial phase of oxidation strongly dependent on the HF treatment time [10]. Moreover, our results clearly indicate that the kinetics of initial oxidation process is related to the state of oxidation induced by the pre-treatment.

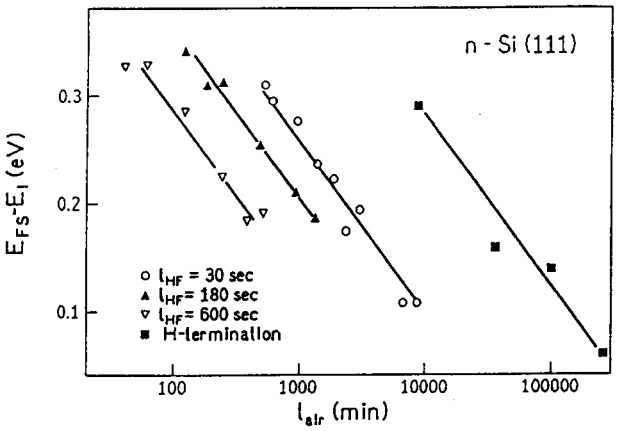

Fig. 6: Surface Fermi level during native oxide growth

References

1. G. S. Higashi, R. S. Becker, Y. J. Chabal, A. J. Becker, Appl. Phys. Letters 58 (15) (1991) 1656.
2. T. Bitzer, M. Gruyters, H. J. Lewerenz, K. Jacob, Appl. Phys. Letters 63 (3) (1993) 397.
3. D. Gräf, M. Grundner, R. Schulz, J. Appl. Phys. 68 (10) (1990) 5155.
4. M. Morita, T. Ohmi, E. Hasegawa, A. Teramoto, Jap. J. Appl. Phys. 29 (12) (1990) L2392.
5. K. Heilig, Surf. Sci. 44 (1974) 421.
6. Th. Dittrich, M. Brauer, L. Elstner, phys. stat. sol. (a) 137 (1993) K29.
7. H. Flietner, Surf. Sci. 46 (1974) 251.
8. H. Flietner, Surf. Sci. 200 (1988) 463.
9. H. Flietner, Proc. 7th Conf. Insulating Films on Semiconductors (INFOS) 1991, Ed. W. Eccleston and M. Uren, A. Hilger, Bristol/Philadelphia/ New York 1991 (pp. 151 to 154).
10. Th. Dittrich, H. Angermann, W. Füssel, H. Flietner, phys. stat. sol. (a), 140 (1993) 463.
11. H. Angermann, Th. Dittrich, H. Flietner, Appl. Phys. A 59 (1994) 193.

DEGRADATION OF CLEAN SI-SURFACES DUE TO STORAGE IN CLEAN (?) WAFER BOXES

W. Storm, W. Vandervorst, J. Alay*, M. Meuris, A. Opdebeeck, M.M. Heyns
Imec, Kapeldreef 75, Leuven, Belgium
C. Polleunis, P. Bertrand
PCPM, UCL, Place Croix du Sud 1, Louvain-la-Neuve, Belgium
*presently at Hiroshima University, Faculty of Engineering, Japan

1.INTRODUCTION

Recently a lot of work has been spent on obtaining a very clean surface using cleaning concepts like HF-last clean. Although this does lead to a H-passivated surface, questions arise regarding the stability of this surface during subsequent storage of these wafers in wafer boxes. Storage of wafers can lead to two kinds of problems. First of all the H-passivation will slowly degrade leading to Si-oxide formation. Moreover there exists also the danger of volatile species from the enclosure or the environment adsorbing on the Si-surface.

We have studied these phenomena by analysing the Si-surface using TOF-SIMS and XPS. The main advantage of using TOF-SIMS is, that it not only provides a highly sensitive signal for surface contaminants (for instance detection limits for metallic impurities down to the 10^9 at/cm^2-level have been reported [1]) but its mass spectrum also contains signals which are characteristic for the organic compound adsorbed on the sample surface [2]. Fig 1 illustrates this clearly showing a region of the negative ion spectrum of a hydrophobic Si-surface. Together with $Si_xO_yH_z^-$-fragments some $(M-H)^-$-peaks characteristic for a series of organic acids are detected.

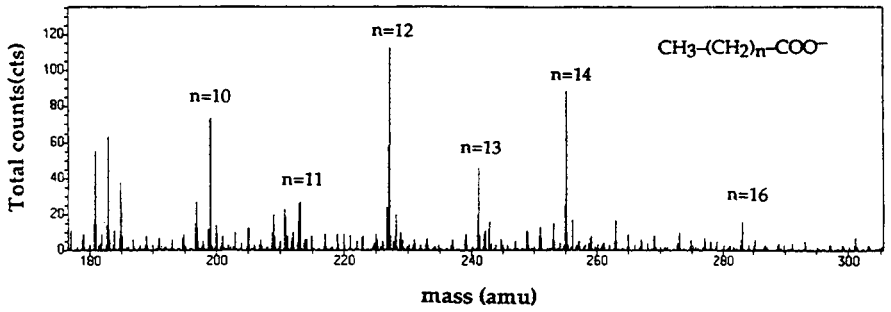

Fig 1: Region of a negative SI spectrum of a hydrophobic Si-wafer stored for 24h in a wafer box.

In our experiments we focused on two aspects. How does the uptake of oxygen and organic contaminants depend on parameters like the initial Si-surface state (hydrophilic, hydrophobic), wafer box material, or storage time? What mechanisms influence the oxidation of H-passivated Si-surfaces?

2. EXPERIMENTAL

To answer these questions two sets of wafers were prepared. One received a RCA-clean (modified FSIb-clean in FSI-mercury) and was stored in different types of wafer boxes for different times. The second set additionally received a HF-last clean (0.5 %

HF followed by a 3 min DI water rinse). For XPS-analyses a SSX-100 spectrometer (Fisons) was applied. The instrument is equipped with a monochromated Al-kα source (1486.6 eV) and a hemispherical electron energy analyser with a multichannel detection system. TOF-SIMS measurements were carried out with a TRIFT spectrometer (Charles Evans & Ass.) using the liquid Ga ion source. Typical parameters were an ion current of 400 pA and an acquisition time of 10 min per spectrum.

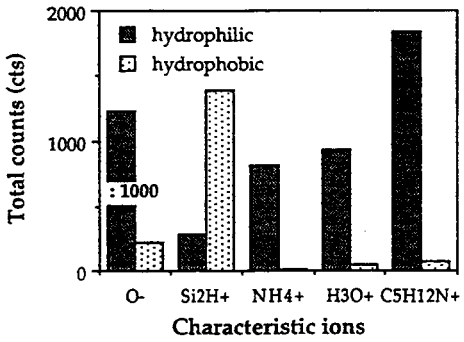

Fig 2: Total counts of some characteristic ions for the hydrophilic and the hydrophobic Si-surface.

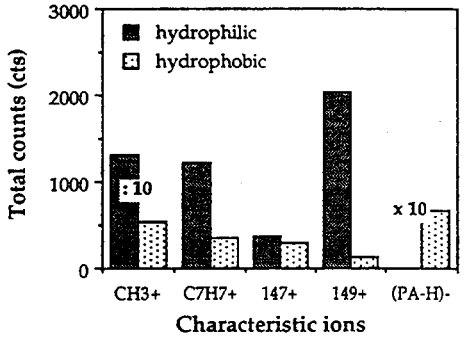

Fig 3: Total counts of some characteristic ions for the hydrophilic and the hydrophobic Si-surface.

3. RESULTS AND DISCUSSION

Both types of surfaces show significant differences. XPS measurements yield oxygen surface concentrations higher than 20 at.% for hydrophilic and smaller than 5 at.% for hydrophobic surfaces. The carbon content is 2 - 3 times higher on the hydrophilic surface. This is confirmed and shown more detailed by TOF-SIMS. Figs 2 and 3 compare several characteristic peaks for both sets of wafers. Additionally to a much higher O^--signal the hydrophilic surface exhibits much more water and ammonium. The still existing H-passivation on the hydrophobic surface is reflected by the strong Si_2H^+-signal. The unspecific CH_3^+-signal and the specific $C_7H_7^+$-peak (characteristic for compounds containing benzene) demonstrate the higher uptake of organic contaminants on hydrophilic Si-surfaces. Some very prominent contaminants have been identified. Ion 147^+ ($C_5H_{15}OSi_2^+$) is characteristic for polydimethylsiloxane (PDMS) and 149^+ ($C_8H_5O_3^+$) for phtalates which are frequently used as lubricants and plasticizers, respectively, for polymers. Whereas PDMS is equally present on both sets the phtalate peak is much more intense on the hydrophilic surface. In contrast to this palmitic acid and other long-chain organic acids are found on the hydrophobic surface exclusively. The comparatively low uptake of a lot of organic contaminants on the latter type of surface is probably due to the fact that on and in the amorphous SiO_2 there are much more bonding sites for contaminants compared to the smooth and H-terminated Si-surface.

Further parameters influencing the presence of oxygen and contaminants at the surface may be wafer box material and wafer storage time. Fig 4 shows the amount of some characteristic contaminants on a hydrophilic wafer surface versus storage time in a wafer box. Obviously the surface is strongly contaminated with increasing storage time which must be due to the wafer box material or the cleanroom air. It must be stressed that the contamination rate can vary significantly from experiment to experiment which indicates that not solely the wafer box material but the actual

state of the wafer box (new or old, frequently cleaned) or a changing level of cleanroom air contamination determines what is adsorbed on a wafer surface.

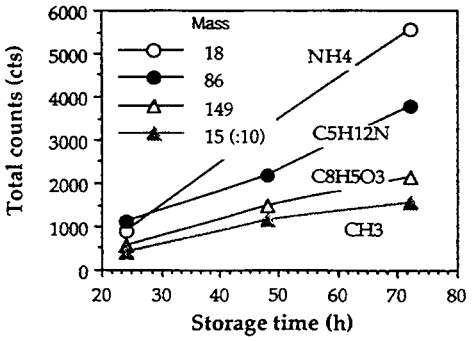

Fig 4: Organic contamination on Si-surface as a function of storage time in wafer box.

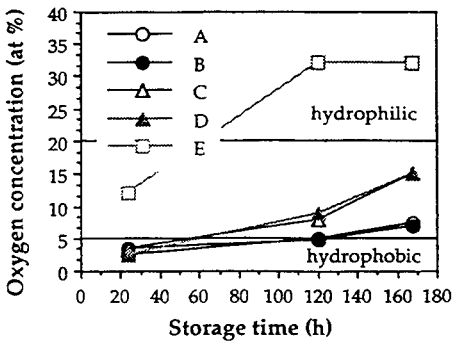

Fig 5: Oxygen concentration as a function of storage time in wafer boxes of different material.

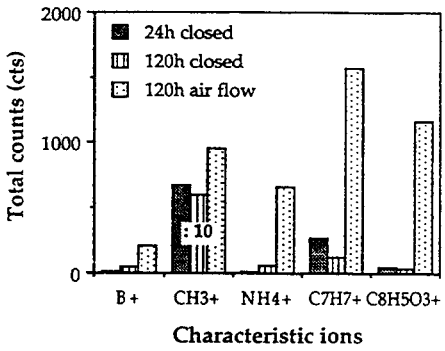

Fig 6: Influence of storage conditions on the surface contamination of a silicon wafer.

In Fig 5 the oxygen concentration of hydrophobic wafers determined by XPS versus storage time in boxes of different materials (A - E) is plotted. Curves A - D show the slow reoxidation of H-passivated Si-surfaces. Curve E represents a wafer which has been stored in an open wafer box under a laminar air flow. The oxidation rate of this wafer is a multiple of that of the others. Responsible for this oxidation is not the box material but the air flow because storing a hydrophobic wafer in a closed box of the same material leads to a curve similar to A-D. With increasing storage time the wafer under laminar flow becomes hydrophilic with respect to the amount of oxygen on the surface (fig 5) as well as to the uptake of characteristic contaminants as it is shown by a comparison with the wafer stored in a closed box of the same material in fig 6.

Characteristic for the hydrophobic wafers is a coverage with halogens which is especially high in fluorine and chlorine. All halogen-signals are decreasing with increasing oxidation of the surface. As an example fig 7 shows the Chlorine coverage versus oxygen concentration. Similar results for fluorine are in accordance with the oxidation model reported by Hirose et al. [3,4]. In this model the fluorine protects chemically reactive sites of the surface like step-edges against oxidation. The similar decrease of the other halogens with increasing oxidation leads to the conclusion that

they might play a similar role in the oxidation process. If this is correct, one should really look at the total halogen concentration on the surface (i.e. the sum of Cl and F) versus the oxygen concentration. Fig 8 indeed shows then a very nice correlation with strongly reduced scatter as compared to for instance fig 7.

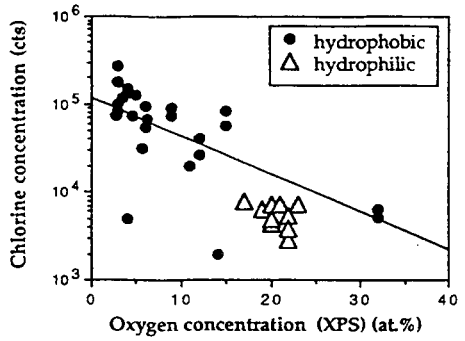

Fig 7: Chlorine concentration (TOF-SIMS) versus oxygen concentration (XPS)

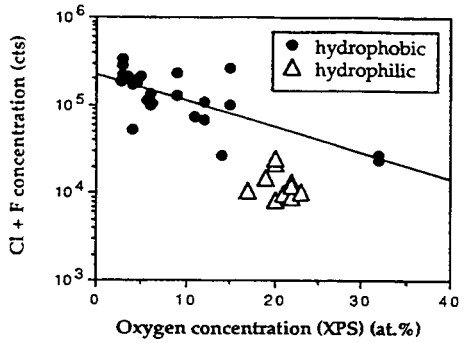

Fig 8: Chlorine + fluorine concentration (TOF-SIMS) versus oxygen concentration (XPS)

4. CONCLUSIONS

Hydrophilic and hydrophobic Si-surfaces exhibit large differences concerning oxidation and uptake of organic contaminants. Hydrophobic wafers have a lower oxygen content and a reduced uptake of organic molecules which may be explained by a larger number of bonding sites for contaminants in or on the oxidized hydrophilic surface. Due to different treatments or a selective susceptibilty different classes of organic molecules are found on the hydrophilic and the hydrophobic surface. Depending on parameters like wafer box material or storage conditions a heavy contamination of the wafer surface may occur. The reoxidation of a Si-wafer is correlated with a strong decrease in halogen-signals from the surface. The correlation between the F + Cl coverage and the oxygen content on the surface indicates that not only fluorine but also Cl plays a role in the oxidation process.

5. ACKNOWLEDGEMENTS

W. Storm receives grants from the Commission of the European Communities within the Human Capital and Mobility Program (ERB CHB GCT 930286) which he gratefully acknowledges.

6. REFERENCES

[1] H.G. Cramer, E. Niehuis, T. Heller, U. Jürgens, R. Möllers, M. Terhorst, and A. Benninghoven: *Proceedings SIMS-IX*, Yokohama (1993)

[2] H. van der Wel, P.N.T. van Velzen, U. Jürgens, and A. Benninghoven, in: *Analysis of Microelectronic Materials and Devices* (Eds. M. Grasserbauer and H.W. Werner), 461, Wiley 1991

[3] H. Hirose, T. Yasaka, M. Takakura, and S. Miyazaki: Solid State Techn. **34(12)**, 43 (1991)

[4] T. Yasaka, M. Takakura, K. Sawara, S. Uenage, H. Yasutake, S. Miyazaki, and M. Hirose: IEICE Trans. Electron. **E75-C**, 764 (1992)

CHEMICALLY TREATED STEPPED SILICON {100} SURFACES

Vishal Nayar, Allan J. Pidduck, Mohammed Idrees and Beverley E. J. Dew
Defence Research Agency, St. Andrews Rd., Malvern, Worcs., WR14 3PS, UK.

ABSTRACT

Ultra-smooth Si {100} surfaces are necessary for advanced deep sub-micron electronics. There is a particular need for chemical cleaning treatments which do not roughen Si {100}. We have compared continuous-contact and intermittent-contact atomic force microscopy (AFM) techniques, on atomically stepped Si {100} specimens, to study the morphological effects of dilute HF (3.5%) etching and subsequent reoxidation, in air and UV/ozone, with sub-Angstrom vertical sensitivity. We show that Si {100} atomic terraces are not detectably roughened during numerous repeated cycles of thin oxide formation by UV/ozone exposure and removal by HF etching.

1. INTRODUCTION

Processes leading to atomically smooth Si surfaces are gaining importance as integration in microelectronics increases. Manufacturing relies on the development of improved metrological tools to gain leverage in understanding process effects. Surface chemical treatments and oxide formation remain critical areas which are pushing the associated analytical tools to their limits. New generation production wafers display microroughness with local root mean square (RMS) values below 0.1nm. AFM, though not able to provide routine atomic resolution, can be applied to very smooth atomically-stepped surfaces in order to study the effects of chemical treatments at the monolayer level. We will describe a series of experiments to optimise AFM measurement conditions and to investigate the effects of dilute HF etching and subsequent re-oxidation by ambient air or UV/ozone exposure.

2. EXPERIMENTS ON STEPPED Si {100} SURFACES

2.1. Continuous-contact AFM

The work reported below was carried out on a Digital Instruments Nanoscope III and Dimension 3000 in air (relative humidity 50-70%). Continuous-contact AFM (C-AFM) measurements were made on epitaxially-grown Si surfaces [1] using pyramidal silicon nitride tips. Fig. 1 shows the changes in contact ("adhesion") force and RMS roughness (evaluated typically over 0.15μm^2 terrace areas) with time after dilute HF etching (180secs.) and a 30sec. DI water rinse. The adhesion force is the cantilever spring force (measured assuming a spring constant of 0.6N/m) which needs to be applied to the AFM tip in order to detach it from the surface. In air, the force is primarily determined by the thin adsorbed water film stabilised by the ambient humidity [2]. Initially after HF treatment, this force is expected to be low because the surface is hydrophobic. Oxidation then results in an increased force. Two plateaus in adhesion force are observed as a function of time, Fig.1. Stable images can be obtained at the first plateau. However, when, as for some Si oxides, the adhesion force exceeds a few

hundred nN, tip-surface bonding and hence wear occurs, resulting in loss of resolution and non-reproducible images. Furthermore, when the measured roughness data in Fig.1 is plotted against the adhesion force as in Fig.2 there is an apparent correlation between the two quantities. One explanation for this is that as the contact force increases, so the tip-surface contact area increases, the lateral resolution becomes poorer and the measured RMS height reduces. The changing contact force, and hence resolution, with time, means that to obtain reliable C-AFM roughness data from HF-etched specimens it is necessary to make measurements either in a non-oxidising ambient or after a certain stabilisation period in air [3].

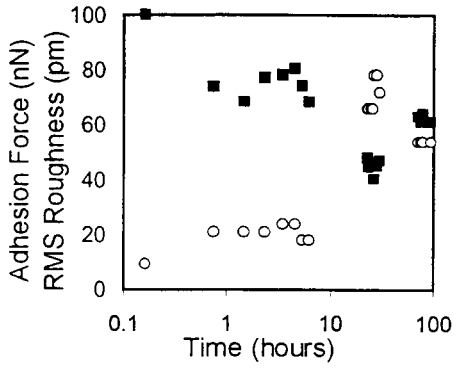

Figure 1 Roughness(■)/adhesion force (o) changes after dilute HF etch

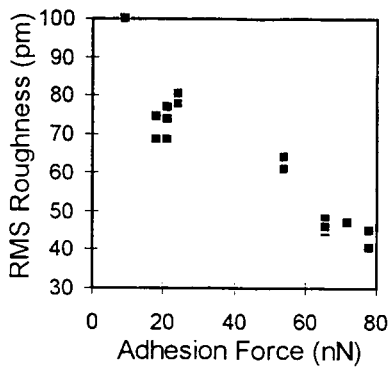

Figure 2 Correlation of adhesion force and RMS roughness values.

2.2. Intermittent-contact or "tapping-mode" AFM (T-AFM)

In T-AFM a microfabricated Si lever is resonated vertically at about 400KHz. At the lowest extent of its motion the tip contacts the surface only for a very short time. T-AFM does not "remove or reduce" surface forces but rather it limits the tip/surface interaction time, hence reducing the possibility of shear-induced tip damage. No direct measurement of adhesion force after the brief T-AFM contact periods is made. However, surfaces which often gave high adhesion forces in C-AFM, such as immediately after UV/ozone oxidation, can be imaged apparently stably and reproducibly by T-AFM.

We have taken stepped Si {100} surfaces, formed by resistively heating Si in ultrahigh vacuum [4], stored in air for several months, and carried out the following surface treatments before imaging with T-AFM:

(a) DI water rinse for approx 2minutes,

(b) 30secs. dilute HF(3.5%)/30secs. followed by 30 seconds DI water rinse

(c) step (b) followed by 10 minutes UV/ozone (UVO) exposure.

Fig.3 shows the starting {100} surface after (a) DI rinsing. Clear, sharply defined steps are evident and the RMS roughness over a single terrace (area ≈ 0.15 to $0.2\mu m^2$) is ≈ 0.05nm. Fig.4a shows a HF etched surface imaged ≈ 30 minutes after the etch. The sample was previously etched and aged in air for 24 hours twice. Although steps are visible the roughness is significantly higher (0.095nm RMS) than the starting surface in Fig.3. The nature of the roughness is also distinct, comprising many minute islands which are not evident

in Fig.3. Most, islands down to 20nm in lateral size are imaged reproducibly in concurrent T-AFM images. Nevertheless, slow tip degradation occurs even in T-AFM, and generally, the image resolution becomes noticeably poorer after several hours of scanning, and the RMS values are consequently lower. Despite this effect, we measured an increase in terrace RMS roughness, up to about 0.11nm, 1.5 hours after etching, Fig.4b. One day later with a new tip the measured RMS roughness had increased further to 0.15nm.

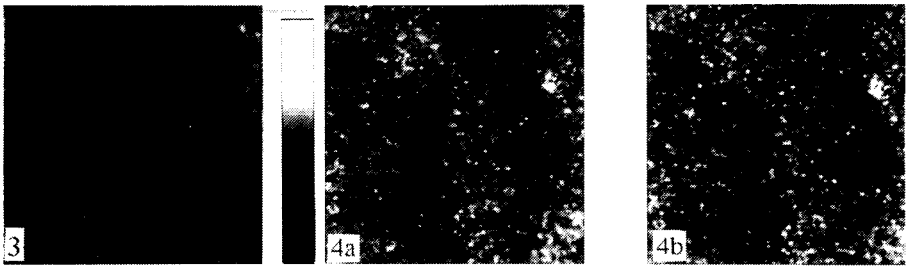

Figure 3 Typical stepped surface, **Figure 4a,b** HF etched and aged surfaces, height range 0 to 1.5nm, image size 0.7 x 0.7μm^2.

We conclude that the native oxide growth on our HF treated Si {100} surface is not step edge dominated, but apparently occurs by the formation of numerous small oxide islands at discrete positions on the terraces. These then appear to grow in height and width during the first 24 hours. This mechanism implies a non-uniform surface oxide which would be detrimental to MOS devices. From the view point of processing, the Si surface may need to be passivated after HF etching to avoid this roughening. The positions of the islands may depend on the distribution of contaminants which may catalyse oxidation.

2.3 T-AFM of repeated HF and UVO treatments

UVO exposure is one possible route to a stable and uniform thin oxide. In the experiment described below we have imaged the same areas before and after chemical treatments. When tested, no significant difference in either the form or amplitude of roughness was observed between areas which had and had not been previously imaged.

Fig.5a shows a stepped area after DI water rinse. The single terrace RMS roughness is 0.06nm. The same area is shown in Fig.5(b) after twice repeating process (c), HF/UVO. Sharply defined steps and smooth terraces are again observed, but there appear to be small contamination islands distributed across the surface. The origin of these is unknown. Possibilities are non-uniform etching or deposition from the etch solution. After a further 5 HF/UVO cycles the surface, shown in Fig.5c, is clear of the contaminants observed in Fig.5b and the RMS roughness is measured to be 0.045nm. It is interesting to note that at the locations of the contaminants in Fig.5b, pits appear in Fig.5c. This suggests that locally enhanced oxidation or etching may be pitting the surface.

Thus we conclude that cycling of HF and UVO steps can be used without significantly affecting the surface roughness, given that contamination is minimised. The absence of a detectable increase in terrace surface roughness after

repeated HF/UVO cycles was also observed on epitaxial Si surfaces. In carrying out 7 HF/UVO cycles at least 3nm (20 atomic planes) of Si was consumed, conservatively assuming 1nm of oxide is formed and removed in each cycle. Preservation of starting roughness levels is possible because of the self-limiting nature of UVO oxidation. This is important for gate oxidation as HF last cleans are developed, since a short UVO exposure may be appropriate to passivate a surface prior to thermal oxidation. Alternatively, a controlled UVO gate oxidation process would not lead to increased roughness. It also provides a means to rapidly and controllably stabilise, and hence to measure, the surface roughness present directly after HF etching.

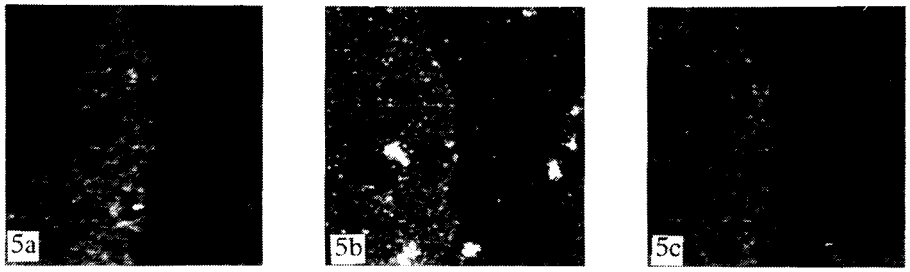

Figure 5 The same area imaged before processing (a), after 2 cycles (b), and 7 cycles of HF/UVO (c), height range 0 to 1.5nm and image size 0.7 x 0.7μm^2.

3. CONCLUSION

We have used stepped Si surfaces to develop optimised measurement conditions for the study of chemical processes affecting roughness. Intermittent-contact AFM with Si tips largely overcomes the tip-surface damage problem encountered with continuous-contact AFM of many Si oxide surfaces when using Si_3N_4 tips. Native oxide growth in air after dilute HF oxide removal led to the appearance of a high density of subnanometre height islands, whereas UVO induced oxide formation provided a stable and uniform oxide. Repeated cycles of UVO oxide growth and HF oxide removal resulted in no detectable roughening of the {100} Si atomic terraces.

ACKNOWLEDGEMENTS
We are grateful to Y. Homma of NTT for the resistively heated stepped sample and to Dr. T. Abe of SEH for low misorientation Si wafers used in epitaxy. This work was partly funded by DTI under the BELPA project.

[1] A J Pidduck, D J Robbins, I M Young and G Patel, Thin Solid Films, 183 (1989), 225.
[2]N A Burnham, R J Colton and H M Pollock, J. Vac. Sci. Technol., A9(4) (1991), 2548
[3] V Nayar, R Jackson, A J Pidduck and C Pickering, in "The physics and chemistry of SiO_2 and the Si-SiO_2 interface 2", Plenum, New York (1993) 299.
[4] Y Homma, Proc. 50th Ann. Meet. Electron Micr. Soc. Amer., (1992), 1286, and Semicon. World (in Japanese), no. 10 (1992), 130.

SELECTIVE ETCHING OF PHOSPHOROUS DOPED OXIDES OVER UNDOPED OXIDES IN A LOW PRESSURE HF VAPOR PROCESS

R.J. Wilhelm, W.J.C. Vermeulen
ASM International, Rembrandtlaan 7, 3723 BG Bilthoven, The Netherlands
H. Watanabe
ULSI Dev. Res. Lab., NEC Corp., 1120 Shimokuzawa, Sagamihara,
Kanagawa 229, Japan

ABSTRACT

A reliable low pressure vapor HF etch process was developed for the selective removal of phosphorous doped silicon oxides. With this process, a high etch selectivity of phospho-silicate glass (PSG) over undoped oxide is obtained. The high etch selectivity is accomplished by controlling the total vapor pressure, the water vapor partial pressure, and the temperature. It was found that the etch rate of undoped oxide is strongly influenced by these parameters while the etch rate of PSG is relatively insensitive for these parameters.
At low vapor pressures and elevated temperatures HF/H_2O adsorption on the oxide surface is suppressed, resulting in a low etch rate of the undoped oxide. On the other hand the formation of an adsorption layer on PSG occurs even at low vapor pressures and elevated temperatures due to the presence of phosphorous.

1. INTRODUCTION

HF vapor etching of silicon oxides has been widely investigated. The previous work on HF vapor etching can be divided in two major categories, cleaning and selective etching. The cleaning method was developed to obtain a clean silicon surface prior to gate oxidation by removing the native oxide [1]. This application generally requires a low etch selectivity, i.e. native oxide should be removed with no or little etching of the other oxides exposed to the HF vapor. Research up until now has shown that the selectivity of the HF vapor process strongly depends on the wafer temperature [2, 3, 4], processing pressure [5, 6], and moisture content [1, 6].
A high etch selectivity is generally undesired in case of cleaning, however it can be used to realize three dimensional structures. Three dimensional cylinder structures have been investigated to increase the surface area of the capacitor electrode in DRAM devices. It was reported that three dimensional structures can be realized by using a low pressure HF vapor etch process to selectively remove the Phospho-Silicate Glass (PSG) that is used as sacrificial layer for the formation of the poly-silicon cylinder, without etching the Chemical Vapor Deposited (CVD) SiO_2 that is used as etch stopper on top of the interlayer silicon

oxide [1].
Here we will report on the influence of the water vapor partial pressure and the temperature on the etch selectivity ratio of PSG over thermal oxide.

2. RESULTS

2.1. Etch Kinetics

The etch rate of different oxides in the HF vapor etch process was determined by SEM observation of a multilayer structure, consisting of stacked layers of silicon, PSG, BSG, BPSG, CVD oxide, and thermal oxide on a silicon substrate. In addition, ellipsometry of blanket thermal oxide layers was used to determine the amount of oxide etched when low etch rate conditions were selected.

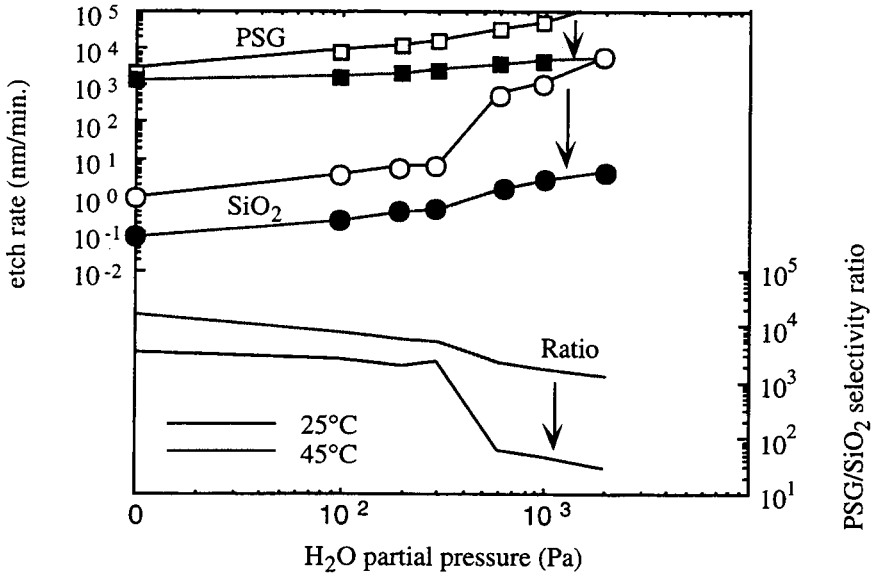

Figure 1. The etch rate and etch rate ratio (selectivity) of PSG and thermal oxide versus the water vapor partial pressure for different etch temperatures.

In figure 1 the etch rate of PSG and thermal oxide as well as the etch selectivity of PSG over thermal oxide is shown as a function of the water vapor partial pressure for different process temperatures. When etching takes place at room temperature, the etch rate of PSG increases monotonically with an increase of the water vapor partial pressure, while the etch rate of thermal oxide shows an abrupt change at a water vapor partial pressure of 600 Pa. This difference in etch behavior affects the etch selectivity of PSG over thermal oxide: the selectivity, i.e. the etch rate ratio, is higher than 1000 for water vapor pressures < 300 Pa, but drops to below 50 for water vapor pressures > 600 Pa. At 45 °C, the etch rate of

PSG is hardly influenced by the water vapor partial pressure and equals approximately 2000 nm/min. The etch rate of thermal oxide increases with an increase of the water vapor partial pressure but, contrary to etching at room temperature, the abrupt change in the etch rate is no longer observed. Furthermore, the etch rate of thermal oxide decreases at elevated temperatures. Based on these findings, it is concluded that the process window for selective etching at 45 °C is wider than at room temperature.

2.2. Etch residues

The composition of the liquid by-products remaining at the wafer surface after etching of 1 μm thick BPSG in a pure HF vapor process was analyzed by means of ion chromatography (see table 1). It is found that the liquid residues contain predominantly phosphorus and that the bonding state of the phosphorus atoms in the liquid residues is mainly PO_4^{3-}.

Table 1. Composition of liquid residues found on PSG and BPSG

	B	P(V) PO_4^{3-}	P(III) HPO_3^{2-}	Si	F
PSG P: 3.9 mol%	-	97.30 wt%	2.67 wt%	0.01 wt%	0.02 wt%
BPSG P: 4.4 mol% B: 10 mol%	5.07 wt%	86.34 wt%	1.48 wt%	0.01 wt%	7.1 wt%

3. DISCUSSION

It is reported that the etch rate of thermal oxide is strongly influenced by the amount of adsorbed water vapor at the oxide surface [6]. At low surface coverage, the amount of adsorbed water linearly increases with the water vapor partial pressure, as does the etch rate. On the other hand, the amount of adsorbed water decreases with increasing temperature. The etch rate of thermal oxide, therefore, can be suppressed by increasing the temperature and decreasing the water vapor partial pressure. The transition from the low etch rate regime to the high etch rate regime (see fig. 1) can also be explained by the adsorption mechanism. The amount of adsorbed water increases with an increasing water vapor partial pressure until the oxide surface is completely covered with water. A further increase in the water vapor partial pressure yields multilayer adsorption where a 'liquid like' layer of HF and H_2O is formed at the silicon oxide surface. Since the transition point is determined by the saturation pressure of the vapor mixture, it will shift towards higher pressures when the temperature is increased.

The etch rate of doped oxides is less affected by the selected process parameters since sufficient HF adsorption is realized by a different mechanism. It is well

known that H_3PO_4 is formed during etching of (B)PSG in an HF solution. This H_3PO_4 is generated in the reaction of H_2O with P_2O_5, the bonding state of phosphorus in (B)PSG films. It is found that H_3PO_4 is also generated in HF vapor etching of (B)PSG. Since H_3PO_4 is highly hygroscopic it readily absorbs water molecules generated in the continuing reaction of HF with SiO_2. The so formed $H_3PO_4(H_2O)$ is a liquid with a low vapor pressure and, thus, does not evaporate at the reactor pressures and temperatures at which the HF vapor process is carried out. The HF dissolves in the $H_3PO_4(H_2O)$ layer and this solution is able to etch the oxide at a high rate (see figure 2).

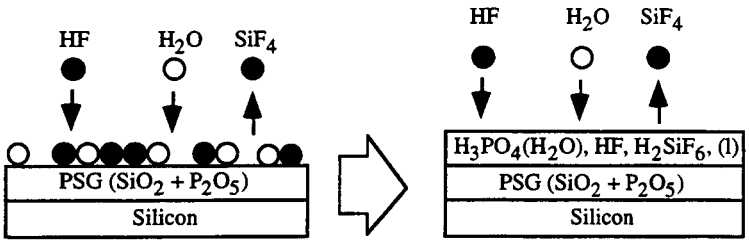

Figure 2. Etch mechanism of (B)PSG

REFERENCES

1. B.E. Deal, M.A. McNeilly, and D.B. Kao, Ext. Abs. of Solid State Device and Materials, Yokohama, (1991) 496.
2. M. Wong, M. Moslehi, and R. Bowling, J. Electrochem. Soc., 140 (1993) 205.
3. C. Galewski, J. Lou, and W. Oldham, IEEE Trans. on Semic. Manuf., 3 (1990) 93.
4. J. Ruzyllo, K. Torek, C. Daffron, R. Grant, and R. Novak, J. Electrochem. Soc., 140 (1993) L64.
5. H. Watanabe, T. Tatsumi, S. Ohnishi, T. Hamada, I. Honma, and T. Kikkawa, International Electron Devices Meeting, (1992) 259.
6. W.J.C. Vermeulen, L.F.Tz. Kwakman, C.J. Werkhoven, E.H.A. Granneman, S. Verhaverbeke, and M. Heyns, abstr. of ECS meeting, October 1993.